Shear Behaviour of Reinforced Concrete Members without Shear Reinforcement

A New Look at an Old Problem

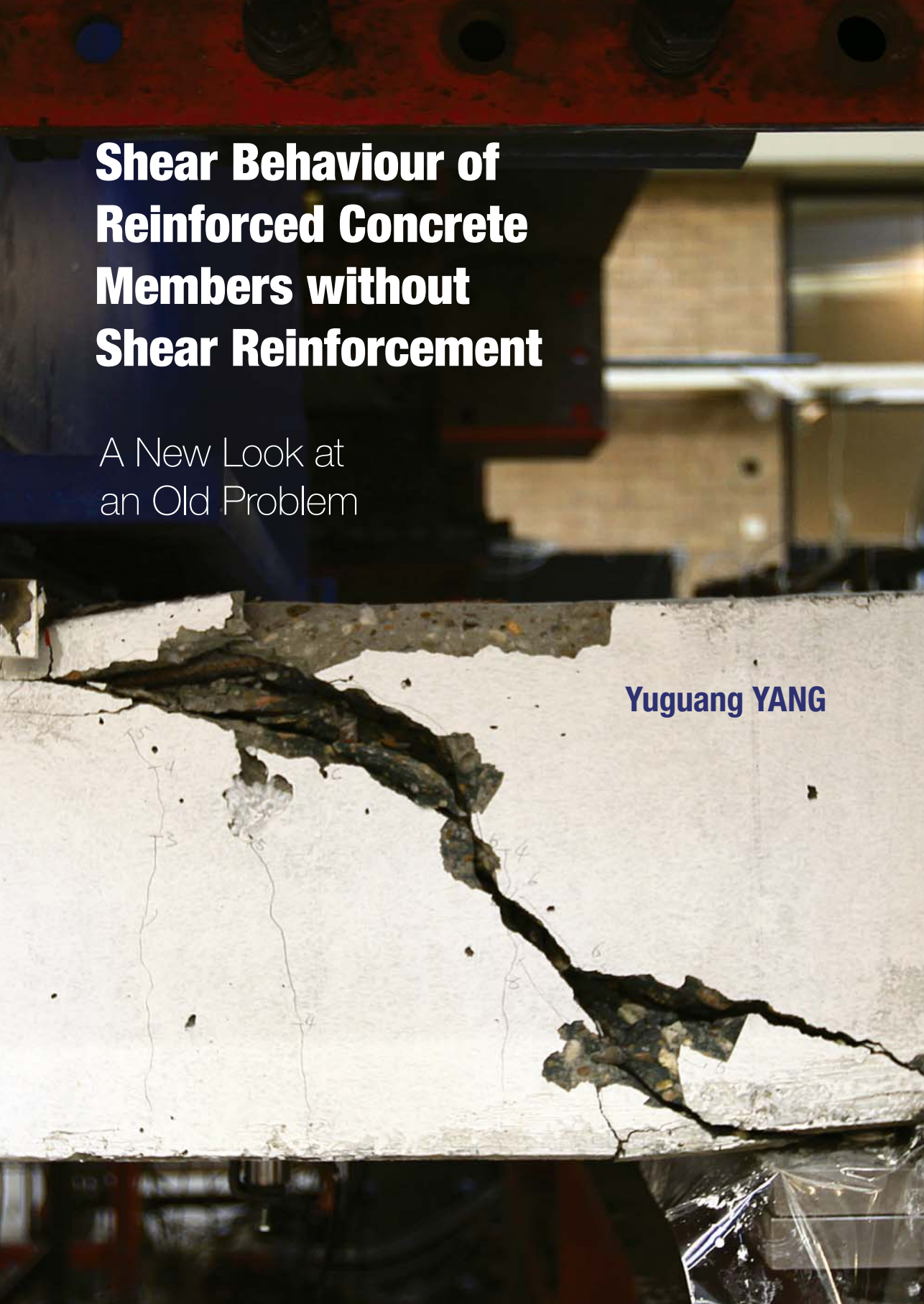

Yuguang YANG

Shear Behaviour of Reinforced Concrete Members without Shear Reinforcement

A New Look at an Old Problem

Yuguang YANG

Shear behaviour of reinforced concrete members without shear reinforcement

A new look at an old problem

Proefschrift

ter verkrijging van de graad van doctor
aan de Technische Universiteit Delft,
op gezag van de Rector Magnificus prof. ir. K.C.A.M. Luyben,
voorzitter van het College voor Promoties,
in het openbaar te verdedigen op
30 april 2014 om 10:00 uur
door

Yuguang YANG

civiel ingenieur
geboren te Jiaxing, Zhejiang - CHINA.

Dit proefschrift is goedgekeurd door de promotor:
Prof. dr.ir. Dr.-ing. e.h. J.C. Walraven

en
Copromotor
Ir. J.A. den Uijl

Samenstelling promotiecommissie:

Rector Magnificus,	voorzitter
Prof. dr.ir. Dr.-ing. e.h. J.C. Walraven,	Technische Universiteit Delft, promotor
Ir. J.A. den Uijl,	Technische Universiteit Delft, copromotor
Prof. Dr. A. Muttoni,	Ecole Politechnique Fédérale de Lausanne
Prof. dr.ir. J.G. Rots,	Technische Universiteit Delft
Prof. dr.ir. D.A. Hordijk,	Technische Universiteit Delft
Dr. R.L. Vollum,	Imperial College London
Dr.ir. A. de Boer,	Rijkswaterstaat
Prof. dr.ir. M.A.N. Hendriks,	Norwegian University of Science and Technology, reservelid

Printed in the Netherlands by Optima
First Printing, 2014.
Digital version 1.00, June 2014.

ISBN 978-94-6169-516-1

Email: yuguangyang@gmail.com

谨以此书献给我的父亲与母亲

Summary

Shear loading on structures has been recognized as one of the most relevant actions determining structural safety since the 19th century. A systematic theoretical study on the shear behaviour of structural members was already carried out by Jourawski in 1856. In the case of reinforced concrete structures, despite the great efforts that have been made through experimental and theoretical research over many years, the nature of the shear failure process of a reinforced concrete beam without shear reinforcement has always, for a substantial part, remained a riddle. Consequently, empirical formulas have been derived and widely applied in design practice for such structures in order to guarantee structural safety.

In the recent years, an increasing number of existing structures approach the end of their technical service life. Their bearing capacity needs to be evaluated accurately against the current traffic load, to determine whether or not strengthening or even demolishing of these existing structures is needed. On the other hand, with the development of numerical methods, the internal forces of a structure can be calculated more accurately, which allows the design of more complex and larger scale new structures. The shear capacity of such structures has to be estimated accurately as well. In both cases, complex loading conditions and material properties are encountered. Without a solid physical background, the conventional empirical methods may be inapplicable in many situations. A better understanding of the nature of the shear failure of reinforced concrete members seems to be more urgent than ever. The research work presented in this dissertation concentrates on this task. Based on the results of the experimental research program, the dissertation presents the researcher's philosophy on the failure mechanism of reinforced concrete structural members without shear reinforcement induced by the opening of an inclined crack in the critical shear span.

Contrary to the various theories on shear known from literature, the present research work takes a new look at this old problem. It builds its theory fundamentally on the study of the cracking behaviour of a concrete beam. With the help of fracture mechanics and non-linear finite element analysis, the develop-

ment of the crack pattern in a beam is simulated with regard to spacing, height and profile of the flexural cracks. The simulation of the crack pattern enables the study of the contribution of the different shear transfer mechanisms of a cracked section under given kinematic conditions for any assumed failure mechanism. On the basis of the study it was concluded that the opening of a critical inclined crack at shear failure is attributed to the unstable development of secondary cracks along the tensile reinforcement and/or the compression zone. Furthermore, the failure criterion is assumed to be related to the shear displacement between the crack faces of a flexural shear crack. Finally, the bearing capacity of the residual structure bounded by the inclined crack is evaluated, which provides a criterion to establish whether the opening of such an inclined crack will result in immediate failure or not.

To be of practical relevance, the possibility of converting a theory into a simplified evaluation procedure is considered to be equally important in the research. Therefore, efforts have been made to develop an evaluation procedure for practical use. The resultant evaluation procedure can be considered as a reference for future design code development. It is based on a critical section defined by a simplified crack profile at a predefined section close to the loading point. A simplified evaluation method is developed in order to calculate the contribution of aggregate interlock, tension softening and dowel action to the shear force transfer along the simplified cracked profile with a given shear displacement Δ. From an inverse analysis of the results of shear tests reported in literature, the critical shear displacement Δ_{cr} was derived. That leads to a shear evaluation procedure for simply supported beams subjected to point loads. A comparison of the calculated shear capacities with experimental results from a database known from literature containing 176 carefully selected results (König & Fischer 1995) showed that the proposed evaluation procedure is able to deliver a very consistent prediction in general, with a coefficient of variation of only 12.2%. Owing to its solid physical background, the evaluation procedure is more generally applicable than the conventional empirical methods when dealing with complex design situations. As examples, several special topics have been dealt within the scope of the presented evaluation procedure. With the physical meaning of each component in the evaluation procedure known, a logical adjustment can be made for the corresponding components in the formula according to the specific situations considered. That conclusion was further confirmed by comparing the model predictions with experimental results of tests that were carried out by the author at TU Delft, and reported in literature investigating these topics. The effects of the special aspects covered are listed in the sequel:

- Fracture of aggregate in high strength concrete or lightweight aggregate concrete beams (Chapter 4);

- Rebar configurations (Chapter 4);
- Scaling effect with regard to the height of the structural member (Chapter 4);
- Complex loading and supporting conditions of the structural member (Chapter 5);
- Spatial variability of the material properties, such as concrete strength (Chapter 6);
- Width of a one-way slab (Chapter 6).

Samenvatting

De afschuifbelasting op constructies wordt als sinds de 19e eeuw gezien als een van de meest relevante inwerkingen die de constructieve veiligheid bepalen. Een systematische theoretische studie omtrent het gedrag van op afschuiving belaste constructieve elementen werd al uitgevoerd door Jourawski in 1856. In het geval van betonconstructies geldt, dat de manier waarop een gewapend betonnen balk zonder schuifwapening op afschuiving bezwijkt, nog steeds raadselachtige aspecten kent. Dat verklaart, waarom empirische formules zijn afgeleid en op grote schaal worden gebruikt om de constructieve veiligheid van constructies te garanderen.

Gedurende de laatste jaren naderen een toenemend aantal bestaande constructies het einde van hun technische levensduur. Het draagvermogen van deze constructies moet worden geëvalueerd met betrekking tot de huidige verkeersbelasting, om vast te kunnen stellen of versterken, of zelfs afbreken, noodzakelijk is. Daarnaast kan door de ontwikkeling van numerieke analysemethoden het krachtsverloop in de constructie nauwkeuriger worden vastgesteld dan voorheen, waardoor het mogelijk wordt meer complexe en grootschalige constructies te ontwerpen. Het afschuifdraagvermogen van zulke constructies moet eveneens zo nauwkeurig mogelijk worden vastgesteld. In beide gevallen krijgt men te maken met complexe belastingcondities en bijzondere materiaaleigenschappen. De beschikbare empirische relaties zijn, door het ontbreken van een degelijke fysische achtergrond, in veel situaties niet toepasbaar. Een beter begrip van de fysische achtergrond van het afschuifdraagvermogen van gewapend betonnen constructiedelen is daarom relevanter dan ooit. Het onderzoek, beschreven in deze dissertatie, richt zich op deze problematiek. Op grond van de resultaten van het uitgevoerde onderzoeksprogramma, wordt in de dissertatie een nieuwe filosofie ontwikkeld voor de beschrijving van het afschuifdraagvermogen van elementen zonder schuifwapening, op grond van de opening van een schuine scheur in het kritische deel van het element.

In tegenstelling tot de diverse theorieën die bekend zijn uit de literatuur, wordt in de voorliggende dissertatie een theoretisch model ontwikkeld op basis van het scheuropeningsgedrag van een betonnen balk. Met behulp van breuk-

mechanische overwegingen en een niet-lineaire eindige-elementenanalyse, wordt de ontwikkeling van het scheurenpatroon in de balk gesimuleerd, waarbij rekening wordt gehouden met de afstand, de hoogte en het profiel van de buigscheuren. Deze simulatie van het scheurenpatroon geeft de mogelijkheid de grootte van de diverse componenten die aan het afschuifdraagvermogen bijdragen te berekenen, rekening houdend met de kinematische condities behorend bij het aangenomen breukmechanisme. Op basis van de uitgevoerde studie werd geconcludeerd dat de opening van de kritische schuine scheur bij het optreden van afschuifbreuk is gerelateerd aan de instabiele ontwikkeling van de secundaire scheuren langs de langswapening en/of de betondrukzone. Verder wordt aangenomen dat het breukcriterium gerelateerd is aan de parallelverplaatsing tussen de scheurvlakken van de afschuifbuigscheur. Uiteindelijk wordt het draagvermogen van het hoofdgedeelte van de constructie bepaald, dat begrensd is door de schuine scheur. Dit levert een criterium, op basis waarvan vastgesteld kan worden of het openen van een dergelijke schuine scheur zal resulteren in onmiddellijke breuk.

Om de praktische toepassing van de ontwikkelde theorie te ondersteunen is in het onderzoek nagegaan of het ontwikkelde model kan worden omgewerkt naar een vereenvoudigde evaluatieprocedure. Daarom is getracht een evaluatieprocedure voor praktisch gebruik te ontwikkelen. De hieruit resulterende evaluatieprocedure kan worden beschouwd als grondslag voor de ontwikkeling van een toekomstige generatie dimensionerings- en evaluatierichtlijnen. De procedure is gebaseerd op een kritische doorsnede vastgelegd door een vereenvoudigd scheurprofiel ter plaatse van een bij voorbaat aangewezen doorsnede dicht bij het punt waar de geconcentreerde last aangrijpt. Een vereenvoudigde evaluatiemethode is ontwikkeld om de bijdragen van scheurwrijving, tension-softening en deuvelwerking langs het vereenvoudigde scheurprofiel aan het afschuifdraagvermogen vast te stellen als functie van de parallelverschuiving van de scheurvlakken. Door het uitvoeren van een inverse analyse van de resultaten van afschuifproeven, ontleend aan de literatuur, werd de kritische parallelverplaatsing van de scheurvlakken vastgesteld. Dit resulteerde in een evaluatieprocedure voor statisch bepaalde balken onderworpen aan puntlasten. Een vergelijking tussen de berekende waarden van het afschuifdraagvermogen en resultaten uit experimenten, ontleend aan een zorgvuldig samengestelde databank met 175 proefresultaten (König en Fischer, 1995) toonde aan dat de voorgestelde evaluatieprocedure in staat is om een zeer consistente voorspelling van het afschuifdraagvermogen te geven, met een variatiecoëfficiënt van slechts 12,2%. Op grond van het ontwikkelde fysische model is de evaluatieprocedure in bredere zin bruikbaar dan de conventionele empirische methoden, indien het gaat om meer complexe ontwerpsituaties. Als illustratie zijn diverse speciale gevallen behandeld, uitgaande van de in dit

onderzoeksproject ontwikkelde evaluatieprocedure. Omdat de fysische betekenis van elke component in de evaluatieprocedure bekend is, kan een logische aanpassing worden gedaan voor de corresponderende componenten in de formule behorend bij de beschouwde specifieke situatie. Deze conclusie wordt verder bevestigd door het vergelijken van de voorspellingen gedaan met het model met de resultaten van experimenten, uitgevoerd door de auteur van dit proefschrift in het Stevinlaboratorium, en resultaten ontleend aan de literatuur voor vergelijkbare situaties. Het effect van de volgende speciale aspecten werd hierbij onderzocht:

- Breuk van de toeslag in hogesterktebeton of lichtbeton (Hoofdstuk 4)
- Configuratie van de wapening in de trekzone (Hoofdstuk 4)
- Schaaleffect gerelateerd aan variatie van de doorsnedehoogte (Hoofdstuk 4)
- Complexe belasting- en oplegcondities van toepassing op het constructieve element (Hoofdstuk 5)
- Ruimtelijke variabiliteit van de materiaaleigenschappen van beton, zoals de betonsterkte (Hoofdstuk 6)
- De breedte van in één richting dragende platen (Hoofdstuk 6)

Contents

Preface

Being a Ph.D. student (Promovendus) means spending years on studying a specific subject. It might sound awful for many. To me this period is perhaps the most enjoyable part of my life so far. Ph.D. research is one of the very few jobs in the world, in which you are paid to spend your time, energy and other resources freely just to fulfil your own curiosity. The research of shear turns out to be a perfect playground full of unknowns for me. It is such a complex topic that even after more than one hundred years of research with countless experiments, people are still debating on the most fundamentals of this phenomenon worldwide. Although a lot have been discovered, even more are still waiting to be uncovered. That gives me the chance to blend my own theory with the more than enough available ingredients, and to try out with my big toys in the lab (the large scale specimens). Of course, the greatest joy in this journey is that, at certain point, I was able to predict my test results with my own theory, and the same theory worked for most of the tests carried out by others in the literature as well. But sadly, it also indicated that this joyful journey is approaching to its destination. Looking back to the past few years I am really grateful to many.

First of all, I would like to express my gratitude to my promoter, Prof. Joost Walraven, who made this fun period possible by offering me the opportunity of doing this research in the group of concrete structure. His full trust and encouragement allows me explore freely after my own instinct. Not everyone could enjoy such freedom, but it really made me comfortable. His vast knowledge on almost all aspects of concrete structures always brought me the right information. I always get lots of papers and other materials from him, many of which can never be found through modern searching engines on internet.

I am certainly in great debt to my copromoter Joop den Uijl. Joop is the teacher who introduced me to the academic world. As my daily supervisor since my MSc project, he showed me the uncompromised attitude to the scientific research, and taught me patiently how to write a thesis, how to execute experiments and many other things. He is always a wise mentor to me. In China, we

often say your teacher is like your father outside home. Joop has clearly proven this in the past few years. Without him this work could not have been possible.

My graduation committee has to be thanked for the time and effort they spent. Among them, I would like to thank Prof Dick Hordijk for his helpful advice on the crack path calculation, and for his support to me to finalize this thesis work. Dr. Ane de Boer is thanked for his critical comments on my reports and the FEM models in my research. Thanks also go to Prof. Aurelio Muttoni and Dr. Robert Vollum, for the inspiring discussions during the *fib* conferences and for their valuable advice on my thesis.

An exceptionally large amount of full scale tests have been carried out during my Ph.D. study. This is would not be possible without the help from the technicians in Stevin Lab. Special thanks go to Fred Schilperpoort, for his reliable technical support and expertise of measurement equipment. I also would like to appreciate the help from Albert Bosman and Ger Nagtegaal for their help of carrying out some of the experiments. Ton has to be thanked for all the other supporting works. Thanks also go to the former MSc student Stavros Petrocheilos for his help on the weak spot tests.

I am thankful to Jan Gijsbers for sharing his opinion on shear with me, and for allowing me to use the results and the nice photos of the TNO shear tests. My acknowledgement also goes to Arthur Slobbe. His innovative CPA is really the perfect solution for my crack path simulation.

Appreciation also goes to Rijkswaterstaat, for their financial support to make this research possible. The additional financial support from Stichting SOOB is also appreciated.

I own lots of thanks to my officemate Sonja, for giving me many valuable advices patiently, getting me out of the office in the coffee breaks and all those Dutch lessons. During the Ph.D. period, I had the great pleasure to work with many of my wonderful colleagues and Ph.D. fellows in the concrete structure group. To Cor, our discussions on the shear mechanics in the coffee corner are quite inspiring. To Kees, our discussion about 'shear does not exist' are quite helpful. To the other members of the lunch club: Albert, Eva, Kees, Patrick, thanks for all the jokes you made on the lunch table, and the very occasional but helpful academic discussions. The thanks also go to the members of the lunch club from foreign universities: Ryosuke, Pablo, Ana, Susanne, Stefano and more.

I also would like to thank my friends: CUI Haiyang, LIU Xiaochen, LI Sheng, ZHOU Jian, ZHAO Qiaole, Tiago and all the other friends. I cannot list all of your names within this short acknowledgement. The same thanks go to my roommates during this period: ZHANG Lujun, DENG Wenhua, REN Shibo, SHI Haowen, REN Dongya, DENG Shuanghou, and WANG Jingang. You make my life in Delft not only academic research. The thanks also go to Dr. YE Guang for many of his valuable advices.

A special acknowledgement goes to HU Bin, for accompanying me during the whole Ph.D. period. We have been going through a long journey and hopefully it will last forever.

Last but the most important, I would like to give my greatest gratitude to my family, for their endless and unconditional love throughout my life. All the work being presented in this book is undoubtedly the fruit of their support and patience; therefore I would like to dedicate this book to my father and mother.

Yuguang YANG
April 11, 2014
Delft, the Netherlands

Chapter 1

Introduction

1.1 DO WE NEED ANOTHER ANALYTICAL MODEL FOR SHEAR?

The so-called shear failure is usually considered as one of the most critical structural failure modes for reinforced concrete structures, especially for the structural members without shear reinforcement. Unlike other failure modes like flexural failure, almost no warning occurs, signalizing that the structure is at the onset of failing in shear. Therefore, shear failures of structural elements usually lead to catastrophic, loss of casualties and properties, and shall be prevented at high priority.

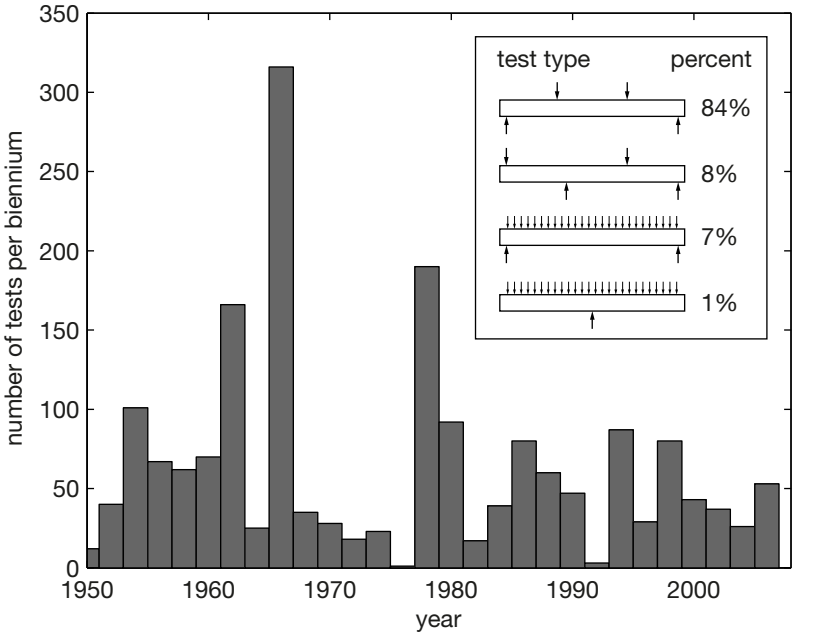

Fig. 1.1. Distribution of number of research programs in terms of date of publication in the past sixty years (Collins et al. 2008).

Good understanding of the shear behaviour of concrete structures is essential to design against shear failure. The fundamentals of shear design of reinforced concrete beams have been established since the beginning of the last century, when Mörsch proposed the first model for concrete beams in shear (Mörsch 1909). At that time it was already assumed that the shear problem had been more or less solved. Thus, not so much research had been done after that until the last fifty years, when two roofs of U.S. air force bases collapsed under their self-weight in 1955 and 1956. The total collapsed area in those cases was more than 900 m^2. (Stamenkovic 1977; Delatter 2009). Both collapses were due to the shear failure of the reinforced concrete girders under the roof. The failure

occurred in the part of girders without shear reinforcement. Investigations showed that in both cases, the design, material and fabrication of the structures were up to date to the design standards of that time. Engineers and researchers at that time had to admit that their knowledge about shear capacity of reinforced concrete structures was still rather limited.

Consequently, lots of attempts have been made to generate a better understanding of the shear carrying behaviour of reinforced concrete structures. Different new models and design methods have been proposed by researchers, a brief review of which is given in Chapter 2. As an indication, the amount of tests on the shear capacity of concrete structures reported in literature in the past 60 years is plotted in Fig. 1.1 (Collins, Bentz et al. 2008). A clear increment on the amount of experiments is observed. Thanks to that, the knowledge of shear has been greatly improved. Besides, advanced non-linear finite element methods have been developed for modelling the fracture behaviour of concrete structures, like Atena (Červenka & Jendele 2009) and Diana (TNO-DIANA 2011). All these aspects seem to indicate that the old problem of shear capacity of reinforced concrete members has been solved. We have already obtained enough models to describe this phenomenon.

Yet, it is still too early to draw such a conclusion. Structural failures caused by shear can still not be fully prevented. Besides, there are more questions from practice, which cannot be solved by the models available. On September 30th 2006, a portion of the de la Concorde Overpass in Laval, Québec, Canada collapsed, resulting in five casualties, see Fig. 1.2. The investigation afterwards led to the conclusion that the collapse was due to the shear failure of the main bridge girders which fulfilled the design regulations when it was designed 40 years earlier (Commission of Inquiry 2007). Further investments resulted in the demolishment of 28 similar bridges, and the strengthening of 25 others. All those bridge girders were reinforced concrete beams without shear reinforcement.

Fig. 1.2. Collapse of the de la Concorde Overpass (Commission of Inquiry 2007).

In the case of the Netherlands, a large portion of the concrete bridges in the Dutch highway system were constructed in the 1960s and 1970s based on the expected traffic loads at that time (Klatter & van Noortwijk 2003). They mostly contain concrete slab decks without shear reinforcement. In 2008, a preliminary analyses carried out by the Dutch Ministry of Infrastructure and Environment (Rijkswaterstaat) with the Eurocode provision (Eurocode 2 2004) showed that many of those bridge decks did not fulfil the code requirements on shear anymore under the actual heavier traffic load. This would mean a national renovation of all those bridges, which is really costly for the country. Nevertheless, traffic is still running on those bridges with no significant damage reported yet.

In both cases the present design methods led to a conclusion which is opposite to the observations in practice. This undoubtedly indicates that up till now our models cannot predict the shear carrying behaviour of concrete beams without shear reinforcement with sufficient accuracy yet. As will be presented later in Chapter 2, the available models show fundamental disagreement on the mechanisms causing shear failure. In case of non-linear finite element methods, the difficulty lies in the modelling of the shear stress in cracks taking into account both normal and tangential stress as observed in experiments, which results in unsymmetrical constitutive matrices. Simplifications have been made to solve this difficulty, which means that calibrations are always needed to get a proper prediction of the overall behaviour by FEM methods.

Taking the aspects listed above into account, the answer to the question raised in the title of the section is still YES. The old problem of the shear behaviour of concrete members without shear reinforcement remains to be solved. In fact, more challenges are encountered. With the structural elements becoming larger and more complex, a model which is more accurate in describing the size effect of the structure capacities and more capable to handle non-conventional loading conditions and material properties is needed. Such a model can only be derived based on a solid understanding of the mechanisms behind the phenomenon.

For the 50 to 60 years old concrete bridge decks, a more accurate assessment procedure for the structural shear capacity is in demand to deal with the spatial variability of concrete properties, loading history and complex load combinations under traffic loads. Therefore, the Dutch Ministry of Infrastructure and Environment started a research project investigating the residual shear capacities of existing concrete bridges. The work presented in this dissertation is based on the research carried out by the author in the past 4 years at Delft University of Technology within the scope of that project. It is hoped that this work may contribute to the knowledge of shear design of concrete structures.

1.2 SCOPE OF THE RESEARCH

The large number of experimental research programs in the last sixty years has shown that the shear capacity of reinforced concrete structures can be effected by lot of factors (Regan 1993; ACI-ASCE Committee 445 1998; Collins, Bentz et al. 2008). Within this research, the author would like to restrain his research to the following aspects:

First of all, only the shear behaviour of reinforced concrete elements without shear reinforcement is addressed. This includes concrete beams, wide one-way concrete slabs loaded by a line load in width direction, etc. There should be no internal shear reinforcement such as stirrups, or any other external reinforcement along the depth direction of the elements. The elements are not prestressed. Besides, the reinforcing bars are conventional steel rebars. Fibre Reinforced Polymer (FRP) or any other types of reinforcing bars are studied in this research because of the different bond properties. This type of structure is often considered as shear critical in structural design. They can be found in many places, such as concrete slab decks, strip footings, underground tunnel roofs or walls, thick concrete transfer floors in buildings, etc.

Secondly, the structural elements are made of normal concrete mixtures. Although special types of concrete such as high strength concrete and lightweight aggregate concrete are also discussed in this research work, they are only included in general examples to illustrate the function of certain mechanisms such as aggregate interlock. The effect of using a specific special concrete type will not be investigated in this research. Also, the shear behaviour of fibre reinforced concrete elements is not discussed in this research either, since fibres can be considered as a type of shear reinforcement as well.

Third, although the influence of the position of the load on the shear capacity (Kani 1964) is one of the important aspects to be studied in this research, loads very close to the support have not been regarded in this research program. In that case, the load is directly transferred to the support through a different mechanism. Within this research, a criterion will be given to distinguish when the direct load transfer mechanism is dominating. It is considered as the boundary conditions for this research. However, further study on the direct load transfer mechanism is not considered as the emphasis of this research because of the limited time and resources.

Furthermore, preliminary studies have shown that with regard to the shear capacity of concrete slab bridges, there are several aspects which have been ignored or inaccurately implemented in the design codes, such as the distribution effect of a point load close to the slab support (Regan & Rezai-Jorabi 1988; Lantsoght et al. 2011; Lantsoght 2013), the compressive membrane action in slabs (Rankin & Long 1997; Amir 2012), the long term effect on the shear be-

haviour of concrete structures (Sarkhosh 2012) etc. Many of them are included in the other parts of the Rijkswaterstaat research project. For those topics reference is made to corresponding reports.

1.3 EXPERIMENTAL PROGRAM AND OTHER RESEARCH METHODOLOGY

As mentioned above, the research is based on experimental work carried out at the Stevin Laboratory at Delft University of Technology with several different topics assigned by Rijkswaterstaat between 2009 and 2012. Not all of those experiments are closely related. Nevertheless, they are all developed and carried out based on the same philosophy about the shear phenomenon of concrete structures supported by the author and his colleagues. Therefore, it is decided that this dissertation is mainly dedicated to the presentation of this general philosophy on the shear behaviour of reinforced concrete structures, and its application in design practice. The explanation of the theory is mainly proceeded by reasoning on what is shear failure in this dissertation. The details of the experiments and the findings from the experiments are treated as examples or proofs of the theory. For readers who are willing to learn more on the details of the experiments, several Stevin reports submitted to Rijkswaterstaat are referred to, where the large amount of experimental results derived from the measurement equipment and the evaluation of the results are explained in great detail. These experimental programs and the relating reports are listed below:

- Experimental Work on Comparing the Shear Capacities of 50-Years Old and New Concrete Beams (simply supported), 2009-2010 (den Uijl & Yang 2009; Yang 2009; Yang 2009; Yang & Den Uijl 2010);
- Experimental Research on Shear Capacity of Beams Close to Intermediate Supports, 2010-2011 (Yang & den Uijl 2011);
- Study on Shear Capacity of Old Concrete Beams with Continuous Supported Conditions, 2011-2012 (Yang & Den Uijl 2012);
- Experiments on Concrete Slabs with Weak Spots along the Width Direction, 2012 (Yang & den Uijl 2012);

Besides, non-linear Finite Element Method (FEM) Models are used in the research program. Most of the experimental programs have been developed incorporating FEM simulations. The results derived are evaluated with FEM models afterwards so that experiences are gained for a better selection of material properties for the simulation of the behaviour of similar structures in the future. The FEM models with material models and calculation procedures that were validated by previous experimental results are also used in simulating tests which could actually not be conducted. Other than that a special algorism called Sequential Linear Analysis is used in Chapter 3 to calculate the crack path

expression. The two FEM packages that have been used within this research work are Atena (Červenka & Jendele 2009) and Diana (TNO-DIANA 2011).

1.4 OUTLINE

In total, this dissertation includes 7 chapters. As a guide for the readers, a brief introduction of each chapter is provided here.

Chapter 2 provides the state of the art of the research on the shear capacity of concrete members without shear reinforcement, in which the terminology on the shear failure modes is clarified first. Flexural shear failure is distinguished from the other failure modes. The mechanisms that have been agreed by most researchers as the basic shear force transferring mechanisms in concrete beams with flexural cracks are discussed. The most influential theories are presented afterwards. They are categorised by the dominating failure mechanisms from which they were derived. As shown in Chapter 2, fundamental differences still exist between different theories about what is the dominating shear failure. It shows the necessity of investigating the failure process again. By the end of the chapter, the available shear databases are reviewed.

Chapter 3 is dedicated to exploring the shear failure process of a reinforced concrete beam fundamentally. The author tries to explain the reason why the flexural cracks in a reinforced concrete beam start to incline under a given shear force and bending moment combination, and more importantly, what is the cause of shear failure at a specific inclined crack profile observed in laboratory tests. Therefore, the profile of major flexural cracks is studied first. A general function is proposed with the help of FEM analysis, which describes the spacing, height and profiles of the major flexural crack pattern at given boundary conditions of a beam. With the crack profile expressed, the main shear transfer mechanisms along a free body formed by any flexural crack with known cross sectional force are studied, so that the driving forces for shear failure at a specific crack profile are checked. By exploring the ultimate cause of shear failure step by step, a new mechanism on shear failure shows up. By the evaluation of the residual capacity after the opening of the critical inclined crack, it is also possible to distinguish the two failure modes observed in the experiments.

The intention of Chapter 4 is to translate the shear failure mechanism derived in the previous chapter into an applicable design method. A new failure criterion is formulated with simplified assumptions, and calibrated by experimental data. The new design method is further implemented by taking into account the influence of reinforcement configuration, concrete type and size effect. The proposed method prevails regarding its accuracy, flexibility and practical relevance over existing shear models.

Chapter 5 treats the influence of complex boundary conditions to the shear capacity of concrete structures. The consideration is that for most real structures, the boundary conditions are more complex than the laboratory conditions, based on which the design formulas are derived. Thus those design formulas derived from simplified boundary conditions shall always be validated in more realistic scenarios. In this chapter, three criteria are proposed to evaluate the applicability of the new design method on new boundary conditions. Adjustments are suggested when necessary. The approach is evaluated in three specific loading conditions. Those are continuous beams with point loads, simply supported beams with uniformly distributed load, and continuous beam with uniformly distributed load. Recommendations regarding the proposed design method for these loading conditions are given.

In Chapter 6, the spatial variability of material properties is studied with the shear failure mechanism proposed in this study. The consideration of spatial variability becomes especially important when assessing the residual capacity of existing structures. This problem is decomposed into longitudinal (length) direction, vertical (depth) direction and transverse (width) direction in this chapter. The evaluation in each direction is validated by experimental research programs related to practical questions. Similarly, recommendations are made to deal with specific situations under the respective scenarios.

Chapter 7 summarizes the shear failure mechanisms and the corresponding design method proposed in the research with respect to all the situations presented in the preceding chapters. Moreover, several special topics are regarded which do not fully reflect the experimental observations or seeming to be consistent with other current theories. Based on the discussion further experimental and theoretical input for the model is suggested.

As a general guidance, for readers who are more interested in the development of the theory and how it is translated into the design procedure, Chapter 3 and 4 form a self-consistent part. They explain the basics of the whole theory, thus can be read independently, or with the implementation of Chapter 2. Chapter 5 and 6 serve as extensions of the theory to special applications. They are written for the readers who have specific interests in the related topics.

Chapter 2

Shear Failure of Reinforced Concrete Beams in Literature

2.1 INTRODUCTION

Although after the first initiatives taken by Mörsch (Mörsch 1909), research on the behaviour of concrete members loaded in shear has been carried out for more than 100 years, a consistent definition of shear failure of reinforced concrete beams without shear reinforcement does not exist yet. A commonly accepted phenomenological definition of shear failure is that it is a brittle failure occurring under a shear force, with diagonal cracks developing in the span. The most important elements in this type of failure are the shear force and the diagonal cracks in the span. According to the classic beam theory (de Saint-Venant 1856; Jourawski 1856), the maximum shear stress locates at the neutral axis of a linear elastic beam section. As a result the direction of the first principal stress is in the diagonal direction. When diagonal cracks are observed in concrete members at the neutral axis of the cross section, researchers linked those cracks to the principal stress distribution described in classic beam theory. They thought it was the maximal shear stress close to the neutral axis that results in opening of the diagonal cracks. Thus, this type of failure is denoted as shear failure.

However, diagonal crack opening as a result of the principal stress exceeding the concrete tensile strength at mid-height of the specimen section only occurs in a limited number of structural elements, like prestressed hollow core slabs or T beams, in which the flexural cracking is limited, and the width of the cross-section is small at mid-height of the cross section, see Fig. 2.1.

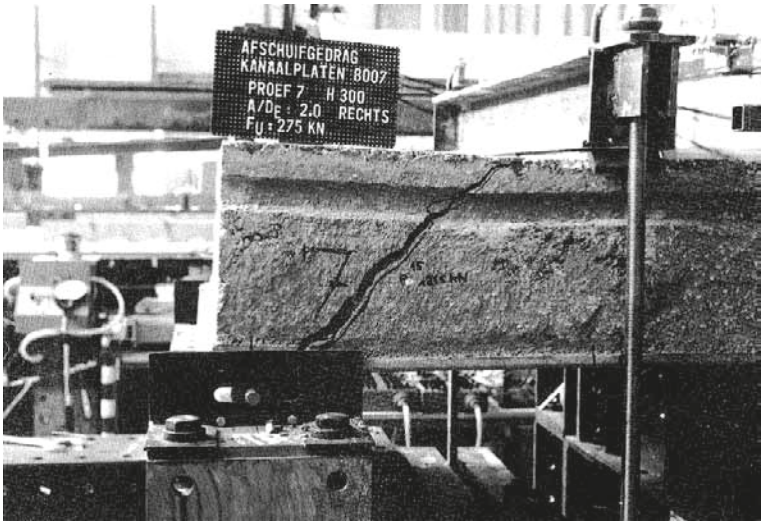

Fig. 2.1. Diagonal tension failure of a hollow core slab (Walraven & Mercx 1983).

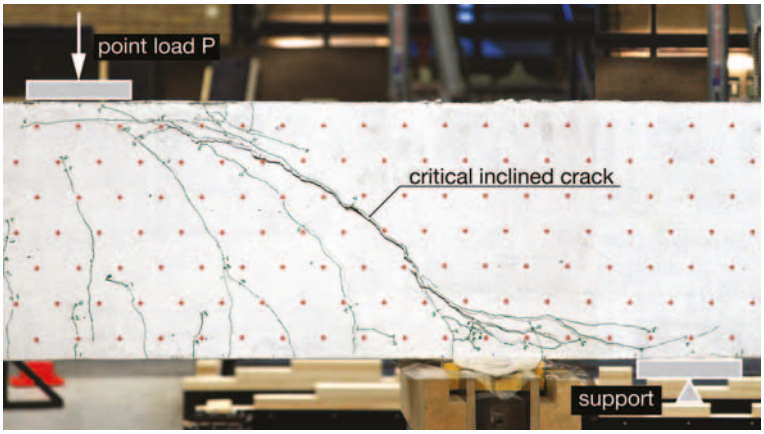

Fig. 2.2. Crack pattern of beam with flexural shear failure (diagonal tension failure according to some literature).

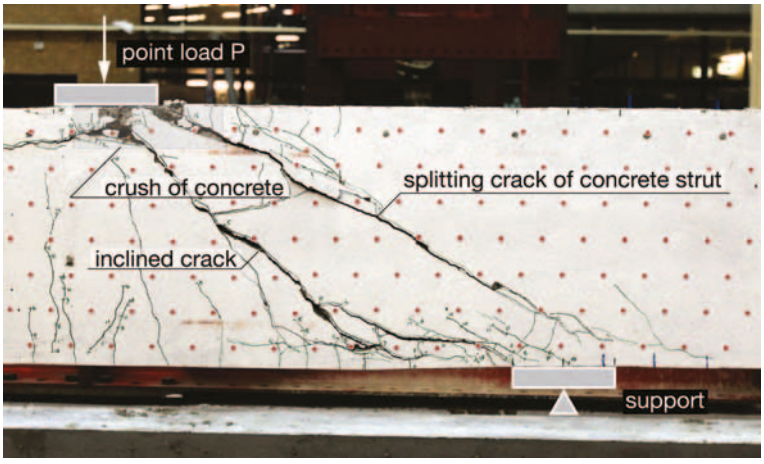

Fig. 2.3. Crack pattern of beam with shear compression failure.

For a reinforced prismatic beam, the failure type 'shear failure' actually stands for more than one type of failure mode. Depending on whether the opening of the diagonal crack results in the collapse of the beam or not, two failure modes can be distinguished. In some literature (Regan 1993; Nawy 2009), those failure modes are called 'Diagonal Tension failure' and '**Shear Compression failure**'. The crack patterns corresponding to the two typical failure modes are illustrated in Fig. 2.2 and Fig. 2.3 respectively. In Fig. 2.3, the diagonal crack, marked as 'splitting crack of concrete strut' developed after the concrete strut crushed, as a secondary effect of failure. However, what has to be clarified is that

only the failure mode shown in Fig. 2.1 is truly caused by the tensile stress in the diagonal direction, thus can be named by **diagonal tension failure**. The so-called diagonal cracks in most reinforced concrete beams are actually **inclined flexural cracks** due to the shear force, or **flexural shear cracks** as described in (ACI-ASCE Committee 426 1973). To be able to distinguish the failure modes shown in Fig. 2.1 and Fig. 2.2, it is more appropriate to denote the latter one as '**flexural shear failure**' in relation to its origin from a flexural shear crack. Besides, those inclined flexural cracks are called inclined cracks to be distinguished from the real diagonal cracks such as shown in Fig. 2.1. Since the real diagonal tension failure only occurs under special conditions it is not discussed anymore in this study. With respect to shear failure modes, only flexural shear failure and shear compression failure are discussed in the study.

Apparently, these two failure modes reflect the different dominating load transfer mechanisms in beams. Fenwick and Paulay (Fenwick & Paulay 1968) suggest that for a beam the transfer of the shear force can be attributed to two general mechanisms:

- Variation in internal forces acting over a constant lever arm;
- Constant internal forces acting over a variable lever arm.

The first load transfer mechanism relates to flexural shear failure, which is often found in beams with large spans. The maximum shear forces corresponding to this failure mode are usually lower than that found with the other load transfer mechanism. Since the loading condition of a concrete member is not always known in advance, the lower bound of its shear capacity defined by the flexural shear failure mode is crucial. Therefore, this research work mostly focuses on the first mechanism and the failure process according to that mechanism.

When the variation of the lever arm is the dominating shear transfer mechanism, this shear force transfer mechanism is also denoted as '**Arch Action**' (Fenwick & Paulay 1968). In that case, the behaviour of the structure can be simulated by the **Strut and Tie method**, representing the flow of forces with concrete struts and steel tensile ties. The method was proposed in the 1980s (Marti 1985; Schlaich et al. 1987). It has been shown to be able to estimate the bearing capacities of beams having the failure mode of shear compression failure with sufficient accuracy (Walraven & Lehwalter 1989; Walraven & Lehwalter 1994; Wight & Parra-Momtesinos 2003; Collins et al. 2008). The method has been implemented in most concrete design codes by now: (AASHTO 2004; ACI Committee 318 2004; CSA 2004; Eurocode 2 2004; fib 2012). Alternatively, Mihaylov et al. proposed the Two-Parameter Kinematic Theory for the shear design of deep beams in (Mihaylov et al. 2013), which will be discussed further in section 3.5.3.

In general, extensive literature is available on this subject, therefore no further discussions on the ultimate capacity of beams with shear compression failure will be included in this research. Only the shear cracking of deep beams is studied in this research as an extension of the research on slender beams.

2.2 MECHANISMS OF SHEAR TRANSFER IN BEAMS CRACKED IN FLEXURE

2.2.1 Overview

Given the fact that the tensile strength of concrete is lower than its compressive strength, flexural cracks are generally present in a normal reinforced concrete member before shear failure. Although there are still discussions on the mechanism of the failure process in beams with flexural cracks, it has been widely accepted that there are four types of mechanisms that can transfer the shear force in a cracked concrete beam since 1970s (ACI-ASCE Committee 426 1973; ACI-ASCE Committee 445 1998). They are:

- Shear stress in the uncracked concrete zone;
- Aggregate interlock caused by tangential displacement of the crack faces;
- Residual tensile stress occurring at limited normal opening of the cracks;
- Dowel action caused by the longitudinal reinforcing bars.

The research on the four mechanisms in literature is introduced briefly in the following sections. In Chapter 3, a more detailed treatment of the mechanisms will be given, based on which the shear failure process is analysed.

2.2.2 Shear Stress in Uncracked Concrete

In the uncracked part of a reinforced concrete cross section, the stress distribution still follows the theory of elasticity. Once the boundary conditions of the uncracked concrete are known, the shear stress transferred in the uncracked concrete compression zone can be calculated. Taking into account that an exact description of the boundary conditions is almost impossible, approximations have to be made. Depending on whether the height of the compression zone varies along the beam axis or not, the simplification shall be done differently.

In the part of a beam with varying depth of the compression zone, the shear force is transmitted mainly by the inclination of the principal stress. That complies with the second shear transfer method, explained in 2.1, for which the use of the strut and tie method is suggested. Such a part of the beam is usually defined as a D (disturbed) region according to (Schlaich, Schäfer et al. 1987).

When the compression zone of the beam is more or less constant, the simplification of the boundary conditions of that zone has to regard the comb-like

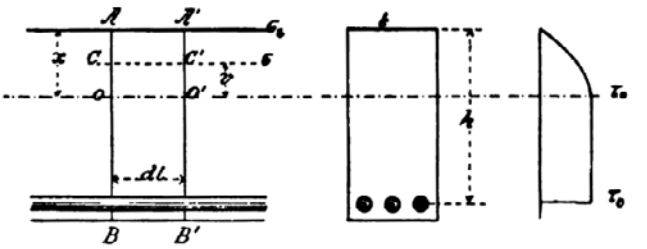

Fig. 2.4. Parabolic shear stress distribution assumed by Mörsch (Mörsch 1909).

teeth structure formed by the flexural cracks. A simplified expression of the shear stress distribution has been given by Mörsch in the early 1900s (Mörsch 1909), assuming a parabolic shear stress distribution above the neutral axis, see Fig. 2.4. The basic principle has not been changed since then. Reineck (Reineck 1991) adopted the same expression for the calculation of the shear force contribution in the compression zone V_c. Hamadi and Regan (Hamadi & Regan 1980), Taylor (Taylor 1974) suggested a change of the shear stress distribution curve. Fenwick and Paulay (Fenwick & Paulay 1968) derived a complex formula based on experimental results of beams eliminating aggregate interlock. Sherwood, Bentz and Collins measured differences of the compressive strain distribution in the compression zone in experiments, and convert them into a shear force (Sherwood et al. 2007) with the classical principle of shear force transfer proposed by (Jourawski 1856). The comparison showed that the shear force calculated based on Mörsch's formula provides sufficient accuracy on the V_c prediction with measured value: $V_c = 24\%V$ and Mörsch's formula: $V_c = 21\%V$. Those more complex expressions seem not necessary, since the simplified Mörsch's formula can already provide a very good accuracy. A similar conclusion was drawn by Taylor on the basis of his tests (Taylor 1974).

2.2.3 Aggregate Interlock

The term '**Aggregate Interlock**' stands for the effect that generates shear stress as a result of the relative tangential displacement Δ of two cracked surfaces. The name implies that the cause of this effect is the friction or contacting forces between the protruded aggregate particles in the crack.

Fenwick and Paulay (Fenwick & Paulay 1968) showed the importance of the crack surface roughness firstly by comparing the shear capacity of specimens with smoothened cracks and naturally developed cracks. They proposed an aggregate interlock formula based on a regression analysis. Gambarova proposed a more refined model assuming that aggregate interlock is generated by slip of two rough surfaces (Bažant & Gambarova 1980; Gambarova 1981). It relates the four components involved in the shear transfer process of a crack,

which are: shear stress, normal stress, tangential displacement and normal displacement.

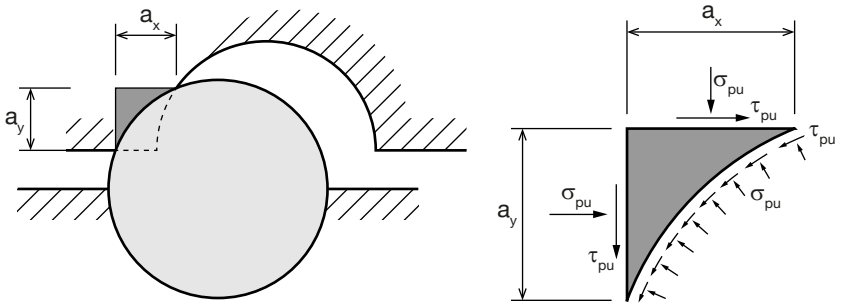

Fig. 2.5. Schematic model for the mechanism of aggregate interlock (Walraven 1981).

The most comprehensive experimental research on aggregate interlock was carried out by Walraven (Walraven et al. 1979; Walraven 1980). In his experimental program, all the four basic components mentioned above were taken into account in the same test. In total, 32 tests were carried out on concrete cracks not intersected by reinforcement, which covered most variables influencing the aggregate interlock effect. Based on the numerous test data, a mechanical model was proposed (Walraven 1980; Walraven 1981). The model will be explained further in Chapter 3. In the model, the aggregates particles are simplified by rigid spheres with random diameters and locations. The cement matrix crushes upon contact with the aggregates. Slip and crushing at the interface between the two components at the contact area generate shear stresses and normal stresses. A schematic model is shown in Fig. 2.5. The model reflects the physical background of aggregate interlock to a certain extent. In the meantime it is able to reproduce the experimental results accurately. This was approved further by Millard and Johnson in their tests (Millard & Johnson 1984; Millard & Johnson 1985). Other than the crack surface displacements, the main variables in the model are the concrete strength f_c and the maximum aggregate size $D_{\max}$. It has to be pointed out that the assumptions of rigid aggregate particles in Walraven's model should be considered as a way to simplify the roughness of the crack surfaces. In high strength concrete and lightweight aggregate concrete members, however, the aggregates break at the crack, as such reducing the shear resistance. It was shown in (Walraven & Stroband 1999) that for high strength concrete f_c = 110 MPa, the model still describes aggregate interlock properly with a reduction factor if the aggregate fracture is introduced.

Based on a regression analysis of Walraven's test results, Vecchio and Collins derived a simplified formula (Vecchio & Collins 1986):

$$\tau = 0.18\tau_{\max} + 1.64\sigma - 0.82\sigma^2 / \tau_{\max} \tag{2.1}$$

where

$$\tau_{\max} = \frac{\sqrt{f_{cm}}}{0.31 + 24w / (D_{\max} + 16)} \tag{2.2}$$

and

σ : is the normal stress in the crack surface, in N/mm²;
$\tau_{\max}$: is the maximum allowable shear stress, in N/mm²;
w : is the crack width in the normal direction to the crack profile.

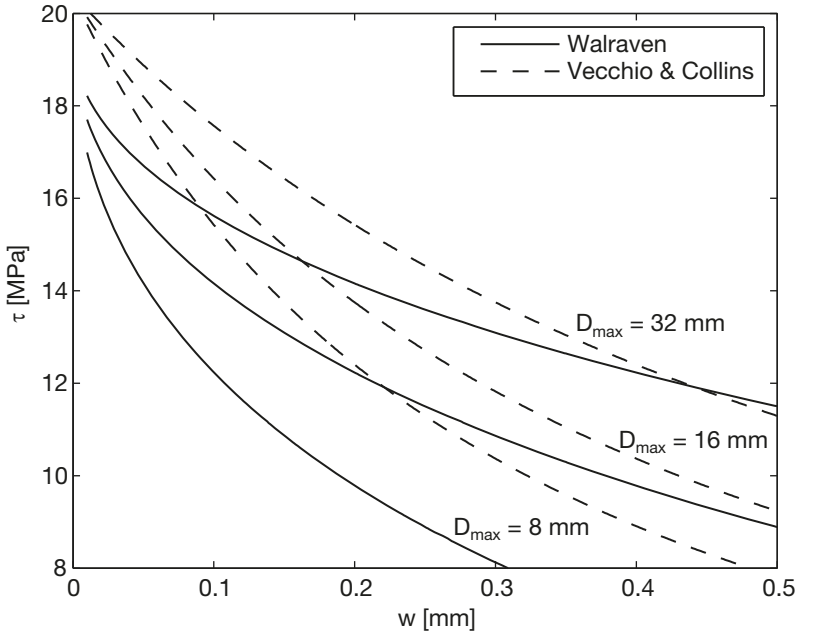

Fig. 2.6. Comparison between Walraven's model (upper bound) and Vecchio and Collins' model.

Eq. (2.2) is an approximation of the maximum shear stress level derived from Walraven's tests. A comparison between the upper bound of Walraven's model and Vecchio and Collins' simplification is given in Fig. 2.6. It shows that the later one tends to give a higher value for $\tau_{\max}$ at smaller value of w than Walraven's model.

The drawback of Eq. (2.2) is that the calculation of the shear stress has to rely on the normal stress rather than the tangential displacement Δ, which is supposed to be the resultant of the total displacements in both directions according to most physical models. That makes the formula not practical in beams without transverse reinforcement, in which the normal stress cannot be determined due to the complex stress state. To solve the problem, Eq. (2.1) was further simplified

by eliminating the normal stress terms by Bentz et al. (Bentz et al. 2006) in the Simplified Modified Compressive Field (SMCF) theory. The final simplified equation is only related to the crack width. It is employed in many constitutive equations (CSA 2004; Červenka & Jendele 2009; fib 2012) as the failure criterion for the crack surface. Apparently, compared to Eq. (2.2), it significantly underestimates the maximum shear stress of the crack at a given crack width. Despite the obvious inconsistency the equations utilizing the criterion have been shown to give reasonably accurate approximations.

To explain this, the failure criterion formula in SMCF theory should be understood in a different way. This can be revealed by comparing the SMCF equations with Walraven's model, see Fig. 2.7. The intersection points of the SMCF theory and Walraven's model indicate the tangential displacements Δ of the crack at given crack widths w and shear stresses τ. The comparison shows that the ratio of Δ/w seems to remain constant at around 0.55. Thus, the SMCF criterion actually limits the maximum tangential displacement Δ under a given crack width w implicitly to: $\Delta \leq 0.55\, w$.

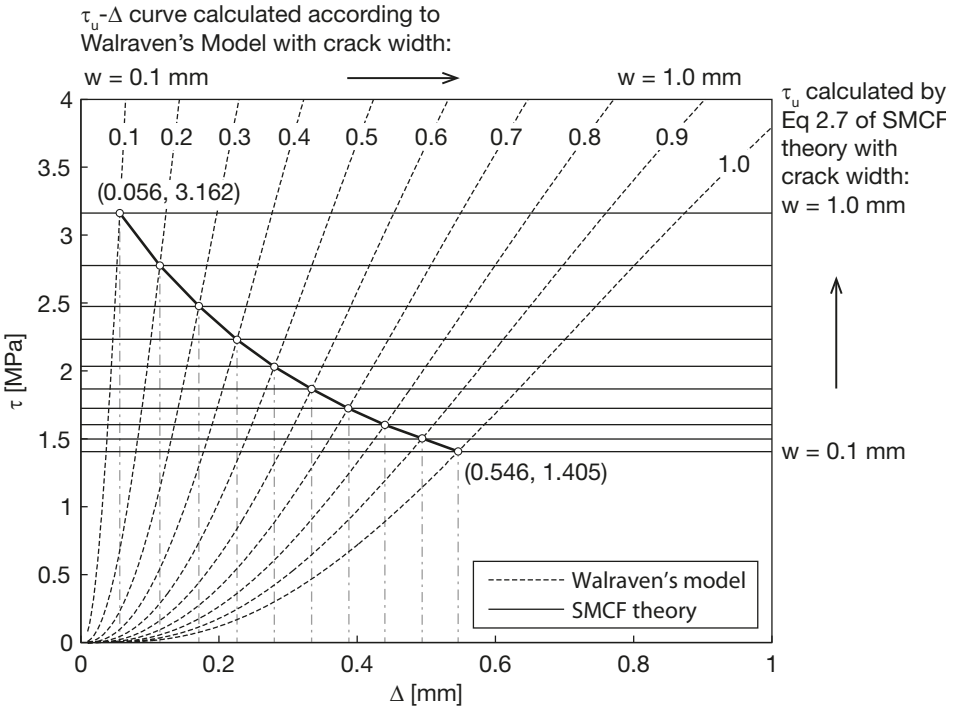

Fig. 2.7. Comparison between Simplified Modified Compression Field (SMCF) theory and Walraven's model for the same crack widths and shear stresses.

2.2.4 Residual Tensile Stress

Further than by aggregate interlock, tensile stresses can be transmitted across cracks when the crack width is smaller than 0.1 mm. The tensile stress – crack width relationship was firstly measured in 1960s by Evans and Marathe (Evans & Marathe 1968). The importance of the concrete softening relationship in structural analysis was not recognized, until Hillerborg introduced his Fictitious Crack Model simulating the bending behaviour of concrete beams (Hillerborg et al. 1976; Petersson 1981). Since then, systematic research on the tension softening behaviour of concrete has been carried out. A widely accepted tensile stress – crack width relationship is the exponential relationship proposed by Hordijk and Reinhardt in (Reinhardt & Hordijk 1986; Hordijk 1991). Significant progress has been made in the last few decades regarding to concrete fracture mechanics. Comprehensive overviews are given in (ACI Committee 446 1989; Shah et al. 1995; Bažant & Planas 1998; van Mier 2013).

With respect to the shear behaviour of concrete beams, the function of tensile stress after cracking is not agreed yet between researchers. In the shear modes based on fracture mechanics, the tensile stress across the crack is the major mechanism for shear transfer. Examples of such models are Jenq and Shah's model (Jenq & Shah 1990), or Gustafsson and Hillerborg's model (Gustafsson & Hillerborg 1988). More explanations on fracture mechanics approaches will be given in 2.3.3. According to other researchers the significance of tensile stress in shear cracks is very limited. Reineck mentioned in the discussion of (Reineck 1991) that the concrete tensile stress is only activated in the fracture zone near the tip of the crack, thus it is only relevant in very shallow beams.

2.2.5 Dowel Action

A dowel force is generated as a result of the interaction between the reinforcing bars and the surrounding concrete when there is differential tangential displacement in the crack plane of the concrete. For beams without shear reinforcement, **dowel action** occurs at the longitudinal reinforcement at the bottom of the beam. The dowel action at that location is different from the interaction between stirrups and concrete normally measured in push off tests (Millard & Johnson 1984; Pruijssers 1988). A large rebar area can be expected locally, thus a large tensile force may be expected, due to the rotation of the crack faces under bending. Krefeld and Thurston firstly investigated the mechanism of dowel action on specimens with configuration approximating the condition in beams (Krefeld & Thurston 1966), see Fig. 2.8. With similar a test configuration, Baumann and Rüsch (Baumann & Rüsch 1970) carried out an extensive experimental program on dowel action of longitudinal reinforcement. In their tests, the post peak behaviour was measured as well. They showed that

extensive experimental program on dowel action of longitudinal reinforcement. In their tests, the post peak behaviour was measured as well. They showed that even for beams without shear reinforcement, a large plastic deformation can be expected after the peak load. They derived a regression formula based on their test results, which will be discussed further in Section 3.3.2.2 in Chapter 3. Taylor carried out dowel action tests with similar configurations but with different specimen dimensions in (Taylor 1971). Houde and Mirza evaluated the dowel behaviour of longitudinal rebars in a different configuration in (Houde & Mirza 1974). The latter two research programs resulted into relationships with a quite comparable maximum dowel force as following from Baumann and Rüsch's equation. However, regarding the transverse displacement Δ at maximum dowel force, there are larger disagreements. The measured values of Δ vary from about 0.01 mm to 0.1 mm.

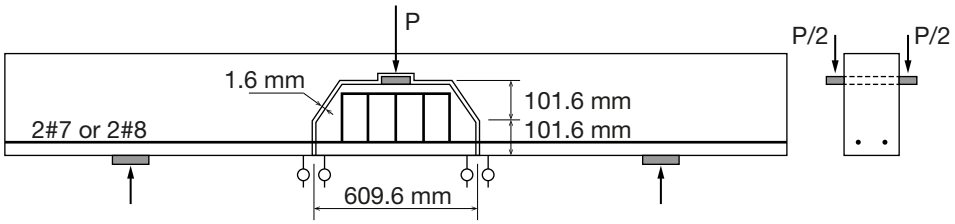

Fig. 2.8. Dowel action test setup of Krefeld and Thurston (Krefeld & Thurston 1966).

Theoretically, Vintzeleou and Tassios categorised the failure of dowel action into two modes: Crushing of Concrete and Concrete Splitting, and derived theoretical models for both modes (Vintzeleou & Tassios 1986). Their formula for Mode II is in principle the same as Baumann and Rüsch's formula. For concrete beams without shear reinforcement, Mode II is dominating.

Since the shear force contribution of longitudinal rebars is usually small compared to the overall shear capacity, typically about 15-25% according to Regan (Regan 1993), the function of dowel action was not recognized by many researchers. Chana showed for the first time the importance of dowel action (Chana 1987). He measured the change of crack widths of the critical inclined crack during the shear failure of beams with crack gauges at a high sampling rate. The measurement showed that dowel cracking along a longitudinal rebar always starts first before the opening of the critical inclined crack. Based on this observation, he concluded that: 'the mechanism of shear failure is closely associated with the loss of the dowel force.' However, how to link the dowel cracking to the overall shear force remained an open question.

2.3 SHEAR FAILURE FROM DIFFERENT PERSPECTIVES

Although the basic mechanisms that enable shear force transfer in beams with flexural cracks have been recognized and studied thoroughly, without a clear vision on the interaction between the basic mechanisms and the failure mechanism, the discussion about the shear capacity of concrete beams will continue. Therefore, there is still no general agreement on the reason of shear failure among researchers. Fundamentally different explanations on the mechanism of shear failure can be distinguished in literature, based on which different approaches have been proposed to calculate the shear capacity of concrete beams without shear reinforcement. Recently several researchers were trying the evaluate the contributions of the basic shear transfer mechanisms through experimental measurement on the kinematics of a critical crack, examples of such researches are (Yang et al. 2010; Campana et al. 2013). However, because the opening of a critical inclined crack happens in a very short time, in the meantime, the critical cracks cannot always be foreseen, measurement of the kinematic of a critical major crack during the failure process seems to be very difficult. For that reason, direct experimental proof is not yet available to support any of these approaches. In this section, a selection of representative approaches is presented in several categories, depending on the failure mechanism they are based on.

2.3.1 Prelude

The attempts of formulating the shear capacity of a concrete beam started with Mörsch's truss model (Mörsch 1909). The model assumes a truss structure in a reinforced concrete beam with shear reinforcement. To transfer the shear force, the tensile force is carried by the shear reinforcement, while the compression force is taken by the concrete. To explain the shear capacity of concrete beams without shear reinforcement, the tensile stress in the concrete has to replace somehow the role of shear reinforcement. Therefore, Mörsch related the shear capacity of concrete beams without shear reinforcement to the tensile strength of concrete. The contribution of shear resistance from concrete tensile strength was treated as an additional term, denoted as shear resistance by the concrete in his model. This can be considered as the common root of both the empirical methods and physical models on the shear capacity of concrete beams.

2.3.2 Empirical Methods

The empirical methods stand for a design approach based mainly on formulas derived from regression analysis of experimental results. The main difference between the various empirical methods lies in the choice of the variables that are taken into account in the formulation, and the structure of the formula. There is

not necessarily a physical explanation behind the formula. This type of approach has been the major practice for the derivation of code formulas in the past. Numerous empirical expressions have been proposed meanwhile. A comprehensive review is given in (ACI-ASCE Committee 426 1973) by ACI-ASCE Committee 426. Among them only a few most representative ones are discussed here, including the ACI shear formula and the Eurocode formula.

The ACI shear design method is inherited from Mörsch's model (ACI Committee 318 2004). The shear capacity of a shear reinforced concrete beam is split into the contribution of shear reinforcement and the contribution of concrete tension. The later one is also used to represent the shear capacity of concrete beams without shear reinforcement:

$$\tau_u = \frac{\sqrt{f_{cm}}}{6} \tag{2.3}$$

with

f_{cm} : is the mean concrete strength;
τ_u : is the ultimate shear stress in the beam cross-section at failure.

According to the ACI formula Eq. (2.3), the shear capacity is only related to the square root of the concrete compressive strength. The formula shows a clear influence from Mörsch. However, based on the knowledge developed after the formula was proposed, one may find that several key elements are missing in the formula. Those are the configuration of the longitudinal reinforcement, the beam height and the loading condition. Because of that, the accuracy of the formula is poor compared to experimental results. The formula can be seen as an indication of the lower bound of the shear capacity.

The Eurocode formula (Eurocode 2 2004) represents a significant improvement compared to the ACI code. The basic structure of the Eurocode equation is:

$$\tau_u = C_{Rd} k_h \sqrt[3]{100 \rho_s f_{cm}} \tag{2.4}$$

where

k_h: is the size effect factor, $k_h = 1 + \sqrt{200 / d}$, with d in mm;
C_{Rd}: is a regression factor to be determined by test results;
ρ_s: is the reinforcement ratio, $\rho_s = A_s / bd$.

For the prediction of the mean value of the shear capacity, the factor C_{Rd} is replaced by C_{Rm}. The value of C_{Rm} was firstly determined by Regan as $C_{Rm} = 0.15$. Later, König & Fischer evaluated the formula with 176 carefully selected shear tests in (König & Fischer 1995). In their analysis the mean calculated shear resistance is 0.92 smaller than the reported test results, thus increasing the value

of C_{Rm} to 0.163 results in better fitting according to their database. This result was used to derive the design equation as found in the Eurocode for Concrete Structures (Eurocode 2 2004), assuming a reliability index equal to 3.8. On this basis, the factor C_{Rd} = 0.12 was found, suggested as a default value in the code. Moreover, the influence of the shear slenderness ratio (a_v/d, with a_v being the ratio between the edge of the loading plate and the edge of the support), is included in the Eurocode formula by introducing a reduction factor on the load applied at a distance smaller than $2.0a_v$. A reduction factor of $(a_v/d)/2$ is used to reduce the load in that case. In this research, when the Eurocode formula is addressed, the roundup value from Regan C_{Rm} = 0.15 is chosen and the shear slenderness factor is changed to $\beta_a = 2/(M/Vd)$ to including continuous beams. The factor β_a is added to Eq. (2.4), so that it is turned into a capacity-increasing factor.

Another interesting empirical method is the TNO-IBBC method, which is based on experimental research on beams with complex boundary conditions loaded by a uniformly distributed load (IBBC-TNO 1977c; IBBC-TNO 1985). The method treats the failure of the two shear transfer mechanisms explained in Section 2.1 separately. The capacity according to the two failure modes is denoted as τ_1 and τ_2, the values of which are expressed by formulas relating to the varying ratio M/V along the beam. By comparing the values of τ_1 and τ_2 at each section of the beam, the maximum shear force and the critical section are determined. The method works well for concrete members with complex boundary conditions, such as cut-and-cover tunnel segments.

A more recent empirical method was proposed by Bažant and Yu (Bažant & Yu 2005; Bažant & Yu 2005). The expression is based on Bažant's size effect theory derived from fracture mechanics (Bažant & Planas 1998; Bažant 2005). The factors in the formula were determined by regression analysis:

$$\tau_u = 1.33\rho_s^{3/8}\left(1+\frac{d}{a}\right)\sqrt{\frac{f_{cm}}{1+d/d_0}} \tag{2.5}$$

where

d_0 : is a constant, $d_0 = \kappa_B f_c^{-2/3}$, with $\kappa_B = 3.8\sqrt{D_{\max}}$, if the maximum aggregate size $D_{\max}$ is known, otherwise κ_B = 3.330.

Since the formula itself is not derived from a specific mechanism with a physical meaning, it still falls into the category of empirical formulae according to the definition given in the beginning of this section. On the other hand, the basic relationship is based on fracture mechanics. It indicates that the fracturing process of the critical inclined crack determines the shear failure of the beam according to the formula.

The problem of most empirical methods is that they are purely based on the experimental results available when the formula was derived. Since they do not reflect the fundamental nature of the shear failure process, the formulas cannot be extended outside the scope of the tests and do not always match design situations encountered in practice.

2.3.3 Methods Based on Fracture Mechanics

As explained above, Bažant's equation can be considered as a semi fracture mechanics approach. There are several more researchers attributing the flexural shear failure to the fracturing process of the critical inclined crack. Because of the complex expressions for the fracturing behaviour of concrete in tension, analytical expressions for the shear capacity based on fracture mechanics approach are seldom. Therefore the principles of fracture mechanics are mostly used in combination with finite element analysis, or regression analysis. Most analytical expressions relating to fracture mechanics are determined from regression methods. To be distinguished from the empirical method, in the fracture mechanics approach the derivation of the formula is still based on the analysis of the fracturing of a specified crack path, although the final expression is similar to an empirical formula. Thus, the method usually needs to specify a crack path or failure mechanism in advance.

Gustafsson and Hillerborg were the first to model the fracturing process of the critical inclined crack with concrete fracture mechanics (Gustafsson & Hillerborg 1988). They assumed a parabolic crack path in a beam, and calculated the fracturing process of the crack with their Fictitious Crack Model, see Fig. 2.9. Based on the simulation results, they derived a shear capacity formula.

Jenq and Shah employed the concept of fracture mechanics with another

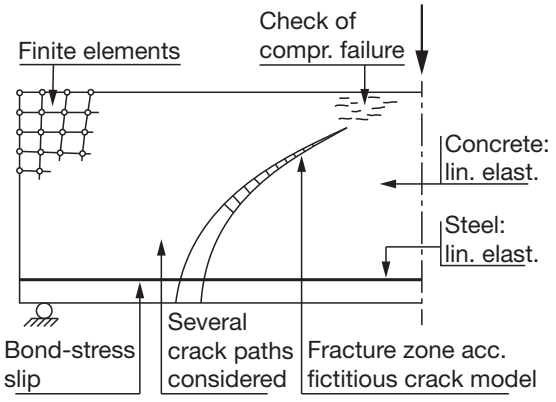

Fig. 2.9. Fictitious crack model for shear cracking simulation (Gustafsson & Hillerborg 1988).

approach. In their two-parameter model, the formulation of Linear Elastic Fracture Mechanics (LEFM) was adopted for the fracture of concrete (Jenq & Shah 1985; Shah, Stuart et al. 1995). To model flexural shear cracking, a straight diagonal crack path with inclination angle θ was assumed. Subsequently, the force needed to open the crack was calculated with their model (Jenq & Shah 1990).

A common feature in the models discussed above is that to simulate the fracture process, a simplified crack path has to be assumed. It is necessary that the derivation of the model should be based on a crack path assumption reflecting the experimental observation properly. On the other hand, to derive an applicable calculation method requires a simple crack path expression. The two conflicting requirements cannot be solved within the scope of the approach. Besides, by definition, the fracture mechanics approach assumed for the fracturing of the critical inclined crack is the dominating shear failure mechanism, while the other shear transfer mechanisms such as aggregate interlock and shear stress transfer in compressive zone are mostly ignored in a typical fracture mechanics models. In slender beams with relatively high reinforcement ratio, the critical shear crack may develop from pure flexural cracks, such as observed in the tests reported by Yang (Yang et al. 2012), see also Section 5.3.5 in this research work. In that case, the critical crack is composed of the flexural crack and secondary crack branch developing further along the compression zone and the longitudinal reinforcement. Because of this crack shape, the shear stress generated by aggregate interlock under a tangential displacement of the flexural crack faces cannot be ignored anymore.

2.3.4 Teeth Model

The problem addressed in case of fracture mechanics methods is basically nothing else than addressed already before by the Teeth Models. They represent one of the first attempts towards a totally rational explanation of the flexural shear failure mode. The first of this type of models was proposed by Kani in his well-known paper 'The Riddle of Shear Failure and Its Solution' (Kani 1964). In Kani's model, he focused on the shear capacity of a beam with a fully developed flexural crack pattern. The flexural cracks shape the beam into a teeth-like structure, see Fig. 2.11. Taking a single teeth apart, it is loaded like a corbel by the shear force generated by the longitudinal reinforcement at the tensile side and a compression force in the concrete compression zone. Kani assumed that the shear failure of such a beam occurring due to breaking off of the concrete corbel under the local shear forces. With the teeth model and an arch analogy, Kani explained the influence of shear slenderness ratio to the shear capacity, which is often referred as Kani's Valley (Fig. 2.10) by other researchers. The

model regards the initiation of inclined cracks from a different perspective, which turns out to be inspiring till now.

Fenwick and Paulay evaluated Kani's model in (Fenwick & Paulay 1968) by experiments on beams with manually arranged teeth structures with and without aggregate interlock. They showed that aggregate interlock cannot be ignored in a teeth structure. Taylor (Taylor 1974) came to a similar conclusion on the basis of his tests. He suggested that dowel action should also be taken into account. These experimental observations cannot be explained by the fracture mechanics models either.

Kani's model was further improved by MacGregor and Walters (MacGregor & Walters 1967) introducing a simplified dowel action expression and shear stress distribution between cracks. Both simplified relationships were not validated by experiments yet. However, they showed that the development of the inclined crack is due to the bending of the concrete teeth.

Hamadi and Regan (Hamadi & Regan 1980) implemented the teeth model with a more complex shear stress distribution in the compression zone, and the rebar dowel force was calculated based on experimental results in their paper. Regarding the shear stress distribution in the crack, a simple bilinear shear stress distribution was assumed.

Reineck (Reineck 1991) derived a simplified aggregate interlock relationship derived from Walraven's research (Walraven 1980), assuming there is no compressive normal stress in the crack due to aggregate interlock. Under that condition, the maximum shear stress according to Walraven's model determines the capacity of aggregate interlock, which determines the shear capacity of the whole cross section. The teeth inclination is assumed to be 60° in Reinecks's

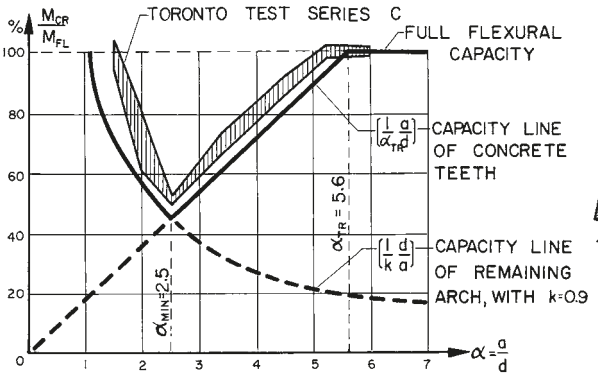

Fig. 2.10. Influence of *a/d* on the beam capacity known as Kani's Valley (Kani 1964).

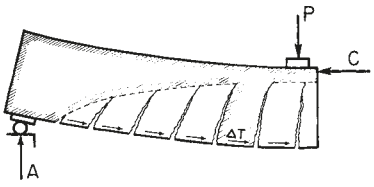

Fig. 2.11. Illustration of Kani's teeth model (Kani 1964).

model. Other assumptions are that the height of the concrete compression zone is $0.4d$, the average crack spacing is $0.42d$, etc. According to his study, the tensile stress of concrete at small crack width can be neglected. Although some of his simplifications mentioned above still need experimental evidence, the accuracy of the model prediction is comparable with that of empirical formulas.

Based on the teeth model, the shear failure mechanism has evolved from the break of the teeth to the failure of aggregate interlock between the crack surfaces. The teeth analogy still turns out to be a reasonable framework to include the basic shear transfer mechanisms as previously discussed in Section 2.2.

2.3.5 Crack Width Based Models

The studies on the shear transfer mechanism based on teeth models eventually evolved towards shear failure criteria based on aggregate interlock. Since the shear stress generated by aggregate interlock is determined by the displacement of the crack faces in normal and tangential direction, the failure of aggregate interlock can be related to the crack width of the critical section. It is logical to relate the overall shear capacity to the crack width directly. This possibility has been validated by Lubell et al. in (Lubell et al. 2009) and Muttoni (Muttoni 2003). Typical models that rely on the crack width of the beams are the Modified Compressive Field Theory (MCFT) proposed by Collins et al. (Vecchio & Collins 1986; Adebar & Collins 1996; Bentz, Vecchio et al. 2006) and the Critical Shear Crack Theory (CSCT) proposed by Muttoni (Muttoni & Ruiz 2008). Besides, Reineck's model (Reineck 1991) discussed in the previous section also relates the shear capacity partly to the crack width.

Among the crack width based models discussed above, the CSCT proposes that the shear capacity of a beam can be completely related to the crack width at a predefined critical cross section. It defines the critical section at a distance of $d/2$ from the loading point for point loading, and relates the crack width of the cross-section to the longitudinal strain of the beam at $0.6d$ from the top surface. By comparing the longitudinal strain of test results reported in literature at failure load with the average cross sectional shear stress, the following regression formula was derived:

$$\tau_u = \frac{1}{6}\frac{2}{1+120\dfrac{\varepsilon_x d}{16+D_{\max}}}\sqrt{f_{cm}} \tag{2.6}$$

where

ε_x : is the average strain calculated at the critical point.

It has been shown that the formula is able to provide an accurate prediction of the shear capacity in general (Muttoni & Ruiz 2008; Caldentey et al. 2012). In principle, it is still an empirical approach, since Eq. (2.6) can hardly be traced back to a rational explanation of the failure mechanisms, so that the failure criterion is generally nothing more than the definition of a certain maximum crack opening at a critical section.

The modified compressive field theory approaches the problem from a quite different perspective. It was firstly proposed by Collins as Compressive Field Theory in (Collins 1978). The theory was derived to determine the principal direction of the compressive stress in shear reinforced concrete specimens as an alternative for Mörsch's truss analogy. Eq. (2.1) was later added to take into account aggregate interlock in the improved theory called modified compressive field theory, suggested by Vecchio and Collins (Vecchio & Collins 1986). The theory was extended to beams without shear reinforcement by Adebar and Collins (Adebar & Collins 1996). In case of beams without shear reinforcement, the shear capacity along the crack is directly related to the shear stress transferred across flexural cracks:

$$\tau_{ai} \leq \frac{0.18\sqrt{f_{cm}}}{0.31 + 24w / (D_{\max} + 16)} \tag{2.7}$$

The equation has been discussed before in 2.2.3. It was derived by removing the normal stress across the crack surface. Thus, in principle, it should be equivalent to the equation proposed by Reineck. Bentz, Vecchio and Collins further simplified the procedure of calculating the direction of the principal compressive stress in (Bentz, Vecchio et al. 2006), which yields the following expression for the shear capacity:

$$\tau_u = \frac{0.4}{1 + 1500\varepsilon_x} \frac{1300}{1000 + l_{cr,m}} \tag{2.8}$$

where,

$l_{cr,m}$: is the average crack spacing, expressed by $l_{cr,m} = \frac{32z}{16 + D_{\max}}$, where z is the length of the internal level arm, $z = 0.9d$;

ε_x : is the longitudinal strain of the beam at mid-height of the predefined critical section.

The advantage of the model is that it is able to unify the design of beams with and without shear reinforcement within the same framework. Besides, comparing to the CSCT a link between the formulation and the specific failure mechanism can be traced. As explained before, the advantage of a physical model is its possibility of extending to more general conditions. This has been

approved in case of large, lightly reinforced beams by experiments (Collins & Kuchma 1999; Collins, Bentz et al. 2008; Lubell, Bentz et al. 2009), in which cases empirical formulas such as Eurocode and ACI provisions give less conservative predictions according to (Collins et al. 2008; Lubell, Bentz et al. 2009). Because of the advantages stated above, the theory has been implemented into design provisions such as the Canadian CSA code (CSA 2004), and the new fib Model Code 2010 (fib 2012).

In crack width based models, the basic assumption is that the failure of aggregate interlock determines the shear failure of the beam. Regarding to the capacity of aggregate interlock, a common assumption is that there is no normal stress perpendicular to the cracks. This assumption is questionable, since the uncracked concrete parts at both sides of the crack remain solid elements connected by the longitudinal reinforcement and the uncracked concrete compression zone. Thus the displacement perpendicular to the crack plane is still limited, especially at the region close to the tip of the crack. As pointed out by Bažant and Yu in (Bažant & Yu 2005), in that case the allowable shear stress in the crack should be much higher than what was observed in most shear tests. On the other hand, as shown in Fig. 2.7, the shear failure criterion in the MCFT is equivalent to a limitation of the transverse displacement with respect to a given crack width being $\Delta \leq 0.55\, w$. That may be considered as a rational explanation for the criterion on the shear stress in the crack. It makes sense to investigate whether this criterion can be improved in order to make a further step towards a complete solution to the riddle of shear capacity.

2.3.6 Secondary Crack Models

The term **secondary crack** represents the dowel crack along the longitudinal reinforcenet and the splitting crack in the concrete compression zone.

Although it has already been pointed out by Bresler and MacGregor in (Bresler & MacGregor 1967), Chana has firstly shown with tests that the opening of the flexural shear crack is initiated by the development of a dowel crack along the longitudinal rebar at the bottom of a beam (Chana 1987). This observation opened another possibility to explain the mechanism of shear failure, which is the development of a dowel crack in the horizontal direction. The importance of dowel cracking along the longitudinal rebar was further confirmed by Kim and Wight through their comprehensive test program in (Kim & White 1999).

Kim and White derived the first shear cracking formula based on the dowel crack development along the longitudinal rebar in (Kim & White 1991). In their model, they related the initiation of the dowel crack to the maximum bond stress between rebar and concrete, and compared the cross-sectional cracking moment with the development of maximum bond stress to derive the inclined cracking

load. The formula is comparable with the empirical formula proposed by Zsutty (Zsutty 1971) according to Kim and White. An equation to predict the position of the flexural crack was given as well in this research. However, relating the opening of the dowel crack to maximum bond stress is questionable. First of all, Baumann and Rüsch's tests (Baumann & Rüsch 1970) showed that the opening of the dowel crack along a longitudinal rebar is a plastic process. Sudden opening of the flexural shear crack cannot be related to the dowel crack solely. Moreover, in the experiments executed by Kim and White (Kim & White 1999) they compared the shear capacity of test series disabling the bond between concrete and steel in two different ways: introducing a PVC tube or removal of concrete locally. The two approaches generated completely opposite results. Thus the shear stress cannot be the only reason of shear failure.

Gastebled and May established their theory upon the same mechanism through a different approach (Gastebled & May 2001). The concept from fracture mechanics was employed. However, unlike the conventional fracture mechanics methods introduced in 2.3.3, the formulation avoided the calculation of the tensile stress in concrete. It is based on the total energy balance of an assumed crack pattern in the beam. They derived a rather simple formula which was comparable to the Eurocode formula Eq. (2.4). In their model a straight diagonal crack with 45° inclination is assumed. Xu et al. further developed the model by replacing the mode I fracture energy $G_{f,I}$ as used by Gastebled and May with mode II fracture energy $G_{f,II}$ (Xu et al. 2012).

The two methods discussed in the section show the significance of relating shear failure to the opening of a dowel crack along the longitudinal reinforcement. However, the common questions that have to be solved for shear design methods that attribute dowel cracking as failure mechanism are the following:

- How to take into account the other shear transfer mechanisms, which have been proven to be influential to the overall shear capacity from experimental observations?
- What is the criterion to determine the abrupt opening of the flexural shear crack observed in experiments?

Further to the two aforementioned methods, Zararis proposed a totally different rational method in (Zararis & Papadakis 2001; Zararis & Zararis 2009), in which he suggested that the flexural shear crack is initiated by the development of a splitting crack in the concrete compressive zone. He divides the critical inclined crack into two branches, the first part of which is the flexural crack, whose height is stabilized quickly due to cross sectional force equilibrium. The second branch develops along the centre of the compressive strut towards the loading point, the opening stress of which is the secondary tensile stress due to the Poisson's effect in the strut. The distribution of the stress along the centroid of the strut is assumed to be similar to the one in a splitting cylinder test. The

method provides an interesting perspective in explaining the opening of the flexural shear crack close to the loading point. An apparent deviation from experimental observation is that the tips of flexural cracks are usually not in the centroid of the compressive strut. A similar approach was also followed by Choi et al. in (Choi & Park 2007; Choi et al. 2007). The difference lies in the way the two-dimensional stress state in the concrete compressive zone was treated.

2.3.7 Missing Links

The shear capacity of reinforced concrete beams without shear reinforcement is one of the most interesting research topics in the whole structural concrete theory. This is already clearly demonstrated in this short review of the theories proposed in the last 50 years. With respect to the same phenomenon, hundreds of papers have been published (ACI-ASCE Committee 426 1973; ACI-ASCE Committee 445 1998; Collins, Mitchell et al. 2008), in which different theories have been proposed. However, there is still fundamental disagreement on the governing mechanisms in the shear failure process. As a summary to the presented theories, shear failure can be attributed to:

- Fracturing process of the critical inclined crack;
- Breaking of concrete teeth formed by flexural cracks;
- Loss of aggregate interlock capacity;
- Dowel cracking along the longitudinal rebar;
- Splitting cracking in the concrete compression zone.

There are even more theories that have been reported in literature based on other failure criteria, such as the plasticity theory proposed by Zhang (Zhang 1997), etc.

As mentioned before, none of them is able to give a sound explanation yet. Thus the biggest challenge in the field of shear research remains unchanged: to find a model that is able to explain the fundamental mechanism of flexural shear failure. Nevertheless, the understanding of the phenomenon denoted as flexural shear failure has been pushed forward indeed with regard to various sub-mechanisms. How to link the knowledge that is available is a crucial challenge towards the final solution of the problem. The following aspects have been learnt from the exploring works discussed in this section:

- The pure regression analysis of experimental data shows that the major variables that influence the shear capacity of concrete beams are: the concrete strength f_c, the effective beam height d, the reinforcement configuration and the load configuration.
- The development of the critical inclined crack follows the laws of the fracture mechanics.

- The inclination of the flexural crack should be related to the bending of the concrete teeth.
- To model the shear capacity properly, it is necessary to take into account all the shear transfer mechanisms in the teeth model: the conclusion holds true for the other models as well.
- The longitudinal strain ε_x or alternatively the crack width w, is proven to be strongly related to the shear capacity of concrete beams by the comparison of test results. That indirectly indicates that the aggregate interlock cannot be ignored.
- However, aggregate interlock cannot be the governing criterion of shear failure either. Instead, the tangential displacement of the crack faces can be used as a failure criterion to calculate the critical shear stress in the cracks.
- The development of secondary cracks in the longitudinal direction at both ends of the flexural cracks is important in the shear failure process.

2.4 SHEAR DATABASES

The previous section about shear capacity theories has clearly shown that most of the shear design methods still rely on regression analysis of test results in order to determine the factors included in the theoretical models they represent. Hence, a collection of shear tests data is essential. Most researchers collect their own database for their models, such as (Rafla 1971; Zsutty 1971). However, this may become a problem when comparing different models derived from different data collections. The procedures to select the data and to process it were different, such as the choice of concrete strength between cylinder strength and cube strength, whether or not the self-weight of the specimen is taken into account. To avoid such problems, several researchers have been working on collecting as much shear test data as possible, and process them in a uniform manner, so that the difference introduced by the person who analyses the set of data is minimized.

One of the noticeable databanks is the collection reported by Collins and Bentz in (Collins, Bentz et al. 2008), in which 1849 shear tests have been included. The databank includes the maximum aggregate size, and type if known. The loading plate sizes are included as well. Another databank with a large collection is Reineck's Database collected by Reineck et al. in (Reineck et al. 2003). It was extended further to the ACI-DAfStb Database reported in (Reineck et al. 2013). The database includes 1365 shear tests with point loading and 128 tests with distributed loading. In the ACI-DAfStb Database, more detailed longitudinal reinforcement information is included. Both test databases are used in this

research work with certain selection criteria depending on the specific requirement in the research.

However, as pointed out by Bažant in (Bažant 2004; Bažant & Yu 2005), trying to fit a formula with an entire database with the parameter variation of the test data not well distributed, or including other types of failure modes which are not corresponding to the model will lead to incorrect results. As shown in Fig. 2.12, most shear tests reported in literature were carried out on a laboratory scale, and were heavily reinforced to guarentee shear failure, moreover, a large percentage of the specimens have a concrete strength lower than 45 MPa, which are apparently quite different from the current design practice. A formula which fits best with a database mostly composed of such tests is not necessarily to be the best fitting formula for all conditions. A proper selection of the test data is important. Taking that into account, König and Fischer evaluated the Eurocode formula with a small database with a carefull selection (König & Fischer 1995). It is composed of 176 tests with only flexural shear failures. Tests with higher concrete strength and larger cross-sectional depth take up a reasonable percentage in the collection, see the comparison in Fig. 2.12. That database is therefore used as an evaluation tool to compare the accuracy of different model predictions.

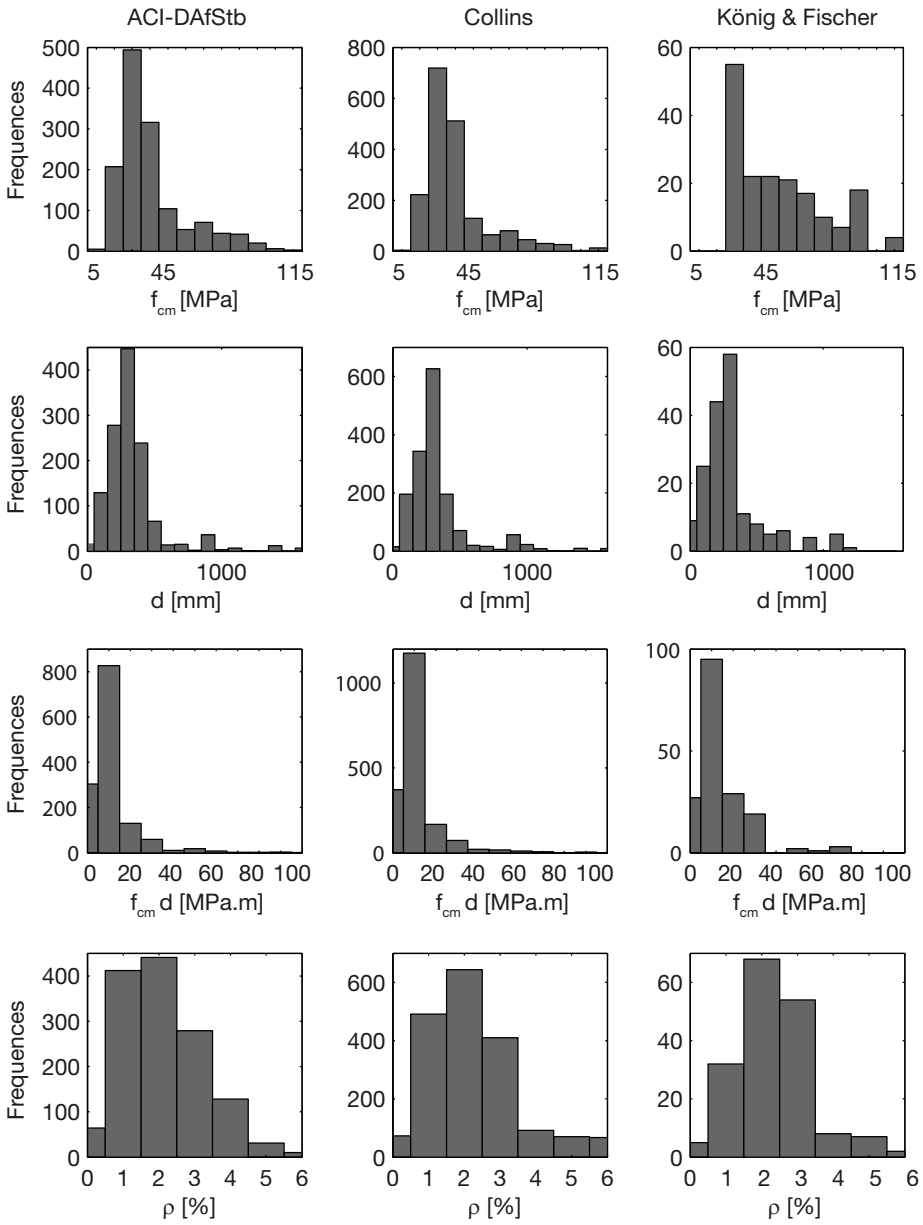

Fig. 2.12. Comparison of data distribution between databases.

Chapter 3

Failure Process of a Reinforced Concrete Beam without Shear Reinforcement

3.1 INTRODUCTION

The central issue of this chapter is to explain the failure process of a reinforced concrete beam without shear reinforcement under shear loading. The survey of literature in Chapter 2 has shown that there is general agreement on the mechanisms which contribute to the shear capacity of a reinforced concrete beam with flexural cracks, namely, shear resistance in the uncracked compressive zone, residual tensile stress through the crack, aggregate interlock and dowel action. Nevertheless, there is no agreement yet on how those components influence the overall shear failure process, and which one is the governing mechanism in the failure process.

In this chapter the shear failure process is explored by studying the formation of a critical inclined crack generated by the combination of the flexural moment and shear force at a given cross section. The study starts from the opening of a crack under the local cracking moment M_{cr}. Key aspects relating to the crack pattern, including the crack spacing, crack height and profile are involved in the study. Corresponding expressions are given. Along a given crack, a part of the beam specimen is regarded as a free body, the forces applied on this body are analysed, which includes the aforementioned effects such as the aggregate interlock, dowel action, and direct shear transfer in the compressive zone. By quantifying those components through equilibrium and kinematic conditions, the failure process of a beam under shear force is explained step by step. Based on that, a new type of shear failure criterion is proposed which can be used to develop a new model for the shear capacity of structural members. By the end of this chapter, the behaviour of the structural member after the opening of a critical inclined crack is discussed. That is presented as the governing loading bearing mechanism at that stage. It is shown that the capacity of the structural member in that stage determines the shear failure mode.

In order to simplify the research question, within this chapter, the study is strictly confined by certain boundary conditions. A standard structural member is defined, which is a prismatic beam with a cross-section of 300×500 mm. It is simply supported and loaded by a single point load, where the closer centre-to-centre distance between the support and the point load is the **span length** denoted as a. The span length a may vary in different cases. The longitudinal reinforcement at the tensile side of the beam consists of three ribbed rebars of Ø32 mm. They are properly anchored at the edge of the beam. No shear reinforcement is present in the shear span. It is assumed that the amount of reinforcement is always sufficient to guarantee shear failure. The concrete cover is assumed to be 25 mm, which makes the effective height of the beam d about 460 mm. The concrete strength is assumed to be f_c = 40 MPa, with a maximum

aggregate size of 16 mm. This configuration is partly based on the specimens of the experimental research reported in (Yang & den Uijl 2011; Yang et al. 2011).

3.2 CRACK DEVELOPMENT UNDER THE CRACKING MOMENT

In this section the development of cracks under the combination of a bending moment M and a shear force V is studied. It is of interest why and how a certain crack pattern forms in a beam under given loading condition. The term crack pattern stands for the height, spacing and profiles of the cracks. Experimental research has been shown that the shear capacity of a reinforced concrete beam is strongly related to the development of the critical inclined crack in the shear span (Yang et al. 2011; Yang, den Uijl et al. 2012), which is certainly the most essential part of the whole crack pattern. Therefore the first step to understand the shear phenomenon should be to explain how cracks, especially inclined cracks develop.

3.2.1 Stability of Crack Height under Flexural Moment

Before cracks develop, the beam follows the theory of elasticity, which says that for an uncracked concrete beam with a rectangular cross section, the crack will always initiate from the ultimate tensile fibre of the specimen due to the moment at the cross-section when the tensile stress there reaches the tensile strength of the concrete. At the ultimate fibre of the beam, the tensile stress reaches the maximum value in x direction, while the shear stress is zero there. It is assumed that the direction of the crack faces is perpendicular to the maximum principal stress direction. Due to the tension softening character of the concrete, the opening process of the crack is quite unstable. This can be illustrated by a simplified layered model.

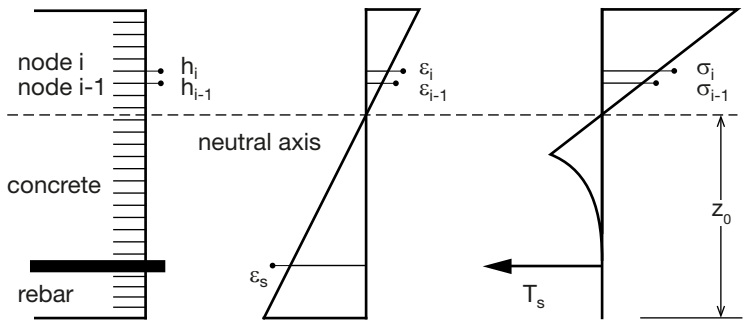

Fig. 3.1. Illustration of layered model

The simulation of the cracking process with a layered model was proposed by Hordijk in (Hordijk 1991). The basis of the model is dividing the vertical plain of the cross-section into multiple horizontal layers. The stress-strain (crack opening) relationship of concrete is assigned to each layer. The deformation in the height direction is assumed to be linear. The crack width is converted into strain by a characteristic length l_{ch}. In this model the value of l_{ch} is chosen to be 250 mm, which is half the beam height according to Hordijk (Hordijk 1991). For any given curvature κ, by solving two equations describing the equilibrium of forces and moment, the height of the neutral axis z_0, and the external moment that applies on the cross-section is calculated. Since the model is rather easy to be implemented, it has been widely applied to study the propagation of a crack in tension-softening materials such as concrete.

$$\begin{aligned} F &= \sum \frac{1}{2}(\sigma_i + \sigma_{i-1})(h_i - h_{i-1}) = 0; \\ M &= \sum \frac{1}{4}(\sigma_i + \sigma_{i-1})(h_i - h_{i-1})(h_i + h_{i-1}). \end{aligned} \tag{3.1}$$

where,

h_i : is the position of node i in the cross section;
σ_i : is the stress at a given node i, it is calculated by the strain of the layer, with the constitutive relationship of the material;
ε_i : is the strain at a given node i, $\varepsilon_i = \kappa\ (h_i - z_0)$;
κ : is the curvature of the cross section.

The prototype beam specified in Section 3.1 is modelled here. The reinforcement area is chosen as the variable. Three reinforcement configurations are specified, being 1 Ø32 mm, 2 Ø32 mm, 3 Ø32 mm. The corresponding reinforcement ratios are ρ_s = 0.59%, 1.18% and 1.77%. The concrete tensile strength in the model is f_{ctm} = 2.9 MPa, a fracture energy of G_f = 0.0579 N/mm is chosen (fib 1993), and a linear softening curve for the post cracking behaviour of concrete is adopted to keep the simplicity of the whole model. For each beam by assuming a curvature κ, the height of the cracked concrete layers is calculated as well as the cross-sectional moment M. The relationship between crack height from the level or the reinforcement s and moment M that can be resisted by the cracked cross-section is plotted in Fig. 3.2.

Comparing the crack height of the concrete cross-section and the corresponding maximum moment in Fig. 3.2, one may find that shortly after the moment is higher than the cracking moment M_{cr} (see point 1 in Fig. 3.2), further development of crack height will result in the reduction of the moment resistance over the cross section. This means that once the moment applied at the

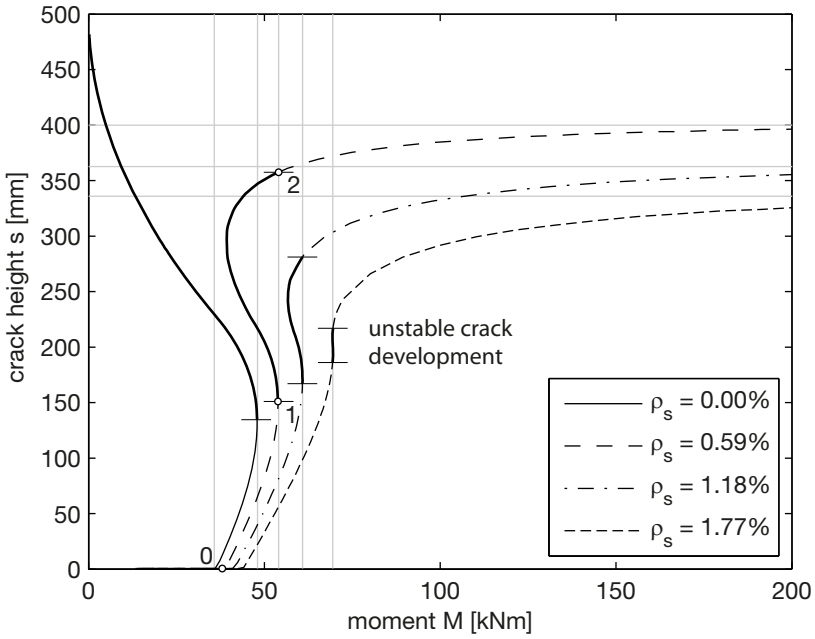

Fig. 3.2. Crack height *s* versus cross-sectional moment *M* relationship for beams with different reinforcement ratios.

cross-section is higher than that value M_1, or the crack height is larger than s_1, further development of the crack height does not ask for any additional loading. The crack opening will become unstable until the moment resistance of the cross-section gets higher than the previous peak point (see point 2 in Fig. 3.2): the crack height becomes stable after reaching the level s_2. The values s_1, s_2 and M_1 depend on the reinforcement ratio and the fracture energy G_f of the concrete and the beam height. A higher reinforcement ratio and larger fracture energy result in a lower stabilized crack height s_2 and a lower critical moment M_1. Other than that the height of the beam affects the values of s and M_1 as well, due to the constant l_{ch} for a specific concrete type. It is usually denoted as the size effect in literature. This has been proven by Walraven in (Walraven 1978). Further discussions on this topic will be given in Section 4.7.

Fig. 3.2 also shows that, between the points 1 and 2, the equilibrium of the internal forces does not balance with the external load, thus, in principle it is not possible to acquire the exact value of the stress distribution around the crack tip with conventional equilibrium methods. The same conclusion holds true for conventional non-linear finite element methods, with which the inner force equilibrium has to be balanced with the external force as well.

After the crack height has reached s_2, the curve becomes almost flat. This indicates that a further increase of the moment over the cross-section will not change the crack length significantly. The crack height approaches to a constant value in the ultimate state. The **stabilized crack height** s_{cr} can be calculated from the equilibrium of forces expressed by Eq. (3.1), assuming that there is no tensile stress in the concrete. The value of s_{cr} is expressed by

$$s_{cr} = \left(1 + \rho_s n_e - \sqrt{2\rho_s n_e + (\rho_s n_e)^2}\right) d$$

where

ρ_s : is the reinforcement ratio $A_s / b_w d$;
n_e : is the ratio between E_s and E_c.

Eliminating the smaller term $\rho_s n_e^2$, the ultimate crack height s_{cr} may be estimated by (Braam 1990):

$$s_{cr} = (1 - 1.05(\rho_s n_e)^{0.45}) d \tag{3.2}$$

Thus, assuming the height of the compressive zone $z_c = d - s_{cr}$, the internal level arm of a given cross-section z can be calculated with s_{cr} by

$$z = \frac{2}{3} d + \frac{1}{3} s_{cr} \tag{3.3}$$

For beams with a relatively large effective height, the critical moment M_1 is quite close to the cracking moment M_{cr}. Moreover the cracking height in vertical direction is mostly related to the stress distribution in longitudinal direction, thus to the moment in the cross section. It is reasonable to conclude that for a cracked cross-section in a reinforced concrete beam, once the moment reaches the cracking moment, a crack with a height s_{cr} is formed. The crack height s_{cr} may be considered to be independent to the shape of the crack. In the case of the beam example presented previously, with 3-Ø32 mm reinforcement, the height of the crack will be s_{cr} = 297.4 mm

3.2.2 Crack Spacing

With the load applied on the concrete member increases, there will be multiple cracks over the span where the moment is higher than M_{cr} locally. The distribution of the cracks is of interest here. Once a crack is formed, the stresses in the region adjacent to the crack are significantly released. Consequently, it is not possible to develop sufficient stresses to generate another crack adjacent to the first one. Therefore, cracks are always developed at certain distances.

The study of crack spacing is closely related to the crack width control in most studies in literature, see (Noakowski 1985; Frosch 1999; Borosnyói & Balázs 2005). Thus the crack spacing is mostly of concern at the level of reinforcement. For flexural members, the surface reinforcement and an effective concrete area $A_{c,eff}$ surrounding it, can be considered together as a tensile member. The tensile deformation is mainly localized in the tensile reinforcement. The tensile stress in the concrete surrounding the reinforcement is developed through the bond stress between concrete and reinforcement. Despite the different definitions of the average bond stress τ_{bm} from different theories, the minimum crack spacing l_t, also defined as transfer length, is calculated by:

$$l_t = \frac{f_{ctm} A_{c,eff}}{\tau_{bm} \Sigma u} = \frac{f_{ctm} \phi}{4 \tau_{bm} \rho_{eff}} \tag{3.4}$$

where:

τ_{bm} : is the average friction between rebars and concrete;
ρ_{eff} : is the effective reinforcement ratio, $\rho_{eff} = A_s / A_{c,eff}$;
ϕ : is the diameter of the rebar;
f_{ctm} : is the mean tensile strength of the concrete.

The **mean crack spacing** l_{cr} at the level of tensile reinforcement, on the other hand, is $l_{cr} = \Psi_s l_t$. The value of Ψ_s varies from 1.3 to 1.5 in different publications, while for the maximum crack spacing $l_{cr,max}$, the value of Ψ_s is always 2.0.

However, concrete beams with reinforcing bars only located at the tensile side behave differently from tensile members. With the increase of the depth of the member the gradient of deformation from the level of reinforcement to the other edge cannot be neglected. Accordingly, the stressed area of the uncracked concrete has to build up again from the region adjacent to the reinforcement level at the crack face towards the whole cross-section along a certain length. The boundary of the stressed area in the stress recovery length can be simplified by a stress line, see Fig. 3.3. According to Krips' FEM study (Krips 1985), the inclination of the stress line is 52°, which gives k_c = 1.28.In the CUR report (CUR 1978) it is simplified to 45°, with k_c = 1.0.

The stress line defines the part of the beam where stress can develop, according to which it is clear that not all the cracks at the reinforcement level can actually develop till the neutral axis. This conclusion applies in more general conditions, Bažant et al. (Bažant & Ohtsubo 1977; Bažant & Wahab 1980) have shown that in the case of a parallel crack system, it is not possible that all the cracks have the same height in order to fulfil the stability condition of the whole system.

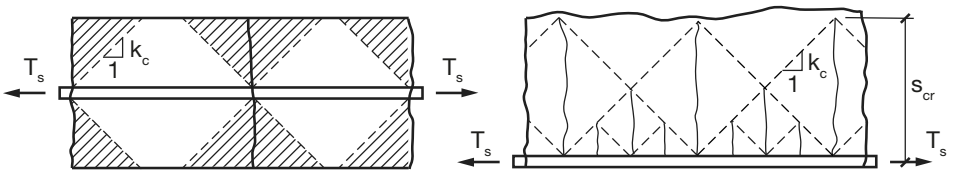

Fig. 3.3. Stress lines and crack patterns of tension members with reinforcing bars in the middle (left) and at the bottom (right).

Therefore, it is important to make a difference between cracks that can develop up to s_{cr} as defined in Section 3.2.1 after M_{cr}, and cracks that cannot. Only the former ones are critical to the shear capacity of the beam. They are denoted as the **major cracks**. As described previously, the spacing of the major cracks cannot be defined by the crack spacing theory based on a tensile member anymore. Instead, it is more related to the stress line starting from the crack face.

Assuming a perfect bond between the reinforcement and the concrete, with the increase of the tensile strain along the reinforcement, a self-similar crack pattern is formed in the concrete member. The increase of strain along the reinforcement only results in new cracks between the existing ones. The tips of the cracks fall in the stress lines starting from the crack faces. An illustration of such a crack pattern is given in Fig. 3.3. The **spacing of the major cracks** (the ones in the mid height of the beam) is defined by:

$$l_{cr,m} = \frac{s_{cr}}{k_c}. \tag{3.5}$$

The expression indicates that the spacing of the major cracks is only dependent on the crack height s_{cr}, and the inclination of the stress line k_c, whereas it is independent of the load level applied on the specimen, the reinforcement ratio or the bonding between reinforcement and concrete.

The increase of the load applied on the member will only result in the development of new cracks at the reinforcement level in case of perfect bond. If the bond-slip relationship between concrete and steel bars is taken into account, this process stops when the crack spacing at the reinforcement level is between l_t and $2.0l_t$. Further increase of the load level only increases the crack width.

Taking into account the relative displacement between rebar and concrete will not change the inclination of the stress line, thus does not influence the crack spacing. This is validated by the comparison of FEM models. Two analyses are carried out with Atena2D. The concrete is modelled with a perfect linear elastic material, and the reinforcement is modelled by bar elements. In the reference model, the reinforcement and the concrete have perfect bond, while the other model takes into account the bond stress displacement relationship between

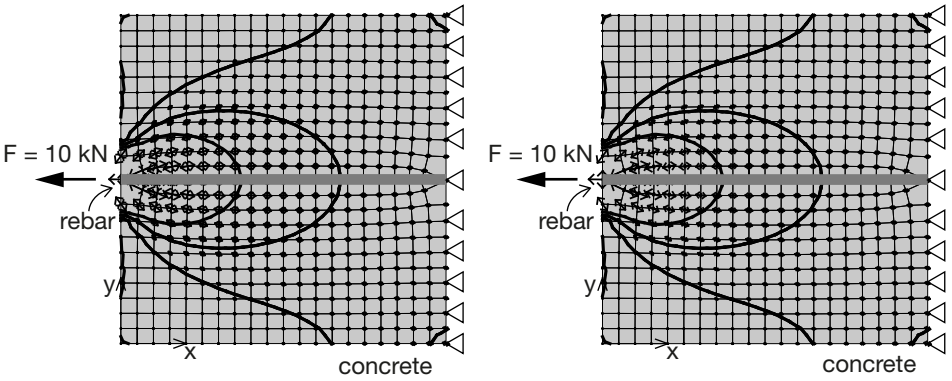

Fig. 3.4. Comparison of principal stress distribution of reinforcement-concrete interaction with perfect bond model (left) or with the bond mode model according to (fib 1993) (right), calculated by Atena2D.

concrete and steel according to fib Model Code 1990 (fib 1993). A tensile force of 10 kN is introduced at the level of the reinforcement. Moreover the displacement of the whole specimen is confined in x and y direction along the other edge. One may compare the principle stress distribution shown in Fig. 3.4.

To validate eq.(3.5), the beam specimen proposed in Section 3.2.1 is regarded. k_c = 1.28 is used in the equation. That will result in a crack spacing of 232 mm at mid height of the beam. The results compare well with the experimental findings reported in (Yang & den Uijl 2011). An example is given in Fig. 3.5, in which an average crack spacing of 214 mm is measured.

Another example is shown in Fig. 3.6, whereas, the crack patterns of three shear tests carried out by Shioya (Shioya 1989) are shown. The specimens were designed to evaluate the size effect on the shear capacity of concrete beams. Therefore, the concrete strength, the reinforcement ratio and the loading conditions of them are all proportional. The heights of the specimens vary from 100 mm to 3000 mm. According to Eq. (3.2) and Eq. (3.5), the height and the spacing of the major cracks should be proportional to the beam effective depth d. Fig. 3.6 shows that the major crack patterns of beams with 3000 mm and 1000 mm

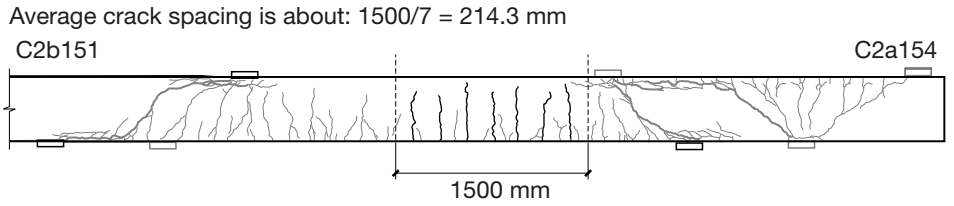

Fig. 3.5. Crack pattern after failure of test C2a154 and C2b151 in (Yang & den Uijl 2011).

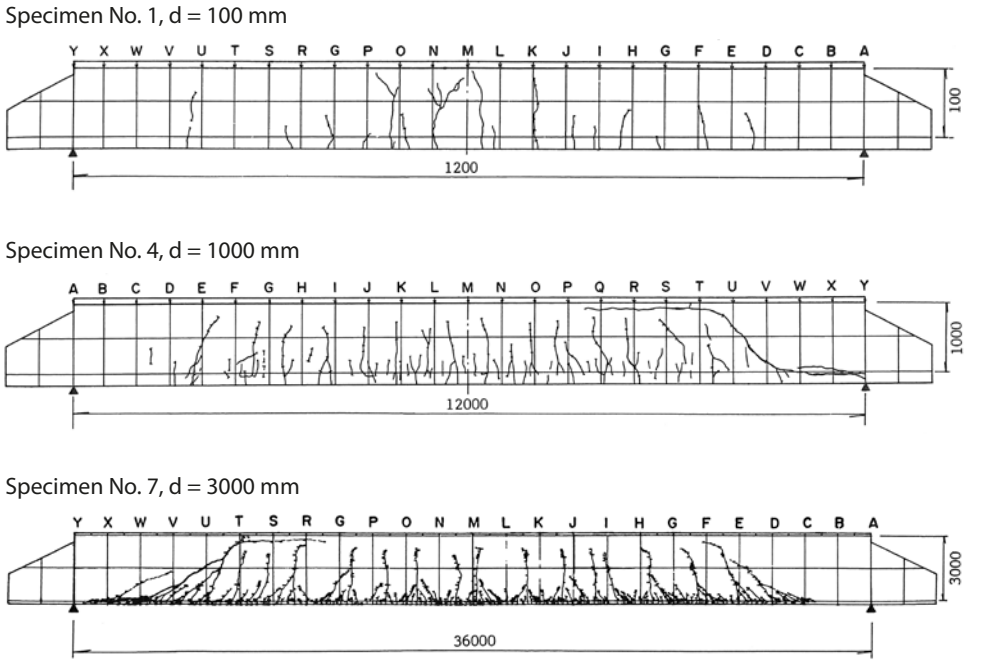

Fig. 3.6. Crack patterns of tests specimens with various effective depths (Shioya 1989), the effective heights of the specimens from the top are 100 mm, 1000 mm and 3000 mm respectively.

effective heights are more or less the same. Whereas the cracks at the reinforcement level are quite different, in case of the beam with a height of 3000 mm, the cracks at reinforcement level only form at a very limited height of the beam comparing the total effective height of the beam, whereas for the beam with d = 1000 mm, the cracks developed at the reinforcement level proceed to a larger height. This clearly confirms the theory on the distribution of major cracks presented above.

On the other hand, the beam with d = 100 mm has a different crack pattern. In that case, because of the smaller beam height, the maximum strain of the beam at the tensile side is smaller, so do the crack widths. As a result, the crack opening in this case is significantly influenced by the tension softening behaviour of the concrete. It indicates that Eq. (3.2) and Eq. (3.5) are not valid any more. According to Bažant (Bažant & Planas 1998), the influence of tension softening behaviour becomes pronounced when the beam height is smaller than 70 mm in case of three point bending. That can be used as a reference for shear tests as well. The result has been confirmed as well by the size effect tests on shear capacity of reinforced concrete beams from Bažant an Kazemi (Bažant & Kazemi 1991). Taking into account the observation of Shioya's tests shown in Fig. 3.6, 100

mm seems to be appropriate as a lower bound of the effective height that the crack pattern of the major cracks is influenced by the tension softening behaviour of the concrete.

3.2.3 Inclination of a Flexural Crack under Shear

3.2.3.1 What is the Reason of Crack Inclination?

With the height and spacing of the major cracks known, the following step is to derive the profiles of the major cracks. However, before that the basic question to be answered is "What is the Reason of Crack Inclination?" One of the popular deductions on the reason of crack inclination is as follows: Experimental observations show that for reinforced concrete beams, cracks start to incline when a shear load has to be transferred through a cross section. Usually, for an uncracked beam, the maximum shear stress is located at the height of neutral axis, where only shear stress exists. From the theory or elasticity, the principal stress of a solid block under pure shear in x and z direction should incline to 45° of the main axis. Since the crack follows the maximum principal stress direction, a crack path should follow the trajectories of the maximum principal stress lines as well. It seems to be natural to conclude that the shear stress at mid-height of the beam results in the inclination of flexural cracks.

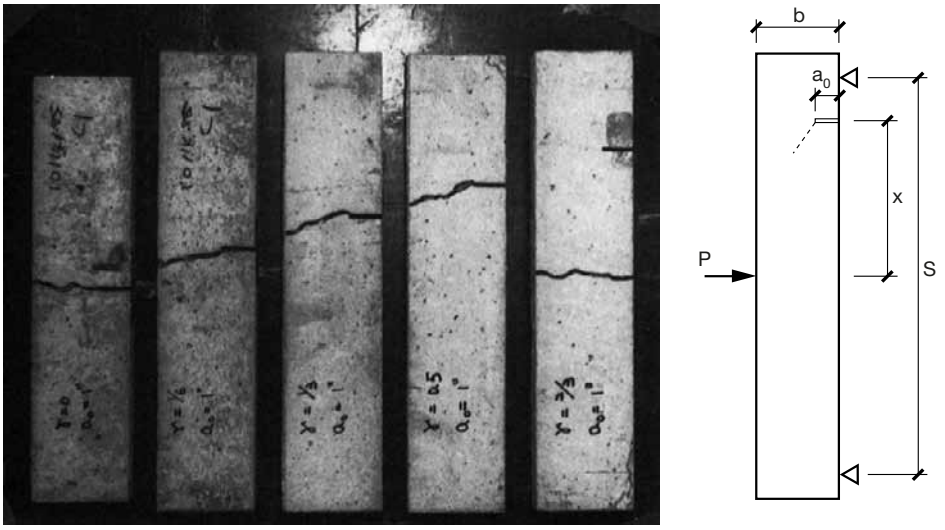

Fig. 3.7. Crack patterns of specimens with different crack initiating location in Jenq and Shah's tests (Jenq & Shah 1988). The notations of the dimensions are according to the original paper. The values of them can be found in the original paper.

However, this logic is questionable if one regards the process of crack growth more carefully. The development of cracks changes the stress distribution of the beam continuously. Thus, the stress state has already changed when the crack tip moves to the location where a change of principal stress direction was expected before cracking. Apparently, the change of stress state due to the cracking process is quite significant in plain concrete beams. Since in plain concrete beams, the assumption proposed previously shall work exactly, in reinforced concrete, the crack shape should follow the principal stress trajectories. That conclusion is not supported by experimental results. The shear test series carried out on plain concrete beams by Jenq and Shah (Jenq & Shah 1988) showed only straight crack paths in most cracking locations, see Fig. 3.7. The specimens are loaded by three point bending. Notches are made in different locations regarding to the loading point.

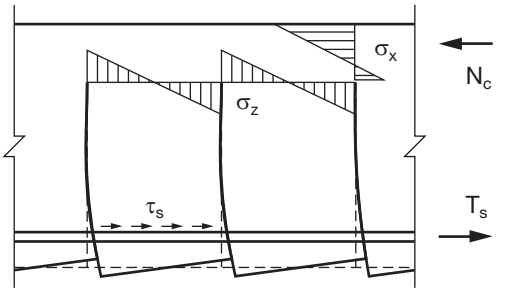

Fig. 3.8. Indication of stress distribution in Kani's Teeth model.

On the other hand, in reinforced concrete specimens, the inclination of cracks is always observed in experiments. The only possible conclusion is that the existence of longitudinal reinforcement influences the crack development in the shear failure process. This influence can be illustrated by Kani's teeth model (Kani 1964). The background of the model has been explained in Chapter 2. The model says that the flexural cracks develop perpendicular to the longitudinal rebars dividing the reinforced concrete beam into a teeth-like structure. The difference of tension between two cracks generates a secondary bending moment along the vertical direction in the teeth. The stress distribution of such a structure is demonstrated in Fig. 3.8. Kani assumed that only when σ_z at the crack tip reaches f_{ctm}, the corbel in the teeth structure breaks, and the structure fails. However, the process is more complex than that. Earlier than σ_z reaches f_{ctm}, a large difference in σ_z between the both sides of the crack tip already forms, as is clearly shown in Fig. 3.8. That results in a localized shear stress in the crack tip. Together with the normal stress σ_x, this shear stress influences the propagation of the crack. Therefore it can be conclude that the stress in z direction σ_x caused

by the bending of the concrete teeth is the main driving force in the inclination of the crack.

3.2.3.2 Basic Assumptions

Because the inclination of the flexural crack is due to the combined action between tension in the longitudinal direction, and shear in the vertical direction, it is important to understand the stress state at the crack tip under such a loading condition to predict the crack propagation. Because of the complexity of the problem, the intention in this study is not to derive an accurate solution under specific boundary conditions, which will not be so useful in reality, since the boundary conditions of the corbel in the teeth structure changes constantly during the cracking process. Moreover, the cracking process itself is also influenced by many other effects, such as the variation of material properties, directional stability of crack (Melin 1992; Xu & Needleman 1994; Broberg 1999). An estimation of the stress state with a proper theoretical background and sufficient accuracy is of more practical importance. As a brittle material, the fracture of concrete follows Tresca's criterion in principle. Thus, at a given crack height s, only the direction in which the maximum principal stress is oriented at the tip of a crack is of interest. That determines the direction of the crack when it develops further. To determine the direction of the principal stresses, concepts from Linear Elastic Fracture Mechanics (LEFM) are adopted here. Before that, several simplifications are needed.

- As explained in 3.2.1, most of the crack development in the height direction

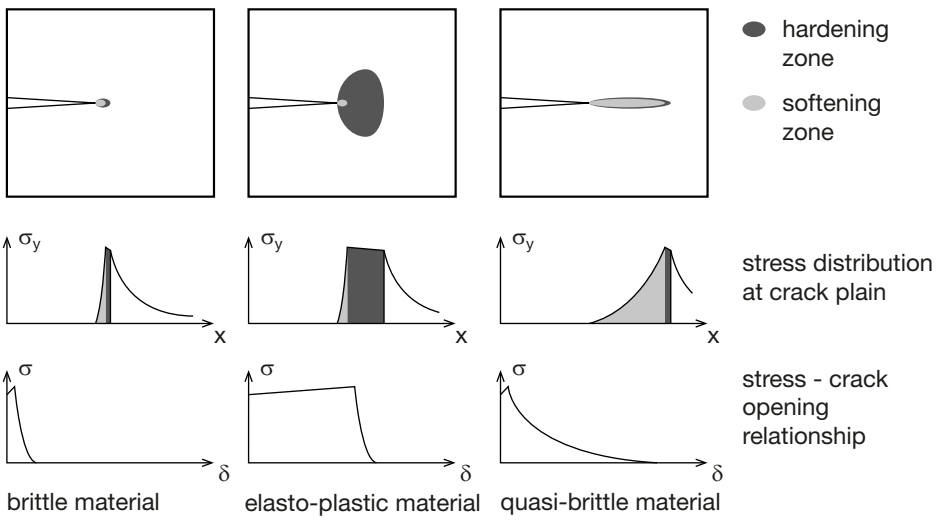

Fig. 3.9. Fracture process zone of different materials (Bažant & Planas 1998).

occurs shortly in an unstable process. Ignoring the additional moment needed to achieve M_1 stated in Fig. 3.2, it is reasonable to assume that when the crack is opening, the remote forces that drive the growth of the crack tip are constant, with the cross sectional moment $M = M_{cr}$.

- Another aspect is that, during crack opening, the relative shear displacement between two teeth is usually small, especially at the beginning when the direction of the crack is vertical. According to the experimental research carried out by Walraven (Walraven 1980), the shear stress that may be generated in the crack is negligible.
- Since the remaining part of the structure stays uncracked, the uncracked concrete outside the crack tip region is assumed to behave as a linear elastic material.
- In the crack tip region, the concrete behaves as a quasi-brittle material with a large tension softening strength after cracking. The inelastic zone according to Irwin's plastic zone correction (Irwin 1958) is not negligible compared to the size of the structure itself according to (Bažant & Planas 1998). Thus direct application of LEFM will lead to a considerable deviation from experimental observation quantitatively. Nevertheless, only regarding the fracture processing zone in concrete, see Fig. 3.9, the direction of the crack propagation can still be considered to coincide with the direction of the principal stress. Moreover, in a quasi-brittle material like concrete, the crack processing zone is actually much more localized than would be the case in the other materials. Thus, considering the aim set previously, it is correct to assume that the stress distribution determined by LEFM still appropriately represents the stress distribution surrounding the end of the fracture process zone.

3.2.3.3 Stress State at Crack Tip

Depending on the type of loading, the fracture processes of a solid are categorized into three modes. In this section Mode I (tension) and Mode II (shear) fracture are of interest. The assumption of linear elastic behaviour allows superposition of load cases of the same mode. The stress distribution of Mode I and Mode II in the vicinity of the crack tip can be formulated with the method of Westergaard (Westergaard 1939).

Mode I:

$$\begin{aligned}\sigma_x &= \frac{K_I}{\sqrt{2\pi r}}\cos\frac{\theta}{2}\left(1-\sin\frac{\theta}{2}\sin\frac{\theta}{3}\right)+\sigma_{x0}+O\left(r^{1/2}\right)\\ \sigma_y &= \frac{K_I}{\sqrt{2\pi r}}\cos\frac{\theta}{2}\left(1+\sin\frac{\theta}{2}\sin\frac{\theta}{3}\right)+O\left(r^{1/2}\right)\\ \tau_{xy} &= \frac{K_I}{\sqrt{2\pi r}}\sin\frac{\theta}{2}\cos\frac{\theta}{2}\cos\frac{3\theta}{2}+O\left(r^{1/2}\right)\end{aligned} \tag{3.6}$$

Mode II:

$$\begin{aligned}\sigma_x &= -\frac{K_{II}}{\sqrt{2\pi r}}\sin\frac{\theta}{2}\left(2+\cos\frac{\theta}{2}\cos\frac{3\theta}{2}\right)+\sigma_{x0}+O\left(r^{1/2}\right)\\ \sigma_y &= \frac{K_{II}}{\sqrt{2\pi r}}\sin\frac{\theta}{2}\cos\frac{\theta}{2}\cos\frac{3\theta}{2}+O\left(r^{1/2}\right)\\ \tau_{xy} &= \frac{K_{II}}{\sqrt{2\pi r}}\cos\frac{\theta}{2}\left(1-\sin\frac{\theta}{2}\sin\frac{3\theta}{2}\right)+O\left(r^{1/2}\right)\end{aligned} \tag{3.7}$$

where,

K_I and K_{II} : are the stress intensity factors related to the fracture mode. They are determined regarding the boundary conditions of the fracture specimens;

r,θ: are coordinates in a polar coordinate system with the origin at the tip of the crack and the principal axis along the axis of the crack;

$O(x)$: are higher order terms that can be ignored.

Eq. (3.6) and Eq. (3.7) show that the two variables in the equations θ and r are independent of each other. It implies that the direction where the maximum principal stress rises is independent of the distance r. This enables the possibility of using the Westergaard equations to search for the crack direction even in a quasi-brittle material like concrete.

In mixed mode fracture problems (Mode I and Mode II), several criteria have been proposed by researchers to determine the direction of the crack propagating direction. The criteria are summarized in (Bergkvist & Guex 1979; Bažant & Planas 1998; Broberg 1999). The three most popular principles are:

- Crack propagation perpendicular to the direction of the maximum principal stress (Erdogan & Sih 1963);
- Crack propagation in the direction of minimum strain energy density (Sih 1974);
- Crack propagation in the direction of the maximum strain energy release rate (Strifors 1974).

It was not possible to validate through experiments so far which of those principles is the most realistic. Nevertheless, Bergkvist and Guex show that all the principles provide almost equivalent criteria within a certain accuracy (Bergkvist & Guex 1979). Regarding for example the first principle, it is possible to find the direction where the shear stress in the polar systerm is equal to $\tau_{r\theta} = 0$ in the stress field. Converting Eq. (3.6) and Eq. (3.7) from Cartesian coordinates into cylindrical coordinates generates

$$\tau_{r\theta} = \frac{\cos\theta / 2}{2\sqrt{2\pi r}}\left(K_I \sin\theta + K_{II}(3\cos\theta - 1)\right) \tag{3.8}$$

By taking $\tau_{r\theta} = 0$, the increment of the cracking direction $\Delta\theta$ where the maximum principal stress is oriented is derived by solving Eq. (3.8). For a small change of the crack inclination the solution is simplified into

$$\Delta\theta = -2\frac{K_{II}}{K_I} \tag{3.9}$$

Therefore, once the stress intensity factors K_I and K_{II} are known, it is possible to determine the change of crack inclination $\theta = \mathrm{d}x/\mathrm{d}s$, which results in

$$\frac{\mathrm{d}^2 x}{\mathrm{d}s^2} = -2\frac{K_{II}}{K_I} \tag{3.10}$$

Here, x and s are the distances to the crack initiation location in longitudinal and vertical directions respectively.

3.2.3.4 Crack Path Function

It has been shown that to determine the crack path function of a mixed mode fracture the stress intensity factors K_I and K_{II} are necessary. Thus, they are discussed first under given loading conditions.

K_I Function

Isolating a part of the concrete beam surrounding a developing crack, two fracturing modes can be examined separately.

In the case of Mode I fracture, the model proposed by Carpinteri is employed (Carpinteri 1984; Bosco & Carpinteri 1992), in which the load applied at the concrete part of the reinforced concrete beam is simplified into the eccentric crack closing force T_s given by the reinforcement, and the remaining bending moment M applied at the concrete cross section, see Fig. 3.10.

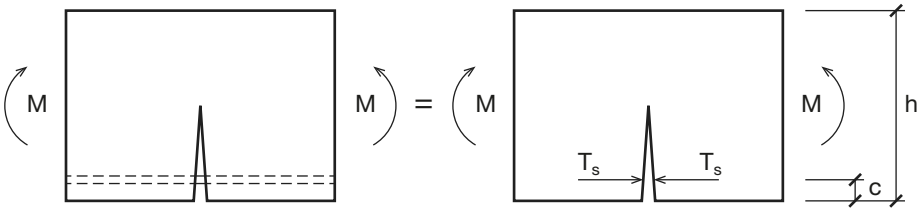

Fig. 3.10. Forces applied on the concrete part of RC beams. Adapted from Carpinteri (Bosco & Carpinteri 1992).

According to LEFM, the K_I of both load cases is found by sound analytical solutions (Tada et al. 2000):

$$K_{I,M} = \frac{M}{h^{3/2}b}\psi_M(\xi)$$
$$K_{I,T} = \frac{T_s}{h^{1/2}b}\psi_T(\frac{c}{h},\xi)$$

where

h : is the height of the beam;
c : is the thickness of the concrete cover;
b : is the width of the beam;
ξ : is the ratio between crack height s and beam height h, $\xi = s/h$;

$$\psi_M(\xi) = 6(1.99\xi^{1/2} - 2.47\xi^{3/2} + 12.97\xi^{5/2} - 23.17\xi^{7/2} + 24.80\xi^{9/2});$$

$$\psi_T(\frac{c}{h},\xi) = \frac{2}{\sqrt{\pi\xi}}\left(\frac{3.52(1-c/s)}{(1-s/h)^{3/2}} - \frac{4.35-5.28c/s}{(1-s/h)^{3/2}} + \left(\frac{1.30-.30(c/s)^{3/2}}{(1-(c/s)^2)^{1/2}} + 0.83 - 1.76c/s\right)\left(1-(1-c/s)s/h\right)\right)$$

Both ψ_M and ψ_T are regression functions. The overall K_I factor of a reinforced concrete beam becomes

$$K_I = K_{I,M} - K_{I,T} = \frac{M}{h^{3/2}b}\psi_M(\xi) - \frac{T_s}{h^{1/2}b}\psi_T(\frac{c}{h},\xi) \tag{3.11}$$

According to the assumptions given previously, during the crack formation process, the moment applied at the cross-section is $M = M_{cr}$, in Eq. (3.11). The value of T_s is still unknown. As shown in 3.2.1, the cracking process is unstable for a reinforced concrete cross section. At the snap back branch the external moment cannot be balanced by the internal force. What can be anticipated is the value of T_s before cracking and after the crack stabilizes. As a rough estimation

T_s is calculated from balancing the external moment with the internal level arm z derived from crack height s. So Eq. (3.11) becomes:

$$\begin{aligned} K_I &= \frac{M_{cr}}{h^{3/2}b}\psi_M(\xi) - \frac{M_{cr}}{h^{3/2}b}\frac{3}{(2+\xi)(1-\frac{c}{h})}\psi_T(\frac{c}{h},\xi) \\ &= \frac{M_{cr}}{h^{3/2}b}\psi_I(\frac{c}{h},\xi) \end{aligned} \tag{3.12}$$

Here the expression for K_I is combined into one formula, whereas the other geometry related functions ψ_M, ψ_T etc. are put together as a general function ψ_I, which is independent of the load condition.

K_{II} Function

Based on the experience of K_I, it is hoped that a similar formulation can be formed with regard to K_{II}. The load applied at the concrete relating Mode II fracture is illustrated in Fig. 3.11. The forces applied at the concrete include the remote shear force V, the local dowel shear force V_d, and the change of the tension force in reinforcement ΔT_s. As shown in Section 3.2.3.1, the influence of the remote shear force V to the cracking process is quite limited compared to the other effects, thus it is not considered here. At the crack opening stage, the relative displacement between the two crack surfaces is negligible, thus the component of V_d is neglected at this stage as well.

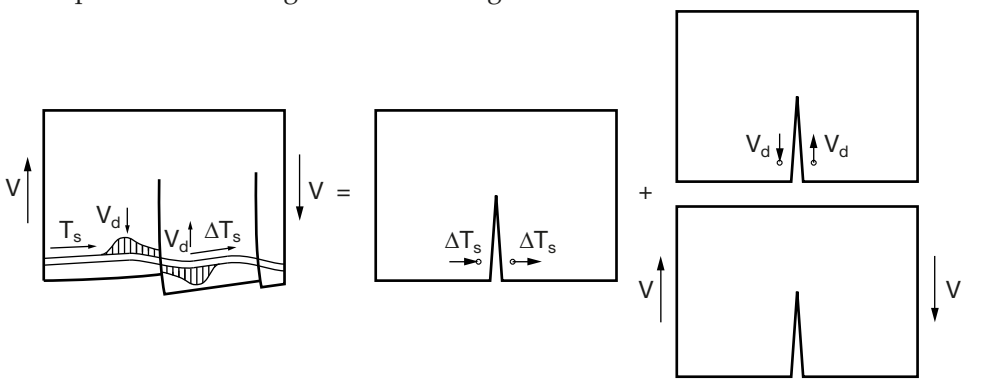

Fig. 3.11. Forces applied at the concrete part of a RC beam

Unlike the Mode I case, other than the load case of V_d, there is no analytical solution for the other Mode II load cases yet. It is not the intention of this research to derive one either. Nevertheless the general form of the K_{II} factor of concrete under ΔT_s can still be estimated by checking the energy dissipation during the crack progressing process. Assuming that the concrete teeth can be considered as beams, the strain energy stored can be estimated by beam theory

(Timoshenko 1956). Upon its release, the strain energy release rate G_{II} can be estimated with:

$$G_{II,est} = \frac{12T_s^2 s^2}{Eb^2 l_{cr,m}^3}$$

The stress intensity factor K_{II} is therefore determined with $K_{II}^2 = G_{II}E$. Considering that it is a rough estimation of K_{II}, the deviation between the estimation and reality is included in the function ψ_{II}. K_{II} and is expressed as:

$$K_{II} = \frac{\Delta T_s s}{l_{cr,m}^{3/2} b} \psi_{II}(\xi, l_{cr,m}) \tag{3.13}$$

with

ΔT_s: the difference of tensile force in reinforcement between two major cracks.

ΔT_s is related to the shear force V in the span by $\Delta T_s = Vl_{cr,m}/z$ between the major cracks. In the crack progressing section, the same problem of determining the value of T_s locally comes across. A similar approach as was used for determining K_I is used here, which results in an expression for K_{II}

$$\Delta T_s = \frac{3Vl_{cr,m}}{h(2+\xi)} + \frac{3M_{cr}(\xi_0 - \xi)}{h(2+\xi)^2} \tag{3.14}$$

Substituting Eq. (3.14) into Eq. (3.13) generates

$$K_{II} = \left(\frac{3\xi}{(2+\xi) l_{cr,m}^{1/2} b_w} V + \frac{3(\xi_0 - \xi)\xi}{(2+\xi)^2 l_{cr,m}^{3/2} b_w} M_{cr} \right) \psi_{II}(\xi, l_{cr,m}) \tag{3.15}$$

Here $\xi_0 = s_{cr}/h$, where s_{cr} is the stabilized crack height given by Eq. (3.2)

Basic Differential Equation

Having derived the expressions for K_I and K_{II}, the differential equations given by Eq. (3.10) can be expressed analytically. Substituting Eq. (3.12) and Eq. (3.15) into Eq. (3.10), and replacing the value of $l_{cr,m}$ by Eq. (3.5) generates:

$$\frac{\mathrm{d}^2 x}{\mathrm{d}s^2} = -2 \left(\frac{3\xi}{2+\xi} \left(\frac{3k_c}{2+\xi_0} \right)^{1/2} \frac{Vh}{M} + \frac{3(\xi_0 - \xi)\xi}{(2+\xi)^2} \left(\frac{3k_c}{2+\xi_0} \right)^{3/2} \right) \frac{\psi_{II}}{\psi_I} \tag{3.16}$$

In Eq. (3.16), the second term in the brackets is much smaller than the first one. Taking the prototype beam proposed in Section 3.1 as an example, the second term is only about 2.5% of the first one at the location which is about 2.0d from the support. Thus, the second term can be neglected, which leads to a simplified expression of the basic differential equation for the crack path

$$\frac{\mathrm{d}^2x}{\mathrm{d}s^2} = \frac{Vd}{M}\psi(\xi, \xi_0, k_c, \frac{c}{h}, \frac{M}{Vd}) \tag{3.17}$$

In Eq. (3.17) the beam height h is replaced by the effective height d. The influences of k_c, ξ, ξ_0 and c are covered by a function ψ in general.

Eq. (3.17) reveals how a crack path is inclined under the influence of the loading condition and the geometry of a reinforced concrete beam. It turns out that for a given structural member, the value of M/Vd at the cross-section will directly influence the inclination of the crack generated at the section. It also shows that for a simply supported beam loaded by point loads, the crack pattern is independent of the actual location of the loading points. Other than the cracks in the vicinity of the loading point, in most cases, the crack path function is only related to the value of M/Vd locally. For beams loaded by point loads, the value of M/Vd is equal to the distance to the location where the moment equals to zero.

The other influencing factors include the beam height h, the concrete cover c, the inclination of stress relief line k, the height of the stabilized major crack $\xi_0 = s_{cr}/h$ and the height of a developing crack $\xi = s/h$. They are all included in the function ψ. Among them, the values of c and ξ_0 do not vary significantly in practice.

However, as stated previously, due to the complexity of the problem, even with the significant simplifications stated during the derivation, it is still rather difficult to get an analytical solution for ψ that can be easily handled in practice. Besides, the expressions for ψ_M and ψ_T in Eq. (3.11) are results of a regression analysis with a certain inaccuracy already. The multiplication of these expressions will increase this inaccuracy inevitably. Taking these aspects into account, numerical simulations are employed in this research. Instead of trying to determine the complex expressions of ψ_I and ψ_{II}, the value of ψ is directly derived from the study of the numerical simulations.

3.2.4 FEM Models

3.2.4.1 Introduction

In the previous section, the crack path was formulated by the differential equation Eq. (3.17). However, it is rather difficult to derive an expression for the function ψ analytically. Even if it exists, the possible solution would be too complex for practical application. An alternative solution is to calculate a crack

path numerically with a model following exactly the same assumptions needed to determine an analytical model, and derive an expression for the crack path directly from the numerical solutions, eventually determining an expression for ψ.

Following this strategy, a Non-Linear Finite Element analysis is set-up taking into account the variables defined previously. The analysis of Eq. (3.17) previously showed that the main influencing factors of ψ are the crack height ξ and the height of the beam h. Thus, they are the main variables in the study. Other than that, the value of M/Vd is certainly a main variable as well. The expected output of the numerical studies is the value of d^2x/ds^2 expressed by Eq. (3.17).

Several special requirements are asked for in the analysis. Firstly, it is necessary to determine the crack path explicitly. This cannot be done by the conventional smeared crack approach used in engineering practice, which can only be used to indicate certain cracked area by smearing the crack opening over a 'cracked' element. Secondly, since the second derivative of the crack path is needed, it is more convenient to make the calculated crack path as continuous as possible. Thirdly, to investigate the variables discussed within the scope of the teeth model, the crack path has to develop at specific location, in addition, other than the specified crack, no other crack can develop in the model. To fulfil all these requirements **Sequentially Linear Analysis** with **Crack Propagation Algorithm** is utilized in this study.

3.2.4.2 Sequentially Linear Analysis (SLA) with Crack Propagation Algorithm (CPA)

Sequentially Linear Analysis

Fig. 3.2 has demonstrated that for a reinforced concrete element, its cracking process can be considered as a snap-back process (between point 1 and 2 in Fig. 3.2). When the moment at the cross-section reaches M_1, the crack will always jump from point 1 to point 2 even if the load or the displacement of the structure is kept constant at that moment. This behaviour cannot be simulated by the conventional non-linear finite element methods with the most widely used solving strategies such as the Newton-Raphson method, which approaches the solution of an equation system by solving the whole system at designated load/displacement steps. In each iteration, the Newton-Raphson method solves the stress field of the structure as a whole. Then, it simply tags all the integration points as cracked where the calculated principal strain level is higher than the crack strain. This procedure neglects the influence of the existing crack path to its future development within a single iteration. When the development of the crack follows the increase of the load or displacement, this strategy can approximate the crack development quite well. However, when the whole crack

develops within one iteration, it is not possible to derive an accurate crack path correctly anymore, which is the case for the unstable crack development at M_1. Similar problems will be faced even with the other solving strategies like the Arc-Length method, which tags cracked integration points in the same way.

To take into account the whole evolution process of the crack at M_{cr}, the definition of the load step shall be based on the increase of the crack length. Therefore crack path tracking calculation in this section uses sequential linear analysis (SLA) proposed by Rots et al. (Rots & Invernizzi 2004; Rots et al. 2008) to replace the conventional Newton-Raphson method. With the SLA, the non-linear behaviour of a structure is captured by applying a series of scaled linear elastic analyses up to predefined 'critical events' at the most critically loaded integration point of the model. The critical events are defined by crack initiation and crack propagation. For quasi brittle materials such as concrete, its crack propagation is related to a post tension softening law (tensile stress – crack opening relationship). In SLA, the crack opening is smeared out over the cracked element like other smeared crack FEM models, while the softening curve is discretised by a saw-tooth constitutive law. Each node on the saw-tooth curve is defined as a critical event. On the other hand, it is still possible to discretise the structure using standard elastic continuum elements. Thus, unlike the lattice models (Schlangen & van Mier 1992; Schlangen & Garboczi 1996), which was also widely used to simulate the fracture process of concrete, it is more convenient to interpolate the crack path between the integration points in continuum elements. The calculation process is summarized according to (Rots, Belletti et al. 2008) as follows

- Add the external load as a unit load.
- Perform a linear-elastic analysis.
- Extract the 'critical integration point' from the results. The 'critical integration point' is located in a element for which the stress level divided by its current strength is the highest in the whole structure.
- Calculate the ratio between the strength and the stress level in the critical element: this ratio provides the 'global load factor'. The present solution step is obtained rescaling the 'unit load elastic solution' times the 'global load factor'.
- Increase the damage in the critical integration pointby reducing its stiffness and strength, i.e. Young's modulus E and tensile strength f_t, according to a saw-tooth constitutive law extracted from the constitutive law of the target material. This corresponds to a local damage 'event'.
- Repeat the previous steps for the new configuration. Trace the next critical saw-tooth in some element, repeat this process till the damage has spread into the structure to the desired level.

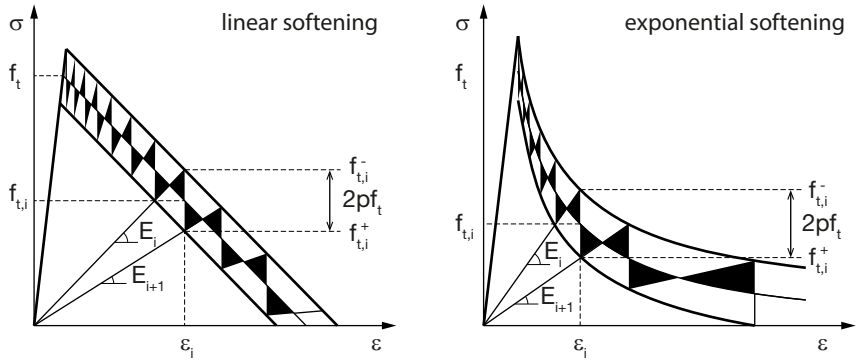

Fig. 3.12. Examples of a saw-tooth descritised law on the concrete softening law, left: linear softening, right: exponential softening (Rots, Belletti et al. 2008).

Two examples of saw-tooth discretisation on concrete softening laws are shown in Fig. 3.12. The basic principle is that the initial stiffness E, the tensile strength f_t and the fracture energy G_f (the area covered by the curve) shall remain the same after the discretization. As is illustrated in Fig. 3.12, the more saw-teeth are used, the more accurate the discretised constitutive law is, but at the meantime, the calculation time is increased enormously. This method has been successfully applied by Slobbe, Hendriks et al. in (Slobbe et al. 2012) to simulate the shear failure of reinforced concrete beams without shear reinforcement.

The drawback of such type of analysis is that for some reinforced concrete structures with multiple cracks, the unloading and reloading stiffness of the cracked concrete cannot be represented anymore, while this type of behaviour can be critical in concrete structures with a multiple crack system. However, as will be shown later, in the model presented in this section, only one cracking process is modelled. It is assumed that there is no reloading during the cracking process.

Delayed C^1 - Continuous Propagation Algorithm

In addition to the SLA, the analysis presented in this chapter also includes a Crack Propagation Algorithm (CPA) as proposed by Slobbe et al. in (Slobbe et al. 2014). The algorithm was developed to solve the problem of mesh induced directional bias addressed by Slobbe et al. in (Slobbe et al. 2013). Instead of having the crack opening smeared out over the element according to the conventional smeared crack method, the algorithm calculates the propagation of the crack path explicitly. In addition, the algorithm ensures C^1 continuous to the calculated crack path. An illustration of the crack propagation algorithm is given in Fig. 3.13. The algorithm works as follows.

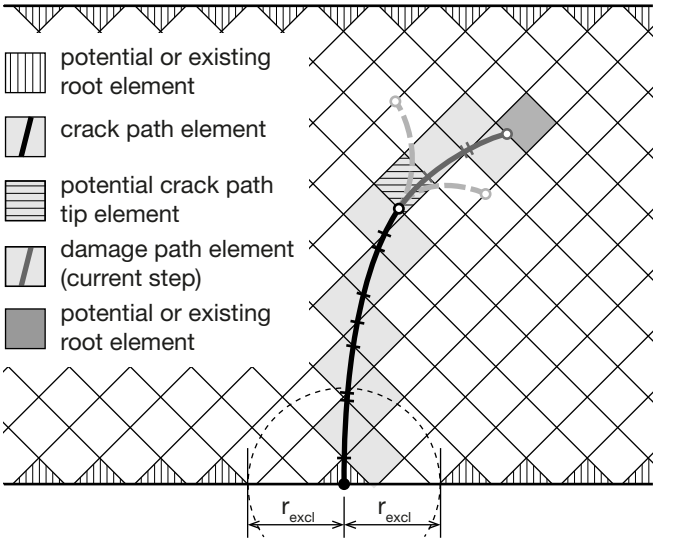

Fig. 3.13. Illustration of a propagating crack path in the delayed C^1 - continuous propagation algorithm and the corresponding labelled element (Slobbe, Hendriks et al. 2014).

Firstly a crack path initiates from one of the root elements predefined in the mesh, which are usually located at the edges of the mesh, excluding the elements within r_{excl} from an already cracked root element, see Fig. 3.13. For a propagating crack path, the potential trajectory of the crack path is calculated as damage path in the damage path elements in front of the already fixed crack path. Only when the relative stiffness reduction of the damage path elements is larger than the predefined threshold $d_{crit,crk}$, the part of the damage path is fixed as crack path.

Within a damage path element, the position and the direction of the starting point of the crack path is defined by the intersection of the crack path calculated from the previous cracked element. The crack propagation directions are firstly evaluated at the Gauss Points of the elements as the orthogonal direction of the principal strain direction. The propagation directions at the Gauss Points are then used to calculate a crack path propagation field within the elements. The procedure basically extrapolates the directions calculated at the Gauss Points into a linear distribution of crack directions including a weight function that take into account the damage level of the material at different Gauss Points. The crack path is than calculated by simulating the streamline of a particle in a two-dimensional steady flow field with Euler method. As shown here, the calculation procedure is based on the crack directions; therefore it guarantees C^1 continuous for the crack path intrinsically, although the outputs of the crack path are the intersection points of the crack path and the element boundaries.

The described procedure have been demonstrated in (Slobbe, Hendriks et al. 2014) that it is able to evaluate the crack paths of mixed mode cracking specimens under complex loading conditions with very good accuracy.

3.2.4.3 Model Configurations

The analysis is carried out with a code developed in the TNO Diana platform. The finite element mesh is generated by the pre/post processor iDiana. Thus some of the terminologies used here are in accordance with the aforementioned software package.

Boundary Conditions

The crack path is modelled in a simply supported beam with two point loads applied in the middle of the span. Taking advantage of the symmetric configuration, only half of the beam is modelled. The cross-section of the beam is the same as is described in Section 3.1 for the reference specimens. A sketch of the beam model is given in Fig. 3.14.

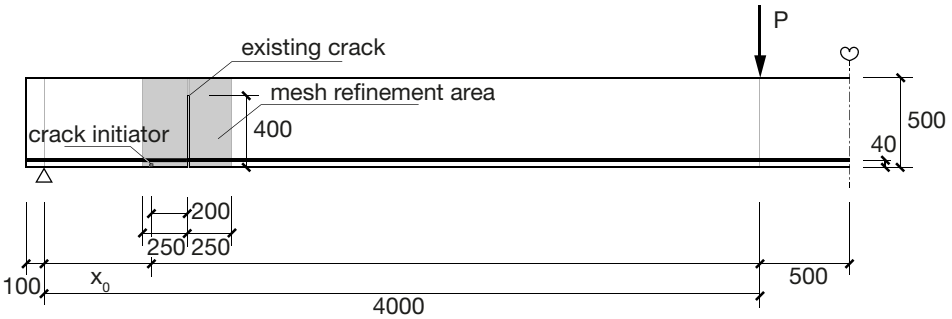

Fig. 3.14. Sketch of the model configuration.

Since the actual location of the loading point is not influencing the crack path according to the theory described in the preceding section, a rather long span is taken, so that relatively more M/Vd situations can be studied with more or less the same configuration. The centre-to-centre distance between the loading point and the support is 4000 mm. The centre of the reinforcement to the tensile edge of the beam is 40 mm. It allows the maximum M/Vd to be 8.0.

The boundary conditions described in Section 3.2.3.4 are realized in the following manner. The existing flexural cracks are modelled by an opening gap in the beam. At the location of the reinforcement, the gap is kept connected by steel bars. In this way a crack without residual tensile stress is modelled. The height of the existing crack is 300 mm, which is 65% of the effective beam height, from the observation of experiments. The propagating crack path to be evaluated, is initiated at 200 mm from the existing crack. The distance of 200 mm is an estimation derived from on the average crack space $l_{cr,m}$, see Section 3.2.2. The

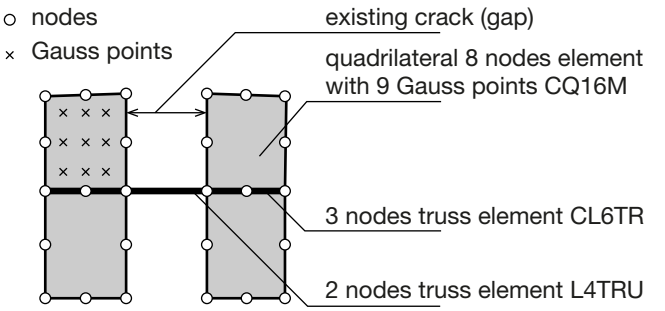

Fig. 3.15. Detail of elements at the existing crack, the name of the elements being defined in Diana, see Diana Manual (TNO-DIANA 2011).

location of the crack path is fixed by manually assigning an exceptionally low material strength f_{ct} to the root element at a specific location. Other than that, the value of r_{excl} is set to be longer than the length of the specimen, to supress the opening of any other crack in the model according to the delayed C^1 - continuous propagation algorithm described previously. The distance between the predefined root element (crack root in Fig. 3.14) and the support is denoted by x_0. x_0 is equivalent to the value of M/Vd at the cross section. It varies from 300 mm to 1900 mm, which results in variation of M/Vd between 0.66 and 4.14 in this study.

Mesh

Quadrilateral 8 nodes elements are used to model the concrete. 3×3 integration points (Gauss Point) are used with each element. The reinforcement is modelled by 3 nodes truss elements. The nodes of the truss elements are connected to the nodes of the quadrilateral elements. Thus perfect bond is assumed between the reinforcement and the concrete. To simulate the reinforcement in the existing crack modelled by the gap, a 2 nodes straight truss element is used to connect the nodes of the two adjacent concrete elements. A demonstration of the elements is shown in Fig. 3.15. Besides, an example of the mesh configuration is given in Fig. 3.16.

The mesh is refined within 250 mm from the existing crack, where the mesh size is 10 mm. Thus there are about 50 elements over the height of the beam. A mesh sensitivity study has been carried out by enlarging the mesh size twice in the refined zone, which will be discussed further in Section 3.2.4.4. The resulting crack path is not influence by the mesh configuration. Thus it may be concluded that there is no significant mesh dependency in the analysis described in this study, which can be understood as the benefit of the crack propagation algorithm as well.

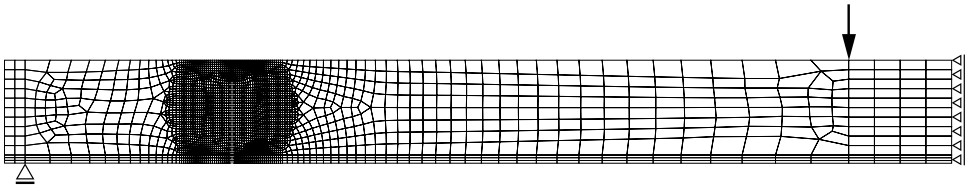

Fig. 3.16. Mesh configuration and boundary conditions of model with x_0 = 700 mm.

Material Properties

The uncracked concrete is modelled as a linear elastic material, with an initial modulus of elasticity equal to E_c = 34 GPa. The reinforcement is assumed to be a linear elastic material. The modulus of elasticity of the steel is assumed to be E_s = 210 GPa.

The cracking behaviour of the concrete is modelled by means of smeared crack elements. The tensile strength of the concrete is f_{ctm} = 2.8 MPa. The fracture energy is G_f = 7.08·10^{-4} Nm/m, which is calculated based on fib Model Code 1990 (fib 1993). Hordijk's curve (Hordijk 1991) is used to define the tension softening law. The softening curve is discretised by 25 saw teeth to make use of the SLA method. The shear retention factor is assumed to be 0.05, so that the reduction of shear stiffness of the element due to cracking is taken into account. For the root element of the propagating crack path, the tensile strength and the fracture energy are 10 times smaller than in the other elements. That element is used to introduce the crack path at the specific location in the model.

Calculation Scheme

In the SLA used in this study, 6000 load steps were applied in the evaluation of a single model. The number of steps is based on the estimated length of the crack. With 9 integration points per element and 25 teeth for each integration point, 225 steps are needed to completely crack an element.

With regard to the CPA, preliminary analysis (Slobbe, Hendriks et al. 2014) showed that the delayed procedure did not have significant influence on the crack path when the shear stress at the crack tip is large. Therefore $d_{crit,crk}$, is set to be 1.0 in the simulation.

3.2.4.4 Results

With the analytical procedure described before, it is possible to calculate the crack path initiated at any given cross-section under the idealized boundary conditions. As an example, two simulated crack paths are plotted in Fig. 3.17. The contour plot of the maximum principal strain is shown in Fig. 3.19, where the crack path is also indicated by large local strains. Both plots show that the

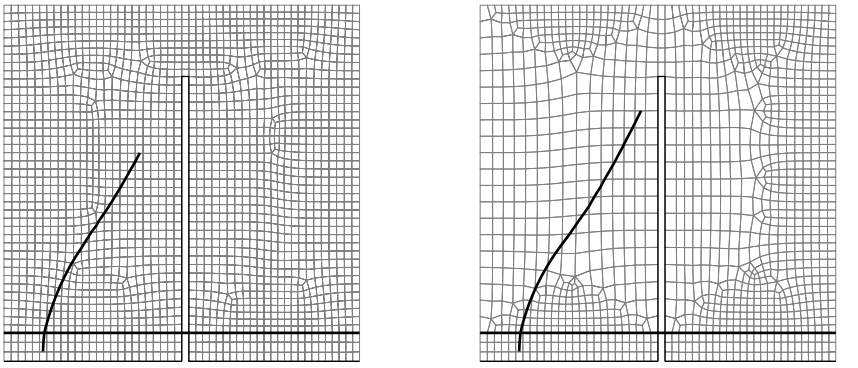

Fig. 3.17. Influence of mesh size to simulated crack paths from SLA (x_0 = 600 mm).

simulated crack paths seem quite comparable with crack paths observed in experiments. By defining the exact crack path with CPA it is possible to refine the calculation of the smeared crack over multiple elements more effectively. Thus it improves the mesh bias if the crack path is skewed or close to the boundary of the element. The two crack paths shown in Fig. 3.17 are simulated by two models with the same boundary conditions but different mesh sizes. The mesh size of the right model is two times larger than that of the left one. The differences of the two crack paths are negligible. This demonstrates that when the mesh presented in Section 3.2.4.3 is fine enough, the simulated crack path is mesh-independent.

However, Fig. 3.17 also shows that when the crack height increases further the crack path becomes more unrealistic. This is due to the simplification of the existing crack with a gap which ignores the tension softening of concrete at small crack width. This effect should be taken into account. Therefore, only a part of the calculated crack path which is less influenced by this simplification is used in the study.

In Fig. 3.18, the relationship between the load factor for the SLA step and the deflection at the loading point is plotted for a crack generated at a cross-section with M/Vd = 2.6. As explained previously, in SLA, the load factor applied per load step reflects the external load on the structure. At large M/Vd the crack path is comparable with straight cracks orthogonal to the longitudinal direction being simplified in Section 3.2.1, accordingly, the presented results are consistent to the layered model analysis at the cross sectional level shown in Fig. 3.2.

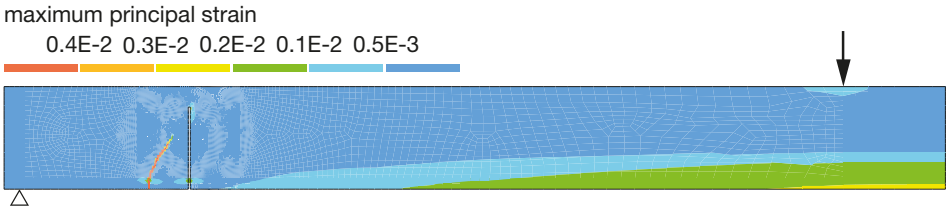

Fig. 3.19. Distribution of maximum principal strain of model with x_0 = 600 mm.

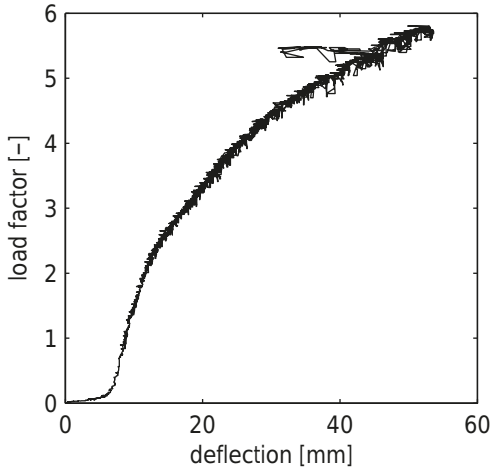

Fig. 3.18. Load factor - deflection for a model with x_0 = 1200 mm.

Crack Path Expression

According to Eq. (3.17), the curvature of a crack path developed at a given cross-section is strongly influenced by the value of M/Vd locally. Thus, the value of M/Vd is considered to be the major variable in the study. With the model presented above, the crack paths generated from x_0 = 200 mm to 1800 mm are calculated; they are plotted in Fig. 3.21. The detailed information of each simulation and the results are listed in Appendix II.

To evaluate the crack paths derived from the numerical analysis, the crack paths shown in Fig. 3.21 are plotted together with the cracks marked from experiments. It has to be remarked that unlike the marked cracks from experiments, the black lines shown in Fig. 3.21 and Fig. 3.20 are simply the assembly of the calculated crack path from different FEM models like the one shown in Fig. 3.16. Therefore, in these models, only a single crack is simulated at each time.

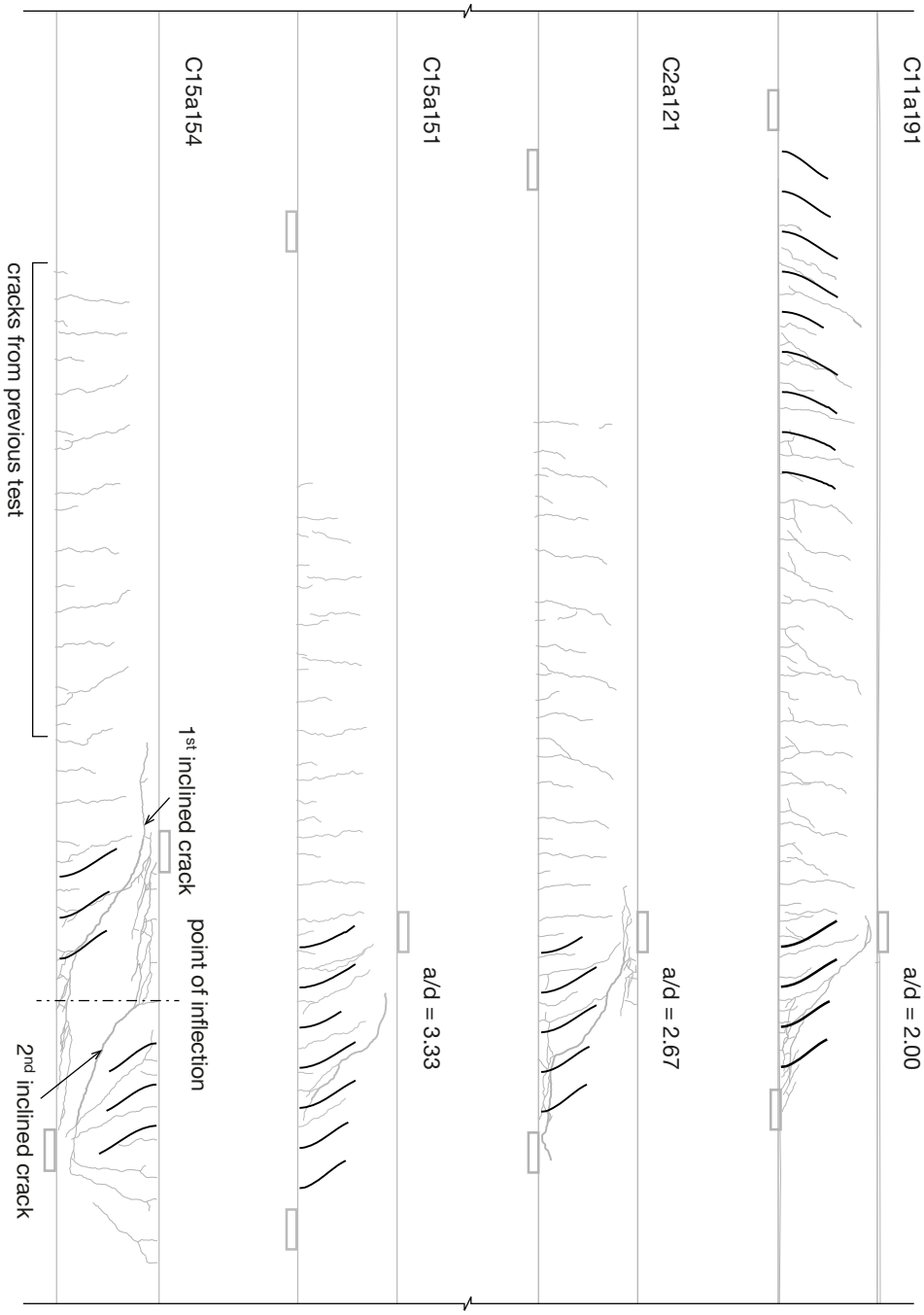

Fig. 3.20. Comparison between simulated crack path and marked ones from experiments. The grey lines in the figures are marked cracks in experiments, the black lines are the assembly of the simulated crack paths from different models.

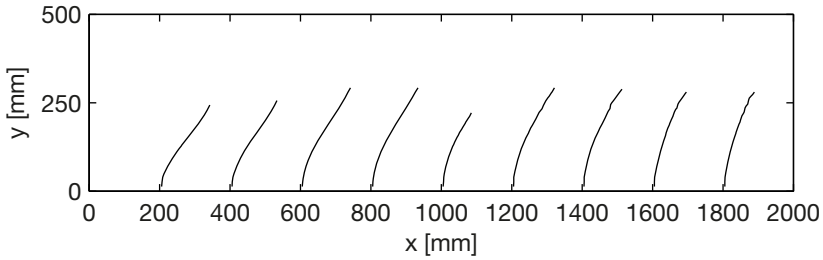

Fig. 3.21. Simulated crack paths with x_0 from 200 mm to 1800 mm.

The plotted crack paths do not imply that the cracks have to develop to the height and the location as they are indicated in Fig. 3.20. Instead, it should be understood in such a way that if there is a major crack developing at the location where the crack path is simulated with a height s_{cr}, then its profile looks like the one plotted in the figure up to the crack height s_{cr}.

Four beams from the continuous beam test series (the test program with be explained in Section 5.3.2) are selected and their crack patterns after failure are plotted in Fig. 3.20. The dimensions and the reinforcement configurations of the test specimens are in general the same as the models. Among them, three specimens are simply supported and loaded with a single point load, while the last one was loaded in a way to simulate a continuous supported moment distribution. The point of inflection is marked in Fig. 3.20.

Despite the roughness of the crack path due to variation of material properties, the direct comparison clearly shows that the crack paths simulated with SLA models are capable to represent the crack pattern of reinforced concrete beams without shear reinforcement with a quite reasonable accuracy. It also works in case of continuous supported beams with more complex moment distribution. Besides, the comparison clearly shows that there is in principle no difference regarding to the crack profile in beams with different loading condition as long as the crack is initiated from the cross-section with the same M/Vd.

Here, the second inclined crack in C15a154 shall be treated separately, since it is developed after the beam was heavily damaged by the first inclined crack at lower load level. That results in a significantly stress redistribution in the span. Thus, the boundary conditions applied in the models are not valid any more. The other point that has to be noticed is that for cracks with a large M/Vd, the crack paths from simulation could be slightly overestimate the inclination of the crack.

The crack paths calculated from numerical simulations are then utilized as original data to derive a more general expression of the crack path in accordance to the expression explained in Section 3.2.3.4. Before that, the crack paths are

re-formulated with a dimensionless expression with the beam height, and the coordinates are reversed. In addition, the value of $\zeta = x/h$ shall be limited to 0.16 (x_0 < 80 mm). This is necessary to limit the influence of the local effect due to the simplification of the existing crack as discussed previously. Another reason is that Fig. 3.18 shows that a further increase of the crack length requires a larger increase of the external load, which is in conflict with the assumption made in Section 3.2.3.2: only crack development at M close to M_{cr} is studied. With the treatment mentioned above, a regression analysis is applied for the crack paths.

The analysis shows that in most cases a quadratic function is able to express the crack path with sufficient accuracy. Two examples of the results are given in Fig. 3.22. In both cases the value of R^2 is larger than 0.99. The same level of accuracy holds for the other 9 analyses, see Table 3.1. Besides, Table 3.1 also confirms that the curvature of the crack paths is indeed strongly related to the value of M/Vd at the considered cross-section. The numerical analysis clearly proves that Eq. (3.17) describes the crack path properly. The results of all the other models can be found in Appendix II.

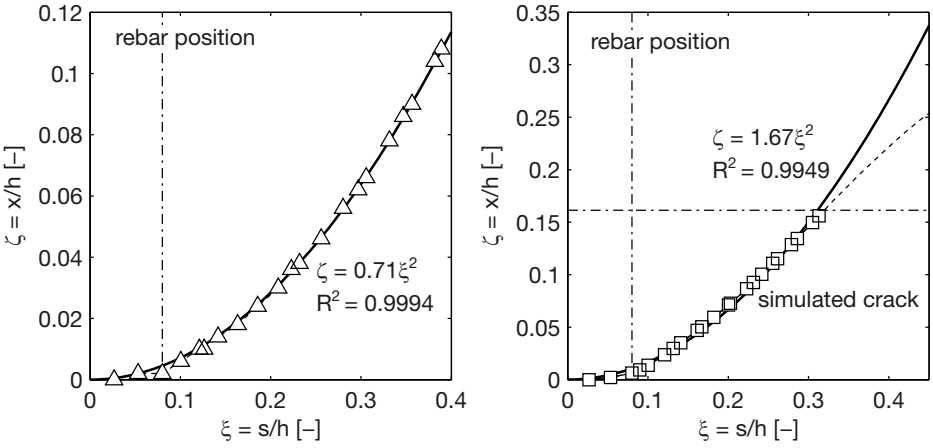

Fig. 3.22. Regression analysis of two crack paths. Left: x_0 = 1400 mm. Right: x_0 = 200 mm.

By comparing the simulated crack paths with the ones derived from the experiments in Fig. 3.20, the influence of another simplification is shown. In the simulation, the existing crack is modelled by a gap being perpendicular to the longitudinal axis, which is apparently inappropriate. The existing crack should have a similar expression as well. However, because most cracks still start perpendicular to the axis of the member, at a lower level the simplification of a vertical crack face remains a good approximation. The comparison shown in Fig. 3.20 confirms this. The difference is only obvious when the crack height ap-

proaches s_{cr}. In that case the simulated cracks start to become parallel, because the influence of the imposed vertical crack used in the simulation stopped the further development of the crack towards the loading point. In the experiments, the cracks develop more freely towards the existing cracks, as is shown in Fig. 3.20, and even alignment of two cracks is possible. Nevertheless, the influence of this difference is limited since that part of the crack branch has been discarded in the analysis, as explained before.

Since the crack path can be expressed by a quadratic function, the function ψ in Eq. (3.17) becomes a constant independent of the value of ξ. This indicates that the ratio between K_{II} and K_I remains constant during the development of the crack. This might be attributed to the constantly changing crack inclination, because it changes the boundary conditions that influence the crack tip stress state under the same moment shear force combination. From the results derived from regression analysis, it is possible to calculate the values ψ for each crack path, see Table 3.1. They are plotted against M/Vd in Fig. 3.23.

Table 3.1. Summary of regression analysis.

x_0	M/Vd	$d\xi^2/d^2\zeta$	R^2	ψ
[mm]	[-]	[-]	[-]	[-]
200	0.43	1.6660	0.9949	1.4487
400	0.87	1.3120	0.9977	2.2817
600	1.30	1.0540	0.9987	2.7496
800	1.74	0.9184	0.9992	3.1944
1000	2.17	0.8533	0.9994	3.7100
1200	2.61	0.7715	0.9991	4.0252
1400	3.04	0.7100	0.9994	4.3217
1600	3.48	0.6248	0.9914	4.3464
1800	3.91	0.5836	0.9961	4.5673

Combining the regression results of ψ as shown in Fig. 3.23 and Eq. (3.17), an expression for the crack path under the specific condition described in this section can be derived:

$$\zeta = 1.22\left(\frac{M}{Vd}\right)^{-0.5}\xi^2 \tag{3.18}$$

The validation of this equation to more general boundary conditions has to be checked with more parametric studies.

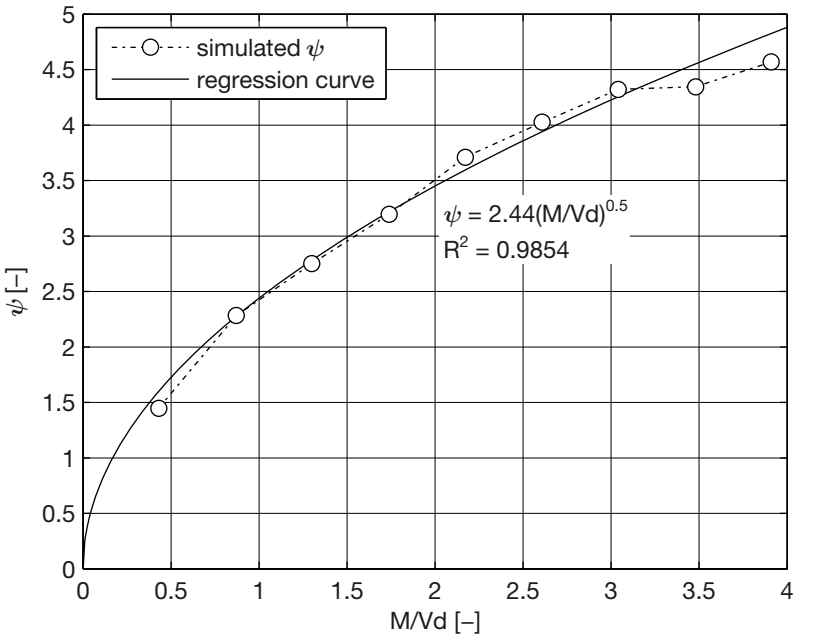

Fig. 3.23. Resulting ψ from simulated crack paths

Other Variables

In addition to the major variable M/Vd, other aspects or variables may influence the development of the cracks. Some of the variables are also included in the expression for ψ in Eq. (3.17). They are summarized below. Regarding to each variable, several models are set-up. Most of the parametric studies are based on the reference model with x_0 = 600 mm. The most important variables are supposed to be:

- Reinforcement ratio ρ_s.
- Tensile strength f_{ct}, fracture energy G_f and shear retention factor of concrete.
- Beam height h, (size effect).
- Thickness of concrete cover c.
- Crack spacing $l_{cr.m}$.
- Height of the existing crack $\xi_0 = s_{cr}/h$.

Comparing the models with different variables with the reference models shows that not all the variables have a significant influence on the crack path development. Among them, the concrete properties such as tensile strength f_t, fracture energy G_f, shear retention factor, and the height of the specimen h have almost no influence on the crack path. The concrete cover determines where the crack inclination starts, however, since the difference of c is usually rather small compared to the beam height, this effect is almost negligible.

The height of the existing crack ξ_0 only affects the crack path when the value of ξ_0 is very small. In that case, the crack becomes considerably steeper. This effect is demonstrated in Fig. 3.24, where four simulated crack paths with different existing crack height ξ_0 are plotted. The crack path with existing crack height s_{cr} = 100 mm (ξ_0 = 0.2) is clearly different from the other three, while the other three crack paths are quite close to each other. Since the flexural crack heights of normal reinforced concrete beams are usually higher than 0.5h, the effect of crack height ξ_0 can be neglected as well. This actually shows that it is necessary of having an existing crack to make the flexural crack inclined as was concluded previously in Section 3.2.3.1.

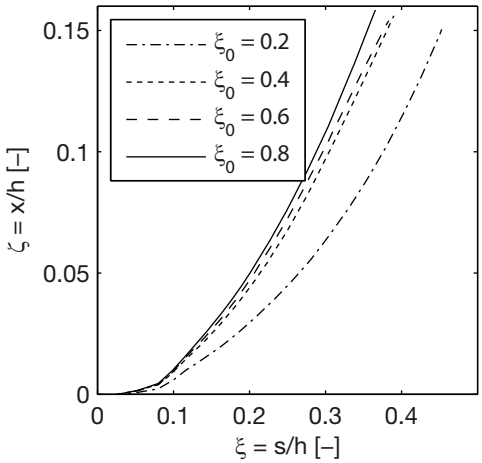

Fig. 3.24. Influence of existing crack height ξ_0 to the crack path.

The reinforcement ratio has a similar effect on the crack path as the height of the existing crack ξ_0. Its stiffness affects the crack opening under a certain moment, thus it influences the crack path. However, such an influence is only pronounced if the number of rebars is very low. In practice, the reinforcing steel will yield upon the cracking of the specimen. Therefore, one may assume that the reinforcement ratio ρ does not affect the crack path.

The crack spacing, on the other hand, has the most significant effect on the crack path. As already shown by Eq. (3.15), the value of K_{II} is related to crack spacing l_{cr}. A similar regression analysis is carried out to check the effect of l_{cr}. Models are set-up with a crack spacing of 100 mm, 200 mm and 300 mm. l_{cr} is normalized by specifying $\delta_{cr} = l_{cr}/h$. It is found that ψ is related to $1.2\delta_{cr}^{-0.2}$.

3.2.5 Conclusions

The application of Sequentially Linear Analysis with a Crack Propagation Algorithm makes it possible to calculate the crack path explicitly under idealized boundary conditions. That makes it possible to derive a generalized crack path expression. The crack paths simulated from numerical analysis are used directly to approach an estimation of the crack path based on fracture mechanics. This process makes the complex stress field analysis usually needed to derive stress intensity factors superfluous. A rather simple expression for the crack path is derived by combining the analysis of other variables and Eq. (3.18).

$$\zeta = \delta_{cr}^{-0.2}\left(\frac{M}{Vd}\right)^{-0.5}\xi^2 \tag{3.19}$$

where

$\zeta = x/d$: is the normalized coordinate of the crack in the longitudinal direction

$\xi = s/d$: is the normalized coordinate of the crack in the height direction

$\delta = l_{cr}/d$: is the normalized crack spacing

Because the value of the concrete cover c is usually much smaller than the beam height h and the effective height $d = h - c$, h is approximated by d in Eq. (3.19). Taking into account the large variation of material properties in a concrete beam, the derived crack path expression offers sufficient accuracy for further analysis.

3.3 EQUILIBRIUM SYSTEM OF A CRACK

3.3.1 Free Body Element Formed by a Crack

In the previous study a crack pattern was derived mainly dependent on the location where the crack is initiated. It is assumed that at a given cross section, as soon as the moment locally reaches the cracking moment M_{cr}, a major flexural crack will spontaneously develop up to a certain height s_{cr}, with a predefined shape expressed by Eq. (3.19) if there is no other major crack located at about $l_{cr,m}$ from that section. Based on that assumption, it is possible to cut the concrete member along the predefined crack at any location including the compressive zone. The concrete part closer to the support together with the longitudinal rebar is considered as a **free body**. The free body element and the forces applied on it are shown in Fig. 3.25. In this free body element, the equilibrium conditions and kinematic conditions have to be fulfilled.

In Fig. 3.25, the beam is loaded from its top surface, thus the direction of the load is denoted as the **vertical direction**. Respectively, the direction of the beam

axis is denoted as the **horizontal direction** or the **longitudinal direction**; besides the beam is in tension at the bottom side and in compression at the top side, thus within this chapter, the term '**bottom side**' of the beam means the **tensile side** of the member in a more general case, and the '**top side**' stands for the **compressive side** of the member.

The forces applied on the free body shown in Fig. 3.25 include the following components:

- V : is the reaction force, which is equal to the shear force at the cracked cross section;
- V_c, N_c : are the shear component and the normal component of the forces in the uncracked concrete;
- V_{ai}, N_{ai} : are the total vertical and horizontal components of the aggregate interlock effect along the crack. They are calculated by the shear stress τ_{ai} and normal stress σ_{ai} distribution along the shear crack;
- V_d : is the shear force transmitted through dowel action perpendicular to the rebars;
- T_s : is the tensile force in the rebars.

In addition, the following terms can be found in Fig. 3.25 as well. Some of them have already been defined before. The distance between N_c and T_s is defined as the internal level arm z. The longitudinal component of the total force derived from aggregate interlock N_{ai} is applied at a distance of z_{ai} from N_c. The height of the crack is defined as s_{cr}, and the height of the compressive zone in the concrete is referred as z_c.

For the convenience of the formulation, within this section, the longitudinal and vertical directions of the beam are defined as x and y direction respectively.

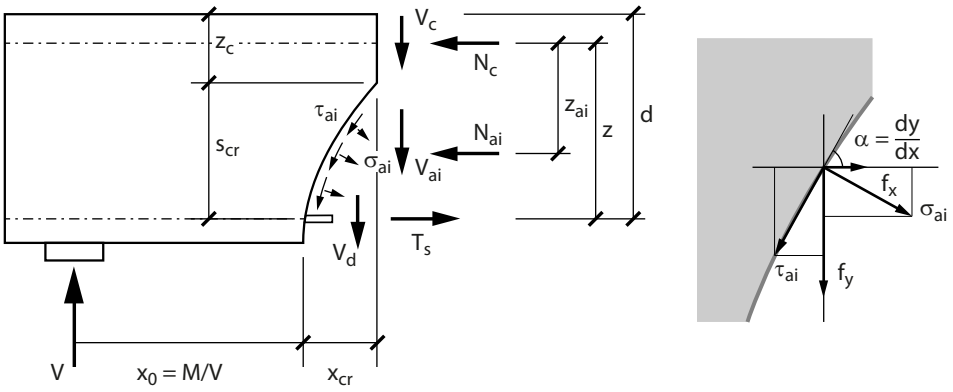

Fig. 3.25. Part of a reinforced concrete member (free body) cut along a crack ($x_0 = d$)

In x direction, the distance between the centroid of the support and the initial location of the crack is x_0. The horizontal distance between the bottom and the tip of the crack is defined as x_{cr}. For the vertical component of the aggregate interlock force V_{ai}, its horizontal distance to the start of the crack at the bottom is x_{ai}. This is not indicated in Fig. 3.25.

3.3.1.1 Equilibrium Conditions

The forces applied on the free body element have to be in equilibrium in all directions for a stable structure. In vertical direction the force equilibrium equation is formulated as:

$$V = V_c + V_{ai} + V_d \tag{3.20}$$

The longitudinal force equilibrium is achieved by:

$$N_c + N_{ai} + T_s = 0 \tag{3.21}$$

The moment equilibrium is calculated around the position where N_c is applied. As a result, the equation is formulated as follows:

$$V(x_0 + x_{cr}) = V_d x_{cr} + V_{ai} x_{ai} + T_s z - N_{ai} z_{ai} \tag{3.22}$$

Here the longitudinal component of the aggregate interlock effect is assumed to be compression along the crack.

3.3.1.2 Kinematic Conditions

For any crack generated in the loading process, the study of the crack pattern has shown that after the crack development stage, it can hardly have any further extension in vertical direction. Further increase of the external load may result in the opening of the crack mouth or the development of a crack in longitudinal direction. Consequently, the possible movement of the two surfaces along the crack curve can only be the rotation θ around the crack tip, or the relative displacement Δ_0 in vertical direction. The corresponding displacements are demonstrated in Fig. 3.26. For the convenience of the formulation, a coordinate system is set within this section with the origin at the tip of the crack, the positive directions of x and y are indicated in Fig. 3.26. Another simplification in the analysis is that the uncracked concrete adjacent to the crack faces is assumed as rigid body; therefore the crack profile is not influenced by the local forces. This simplification will be further discussed in Chapter 4.

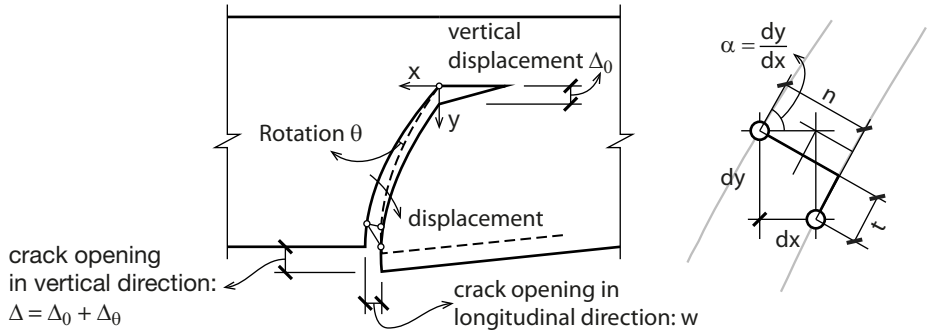

Fig. 3.26. Kinematic conditions of a crack.

For any points along a random crack curve expressed by the function $y = s(x)$, the rotation and relative displacement of the crack curve are basically the rotation and translation of the coordinate system. Thus, the new coordinates after movement can be expressed as follows:

$$\begin{pmatrix} x' \\ y' \end{pmatrix} = \begin{pmatrix} \cos\theta & -\sin\theta \\ \sin\theta & \cos\theta \end{pmatrix} \begin{pmatrix} x \\ y \end{pmatrix} + \begin{pmatrix} \Delta_x \\ \Delta_y \end{pmatrix} \tag{3.23}$$

For the free body element formed by a crack defined in this section, the values of the translated displacements are $\Delta_x = 0$, and $\Delta_y = \Delta_0$, with Δ_0 being the vertical displacement at the tip of the crack. For a crack in a concrete structural element, its opening in longitudinal and vertical directions (w and Δ) at the level of reinforcement are directly measureable variables, therefore they are of more interest than the rotation and vertical displacement at the tip. They can be expressed by $w = x' - x$, $\Delta = y' - y$. The two types of movements are therefore converted to crack opening parameters in two directions with Eq. (3.23) by further assuming $x = x_{cr}$, $y = s_{cr}$ according to the kinematic conditions shown in Fig. 3.26:

$$\begin{aligned} \theta &= \frac{w^2 + 2x_{cr}w}{2s_{cr}(x_{cr} + w)} \\ \Delta_o &= \Delta - (\sin\theta \cdot x_{cr} + \cos\cdot\theta s_{cr} - s_{cr}) \end{aligned} \tag{3.24}$$

On the other hand, for a crack curve moved by θ and Δ_0 from its original position, the tangential and normal displacement of each point along the curve can be derived from the relative displacement in x and y direction. The relationship between (dx, dy) and (n,t) is illustrated in Fig. 3.26. It can be calculated by:

$$\begin{pmatrix} n \\ t \end{pmatrix} = \begin{pmatrix} \sin\alpha & -\cos\alpha \\ \cos\alpha & \sin\alpha \end{pmatrix} \begin{pmatrix} \mathrm{d}x \\ \mathrm{d}y \end{pmatrix} \tag{3.25}$$

The value of (n,t) is directly linked to the normal and shear stress along the crack due to the aggregate interlock effect. The vertical and longitudinal displacement of the crack bottom is related to the dowel action and the tensile force in the rebar. The constitutive relations of the effects referred to are given in the following section.

3.3.2 Constitutive Relations

3.3.2.1 Shear Force Component in the Concrete Compressive Zone

In the stabilized cracking stage, the stress distribution of the concrete compressive zone can be well described by the classic beam theory. Since the compressive zone is dominating the uncracked area of the concrete beam, see Fig. 3.27, it is reasonable to assume the shear force in the concrete compressive zone to be a close estimation of the contribution of the whole uncracked area concrete. The amount of shear force transferred in the compressive zone has been estimated by Mörsch in (Mörsch 1909), and has been approved by experiments(Sherwood, Bentz et al. 2007). A simplified derivation is repeated here.

Examining a concrete block formed by two following cracked concrete cross sections at x_1 and x_2, and the neutral axis in Fig. 3.27 (assuming that the neutral axis keeps constant between the two cracks), the difference of the resultant compressive forces is generated by the shear stresses along the neutral axis. The average shear stress τ_m along the neutral axis turns out to be $\tau_m = \mathrm{d}N/\mathrm{d}x$. Based on the beam theory, the maximum shear stress at the neutral axis equals τ_m, that gives for the total shear force carried by the concrete compressive zone:

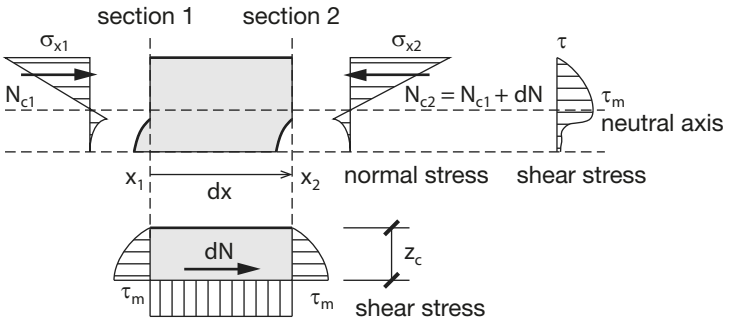

Fig. 3.27. Stress distribution in concrete compressive zone. Adopted from (Reineck 1991).

$$V_c = \frac{2}{3}\tau_m z_c b_w$$

Since the compressive force in the cross-section can be estimated by $N_{c,i} = M_i/z$, this gives:

$$\tau_m = \frac{1}{bz}\frac{dM}{dx} = \frac{V}{bz}$$

By substituting this into the previous expression, the shear force carried by the concrete compressive zone can be expressed by

$$V_c = \frac{2}{3}\frac{z_c}{z}V \tag{3.26}$$

with

z_c : the height of the compressive zone, $z_c = d - s_{cr}$;
z : the internal level arm expressed by Eq. (3.3).

3.3.2.2 Force in Rebars

In a cracked concrete beam, the forces carried by the rebars include the tensile force T_s in longitudinal direction and the dowel action V_d in vertical direction. The two components are discussed in this section.

Tensile Force

In most cases, the rebars in a concrete beam are in the linear elastic stage, thus the tensile force T_s can be calculated directly by the strain of the reinforcement $T_s = \varepsilon_s A_s E_s$. On the other hand, the crack width w at the reinforcement level is calculated by:

$$w = (\varepsilon_{sm} - \varepsilon_{cm})l_{cr} = \frac{(T_s / A_s - \sigma_{sr})l_{cr}}{E_s} \tag{3.27}$$

where

l_{cr} : is the average crack spacing, which equals $l_{cr} = \Psi_s l_t$, where l_t is calculated by Eq. (3.4);
ε_{sm}, ε_{cm} : are the average strains in reinforcement and concrete between two adjacent major cracks respectively;
σ_{sr} : is the cracking stress of reinforcement at the onset of the formation of a new crack, and is expressed by:

$$\sigma_{sr} = \frac{f_{ctm}}{\rho_{eff}}(1 + n_e \rho_{eff})$$

The crack width will be large if the dowel action results in the detachment of the longitudinal reinforcement due to the dowel cracking in the concrete along the longitudinal reinforcement. This phenomenon will be discussed in the following sections.

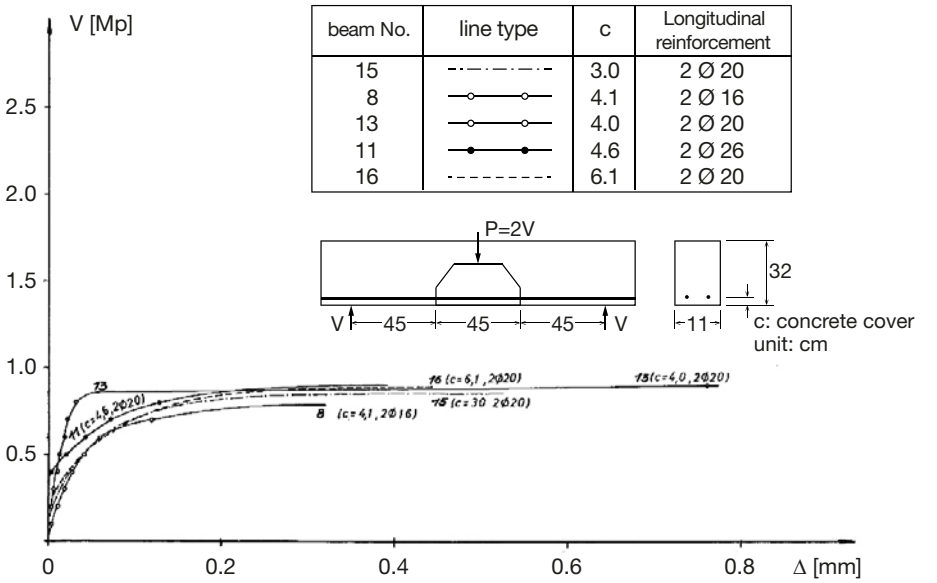

Fig. 3.28. Shear displacement — dowel force relationship of tests carried out by Baumann and Rüsch, adapted from (Baumann & Rüsch 1970).

Dowel Action

For the dowel action, Baumann and Rüsch's model is employed (Baumann & Rüsch 1970). Their experiments show that the relationship between vertical displacement along the crack opening and the shear resistance from dowel action can be assumed to be linear elastic before the maximum shear force V_{dmax} is reached. After that, the shear resistance provided by dowel action becomes constant with respect to any further shear displacement. The load – displacement relationship for tests specimens without shear reinforcement is given in Fig. 3.28.

The maximum shear force which can be carried by dowel action is:

$$V_{d\max} = 1.64 b_n \phi \sqrt[3]{f_c} \tag{3.28}$$

where

b_n : is the clear width of the beam (b - $n\phi$).

The vertical displacement Δ at the peak shear force was found to be 0.08 mm in the experiments (Baumann & Rüsch 1970). Thus, the linear relation before yielding is expressed by:

$$V_d = \frac{\Delta}{0.08} V_{d\max}, \ \Delta < 0.08 \text{ mm} \tag{3.29}$$

For the maximum vertical displacement, a large scatter is found between different experiments. Taylor reports 0.013 mm in (Taylor 1971). Further investigation is needed regarding to the failure displacement of dowel action.

3.3.2.3 Residual Stresses in Cracks

The fact that there are stresses in a crack in concrete structures has been well accepted. From a general perspective, two types of phenomena are possible. They are the tension softening effect and the aggregate interlock effect. As was shown in Chapter 2, both effects have been well studied in literature. With given (n,t), the stresses (τ,σ) that are transmitted across the crack can be calculated.

Aggregate Interlock

The so-called aggregate interlock effect describes the relationship between the shear stress, the compressive normal stress (τ,σ) and the normal and tangential displacement along a crack (n,t). The model proposed by Walraven (Walraven 1980; Walraven 1981) is utilized here. It has been validated by extensive experimental results, and has been implemented in several models (Vecchio & Collins 1986; Reineck 1991) describing the shear phenomenon. The original formula cannot be evaluated analytically, therefore numerical integration is asked for:

$$\begin{pmatrix} \sigma \\ \tau \end{pmatrix} = \sigma_{pu} \begin{pmatrix} A_y + \mu A_x \\ A_x - \mu A_y \end{pmatrix} \tag{3.30}$$

where

σ_{pu} : is the crushing strength of the cement matrix under confinement, $\sigma_{pu} = 6.39 f_c^{0.56}$;

μ : is the coefficient of the friction between aggregate and the matrix material;

D : is the diameter of the aggregate;

A_x, A_y : are the projected contact areas for a unit crack length, which are functions of the normal and tangential displacement (n,t) of the two crack faces. Their expressions are:

$$t < n$$

$$A_y = \int_{\frac{n^2+t^2}{t}}^{D_{\max}} p_k \frac{4}{\pi} F\left(\frac{D}{D_{\max}}\right) G_1(n,t,D)\mathrm{d}D$$

$$A_x = \int_{\frac{n^2+t^2}{t}}^{D_{\max}} p_k \frac{4}{\pi} F\left(\frac{D}{D_{\max}}\right) G_2(n,t,D)\mathrm{d}D$$

$$t > n$$

$$A_y = \int_{2n}^{\frac{n^2+t^2}{n}} p_k \frac{4}{\pi} F\left(\frac{D}{D_{\max}}\right) G_3(n,t,D)\mathrm{d}D + \int_{\frac{n^2+t^2}{n}}^{D_{\max}} p_k \frac{4}{\pi} F\left(\frac{D}{D_{\max}}\right) G_1(n,t,D)\mathrm{d}D$$

$$A_x = \int_{2n}^{\frac{n^2+t^2}{n}} p_k \frac{4}{\pi} F\left(\frac{D}{D_{\max}}\right) G_4(n,t,D)\mathrm{d}D + \int_{\frac{n^2+t^2}{n}}^{D_{\max}} p_k \frac{4}{\pi} F\left(\frac{D}{D_{\max}}\right) G_2(n,t,D)\mathrm{d}D$$

with

$$G_1(n,t,D) = D^{-3}(\sqrt{D^2-(n^2+t^2)}\,\frac{t}{\sqrt{n^2+t^2}}\,u_{\max} - nu_{\max} - u_{\max}^2)$$

$$G_2(n,t,D) = D^{-3}\{(t-\sqrt{D^2-(n^2+t^2)}\,\frac{n}{\sqrt{n^2+t^2}}\,u_{\max} + (u_{\max}+n)\sqrt{\frac{D^2}{4}-(n^2+t^2)}$$
$$-n\sqrt{\frac{D^2}{4}-n^2} + \frac{D^2}{4}\arcsin\left(\frac{w+u_{\max}}{D/2}\right) - \frac{D^2}{4}\arcsin\left(\frac{2n}{D}\right)dD\}$$

$$G_3(n,t,D) = D^{-3}(\frac{D}{2}-n)^2$$

$$G_4(n,t,D) = D^{-3}(\frac{\pi}{8}D^2 - w\sqrt{\frac{D^2}{4}-n^2} - \frac{D^2}{4}\arcsin\frac{2n}{D})$$

$$F(D) = 0.532\left(\frac{D}{D_{\max}}\right)^{0.5} - 0.212\left(\frac{D}{D_{\max}}\right)^4 - 0.072\left(\frac{D}{D_{\max}}\right)^6$$
$$-0.036\left(\frac{D}{D_{\max}}\right)^8 - 0.025\left(\frac{D}{D_{\max}}\right)^{10}$$

Because of the complexity in formulation, it is not possible to apply the formula into design practice analytically. In most cases the formula is simplified. One of the well-known examples is the equation proposed by Vecchio and Collins in (Vecchio & Collins 1986), explained in Section 2.2.3.

The stress distribution along the crack curve is then decomposed in x and y direction by:

$$f_x = \sigma \sin\beta - \tau\cos\beta$$
$$f_u = \sigma\cos\beta + \tau\sin\beta$$

where, the positive directions of σ and τ are given in Fig. 3.25. The resultant forces and their locations are then calculated by integration along the crack curve:

$$\begin{aligned} F_i &= \oint f_i \mathrm{d}l \\ x_i &= \oint f_j x_i \mathrm{d}l \,/\, F_j,\ i = x \text{ or } y \end{aligned} \tag{3.31}$$

Due to the complexity of the problem, the integration has to be carried out numerically. Nevertheless, the resultant forces $V_{ai} = F_y$, $N_{ai} = F_x$ and their locations $x_{ai} = x_{cr}\text{-}x_x$, $z_{ai} = z - x_y$ are functions of crack opening w and Δ. For a crack initiated at $x_0 = 2d$, a beam with d = 465 mm, b = 300 mm, the relationship between (w, Δ), and the resultant forces (V_{ai}, N_{ai}) are plotted in Fig. 3.29.

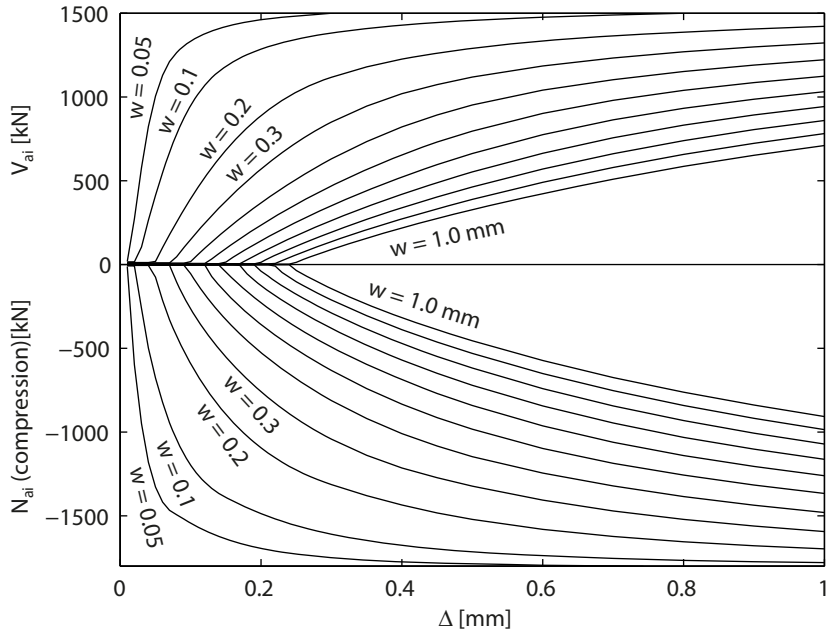

Fig. 3.29. Relationship between resultant forces in x, y direction and crack bottom displacements (w, Δ) of a concrete beam.

Fig. 3.29 shows that the aggregate interlock effect predicted by Walraven's model actually provides significantly higher shear forces than what is really measured in usual shear beam tests. Further to that, to reach that shear force, an even larger normal force is needed. That normal force should not be neglected in the moment equilibrium equation Eq. (3.22).

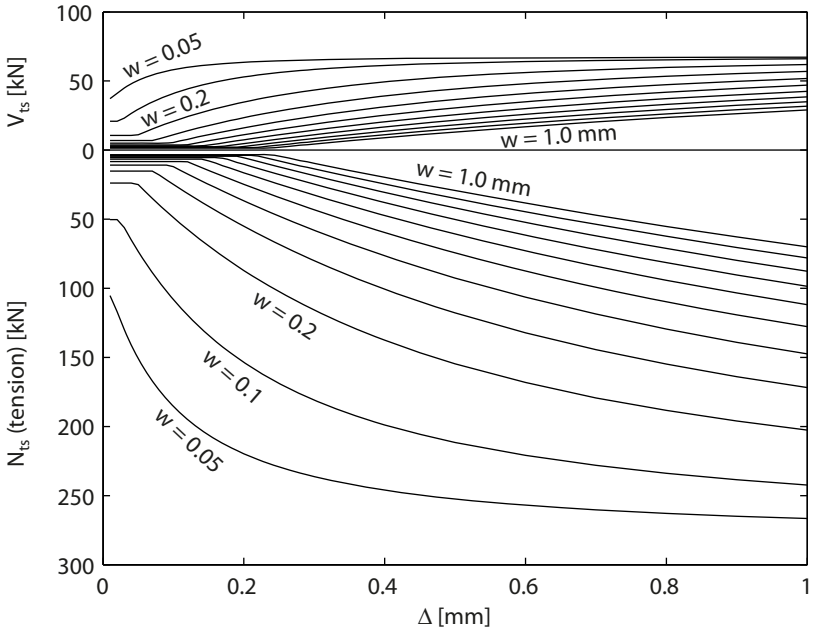

Fig. 3.30. Relationship between resultant forces from tension softening effect in x, y direction and crack bottom displacement (w, Δ).

Tension Softening

With respect to the normal stress in the crack, other than aggregate interlock, which provides compressive stresses across the crack, when the crack width is small, a crack can also transmit tensile stress, which is defined as the tension softening effect. The tension softening behaviour of concrete has been studied extensively by bending tests or direct tension tests (Hillerborg, Modeer et al. 1976; Hordijk 1991). Experimental research carried out by Keuser and Walraven (Keuser & Walraven 1989) shows that when the crack width is smaller than 0.2 mm, and the tangential displacement is smaller than the normal displacement, it is possible to neglect the influence of aggregate interlock to the tension softening relationship. Nevertheless, when the shear displacement is smaller than the crack width, the normal stress is very small according to Walraven's model anyway. On the other hand, if the shear displacement is comparable or even larger than the crack width, it is very difficult to generate such type of shear crack from a plain concrete according to (van Mier et al. 1991). The other alternative is to open a crack first and the close it to very small crack width; in that case, the tension softening stress is significantly reduced. The latter case is possible with regard to the tip of the flexural cracks when a secondary crack develops in the horizontal direction due to increasing shear forces. To simplify

the calculation process, it is assumed that it is possible to superpose the two effects, since the normal stress due to aggregate interlocking at that stage is very small anyway. A linear softening relationship is adopted as explained previously.

Similar to the aggregate interlock effect, the normal stress in the crack is decomposed in vertical and longitudinal directions, and integrated along the crack curve as expressed in Eq. (3.31). Similarly, the resultant shear and normal forces in the crack are dependent on the crack opening at the bottom of the crack. The relationship between (V_{ts}, N_{ts}) and (w, Δ) of the same crack in the beam configuration specified previously is plotted in Fig. 3.30. Compared to the aggregate interlock effect, the contribution of tension softening force to the shear resistance is about 10 times smaller, thus it can be neglected when the crack width is larger than 0.1 mm. Similarly, the tensile force generated by the tension softening stresses is relatively small.

In general both effects are considered as residual stresses in a crack. The resultant forces are functions of crack bottom displacement (w, Δ), and are calculated by summation of both effects. Moreover, without considering redistribution, the normal force in longitudinal direction seems to be substantial, so that it should not be neglected in the equilibrium formula.

3.4 FAILURE MECHANISM

3.4.1 Assemble of Equilibrium Equations

By applying the constitutive relations described in 3.3.2, the equilibrium equations Eq. (3.20) and Eq. (3.22) become:

$$V(x+x_{cr})-V_d(\Delta)x_{cr}-V_{ai}(w,\Delta)x_{ai}(w,\Delta)-T_s(w)z+N_{ai}(w,\Delta)z_{ai}=0 \quad (3.32)$$

$$(1-\frac{2}{3}\frac{z_c}{z})V-V_{ai}(w,\Delta)-V_d(\Delta)=0 \quad (3.33)$$

Here the two equations are dependent on the vertical and longitudinal directions of crack opening (w, Δ). If the crack profile is given, by introducing a total shear force V, the crack opening in both directions (w, Δ) can be solved with the set of equations, vice versa.

The set of equations cannot be solved directly due to the complexity of the problem. Instead, the two variables are solved by iterations. The whole process is illustrated in Fig. 3.31. The relationship between the maximum allowable shear force calculated from the sets of equations and the crack opening in

vertical and horizontal direction (w, Δ) is determined, with which the failure process of a reinforced concrete beam is studied as follows.

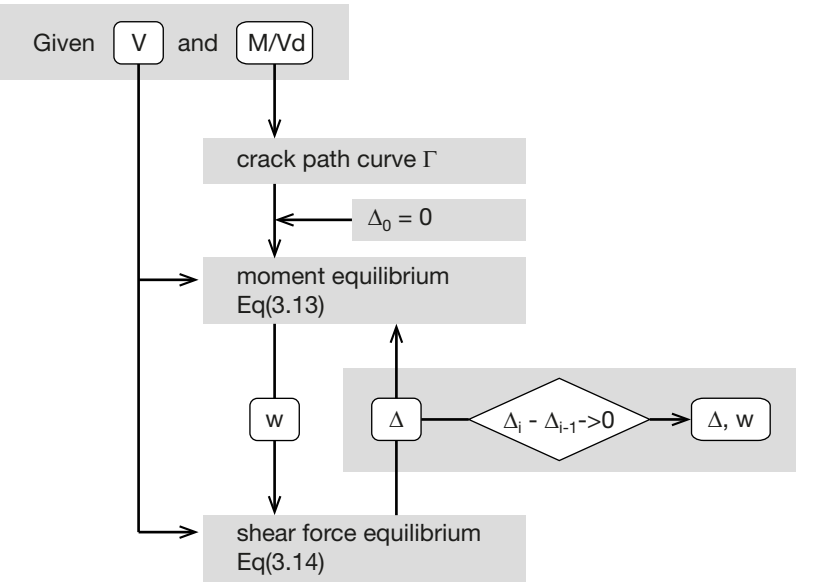

Fig. 3.31. Procedure to solve equation system Eq. (3.32) and Eq. (3.33).

3.4.2 Failure Criteria

To understand the failure process, the most important question to be answered is: what triggers the collapse of a concrete beam at a given cracked section under a shear force? An attempt is made in this section to search for an answer on this research question. It starts with the most basic mechanism: the opening of a crack around its tip.

3.4.2.1 Crack Opening around Its Tip

Due to the curved shape of a major crack, the rotation of the crack around its tip will generate a tangential displacement locally, which activates aggregate interlock and dowel action. By assuming only rotation of the two cracked surfaces, the shear force that is carried by aggregate interlock and dowel action is plotted in Fig. 3.32 versus the crack width. Crack curves for M/Vd of 1.0 and 2.0 are taken as two examples.

The comparison shows that the magnitude of the shear force that can be transmitted by the crack depends on the shape of the crack. The shear force V_{ai} in the crack generated at M/Vd = 1.0 is more than 3 times larger than that in the crack at M/Vd = 2.0. However, for a crack generated in most moderated locations, the shear resistance raised in the crack is not sufficient to compensate the

shear force at the cross-section even at relatively small crack width. The force equilibrium in vertical direction described by Eq. (3.33) cannot be fulfilled. Besides, in all cases, V_{ai} drops quickly with the increase of the crack opening w. Both observations are contradictory to the experimental findings, thus the assumed crack opening mechanism cannot guarantee a stable system along the cross section. Additional shear resistance has to be provided by another mechanism.

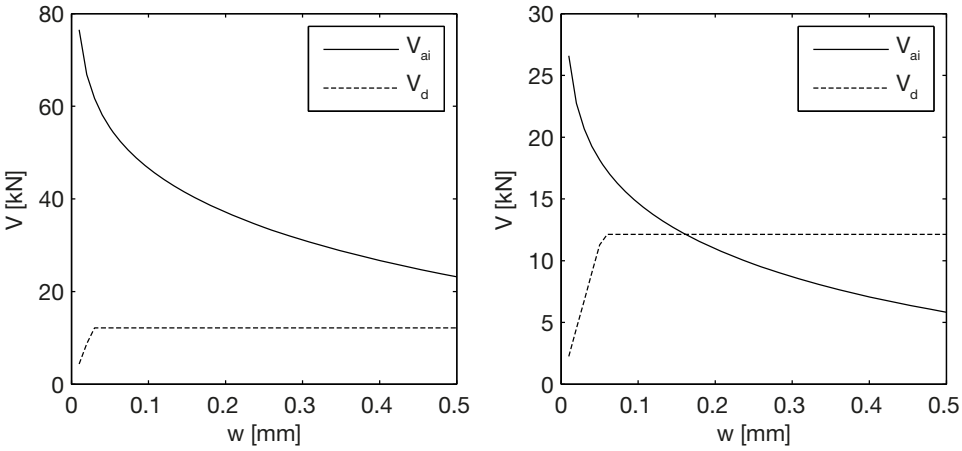

Fig. 3.32. Relationship between crack width and shear force carried by aggregate interlock V_{ai} and dowel action V_d (left: M/Vd = 1.0, right: M/Vd = 2.0).

3.4.2.2 Vertical Crack Opening

Since it is not possible to achieve equilibrium only with rotation of the crack faces around the tip, the other possible movement of the two crack faces is translation in vertical direction according to the kinematic conditions described in Fig. 3.26. It is shown in Fig. 3.29 that the increase of vertical crack opening Δ quickly increases the shear force and the normal force that is carried by the crack. Therefore to generate the magnitude of shear resistance as observed in experiments, the additional displacement of the two crack surfaces in vertical direction Δ_0 is necessary.

In this study, it is assumed that the vertical displacement Δ can be superposed onto the rotation θ of the same crack in the free body analysis. Only when the vertical displacement Δ is introduced, it becomes possible to solve Eq. (3.33) under the most realistic shear force V and M/Vd combinations. As an example, the crack opening combinations of the beam cross sections used in Section 3.3.2.3 under shear force values from 100 kN to 300 kN with M/Vd varying from 1.0 to 4.0 are plotted in Fig. 3.33. Experimental results of the specimens with the same

configuration (Yang & den Uijl 2011) showed that the ultimate shear capacity of such specimens varies between 150 kN and 300 kN.

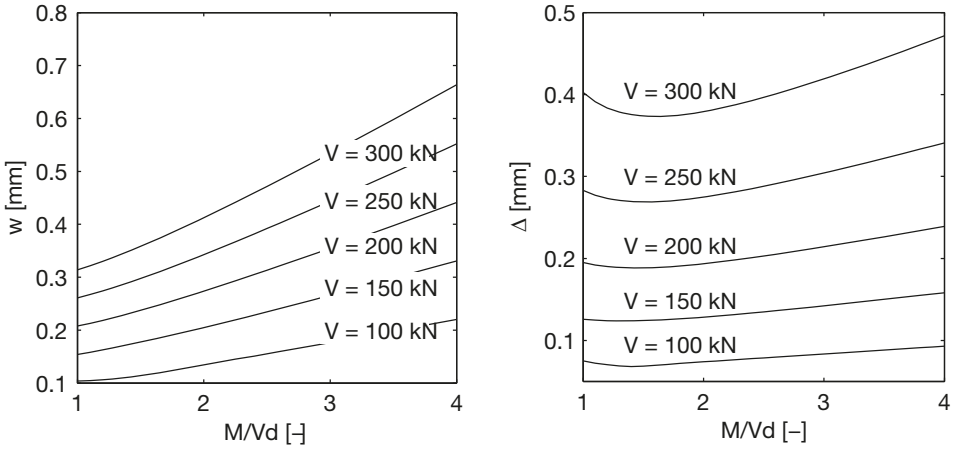

Fig. 3.33. Crack opening combination of cracks generated at *M/Vd* from 1.0 to 4.0 under different shear forces (left: crack opening w in longitudinal direction; right: crack opening Δ in vertical direction).

In simply supported beams, the value of M/Vd is equivalent to x_0/d of the cracked cross section, therefore, Fig. 3.33 actually indicates the relationship between the shear resistance, the crack openings and the location of the cracked section to be evaluated. It shows that w always increases with the crack location, whereas Δ has the lowest value at sections with M/Vd between 1 and 2. From that location any other cracked sections closer to or farther from to the support of the beam will generate a larger vertical displacement Δ at the same shear force. The increase of Δ with respect to the decrease of M/Vd is because of the larger inclination of the crack profile, while when the cracked section moves further from the support, the increase of Δ is due to the larger cross sectional moment, which is less steep than in the other situation.

On the other hand, regarding the shear force, it is always possible to find a crack opening combination in both directions when increasing the shear force V. Recalling to the simulation results of Fig. 3.29, it turns out that the shear resistance that is generated by increasing the value Δ of the crack can reach an extraordinary high value. This is obviously in conflict with the experimental findings in the laboratory. The maximum shear resistance found from laboratory experiments is close to 150 kN for specimens with M/Vd larger than 2.0 (10 times smaller than the maximum shear resistance according to Fig. 3.29). Once the shear force reaches that level, the width of one of the flexural cracks grows rapidly, meanwhile the force that can be applied on the beam drops. That defines the failure of the beam. The crack pattern of such a specimen is demon-

strated in Fig. 3.34, in which the crack width can reach centimetres at failure. However, according to the model presented in this chapter, if the longitudinal reinforcement does not yield, the value of w is more or less stable in certain range. In that situation, further increase of shear force level can easily be compensated by the increase of Δ. Besides, when the maximum value of the shear force is reached, it remains constant with the increase of Δ, which means that it is not possible to obtain an unstable failure as shown in Fig. 3.34. The only explanation to this is that the mechanisms described in this chapter are not sufficient to describe the failure process. Additional mechanisms have to be included into the system to allow the unstable displacement along the crack curve.

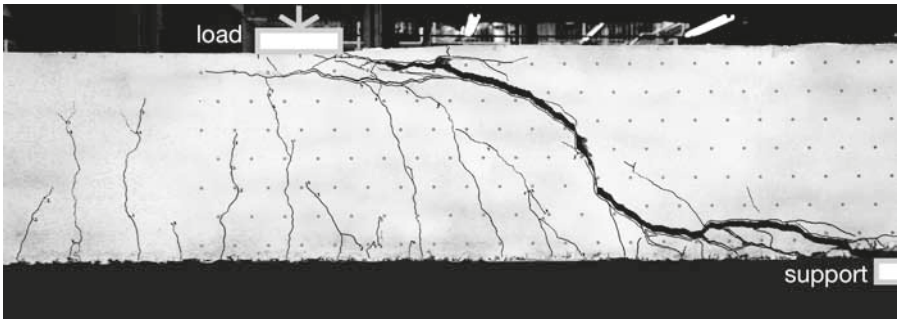

Fig. 3.34. Crack pattern of a concrete beam with M/Vd = 3.0 after failure. Specimen C2b151 from continuous beam tests, from (Yang & den Uijl 2011).

3.4.2.3 Dowel Cracking due to Dowel Force

To reduce the shear force generated by aggregate interlock, an additional increase of the crack width w has to be allowed. This can be done by introducing a horizontal crack at the reinforcement level, and in the compression zone, in which the first one allows the detachment of the rebar from the concrete beam. Consequently, the crack width of the major flexural crack shall be calculated directly from the elongation of the detached longitudinal reinforcement instead of Eq. (3.27). The crack width can increase more than one order of magnitude. This additional mechanism allowing catastrophic opening of the critical crack is related to the dowel action.

For most reinforced concrete beams the concrete cover of the rebars is relatively small at the side, thus the dominating failure mechanism of the dowel action is splitting of the concrete cover across the width of the beam (Vintzeleou & Tassios 1986). Based on the experimental observations of Bauman and Rüsch (Baumann & Rüsch 1970), after the maximum dowel force $V_{d,\max}$ is reached, plastic behaviour is expected, see Fig. 3.28. With respect to the propagation of the dowel crack, as long as the shear force applied at the rebar can be kept

constant, the crack can keep propagating until it reaches the support where the compressive stress stops the further opening of the crack. In most cases, the maximum dowel force is relatively small compared to the other actions. Thus, its limit of linear elastic behaviour can easily be reached. After that, the opening process is dependent on the energy balance of the whole system. During the propagation of the dowel crack, when the energy releasing rate of the system is larger than the fracture energy of the crack propagation, the process is unstable.

Assuming that the dowel crack has reached the support, the length of the detached reinforcement equals to x_0, so the width of the major crack is expressed by:

$$w = \varepsilon_s x_0 = \frac{T_s}{A_s E_s} x_0 \tag{3.34}$$

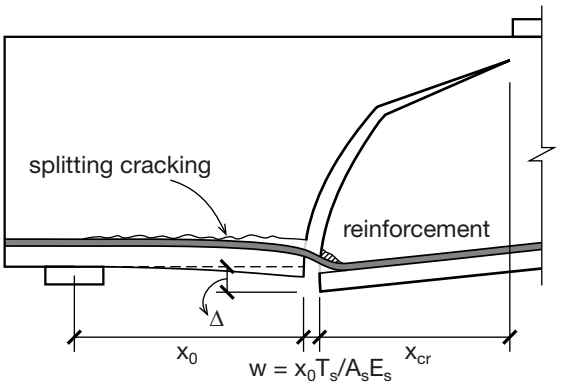

Fig. 3.35. Dowel cracking initiated from the root of a major crack under shear.

At the compressive side of the beam, the shear displacement Δ of the crack path also accompanies with the development of a secondary crack branch at the crack tip towards the loading point. Similarly, the development of the horizontal crack branch in the compressive zone is an unstable process, which continues until it reaches the loading point. The progress of the crack tip in the concrete compressive zone results in an increase of x_{cr} in Eq. (3.32), see Fig. 3.35. Eventually the value of x_{cr} will be $x_{cr} = a - x_0$, when a being the centre to centre distance between the support and the loading point. In that case the reinforcing bars become a tension chord in the beam system. The load applied on it shall be calculated at the loading point. Thus the value of T_s can be formulated by

$$T_s = \frac{1}{z}\left(Va - V_d(a - x_0) - M_{ai}\right) \tag{3.35}$$

where,

M_{ai}: is the moment raised by the aggregate interlock effect to the centre of N_c under the loading point.

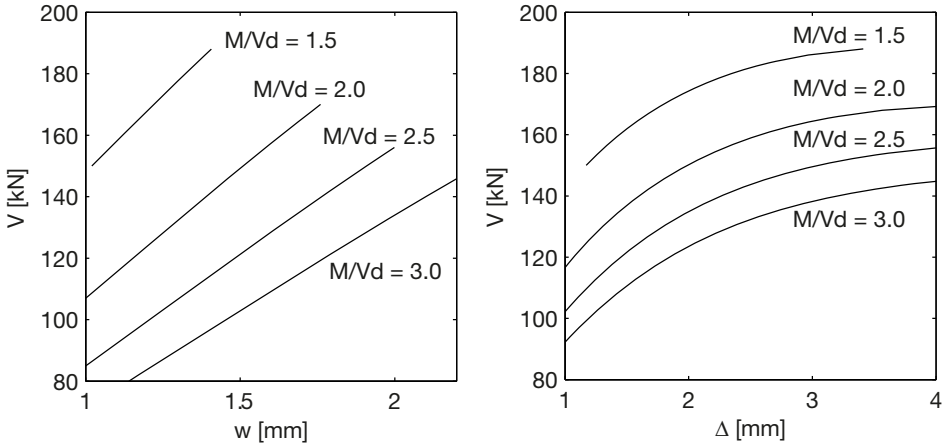

Fig. 3.36. Shear force crack bottom displacement relationship according to Eq. (3.34) (left: crack opening w in longitudinal direction; right: crack opening Δ in vertical direction).

Both cracks discussed in this section are denoted as **secondary cracks** caused by the increase of shear displacement of the major crack. The consequence of these cracks described by Eq. (3.34) and Eq. (3.35) are introduced into the program to simulate the cracking process, with which the failure process is illustrated. It is demonstrated in Fig. 3.36, where the openings of the crack in both directions are plotted against the shear force applied in the span. The cracking behaviour after the development of the dowel crack is quite different. As stated before, the additional crack opening caused by the secondary cracks reduces the maximum shear force in the crack enormously. The shear force transferred through the cracks cannot always be increased further by generating more vertical displacement Δ anymore. Besides, comparing to Fig. 3.33 the vertical crack opening Δ occurring after the dowel crack has developed is more than 100 times larger at the same load level which indicates a large reduction of the member stiffness.

That explained the observation of a typical flexural shear failure of a normal reinforced concrete beam: the secondary crack branches propagate at both sides of a cracked beam section accompanied by a significant increase of the width of the relating major crack. The unstable opened crack is defined as the critical inclined crack, and the shear force level under which the process described in this section develops is defined as the **inclined cracking load**.

3.4.3 Discussion

In the study up to this section the contributions to the shear resistance have been investigated from the corresponding mechanisms along a crack in a reinforced concrete beam, such as the aggregate interlock and dowel action. It reveals that, although the aggregate interlock contributes for a substantial proportion to the shear resistance, the final failure is eventually triggered by the development of a dowel crack relating to the dowel action of the reinforcement. Only when the dowel cracking is taken into account, the following steps in the failure process are possible. Thus to evaluate the inclined cracking load of a reinforced concrete beam, the development of this type of crack can be considered as the failure criterion as pointed out by Chana in (Chana 1987).

3.4.3.1 Unstable Opening of the Dowel cracks

Experimental results have shown that the force needed to open the dowel crack is constant after the linear elastic limit has been reached. Besides, the shear resistance contributed by the dowel action is quite limited, so that during the loading process, the maximum dowel action force is easily reached while the development of the dowel crack remains stable. Therefore the force criterion is not suitable to determine the moment at which the development of the dowel crack becomes unstable. On the hand, the vertical crack opening or to be more general: **the shear displacement of the crack faces at the tensile reinforcement level** (the term is simplified as **shear displacement** in the remaining part of the dissertation) Δ always increases with the cross sectional shear force, and it is directly linked to the other shear resistance effects such as the aggregate interlock. Thus, it is logic to relate the moment at which the unstable dowel cracking process starts to Δ, instead.

In principle, the development of the dowel crack always has to correspond to the general energy balance, based on which, the critical shear displacement Δ_{cr} should be determined. Considering the cracked beam as a whole system, the energy releasing rate per crack length G has to be no smaller than the fracture

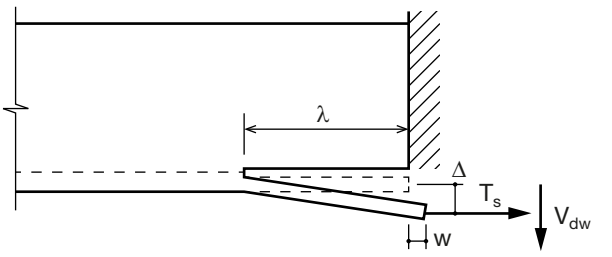

Fig. 3.37. Detachment of a tension bar attached to a deep beam.

energy G_f to allow the crack to develop. In the most simplified manner, the detachment of the longitudinal reinforcement can be considered as the development of a crack between a tensile bar and a large beam as shown in Fig. 3.37:

With the length of the crack expressed by λ, the energy release rate of the tensile bar can be expressed by $G = \mathrm{d}U^*/\mathrm{d}\lambda$. Neglecting the complimentary strain energy in the large beam, the additional U^* due to the elongation of the crack can be expressed analytically with classic mechanics such as (Timoshenko 1956). The complementary strain energy U^* and the strain energy U are:

$$U^* = \frac{T_s^2}{2A_sE_s}\lambda = U = \frac{w^2A_sE_s}{2\lambda}$$

Assuming that during the dowel cracking process, the tensile force in the rebar T_s and the shear force V_d are constant, the energy release rate G may be expressed by:

$$G = \frac{dU^*}{d\lambda} = \frac{T_s^2}{2A_sE_s} = \frac{dU}{d\lambda} = \frac{A_sE_s}{2\lambda^2}w^2 \geq G_f \tag{3.36}$$

Here the value of w is expressed by Eq. (3.27). When the energy releasing rate G becomes is larger than the fracture energy G_f along the longitudinal rebar, unstable crack development of the dowel crack starts. In the case of pure tension in the bar, the value of G_f should be the mode II fracture energy $G_{f,II}$. The cross sectional moment in a normal reinforced concrete beam at the cracking surface is normally large, so that a large T_s is expected. According to Eq. (3.36), if T_s is large enough, it is possible to obtain a sufficiently large energy releasing rate to get unstable crack development along the longitudinal rebar. That explains why some researchers are able to simulate the dowel crack with rebars only modelled as a truss element (no transverse stiffness) in Non Linear Finite Element programs (Slobbe, Hendriks et al. 2012). As it is shown below, depending on the stiffness of the rebar itself, this simplification underestimates the total energy releasing rate G.

In this very simplified case, the reinforcing bars are considered as pure tension elements, whereas their flexural stiffness is neglected. When the flexural stiffness of the rebars is taken into account, the additional strain energy introduced by the dowel shear force V_d is :

$$\frac{dU^*}{d\lambda} = \frac{V_{dw}^2\lambda^2}{EI} = \frac{dU}{d\lambda} = \frac{9E_sI_s}{\lambda^4}\Delta^2 \tag{3.37}$$

With the energy of the flexural stiffness of the rebar taken into account, Eq. (3.36) is updated to:

$$G = \frac{A_s E_s}{2\lambda^2} w^2 + \frac{9 E_s I_s}{\lambda^4} \Delta^2 \geq G_f \tag{3.38}$$

As shown previously, only before the horizontal branch of the flexural cracks develops, the vertical crack opening Δ and the horizontal crack opening w are related to each other. Since the development of that horizontal branch is always needed for slender beams, the value of Δ has to be determined independently.

The two examples shown above are quite simplified models. Considering the components acting along the cracked surface as inner forces, the construction of the energy release rate G of the critical inclined crack has to involve more aspects. Being inspired by Griffith (Griffith 1921), an attempt is made to formulate the energy balance of the whole cracked beam based on the vertical displacement Δ and the total shear force V. In the system, the uncracked concrete can be considered as a linear elastic material. Nevertheless, the energy dissipated by the aggregate interlocking effect cannot be neglected. That makes the basic energy balance equation (Shah, Stuart et al. 1995) as follows:

$$V d\Delta = (V_c + V_d + V_{ai}) d\Delta = G_f d\lambda + dU$$

$$G_f = \frac{dU_d^*}{d\lambda} + \frac{dU_{ai}^*}{d\lambda} \tag{3.39}$$

In the energy balance equation, the total shear force V is composed of three components, among which V_c remains constant with respect to the crack development, thus its derivation against $d\lambda$ is made zero. The contribution of the longitudinal rebars: $dU_d^* = V_d d\Delta - dU_d$ can be estimated with Eq. (3.38). The additional component in the energy balance equation is the aggregate interlocking component. Here the expression applied to solid materials: $U^* = Fu - U$ is not valid anymore, since a large part of the deformation under V_{ai} goes to friction between the aggregates. It is a highly nonlinear process. The remaining part, stored as strain energy in the uncracked concrete, does not equal the complementary strain energy. Taking into account the complex expression of V_{ai} and the uncertainty in crack trajectory, an analytical solution of Δ_{cr} is not practical.

The idea of introducing the energy balance principle into the crack propagating process has been employed by Gastebled and May in (Gastebled & May 2001). In their study, they linked the value of w and Δ in Eq. (3.38) by forcing the crack profile to a 45° straight line, relating the shear displacement of crack faces at the longitudinal rebars Δ to the shear deformation of the bars linearly and neglecting the aggregate interlocking effect. As shown in the preceding discussion in this study, some of these simplifications can still be criticized.

3.4.3.2 Location of the Critical Inclined Crack

With Δ as a failure criterion, the remaining question is which crack will develop into the critical shear crack? The relationship between the shear displacement Δ and the shear force V presented in Fig. 3.33 is examined again. It shows that under the same load level, the minimum vertical displacement is close to the cracks developed under $M/Vd = 2.0$. Under the same shear force, the values of Δ increase with M/Vd when the value of M/Vd is larger than the one at the lower point. That indicates that at the same shear force the shear displacement Δ of cracked sections closer to the loading point will always reach Δ_{cr} earlier. Nevertheless, a certain distance between the crack tip and the centre of the loading point is still necessary to guarantee a sufficient length of the horizontal branch to generate Δ at the crack tip. When the shear span is large, this distance can be neglected, because the difference between the shear resistances of sections with large M/Vd values is small according to experimental observations.

On the other hand, when the value of M/Vd at the cracked section is smaller than that of the lowest point in Fig. 3.33 (left), Δ increases with the decrease of M/Vd due to the larger inclination of the crack profile. That implies that the cracks that are initiated at sections closer to the support can carry less shear force than the ones further away when the M/Vd is very small. Assuming a constant critical shear displacement Δ_{cr} along the span, the shear force that is needed to make $\Delta = \Delta_{cr}$ for the corresponding crack initiated at x_0 from the support can be indicated as the shear resistance of the section. It is indicated as the solid line in Fig. 3.38 qualitatively.

It sounds contradictory to the experimental observation that the shear resistance of the cracked sections closer to the support become lower, because most experiments show that for simply supported beams with smaller shear slenderness ratio a/d, the shear capacity is higher than the ones with larger a/d. An explanation is that for cross sections located closer to the support, despite that the shear capacity of an inclined crack is smaller, as long as the crack does not develop, the shear force is still carried by the whole uncracked cross section, which will give a much higher shear resistance than a cracked section. Therefore, the decisive factor in this case is whether a fully developed major crack can be formed in the section or not. This effect can be explained in a very simplified manner. Assuming that the major crack forms immediately when the moment M reaches the cracking moment M_{cr}, the section located at x_0 from the support needs the shear force to be $V_{cr,m}$ to generate a crack

$$V_{cr,m} = \frac{M_{cr}}{x_0} \tag{3.40}$$

The value of $V_{cr,m}$ against the location of the cross-section is plotted in Fig. 3.38 as the cracking shear force line. The part of the shear resistance line between the loading point and the cracking shear force line actually indicates the shear resistance. After the intersection point, the cracking shear force line replaces the other one as the shear resistance line. The position of the lowest point of the curve decides where the critical inclined crack is found.

For beams with large shear slenderness ratio a/d, it is appropriate to assume that the critical section is in the vicinity of the loading point and evaluate the shear force required to cause $\Delta = \Delta_{cr}$ at that section. Once the shear capacity of the crack close to the loading point V_{cr} is known, it is also necessary to check the uncracked span from the support a_0 for the specimen.

$$a_0 \leq \frac{M_{cr}}{V_{cr}} \tag{3.41}$$

When a_0 is very small, the chance that the critical crack is located at the other end of the curve is very high.

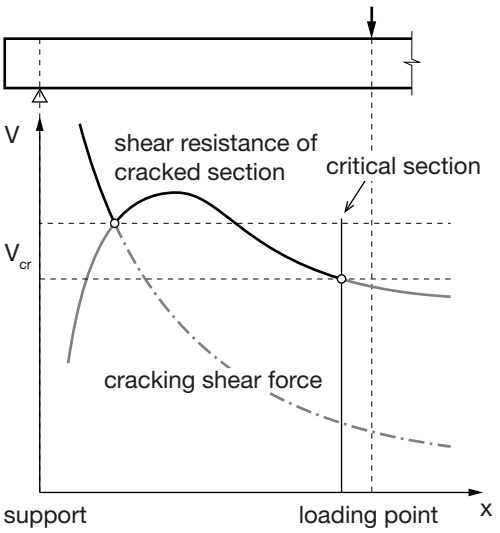

Fig. 3.38. Illustration of shear resistance versus cracking shear force line at shear failure.

It has to be remarked that the shear capacity discussed here defines the load level under which a crack in the shear span opens unstably under the shear force. Considering the fact that the crack is mostly inclined in experiment, this shear force is defined as the **inclined cracking load** V_{cr}. Nevertheless, it is not necessarily the ultimate capacity of the beam.

3.5 RESIDUAL CAPACITY

3.5.1 Arch Structure Formed by Inclined Crack

For beams with a relatively large shear span, section 3.4 has shown that the development of the dowel crack along the longitudinal reinforcement results in a significant reduction of shear resistance of the cracked section, and the overall beam stiffness. This phenomenon is defined as the reason for the final failure. However, the questions being raised constantly before are actually still valid here. Is that really the ultimate failure of the beam? What happens afterwards? If we have a second look at the beam after the opening of the dowel crack, we might find a bearing mechanism in the damaged beam. The debonding of the reinforcing bars results in a great increase of the opening of the critical inclined crack. Consequently, the shear force due to aggregate interlock reduces significantly across the crack. In some cases, it can even be neglected completely. The remaining uncracked part of the concrete beam has to carry the entire load. On the other hand, the longitudinal rebar can be considered as a tension chord. The uncracked concrete part and the fully detached rebar forms a sort of arch-like structure. An illustration of such a structure is shown in Fig. 3.39. In theory, it can still resist the bending moment and the shear force. Thus, it is not necessary that the beam collapses after the opening of the inclined crack.

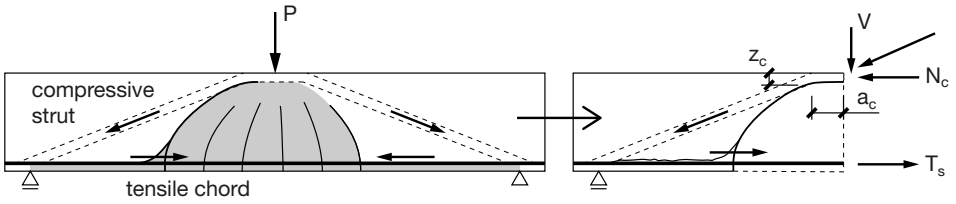

Fig. 3.39. Load bearing structure of a beam after inclined crack developed.

Only when the remaining arch structure is not able to resist the load which causes the opening of the inclined crack, then a catastrophic failure occurs. The tensile chord of the structure is mainly composed of the longitudinal reinforcement, which will not change with the cracking of the concrete beam. Before yielding, the uncracked concrete part of the beam actually determines the residual capacity after the inclined crack develops. If the uncracked concrete part is able to resist the load level that is higher than the load causing the

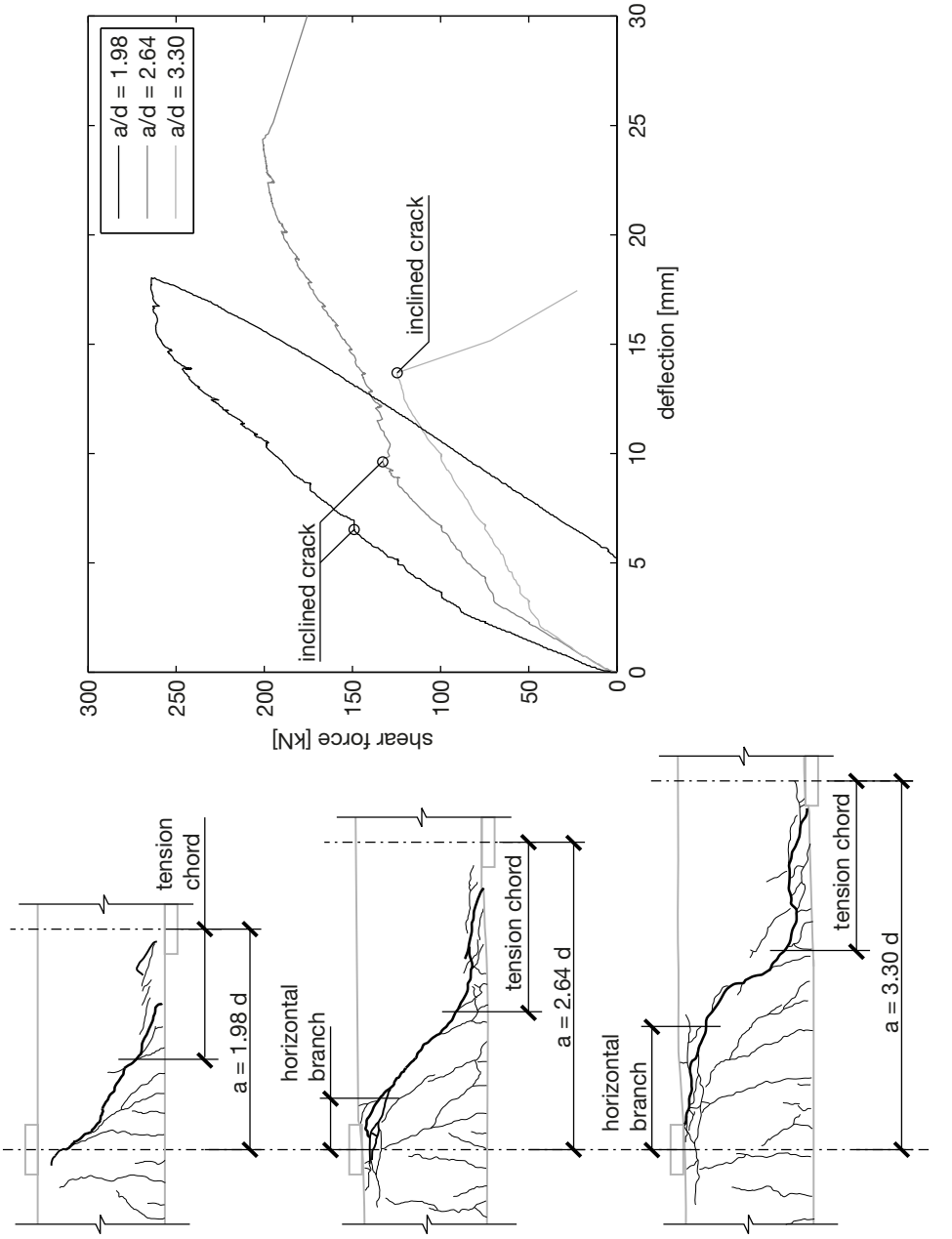

Fig. 3.40. Formation of arch structure by inclined cracks in beams with different shear span, and their influence to the load-deflection relationship. The specimens are C2b151 (see also Fig. 3.5 and Fig. 3.34), C3b121 and C4b091 from the continuous beam test series.

development of the inclined crack, the beam may have a higher capacity after the inclined crack develops. Reflecting on the load-deflection relationship, a certain increment of deflection with constant load can be found in the diagram. Three examples are shown in Fig. 3.40. It includes three load deflection relationships derived from experiments as well as the crack patterns of the specimens after failure.

Fig. 3.40 shows three typical situations. For beams with a = 3.30 d (C5a151 in the tests series explained in Chapter 4), the inclined crack formed at a certain distance from the loading point, that resulted in a relatively long horizontal branch in the compressive zone. The remaining structure could not resist the load causing the inclined crack, thus the structure failed immediately after the formation of the inclined crack. In the second case, a = 2.64 d, the tip of the inclined crack reached the loading point already, thus the remaining uncracked structure is stronger than in the previous case. On the other hand, the bottom of the inclined crack is still at a certain distance from the support. Consequently, the opening of the dowel crack results in a clear reduction of the overall stiffness. A large deformation was observed in the load deflection relationship after the inclined crack developed. Nonetheless, the remaining structure was able to resist a load that is larger than that causing the inclined crack. The ultimate capacity of the beam was defined by the capacity of the arch structure formed by the inclined crack at a higher load level. The last beam had the shortest shear span with a = 1.98 d. When dowel crack developed, the length of the tension chord was so small that an almost negligible increment of deflection was observed regarding the load-deflection relationship. The last case is usually denoted as shear compression failure in literature, see Chapter 2.

The profile of a critical inclined crack consists of the part formed shortly after $M = M_{cr}$ (defined as the **major cracks** before further development), and those parts that propagates at $V = V_{cr}$ (the **secondary cracks**). Because of the non-linearity of concrete behaviour at higher compressive strain, the height of the compressive zone z_c reduces. It results in the secondary crack moving towards the loading point in the compressive zone. Nonetheless, regarding the strength of the concrete arch, the height of the compressive zone where the secondary crack starts to develop is of more importance. It defines the starting point of the horizontal crack branch. From there, a crack path with limited curvature is expected. The uncracked part of the concrete beam formed by the secondary crack can be considered as a cantilever loaded by shear force V_c and compressive force N_c, as illustrated in Fig. 3.39. Since the height of the cantilever cannot vary as much as the remaining part of the concrete arch, the starting point of the horizontal branch with the largest moment is then considered to be the critical

section. The stress at the top fibre of that section defines the ultimate capacity of the beam:

$$\sigma_c = \frac{6V_c a_c}{b_w z_c^2} - \frac{N_c}{b_w z_c} - \frac{6N_c e_c}{b_w z_c^2} < f_{ct} \tag{3.42}$$

where

a_c : is the length of the secondary branch;

z_c : is the height of the compressive zone at the starting point of the secondary branch.

V_c: is the shear force component in the concrete compressive zone, see Eq. (3.26).

N_c: is the resultant compressive force in the concrete compressive zone.

e_c: is the offset of the resultant compressive force to the centroid of the compressive zone. The value of e_c is mostly negligible. Accordingly, the third item in the equation may be neglected.

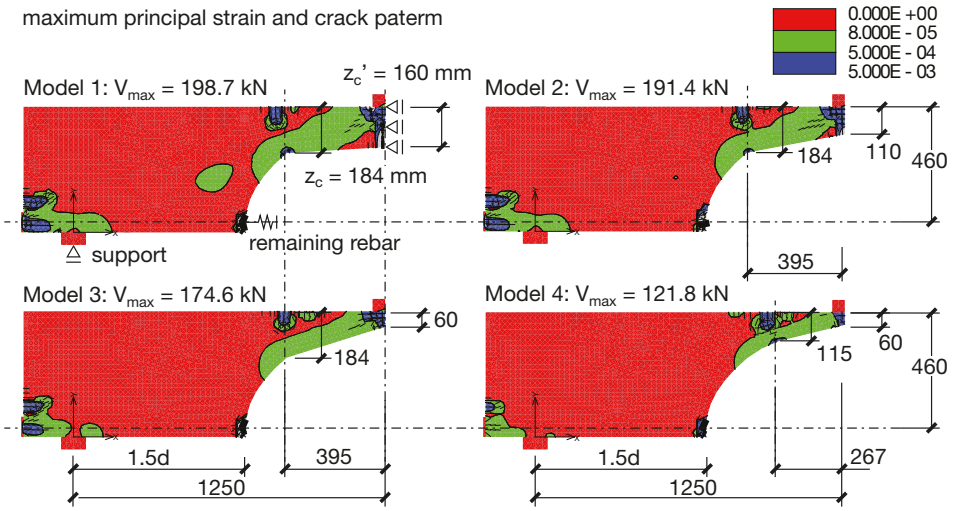

Fig. 3.41. Maximum principal stress distributions and crack patterns of FEM models of arch structure with different horizontal crack branches profiles.

The influence of height variation of the concrete arch due to the variation of secondary crack profile has to be investigated. Because the limited curvature of the secondary cracks, it is assumed that it only rotation around its tip, thus no shear displacement is expected there. Fig. 3.41 illustrates four results of numerical simulations with the nonlinear FEM software package Atena2D using smeared cracking elements. Four possible arch structures of a reinforced concrete beam after the formation of an inclined crack are constructed. A half beam

is modelled. The reinforcement is modelled by external rebars, thus no interaction between concrete and rebar is expected between the ends of the rebars. The models are based on the standard structural members introduced in Section 3.1. The dimensions of the models are summarized in Fig. 3.41 as well. The crack paths of all the four models are initiated at 1.5d from the support. The profile of the major cracks are calculated by Eq. (3.19). Other than the last model, the heights of the cracks are calculated by s_{cr} from Eq. (3.2). It results in a constant height of the concrete arch z_c at the root of the cantilever. The height of the cantilever under the loading point z_c' is the main variable, see Fig. 3.41. In the first three models, the height of the cantilever varies linearly, while in the last one, the cantilever branch of the concrete arch is formed by the extension of the crack profile calculated by Eq. (3.19).

The simulations show that despite the variation of the secondary crack branch, the maximum shear forces that can be reached in the first three models are quite close. Only when z_c is reduced, a significantly smaller shear force is expected. The crack patterns shown in Fig. 3.41, together with the maximum shear force at failure, confirms the conclusion derived previously, that it is the moment capacity at the starting point of the horizontal crack that defines the ultimate capacity of the beam. Besides, the simulations show that Eq. (3.42) may be utilized to judge the failure mode of a beam.

3.5.2 Critical Compressive Zone

The analysis of the residual structure formed by the critical inclined crack implies that under the shear force level where the inclined crack develops, a **critical compressive zone** can be defined. If the tip of the inclined crack is located within $a_{c,c}$ from the loading point, the stress of the top fibre of the beam is always smaller than the tensile strength of the concrete, thus a stable arch structure can still form after the opening of the inclined crack. Otherwise, if it is possible to develop a crack with its tip located at $a_c > a_{c,c}$, one may expect the collapse of the beam directly after the development of the inclined crack. It has to be remarked that unlike the other cases discussed in this research, here the definition of $a_{c,c}$ starts from the edge of the loading plate if the point load is introduced through a plate, which can be considered as the support of the concrete cantilever. The value of $a_{c,c}$ is determined by making $\sigma_c = f_{ct}$ in Eq. (3.42), and is expressed by

$$a_{c,c} = \frac{b_w z_c^2}{6}\left(f_{ct} + \frac{N_c}{b_w z_c}\right) \approx \frac{N_c z_c}{6V_c} \tag{3.43}$$

In Eq. (3.43), e_c is neglected. Besides, since $f_{ct} b_w z_c$ is always much smaller than N_c, this term is neglected as well.

Before further elaboration, it has to be clarified that the height of the uncracked part in the compressive zone should have been slightly higher than z_c in theory, when taking into account the tension softening behaviour of concrete. However, the observations from experiments always show a smaller uncracked zone than the calculated z_c because the 2-dimensional stress state at the crack tip generates a gradual transition between the major crack and the secondary crack rather than a kink. Thus the value of z_c used in Eq. (3.43) may need to be reduced by $\beta_{zc}z_c$. Besides, when the possible secondary crack branch is really long, buckling has to be regarded as a possible failure mode, that also introduces a certain reduction of the maximum allowable length of $a_{c,c}$. Before further calibration this effect is not taken into account, thus β_{zc} = 1.0. Nevertheless, the aforementioned reductions will not influence the conclusion significantly, therefore will not be discussed in detail.

Eq. (3.43) can be further simplified by taking into account that $N_c = M/z$ and regarding Eq. (3.26). It becomes

$$a_{c,c} = \frac{\beta_{zc}}{4}\frac{M}{V} \tag{3.44}$$

where

M, V : are the moment and shear force at the loading point;
β_{zc} : is a reduction factor for the compressive zone.

The beam specimens shown in Fig. 3.40 of this section can be taken as an example. The maximum values of M/Vd of the spans are 3.30, 2.64 and 1.98. The lengths of the critical compressive zone of the beams are 379.5 mm, 308.25 mm and 227.75 mm. The value of z_c in the specimens are $z_c = d\text{-}s_{cr}$ = 157.6 mm. The maximum crack height is then $s_{max} = h - \beta_{zc}z_c$ = 373.9 mm. With a beam height h = 500 mm it is found that ξ = 0.748. For each beam, it is assumed that the crack may develop at any location of the span. If all the cracks can reach the crack height ξ as calculated here. The distance between the crack tip and the support x_{tip} can be calculated with Eq. (3.19). The value of x_{tip}/d of a crack is plotted against the location x_0/d where the same crack initiates, see Fig. 3.42, which is independent of the load cases as long as the beam is loaded by point loads. In Fig. 3.42, the boundaries of the critical compressive zones of the three beams are plotted as well. For each loading case, if the crack tip enters $a_{c,c}$ from the loading point, it is possible to form a stable arch structure, even after the opening of the inclined crack. In Fig. 3.42 it means that the curve is higher than the boundaries of the corresponding loading case.

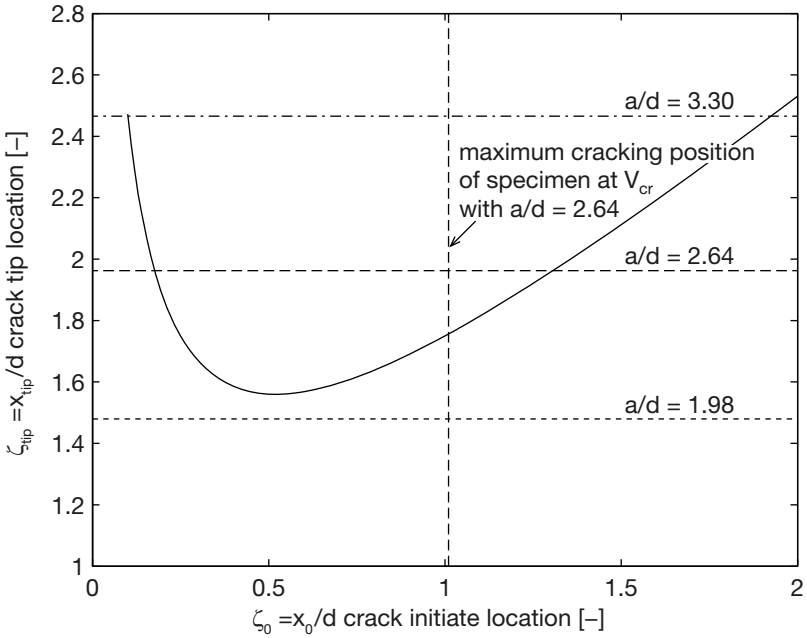

Fig. 3.42. Relationship of crack tip location and crack initiation location according to Eq. (3.19).

Fig. 3.42 clearly shows that with the configuration presented in this example, if the shear slenderness ratio of the beam is a/d = 1.98, the crack will always enter the critical compressive zone. Therefore it is not possible to have the so-called flexural shear failure for that loading case. On the other hand, for the specimen with a/d = 3.30, any crack that initiates between x_0 = 0.10d and 1.93d from the support can become a critical inclined crack, the opening of which will result in the collapse of the whole structure directly.

In the case of a/d = 2.64, it is more complicated. Fig. 3.42 indicates that if the crack initiates at 1.31d or closer to the support the beam will fail immediately after the crack opens. However, considering the tensile strength of the concrete, the cracking moment of the beam is M_{cr} = 61.3 kNm (f_{ctm} = 4.9 MPa). At the measured V_{cr} = 132.4 kN, the crack only starts to develop at 1.01d from the support. Taking that into account, the length of the actual zone along the axis of the beam where a critical inclined crack may develop is about 138 mm. However, the average crack spacing $l_{cr,m}$ of the major cracks is 232 mm according to Eq. (3.5) or 214 mm based on measurement in Fig. 3.5. Both are larger than 138 mm. It means that a principal inclined crack will not always develop within this region. Depending on whether the crack will develop or not, the shear failure mode may

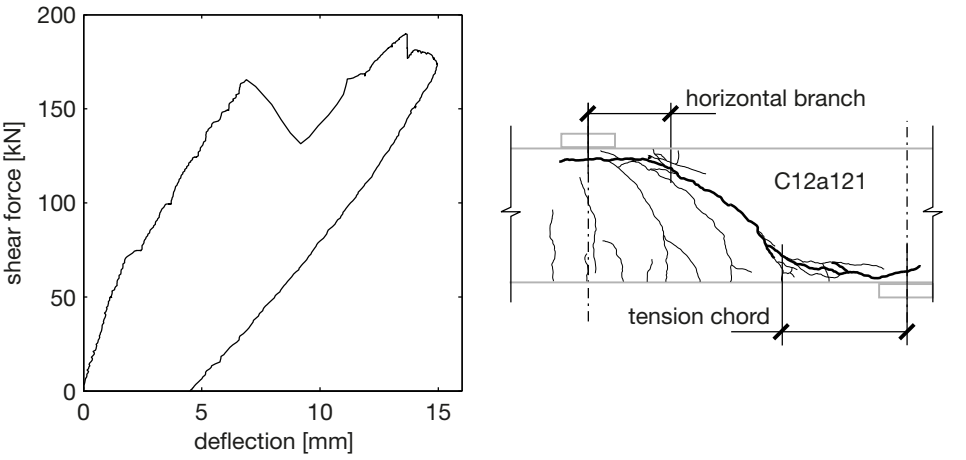

Fig. 3.43. Load deflection and crack pattern of specimen C12a121 with a/d = 2.64. Check Fig. 3.40 for specimen with the same boundary conditions but different failure mode.

switch. Indeed, both failure patterns were observed in the experimental program of continuous beams.

As a complement to Fig. 3.40, the crack pattern of a beam with the same a/d but different failure mode is shown in Fig. 3.43. It has to be mentioned that the boundary conditions and the geometry of both beam C3b121 and C12a121 are identical, except that the reinforcement ratio of the two beams are different, see Table 5.1. That difference might introduce a certain difference in behaviour. Nevertheless an impression on the influence of the crack pattern may be derived from the comparison. In beam C12a121, the critical inclined crack developed at a distance of about 1.0d from the support. Consequently the arch structure formed by the crack was not able to withstand the load directly after the development of the major inclined crack. After a considerable deformation, the load level was able to be increased again to a slightly higher level by virtue of the top reinforcement. The position of the inclined crack clearly influences the failure modes in the two cases shown here.

If the theory presented here reflects the mechanism properly, another conclusion that can be drawn is that for beams with the same a/d but with smaller concrete tensile strength f_{ctm}, the area where a critical inclined crack may develop becomes larger. When the length of the critical cracking zone is larger than the average crack spacing, the chance of having flexural shear failure will be 100%.

Another conclusion that can be derived by the theory is that it is the profile of the inclined crack that forms the arch structure. If it is possible to affect the shape of the inclined crack or even construct the shape of the arch structure manually

rather than letting the inclined cracks do so, the shear capacity of the beam can be improved. It will be the strength of the concrete arch that defines the capacity eventually. This conclusion has been proven by Beeby by experiments reported in (Walraven 2007). Beeby designed a reinforced concrete beam with a part of the concrete at mid span replaced by polystyrene. The remaining concrete and rebar forms a simple arch structure similar to what can be expected after the formation of the inclined crack. The artificially formed arch structure has a larger slope than that normally formed by cracking (Fig. 3.39), which was limited by the compressive force distribution. The test results showed that the specimen with an artificially formed arch structure is about 60% stronger than the reference beam with normal rectangular section (more concrete) and the same amount of reinforcement: 202 kN for Beeby's beam versus 129 kN (average) for the reference beams. The configurations of Beeby's arch-like beam and the reference are shown in Fig. 3.44.

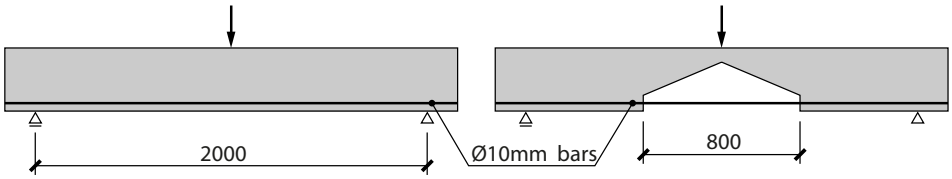

Fig. 3.44. Configurations of Beeby's beams adopted from (Walraven 2007).

3.5.3 Shear Force in Concrete Compressive Zone

The shear force in the concrete compressive zone of a concrete beam with flexural cracks was discussed in Section 3.3.2.1. The shear force was calculated by the shear stress distribution as proposed by Mörsch (Mörsch 1909). For the remaining arch structure after the opening of the inclined crack, that formula was still utilized in the previous sections. However, whether the formula is still valid or not is not clarified yet. Apparently the arch-like structure formed by the inclined crack and the longitudinal crack along the rebar is quite different from the teeth structure of a reinforced concrete beam with only flexural cracks. For that reason the same topic is picked-up again in this part of study. The assumptions presented in Section 3.3.2.1 are re-examined and adapted if necessary.

An obvious difference between the two situations is the opening of the horizontal crack branch. It removes the interaction between the concrete compressive zone and the tension zone. The opening direction of the crack is perpendicular to the longitudinal direction of the beam. No tangential displacement can develop along the crack, thus no shear stress is expected along the crack. While in a beam with only flexural cracks, the maximum shear stress

is expected at the neutral axis, the proposed stress distribution shown in Fig. 3.27 is not applicable anymore to the arch structure. Since no shear stress is expected through the crack, the shear force in the cantilever remains constant. It is governed by the shear force that is at the tip of the crack.

Here two possibilities may be expected. If teeth structures can still be formed by other major cracks between the tip of the secondary crack branch and the loading point, for example the crack patterns for a/d = 3.30 and 2.64 as shown in Fig. 3.40 and Fig. 3.43, the Mörsch's shear stress distribution may still describe the stress state properly. V_c can still be calculated by Eq. (3.26). On the other hand, if the crack tip already reaches the loading point, a rather complex stress state is generated there. In principle the uncracked compressive zone of the arch structure shall carry all the shear force that is not transmitted through the aggregate interlock effect and dowel action. Thus, depending on the crack profile this contribution may approach to 100% V. In that case the value of $a_{c,c}$ has to be adjusted, the lower bound of which is determined by replacing V_c with V in Eq. (3.43). It delivers:

$$a_{c,c} = \frac{z_c}{6z}\frac{M}{V} = \frac{\beta_{zc}}{4}\frac{M}{V}, \qquad \beta_{zc} = \frac{2}{3}\frac{z_c}{z} \tag{3.45}$$

In principal, the components of the region with an inclined crack can be schematized by Fig. 3.45. Before the crack tip reaches the loading point, the shear force available in the compressive zone V_c is limited by the shear stress distribution in the flexural cracked zone. After the crack tip reaches the loading point, the value of V_c is not limited anymore. The stiffness of the different components in the system shown in Fig. 3.45 determines the distribution of the shear force.

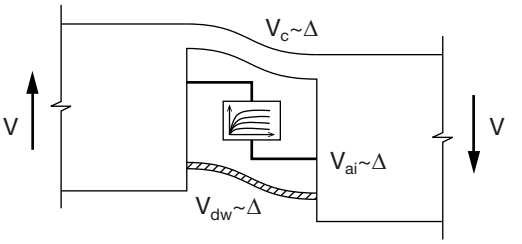

Fig. 3.45. Shear resisting components in an inclined cracked region of a reinforced concrete beam.

The uncracked concrete part has a varying cross section, so that under a unit load, the deflection of it has to be calculated by solving the differential equation:

$$\left(\frac{M}{E_c I}\right)' = \left(\frac{d^2 y}{dx^2}\right)'$$
$$\frac{V_c}{E_c} = \left(y'' I\right)' = Iy''' + I'y'' \tag{3.46}$$

where

I : is the moment of inertia of the cross-section above the crack;
y : is the deflection of the beam.

Since the crack profile varies along the longitudinal direction, I is a function of x as well:

$$I(x) = \frac{1}{12} bh(x)^3 = \frac{1}{12} b\left(h - s(x)\right)^3$$

with,

$s(x)$: is the expression of the crack profile;
h: the height of the beam.

The value of $s(x)$ is defined by Eq. (3.19), it is expressed as follows:

$$I(x) = \frac{bh^3}{12}\left(1 - \sqrt{\alpha_c \frac{x}{h}}\right)^3, \quad \alpha_c = \frac{1}{\delta_{cr}^{0.2}(M / Vd)^{-0.5}} \tag{3.47}$$

With the boundary conditions known, Eq. (3.46) can be solved in theory. However, due to the complexity of Eq. (3.47), the solution is not analytical. To get a general impression for the stiffness of the remaining arch structure, Eq. (3.47) is further simplified by replacing the expression of $s(x)$ by a linear crack path: $s(x) = h - t_c x$, where t_c defines the inclination of the crack path, $t_c = s_{cr}/x_{cr}$. With the simplified expression, Eq. (3.46) can be solved analytically, resulting in:

$$y(x) = -\frac{12V_c \ln(h - t_c x)}{t_c^3 E_c b} + \frac{C_1}{2(h - t_c x)} + C_2(h - t_c x) + C_3$$
$$C_1 = -\frac{12V_c h}{t_c^3 E_c b}; \quad C_2 = \frac{6V_c(h - 2t_c x_{cr})}{t_c^3 E_c b(h - t_c x_{cr})^2}; \tag{3.48}$$
$$C_3 = \frac{6V_c\left(2\ln(h)(h - t_c x_{cr})^2 + t_c^2 x_{cr}^2\right)}{t_c^3 E_c b(h - t_c x_{cr})^2};$$

The values of C_1 to C_3 are solved assuming the following boundary conditions $y(x_{cr}) = 0$, $y(0)' = 0$, and $y(x_{cr})'' = 0$. With the expression of $y(x)$ known, the stiffness of the residual structure can be expressed:

$$k_r = \frac{x_{cr}^3}{E_c b}\kappa_r(h, s_{cr}); \tag{3.49}$$

where

$$\kappa_r(h, s_{cr}) = \frac{6\left(s_{cr}(3s_{cr} - 2h) + 2\left(\ln(h) - \ln(h - s_{cr})\right)(h - s_{cr})^2\right)}{s_{cr}^3(h - s_{cr})^2}$$

The structure of Eq. (3.49) is quite simple, in which the length of the crack in longitudinal direction can be subtracted from the remaining equation. The same formulation structure can be extended to a more general scaling rule. For any beam like structure with a given expression of cross sectional function in its longitudinal direction, its vertical deflection stiffness is proportion to the 3rd power of the length of the beam x_{cr}.

When the shear span of the beam a is small, the length of the crack in longitudinal direction is related to the shear span. Assuming that x_{cr} is proportional to a, k_r is proportional to $(a/d)^{-3}$. For beams with smaller shear slenderness ratios, the analysis presented in this section shows that after the opening of the critical inclined crack, the proportion of V_c within the total shear resistance increases tremendously, being proportional to $(a/d)^{-3}$. Thus the study of the shear force that can be carried by the residual concrete arch structure will deliver sufficient information on the ultimate capacity of the member.

Such a analysis can be carried out by strut and tie models as proposed by (Marti 1985; Schlaich, Schäfer et al. 1987; Walraven & Lehwalter 1989; Collins, Bentz et al. 2008). Alternatively, Mihaylov et.al. proposed the theory called Two-Parameter Kinematic Theory (2PKT) in (Mihaylov, Bentz et al. 2013) shortly before the present thesis work was finished. Similar to the theory proposed in this thesis, the shear displacement of the critical major crack, is adapted as a criterion for the shear failure. The theory showed remarkable accuracy in comparison with the conventional strut and tie method. However, it has to be clarified that the shear displacement in the 2PKT is mainly caused by the shear deformation of the concrete arch close to the loading plate when the concrete is crushed there.

3.6 CONCLUSIONS

This chapter focuses on giving a rational description of the shear failure process of a simply supported prismatic reinforced concrete beam without shear reinforcement loaded by a point load. Considering inclined cracks as the most prominent feature of shear failure, the study is subdivided into three parts,

namely: the pattern of the major cracks before inclined cracking, the mechanism of the opening of the critical inclined crack and the residual structure after inclined cracking. The mechanism in each stage of the failure process is studied and formulated, so that it can be extended to more general cases. What has been learnt is summarized in this section.

Formation of the Major Crack Pattern

Because of the equilibrium condition of the forces in the cross section, the height of a crack becomes stabilized quickly after the cross sectional moment M has exceeded M_{cr}. By then, the height of the cracks can be approximated by s_{cr}. Thus, the shape of the crack is determined at $M \approx M_{cr}$. If the height of the crack can reach s_{cr} it is defined as major crack and is important for the shear resistance of the member.

The spacing of the major cracks occurs mainly determined by the crack height s_{cr} when the height of the member is larger than 100 mm.

For a major crack, its inclination occurs mainly because of the normal and shear stresses at its tip during the propagation process, among which shear stresses in the crack tip are generated by the bending of the concrete corbel in the teeth model formed by two adjacent major cracks by the longitudinal reinforcement.

During the crack propagation, the change of the crack inclination is strongly influenced by the value of M/Vd in the cross-section where the crack initiated, according to LEFM analysis.

By applying a Sequentially Linear Analysis (SLA) with Crack Propagation Algorithm (CPA), it is shown that the crack path can be approximated by a quadratic function. The major factors of the function are M/Vd and crack spacing.

Opening of the Critical Inclined Crack

Once the shape of the crack is known, it is possible to cut a part of the concrete beam along a given crack, considering it as a free body and evaluating the forces that apply on it. The study is aimed at revealing what is the reason of the sudden opening of a certain crack.

If the major cracks stay as what they were at their formation, and only allow opening by rotation around the tip, the shear resistance that can be generated along the crack path is not sufficient to balance the shear force.

A secondary crack branch starting from the original tip of the major crack in the longitudinal direction is necessary to generate additional tangential displacement Δ along the crack. This results in the increase of shear resistance by

aggregate interlock, which can balance the additional shear force that is higher than the resistance that can be generated from the original crack path.

If the crack width in the longitudinal direction w remains the same, the maximum shear force that can be resisted by aggregate interlock in a given crack is far beyond the normally expected shear capacity. Besides, the failure mode is plastic, rather than characterized by a sudden break as observed in experiments.

The sudden loss of the shear resistance can only be explained when the significant increase of the crack width due to the detachment of the longitudinal rebar under a dowel force is taken into account. It is suggested to take the shear displacement of the crack faces at the level of longitudinal reinforcement Δ as the criterion for the initiation of the dowel cracks. The shear force at which the sudden opening of the dowel crack along the longitudinal rebar starts is defined as the inclined cracking load V_{cr}.

The critical shear displacement (simplified from the critical shear displacement of crack faces at reinforcement level) Δ_{cr} should be determined by the overall energy balance of the whole beam. For a beam with known Δ_{cr}, both the bending moment of the crack and the profile of the crack influence the value of Δ in the crack at a given shear force. The crack with the largest vertical displacement Δ will become the critical inclined crack. Its position is either close to the loading point (when a/d is large), or to the support.

Residual Structure after Inclined Cracking

After the dowel crack along the longitudinal rebar has been developed, an arch structure is formed by the uncracked concrete and the detached longitudinal rebar.

The stiffness and the capacity of the remaining arch structure determine the behaviour of the beam after the opening of the inclined crack.

Whether or not the beam can withstand a larger load after the inclined cracking load is determined by the location of the tip of the major crack when it is stabilized after $M > M_{cr}$. If the crack tip is located within the critical compression zone defined by $a_{c,c}$ according to Eq. (3.44) from the edge of the loading plate, a higher residual capacity is expected.

Artificially influencing the shape and position of the critical inclined crack may influence the ultimate shear capacity of the beam.

The stiffness of the concrete arch structure is highly dependent on the profile of the inclined crack. When the crack reaches the loading plate directly, the stiffness also determines the portion of V_c in the concrete compressive zone. The magnitude of V_c is proportional to $(a/d)^{-3}$, thus increases quickly with a reduction of the shear span.

Chapter 4

Evaluation of Shear Capacity of Reinforced Concrete Beams Based on Critical Vertical Displacement

4.1 INTRODUCTION

This chapter presents the possibility to translate the shear failure mechanism described in Chapter 3 into an evaluation procedure which is applicable in engineering practice as most design codes, with comparable or even better accuracy, but wider applicability.

Chapter 3 has shown that the failure of a given cracked section under a shear force is due to the opening of the dowel cracks along the longitudinal reinforcement and the compression zone. Furthermore, it was assumed that the phenomenon occurs when the shear displacement of one of the major cracks reaches the critical displacement Δ_{cr}. That assumption indicates that the calculation of the inclined cracking load can be related to the shear displacement between the crack faces of a major crack.

Although the crack profile expression Eq. (3.19) has been greatly simplified, to calculate all the forces acting on such a parabolic profile is still far too complex for engineering calculation. A logical and safe solution is to focus on the simplified evaluation procedure for the most dangerous situation. Regarding the critical section, Chapter 3 showed that for beams with a larger shear slenderness ratio, the shear capacity of a crack being closer to the loading point is often lower than that of others (see Fig. 3.38), where the influence of the crack profile by M/Vd is minimized as well. Therefore it is appropriate to choose a crack profile at a section with very large M/Vd as the standard crack profile, and develop the shear evaluation procedure based on such a crack.

In a cracked section of a beam, the total shear force is carried by three different mechanisms: the shear forces in the uncracked compression zone V_c, the aggregate interlock between the crack faces V_{ai}, and the dowel action at the longitudinal reinforcement V_d, see Fig. 4.1. The three mechanisms can be considered as a paralell system carrying the total shear force V. Among them, V_c is related to the height of the compressive zone, and the total shear force V. It can be evaluated with Eq. (3.26). The value of V_d has already reached $V_{d,\max}$ ex-

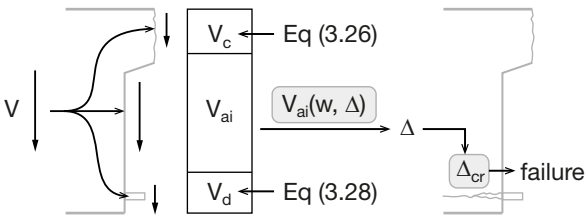

Fig. 4.1. Scheme of inclined crack evaluation, where the items in the boxes have to be evaluated.

pressed by Eq. (3.28) before $\Delta = \Delta_{cr}$. The part of the shear force carried by aggregate interlock V_{ai} is essential to determine the total shear resistance V. To calculate V_{ai} at the inclined cracking load, it is necessary to derive a relationship between V_{ai} and Δ for a given crack profile, and to determine the critical shear displacement Δ_{cr}. The two issues are dealt with in section 4.2 and 4.3 respectively. Based on that, an evaluation procedure for the inclined cracking load of a concrete member without shear reinforcement is provided in section 4.4.

The basic evaluation procedure is extended in section 4.5 - 4.7, where three special topics are dealt with respectively. They are the fracture of aggregate, the reinforcement configuration and the size effect.

4.2 SHEAR FORCE-DISPLACEMENT RELATIONSHIP

The principle of calculating V_{ai} under given w and Δ has been demonstrated in Chapter 3. The value of V_{ai} can be calculated by integrating the shear and normal stress under given displacement distribution along the crack profile with Walraven's formula Eq. (3.30). That procedure asks for a specific crack profile, which is dependent on the location of the cross-section where the crack initiates and the loading condition. In some load cases, when the critical section of the member cannot be determined, the shear resistance of each section of the member has to be evaluated. On the other hand, because Eq. (3.30) has to be solved with numerical integration, on a parabolic crack profile, the displacements in two directions are strongly coupled, which makes the solution of V_{ai} under given Δ_{cr} not always possible. Both aspects are not practical when the procedure introcduced in Chapter 3 is applying in engineering practice directly. A simplified relationship between V_{ai}, w and Δ is needed. Such a relationship can be based on the most common crack profile, and can be applied with a relatively simple calculation procedure.

4.2.1 Simplified Crack Profile

Fig. 3.33 has shown that for cracks initiated at a section with a relatively large M/Vd, the influence of the crack profile on the shear crack opening Δ is quite limited. For cross sections with a large M/Vd, the effect of the moment distribution in the longitudinal axis is dominating, the curvature of the crack profile at that condition is very small, thus the crack can be treated as a plane perpendicular to the longitudinal axis at M_{cr}. For the major cracks, after their formation, further increase of the external load can hardly increase the crack height s_{cr} in vertical direction, while the increase of the shear force in the cross-section will increase the stress σ_y in the beam height direction. The crack direction changes

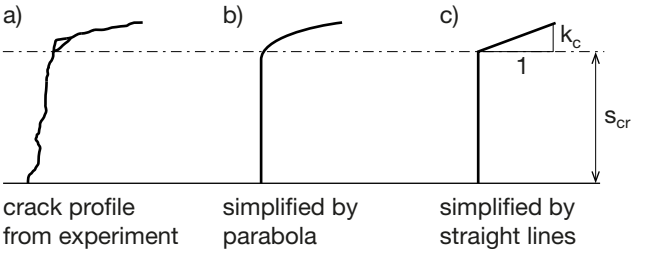

Fig. 4.2. Crack profile simplifications, based on the crack profile found in test D18a121 (see Fig. 5.13).

towards the longitudinal direction forming a secondary crack branch towards the loading point. Only after that, additional vertical displacement between the crack faces is possible, thus a larger shear force can be transferred through the vertical crack plane.

Taking that in to account, a potential critical inclined crack before shear failure shall be composed of a vertical major crack and a more or less horizontal secondary branch. An example of such a crack is shown in Fig. 4.2 (a). The crack pattern is derived from test D18a121 (in the test series discussed in Chapter 5) at failure. It can be approximated by a straight line connected to a parabolic curve as is shown in Fig. 4.2 (b).

The crack pattern shown Fig. 4.2 (a) can be described by the simplified formulation:

$$x = 0, \qquad 0 < s < s_{cr}$$
$$x = 0.2s^2, \; s_{cr} < s < 45 \text{ mm}$$

With this assumed crack profile, the shear displacement Δ and the crack width w are determined by the length of the parabolic branch and the rotation of the crack. The shear force transferred through the crack path due to aggregate interlock is calculated by making the crack rotate around the crack tip. As an example, assuming that the length of the parabolic branch is 20 mm, the height of which is 10 mm, and the crack width is 0.045 mm, the stresses generated by aggregate interlock can be calculated. The component of V_{ai} along the height direction is plotted in Fig. 4.3. The shaded area in the figure shows the contribution of the secondary branch. A peak is developed at the end of the straight crack path. The large normal stress increases further after that point, see Fig. 4.4. Despite of that, the shear force degrades to zero quickly in that branch. Compared with the shear force carried by the major crack, the contribution of the secondary crack branch is rather limited. On the other hand, the randomness of the material properties generates a large variation in the crack path anyway. The

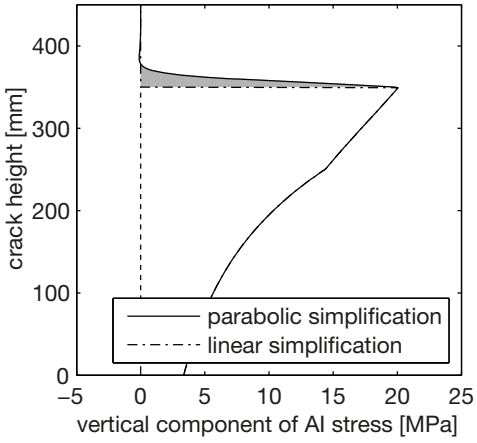

Fig. 4.3. Distribution of vertical component of V_{ai} along the height direction.

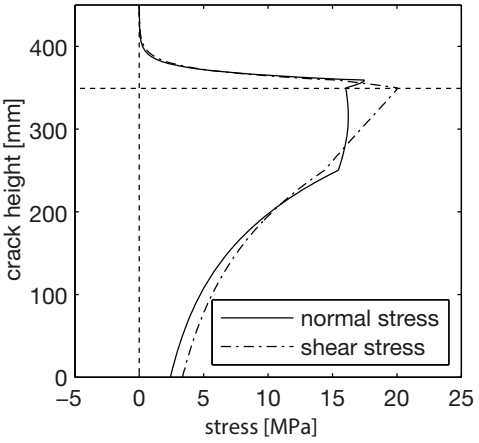

Fig. 4.4. Distribution of normal stress and shear stress due to aggregate interlock effect along the crack height (parabolic simplification).

contribution of a perfect crack path with regard to the accuracy of prediction for the shear force-displacement relationship is limited.

Based on the consideration mentioned before, the design crack profile is simplified further. A straight line is used to describe the secondary crack branch. The simplified crack path is shown in Fig. 4.2 (c). With this simplification, the shear force transferred through the secondary crack can be neglected, see Fig. 4.3. With the slope of the crack branch given, the relationship between the shear displacement Δ and the crack width w_t at the top of the major crack is fixed:

$$w_t = k_s \Delta \tag{4.1}$$

where

k_s : is the slope of the secondary crack branch.

The adoption of linear simplification of the crack profile can considerably simplify the calculation of V_{ai}. In this way, the value of V_{ai}.is directly related to the shear stress τ calculated from Walraven's formula, thus the curve integration expressed by Eq. (3.31) is simplified into the integration of τ over the crack height. The curvature dependant calculation based on the integration of τ and σ along a complex crack profile is not needed anymore:

$$V_{ai} = \int_0^{s_{cr}} b\tau(\Delta, w) ds \tag{4.2}$$

In addition, because the critical vertical displacement Δ_{cr} is predetermined as failure criterion, the crack width at the tip of the vertical crack path is known as well with Eq. (4.1). Wheras, the crack width at the reinforcement level is related to the reinforcement strain. Once the crack width distribution along the crack height s is known, conbining with the crack widths at the boundary of the crack makes the formulation of V_{ai} is possible. The choice of crack width distribution is discussed in the next section.

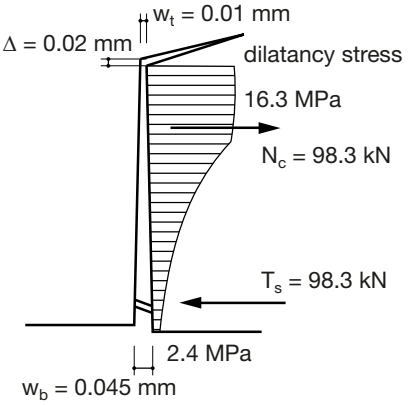

Fig. 4.5. Normal stress/force distribution along crack height.

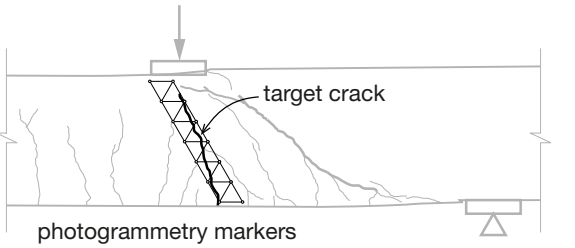

Fig. 4.6. Measurement of the crack opening of a major crack (C3b121).

4.2.2 Crack Width Distribution

To serve the purpose of deriving an expression describing the relationship between shear force and displacement, the crack width distribution has to be studied as well. Here the term **crack width** stands for the normal displacement of the two crack faces at a given point of the crack profile. However, because of the simplification of the crack profile, it actually stands for the crack opening in the longitudinal direction of the beam.

In the aforementioned analysis this problem was neglected by assuming the uncracked concrete as a rigid body. That implies that the crack opening changes linearly along the beam height. That assumption is not totally true in reality, because considering the crack profile as the boundary of the uncracked concrete, the deformation of the concrete under loading will certainly influence the crack profile. Taking the simplified crack profile described above as an example, the normal compressive stress distribution obtained from aggregate interlock is plotted along the vertical crack in Fig. 4.5. The normal stress rises due to the

dilatancy effect with aggregate interlock, and the large localized force transferred through the reinforcement may change the crack opening.

Laboratory measurements of the crack width distribution show that before a failure mechanism develops the crack width distribution is basically linear. An example is given in Fig. 4.6, where the crack opening of a major crack is measured by a photogrammetric measurement. Such a measurement was carried out over the surface of the critical shear span in all the tests of the series of continuous beams loaded by point loads discussed in Chapter 5. More details can be found in the separate report written by the author (Yang 2009). The crack opening is calculated by checking the displacement of measurement targets glued on the beam surface. In Fig. 4.6, the target crack and related measurement markers are shown. The crack opening distribution of the target crack is plotted in Fig. 4.7. It shows that the tensile force applied through the rebar has a considerable influence on the crack profile locally. Nevertheless, the influenced area is quite limited. When the crack height becomes larger than 120 mm, the crack opening becomes linear again. The influence of the level of the reinforcement is dependent on the reinforcement ratio and the beam height. At the reinforcement level, the crack opening is already rather large, thus the shear force that can be

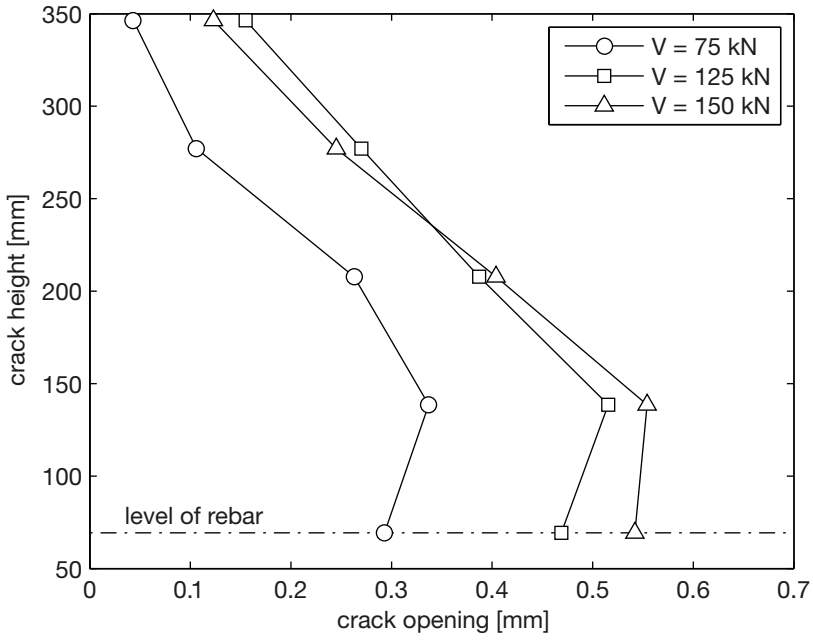

Fig. 4.7. Crack profile measured by photogrammetric measurement (Crack marked in Fig. 4.6)

transferred there is rather limited. Whereas the linear crack width distribution is still valid at the crack tip.

On the other hand, the influence of the crack dilatancy effect is very difficult to be determined. The crack opening at the crack tip is mostly too small to measure. However, since a large proportion of the normal stress from aggregate interlock is localized at the tip of the major crack, see Fig. 4.5, these stresses can be replaced by a localized force applied at the major crack tip. The magnitude of this force merely has an effect on the crack opening at the tip, which enlarges the crack width there so that the tension softening effect is weakened. Based on that consideration, neither the influence of the dilatancy effect or the tension softening of concrete on the crack shape is taken into account.

Taking the discussions above into account, in this study, the crack width is assumed to be a linear function of the crack height s. The crack opening at the level of the tensile reinforcement (defined as **bottom side** here) is estimated by neglecting the smaller cracks develop due to the confinement of the tensile reinforcement:

$$w_b = l_{cr,m}\varepsilon_s \tag{4.3}$$

where

$l_{cr,m}$: is the crack spacing of the major cracks, see Eq. (3.5);
ε_s : is the average strain of reinforcement at that cross section.

This simplification may lead to an overestimation of the value of V_{ai} at the same Δ. However it significantly simplifies the calculation procedure, since the estimation of the influencing height of the reinforcement is not necessary with this formulation.

The crack width at the top of the crack, on the other hand, is related to the critical vertical crack opening Δ_{cr}, because of the simplification of the secondary crack branch. As a rough estimation, the value of w_t is predefined to be w_t = 0.01 mm, which is of the same order of magnitude as the value of Δ_{cr} according to (Baumann & Rüsch 1970; Vintzeleou & Tassios 1986).

4.2.3 Simplified Shear Force Displacement Relationship

With the simplified crack width distribution and the crack profile, the total shear force applied over the crack still has to be calculated through integration with Eq. (4.2). This procedure can be further simplified for practical application.

Taking the simplified crack profile into account, the shear displacement Δ is constant along the vertical crack, and it is predefined in the calculation. The value of Δ_{cr} is between 0 and 0.1 mm. That limit will be refined further in the next section.

On the other hand, the crack opening w is linearly distributed along the height of the crack, thus may be expressed by

$$w(s) = \frac{w_b - w_t}{s_{cr}} s + w_t$$

After the substitution of the expressions for w and Δ into Eq. (4.2), the expression can be simplified to:

$$\begin{aligned} V_{ai} &= \int_0^{s_{cr}} \tau(\Delta, w) b_w \, ds \\ &= \sigma_{pu} b \int_0^{s_{cr}} A_x\left(\Delta, w(s)\right) - \mu A_y\left(\Delta, w(s)\right) ds \\ &= \sigma_{pu} b s_{cr} \int_0^1 A_x\left(\Delta, w(s')\right) - \mu A_y\left(\Delta, w(s')\right) ds' \end{aligned} \tag{4.4}$$

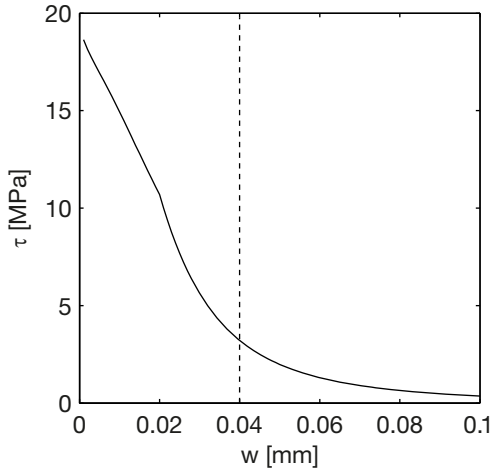

Fig. 4.8. Shear stress as a function of crack width w at Δ = 0.02 mm.

The integration term in Eq. (4.4) is only dependent on the crack width distribution. At a given shear displacement Δ, the aggregate interlock shear stress is shown in Fig. 4.8. This can be also considered as the shear stress distribution over the crack height. The shear stress is significantly higher when the crack width is small, where a larger contacted area is expected according to Walraven's theory. This distribution clearly indicates that the largest proportion of the shear force V_{ai} is actually determined by the shear stress at the part of the crack with small crack width.

The crack width w_{b0} = 0.04 mm is taken as a lower bound. The crack width of a reinforced concrete beam at failure is usually larger than that value. For beams with a larger crack width at failure, the contribution of the crack width larger than w_{b0} is assumed to be zero. Since the crack width at the top of the crack is

fixed at 0.01 mm at failure, for any cracks with edge crack width w_b larger than 0.04, the boundaries of w in the integration of Eq. (4.4) is constant, which makes this term only dependent on the shear displacement. Therefore, the expression of V_{ai} can be further simplified to:

$$\begin{aligned} V_{ai} &= \sigma_{pu} b \frac{w_{b0} - w_t}{w_b - w_t} s_{cr} \int_0^1 A_x\left(\Delta, w(s')\right) - \mu A_y\left(\Delta, w(s')\right) ds' \\ &= 6.39 f_c^{0.56} b \frac{0.03}{w_b - w_t} s_{cr} v_{ai}(\Delta) \end{aligned} \tag{4.5}$$

with

$$\begin{aligned} v_{ai}(\Delta) &= \int_0^1 A_x\left(\Delta, w(s')\right) - \mu A_y\left(\Delta, w(s')\right) ds' \\ &= \int_{0.04}^{0.01} A_x\left(\Delta, w\right) - \mu A_y\left(\Delta, w\right) dw \end{aligned}$$

In Eq. (4.5), v_{ai} is a function of a single variable Δ, and the expression of v_{ai} cannot be solved analytically. Since Δ only varies within a quite limited range, it is not necessary to calculate the equation of Walraven's aggregate interlock equation every time. A more simplified relationship based on regression analysis can make the process much simpler. Therefore, the expression of $v_{ai}(\Delta)$is simplified to:

$$v_{ai}(\Delta) = -978\Delta^2 + 85\Delta - 0.27 \tag{4.6}$$

This expression is valid when Δ varies from 0.005 mm to 0.04 mm. It is compared with the results calculated by Walraven's formula in Fig. 4.9. After substitution of Eq. (4.6) into Eq. (4.5), a simplified formula for the value of V_{ai} is derived.

$$V_{ai} = f_c^{0.56} s_{cr} b \frac{0.03}{w_b - 0.01}(-978\Delta^2 + 85\Delta - 0.27) \tag{4.7}$$

With Eq. (4.7), the shear force transferred through the simplified crack profile example presented in 4.2.1 is calculated at Δ = 0.02 mm. The result is plotted in Fig. 4.10 together with the prediction from Walraven's formula. In Fig. 4.10, the crack width w_b varies from 0.02 mm to 0.1 mm. The comparison shows that the simplified formula gives close estimations to the shear force transferred through aggregate interlock when the crack width is larger than 0.04 mm. From that crack width, the simplified equation is valid. As is expected, Eq. (4.7) underestimates the value of V_{ai} by neglecting the contribution of the part of the crack with large crack width. The percentage of underestimation increases when the value of w_b increases. On the other hand, when the bottom crack width w_b is smaller than 0.04, Eq. (4.7) tends to overestimate the value of V_{ai}. The error is

acceptable if the crack width is not smaller than 0.03 mm, which under most circumstances is reached before the failure of a beam.

As an alternative, for beams with expected crack width smaller than 0.03 mm, such as beams with very small heights, or very large reinforcement ratios, it is still necessary to calculate the value of V_{ai} through the full integration over the simplified crack profile Eq. (4.4). It is supposed to reflect the relationship between V_{ai}, Δ and w better, which has been done in the most part of this dissertation for a better accuracy.

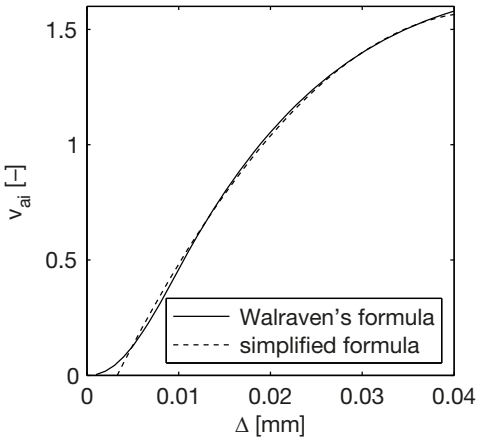

Fig. 4.9. Relationship between v_{ai} and Δ derived from Walraven's formula and the simplified relationship.

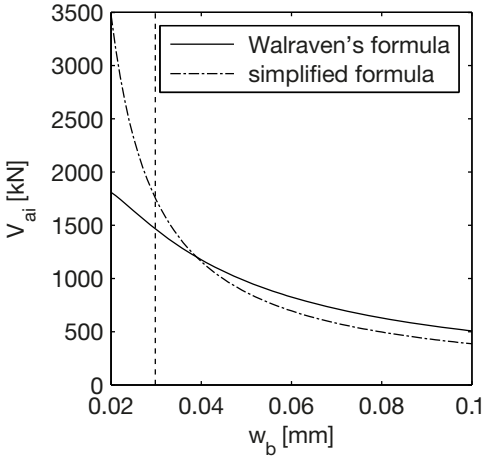

Fig. 4.10. Relationship between V_{ai} and w_b derived from Walraven's formula and simplified formula at Δ = 0.02 mm.

4.3 CRITICAL SHEAR DISPLACEMENT

4.3.1 Determination of Δ_{cr} from Test Results

With the expression Eq. (4.7) for V_{ai} derived in Section 4.2, it is possible to calculate the shear displacement Δ at the cracked cross-section under any given shear force V. Once the critical shear displacement Δ_{cr} is known, the maximum shear capacity may be calculated. However, in literature, the values of Δ_{cr} vary in a rather large range.

According to Baumann & Rüsch (Baumann & Rüsch 1970), the value of Δ_{cr} may vary between 0.06 mm and 0.16. They took the average value of Δ_{cr} = 0.08 mm in their formula, while Taylor (Taylor 1971) reports that it should be about 0.01 mm, which is almost 10 times smaller. His test series consists of several specimens with smaller sizes than used in Baumann & Rüsch's tests. Besides, the

load condition of the dowel action tests cannot fully represent the load condition in a beam specimen. At failure, a smaller tensile force is present in those tests compared to normal beams. Since there is no applicable result from literature, it is decided to derive the critical vertical displacement directly from the shear tests in literature.

The shear database collected by Collins et al. (Collins, Bentz et al. 2008) is used to derive the value of Δ_{cr}. The database includes 1849 tests from 114 publications. Among them, 410 tests are selected. The advantage of the database is that the maximum aggregate size is collected in the database. The following selection criteria have being applied:

- The observed failure mode of the specimen has to be shear failure;
- The concrete strength is smaller than 80 MPa;
- The cross-section of the beam is rectangular, which means that the effective width of the beam is equal to the maximum width of the beam;
- The width-effective depth ratio b/d is smaller than 2.0;
- The value of maximum M/Vd in the critical shear span is at least 3.0.

The first three criteria are defined to guarantee that the derived formulas are still applicable. The criterion for the strength of concrete has been formulated to make sure that fracture of aggregate, as often observed in experiments (Walraven & Stroband 1999) does not have any significant influence on the value of V_{ai}. Further discussions on the fracture of aggregate will be given in Section 4.5. For specimens with different cross sectional configuration, such as I-beams or inverse T-beams, the dowel crack may develop at the bottom of the web instead of at the level of the longitudinal reinforcement. The fourth criterion excludes one-way slabs, which will be discussed separately in Section 6.4. The last criterion guarantees that the evaluation is carried out on the design crack profile.

Since in Collins' database only the reinforcement ratio is provided, and not all the rebar configuration can be found back from the origin literature, the diameter and the number of the bars is estimated in the calibration process. However, the influence of rebar configuration will be discussed further in section 4.6 with the ACI-DAfStb database (Reineck, Bentz et al. 2013). The first assumption is that a beam has three rebars, the diameter of which is calculated from the reinforcement ratio. For unrealistic diameters, the number of the rebars is increased or decreased accordingly.

For all the test data, the measured shear force V_u from the database is applied on a cracked surface at $l_{cr,m}$ from the loading point. The shear displacement Δ_{cr} at V_u is calculated as follows:

Step 1: Calculate the shear component in the compressive zone and the maximum dowel force with:

$$V_c = \frac{2}{3}\frac{z_c}{z}V \tag{3.26}$$

$$V_{d\max} = 1.64 b_n \phi \sqrt[3]{f_c} \tag{3.28}$$

Step 2: Get the shear force component by the aggregate interlock effect:

$$V_{ai} = V_u - V_c - V_d$$

Step 3: Calculate the moment at the critical cross-section M according to Section 3.4.3 and thus the bottom crack width w_b:

$$M_d = V_u d \frac{M}{Vd},\ w_b = \frac{M_d}{zA_s E_s} l_{cr,m} \tag{4.8}$$

Step 4: Calculate the critical shear displacement Δ_{cr} under V_u by updating V_{ai} with varying Δ iteratively with Eq. (4.4), until the total shear force converges to V_u. The value of V_{ai} is calculated for the simplified crack profile and crack width distribution described in 4.2.2 and 4.2.3:

$$V_{ai} = \sigma_{pu} b s_{cr} \int_0^1 A_x\left(\Delta, w(s')\right) - \mu A_y\left(\Delta, w(s')\right) ds' \tag{4.4}$$

4.3.2 Calibration of the Results

The shear displacement Δ under the measured V_u of all 410 test results reported in the data base is calculated with the procedure described above. The derived Δ_{cr} varied between 0.0048 mm and 0.0444 mm. As explained in Section 2.3, reliable measurement of the kinematics of a critical major crack during the failure process is very limited. The calculated Δ_{cr} can hardly be compared systematically with experimental data yet. Before that, it can only be considered as an intermediate variable during the calculation process. Nevertheless, comparing to the values of Δ_{cr} reported by dowel action tests in the literature, the calculated Δ_{cr} is of the same order of magnitude, but at the lower side. That is probably because of the underestimation of the crack width introduced by simplifying the crack width distribution to a linear function discussed in 4.2.2, and the overestimation of the aggregate interlock stress with smaller crack width at the major crack tip.

There is a relatively large scatter among the calculated values of Δ_{cr}. This can partly be attributed to the fact that the information of the reinforcement config-

uration is missing. Nevertheless, it is still clear that the value of Δ_{cr} is influenced by the effective height d of the specimen. In Fig. 4.11, Δ_{cr} is plotted against d. The graph clearly shows that Δ_{cr} increases with d. That tendency is more pronounced with specimens with smaller d. Possible explanations are that for specimens with a smaller height, the influencing height of the crack width by the localized force due to the reinforcement is more significant. On the other hand, Section 3.2.1 has pointed out that the tension softening behaviour of concrete has an effect on the crack pattern. These effects are corrected through a linear regression analysis between Δ_{cr} and d. From the analysis, the value Δ_{cr} is expressed by

$$\begin{aligned} \Delta_{cr} &= 3.3555 \cdot 10^{-5} d + 0.005 \\ &\approx d \,/\, 29800 + 0.005 \leq 0.025 \end{aligned} \tag{4.9}$$

where

d : is the effective height of the specimen.

An additional requirement is that the value of Δ_{cr} shall not be larger than 0.025 mm, which limits the effect of the specimen size to a certain extent, since the influence of the crack width distribution from the reinforcement is more limited in beams with larger height.

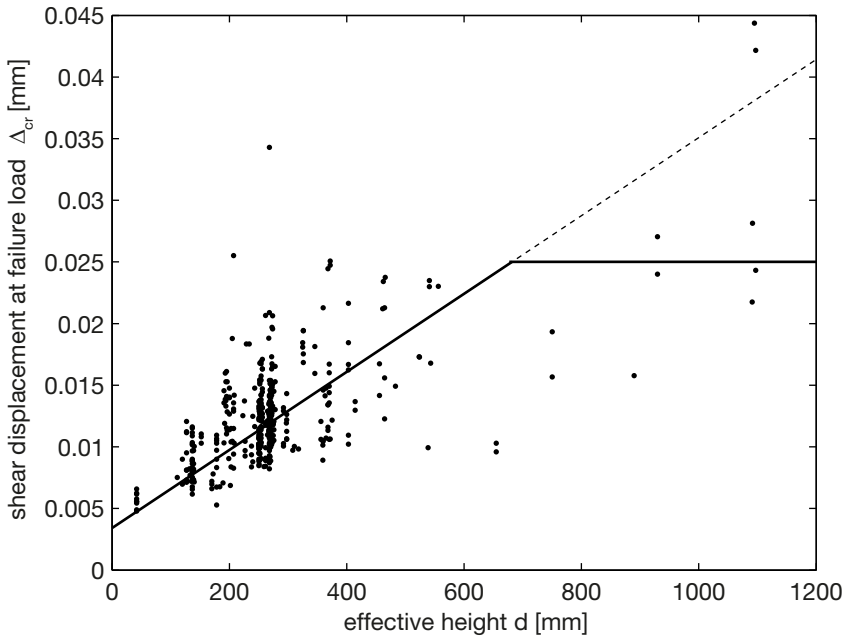

Fig. 4.11. Calculated critical vertical displacement against effective height.

4.4 EVALUATION PROCEDURE

4.4.1 Evaluation Procedure

With a shear force-displacement relationship and failure criterion, the evaluation procedure described in Section 4.1 becomes possible. In this section, the relationships explained previously are assembled together to form a calculation procedure that evaluates the shear capacity of a reinforced concrete beam without shear reinforcement under point loads. The evaluation of beams with more complex loading conditions will be discussed separately in other chapters.

When it is applicable, the evaluation cross-section of the structure to be evaluated is at the loading point according to Section 3.4.3. Although a more accurate estimation would be at $l_{cr,m}$ from the loading point to guarantee the possibility of sufficient shear displacement Δ between the crack surfaces, that choice has been made to guarantee the consistency of the results at small shear span. The evaluation procedure of a beam with known loading position is described as follows:

Step 1: Calculate the maximum shear force carried by dowel action:

$$V_{d\max} = 1.64 b_n \phi \sqrt[3]{f_c} \tag{3.28}$$

Step 2: Start with a shear force value V_u, calculate the moment at the design cross section, and the crack width w_b at that cross section:

$$M_d = V_u d \frac{M}{Vd},\ w_b = \frac{M_d}{z A_s E_s} l_{cr,m} \tag{4.10}$$

Step 3: Determine the critical shear displacement Δ_{cr}:

$$\Delta_{cr} = d / 29800 + 0.005 \le 0.025 \tag{4.9}$$

Step 4: Evaluate the shear force carried by aggregate interlock effect with the calculated Δ_{cr} and w_b:

$$V_{ai} = f_c^{0.56} s_{cr} b_w \frac{0.03}{w_b - 0.01}(-978\Delta^2 + 85\Delta - 0.27) \tag{4.7}$$

Or alternatively:

$$V_{ai} = \sigma_{pu} b s_{cr} \int_0^1 A_x\left(\Delta, w(s')\right) - \mu A_y\left(\Delta, w(s')\right) ds' \tag{4.4}$$

Step 5: Calculate the shear force carried in the concrete compressive zone:

$$V_c = \frac{2}{3}\frac{z_c}{z}V \tag{3.26}$$

Step 6: Update the overall shear force V_u of the whole cross section, and repeat this from Step 2 to Step 6 till the value of V_u converges.

$$V_u = V_c + V_d + V_{ai}$$

The evaluation of the maximum allowable shear force needs iteration since the load applied on the beam is not known in advance. This procedure can also be used for a safety check if the load applied on the beam is known. In this case, the known shear force V is assumed in Step 1, and is compared with V_u calculated in Step 6.

In addition, as shown in Fig. 4.10, the simplified aggregate interlocking equation Eq. (4.7) is an estimation of the integration expressed by Eq. (4.4). For a more accurate prediction, the original Eq. (4.4) is suggested to be used in step 4. The calculation procedure incorporating Eq. (4.4) has been implemented with a Matlab code attached in Appendix I.

4.4.2 Comparison with Test Results

The accuracy of the procedure described here has to be evaluated with the experimental results reported in literature. Other than that, the Eurocode (Eurocode 2 2004) has been used as a reference. The comparison is based on the shear database collected by König and Fischer (König & Fischer 1995) based on which the Eurocode shear formula was calibrated. The adoption of a different database is to avoid the usage of the same set of data in both deriving the formula and evaluating it. 176 tests are included in the database, which were selected in such a way that the key parameters influencing the shear capacity like the beam sizes, concrete strength and reinforcement ratio are distributed evenly over a practical range. All the specimens selected have a shear slenderness ratio (a/d) of at least 3.0.

The calculated shear capacity is denoted as V_{cal}. The mean calculated cross sectional shear stresses V_{cal}/bd are compared with test results V_u/bd in Fig. 4.12. In addition the distribution of V_{cal}/V_u is plotted as well. The comparison clearly shows that the own Δ_{cr} model provides a consistent prediction over the full mean shear stress range. The mean value of V_{cal}/V_u of the model is 1.06, with a **Coefficient of Variation** (COV) of 14.6%. For the Eurocode, the mean value of V_{EC}/V_u is 0.87, with a COV of 16.0%. The comparison shows that the Δ_{cr} model can already give a reasonably accurate prediction even compare to the current design codes. However, it has to be remarked that regarding to the Eurocode formula, the lower mean value and the larger scatter is partly due to the limita-

tion on the size effect factor $k \leq 2.0$, which was applied for additional safely of the structures. Without that limitation, the mean value of V_{EC}/V_u becomes 0.91 with COV(V_{EC}/V_u) = 13.1%. Note that the calculation with the own model was carried out with the exact aggregate interlock method Eq. (4.4) in step 4. When Eq. (4.7) is used, the mean value and COV of the prediction becomes 0.99 and 16.4%, which indicates that there are certain number of tests with small crack widths see Section 4.2.3. They are mostly small beams. Nevertheless, it still gives quite reasonable results.

Compared to the Eurocode, Fig. 4.12 also shows that when the mean shear stress is large, the model seems to overestimate the shear capacity. The reason is that for high strength concrete, the reduction of the aggregate interlocking effect due to the fracture of aggregates is not taken into account in this model. This effect will be discussed in the next section.

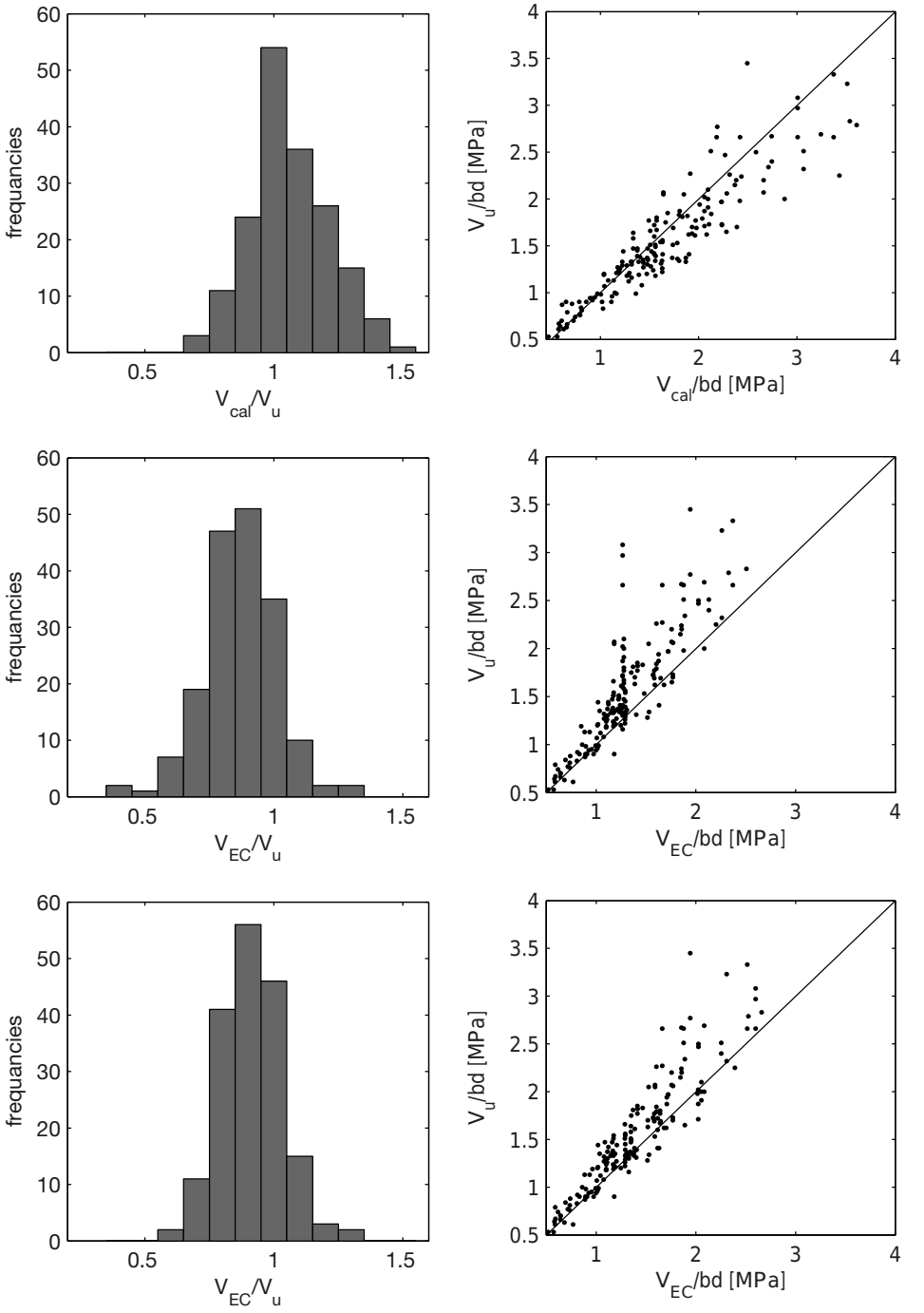

Fig. 4.12. Comparison of predicted shear capacities and test results based on König and Fischer's shear database. From top to bottom: results of own Δ_{cr} model, Eurocode and Eurocode without limitation on $k \leq 2.0$.

4.5 CORRECTION FOR AGGREGATE FRACTURE

4.5.1 Influence of Aggregate Fracture on Aggregate Interlock

The study carried out in Chapter 3 has clearly shown the role that aggregate interlock action plays in a cracked section of a beam loaded by a shear force. In the simplified design procedure presented in this chapter, the aggregate interlock force V_{ai} is calculated with Walraven's formula, which was derived based on experiments carried out on concrete specimens with cylinder strength between 10 and 50 MPa. One of the basic assumptions in the derivation of the formula according to (Walraven 1980) is that the aggregates do not fracture. Thus cracks only occur in the cement matrix and the interface between cement and aggregate. The shear force is generated by the contact between aggregates and cement matrix. Such an assumption may not be valid anymore for concrete specimens with high strength concrete or lightweight aggregate concrete. In both cases, the strength of the cement matrix may be stronger than the aggregates. As a result, cracks may develop through the aggregates. This effect has to be considered in evaluating the shear capacity of corresponding concrete structures.

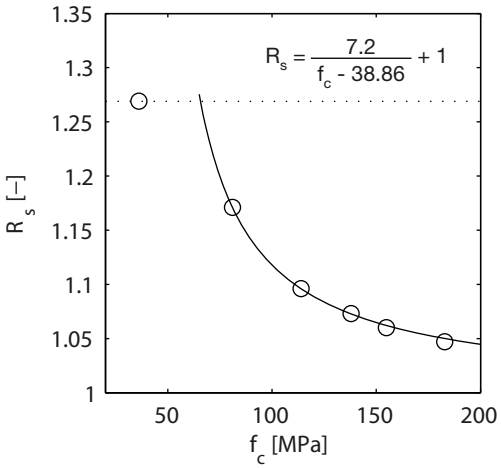

Fig. 4.13. Influence of concrete strength to fractured surface roughness, adapted from (Perera & Mutsuyoshi 2013).

Perera and Mutsuyoshi scanned the cracked surface of concrete splitting tensile specimens with different strength using a laser confocal microscope in (Perera & Mutsuyoshi 2013), see Fig. 4.14. The surface roughness index $R_s = \Sigma A_i / \Sigma A_p$ is calculated from the measurement, where, A_i is the measured fractured surface area, and A_p is the projected surface area. They have shown that the surface roughness of the crack is related to the concrete strength when the

maximum aggregate size is constant, see Fig. 4.13. It indicates that more aggregates may fracture when structures with a higher concrete strength crack. Consequently, the fracture surface is smoother. This is related to the elastic strain energy stored in the concrete at fracture. Fracturing at higher tensile strength, means more strain energy is released, which will result a in a faster crack propagating speed, and a smoother crack surface. Similar results have been reported by Mechtcherine and Müller in (Mechtcherine & Müller 2002; Mechtcherine 2009)

Many research programs have been reported in literature regarding the shear transfer across cracks in reinforced concrete or plain concrete. Walraven (Walraven & Reinhardt 1981), Mattock, Li and Wang(Mattock et al. 1976), Emiko

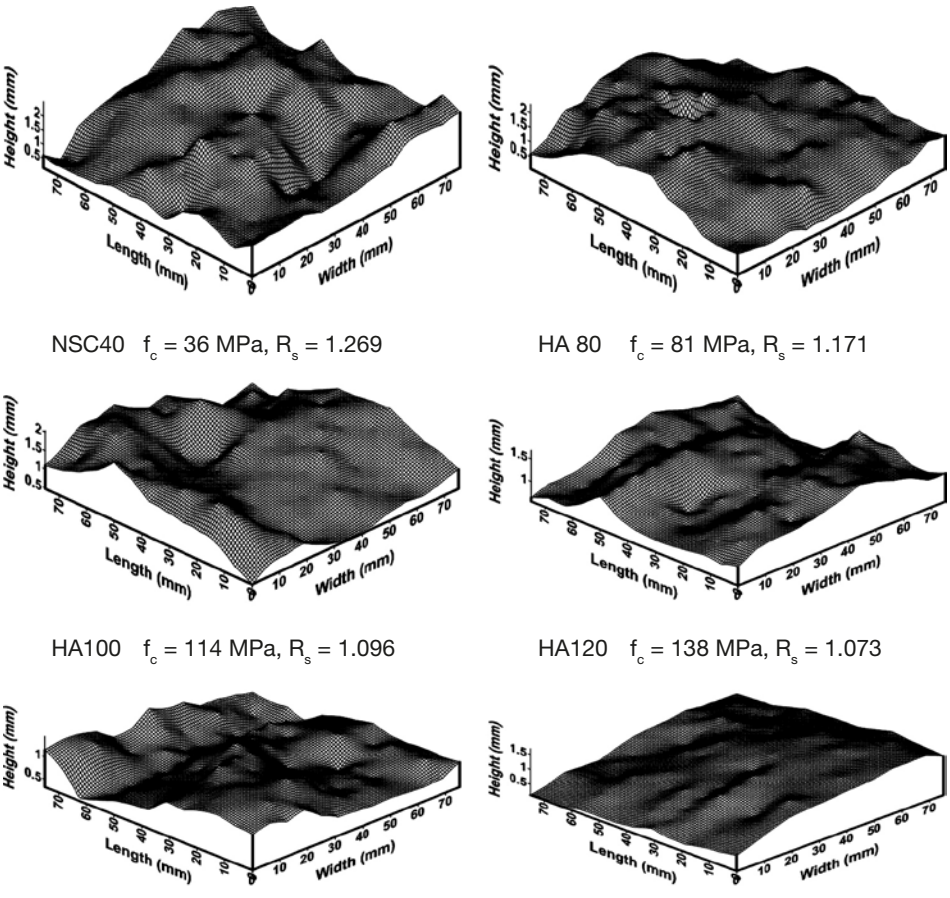

Fig. 4.14. Fractured surfaces of splitting tensile tested specimen; the names of the specimens are according to the original paper (Perera & Mutsuyoshi 2013).

et al.(Emiko et al. 2011), Hamadi and Regan (Hamadi & Regan 1980), have carried out push-off tests on reinforced lightweight aggregate specimens. They have shown that the maximum shear stress that can be transferred across a crack in reinforced lightweight concrete specimens is indeed smaller. Besides, more transverse displacement is needed in lightweight aggregate concrete specimens. Similar observations have been done in push-off tests on high strength concrete specimens executed by Walraven, Frénay and Pruijssers (Walraven et al. 1987), Walraven and Stroband (Walraven & Stroband 1994). This indicates that a reduction of the calculated V_{ai} might be needed. However, as pointed out by Walraven and Reinhardt in (Walraven & Reinhardt 1981), the result of shear transfer in reinforced concrete cannot be applied to shear transfer of cracks in plain concrete.

The evaluation of V_{ai} on beams shall be based on the test results of shear stress transfer across cracks in plain concrete. However, very few experimental research programs have been carried out to investigate the shear force transferred across cracks in plain concrete with high strength concrete or lightweight aggregate concrete. To adjust Walraven's formula for different types of aggregate, results of similar tests are needed. Walraven and Stroband reported a comparative study between concrete specimen with $f_{c,cube}$ = 59.1 MPa and $f_{c,cube}$ = 110 MPa in (Walraven & Stroband 1999). They found that the measured shear stress in cracks of high strength specimen is only 35% of the predicted value given by Walraven's formula for concrete with unbroken aggregates. It indicates that for plain concrete, the fracture of aggregate has a significant influence on the aggregate interlock effect.

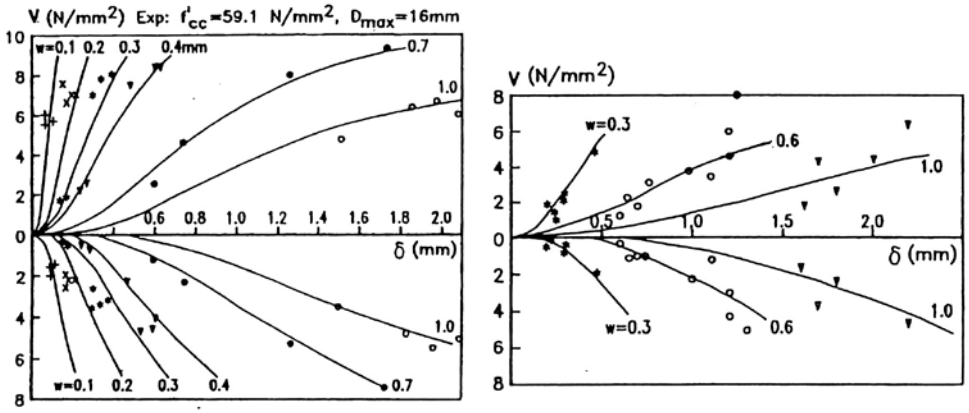

Fig. 4.15. Relationship between shear stress, normal stress, shear displacement and normal displacement of a crack in a plain concrete specimen (left: f_c = 59.1 MPa, right: f_c = 110 MPa), adopted from (Walraven & Stroband 1999).

4.5.2 Effect of Aggregate Fracture on Overall Shear Capacity

High Strength Concrete

According to the failure process described in Chapter 3, the reduction of aggregate interlock action due to the fracture of coarse aggregate will eventually influence the overall shear capacity of the structure. To evaluate that effect, a database of shear test results covering both high strength and low strength concrete specimens is compared.

Many of the concrete structures nowadays use concrete with a compressive strength of 60 MPa or higher and have a the cross sectional height larger than 500 mm. A pre-selection has to be done to guarantee that the parameters of the tested specimens are balanced within a practically relevant range. The selected database is based on the database collected by König and Fischer in (König & Fischer 1995). It also comprises several additional experimental data reported after 1995, in which specimens with higher concrete strengths and large beam sizes are included. The database is described in Appendix III.

To compare the influence of aggregate fracturing with the increase of concrete strength, the ratio between the tested shear capacity and the prediction given by the proposed formula is plotted against the concrete strength in Fig. 4.16. In the figure, it is clear that, when the concrete strength is higher than 60 MPa, the proposed Δ_{cr} method may overestimate the overall shear capacity. The tendency is more pronounced with the increase of the concrete strength. For structures with a concrete strength higher than 100 MPa, the predictions with the proposed evaluation procedure can overestimate the test results significantly. It shows that the fracturing of aggregate of high strength concrete has to be dealt with.

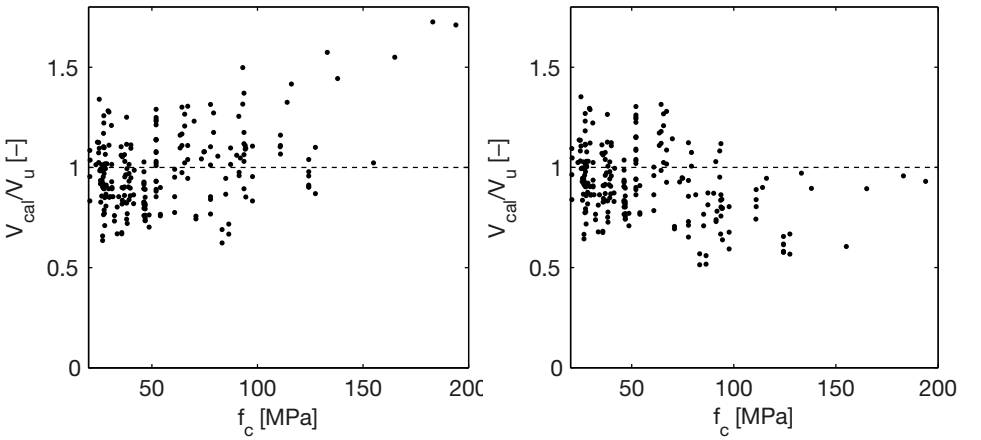

Fig. 4.16. Influence of concrete strength to the shear capacity prediction. (left: without aggregate fracture correction, right: with aggregate fracture correction).

As was already pointed out before, the reduction of aggregate interlock action in high strength concrete can be explained as follows. In high strength concrete structures, the course aggregates fracture together with the cement matrix. Because of the fracture of aggregate, the amount of additional contact area within the crack that can be used to generate aggregate interlock is reduced. In Eq. (3.30) this is expressed by A_x and A_y. Thus, the influence of aggregate fracture to aggregate interlock action can be counted as a reduction of A_x and A_y.

For a rough cracked surface, it is logic that the values of A_x and A_y are related to the crack roughness. Based on that consideration, an assumption is made here to take into account the reduction of contact surface due to aggregate fracture. It is assumed that the value of A_x and A_y are proportional to the additional area due to the roughness R_s-1. When the cracked surface is perfectly smooth (R_s-1 = 0), no aggregate interlock action is possible. Assuming that the fracture of aggregates occurs when the concrete strength is larger than 65 MPa (according to the regression analysis explained later), the values of A_x and A_y are reduced by a factor R_a.

$$R_a = \frac{R_s - 1}{R_{s0} - 1} \tag{4.11}$$

Regarding the roughness index R_s, the test results of Perera & Mutsuyoshi reported in (Perera & Mutsuyoshi 2013) are employed as a preliminary analysis. Since they did not test any cracked surface between f_c = 36 MPa and f_c = 81 MPa, it is not clear from which concrete strength the crack surface roughness starts to reduce, which is defined as the lower bound of the R_a-f_c reinlationship. Therefore, a regression analysis is carried out by assuming that only when the concrete strength is higher than the lower bound the course aggregate starts to crack. It shows that the lower bound of f_c when the R_s reduction starts from f_c = 65 MPa, with the increase of concrete strength, the roughness of the cracked surfaces can be estimated with the following equation (see Fig. 4.13):

$$R_s = \frac{7.2}{f_c - 38.86} + 1 \tag{4.12}$$

With Eq. (4.11) and Eq. (4.12), the value of R_a can be evaluated. Here, R_{s0} = 1.269 at f_c = 65 MPa. If f_c > 65 MPa, R_a is expressed by:

$$R_a = \frac{26.77}{f_c - 38.86} \tag{4.13}$$

Accordingly, Eq. (4.4) and Eq. (4.6) have to be updated by multiplying R_a with V_{ai}. With the correction of R_a, the data set presented in Fig. 4.16 (left) is

updated. The comparison of calculated shear capacity taking into account the aggregate fracture and the test results are plotted in Fig. 4.16 (right). Compared to the original formula, the tendency of overestimation of the shear capacity of beams of higher strength concrete is corrected.

The proposed method provides a workable evaluation procedure to take into account the reduction of the aggregate interlock effect with a proper physical background. However, it has to be remarked that the formula of the surface roughness index R_s was derived from cracks generated by splitting tests. The loading condition is not exactly the same as for the cracks generated in beams. Only one type of concrete mixture was used at each category of concrete strength. Besides, the amount of test date available is quite limited. Therefore, additional validations regarding a more realistic loading condition and a larger variety of concrete/aggregate types are still needed before the resultant regression formula can be applied in design practice.

Since the fracture of aggregate is not only related to the concrete strength but also the strength of the aggregate, while regarding the aggregate, a large variation can be expected. For example in the Netherlands, the fracture of aggregate only starts when f_c is larger than 80 MPa with glacial river aggregates, while according to Sherwood (Sherwood, Bentz et al. 2007) the influence of aggregate fracture starts from f_c = 60 MPa already. A safe strategy to handle this large variation is to simply limit the concrete strength to a constant value when the concrete strength is higher, in calculating V_{ai} with Eq. (4.7) or Eq. (4.4). That method has been applied in some design codes. In the Canadian Code, the concrete strength that is used to calculate the aggregate interlocking force cannot be higher than 64 MPa. The argument is that the shear force due to aggregate interlock does not increase with the increase of concrete strength when the strength of the cement matrix becomes stronger than that of the course aggregate. With that principle, the data collection presented above is evaluated. The calculated results using a limiting strength f_c of 45 MPa are shown in Fig. 4.17. When the concrete strength is smaller than 150 MPa this correction is quite effective. The mean value of V_{cal}/V_u becomes 0.99. However, the limiting strength of 45 MPa is a rather low value. An extensive study showed that it can be raised up to 60 MPa without influencing the overall accuracy significantly. In that case, the mean value of V_{cal}/V_u is 1.04.

However, only limiting the concrete strength to a constant value cannot fully cover the reduction of aggregate interlock caused by the reduction of contact area in crack generated in concrete with very high strength, as discussed previously. This has been shown in Fig. 4.17 already. As the concrete strength of the specimens becomes smaller (close to 80 MPa), the procedure with concrete strength limitation underestimates the test results. When the concrete strength is very high, it still overestimates the test results. The reductions of A_x, A_y and f_c

have to be taken into account as well. To achieve this further study on this topic is needed.

The calculation process presented within this section has not yet taken into account other effects such as the rebar configuration presented in the following sections. The limiting concrete strength may need further adjustment when the other aspects have been taken into account.

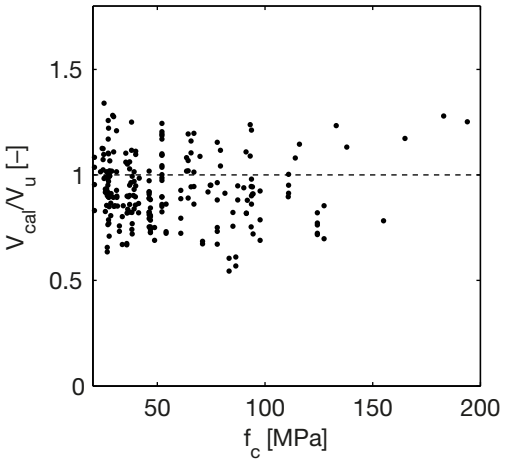

Fig. 4.17. Influence of concrete strength to the shear capacity prediction after limiting the concrete strength when f_c > 45 MPa.

Lightweight Aggregate Concrete

In the case of lightweight aggregate concrete beams, the strength of the aggregates is always lower than the cement matrix. Thus the crack surface will always develop through the aggregates. Comparative studies on the shear capacities of lightweight aggregate concrete beams and normal weight concrete beams have been carried out by Ivey and Buth (Ivey & Buth 1967), Taylor and Brewer (Taylor & Brewer 1963), and Hanson (Hanson 1961) in the 1960s; Walraven evaluated the size effect of LWA beams in (Walraven 1978). The comparative tests revealed that the overall shear capacities of beams with lightweight aggregate concrete are lower than those of normal concrete beams. The reported shear test data from the aforementioned literature have been collected as an additional shear database for LWA concrete specimens, see Appendix III. The reported shear capacity in the database is compared with the prediction by the proposed Δ_{cr} model in Fig. 4.18. As expected, the formula proposed in this chapter overestimates the shear capacity of lightweight aggregate specimens. The mean values of V_{cal}/V_u for lightweight concrete and normal concrete are 1.23 and 1.05 respectively.

Because lightweight aggregate breaks together with the concrete matrix, the cracked surface will not develop surrounding the unbroken aggregate-cement matrix interface, as was assumed by Walraven in (Walraven 1980). In that case, the shear resistance in the crack is mainly caused by the roughness on a meso-level of the crack surface as reported in (Sagaseta & Vollum 2011).

Thus, to take into account the effect of lightweight aggregate to the shear capacity of a beam, a similar strategy as used for high strength concrete beams is suggested. The principle is that the contact areas A_x and A_y shall be reduced in order to reflect the smoother cracked surface due to the fracture of aggregate. Based on the limited test results collected in this section, it is suggested to use a reduction factor R_a = 0.75 for the aggregate interlock effect in the LWA concrete. The comparison with test results with correction by R_a is shown in Fig. 4.18 right. The overestimation on the shear capacity of lightweight concrete members is improved. The mean value of V_{cal}/V_u is 1.09 after correction. It has to be mentioned that the reduction of aggregate interlock action is related to the type of aggregate. Therefore, the scatter in Fig. 4.18 is still large than for normal concrete beams. For a specific type of lightweight aggregate, additional tests may still be needed to obtain the corresponding R_a.

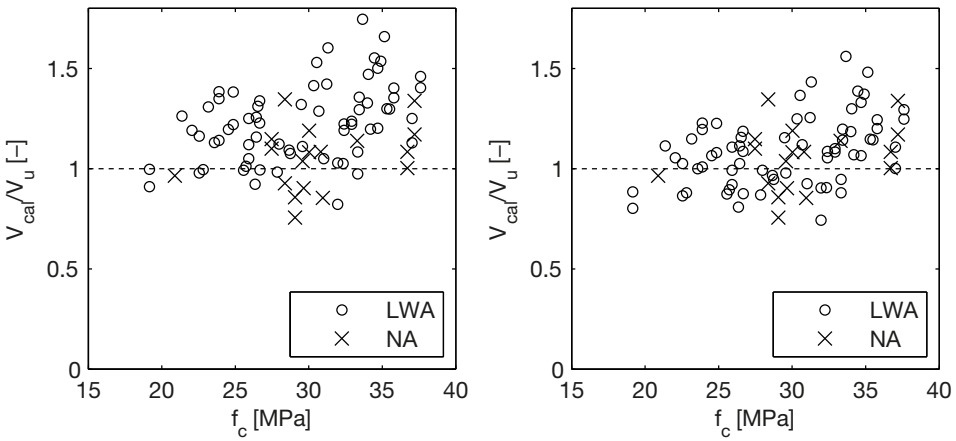

Fig. 4.18. Comparison of shear capacity prediction and experimental results. (left: before contact area correction, right: contact area corrected by a factor 0.75, LWA: lightweight aggregate concrete specimens, NA: normal aggregate specimens).

Moreover, the reason why a relatively larger R_a is chosen is that according to Fig. 4.8, a large proportion of the shear stress at a given shear displacement Δ is generated close to the tip of the major crack, where a relatively small crack width is expected. According to Walraven's aggregate interlock tests (Walraven & Reinhardt 1981), although the stress of aggregate interlock is significantly reduced at larger crack width, when w is small, the crack in LWA concrete can

still transmit a substantial portion of the shear stress compared to normal concrete with the same compressive strength and aggregate sizes. The LWA concrete specimens in his test program can carry about 66% of the shear stress compared to that of the normal concrete specimens at w = 0.1 mm. Further explanation on the regression analysis result will be given in section 4.7.2.

4.6 EFFECT OF REBAR DIAMETER ON CRITICAL SHEAR DISPLACEMENT

4.6.1 Leonhardt's Shear Tests with Varying Rebar Configuration

The effect of the longitudinal rebar to the shear behaviour of reinforced concrete beams is classically related to the tensile force in the rebar. Therefore, in almost all design methods so far, when the effect of the longitudinal reinforcement is concerned, it always appears through the reinforcement ratio $\rho = A_s/bd$. Examples are (CSA 2004; Eurocode 2 2004; fib 2012). An explicit explanation given by Collins et al. (Vecchio & Collins 1986; Bentz, Vecchio et al. 2006) is that the tensile deformation of the longitudinal rebar governs the flexural crack width, which influences the aggregate interlock contribution to the shear force across the crack. A higher reinforcement ratio means a smaller crack width under the same cross sectional moment, and eventually a larger shear capacity. That consideration leads to the conclusion that as long as the reinforcement ratio of a beam remains constant any variation of the reinforcement configuration will not affect the shear behaviour of the beam.

That conclusion has been proven to be wrong experimentally by Leonhardt (Leonhardt & Walther 1962; Leonhardt 1978). He carried out a comparative study on two beams with the same reinforcement ratio ρ_s = 1.88%, but different rebar configurations, EA1: 2Ø24 + 1Ø16; EA2: 2Ø14 + 3Ø16. The shear capacity found for specimen EA2 is about 28% higher than that was found for EA1. A similar trend has been observed in tests on slab specimens of the same reinforcement ratio but with different reinforcement configurations, see Fig. 4.19.
Considering the fact that all the other configurations of the specimens are identical in the test series, the increment of the shear capacity cannot be explained with a theory only involving the total area of the longitudinal reinforcement. Leonhardt attributed this effect to the bond between reinforcement and concrete. He explained that rebars with smaller diameters have better bond, thus smaller crack spacing and a smaller crack width. As a result, the larger aggregate interlock force leads to a larger shear capacity. However, direct observation of the crack pattern does not show a clear difference between the specimens. Moreover, the paradox with this explanation is that if it is the larger bond strength between rebar and concrete that improves the shear capacity of

the specimens, it is not possible to explain that in the same test series, the specimens with plain bars had an even higher shear capacity than the rest. In Table 4.1, it is shown that the two specimens EB1 and EB2 with plain bars are more than 30% stronger than EA2. From these two test results totally contradictory conclusions can be drawn.

The difficulty in explaining the experimental findings comes from improper understanding of the shear failure mechanism. Apparently, other than the two mechanisms discussed in this section, the rebar diameters influence the shear failure process through other mechanisms.

Table 4.1. Test results Leonhardt's tests with varying reinforcement configuration. Translated from (Leonhardt & Walther 1962).

Test No.	Reinforcement Configuration	ϕ_{eq}[1] [mm]	ρ_s [%]	a/d [-]	d [mm]	$f_{cm,cube}$ [MPa]	P_u [kN]	V_u [kN]
EA 1	2Ø24 + 1Ø6	22.1	1.89	2.78	270	24.6	116.6	58.3
EA 2	2Ø14 + 3Ø16	15.1	1.88	2.78	270	24.6	149.0	74.5
EB 1	2Ø25	25.0	1.91	2.78	270	24.6	226.4	113.2
EB 2	5Ø14 + 1Ø16	14.4	1.88	2.78	270	24.6	198.0	100.0

[1] ϕ_{eq} is the equivalent diameter of the reinforcement configuration, $\phi_{eq} = \sum \phi^2 / \sum \phi$. ϕ is the diameter of each rebar.

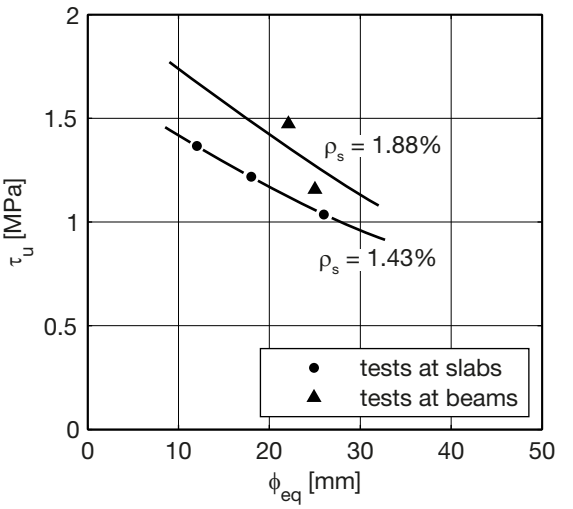

Fig. 4.19. Influence of diameter and spacing of bars on shear strength of beams with the same reinforcement ratio, adapted from (Leonhardt 1978).

4.6.2 Influence of Rebar Diameter on Δ_{cr}

With the procedure introduced in this study, the difficulties in explaining the effect of longitudinal rebar configuration can be solved. As presented previously, although the contribution of the dowel force is not dominating the shear resistance, the failure of the whole specimen is strongly related to the development of the dowel crack along the longitudinal reinforcement. The longitudinal rebars are not only influencing the aggregate interlocking effect which largely contributes to the shear resistance, but certainly affect locally the dowel cracking process along itself as well. As explained before, during the development of the dowel cracking process, the maximum shear force is determined by the concrete tensile strength f_{ct}, so that it remains more or less constant. On the other hand, the critical shear displacement Δ_{cr} is influenced by the reinforcement configuration.

Considering the simplified energy balance equation Eq. (3.38) shown in Chapter 3, under the same crack length λ, the energy release length is not only related to the area of the reinforcement but also to the bending stiffness of it. The larger the rebar diameter, the larger energy releasing rate is expected. Consequently a smaller crack width is needed to get the crack developed. Considering that the items relating to the crack widths are quadratic terms, it is reasonable to relate the actual critical vertical displacement to a function of ϕ^2 and ϕ.

As explained before, because of the complex nature of the problem, it is not possible to derive an accurate analytical solution directly through the energy principle. A more practical solution is to evaluate the vertical displacement from executed test results. To serve that purpose, a different selection of data compared to the ones used in the preceding sections is used here. The database is based on a selection of published test results from the database of Reineck (Reineck, Bentz et al. 2013), in which the configuration of the longitudinal reinforcement of the tests are reported. The selection is based on the diameter size of the longitudinal reinforcement. All the tests with only a single type of rebar are placed into one group. The shear slenderness ratios of the specimens are at least 3.0. The selected tests are subdivided into several groups with rebar diameter of 12 mm, 16 mm, 22 mm, 25 mm, 28 mm, and 32 mm, among which the group with Ø25 mm rebar includes most tests. It has 92 tests out of the total 312 selected test results.

Following the procedure presented in Section 4.3, the shear displacements Δ at the failure loads of each test are calculated. Fig. 4.20 shows the results of the group of beams with Ø25 mm bars. As revealed in Section 4.3, the values of Δ_{cr} are related to the depth d of the specimens. Only comparing the test result of beams with one size of diameter, this trend is much more pronounced. Similar results are observed in the other groups as well. To eliminate the effect of d, the

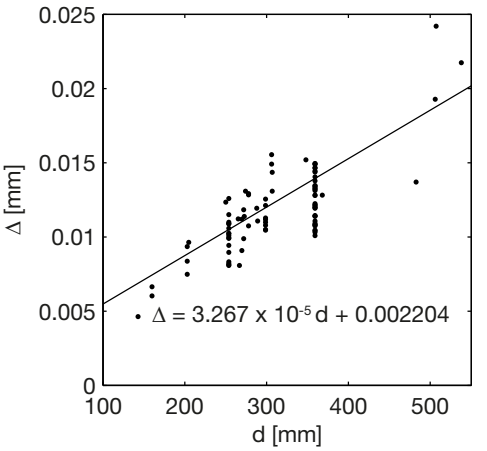

Fig. 4.20. Relationship between beam height d and critical shear displacement Δ_{cr} for beams reinforced by Ø25 bars.

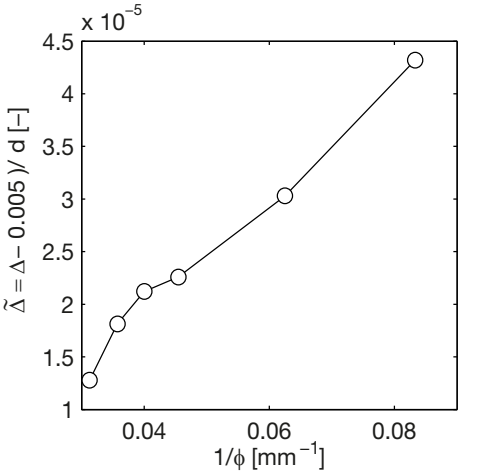

Fig. 4.21. Relationship between rebar diameter and critical shear displacement Δ_{cr}.

calculated value Δ_{cr} is first normalized with Eq. (4.9). Within each rebar size group, the mean values of the **normalized shear displacement** $\tilde{\Delta}$ are evaluated. They are plotted against $1/\phi$ in Fig. 4.21. The influence of rebar diameter on the critical vertical displacement is clearly revealed. Considering the scatter of the test results, a linear relationship is sufficient to evaluate the influence.

Apparently the influence of rebar diameter cannot be ignored. Hence, the derivation process presented in Section 4.3 has to be revised. The rather large scatter of Δ shown in Fig. 4.11 can partly be attributed to the ignorance of the rebar diameter. The accuracy of the prediction can be greatly improved if one can introduce the influence of the rebar diameter. However, a large portion of the reported test beams are reinforced by multiple sizes of rebars. To limit the possible influence from unexpected variables, instead of including all the tests with different rebar types, it is better to evaluate tests on beams only comprising one size of reinforcing bar, and extend the results to the other rebar sizes. Based on that consideration the test group with Ø25 mm rebars is chosen, since it includes the largest number of tests within the test data base. A regression analysis for the group of beams with rebar diameter Ø25 mm gives the following relationship:

$$\begin{aligned} \Delta_{cr,25} &= 3.267 \cdot 10^{-6} d + 0.002204 \\ &= d \,/\, 30610 + 0.0022 \end{aligned} \tag{4.14}$$

With the relationship between the normalized critical shear displacement $\tilde{\Delta}$ and rebar diameter $1/\phi$ shown in Fig. 4.21, Eq. (4.14) can be extended to:

$$\Delta_{cr} = \frac{25d}{30610\phi} + 0.0022 \leq 0.025 \text{ mm} \tag{4.15}$$

where

d : is the effective height of the beam;
ϕ : is the diameter of the longitudinal reinforcing bars.

In the case that there is more than one size of steel bars in the same beam, one may use the equivalent diameter suggested by Leonhardt (Leonhardt & Walther 1962). Before a more sophisticated relationship is derived, it offers sufficient information on the rebar configuration further than the total area A_s.

$$\phi_{eq} = \sum \phi_i^2 \,/\, \sum \phi_i \tag{4.16}$$

Once more detailed information of the longitudinal reinforcement is available, Eq. (4.9) recommended in section 4.4.1 should be replaced by Eq. (4.15). To compare the difference with between the two methods, the test results of the selected tests database shown previously are calculated with both Eq. (4.9) and Eq. (4.15). The ratio between the calculated shear capacity and the measured results of each rebar group are summarized. The mean prediction of each rebar group and their standard deviation are plotted against the rebar diameter in Fig. 4.22.

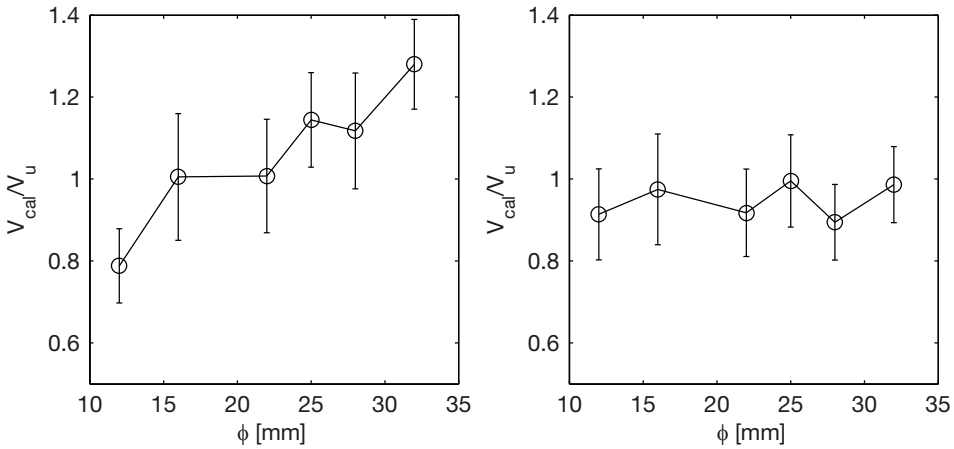

Fig. 4.22. Comparison between prediction accuracy with Eq. (4.9) (left) and Eq. (4.15) (right).

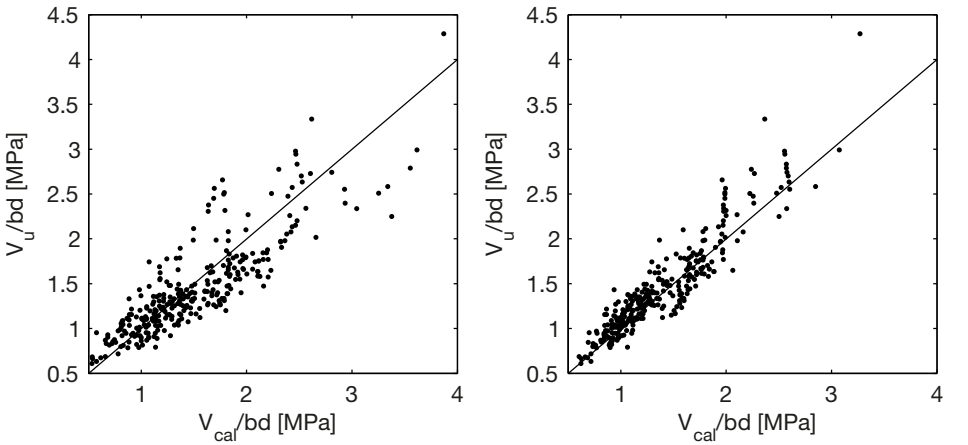

Fig. 4.23. Comparison of predicted and tested shear strength with Eq. (4.9) (left) and Eq. (4.15) (right).

The comparison with the original evaluation procedure clearly shows that the predicted shear capacity is strongly dependent to the rebar diameter, while by introducing Eq. (4.15) the mean values of the V_{cal}/V_u in each rebar diameter group all move to values close to 1.0. In the other words, they may be considered to be independent of the rebar configuration with that correction. Besides, the scatter within each rebar diameter size group is significantly improved. With respect to the overall performance, the introduction of Eq. (4.15) significantly improves the accuracy of the prediction. The COV calculated from the database comprised by all the rebar diameter size groups used within this section improves from 18.2% to 12.3%. The difference regarding the prediction accuracy can be directly observed through the comparison of predicted shear stress and measured ones in Fig. 4.23.

Considering the limit concrete strength discussed in Section 4.5.2 for high strength concrete, by comparing the test results of the database with the procedure implementing the improved evaluation procedure, it is confirmed that the limit concrete strength of 60 MPa is able to provide more accuracy rather than 45 MPa as was suggested in Section 4.5.2. In Section 4.5.2, the lower limit strength is probably because of the influence from rebar configuration in the selected test series. Even in that case, 60 MPa is still an acceptable value. Thus, overall speaking, to take into account the effect of high strength concrete it is more appropriate to adopt a limit strength f_c = 60 MPa.

Taking into account the reinforcement configuration in the critical shear displacement Δ_{cr}, Leonhardt's test series introduced at the beginning of this section is reviewed. The new calculation procedure makes it is possible to explain the difference between the tests. The predicted shear capacities of EA1 and EA2 are

126.9 kN and 142.7 kN respectively. The ratio between the calculated capacity and the tested ones are 1.09 and 0.95 respectively. Regarding the plain bars, as suggested by Muttoni in (Muttoni & Ruiz 2008) their bond capacities are so low that it is not possible to generate a critical crack with its tip outside a_{cc} described by Eq. (3.44) in Chapter 3. Similar to beams with smaller a/d ratio, in that case the contribution of V_c is significantly increased. Thus the formula cannot be applied directly anymore. This effect will be discussed further in the next chapter. Other than that, the effect of bond strength is quite limited.

As discussed in Section 4.4.2, to compare the accuracy of the adjusted evaluation method with the original one at the same level, a different set of test results has to be used for evaluation. Therefore the database of König and Fischer discussed in Section 4.4.2 is adopted again to be evaluated with the adjusted method. The result is plotted in Fig. 4.24, which can be compared with the results plotted in Fig. 4.12. The only difference is that in Fig. 4.24 the test series reported by Bažant in (Bažant & Kazemi 1991) has been discarded. In their tests, a very unconventional rebar configuration has been used. When more than one type of rebar is used in the specimen, Eq. (4.16) is used. Compared to the original method, the COV of V_{cal}/V_{test} has been significantly improved to 12.2%. With the same dataset, the COV of V_{cal}/V_{test} calculated by Eurocode formula without limitation is 13.1%, which was the best predict before the method proposed here was developed.

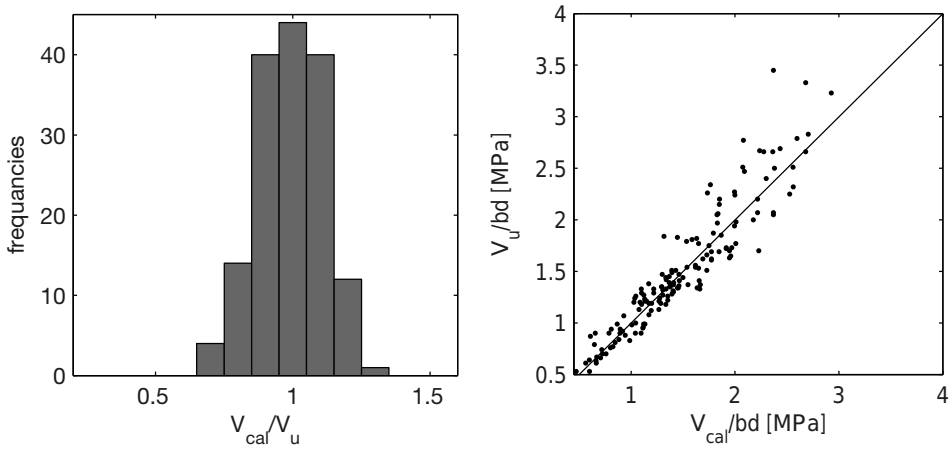

Fig. 4.24. Comparison of predicted shear force and test results based on König and Fischer's database taking into account the rebar configuration.

4.7 EFFECT OF BEAM DEPTH ON SHEAR CAPACITY

4.7.1 Size Effect in Shear Failure of Concrete Members

Scaling has been widely applied in engineering practice and scientific research (Barenblatt 1996). It intends to enable the extension of experimental results derived through experiments within limited conditions to much wider applications. In structural analysis, the calculations of the capacity of a structural member are usually based on the strength of the material of the member, which is considered to be a material property, and therefore independent of the size of the structure. That hypothesis enables the scaling relationship in structural analysis. Thus, it is possible to up-scale the test results from small scale lab tests to big scale structures.

However, the shear capacity of concrete beams without shear reinforcement has been proven to be one of the exceptions of the preceding hypothesis. In the 1960s, Leonhardt and Walther (Leonhardt & Walther 1962) investigated the shear capacity of concrete beams of different scale regarding to all the dimensions. They observed that the scaling-up of the beam specimen will reduce the equivalent **nominal shear strength** ($\tau = V/bd$) of the specimens at failure. Kani showed further through experiments (Kani 1967) that it is the depth that influences the equivalent nominal shear strength. What has to be mentioned is that Kani concluded that the width does not influence the shear strength based on results from specimens with a width of maximum 0.6 m. As will be shown later in Chapter 6, the influence of specimen width becomes pronounced in specimens with a much larger width due to the variability of the material. Besides, neglecting the influence of width is at the safe side, thus it is not discussed in this section. In this section, the term **size effect** only stands for the influence of specimen depth to the average cross sectional shear strength of concrete beams. More experimental proof of the effect of beam height has been observed even since (Walraven 1978; Chana 1981; Shioya 1989; Bažant & Kazemi 1991; Collins & Kuchma 1999). Without a clear image on the size effect relationship, the up-scaling strategy widely applied in structural design will result in a dangerous situation when it is applied in calculating the shear capacities of large scale structures. For that reason, research has been carried out to explore the reason for it and to determine the scaling relationship regarding the effective height of the beam. Some of the theories on size effect of shear capacity are presented here.

Statistical Size Effect

Since the shear flexural failure was attributed to the tensile stress reaching the tensile strength in the diagonal direction (see the discussion in Section 2.1).

Following the analysis of uniaxial tensile tests (Kittl & Díaz 1988; Carpinteri 1989; Kittl & Díaz 1990), the size effect in shear capacity was firstly related to Weibull's theory, also called the Weakest Link Theory (Weilbull 1951). It attributes the influence of beam height to the statistical distribution of concrete strength. Assuming more defects due to a larger beam height results in a lower nominal shear strength of the beam. It was shown by Walraven (Walraven 1978) that it is not possible to apply the same rule derived from Weibull's theory to describe both flexural shear failure and tension failure. This conclusion was also confirmed by Bažant in (Bažant et al. 1991). They showed that the size effect of flexural shear failure observed in tests is stronger than what is predicted by Weibull's theory. Besides, the stress redistribution due to the tension softening behaviour of concrete is different from the assumption of Weibull's theory.

Size Effect from Fracture Mechanics

The other classical theory of size effect comes from Linear Elastic Fracture Mechanics, according to which the crack opening criterion is the energy release rate along the crack, rather than the stress. Dimensional analysis of the main variables involved in the formulation shows the following relationship (Barenblatt 1996):

$$l = \text{const}\,\frac{K^2}{\sigma^2} \tag{4.17}$$

where

- l : is the characteristic length of the structure, with unit: m;
- K : has the same unit of fracture toughness: $N/m^{3/2}$, and can be considered as material property in LEFM such as: K_{IC} or $(EG_f)^{1/2}$.
- σ : is the stress at unstable crack development, with unit: N/m^2.

Eq. (4.17) shows that the critical stress of a structure is related to the square root of the specific dimension of the structure. This relationship can be derived through other approaches as well, see (Bažant 2005).

However, experimental results show that such a relationship holds true only for very large structures or very brittle materials such as ceramics, which can be approximated with LEFM. For quasi-brittle materials like concrete, there are residual tensile stresses in the cracks even for relatively large crack widths: therefore the idealization is not applicable anymore for structures with normal size. K cannot be considered as a constant anymore.

Experimental evidences show that the tension softening property of concrete plays an important role in the propagation of cracks in beams under shear loading. A notable experimental proof followed from the size effect tests carried

out by Walraven in (Walraven 1978). Walraven marked the crack patterns of the three specimens from the same test series with different beam heights at the same nominal shear stress, among which, the crack patterns of beams in A series at τ = 0.42 MPa are plotted in Fig. 4.25, where it is shown that although the configurations of the three specimens are strictly scaled in the test series, the difference among the crack patterns are remarkable. This can be explained by the fact that although the strain gradients along the cross sections of the beams are comparable, the scaled tensile deformation dose not result in the same cracking. The strain criterion for the fracturing of concrete is always constant. Accordingly, due to the fracturing of concrete, the stress redistributes in the beams, and consequently the overall behaviour of the beams deviates.

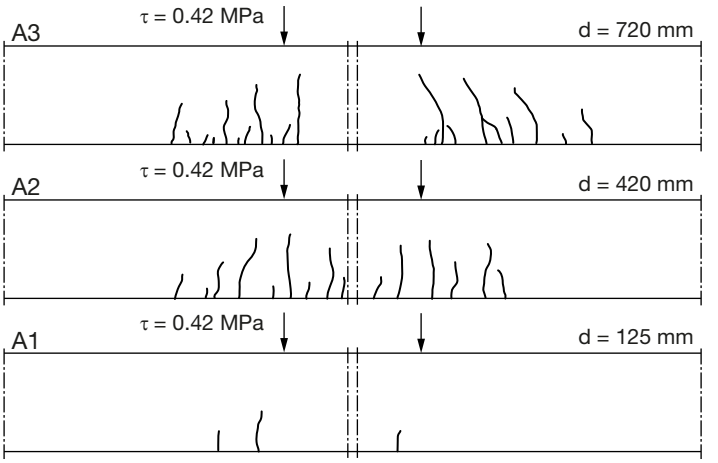

Fig. 4.25. Comparison of the scaled crack patterns for beam A1, A2 and A3 at τ = 0.42 MPa (Walraven 1978)

However, the shear failure of concrete beams is a more complex process comprising several different mechanisms rather than the fracturing process of the inclined crack alone. One of the efforts to describe this complex behaviour is from Bažant. He tried to bridge the gap between the theoretical expression from LEFM and experimental observations with a transitional scaling relationship between LEFM and strength criteria through regression analysis, see Fig. 4.26. Accordingly, a size effect relationship for shear capacity was proposed in (Bažant & Kim 1984; Bažant & Yu 2005; Bažant & Yu 2005):

$$\tau_u = \frac{1}{\sqrt{1 + d / d_0}} \tau_c \tag{4.18}$$

Where d_0, τ_0 are constants from regression analysis.

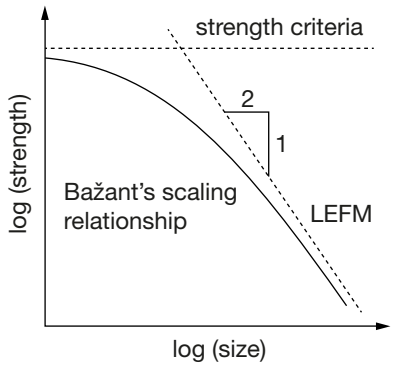

Fig. 4.26. Illustration of Bažant's transitional scaling effect relationship (Bažant 2005).

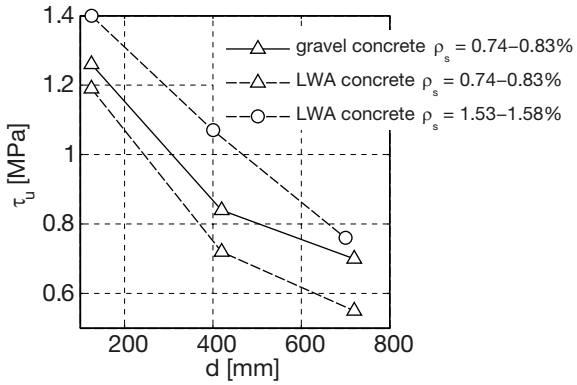

Fig. 4.27. Results of Walraven's size effect test on gravel and light-weight aggregate concrete, adopted from (Walraven 1978).

The procedure improves the first question regarding the LEFM approach. In fact, although Eq. (4.18) was initially based on the assumption that only the residual tensile strength is the reason of this size effect relationship, the regression analysis implicitly covers the effect of all the other mechanisms acting during shear failure as well. However, as shown before, the shear failure of concrete beams is the consequence of several mechanisms. To derive a single scaling relationship covering the size effect of shear strength due to several failure mechanisms with probably different scaling relationships is a fundamental challenge.

Size Effect from Aggregate Interlock

Another explanation of the size effect of shear strength comes from the Modified Compressive Field Theory as proposed by Collins and Vecchio (Vecchio & Collins 1986), which has been introduced in Chapter 2. They suggest that the shear capacity of concrete beams is related to the aggregate interlock effect in a crack. Thus the average width of the inclined crack w determines the size effect of shear strength. The crack width is expressed by $w = l_{cr,m} \cdot \varepsilon_x$ where $l_{cr,m}$ is the crack spacing in the beam. For beams with only longitudinal reinforcement at the tensile side, $l_{cr,m}$ is assumed to be equal to the internal lever arm of the beam z, which is further assumed to be $0.9d$. In this way the shear strength of the beam is related to the beam depth implicitly. The calculation was simplified further in the Simplified Modified Compressive Theory proposed by Bentz, Vecchio et al. in (Bentz, Vecchio et al. 2006), where, the longitudinal strain ε_x and crack spacing $l_{cr,m}$ are separated in Eq. (2.8). According to Collins and Kuchma (Collins & Kuchma 1999), the size effect of shear strength can be attributed to $l_{cr,m}$ in Eq. (2.8). They proved that supposition by comparing beam tests with distributed

longitudinal rebars over the beam depth. By using the rebar space $l_{cr,m}$ as the variable instead of the beam depth $0.9d$, they got a strong correlation between $l_{cr,m}$ and the measured τ_u. In the next section, the relationship between the crack width and the size effect will be elaborated in another way giving slightly different results.

However, following the theories relating the size effect of shear strength solely to aggregate interlocking, one may expect that once the aggregate interlock action is eliminated, the size effect is eliminated as well. To evaluate the influence of aggregate interlock to size effect, Walraven studied the size effect of shear beams with both normal concrete beams and Light-Weight Aggregates (LWA) concrete beams in (Walraven 1978). It was expected that in the LWA concrete beams, the fracture of the course aggregates reduced the contact area in a given crack, thus decreasing the stresses generated by aggregate interlock. Expectedly the size effect in LWA concrete beams should be less pronounced. The results of the tests are given in Fig. 4.27. It clearly shows that LWA concrete beams follow almost the same scaling relationship as normal concrete beams. The experimental observation turns out to be in conflict with the preceding conclusion deducted from the theory. Another experimental evidence is the shear tests series carried out by Chana (Chana 1981). In his specimens, the aggregate sizes were scaled with the beam height as well. Nevertheless, a similar scaling relationship was found in his tests. This shows indirectly that the size effect of shear strength is a comprehensive effect due to more than one type of mechanism related to the beam size.

Empirical Approaches

As shown above, a generally accepted rational explanation on the size effect of shear strength is not available yet. Consequently, regression analysis has been widely carried out by researchers based on the large amount of test results reported in literature, from which empirical formulas have been derived. The basic assumption behind these methods is that it is possible to derive a scaling relationship for the size effect of shear strength. Those formulas have been widely used in design codes. The scaling relationships of several typical formulas are listed in Table 4.2.

In Table 4.2, the scaling relationships in the empirical formulas are significantly different from each other. This can be explained by the fact that they were derived from different data collections. However, since totally different relationships can be concluded from different data collections, the question may be raised: whether it is possible to derive a specific scaling relationship separately in the shear formula? The other aspect is that as shown in Section 2.4, the majority of the test results in literature are laboratory tests on beams with relatively small depths. Therefore, as long as the empirical formulae are able to calculate

the shear capacity of those small scale beams, it gives good regression accuracy in general. The size effect relationship may be easily suppressed with such types of database. That problem has been addressed in Section 2.4 previously.

Table 4.2. Empirical scaling relationship of size effect.

Formula	Eurocode[1]	Rafla[2], Niwa[3]	Bažant[4]	Remmel[5]
Scaling Relationship	$1 + (d/200)^{-1/2}$	$d^{-1/4}$	$(1 + d/d_0)^{-1/2}$	$d^{-1/3}$

[1] Eurocode formula from (Eurocode 2 2004);
[2] Rafla's regression formula from (Rafla 1971);
[3] Shear Formula from Niwa et al. (Niwa et al. 1987), it is also used in JSCE code;
[4] Bažant's size effect relationship from (Bažant & Kim 1984; Bažant & Yu 2005; Bažant & Yu 2005);
[5] Regression formula from Remmel's work in (Remmel 1992).

4.7.2 Size Effect according to Δ_{cr} Model

It was shown in the preceding subsection, that the procedure of deriving a simple scaling relationship and multiplying it to the shear strength is not appropriate to cover the mechanisms with different scaling relationship. Understanding the mechanisms behind it seems to be critical to solve the riddle of the size effect. On the other hand, the good agreement shown in the comparison with the test database in Section 4.4.2 and 4.6.2 indicates that within the shear evaluation method presented in this chapter, the influence of depth has already been integrated. It partly confirms that the theory reflects the reality properly without additional adjustment needed. Since an explicit expression of the scaling effect is not present in the theory, the task of this section is to find out the causes of the size effect within the scope of the shear evaluation procedure explained previously.

The calculation procedure as explained in section 4.4.2 subdivides the total shear capacity V into the three parts V_d, V_{ai} and V_c. The influence of beam effective height d to them will be explained separately. In addition, the role of the tension softening behaviour of concrete in the model is discussed in the end.

Concrete Compressive Zone

The shear force carried by the compressive zone V_c is not subject of a size effect. The two terms in Eq. (3.26): z and z_c are both related to the beam depth d, thus they are eliminated. Assuming a linear normal stress distribution in the compressive zone and simplifying Eq. (3.2) into $s_{cr} = k_{cr}d$, Eq. (3.26)is simplified into:

$$V_c = \frac{2(1-k_{cr})}{2+k_{cr}} V$$

with

$$k_{cr} = 1 - 1.05(\rho_s n_e)^{0.45}.$$

Since k_{cr} is independent of d, the term V_c can be eliminated from Eq. (3.20), so it becomes

$$\frac{3k_{cr}}{2 + k_{cr}} V = V_{ai} + V_d \tag{4.19}$$

Therefore, although the height of the compressive zone is related to the beam depth, the shear force transferred within the compressive zone is independent of beam depth for slender beams.

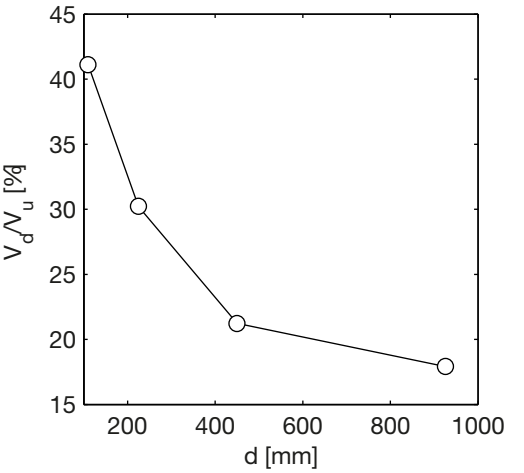

Fig. 4.28. The influence of beam depth on the contribution of dowel action in the ultimate capacity as reported by (Collins & Kuchma 1999).

Dowel Action

The dowel action term V_d expressed by Eq. (3.28) is independent of the beam depth. However, because of that, a different scaling relationship should be considered when the shear strength is concerned. In that case, the shear strength contributed by dowel action τ_d is related to d^{-1}:

$$\tau_d = \frac{V_d}{bd}$$

For the shallow beams in the size effect tests, like the smallest specimens in the tests reported in (Kani 1967; Bažant & Kazemi 1991; Collins & Kuchma 1999), the effect of dowel action can be pronounced. As an example, the BN series test reported by Collins and Kuchma are regarded. The widths of the specimens are

all 300 mm, and the depth varied from 110 mm to 925 mm. Assuming that Eq. (3.28) predicts the dowel force accurately, the percentage of V_d to the total measured shear capacity V_u changes significantly, see Fig. 4.28.

Aggregate Interlock

Compared to the other components, the role of aggregate interlock is much more complex. In the design method, a relatively accurate estimation of the shear force generated by aggregate interlock should be calculated by integrating the shear stress generated at the critical shear displacement Δ_{cr} and the normal crack opening w with Eq. (4.4). Since the normal crack opening at failure is unknown beforehand, an iteration process is required to determine the ultimate capacity. The complex process makes it almost impossible to determine the influence of beam depth explicitly.

In principle there are several effects involved in the mechanism. To clarify the effect of beam depth some simplification is made, in order to demonstrate the influence of beam depth clearly.

First of all, when the crack width is involved in the formulation of the shear capacity, the beam depth is automatically included. This conclusion is given in (ACI Committee 446 1989). It can be illustrated in a simplified way. Most experimental observations show that the shear stress in the crack is inversely proportional to the crack width. In the most simplified manner, the shear stress by aggregate interlock can be expressed as:

$$\tau_{ai} = \frac{w_0}{w}\tau_0 \tag{4.20}$$

On the other hand, the crack width is expressed by Eq. (4.10). Since both z and l_{cr} in the equation are proportional to d, Eq. (4.10) is simplified into:

$$w = \frac{M_d}{zA_sE_s}l_{cr,m} = \frac{l_{cr,m}}{zE_s}\frac{Vd\left(\frac{M}{Vd}\right)}{bd\rho_s} = \text{const}\frac{V}{E_sb} = \text{const}\frac{d\tau}{E_s} \tag{4.21}$$

The relationship between crack width and beam depth holds for most slender beams with reasonable beam height. Assuming that aggregate interlock is the only cause of shear resistance ($\tau = \tau_{ai}$), combining Eq. (4.20) and Eq. (4.21) leads to the conclusion that the shear stress τ is related to the square root of the beam depth d: $\tau \sim d^{-1/2}$. Because the crack width is related to the total shear force rather than the shear stress, as long as it is included in the formulation of the aggregate interlock force, the effect of beam depth d will always be included.

However, the actual expression for the aggregate interlock force is more complex than the simplification in Eq. (4.20). As shown in this chapter, the shear force carried by aggregate interlock is calculated by integrating the shear stress generated along a crack with a certain crack opening and shear displacement combination. Although it is possible to estimate the shear force generated by aggregate interlock in a simplified expression, it is still not possible to separate the scaling relationship from the final expression. As was demonstrated before, this approach is helpful either. Nevertheless it is still useful to discuss how the aggregate interlock force is influenced by the beam depth.

First of all, as illustrated by Eq. (4.21), the crack width is proportional to the beam depth. With the linear crack width distribution as proposed in section 4.2.1, the shear stress distribution over the crack height does not change with the crack width in principle. A larger crack width at the tensile side only causes an additional part of the shear stress to crack width curve approaching zero. Because the peak of the shear stress at the crack tip of the major crack remains unchanged, the total shear force due to aggregate interlock largely concentrates at the part of the major crack close to the tip, see Fig. 4.29. For beams with a larger depth, their crack widths at the tensile side increase proportionally, nevertheless, most of the shear force due to aggregate interlock is generated at a certain distance from the

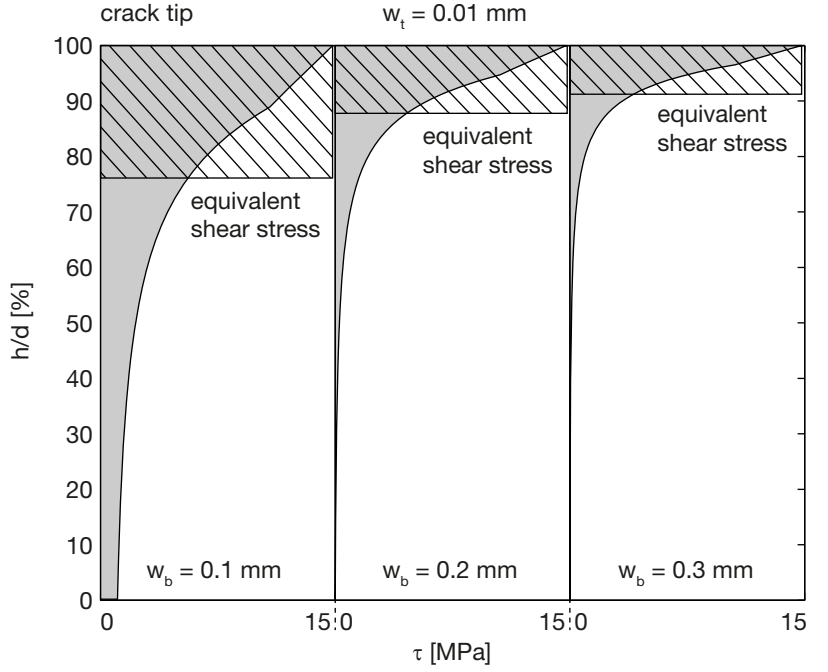

Fig. 4.29. Shear stress distribution calculated from different crack width at the tensile side (w_b = 0.1 mm, 0.2 mm and 0.3 mm respectively, Δ = 0.02 mm, f_{cm} = 40 MPa).

crack tip. It can be defined as the characteristic length l_0, where the crack width at the end of l_0 is $w = w_0$. When w_0 is more or less fixed, the characteristic length from the crack tip is also constant because of Eq. (4.21). Therefore, it is the shear stress distributions close to the crack tip that results in the size effect.

That also explains the observation by Walraven in (Walraven 1978) and Chana in (Chana 1981). The performance of aggregate interlock within l_0 is critical to the size effect relationship. According to Walraven's aggregate interlock test in (Walraven & Reinhardt 1981), the influence of maximum aggregate size is limited at small crack width. Although the minimum crack width w in his tests was limited at w = 0.1 mm, the extension of this conclusion to cracks with even smaller crack width is a realistic assumption regarding the already observed shear stress development for cracks with larger crack width to smaller crack width. Therefore whether or not the aggregate size is scaled with the specimen size, does not influence the size effect relationship of the whole structural member. Regarding the LWA concrete beams, it has discussed in Section 4.5.2, according to Walraven's tests (Walraven & Reinhardt 1981) the shear stress that is generated in cracks of the LWA concrete is not significantly reduced comparing to that of the normal concrete when the crack width is small. At w = 0.1 mm, Δ = 0.15 mm, the experimental observation shows that the τ_{ai} of LWA concretes is about 0.66 times that of normal concrete. A smaller crack width w may even lead to a higher ratio. That also confirms the reduction factor 0.75 applied on V_{ai} for LWA concrete in section 4.5.2, where the value of the reduction factor was derived from regression analysis. Therefore, the application of LWA concrete will not eliminate the size effect due to aggregate interlock either. The size effect of LWA concrete beams can still be explained with the theory presented here.

Another important aspect affecting the aggregate interlock effect is the critical shear displacement Δ_{cr}. The calibration with test results in section 4.3.2 shows that the value of Δ_{cr} should depend on the beam depth as well to correct the error introduced by the simplification of the crack width distribution. Without a correction of the critical shear displacement, the shear stress distribution overestimates V_{ai} in beams with smaller depths, thus enlarging the size effect relationship. This effect is illustrated in Fig. 4.30. In addition, according to section 4.6.2, the rebar configuration needs be taken into account as well when calculating Δ_{cr}. However, the rebar configuration was not always of consideration in the size effect tests for practical reasons. The choice of the rebar configuration when designing the test specimen influences the ultimate shear capacity, and as a result, the size effect relationship derived might be influenced as well.

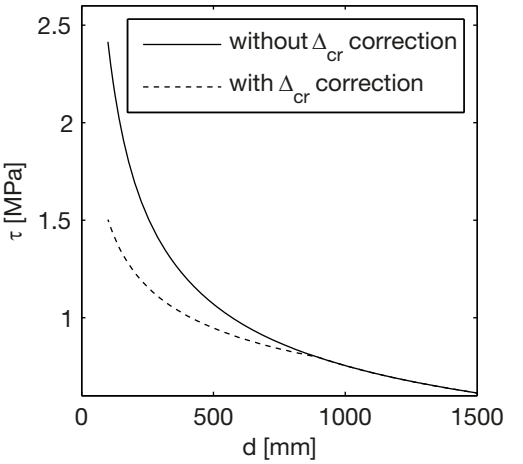

Fig. 4.30. Influence of Δ_{cr} correction on the size effect relationship (f_{cm} = 40 MPa, M/Vd = 3.0, ρ_s = 0.9% with 3 rebars).

Tension Softening

By far the size effect of flexural shear failure of reinforced concrete beams can already be properly described with the aggregate interlock and dowel action in a cracked section of a beam. Nevertheless, the tension softening behaviour of concrete, which is proven as the reason for the influence of beam height to the propagation of cracks (see Fig. 4.25) is still of importance in the model.

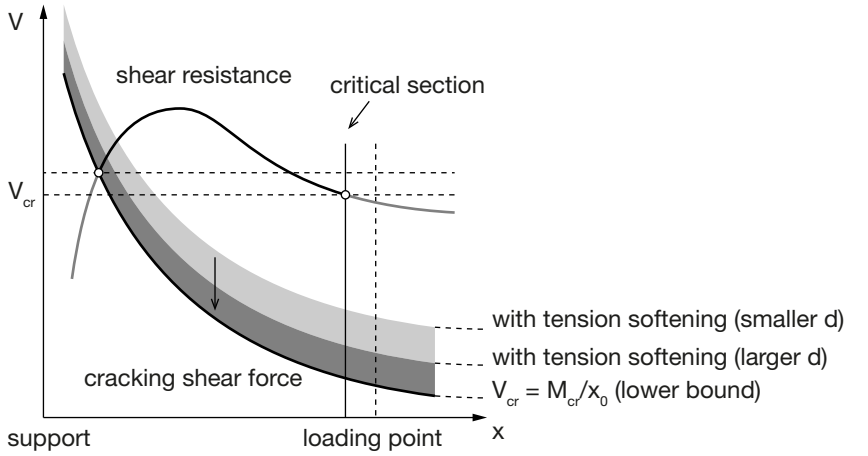

Fig. 4.31. Determination of shear resistance taking into account tension softening.

The effect of tension softening to the shear capacity of concrete beams can be explained with Fig. 4.31 adopted from Fig. 3.38 in Section 3.4.3:

First of all, the tension softening behaviour of concrete influences the propagation of the major cracks, which has been shown in Section 3.2.1. A beam with smaller height needs a larger cross sectional moment M to generate a fully developed major crack.

On the other hand, the shear evaluation model described in this study is based on a fully developed crack profile. Fig. 4.31 indicates that the shear capacity of a beam is determined by the lowest point of the shear resistance line, the boundary of which is defined by the position of the loading point and the cracking shear force line. The later one is significantly influenced by the tension softening behaviour of concrete. In the model described in this chapter, the cracking moment is estimated by completely ignoring the post-peak tensile behaviour of concrete (s_{cr} reached immediately once $M = M_{cr}$), which leads to a lower bound of the cracking shear force line. However, because the cracking shear force line is always much lower than the shear resistance line, the major cracks at the critical sections are already fully developed when the inclined cracking load is reached. As a result, a better evaluation on the exact moment when a crack profile is fully developed does not improve the accuracy of the evaluation. An exception is when the shear span of the beam is very small, in that case the lower bound of the shear resistance line can be determined by the cross point at its left side. Nevertheless, it is always on the safe side to evaluate the shear resistance at $M = M_{cr}$ as the lower bound of the shear resistance.

Although the tension softening behaviour also influences the development of a dowel crack, it has already covered implicitly by Eq. (4.15) through regression analysis.

Because of the aforementioned reason, the influence of tension softening to the shear capacity of concrete beams is not less significant in the model, especially for beams with relatively larger shear slenderness ratio. Further validation on the conclusion can be found in the experiments presented in the following chapters.

4.7.3 Discussion

In this section, the influence of beam height to the shear strength of concrete beams has been discussed. It is shown that the term size effect can be traced back to several different mechanisms. Therefore, it is not practical to express this effect with a relatively simple relationship as some researchers proposed. On the other hand, the shear evaluation procedure proposed in this chapter is developed based on the understanding of the shear failure mechanism, and because of that, it is not necessary to add an additional scaling relationship regarding the effect of the beam effective height d. According to the theory presented, the size

effect is generated from the localized aggregate interlock stress distribution and the constant dowel force at the tension bars.

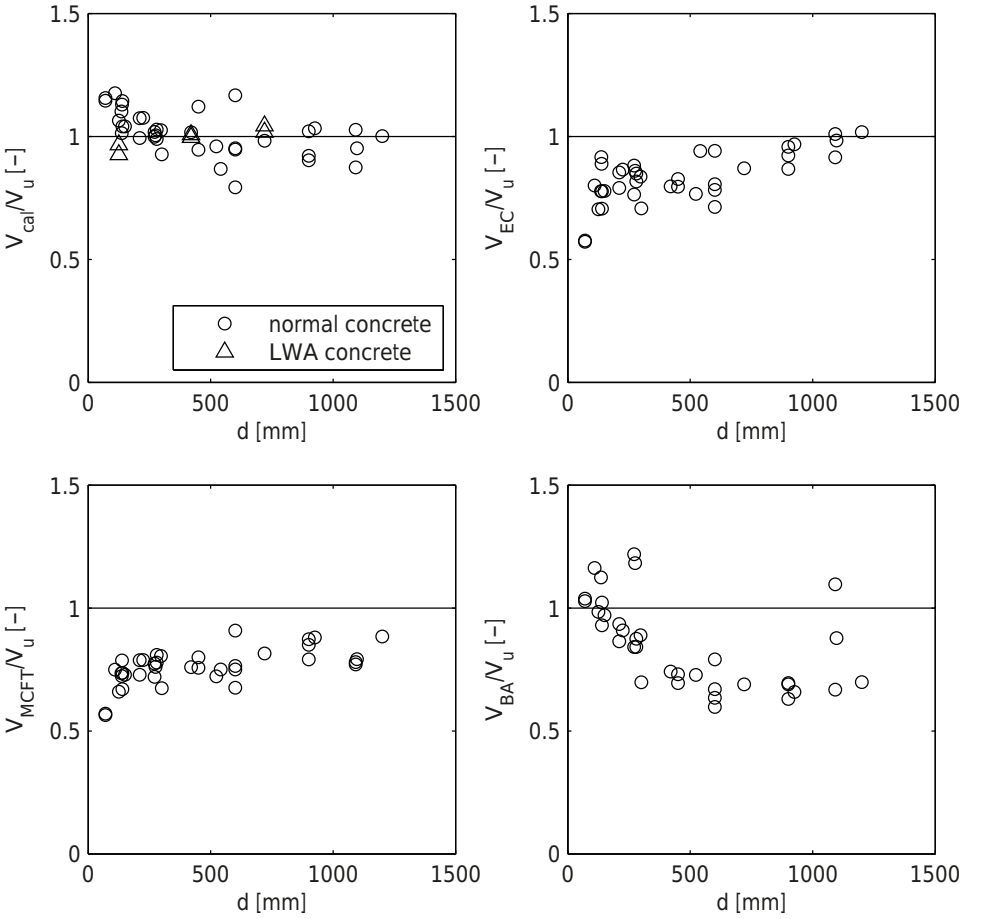

Fig. 4.32. Influence of beam depth on model prediction accuracy (top left: Present Theory; top right: Eurocode; bottom left: Modified Compressive Field Theory; bottom right: Bažant's formula).

To evaluate the present theory with respect to the size effect, experimental results are employed. The bias in the test data distribution is avoided by a selection of small number of test data. Only test data from research aimed at investigating the size effect are chosen. This is done in order to guarantee a good distribution of beam heights and to make sure that the other properties of the specimens do not change significantly. Based on that consideration, 38 tests have been selected from 5 sources: (Leonhardt & Walther 1962; Kani 1967; Bhal 1968; Walraven 1978; Collins & Kuchma 1999). In addition, the 6 size effect tests on LWA concrete beams carried out by Walraven (Walraven 1978) are also included.

Because the material is in general the same as the one tested in (Walraven & Reinhardt 1981), the reduction factor for LWA concrete is chosen to be 0.66 instead of 0.75 according to the test results. The comparison between the model prediction and test results are plotted in Fig. 4.32. For the sake of comparison, the prediction given by Eurocode, MCFT, and Bažant's formula are plotted as well, in which the LWA concrete specimens are not included.

All the models are calibrated with a large set of test data. Good agreements were achieved in the calibrations. Nevertheless, when the large number of tests within a relatively small range of beam depth is removed, the comparison clearly shows that the current theory is able to predict the test results over the whole depth range unbiased, whereas the prediction of all the other models leans towards a certain side of the beam depths range. Besides, as shown in Fig. 4.32, once the reduction of aggregate interlock stress at small crack openings is known, the size effect of LWA concrete beams can be predicted accurately with the present theory as well.

4.8 CONCLUSIONS

Based on the failure mechanism discussed in Chapter 3, a simplified calculation procedure was developed in this chapter. It aims at giving a prediction for the inclined cracking load of simply supported reinforced concrete beams without shear reinforcement with a relatively large shear slenderness ratio (a/d).

In the procedure, the crack profile is simplified to a straight major crack being perpendicular to the longitudinal direction of the beam connected by a secondary inclined branch. With that simplification, it is possible to express the shear displacement Δ and the normal crack opening w independently, which are used to calculate the shear force generated by aggregate interlock based on Walraven's aggregate interlock equations. The procedure is further simplified into an expression that is suitable for hand calculation.

Based on the simplifications, the critical shear displacement Δ_{cr} at the longitudinal rebar is derived by reverse analysis of the vertical displacement Δ at the reported failure loads V_u of 410 experiments reported in literature.

For high strength concrete or lightweight aggregate concrete beams, due to the fracture of aggregates, the aggregate interlocking force V_{ai} has to be reduced. This can be done by taking into account the reduction of the contact area into the aggregate interlock equations. A simplified method is that for high strength concrete the concrete compressive strength used in calculating the aggregate interlocking forces is limited up to 60 MPa, and a general reduction factor R_a = 0.75 is introduced for LWA concrete beams as a rough estimation.

Because the development of the dowel crack along the longitudinal rebar is a complex process, involving both the rebar tensile and flexural stiffness, the rebar configuration plays an important role in the expression of Δ_{cr} in addition to the total cross-sectional area of the reinforcing steel.

The simplified shear evaluation procedure is developed based on a proper understanding of the shear failure mechanism. Therefore, it is able to predict the size effect on the shear capacity without any further modification. According to the model, the inclined crack is generated from a fully developed major crack, and the size effect is mainly due to the aggregate interlock and dowel action at the cracked section. The tension softening behaviour of concrete has limited effects on the shear capacity when the beam span is small.

A comparison with the results found in multiple shear tests databases has shown that the proposed calculation procedure is able to deliver a very accurate prediction of the shear capacity of the target reinforced concrete beams. With regard to accuracy, the method developed is also superior to most of the other design formulas for this type of structure.

Chapter 5

Shear Behaviour of Reinforced Concrete Beams under Complex Boundary Conditions

5.1 INTRODUCTION

In Chapter 3, the shear failure mechanism of a simply supported reinforced concrete beam loaded by single point load has been discussed, based on which a simplified calculation method was proposed in Chapter 4. One of the important messages that have been delivered in the previous chapters is that the shear failure process is strongly related to the cracks initiated by the flexural moment. Therefore, the shear resistance of a structure should not be considered as a material property as is done when it is loaded by a bending moment or a tensile force. For a given structure, the shear resistance has to be evaluated by taking into account its loading condition, which influences the crack trajectories and the crack opening. In the case of a simply supported beam this influence is often related to the so-called **shear slenderness ratio** (a/d), which was firstly demonstrated by Kani in his well-known experiments described in (Kani 1964). With the design procedure specified in Chapter 4, the influence of a/d can simply be explained by the opening of the major crack at the critical cross section. For beams with smaller a/d, the moment at the critical cross-section is smaller under the same shear force, which gives a smaller crack width, thus larger shear resistance at the cracked cross section. The proposed method compares well with experimental results reported in literature. This also implies that the shear failure mechanism reflects the reality properly.

However, most structures in reality are characterized by more complex boundary conditions. Fig. 5.1 shows two examples of structures where shear failure is considered to be critical. The first case is concerned with concrete slab decks, which are widely used in highway bridges with multiple spans. The slab decks are mostly constructed without shear reinforcement, thus vulnerable to shear failure when heavy wheel loads are approaching the support. Also, for tunnel sections, shear reinforcement is usually not provided. Thus shear failure at the corners of tunnel sections is usually a point of concern. In this case the soil/water pressure being simplified as distributed load makes the moment and shear force distribution more complex.

In this chapter, the shear capacity of beams under more complex loading or supporting conditions is discussed. The shear failure mechanism proposed, based on simply supported beams with simple loading conditions, is generalized to more complex boundary conditions first. Three common load cases will be discussed in the section, the design procedures of beams loaded in these load cases are investigated as examples. With increasing complexity, the load cases to be discussed are continuous beams loaded by point loads, and furthermore the two shear critical load conditions shown above. Validation against experimental results is carried out.

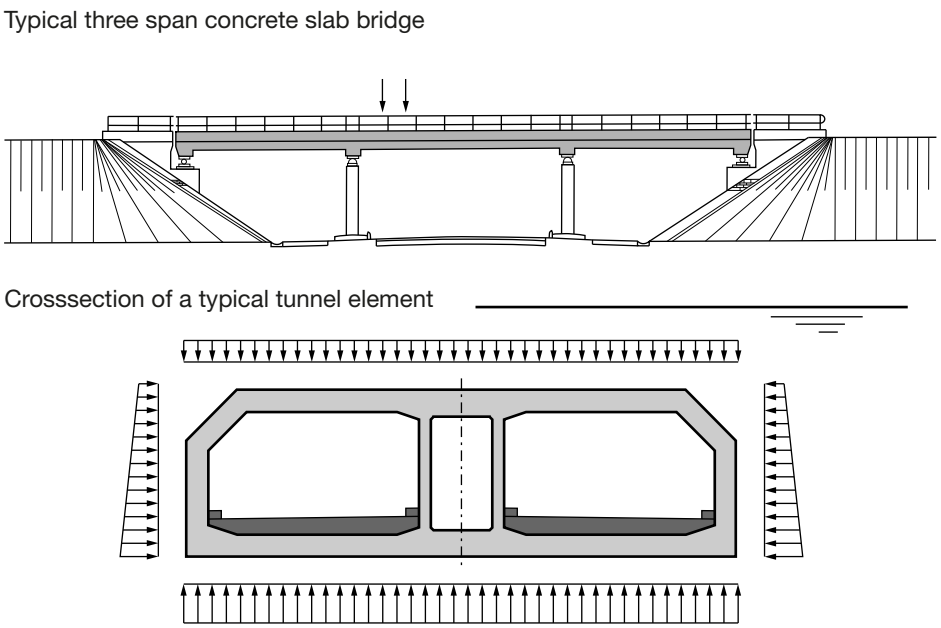

Fig. 5.1. Loading conditions of typical concrete structures vulnerable to shear failure.

For the continuous supported beams loaded by point loads, full scale laboratory studies were executed by the author in the Stevin Laboratory at Delft University of Technology. The experimental program is dealt with in this chapter briefly.

5.2 EXTENSION OF THE SHEAR MODEL TO GENERALIZED BOUNDARY CONDITIONS

For a simply supported beam subject to point loads as described in Chapter 3 and 4, the moment and shear force distribution along the span is rather simple. The shear force along the span is constant between the support and the loading point, which results in a linear moment distribution as shown in Fig. 5.2. Based on this moment and shear force distribution, a crack profile distribution is derived, with which the shear resistance components along a given crack profile can be evaluated, leading to the shear capacity of the whole structure. To extend the same process to more general boundary conditions, as shown in Fig. 5.2 (b) and (c), the derivation of the force components in Chapter 3 based on a relatively simple moment and shear force distribution has to be verified regarding the following questions:

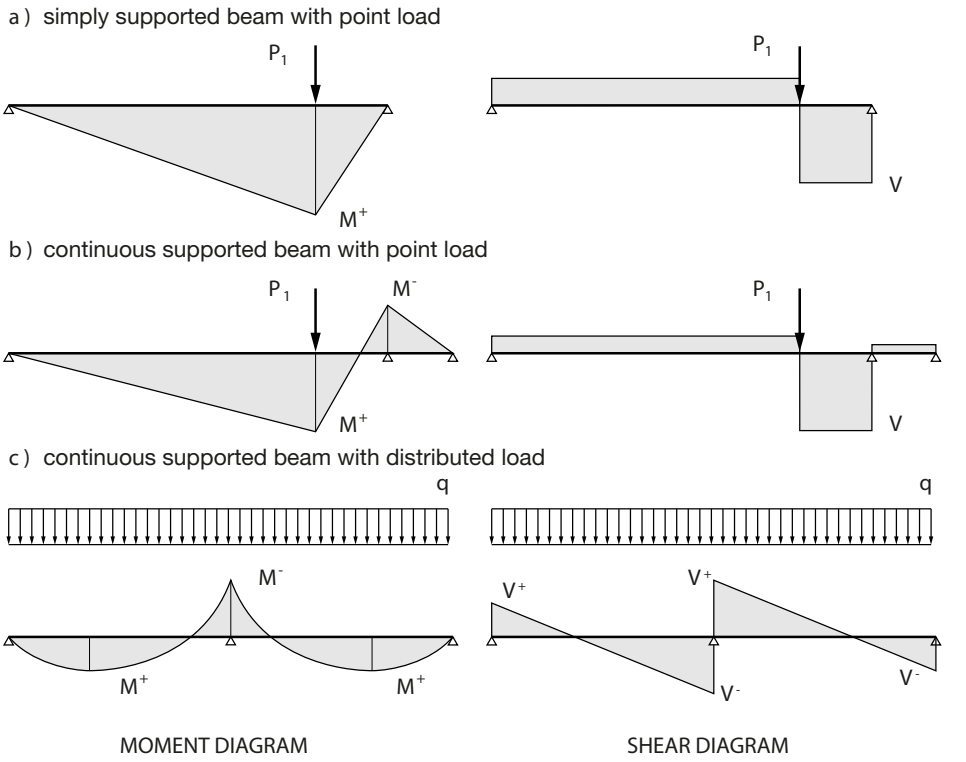

Fig. 5.2. Moment and shear force diagrams of beams under different boundary conditions.

Whether or not a similar crack profile can be obtained at a given moment/shear force ratio?

In Chapter 3 it was concluded that the inclination of a crack in a longitudinally reinforced beam is due to the shear stress developed between the reinforcing bars and concrete at the bottom of the concrete teeth formed by flexural cracks. That statement is independent of the boundary conditions of the whole beam. To get the expression for the crack path, the stress state around the propagating crack tip due to the combination of moment and shear force action has to be calculated. The calculation was done with the help of the sequentially linear analysis including a crack propagation algorithm. Thus the crack path being calculated was based on the condition that the shear force is constant from the section where the crack initiates till the section of the crack tip. When the shear force changes substantially between the two sections, the variation of the shear force will result in a different crack path function.

For beams loaded by point loads and supported by standalone supports, since the shear forces between the supports or the loads are always constant, the

same crack profile expression can be expected. This conclusion may be further extended to beams subjected to uniformly distributed load with a large span. If the inclination of the crack is relatively small, and the distance between the two cracked sections is limited, the change of the shear force can be neglected. In that case, the crack profile expression derived from beams subject to point loads can be considered as a close estimation.

With the same crack profile and crack opening, do the shear force components change?

Since the critical shear displacement Δ_{cr} is only related to the materials and the reinforcement configurations, it is supposed to be independent of the loading condition. If the shear force components along the cracked cross-section remain the same under the same shear displacement Δ, then the shear failure process can be calculated in the same way.

For V_d due to dowel action, it is assumed that at shear failure the maximum value of V_d is reached. Similar to Δ_{cr}, $V_{d,max}$ is a constant value only related to the material properties and the cross-section of the structure. Therefore it is independent of the boundary conditions.

The force V_{ai} is calculated from the shear stress τ_{ai} and the normal stress σ_{ai} at a given crack opening n and t, see Fig. 3.26. Hence, it is related to the crack path and crack opening. As long as the first criterion is fulfilled, the same crack opening should guarantee the same resultant shear force.

In the case of V_c, the stress analysis in Section 3.5.3 has shown that when a concrete teeth structure cannot be formed between the critical inclined crack and the loading point, the shear stress distribution proposed by Mörsch in (Mörsch 1909) is not valid anymore. In that case, it is quite difficult to evaluate the shear stress that is carried by the uncracked zone of the concrete beam. Even when concrete teeth can be formed the value of V_c varies from Eq. (3.26) due to the load distribution. Taking uniformly distributed load as an example, Mörsch's evaluation assumed that the value of V is constant between the two cracked surfaces in the derivation. $V = \mathrm{d}M/\mathrm{d}x$, under that condition. However, when a distributed load is applied on the beam, the relationship between moment and shear force becomes $\mathrm{d}M = \int V(x)\,\mathrm{d}x$. The simplified relationship may not be valid anymore when V varies significantly between the two cracked sections.

Where is the critical section?

Section 3.4.3 suggests that for a simply supported beam the critical cross-section is at the loading point although the real critical section is at a distance $l_{cr,m}$ from the loading point. The determination of the critical section is based on the following reasons. First of all, the cracked cross-section with larger M/Vd

requires a lower shear force to generate the same shear displacement Δ_{cr}. Secondly, the shear displacement Δ is obtained by rotation of the secondary branch at the crack tip, whereas a certain length of the crack branch is necessary to generate Δ under a relatively small rotation. Thus, having the crack tip at $l_{cr,m}$ from the turning point of rotation, it is guaranteed that the development of Δ_{cr} is still theoretically possible. The last one is to check whether a crack can develop at sections with very small M/Vd, where the shear force needed in order to generate an inclined crack can becomes very small again.

The description above explains the criteria to determine the critical cross-section for general loading cases. The location of the critical cross-section must have an M/Vd as large as possible, where the lowest shear capacity is expected. In the meantime it shall be not less than $l_{cr,m}$ from the rotation points. Last but not least, the moment at the section has to be larger than the cracking moment, and there should be a sufficiently large shear force.

Depending on the type of the boundary conditions, the location of the critical section may vary. The choices of critical cross sections will be discussed according to the specific loading cases in the following sections.

To summarize, it is possible to extend the failure mechanism that is based on simply supported beams with point loads to more general boundary conditions. To do so, the critical section where the inclined crack develops has to be updated. Once the critical section is determined, the shear force components along the critical crack have to be checked. Besides, if the boundary conditions of the beam differ from the ones described above, the crack path function and the formula of V_c have to be verified first.

5.3 CONTINUOUS BEAM LOADED BY POINT LOADS

5.3.1 Introduction

Since the solid concrete deck of multiple span bridges is one of the most common structure types that are vulnerable to shear failure, the influence of the boundary conditions of this type of structure is studied in this section. In the Netherlands, an evaluation has been carried out on the concrete bridges in the country's highway system with the Eurocode provisions. The result revealed that a large percentage of those bridges do not fulfil the code provisions under the current traffic load level. However, the Eurocode provision provides a relatively conservative prediction in the case of continuous supported structures, since it treats the shear capacity of beams as a cross sectional property, which is independent of the boundary conditions. Only when a_v/d of the loading point is

smaller than 2.0, the influence of the loading condition is treated as a reduction factor on the applied point load, see also Section 2.3.2.

On the other hand, according to the failure process described in this study, the moment distribution over the shear span has a significant influence on the crack path and crack opening, thus the shear capacity is influenced. In the case of a continuous supported beam, the shear critical span lies often between the loading point and the intermediate support, see Fig. 5.2 (b). In the same span, the moment reaches zero. As explained in 5.2, in this case, the critical section of the beam is located at one of the two sections with a distance $l_{cr,m}$ from the loading point or the support, depending on which one has a larger M/Vd. The shear capacity of the beam is related to the value of the bending moment M and the shear force V at the critical section. Therefore, only regarding inclined cracking load, the beam can be considered as two shear loaded simply supported beams separated by the point where the moment is zero. The relatively smaller moment within the span increases the expected inclined cracking load.

Similar to shear in simply supported beams, experimental results are needed to verify the model dealing with the shear capacity of this type of structures. However, reported test results with regard to complex loading conditions are quite limited in literature. Additional experimental research is needed to get a better insight into this problem. For that reason, a series of experiments with complex loading conditions was carried out in the Stevin Laboratory at Delft University of Technology upon the request of Rijkswaterstaat. In this section the experimental program is explained. More detailed reports can be found in (Yang & den Uijl 2011).

5.3.2 Test Program

5.3.2.1 General Considerations

The aim of the experimental program was to evaluate the influence of the design variables such as the moment distribution, load conditions, reinforcement ratio etc. to the shear capacities of continuous beams. Thus, in the experiments, it is intended to reproduce a moment distribution on a concrete beam in the laboratory which is similar to that in a continuous concrete bridge deck. Both positive and negative moment shall be found in the critical shear span. This type of moment distribution can be generated on either a real continuous beam or a simply supported beam with a cantilever. In this study, the second option is chosen. Nevertheless, because the moment distribution in the critical shear span is chosen to imitate that of a continuous beam, the specimens are still denoted as **continuous beams** in the research to distinguish them from simply supported beams loaded with a point load within the span. In a statically indeterminate continuous beam, once the concrete cracks, the flexural stiffness of the beam

changes along the length. As a result the inner forces, such as the moment distribution, change when the external load level increases. That makes the boundary conditions of the tests indefinite. Besides, the redistribution makes the tested shear capacity higher, while on a simply supported beam with a cantilever, the moment distribution over the target shear span can be kept constant as long as the external load levels are kept constant.

Since the moment distribution is the most distinctive feature for a continuous structure, this is one of the key variables in the research program. The moment distribution can be described by the length of the critical shear span a and the moment ratio between the maximum **positive moment** (sagging moment) and the **negative moment** (hogging moment) M^+/M^-. Both values directly relate to the maximum M/V in the span by

$$\frac{M^-}{V} = a \Big/ \left(\frac{M^+}{M^-} - 1\right); \quad \frac{M^+}{V} = a \Big/ \left(1 - \frac{M^-}{M^+}\right)$$

Therefore, the main variables with respect to the moment distributions involve two variables:

a: is the shear span, which is the distance between the point load and the intermediate support;

M^+/M^-: is the ratio between the maximum positive moment (sagging moment) M^+ and the minimum (sagging moment) negative moment M^- in the shear span a.

The test specimens are designed based on the common practice for Dutch concrete slab bridges, for example the Gestelsestraat Bridge (Yang et al. 2010). The reinforcement of those bridges was originally designed to get flexural failure before shear failure, therefore a large strain is expected on the reinforcement at the ultimate limit state. As reported by Collins et al. in (Collins, Mitchell et al. 2008) beams under such load condition are found to have lower shear capacity than usually expected. On the other hand, a relatively small reinforcement ratio may results in yielding of the rebars before shear failure. For the sake of comparison, an additional test series of specimens with higher reinforcement ratio which guaranteed shear failures was planned to check the influence of the reinforcement ratio ρ_s.

In spite of the single point load tests, an additional test series including two point loads spaced at 1.2 m was planned. This was based on the concentrated loads as specified by Load Model 1 in Eurocode 1 (Eurocode 1 2003). Since the reinforced concrete beams are in general structures with nonlinear behaviour, the superposition principle of a linear elastic structure becomes inapplicable here. For beams loaded by multiple point loads a different shear behaviour was

observed by Bryant et al.(Bryant et al. 1962). Thus, it is necessary to investigate the effect of having multiple point loads on the continuous beam.

5.3.2.2 Test Specimens

Material Properties

The concrete mixture used in the test specimens was a commercial mixture. It was classified as C53/65 by the producer. The maximum aggregate size of the mixture was 16 mm. A typical mixture composition is given in Table 6.5 in Chapter 6. In total 9 casts have been carried out in the lab. Among them, 5 casts were conducted in 2010, and the others in 2011. The last cast was planned almost one year later than the first one. Though the compositions of the mixtures are still the same on paper, the change of the raw materials of the concrete plant might still result in a variation of the final result.

The mean compressive strength f_{cm} and splitting tensile strength $f_{ctm,s}$ were tested with 150 mm cubes after 7 days, 28 days, and on the dates when the experiments were executed. It turned out that the strength was higher than what was expected from Eurocode 2 (Eurocode 2 2004), especially for the first 5 casts made in 2010. The average compressive strength of the first 5 casts on the dates of testing reached $f_{cm,cube}$ = 87 MPa, which corresponds with f_{cm} = 74 MPa. The coefficient of variation was 6.6%. The mean value of the splitting tensile strength was $f_{ctm,s}$ = 5.7 MPa. For the concrete beams from the last four casts in 2011, the $f_{cm,cube}$ value was 80 MPa, corresponding with f_{cm} = 68 MPa with the coefficient of variation being 6.2%. The splitting tensile strength of those specimens was $f_{ctm,s}$ = 4.9 MPa. There was a difference of 7 MPa between the compressive strengths of the two batches of casts, while the coefficients of variations of both groups were relatively low. The two batches of concrete were treated separately.

Geometry and Reinforcement Configuration

As explained before, the dimensions as well as the reinforcement configurations of the test specimens were designed based on the configuration of the Gestelse-straat Bridge (Yang, den Uijl et al. 2010). The dimensions of the beams were uniform in the whole test, being 8 m long, 0.5 m high, and 0.3 m wide. They are also indicated in Fig. 5.3. The specimens were cast with a mould built in the lab. Each time two beams were cast simultaneously. The beams were numbered according to the cast sequence. In total, 18 beams have been cast, among which beams 6-8 were not tested.

Most beams were tested at their ends. Depending on the damage level caused by the first test, it was strengthened before starting the second test. The strengthening frame is composed of six screwed high strength steel bars, and four clampers welded by L shape steel profiles.

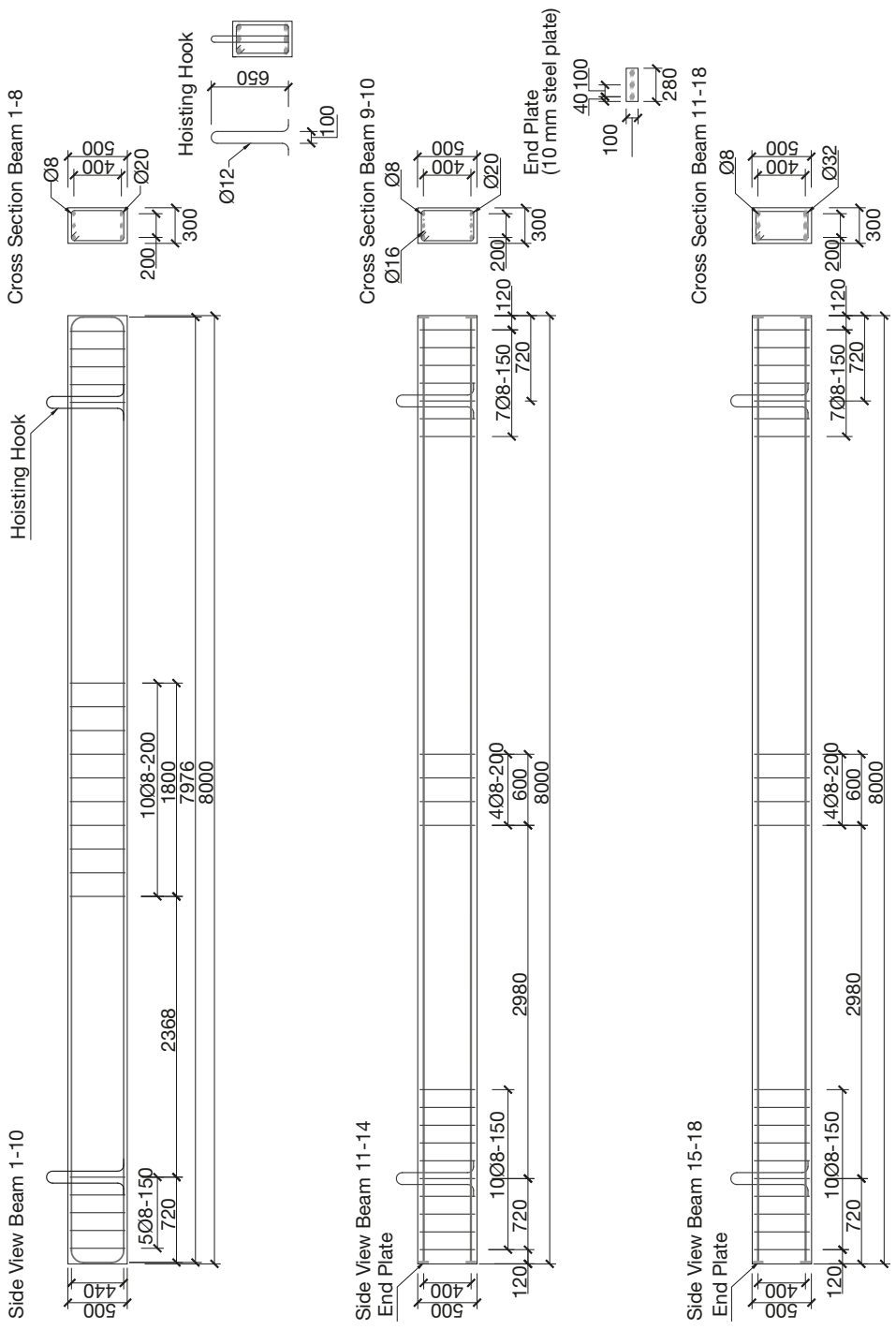

Fig. 5.3. Dimensions and reinforcement configurations of the specimens.

Fig. 5.4. Photo of the test setup with multiple point loads in the main span.

As one of the variables, three reinforcement configurations have been utilized in the test specimens. The reinforcement ratios ρ_s were 0.68%, 0.97% and 1.79% respectively. Among all the 18 beams, the ρ_s of beam 1 to 8 is 0.68%. Three ribbed steel bars Ø20 mm were used both as top and bottom reinforcement. The thickness of the concrete cover was 35 mm. The effective height of the beam d was 455 mm. Beams 9 and 10 had a ρ_s of 0.97%, two additional ribbed bars of Ø16 mm were added on the bases of the rebar cage of beam 1—8. The ρ_s of the rest beams was 1.79%. In those beams, the top and bottom rebars were 3 Ø32 respectively. The effective height d was 450 mm. A few stirrups of Ø8-150 were arranged at the end of the beams and in the middle to support the longitudinal rebars to prevent unexpected shear failure at those positions. In beam 11 to 14, more stirrups were arranged in one end of the beams, to make sure that there would be no shear failure in the cantilever. The configurations of the reinforcement cages are given in Fig. 5.3.

5.3.2.3 Test Setup and Measurement

Test Setup

The moment distribution of a continuous beam was generated by arranging the two point loads on a simply supported beam with cantilever, see Fig. 5.5. The two point loads were generated by two hydraulic actuators with a loading

capacity of 1000 kN. The forces of the actuators were monitored and controlled by a computer, so that the ratio between P_1 and P_2 was kept constant during the whole loading process. The distance between the two actuators was fixed at 2.4 m. For the test series with two point loads, an additional load transfer beam was used to distribute the load equally over the two point loads, which is shown in Fig. 5.5 bottom.

The width of the loading plate and the support plate is 200 mm. Gypsum layers were applied to ensure full contact between the surface of the specimen and the loading plates. In the two wheel loads tests, rubber blocks were used to ensure a certain rotation capacity at the loading positions, and to transfer the load from the steel beam to the specimen.

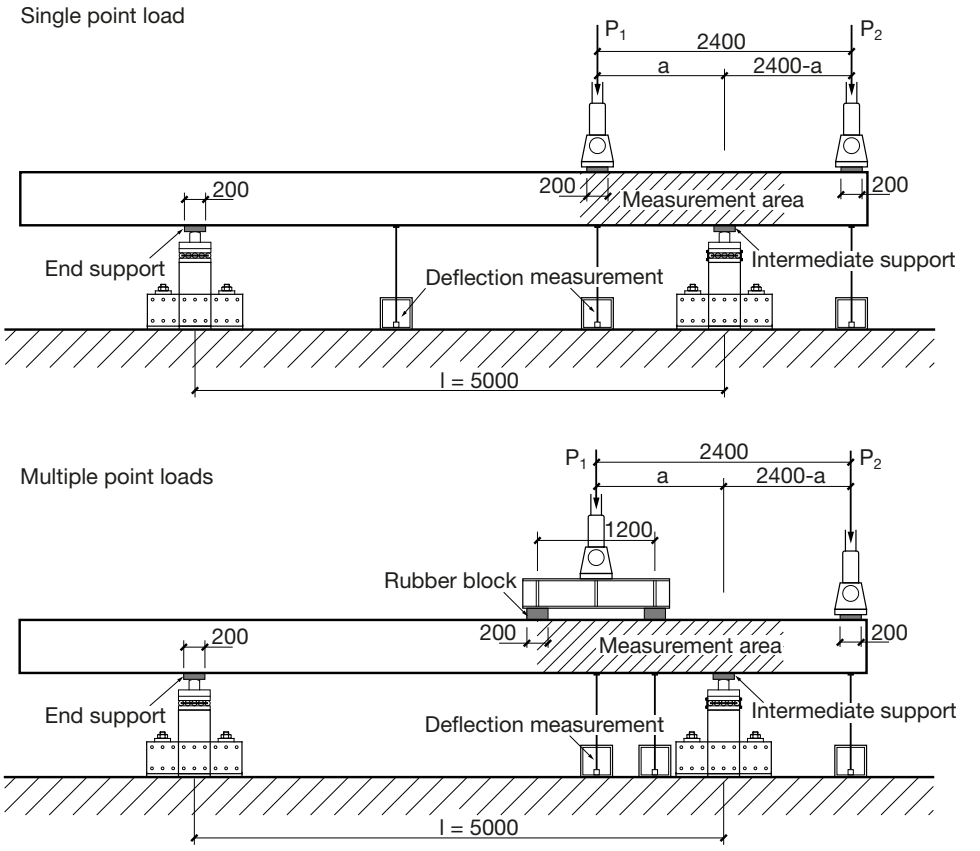

Fig. 5.5. Sketches of test setups with single point load and multiple point loads.

Loading Procedure

With the loading setup presented before, a linear moment distribution with both a positive and negative moment was created. The ratio between the maximum positive moment M^+ and the negative moment M^- is determined by the force ratio P_1/P_2. For each test, a target M^+/M^- was defined first. The force ratio is then calculated according to that target M^+/M^-. The value of P_1/P_2 was kept constant during the test.

$$\frac{P_1}{P_2} = \frac{1}{a}\left(\frac{bl}{(l-a)M^- / M^+} + l_0 - a\right)$$

with l_0 = 2400 mm in all the tests in the program.

The loading procedure was divided into two stages. Firstly, the hydraulic actuators were controlled by the force level measured by load cells, denoted as **force control**. At this stage, the loading process was subdivided into several load steps. For each load step a maximum load level was defined according to the shear force in the shear span a. The ratio between shear force V and P_1 can be calculated with:

$$\frac{V}{P_1} = 1 - \frac{a-(l_0-a)(P_1/P_2)}{l}$$

The forces applied by the actuators P_1 and P_2 were increased under constant loading rates until the predefined load levels. The first load level was defined to be close to the cracking load of the specimen, after that the following load levels were increased by a fixed interval. The loading rate of P_1 was 0.2 kN/s in all tests, and the loading rate of P_2 was determined accordingly. By the end of each load step, the forces were kept constant for 10 minutes, in order to stabilize the deformation of the specimen, and to provide sufficient time for crack marking and other measurements operations.

The force-controlled loading procedure was stopped when unstable inclined crack development was observed, or the specimen showed a significant change of flexural stiffness in the load deflection diagram. The actuator P_1 was then controlled by its displacement, denoted as **displacement control**, while the value of P_2 was still controlled by the force measured from the load cell of P_1 real-time, so that the value of P_1/P_2 was still constant. The value of P_1 was increased stepwisely up to failure of the specimen. An example of the loading history is given in Fig. 5.6. At the end of each load step in the displacement-controlled phase, the displacements of the actuators were also kept constant for a few minutes. Because of the crack propagation, one may find that

the forces in the actuators decrease. The next load level started after the forces of the actuators were more or less stabilized.

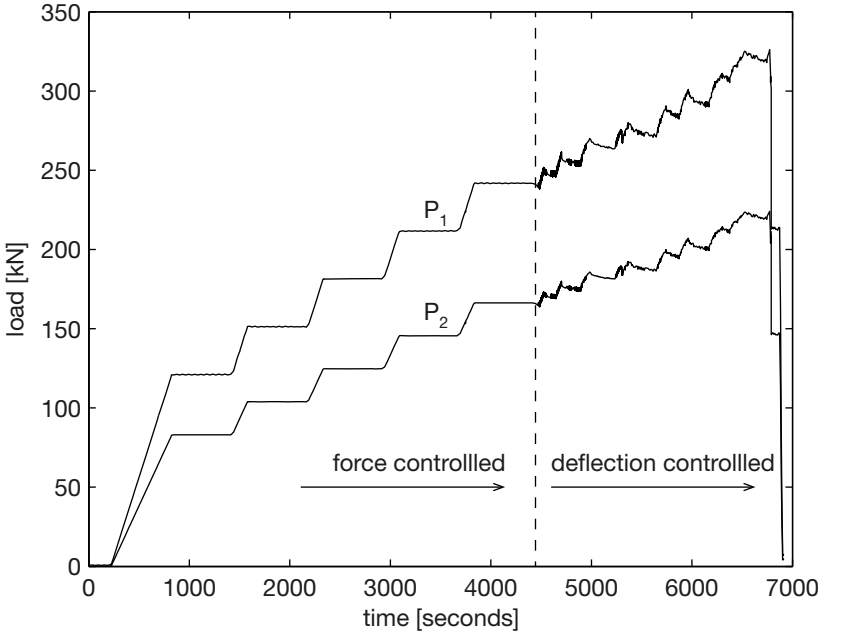

Fig. 5.6. Loading procedure of specimen C2a152.

Measurement

The data that was collected during the experiments includes: the load level in the actuators, the deflection of the specimen, the crack development in the shear span, and the deformation of the beam in the shear span. The following measurement methods were applied.

The loads applied through the actuators were measured with load cells. To ensure the accuracy, the load cell was calibrated again after the whole test program. The variation of the measurement in the period of 1 year was less than 2%. The deflections of the beams were measured by draw-wire displacement sensors through wires connected to the bottom of the beams. The deflections of the specimen were measured at the locations of the actuator P_1, actuator P_2 and the midpoint between P_1 and the end support in the single point load tests, see Fig. 5.5. In the multiple point-loads tests, the displacement sensor between P_1 and the end support was moved to the location of the first point load see Fig. 5.5.

The deformation field or eventually the crack development at the side surfaces in the shear span is of interest, thus it was monitored with two different methods during the tests. At one side of the beam, an LVDT array was glued onto the beam surface. The configuration of the LVDT array was dependent on

the load condition of the specimens and the amount of channels available in the data collection system. An example of the LVDT arrays is shown in Fig. 5.7, the test name shown will be explained in the next section. The arrangement of the LVDT array was designed to record real-time the deformations along the top and bottom longitudinal rebars and the deformations in vertical and diagonal direction, so that the propagations of inclined cracks and flexural cracks can be monitored.

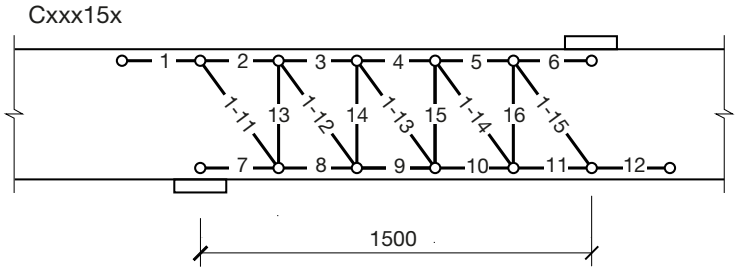

Fig. 5.7. Configurations of LVDT array for beams with shear span a = 1500 mm.

On the other side of the shear span, the so called photogrammetric measurement technology was employed to measure the deformation of the beam by the end of the load steps. It is an optical measurement method developed by the author. More detailed information can be found in (Yang 2009). The deformation gradient at the beam surface can be measured with a very fine grid in a highly automated program based on Matlab. A brief description of the procedure is given here. Before the test, a grid of 8 mm diameter markers was glued onto the surface of the specimen. The grid consisted of equally sided triangular elements with 80 mm side length. In total 7 rows of maximum 24 nodes can be aligned in the grid. The mesh configuration as well as the measurement setup is shown in Fig. 5.8. At the load levels to be measured, photos were made with a digital camera. In this test program the camera used was a Canon 5D MarkII, with a 21.1 megapixel full frame CMOS sensor. The photos made during the tests were processed after the experiment. The locations of all the nodes in the mesh were derived first from the processing images. Comparing the new locations of the nodes with the original locations derived by the photos made before the specimen was loaded, the displacements of the nodes in the grid under the load level was derived. Assuming a linear strain distribution, the nodal displacements can be translated into a strain field of the triangulate mesh with a linear shape function. Compared to the LVDT method, the photogrammetry measurement is able to provide much more detailed information upon the deformation field and crack width distribution over the surface of the specimens at any load step

without contacting the specimen. With the help of this measurement, it is possible to study the development of the critical diagonal cracks in more detail.

Besides, the cracks were carefully marked during the load resting period in each load step. After each test, photos of those cracks were made with an accuracy of 0.5 mm/pixel. The crack patterns of the beam by the end of each load step were then digitized manually based on those photos. By combining the crack position data with the information from photogrammetry measurement, it is possible to calculate the opening of each crack. The output of the measurement has already been applied in the previous studies in the research (e.g. Section 4.2.2).

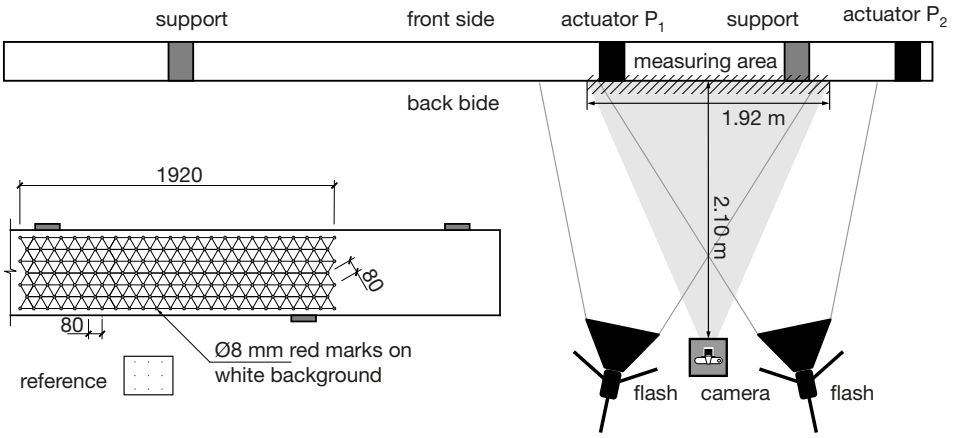

Fig. 5.8. Setup of photogrammetry measurement and mesh arrangement.

5.3.3 Test Series

In total 32 tests have been carried out. The tests are distinguished by the length of the shear span a, the moment ratio within the shear span M^-/M^+, the reinforcement ratio ρ_s, and the number of the loading points. The names of the tests are in accordance with those variables. The identifying rules are illustrated in Fig. 5.9. The first letter stands for the number of loading points in the main span: if the test was loaded by a single point load it is C, otherwise the letter is D. The first one or two numbers after C/D stands for the beam number which is determined by the casting sequence. Not all the cast beams were tested, therefore the numbers are not always continued. The letter a/b indicates the sequence of the tested beam end, a stands for the first test and b is the second. The next two digits indicate the length of the critical shear span a. a may switch among 0.9 m, 1.2 m, 1.5 m and 1.8 m, whereas this number changes from 09 to 18 respectively. The last digit indicates the moment ratio. For each a value four moment ratios M^-/M^+ were tested, $M^-/M^+ = 0, 1/3, 2/3$, or 1. Accordingly the last digit may be distinguished from 1 to 4 in the specimen name.

The tests are categorized into 5 series. The basic test series includes the specimens with ρ_s = 0.68%. The specimens of this series were designed reflecting the existing Dutch bridges. As a reference series, almost all the load cases have been included in this series. However, some of the tests showed flexural failure due to the lower amount of longitudinal reinforcement area. In the second series the specimens have a reinforcement ratio of 0.97%. There are only 4 tests to evaluate the influence of the reinforcement ratio. The specimens of the third series have the largest reinforcement ratio of 1.79%, which guarantees shear failure before yielding of the reinforcing bars. The configurations of tests in this series cover the ones having flexural failure in series 1. Further to that, two additional test series were included. The specimens of tests series 4 and 5 have the same configuration as those in series 3. These two series were designed to evaluate the effect of existing cracks and multiple point loads respectively. A summary of the configurations of all the executed tests is given in Table 5.1.

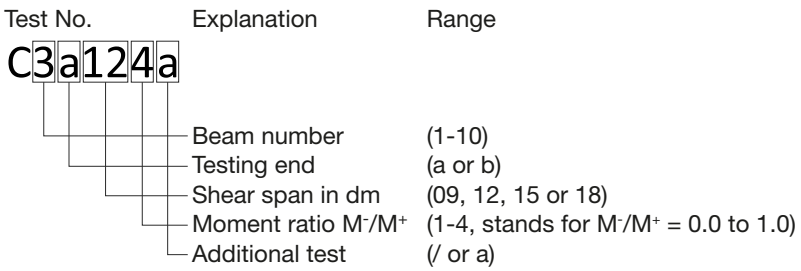

Fig. 5.9. Illustration of test identifying rules.

Table 5.1. Configuration of tested specimens.

Test No.	a [m]	b [m]	a/d [-]	M/Vd [-]	M^-/M^+ [-]	P_1/P_2 [-]	V/P_1 [-]	ρ_s [%]
Series 1								
C1a152	1.5	0.9	3.30	2.47	1/3	3.17	0.76	0.68
C1b153	1.5	0.9	3.30	1.98	2/3	1.89	0.80	0.68
C2a154	1.5	0.9	3.30	1.65	1	1.46	0.82	0.68
C2b151	1.5	0.9	3.30	3.30	0	-	0.70	0.68
C3a123	1.2	1.2	2.64	1.58	2/3	2.97	0.84	0.68
C3a124a	1.2	1.2	2.64	1.32	1	2.32	0.86	0.68
C3b121	1.2	1.2	2.64	2.64	0	-	0.76	0.68
C4a122	1.2	1.2	2.64	1.98	1/3	4.95	0.81	0.68
C4b091	0.9	1.5	1.98	1.98	0	-	0.82	0.68
C4b094a	0.9	1.5	1.98	0.99	1	3.70	0.90	0.68

C5a094	0.9	1.5	1.98	0.99	1	3.70	0.90	0.68
C5b183	1.8	0.6	3.96	2.37	2	1.11	0.75	0.68
Series 2								
C9a123	1.2	1.2	2.64	1.58	2/3	2.97	0.84	0.97
C9b121	1.2	1.2	2.64	2.64	0	-	0.76	0.97
C10a124	1.2	1.2	2.64	1.32	1	2.32	0.86	0.97
C10b154	1.5	0.9	3.30	1.65	1	1.46	0.82	0.97
Series 3								
C11a091	0.9	1.5	2.00	2.00	0	-	0.82	1.79
C11b123	1.2	1.2	2.67	1.60	2/3	2.97	0.84	1.79
C12a121	1.2	1.2	2.67	2.67	0	-	0.76	1.79
C12b094	0.9	1.5	2.00	1.00	1	3.70	0.90	1.79
C13a122	1.2	1.2	2.67	2.00	1/3	4.95	0.81	1.79
C13b092	0.9	1.5	2.00	1.50	1/3	7.76	0.86	1.79
C14a124	1.2	1.2	2.67	1.33	1	2.32	0.86	1.79
C14b093	0.9	1.5	2.00	1.20	2/3	4.72	0.88	1.79
C15a151	1.5	0.9	3.33	3.33	0	-	0.70	1.79
C15b154	1.5	0.9	3.33	1.67	1	1.46	0.82	1.79
Series 4								
C16a123	1.2	1.2	2.67	1.60	2/3	2.97	0.84	1.79
C16b123	1.2	1.2	2.67	1.60	2/3	2.97	0.84	1.79
Series 5								
D17a151	1.5	0.9	3.33	2.00	0	-	0.70	1.79
D17b154	1.5	0.9	3.33	1.67	1	1.46	0.82	1.79
D18a121	1.2	1.2	2.67	1.33	0	-	0.76	1.79
D18b152	1.5	0.9	3.33	1.17	1/3	3.17	0.76	1.79

P_1 is the total force applied through the actuator in series 5.

Table 5.2. Moments and shear forces in specimens of series 5.

Test No.	M_1/M_0	P_1/P_2	V_1/P_1	V_2/P_1	V_3/P_1	V_4/P_1	M_2/M_0	M_3/M_0
D17a151	0	-	-	0.70	0.20	0.30	0.90	0.83
D17b154	1	1.46	0.68	0.82	0.32	0.18	0.20	0.83
D18a121	0	-	-	0.76	0.26	0.24	0.60	0.84
D18b152	1/3	3.17	0.32	0.76	0.26	0.24	0.70	0.83

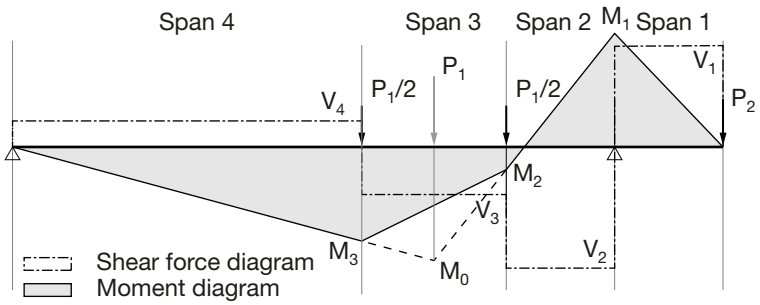

Fig. 5.10. Moment and shear force diagram of two point loads test.

In some tests of serious 5 shear failure was also observed in the spans between the two point loads, or between the second point load and the end support. Therefore, the shear forces in these two spans are also of interest. The values of M_1/M_0, M_2/M_0, $M_2/V_2\,d$, V_2/P_1, V_3/P_1 etc. are listed separately in Table 5.2. The notations of the variables are illustrated in Fig. 5.10.

5.3.4 Test Results

The failure process of the 32 experiments was well recorded by the measurement mentioned above, which generated a huge amount of test data. A brief explanation on the major findings in the tests is given here.

The test results are briefly summarized in Table 5.3. More detailed information on the test results are given in the test report (Yang, den Uijl et al. 2011). Some essential explanations on the tests are still necessary here. The failure modes of the tests are marked in the table. Not all the beams failed in shear. Some specimens with a combination of a low reinforcement ratio and a small shear slenderness ratio showed flexural failure defined by the yielding of the longitudinal reinforcement. Among them, some had moderate damage in the critical shear span, like C3a123 and C4b091. They were unloaded, and reloaded again at a higher moment ratio with a different loading procedure. In that case, the specimens got a new test number, see the remarks in Table 5.3. In some other specimens with a flexural failure such as C9a123 and C9b121, the beam was already loaded by a relatively high load level. Instead of releasing the forces in actuator P_1, it was decided to directly increase the force P_2, while keeping the displacement at actuator P_1 constant. So that the moment ratio and the shear force in the shear span was increased. With those tests, the test numbers are kept the same. But a second record is listed in Table 5.3. In that case the actual shear force in the span and the value of M/Vd has to be updated according to the values of P_1 and P_2 at failure.

Table 5.3. Summary of test results of continuous beam tests.

Test No.	f_{cm} [MPa]	Age [days]	Failure Mode[2]	$P_{1,u}$ [kN]	V_u[3] [kN]	$P_{1,cr}$ [kN]	V_{cr}[3] [kN]
Series 1							
C1a152	68.4	37	FS	198.9	150.5	198.9	150.5
C1b153	68.4	57	FS	336.1	267.3	182.5	146.0
C2a154	68.4	59	FS	326.0	268.5	224.3	184.7
C2b151	68.4	64	FS	178.1	124.7	178.1	124.7
C3a123	74.0	57	F	401.1	337.2	285.5	239.8
C3a124a	74.0	57	O	468.5	404.6	399.4	344.9
C3b121	74.0	75	FS	264.4	200.9	175.6	132.4
C4a122	74.0	76	F	330.0	266.8	204.3	165.2
C4b091	74.0	90	F	322.4	264.3	181.7	149.0
C4b094a	74.0	90	O	561.1	505.6	331.4	298.3
C5a094	78.1	71	F	564.6	508.7	327.4	295.0
C5b183	78.1	138	F	323.2	241.6	183.6	137.7
Series 2							
C9a123	75.5	89	F	529.5	445.2	257.9	216.8
C9a123[1]	75.5	89	O	530.3	494.6	257.9	216.8
C9b121	75.5	90	F	367.5	279.3	177.6	135.0
C9b121[1]	75.5	90	O	475.4	442.4	475.4	442.4
C10a124	75.5	95	F	581.6	502.3	302.9	261.6
C10b154	75.5	96	FS	271.6	223.7	229.9	189.3
Series 3							
C11a091	69.8	35	SC	772.8	633.7	205.6	168.6
C11b123	69.8	41	FS	236.6	198.9	222.8	187.3
C12a121	69.8	42	FS	250.1	190.1	217.9	165.6
C12b094	69.8	43	SC	1002.7	903.5	331.3	298.5
C13a122	69.3	49	FS	488.8	395.2	182.9	147.9
C13b092	69.3	54	SC	827.5	710.5	232.6	199.7
C14a124	69.3	56	SC	463.8	400.6	318.3	274.9
C14b093	69.3	62	SC	821.2	725.6	367.7	324.9
C15a151	66.5	48	FS	220.8	154.6	220.7	154.5
C15b154	66.5	49	FS	290.2	239.0	230.5	189.8
Series 4							
C16a123	66.5	50	SC	611.8	514.3	237.9	200.0
C16b123	66.5	56	FS	301.7	253.6	245.3	206.2
Series 5							
D17a151	66.1	55	FS	303.3	212.3	250.0	175.0
D17b154	66.1	60	O/FS	500.4	161.9	229.6	189.1
D18a121	66.1	61	O/FS	611.9	146.9	250.4	190.3
D18b152	66.1	67	FS	326.8	247.3	326.7	247.2

[1] These results were achieved by keeping the position of P_1 after the yielding moment, and apply P_2 on the cantilevered end at loading rate of 0.01 mm/s.

[2] The failure modes of the specimens are organized in four catalogues abbreviated by: F: Flexural failure (yielding of longitudinal rebar); SC: Shear Compression failure; FS: Flexural Shear failure; O: Others, mainly stands for failure developed in the span such as the cantilever.

[3] The shear force does not include the self-weight. The shear force generated by the self-weight of the specimens is about 8.82 kN. It has to be taken into account during the evaluation process.

In Table 5.3, two critical load levels are recorded. They are the **ultimate capacity** of the specimen denoted by P_u and V_u, and the **inclined cracking load** identified as P_{cr} and V_{cr}. The later one is defined by the moment that the inclined crack in the critical shear span opens due to the development of a dowel crack along the longitudinal rebar. The mechanism of that process has been introduced in Chapter 3. Following the same description, it was always possible to find a critical point during the loading process that fulfils the description within the test series, even when the failure mode of the specimen was flexural failure. The same definition is valid to the other test results that are to be described in the following chapters.

Unlike the ultimate capacity, the definition of V_{cr} varies in the literature per author, especially when the specimen shows shear compression failure. To avoid the inconsistence due to the unclear definition, only inclined cracking loads of the tests carried out within the same research program on the residual shear capacity of concrete bridges are adapted for further analysis. The inclined cracking loads in research program presented are determined from the vertical deformation - shear force relationship diagram measured real-time with the LVDT array shown in Fig. 5.7 during the experiments. The test results in Table 5.3 show that even with a moderate reinforcement ratio of 0.68% in series 1, it is still possible to develop a shear failure in beams without shear reinforcement. Therefore the evaluation of the shear capacity is still crucial in this type of beams.

In Fig. 5.11, the maximum shear forces V_u measured in the tests are plotted against the maximum M/Vd and the shear slenderness ratio a/d of the critical span respectively. The comparison shows that the scatter of the test results is mainly due to the different failure modes of the specimen when the shear slenderness is small. In general the specimens showing shear compression failure form the upper bound whilst the specimens with flexural shear failure form the lower bound. The comparison also reveals that the scatter of the results is reduced when the ultimate capacity of the specimens are plotted against the maximum M/Vd.

However regarding the specimens with failure mode of shear compression failure, V_u is more strongly related to a/d. This can be explained by the residual load bearing structure originating after inclined cracking described in Section

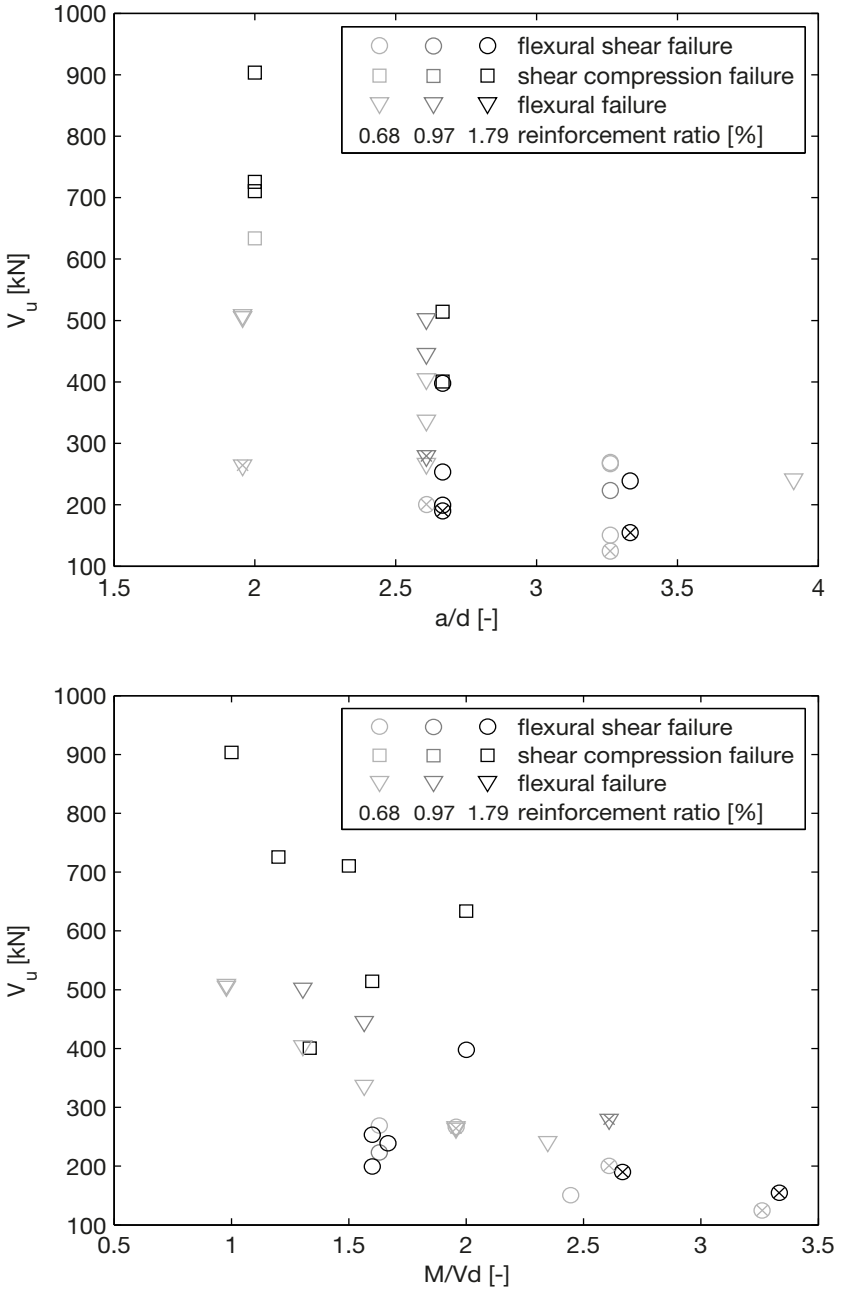

Fig. 5.11. Relationship of maximum shear capacity V_u plotted against a/d (upper) and M/Vd (lower): the additional cross on the markers stands for simply supported beams. The extra sign × on the data point indicates that it is a simply supported test.

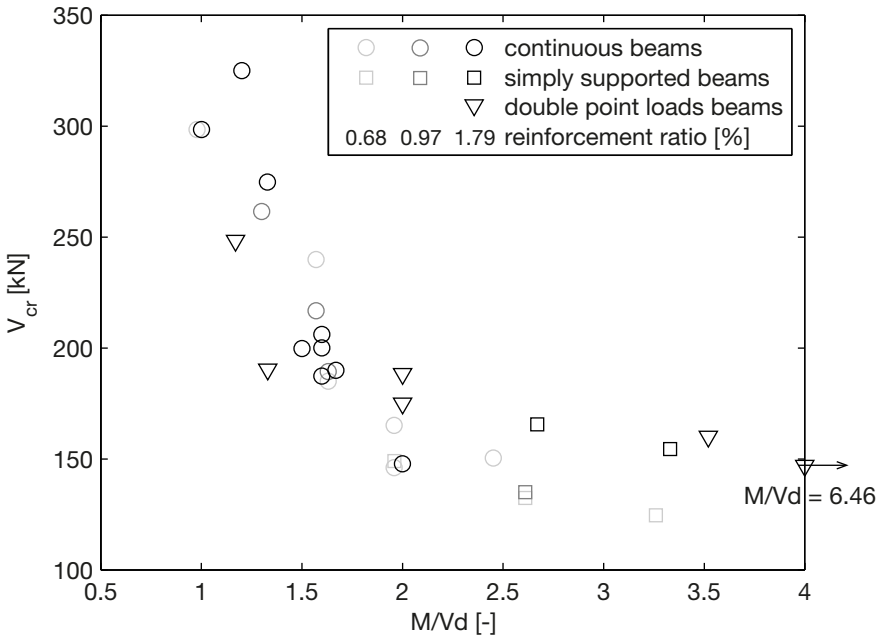

Fig. 5.12. Relationship between inclined cracking load V_{cr} and M/Vd.

3.5.2. In the case of the continuous beams, the loading point also includes the support regarding the moment distribution. Therefore, as long as the tip of the critical crack is within the critical compressive zone a_{cc} from the edge of the loading point, the compressive strut will not fail directly upon the formation of the critical inclined crack. In that case, the strut can develop directly from the loading point to the support through the point of inflection. The critical span should to be considered as one piece. The ultimate capacity has to be calculated according to the shear slenderness a/d.

Fig. 5.12 shows the relationship between the inclined cracking load V_{cr} and the maximum M/Vd. Indeed, compared to the two figures regarding the ultimate shear force V_u in Fig. 5.11, by introducing V_{cr}, a much stronger relationship is observed. The smaller scatter related to the inclined cracking load can be explained by the fact that unlike the ultimate capacity which may be determined by several failure modes, the inclined cracking load is mainly governed by a single failure mode. Therefore, a more robust prediction can be expected regarding to the inclined cracking load rather than trying to get the ultimate capacity of the concrete members involving multiple failure modes.

Furthermore, the formation of the inclined cracks defines the compressive strut. In the case of flexural shear failure, it determines the ultimate capacity of

the specimens directly. Whilst in shear compression failure, the formation of the inclined cracks is always prior to the crush of the compressive strut according. Further discussion in Chapter 6 also shows that considering the presence of the existing cracks and other faults in the beams, whether or not the compressive strut in the residual structure may still be influences by the inclined crack in many cases even at a relatively smaller shear span. In that case, the formation of the inclined crack in a reinforced concrete beam without shear reinforcement can still be considered as the lower bound of the shear capacity.

Based on the results of test series 5, a similar conclusion may be extended to specimens loaded by multiple point loads. In Fig. 5.12, the inclined cracking loads derived from test series 5 are included as well. The results show no difference from the tests with single point loads. In test Series 5, the first inclined crack developed in the critical span in all the four tests. However, unlike the tests with a single point load, in which the inclined crack normally stopped at the edge of the loading point, the cracks extend into Span 3 along the top reinforcement in the tests from series 5. That makes the capacity of the compressive arch structure after the first loading point very low. An example of the crack pattern of a typical multiple point loads test is shown in Fig. 5.13.

Table 5.4. Shear forces over the spans at critical load levels. The shaded cells indicate the critical span.

Test No.	Variable	Span 1	Span 2	Span 3	Span 4	P_1
D17a151	M/Vd	-	2.00	9.76	6.46	
	V_{cr}	-	175.0	50.0	75.0	250.0
	V_u	-	212.3	60.6	91.0	303.3
D17b154	M/Vd	2.00	1.67	3.52	6.46	
	V_{cr}	156.1	188.3	73.5	41.3	229.6
	V_u	340.3	410.3	160.1	90.1	500.4
D18a121	M/Vd	-	1.33	6.56	6.46	
	V_{cr}	-	190.3	65.1	60.1	250.4
	V_u	-	465.0	159.1	146.9	611.9
D18b152	M/Vd	2.00	1.17	6.11	6.46	
	V_{cr}	104.5	248.3	85.0	78.4	326.7
	V_u	104.6	248.3	85.0	78.4	326.8

As two special cases, in tests D17b154 and D18a121, the residual structure of the specimen after the inclined cracking load were still strong enough to carry more load. Because of that, the load applied on the specimen was increased further, until flexural shear failures occurred in another span. The shear forces in each span of the same specimen, corresponding to the occurrence of the inclined crack and failure, are summarized in Table 5.4, whereas the maximum values of

the ratio M/Vd in the corresponding spans are indicated as well. The spans in which the specified event occurred are shaded in the table.

5.3.5 Shear Cracking in a Span with Large *M/Vd*

An additional remark is given on tests D18a121. As shown in Table 5.4, the final failure in this test occurred in span 4 with a maximum M/Vd = 6.46. Compared to the other tests in the same series, the value of M/Vd in the test is much larger. Nevertheless the inclined cracking load found in the experiment is still quite comparable with the other tests with M/Vd close to 3.0. That observation partly proofs that there is a lower limit with respect to the influence of the bending moment, as was illustrated in Fig. 3.38 qualitatively. This can be explained by two facts. First of all, when the crack is developed at an M/Vd larger than 3.0, the influence of M/Vd to the crack pattern is very limited; Secondly, the aggregate interlocking force at the tip of the major cracks (can be simplified with a constant shear stress distributed at a characteristic length l_0 according to Section 4.7.2) contributes mostly to V_{ai}. The length of l_0 is less influenced by the crack opening, when the value of M/Vd is larger.

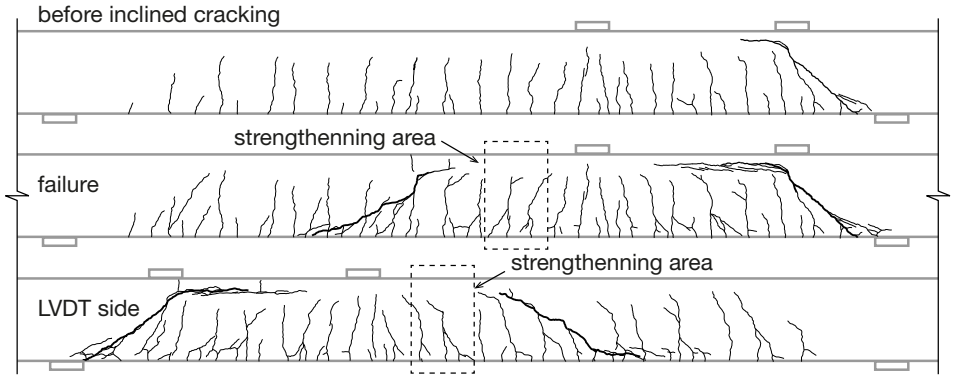

Fig. 5.13. Crack pattern of D18a121 after failure.

As shown in Fig. 5.13, the vertical flexural cracks had been fully developed in D18a121 before the development of the critical inclined crack. Actually at P_1 = 550 kN ($V_{cr,4}$ = 132.0 kN), an inclined crack started to develop from the flexural cracks already formed in Span 4 of the specimen. The test was stopped, and that part of the beam was strengthened, see Fig. 5.13. Nonetheless, the second inclined crack developed quickly afterwards. This experiment validates the hypothesis made in Chapter 3 section 3.4.3.

- The inclined cracks form on the basis of the flexural major cracks. Therefore, the proposition about the opening of a critical inclined crack at one time does not always hold true. The inclination of the crack cannot be 45° either.
- As was proposed in Chapter 3, the failure is due to the fact that the shear force applied at the cross-section results in a large shear displacement between the crack faces so that a dowel crack along the longitudinal reinforcement has to develop;
- When the ratio M/Vd of the span is large, the shape of the flexural major crack does not influence the shear capacity of the beam significantly; the difference between inclined crack locations in different positions is quite limited;
- However, the small difference still causes the inclined crack to develop first at locations with a larger M/Vd.

5.3.6 Shear Cracking in a Span with Small *M/Vd*

5.3.6.1 Evaluation of the Continuous Beam Tests

In principle it is possible to extend the shear evaluation procedure proposed in Chapter 4 to continuous beams loaded by point loads, assuming that the three criteria raised in 5.2 are not violated in this loading case. The test series presented in this chapter are evaluated with the proposed shear calculation procedure. The **calculated shear capacity** V_{cal} is, by definition, the inclined cracking load of the specimens. Thus, they shall be compared with the values of V_{cr} if the development of the inclined crack did not result in the final failure of the corresponding specimen. To evaluate the prediction with the test results, the values of V_{cr}/V_{cal} are plotted against M/Vd in Fig. 5.14.

The comparison shown in Fig. 5.14 should be regarded separately with respect to the maximum M/Vd of the tests. For specimens with an M/Vd larger than 2.0, the model gives quite a good prediction in general. Apart from one test, all the predictions are within 20% of the test results. However, when M/Vd is close to 2.0, the predictions overestimates the capacities of the specimens on average. It actually reflects the discussion on the special cases when determining the critical cross sections in Chapter 3 section 3.4.3. The calculated minimum V_{cal} in the vicinity of the loading point is about 200 kN for beams with shear span of $2.0d$, while at V_{cr} = 150 kN, the cracked section is already at about $0.6d$ from the support, where the resultant shear force that can be generated is significantly reduced due to the large crack inclination. Therefore, the shear capacity is overestimated when the maximum M/Vd is close to 2.0. Nevertheless, as was expected in section 3.4.3, the overestimation is quite limited.

On the other hand, when the maximum M/Vd of the span is smaller than 2.0, the model underestimates the capacities of the specimens. The ratio of V_{cr}/V_{cal}

increases with the decrease of M/Vd. It indicates that the model does not reflect the shear cracking process properly when the maximum M/Vd becomes even smaller than about 2.0. Considering that for continuous beams, it is quite likely to have a very small maximum M/Vd in its critical shear span, additional evaluation under that situation seems to be important.

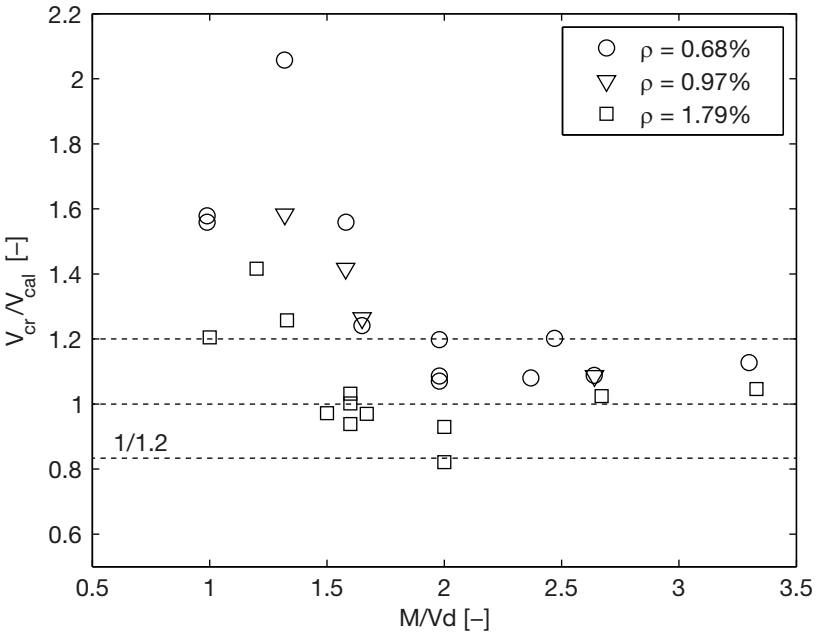

Fig. 5.14. Relationship between V_{cr}/V_{cal} and M/Vd, V_{cal} calculated by the adjusted critical shear displacement shown in Section 4.6.

5.3.6.2 Adjustment for Beams with Small *M/Vd*

With respect to beams with a maximum M/Vd smaller than 2.0 subjected to point loads, the three criteria proposed in 5.2 are checked again. Based on the discussions in Chapter 3 and the observations within the test program, one may conclude that in this case, Criterion 2 is not fulfilled. As explained previously, the calculation model assumed a simple bilinear crack profile, in which the major crack is perpendicular to the longitudinal direction. It is connected by an inclined secondary crack branch in the compressive zone. This is an approximation of the crack path usually observed at cracked sections with large M/Vd. With the reduction of the maximum M/Vd of the span, the inclination of the major cracks in the span increases, the consequence of which is that the formulas of both V_c and V_{ai} at Δ_{cr} cannot describe the behaviour properly anymore.

With respect to the aggregate interlock effect, a larger crack inclination results in an increase of the shear displacement Δ at the position of tensile

reinforcement under the same shear force. This effect has been illustrated in Fig. 3.33. For a given critical shear displacement Δ_{cr}, the shear force that can be generated by aggregate interlock reduces. If the inclination of the crack is large enough, the rotation of the crack around the crack tip before a horizontal crack develops may already make Δ larger than Δ_{cr}. In this case, the propagation of the crack itself leads to splitting cracking along longitudinal reinforcement as shown in section 3.4.3. However, considering that the contribution of V_c to the total shear resistance V is significantly increased at the same time, V_{ai} becomes less important for the loading case being discussed here. A more thorough discussion on this topic will be given in section 5.4.2 for beams loaded by a distributed load. The reduction of V_{ai} under smaller M/Vd will directly affect the ultimate bearing capacity in that case.

The shear force in the concrete compressive zone V_c increases significantly when M/Vd is reduced. This has been illustrated in section 3.5.3. The reason is that when the maximum M/Vd is small, the teeth structure which can be described with Eq. (3.26) to calculate V_c does not exist anymore. In that case, the tip of the inclined crack reaches the loading point directly. The criterion for the residual capacity after reaching the inclined cracking load is illustrated in Fig. 3.42. It also applies for continuous beams with point loads. When the maximum M/Vd is smaller than 2.0, the value of V_c shall be evaluated taking into account the stiffness of the arch structure formed by the inclined crack.

Based on the two aspects mentioned above, the contributions of V_c and V_{ai} to the total shear resistance change significantly when the M/Vd reduces. To illustrate this effect a simplified example is given in Fig. 5.15, where, V_c and V_{ai} are calculated using the beam example introduced in Chapter 3, assuming that the bottom crack opening in both sides is fixed at Δ = 0.02 mm, w = 0.4 mm. The value of V_c is calculated with the simplified formula Eq. (3.49). V_{ai} is calculated by the integration of aggregate interlocking stresses with Eq. (3.31) based on the crack path described by Eq. (3.19), assuming that the critical crack is initiated at $0.6(M/V)$ from the point of inflection. Accordingly, the length of the concrete arch is the remaining part of the span: $0.4(M/V)$. Fig. 5.15 shows that when M/Vd of the span is smaller than 2.0, the proportion of V_c and V_{ai} changes tremendously under the same vertical displacement Δ. The percentage of V_c increases significantly from about 20% at M/Vd = 2.0 towards 100% when M/Vd is smaller than 0.5. The increment of V_c is mainly due to the increase of stiffness of the concrete arch span. The comparison implies that for beams with small M/Vd the aggregate interlocking effect is not decisive anymore as it would be in case of slender beams. This conclusion is valid for all other load cases and structures in which the teeth structure is not able to form.

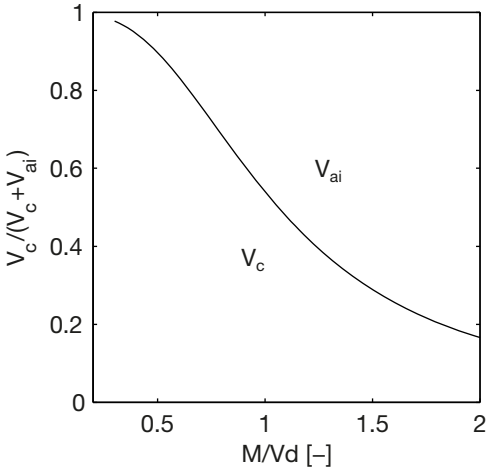

Fig. 5.15. Variation of proportion between V_c and V_{ai} with respect to M/Vd.

It has to be remarked that the calculation procedure utilized in Fig. 5.15 is not directly applicable for the shear capacity evaluation. A more accurate evaluation of the crack width w and the crack profile for V_c calculation is still needed for an accurate evaluation.

In general, the model does not apply in the case of a beam with small maximum M/Vd, since the failure of such beams is often due to the crushing of the concrete arch. The determination of the inclined cracking load in that case seems to be of less significance.

On the other hand, the evaluation on a model predicting the inclined cracking load of beams with small maximum M/Vd is also quite difficult. Because of the fact that the definition of the inclined cracking loading varies from different authors in literature, thus very limited test results can actually be applied for the evaluation process, especially with respect to beams with maximum M/Vd smaller than 1.5.

An engineering approach to this problem is to carry out a general regression analysis as was done by design codes, such as the Eurocode, which shows that with a reduction factor $\beta = 2a/d$ to the shear load, a safe prediction can be obtained. This conclusion was extended by Yang et al. in (Yang, Den Uijl et al. 2011; Yang, den Uijl et al. 2012; Yang et al. 2013). They concluded that for beams loaded by point loads, when the maximum M/Vd in the span is smaller than 2.0, one is able to increase the shear capacity calculated based on $M/Vd = 2.0$ with $\beta = 2(M/Vd)^{-1}$. The conclusion was made based on the Eurocode provision. Nevertheless, it also applies to the model proposed in this research work. The increment of V_{cr} with M/Vd can be understood as the cracking shear force line in Fig. 3.38. In the calculation procedure introduced in section 4.4, two additional

steps shall be added: Check if $M/Vd < 2.0$, make $M/Vd = 2.0$ during the calculation; By the end of the calculation, the resultant V should be increased by $\beta = 2(M/Vd)^{-1}$.

By introducing the adjustment explained above, the accuracy of the prediction is clearly improved. The ratios of V_{cr}/V_{cal}/ are plotted in Fig. 5.16. Compared to the prediction shown in Fig. 5.14, the accuracy is clearly improved in general. The adjusted model turns out to be accurately enough as a lower bound of the shear capacity of the specimens.

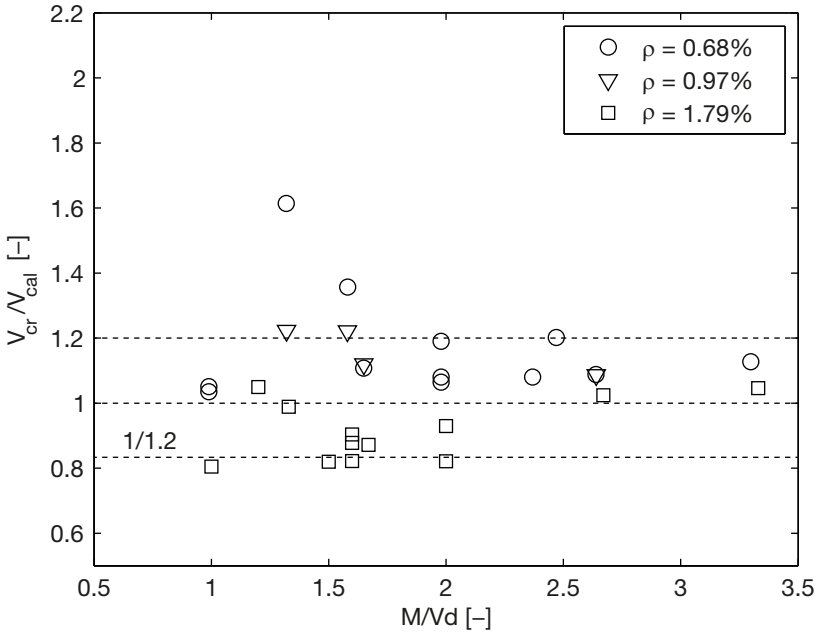

Fig. 5.16. Relationship between V_{cr}/V_{cal} and M/Vd, V_{cal} as calculated with the adjusted critical vertical displacement.

However, it has to be emphasized that one should not be misled by the adjusted method and presume that the shear failure mechanism of specimens with a small M/Vd is the same as in a normal beam. Although the overall shear resistance may be approximated with the same procedure, the contribution of each part of the cracked section is totally different. The reasons for the difference have been explained previously. As a result, some of the conclusions applied to normal beams may not be the same for beams with a small M/Vd. For example, with respect to high strength concrete or lightweight aggregate concrete, the same reduction factor on aggregate interlock proposed in section 4.5.2 may not be applicable anymore. Because the contribution of aggregate interlock effect is very limited in this case. However, the mean tensile strength f_{ctm} and the fracture

energy of the concrete G_f become more important for the inclined cracking load in this case. With the mechanism understood, further adjustment is possible.

5.4 UNIFORMLY DISTRIBUTED LOAD

5.4.1 From Point Loads to Distributed Load

A uniformly distributed load is a regular loading case in tunnels and foundations. Many of those structures are constructied without shear reinforcement, thus are vulnerable to shear failure as well. The evaluation of the shear capacity of beams under a uniformly distributed load is of interest and will be discussed in this section. Based on that, the model is extended to deal with distributed loads.

Compared to point loads, a uniformly distributed load generates a continuously varying shear force distribution along the span. The consequence is that the 2nd and 3rd criteria described in section 5.2 are violated.

Regarding Criterion 2 about the shear force components, the assumptions for the determination of V_c with Eq. (3.26) are not valid. However, since the crack spacing is usually significantly smaller than the beam span, the variation of the shear force between two subsequent cracks is quite limited. As long as the adjacent cracks are of the same height, it is safe to use the simplified relationship described by Eq. (3.26)designed for point loads. In case of a simply supported beam, it is observed that the critical section is located in the vicinity of the support, where no limitation is expected on the development of the secondary crack branch of the critical inclined crack. Criterion 3 is not violated in this case, thus V_c can still be calculated with Eq. (3.26). However, when the beam has an intermediate support or other types of supports with confinement on rotation, the critical inclined crack develops towards the support in the vicinity of the support. In that case, the crack teeth cannot form anymore, thus V_c has to be formulated differently.

For Criterion 3, the determination of the critical section under the loading case of a uniformly distributed load is more complex than for point loads. As an example of a member with simple boundary conditions, a simply supported beam is regarded. The moment and shear force distribution along the beam are given in Fig. 5.17. (a) (b). Under that loading case, the maximum moment is reached at mid-span of the beam. Close to that point, the crack widths are larger. Therefore a lower shear capacity may be expected. However, the shear force in that region is close to zero. Consequently, even though a smaller shear resistance is expected, due to the even lower shear force at the same cross section, the critical section cannot be here. In the vicinity of the support, the maximum shear

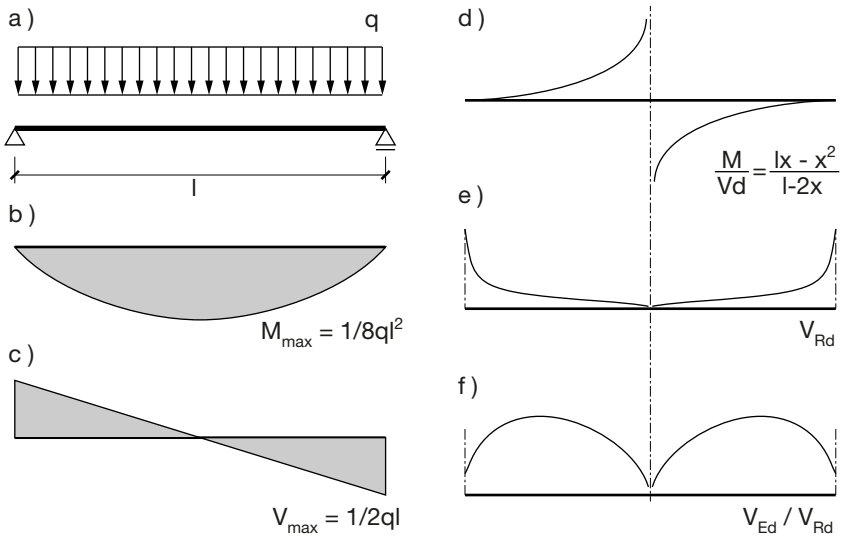

Fig. 5.17. Calculation of shear capacity along simply supported beam loaded by a uniformly distributed load. (a) Boundary conditions. (b) Moment distribution. (c) Shear force distribution. (d) *M/Vd* distribution. (e) Shear resistance assuming straight crack path. (f) Shear force over shear resistance.

force is reached. However, since the moment there is close to zero, the crack widths there are very small. Higher shear resistance is expected there as well. Besides, when the cross sectional moment is smaller than M_{cr}, the flexural cracks cannot develop at the sections very close to the support of the beam; therefore the critical section cannot be there either.

It is assumed that the shear force resistance formula given in Chapter 4 is still valid in the case of beams subjected to a uniformly distributed load, which means that the influence of the crack profile to the shear resistance is eliminated, and the resistance of the cracked section is only related to the moment over shear force ratio (M/Vd) locally. The shear resistance distribution along the span can then be calculated. In the case of a simply supported beam, the shear resistance V_R along the beam is plotted in Fig. 5.17 (e). Considering the linear distribution of the shear load V_E shown in Fig. 5.17 (c), the critical cross-section can be found by checking the location where the value of V_E/V_R reaches the maximum, see Fig. 5.17 (f). A Similar approach has been proposed by Muttoni in (Muttoni & Ruiz 2008). In this loading case, the critical section is located at about $0.15l$ from the support, when l is the length of the total span. The same procedure may be applied to other load cases. In Fig. 5.19, two examples are shown. In these two cases, the critical sections are close to the clamped support, where both the moment and shear forces reach peak values.

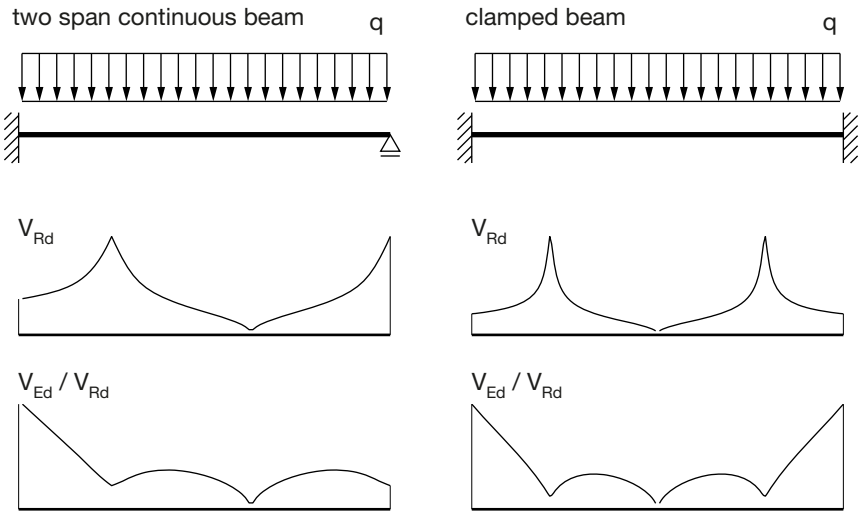

Fig. 5.19. Distribution of V_R and V_E/V_R under statically indeterminate beams.

Another aspect relating to the critical section in beams subject to a uniformly distributed load is how to determine the shear force in the cracked section. Taking simply supported beams as an example, a demonstration of the load distribution and the crack path is shown in Fig. 5.18. The shear force that is transferred across a certain crack should be determined by the location of the crack tip. The part of the distributed load between the crack tip and the support is transferred to the support by the part of the concrete member. Therefore, the shear force that has to be transferred along a crack generated at x_0 is calculated at x_{ct}. With regard to the simple bilinear crack profile defined in Chapter 4, x_{ct} is calculated from the tip of the secondary crack branch, according to Fig. 4.2. The effective shear force at the critical crack is therefore calculated by $V_E = q(l/2 - x_{ct})$.

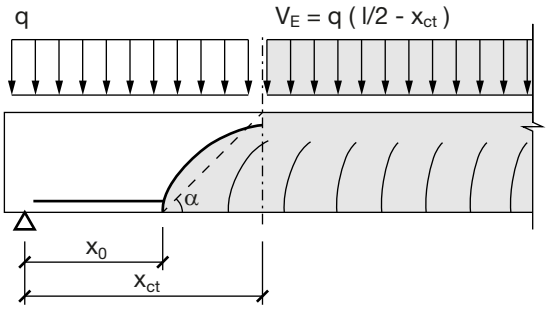

Fig. 5.18. Evaluating shear force V_E for a critical shear crack.

In general, for beams loaded by any type of distributed load, depending on the loading and supporting conditions, the effective shear force has to be calculated by the load applied on the part of the beam that cannot be transferred directly to the support, the boundary of which should always be defined by the tip of the crack. Other examples will be given in the following chapters.

5.4.2 Adjustment of Crack Inclination

The principle discussed in the previous section implies that the shear capacity of cracks initiated from any cross-section of the beam can be predicted with the formulation derived in Chapter 4. In the calculation procedure, the aggregate interlocking force is calculated with a simplified crack shape, which basically ignores the inclination and the curvature of the crack. However, when the value of M/Vd at the critical section is smaller than 1.0, a large inclination is expected when a crack is developed there. In that case, the influence of the crack shape has to be taken into account. Besides, the crack shape may influence the design value of the shear force V_E that has to be checked along the cracked surface, and the shear component in the concrete compressive zone V_c as well. The three aspects are to be discussed in this section.

For beams loaded by point loads, to have a critical crack under a small M/Vd is more difficult because a higher cracking moment is needed in that case. Because the shear force level is constant along the span, at the load level when a crack can develop at sections with small M/Vd, the beam already fails at cracked sections closer to the loading point. However, when a beam is subjected to a uniformly distributed load, a larger part of the sections have very small M/Vd. As an example the simply supported beam shown in Fig. 5.17 is regarded. The distribution of M/Vd is plotted in Fig. 5.17 (d). It shows that in the vicinity of the support, the value of M/Vd is exceptionally low. For a beam with $a/d = 3.0$, the value of M/Vd is smaller than 1.0 at $0.3a$ from the support. For uniformly distributed loaded beams, the shear span a stands for $l/2$. Because the shear force close to the support is larger, the chance of having the crack developed from a section with small M/Vd is high as well. Thus the evaluation of the shear capacities of cracks developed under small M/Vd has to be investigated.

The influence of the crack shape on the shear capacity of a cracked section is shown in Fig. 5.20. In the figure, the shear displacement of the crack faces at the level of reinforcement of a cracked section Δ is calculated under a shear force V = 100 kN according to the procedure described in section 3.4.1, and is represented by the solid line. For the sake of comparison, the dashed line indicates the shear displacement calculated with a constant crack shape at $M/Vd = 4.0$. The figure demonstrates the influence of the crack shape to the shear resistance of the

section qualitatively. It shows a clear drop of the shear resistance when M/Vd is smaller than 1.0.

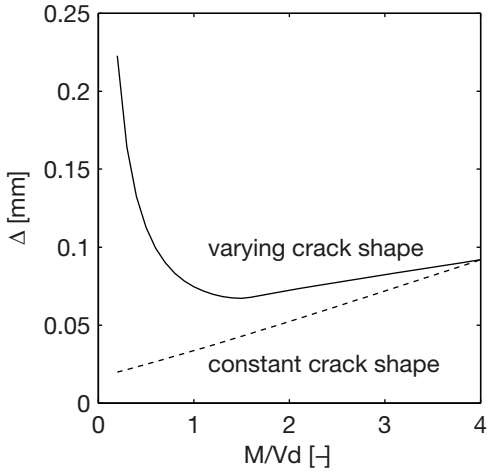

Fig. 5.20. Influence of crack shape to the vertical displacement under V = 100 kN.

However, in order to retain the merit of simplicity by using a straight crack, it is not appropriate to introduce a complex crack shape function to consider this effect. As a compromise, simplification of the crack profile is still needed to get a workable procedure in this case. In this part of the section, two alternatives are provided. Both can describe the change of the crack profile to a certain extent. They are introduced into the evaluation procedure described in Chapter 4.

Crack Inclination Method

The heavily curved crack generated at a cross-section with small M/Vd is simplified by an inclined straight line. The inclination of the line represents the average inclination of the curved crack profile. The advantage of this procedure is that both the simplified aggregate interlock equation Eq. (4.7) and the full expression Eq. (4.4) still apply in this more complex situation. This simplification reflects the reality to a certain extent. What has to be declared is that the average inclination cannot be misunderstood as a replacement of the real curved crack. The inclination of the crack path at the root of the crack still has to be perpendicular to the longitudinal direction for a real crack, see Fig. 5.21, because of the stress state of the cross-section before cracking. For that reason although in Fig. 5.21 the value of Δ_b is not strictly measured along the inclined crack profile, it is still denoted as the shear displacement at the reinforcement level.

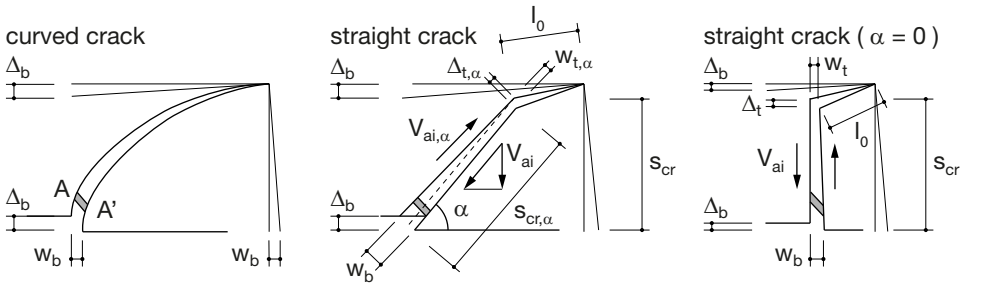

Fig. 5.21. Kinetic condition of an inclined crack.

For inclined cracks, the secondary crack branch defined in chapter 4 is still necessary to generate a tangential displacement in the major crack and to represent the change of inclination of a curved crack properly. It reduces the rotation of the crack under the same Δ_b at the tensile side of the beam when there is sufficient distance between the tip of the major crack and the point of inflection.

By replacing the curved crack profile with a straight crack having an average inclination of α, the input of Eq. (4.7) has to be adjusted. A scheme of the crack is depicted in Fig. 5.21. According to the kinetic conditions shown, the equation is updated:

$$\begin{aligned} V_{ai} &= V_{ai,\alpha} \sin\alpha \\ &= \sin\alpha \cdot f_c^{0.56} s_{cr,\alpha} b \frac{0.03}{w_{b,\alpha} - 0.01}(-978\Delta_\alpha^2 + 85\Delta_\alpha - 0.27) \end{aligned}$$

with $s_{cr,\alpha} = s_{cr}/\sin\alpha$, the equation retains the same structure:

$$V_{ai} = f_c^{0.56} s_{cr} b \frac{0.03}{w_{b,\alpha} - 0.01}(-978\Delta_\alpha^2 + 85\Delta_\alpha - 0.27) \tag{5.1}$$

where

Δ_α, w_α:are the normal and tangential displacement along a crack path, where the additional subscripts b and t stand for the displacement measured at the level of the tensile reinforcement or the tip of the major crack respectively;

$s_{cr,\alpha}$: is the length of the crack, while s_{cr} is the height of the crack in the height direction of the beam

The next step is to convert the crack width w_b and the critical shear displacement Δ_{cr} of the inclined crack into the normal and tangential displacements $w_{b,\alpha}$ and Δ_α required in the formula.

The introduction of the crack inclination results into two effects regarding the formulation of the **vertical displacement** Δ_b (distinguished from the **tangential displacement** Δ_α in the inclined major crack) at the reinforcement level, and the shear displacement Δ_t at the tip of the major crack.

- The additional vertical displacement due to the larger horizontal distance $s_{cr}\cot\alpha$ introduced by the crack inclination is, according to Fig. 5.21:

$$\Delta_b = (l_0\cos\alpha_0 + s_{cr}\cot\alpha)\theta = l_0\theta\cos\alpha_0 + s_{cr}\cot\alpha\cdot\theta \tag{5.2}$$

- The average inclination of the crack path changes the formulation of the normal and tangential displacements $\Delta_{t,\alpha}$, $w_{t,\alpha}$. Assuming that the tangential displacement Δ remains constant along the crack, its value can be calculated by projecting the rotation of the secondary crack branch to the direction of the major crack, which results in:

$$\Delta_\alpha = l_0\theta\cos(\frac{\pi}{2} - \alpha + \alpha_0) \tag{5.3}$$

where

α: represents the average inclination of the major crack;
α_0: is the inclination of the secondary crack branch;
θ: is the rotation of the whole crack profile around the crack tip;
l_0: is the length in the longitudinal direction of the secondary crack branch.

Combining Eq. (5.2) and Eq. (5.3), and taking $\Delta_b = \Delta_{cr}$, gives the following expression for Δ_α:

$$\Delta_\alpha = (\Delta_{cr} - s_{cr}\cot\alpha\cdot\theta)\frac{\cos(\frac{\pi}{2} - \alpha + \alpha_0)}{\cos\alpha_0} \tag{5.4}$$

Since the inclination of the secondary crack branch is usually small due to the confinement in the compression zone, the value of α_0 is set to zero in Eq. (5.4), which results in the following simplified formula:

$$\begin{aligned}\Delta_\alpha &= \Delta_{cr}\sin\alpha - s_{cr}\theta\cos\alpha \\ &= \Delta_{cr}\sin\alpha - (w_{b,\alpha} - w_{t,a})\cos\alpha\end{aligned} \tag{5.5}$$

The simplified aggregate interlocking force formula Eq. (4.7) was derived by regression analysis with a normal crack width w_b = 0.01 mm at the crack tip. To guarantee the validation of the formula, $w_{t,\alpha}$ has to be 0.01 mm. The value of $w_{b\alpha}$

can still be the calculated one by the elongation of the reinforcement expressed by Eq. (4.3).

The additional shear displacement described by Eq. (5.2) can be applied to beams subjected to point loads with short shear span as well. It has been illustrated by Fig. 3.38 in section 3.4.3 qualitatively that the shear resistance of a cracked section reduces for cracks generated with smaller M/Vd. The comparison between experimental results in section 5.3.6.1 confirms that when the shear span is close to $2.0d$, the reduced shear resistance for cracks with smaller M/Vd can be critical. However, in the evaluation procedure developed in Chapter 4, this effect is ignored for beams with large shear span to simplify the evaluation procedure. The argument was that the difference between the reduced shear resistance at smaller M/Vd and the one evaluated in the vicinity of the loading point is limited. For an accurate evaluation of the full shear resistance curve as shown in Fig. 3.38, Eq. (5.2) offers a solution to evaluate the effect of beams with very short span with a similar simplified procedure.

Crack Length Reduction Method

Regarding the original calculation procedure, the introduction of a bilinear crack profile with a vertical first branch (also called major crack) significantly simplifies the calculation procedure. It is appropriate to retain the basic structure of the calculation procedure designed for the case of single point loads. The inclination of the overall crack profile can be imitated by applying a reduction of the major crack height s_{cr} with a crack inclination factor k_α. An illustration of this simplified crack path is shown in Fig. 5.22. The shortened part of the major crack is connected by a longer secondary branch with constant inclination k_s. k_s is the same as it was defined in section 4.2.1. Therefore, the ratio between w_t and Δ_t remains unchanged. Since the pure rotation around the crack tip does not contribute to the shear resistance, the shear force V_{ai} that can be transmitted through the crack path is still calculated only in the vertical crack path but with a reduced length $k_\alpha s_{cr}$. The value of k_α is related to the level of curvature of the original crack. k_α can be related to M/Vd of the section where the crack initiates

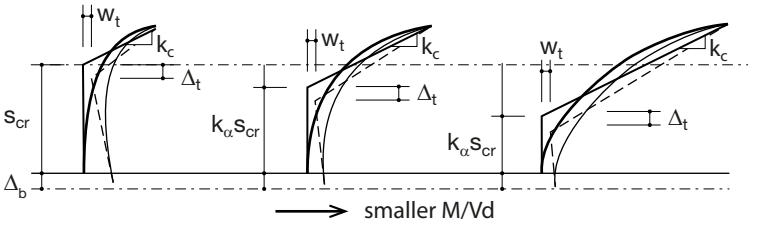

Fig. 5.22. Simplifying curved crack profile by bilinear profile with vertical major crack.

when Eq. (3.19) is taken into account. The crack opening distribution in longitudinal direction w is the same as was proposed in Chapter 4.

By introducing $k_\alpha s_{cr}$ into Eq. (4.7), the shear force transmitted through aggregate interlock becomes:

$$V_{ai} = f_c^{0.56} k_\alpha s_{cr} b \frac{0.03}{w_b - 0.01}(-978\Delta_{cr}^2 + 85\Delta_{cr} - 0.27) \tag{5.6}$$

Similarly, Eq. (4.4) is reformed into:

$$V_{ai} = k_\alpha s_{cr} \sigma_{pu} b \int_0^1 A_x\left(\Delta, w(s')\right) - \mu A_y\left(\Delta, w(s')\right) ds' \tag{5.7}$$

Compared to the formulation described in the first alternative, the procedure of reducing the crack height simplifies the calculation procedure significantly. However, since the assumption of having a crack width at the tip of the vertical crack is set to be 0.01 mm, the rotation of the two parts of the crack has to be different. As a result, the procedure cannot fulfil the kinetic condition, whereas this problem can be neglected in the original model, considering the much smaller length of the secondary branch. For that reason, this alternative can only be applied when proper calibration on test results is available.

5.4.3 Simply Supported Beams

5.4.3.1 General Consideration

By taking into account the inclination of the crack profile discussed in section 5.4.2, the shear failure process of a simply supported beam is re-examined. As shown in Fig. 5.17 (d), the value of M/Vd is really low at the sections close to the support. The influence of the inclination of the critical cracks cannot be neglected anymore. It shall be evaluated from two points of view. On the one hand the shear resistance of the cracked section is reduced by the inclination of the crack profile; on the other hand, the shear force that applies on the crack section should be counted at the tip of the crack profile (x_{ct}), which is also smaller than the shear force at the root of the major crack employed in the original calculation. Thus, it is difficult to evaluate how much the two contradictory effects influence the accuracy of the prediction of the critical crack section.

Regarding the section where the crack initiates, a direct comparison with experimental result has been done with respect to the experimental research carried out by Leonhardt and Walther (Leonhardt & Walther 1962). In the research simply supported beams with different length-depth ratio were loaded

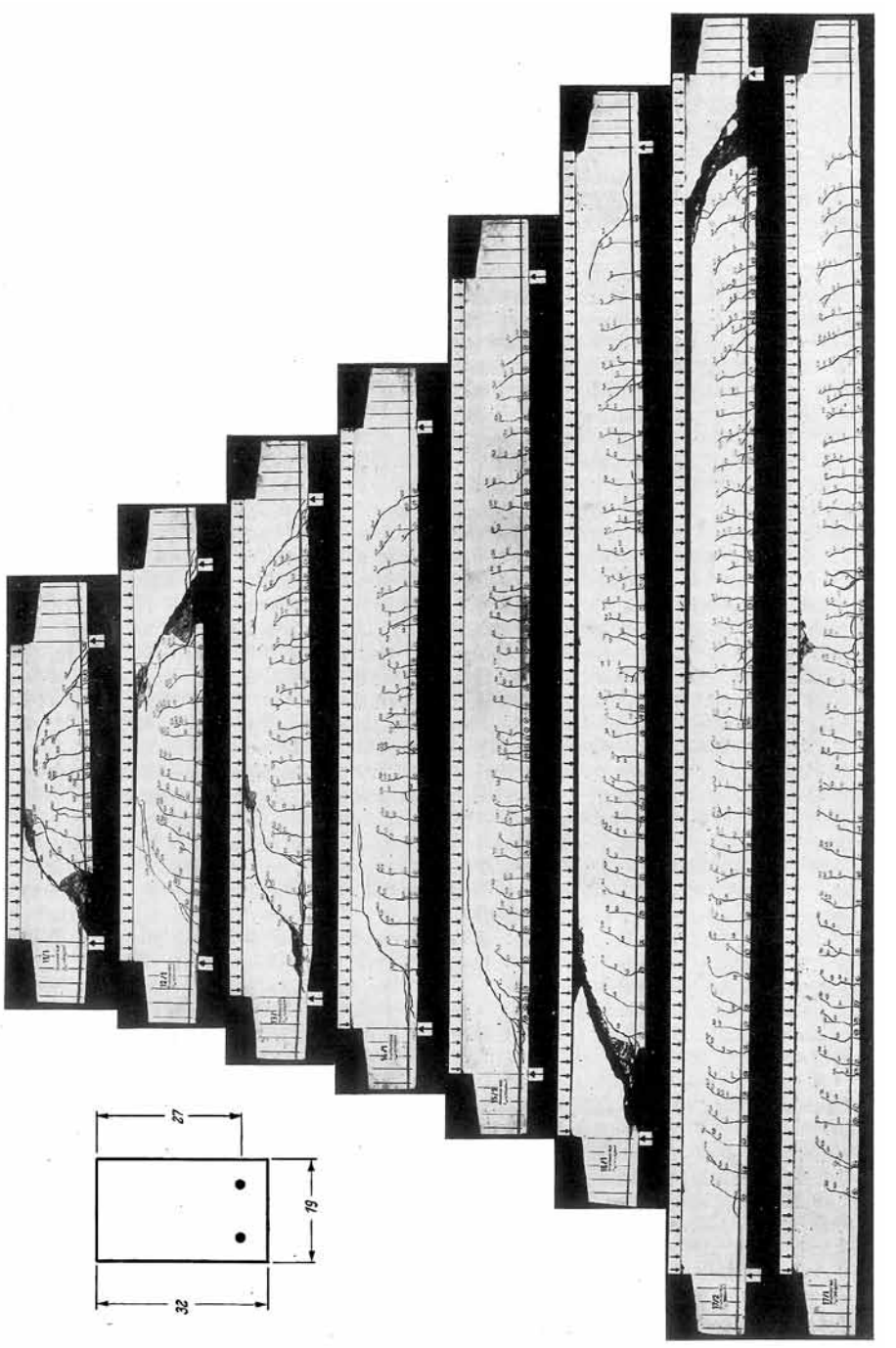

Fig. 5.23. Crack pattern of simply supported beams loaded by uniformly distributed load ((Leonhardt & Walther 1962).

by a uniformly distributed load until shear failure. The crack patterns of the specimens after failure are shown in Fig. 5.23. The figure shows that independent of the beam span, the critical inclined cracks with a large inclination always initiate at sections close to the supports. It is shown that it is appropriate to set the section where cracks initiate at $0.8d$ from the support. The value of M/Vd at the crack initiating section can be used to evaluate the crack profile with Eq. (3.19). It is expressed by:

$$\frac{M}{Vd} = \frac{l \cdot x - 0.5x^2}{0.8(l-x)d} \tag{5.8}$$

However, for the evaluation of the shear resistance, the moment and the shear force must be calculated at the section where the crack tip (secondary crack branch) ends, see Fig. 5.18. Accordingly, the value of M/Vd has to be calculated with Eq. (5.8) at the position of the crack tip.

The position of the crack tip x_{ct} in simply supported beams loaded by a uniformly distributed loads was studied by Reineck, Bentz et al. (Reineck, Bentz et al. 2013). The position of the critical section was directly found on the basis of the failure crack patterns of the specimens reported in literature. According to their definition the position of the critical section is defined as the intersection point of the inclined crack and the neutral axis of the beam. The study showed that the position of the critical section is related to the ratio between the beam span l and the effective depth d. When l/d is larger than 12, the position of x_{ct} is more or less fixed at $2.4d$. For beams with a smaller l/d, a linear regression analysis gives for the expression for x_{ct}:

$$x_{ct} = \left(\frac{2l}{15d} + 0.8\right)d \quad \text{for } l/d < 12 \tag{5.9}$$

The value of x_{ct} has to be converted back to the position of the crack tip again. However, this can be done only when the average inclination of the major crack is known. Before further calibration with experimental results, the value of x_{ct} expressed with Eq. (5.9) is used as an indication of the location of the governing section for the moment and the shear force calculation.

Crack Inclination Method

When the additional crack inclination is taken into account directly by assuming the critical inclined crack as an inclined plane with an angle α, the following adjustment can be considered. For beams with a uniformly distributed load, the tip of the major crack usually locates at a large distance from the centre of the beam, so that the length of the secondary crack branch l_0 is usually rather long. To generate the same critical shear displacement Δ_{cr}, less rotation θ is needed.

Therefore, the additional vertical displacement component due to the inclination of the major crack $s_{cr} \cdot \cot\alpha\theta$ in Eq. (5.2) is less relevant. To avoid convergence problems caused by introducing an additional item related to the output in calculating V_{ai}, that part is neglected. As a result, the expression of Δ_α in Eq. (5.5) becomes:

$$\Delta_\alpha = \Delta_{cr} \sin\alpha \tag{5.10}$$

To sum up, for simply supported beams the following additional steps have to be taken regarding the shear capacity calculation:

- The location of the tip of the critical crack (critical section) shall be calculated by the shear resistance over shear force ratio distribution. As a simplified method, Eq. (5.9) can be used as an alternative.
- The design shear force and moment shall be evaluated at the crack tip x_{ct}. The value of M/Vd is calculated by Eq. (5.8).
- Δ_{cr} being used in Eq. (4.7) or Eq. (4.4) has to be adjusted with Eq. (5.10); further validation should be carried out to obtain an appropriate value of α.

Crack Length Reduction Method

It is also possible to reduce the shear force carried by aggregate interlock by reducing the length of the flexural crack. To do so, Eq. (5.6) or Eq. (5.7) shall be used to replace Eq. (4.7) or Eq. (4.4) in the second step of the procedure presented in 4.4.1. The remaining part of the procedure is the same.

5.4.3.2 Validation

Experiments reported by Leonhardt and Walther (Leonhardt & Walther 1962), Krefeld and Thurston (Krefeld & Thurston 1966) are used to evaluate the shear calculation procedures presented in this section. Both test series include simply supported specimens loaded by a uniformly distributed load. The span to depth ratio l/d of the specimens varies from 4.69 to 22. For beams loaded by uniformly distributed loads, it is quite difficult to distinguish the so-called shear compression failure and flexural shear failure directly. Observation of the tests by Krefeld and Thurston (Krefeld & Thurston 1966) shows that in almost all experiments with uniformly distributed loads, the development of the critical inclined crack does not result in direct collapse of the specimen; additional load increments can be applied afterwards. This is due to the further development of the secondary branch at the major crack tip. However, the larger is the ratio l/d of the specimen, the smaller is the additional load that can be applied. This indicates that for beams with smaller l/d, the uncracked concrete part is able to transmit a larger shear force after the dowel crack forms along the longitudinal reinforcement. Thus the formula presented in Chapter 4, which is aiming at the

development of the critical inclined crack, can only provide a lower bound for this loading condition.

Critical Sections

With the test results, the critical sections are firstly evaluated. The original calculation procedure presented in Chapter 4 is firstly applied to calculate the cross sectional shear resistance, which is then used to determine the position of the critical section. As examples, the configurations of the experiments reported in (Leonhardt & Walther 1962; Krefeld & Thurston 1966) are used the calculate the critical sections. The critical sections determined by the procedure presented are plotted against the span-depth ratio as dots in Fig. 5.24. In the figure, the analysis results show a strong linear relationship. A regression analysis gives the following expression: $x_{ct} = (0.1399\, l/d + 0.3)d$, which has an offset of $0.5d$ from Eq. (5.9) as discussed previously.

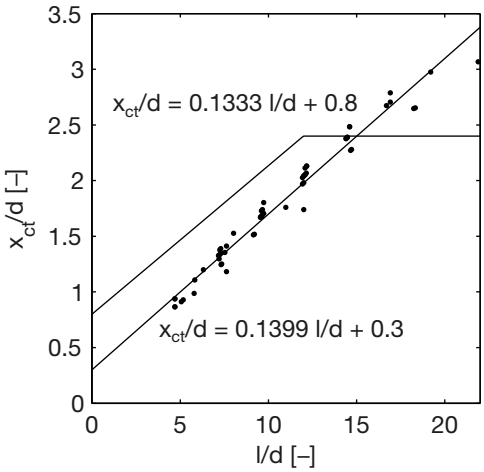

Fig. 5.24. Comparison between the calculated critical sections based on tests reported in (Leonhardt & Walther 1962; Krefeld & Thurston 1966) marked as dots with the simplified model and the regression formula Eq. (5.9).

The offset can be explained by the fact that the moment and the shear force are calculated at the section where the crack is initiated. On the other hand, the reduction of shear resistance by crack inclination is not taken into account either. Both effects results in a certain inaccuracy in the evaluation of the critical section but in different directions. A more accurate evaluation can be achieved by taking into account the reduction of the shear resistance due to the crack profile.

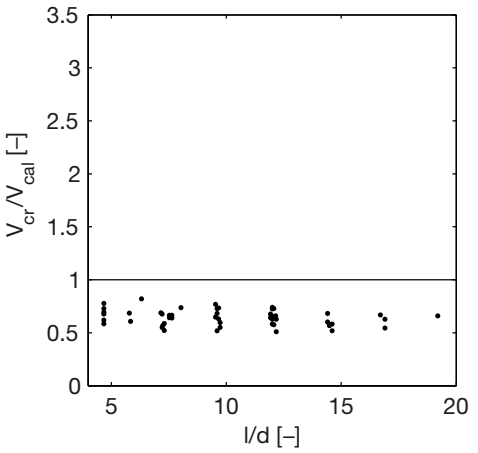

Fig. 5.25. Relationship between V_{cr}/V_{cal} and l/d with the original method.

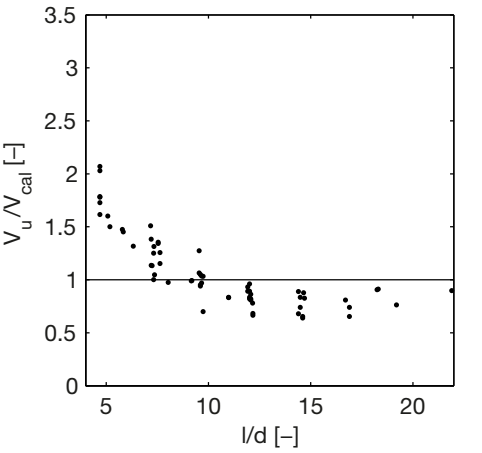

Fig. 5.26. Relationship between V_u/V_{cal} and l/d with the original method.

Shear Capacity

Regarding the shear capacity, the inclined cracking load can be considered as a lower bound for the shear capacity as was done for beams loaded by point loads. Based on that consideration, the inclined cracking loads reported by Krefeld and Thurston are used to evaluate the original calculation procedure at the critical section specified with Eq. (5.9). The choice of a single research program aims at ensuring the consistence of the criterion for inclined cracking. The comparison is plotted in Fig. 5.25. It is shown that on average, the calculation procedure overestimates the inclined cracking load with about 36%. Nevertheless, the level of the prediction is consistent. The coefficient of variation of the prediction is only 11.4%.

In addition, the ultimate bearing capacity obtained in experiments from (Leonhardt & Walther 1962) and (Krefeld & Thurston 1966) is plotted in Fig. 5.26. The comparison confirms that the original simplification gives an overestimation of the ultimate bearing capacity of the beam as well. Thus, the inclination of the major crack has to be taken into account. Besides, the inclined cracking load is the lower bound of the shear capacity of a structure. With decreasing span-depth ratio the shear capacity of the tested specimen increases compared to the calculated capacities. This increase starts at a higher span-depth ratio than in the case of point loaded specimens, because of the different shear force distribution.

Comparisons of test results and the model prediction (Crack Inclination Method) are given in Fig. 5.27 and Fig. 5.28. Regarding the inclined cracking

load, by considering the reduction of the aggregate interlock effect due to the crack inclination, the improved model gives better results, the mean value of V_{cr}/V_{cal} in Fig. 5.27 being 1.00 (COV = 9.7%) and 0.96 (COV = 12.6%) respectively. Besides, with respect to the ultimate capacity, the prediction underestimates the test results in specimens with almost all span/depth ratios.

In addition, with the procedure introduced above, the reduced shear resistance is used to calculate V_R along the length of the beam. The shear capacity of the whole specimen is determined by checking the value of V_R at the section with the maximum V_E/V_R, which is the procedure introduced in Section 5.2 for structural members with general boundary conditions. With this procedure, an accurate prediction can be derived as well: a mean value of V_{cr}/V_{cal} = 1.03 and a COV of 9.6% is obtained regarding the same set of data.

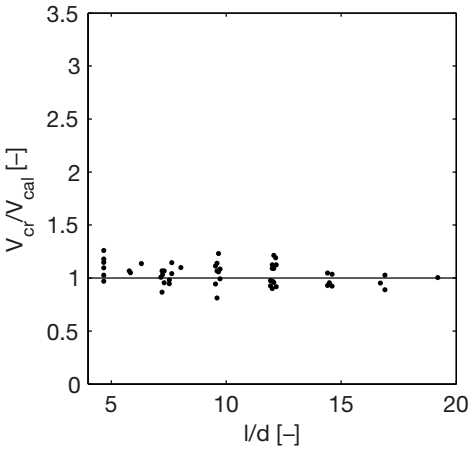

Fig. 5.27. Relationship between V_{cr}/V_{cal} and l/d with the improved simplified method.

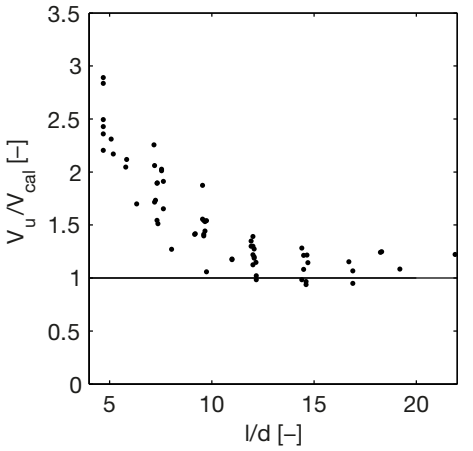

Fig. 5.28. Relationship between V_u/V_{cal} and l/d with the improved simplified method.

5.4.4 General Support Conditions

5.4.4.1 Introduction

In this subsection, the experience gained from simply supported and continuous beams, subjected to point loads and uniformly distributed loads is used to extend the evaluation model to general supporting conditions. For a beam loaded by a uniformly distributed load with any discrete boundary conditions, the moment and shear force distribution within a span can be expressed by a parabolic function and a linear function. An example is shown in Fig. 5.29. In principle, once the moments and the shear forces at the ends of the span are known, the distributions of actions applying along the beam can be determined.

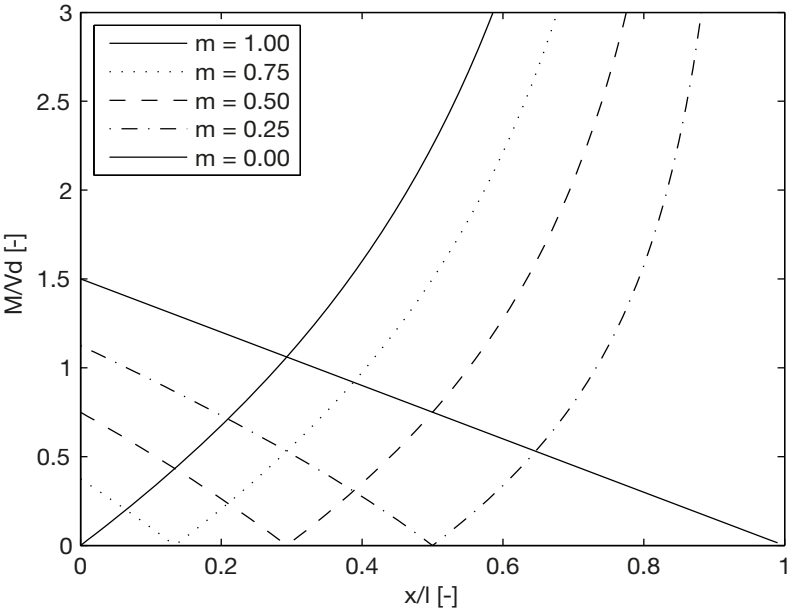

Fig. 5.30. Distribution of *M/Vd* along the longitudinal axis of the specimens in the TNO tests, see the following section.

Furthermore, if the sign of the shear force changes along the span (from V_1 to V_i in Fig. 5.29), the beam can be considered as a part of a beam with the same maximum shear force $V_1 = V_2$ at both ends. To cover all possible moment and shear force combinations, only one variable is needed, which is the ratio between the hogging moment and the total moment difference: $m = M_2/(M_1 + M_2)$. In most practical conditions, the value of m varies between 0 and 1. Several examples of M/Vd distribution of beams with different m value are shown in Fig. 5.30. Those configurations were tested in the research program presented in the following section.

The principle to deal with beams with any moment and shear force ratio at the ends was explained in the previous sections. First of all, the critical section

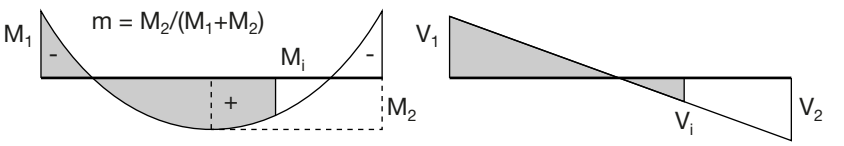

Fig. 5.29. Moment and shear force distribution of a beam loaded by uniformly distributed load with generalized boundary conditions.

has to be found through the V_E/V_R diagram, see the examples shown in Fig. 5.17 and Fig. 5.19. At the critical section, when the maximum ratio V_E/V_R applies, the properties of the crack profile are taken into account if it is necessary. On the basis of the shear resistance at the critical section the overall load level can be determined if required. This procedure has been validated with experimental results of simply supported beams loaded by a uniformly distributed load. In that loading case, the shear force in the span decreases with an increase of the moment. Any part of a beam with only a hogging moment can be considered as a part of a simply supported beam, the critical section and the shear capacity of which has to be checked in the same manner as for simply supported beams loaded by a uniformly distributed load.

For another loading condition, like shown Fig. 5.19, m can be relatively large. The shear force increases with an increase of the moment to the end of the span. In theory the critical section under that condition should be located at the centre of the support. In practice, when there is confinement applied at the support such as by a supporting plate, or a change of the cross section, the development of an inclined crack can be restricted. Based on experimental observation, the recommended minimum cracking distance is d from the centre of the support (IBBC-TNO 1977c). Besides, the design moment and the shear force have to be checked at the initiation position of the crack.

As shown for simply supported beams, the crack profile plays an important role. When crack inclination is expected, the stiffness of the aggregate interlock effect along the crack has to be reduced. Moreover, when there is confinement at the tip of the crack, the shear failure Criterion 3 in 5.4.2 is violated. The actual amount of shear force transferred in the concrete compressive zone V_c has to be enlarged.

This principle is used in the evaluation of beams with different combinations of end moment ratios, to make sure that the chosen boundary conditions are realistic and can be validated. The selection is based on an experimental research program carried out at IBBC-TNO (TNO Institute for Building Materials and Structures) carried out in the 1970s. The research was aimed at understanding the shear behaviour of tunnel segments constructed in the Netherlands at that time. The whole experimental programme is reported in detail in several TNO reports (IBBC-TNO 1977a; IBBC-TNO 1977b; IBBC-TNO 1977c; IBBC-TNO 1985). Since those reports are all in Dutch, a brief introduction of the test programme is given in the section.

5.4.4.2 Evaluation of TNO Tests

The loading condition of the research programme is designed based on the discussion on general boundary conditions of beams subjected to a uniformly

distributed load above. The configuration of the test specimens is plotted in Fig. 5.32. The specimens are simply supported. They are all loaded by a uniformly distributed load generated by water pressure in two fire hoses confined by a stiff steel beam. The two additional supporting blocks are also loaded by the uniformly distributed load. The supports are placed at a distance e from the middle of the specimen on the attachment blocks. That part of the specimen is reinforced with stirrups to prevent unwanted shear failure there. By adjusting the position of the support, the moment at the end of the testing segment is controlled. Fig. 5.31 shows a sketch of the test setup. The main variables in the research are the beam length – depth ratio l/d, the beam end moment ratio m, and the beam height d.

The dimensions of the cross-section of the test segment of the specimens are 180×150 mm, with an effective height d = 150 mm. The length of the test segment l varies among 900, 1350 and 1800 mm, accordingly, the moment ratio m varies from 0 to 1 by every 0.25. 3 Ø14 mm rebars were used as longitudinal reinforce-

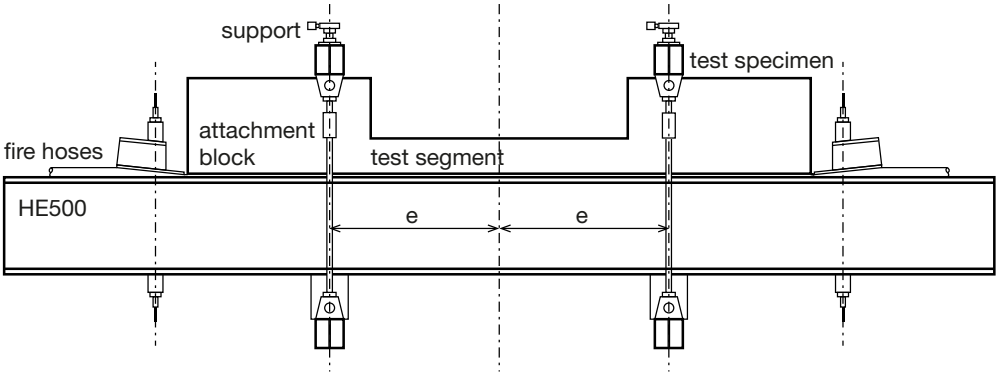

Fig. 5.31. Test setup of TNO shear tests under uniformly distributed load. Adapted from (IBBC-TNO 1977c).

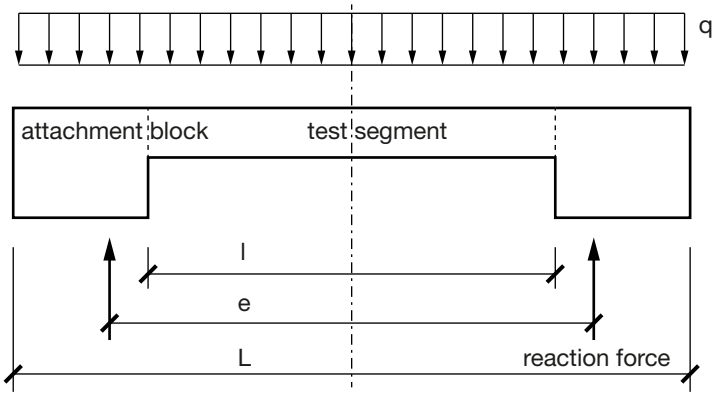

Fig. 5.32. Configuration of TNO test specimens. Adapted from (IBBC-TNO 1985).

ment. Only the test specimens without shear reinforcement in the test segment are selected for the evaluation analysis in this section. Other than the three test series, several additional tests were included later, to check the size effect. In those tests, the effective beam height was increased to 300 and 400 mm. 3 Ø28 mm rebars were employed. The length and the reinforcement of these beams are increased proportionally to keep the same l/d and reinforcement ratio.

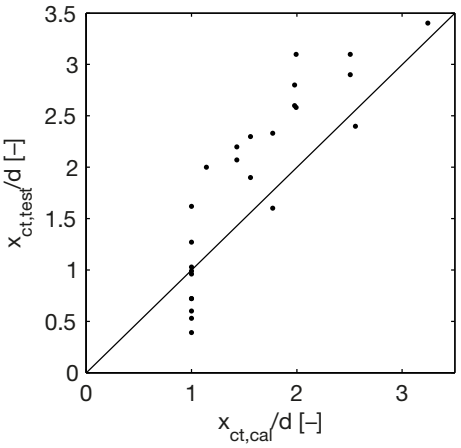

Fig. 5.33. Comparison of measured critical section and critical section used in the calculation.

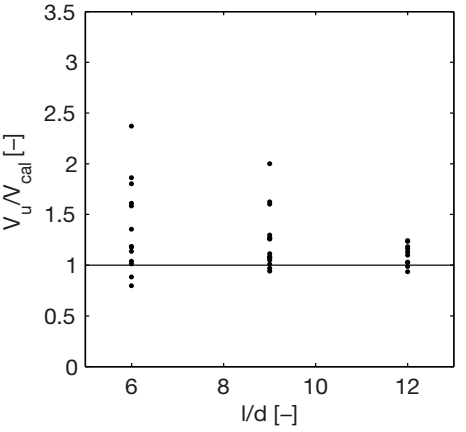

Fig. 5.34. Relationship between V_u/V_{cr} and l/d with the simplified method adjusted for inclined cracks.

The observation of the crack patterns after failure shows that the two possible critical sections discussed in the preceding subsection give quite a good estimation. The locations of the critical section for the test are measured on the basis of the crack pattern. The measured x_{ct} and the values used to calculate the shear resistance are compared in Fig. 5.33. The estimation represents the experimental observation quite well. In addition a set of failure crack patterns is shown in Fig. 5.35. The denotation of the specimens name B1 – B5 corresponds to the moment ratio m of the specimens. From B1 to B5, m = 0.00, 0.25, 0.50, 0.75 and 1.00 respectively.

The shear resistance is evaluated at the two critical sections described in section 5.4.4.1. When the critical inclined crack is generated at a section with M/Vd < 2.0, the aggregate interlocking effect has to be reduced to take into account the effect of the crack profile. Based on the calibration for simply supported beams, the reduction can be done by introducing a crack inclination angle $\alpha = 35^{o}$ for the Crack Inclination Method, or a crack length reduction factor k_{α} = 0.41 to s_{cr} for the Crack Length Reduction Method. In addition, if the teeth structure cannot be developed in the beam, the contribution of V_c has to be increased. The increment is dependent on the stiffness of the residual structure formed by the critical

inclined crack, see the discussions in section 3.5.3. In that case, the value of V_c is suggested to be increased to $2.5V_c$ from the regression analysis of the TNO tests.

With the adjustment described above, the calculated results are plotted against the test results in Fig. 5.34. The result shows that the proposed method is able to predict the behaviour of beams even for more generalized conditions. It should be noted that in the test reports, only the failure loads were recorded. So, in Fig. 5.34 the ultimate loads V_u are compared with the theoretical inclined cracking load $V_{cr,cal}$. The calculated results give a good lower bound. When the

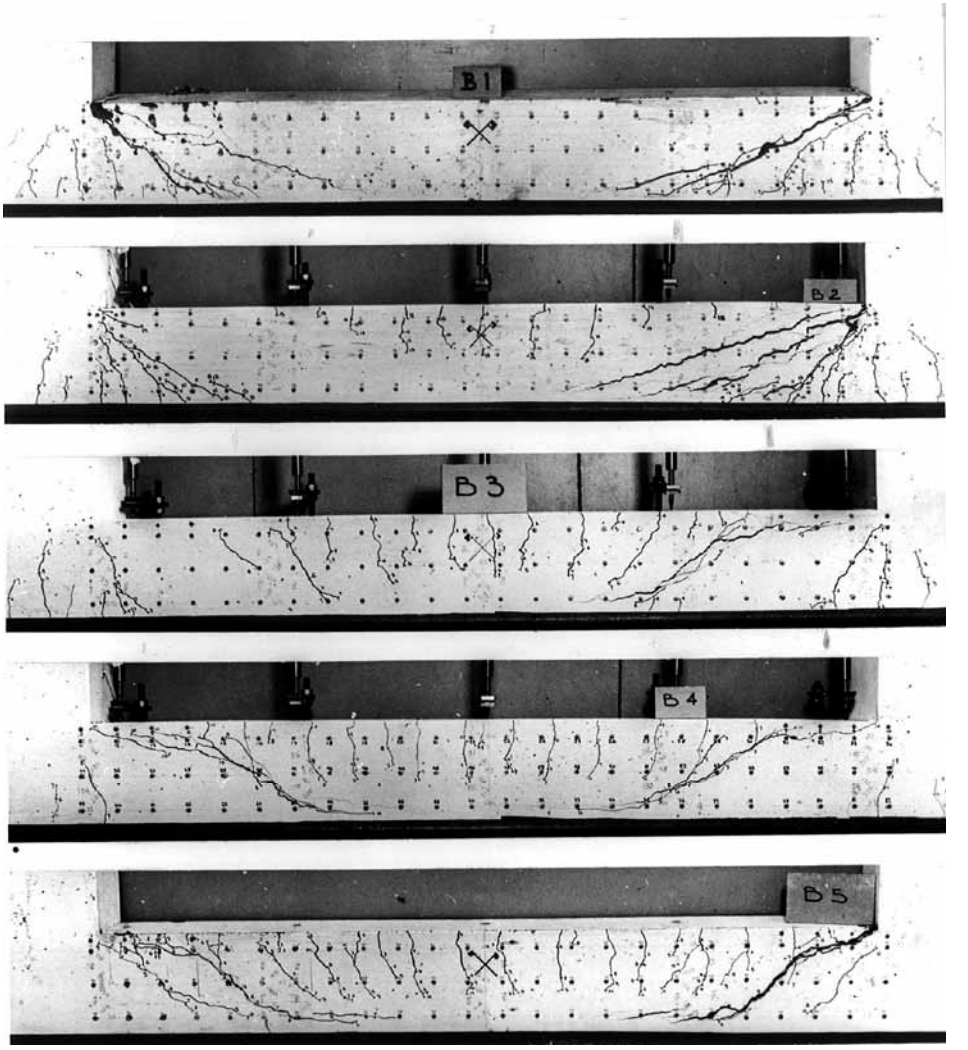

Fig. 5.35. Crack pattern of test series B after failure. l = 1350 mm, from B1 to B5, m = 0.00, 0.25, 0.50, 0.75 and 1.00 respectively (IBBC-TNO 1985).

slenderness of the specimens is small, the span between the two inflection points is not long enough to allow the full development of two inclined cracks with an inclination of 30° anymore. As a result, the remaining part of the uncracked beam forms an arch structure, which is still able to withstand a higher load afterwards. A smaller slenderness of the beam will result in an arch with a larger minimum height, shorter span, and consequently higher stiffness. Therefore the maximum values of V_u/V_{cal} increases with a decrease of the beam slenderness. On the other hand, with regard to the specimens with the largest M/Vd, the opening of the critical inclined crack led to the failure of the specimen, see Fig. 5.36. The adjustment reflects the failure loads found in the specimens with large l/d properly.

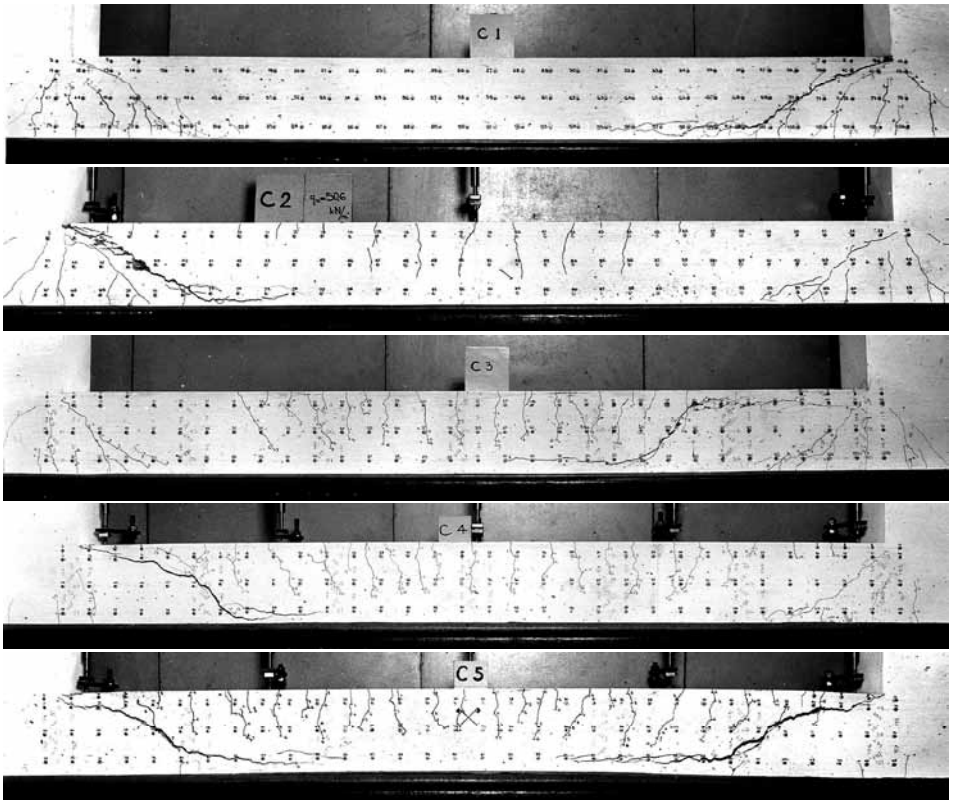

Fig. 5.36. Crack pattern of test series C after failure. l = 1350 mm, from C1 to C5, m = 0.00, 0.25, 0.50, 0.75 and 1.00 respectively (IBBC-TNO 1985).

5.5 CONCLUSIONS

In this chapter the shear evaluation procedure derived in Chapter 4 is extended to more complex boundary conditions. Before the procedure is applied to new boundary conditions, it is suggested that three general criteria have to be checked. If one of the three is not fulfilled, further adjustment to the evaluation procedure should be considered. The three criteria are:

- Whether or not a similar crack profile can be obtained at a given moment/shear force ratio?
- With the same crack profile and crack opening, do the shear force components change?
- Where is the critical section?

Two typical loading conditions are investigated as the examples of the criteria and adjustments suggested in this chapter. Corresponding experimental results are introduced and evaluated.

Point Loads

For continuous beams with point loads, the calculation procedure derived for simply supported beams subjected to a point load can still be applied in principle.

Because the dowel crack along the longitudinal rebar can develop across the point of inflection, the length of the detached tension chord is longer in a continuous beam. The reduction of the stiffness due to the development of inclined cracks is more pronounced. Therefore, the inclined cracking load should be used as a lower bound for the shear capacity, even for beams with a relatively small shear span.

The shear slenderness ratio a/d is not equivalent to the maximum ratio M/Vd in continuous beams anymore. The latter one should be used in order to evaluate the inclined cracking load.

When the maximum of M/Vd is very large, the value of V_{cr} is stabilized. The critical inclined crack is located at flexural cracks close to the loading point (rotation centre).

When the maximum of M/Vd is smaller than 2.0, the teeth structure cannot be formed anymore, and the contribution of V_c is significantly increased with the reduction of the shear span. On the other hand, the contribution of V_{ai} is reduced because of the larger crack inclination. The contributions of the components along the critical inclined crack change.

The opening of the inclined crack of beams with a maximum ratio $M/Vd <$ 2.0 is mostly due to the development of a crack at $M = M_{cr}$. Overall speaking the value of V_{cr} can be estimated by relating V_{cr} to the maximum ratio M/Vd directly.

Uniformly Distributed Load

In a beam subjected to a uniformly distributed load or even more complex loading condition, the shear capacities of the critical sections in the hogging and sagging moment regions need to be checked. The positions of the sections are determined from the peak of the V_E/V_R curve along the span. Here the value of V_R can be determined without taking into account the reduction of crack inclination.

For a simply supported beam loaded by a uniformly distributed load, or any part of a beam under a uniformly distributed load including a sagging moment zone between two points of inflection, the critical section can be determined by a simplified regression formula.

In the hogging moment zone, where the moment increases with the shear force, the critical section is set at d from the support or from any other type of confinement which may prevent the further development of the secondary crack branch. The shear force component transmitted in the uncracked compression zone has to be increased. Based on the TNO tests, a suggested increment factor is 2.5 V_c.

When a uniformly distributed load is applied, the inclined crack usually develops at sections with very small M/Vd ratio, thus a large inclination of the major crack is expected. To take into account the crack inclination, a reduction has to be made when calculating the shear force generated by aggregate interlock at a given vertical displacement Δ. The reduction can be made by introducing a crack inclination angle $\alpha = 36^o$ when using the Crack Inclination Method, or crack height reduction factor $k_\alpha = 0.41$ when using the Crack Length Reduction Method. Both are simplified evaluation procedures proposed in this research and have been evaluated with test results.

The reduction in case of more complex loading conditions has to be evaluated based on test results.

Chapter 6

Influence of Material Variability on the Shear Failure Process

6.1 FUNCTION OF CONCRETE STRENGTH

The contribution of concrete strength to the shear capacity of concrete structures is usually described as being proportional to the cubic root (Eurocode 2 2004) or square root (ACI Committee 318 2004) of the concrete compressive strength f_c based on regression analysis. This simple relationship does not reflect the complex shear failure mechanism of a concrete beam. Based on this, a wrong interpretation may be generated when the material properties of the concrete are not the same as for 'normal' concrete reported in literature. Several examples will be given in the following part of the chapter, regarding shear problems of specimens with abnormal concrete properties, or other shear problems regarding the effect of concrete strength.

Before that, the functions of concrete strength in the shear failure process are summarized. Many of those aspects have already been mentioned in the previous chapters. Further considerations on particular phenomena related to concrete strength are given.

6.1.1 Concrete Tensile Strength

A straight-forward explanation of the role of the concrete strength with regard to shear failure is that for slender beams it is the unstable propagation of the critical inclined crack that defines the shear failure. Finally it is the concrete tensile strength f_{ct} that determines the shear capacity. Since f_{ct} is related to the concrete compressive strength, the compressive strength can also be seen as a governing factor regarding shear capacity. The shear formulation in the former Dutch code NEN 6720 (Nederlands Normalisatie-Instituut 1995) is based on that consideration. This explanation complies with the shear failure criteria proposed in section 3.4.2.1 and 3.4.2.2. In Chapter 3 it has been proven that these two criteria cannot lead to the shear failure of a concrete beam. A secondary crack branch needs to develop at the tip of a major crack to fulfil the cross sectional equilibrium. Additional shear displacement Δ will occur with the opening of the secondary crack branch. Only after that, sufficient shear resistance can be generated by aggregate interlock.

A special case applies when the maximum ratio M/Vd is small. In that case, the shear resistance of the cracks in the vicinity of the loading point is large because of the smaller crack width. Thus, a high shear force level is expected, which results in the opening of a crack at very small M/Vd with a large crack inclination. Because of the large inclination, the critical shear displacement Δ_{cr} at the level of the longitudinal reinforcement can be reached only because of the rotation of the crack around its tip. In this case, the contribution of aggregate interlock to the shear resistance is limited. Therefore, the propagation of a

critical crack will result in the development of the dowel crack, which defines the opening of the inclined crack. However, in this case the chance that the uncracked arch structure still has sufficient capacity is quite large as well. Thus, another failure mode is expected.

The other mechanism related to the concrete tensile strength is the maximum dowel force V_d expressed by Eq. (3.28). However, that does not relate to shear failure directly either, since the value of $V_{d,\max}$ itself is rather small compared to the overall shear resistance. Moreover, as shown in Fig. 3.28, after the maximum value of $V_{d,\max}$ is reached, a yielding plateau will develop. It is the critical shear displacement Δ_{cr} that determines the opening of the dowel crack along the longitudinal rebar, and defines the failure of the beam. Since the value of Δ_{cr} is usually larger than the displacement when $V_{d,\max}$ is reached, it is not dependent on f_{ct} either.

However, the only thing that is really related to the concrete tensile strength is the residual capacity of the arch structure after the development of the dowel crack. The concrete tensile strength f_{ct} influences the strength of the arch structure in the following two manners:

- The tensile strength defines the cracked span in the beam, in other words the boundary of the location where the critical inclined crack may develop. The location of the crack then defines the shape of the arch structure.
- The tensile strength of concrete determines the flexural strength of the uncracked concrete arch. Based on that the critical compressive region $a_{c,c}$ is derived in Eq. (3.43).

Both aspects will influence the failure mode of the beam. For concrete beams with a smaller tensile strength, the length of the cracked span is larger. The critical inclined crack can develop at a large distance from the loading point or the support at the same load level. Moreover, the critical compressive region $a_{c,c}$ is smaller. The chance that the tip of the major crack falls outside $a_{c,c}$ is larger, see the discussion in Section 3.5. Consequently the failure mode of the beam is more likely to be flexural shear failure.

Nevertheless, none of the aforementioned mechanisms relates to the determination of the inclined cracking load V_{cr} directly.

6.1.2 Concrete Compressive Strength

The concrete compressive strength, on the other hand, does influence the shear capacity of reinforced concrete beams in a more direct way. First of all, the capacity of the compressive strut in the residual arch structure after inclined cracking is directly determined by the concrete compressive strength. For beams with small shear slenderness ratio or with any other loading condition under

which the remaining concrete arch structure is not affected by the inclined crack, the ultimate capacity of the whole beam is determined by f_c.

In case of slender beams, the concrete compressive strength implicitly influences the shear capacity. Out of the three shear force components, it is the aggregate interlock force V_{ai} that relates to f_c most. In Eq. (4.7) the term $f_c^{0.56}$ actually represents the yielding strength of the cement matrix. According to Walraven (Walraven 1980), the yielding strength of the cement matrix in normal strength concrete is related to the concrete strength by:

$$\sigma_{pu} = 6.39 f_c^{0.56}$$

In that way the concrete strength is affecting the shear force transmitted across the cracked surfaces.

Moreover, for very high strength concrete, the high concrete tensile strength combined with a higher modulus of elasticity results in the fracture of aggregate along the crack. Consequently the cracked surface is smoother, and a lower aggregate interlock force is expected at the same tangential displacement Δ. This effect was treated in section 4.5.

6.1.3 Effect of Spatial Variability

The concrete strengths in two different loading conditions functions differently. The concrete tensile strength mainly affects the shear failure mode (flexural shear or shear compression), while the concrete compressive strength influences the shear bearing capacity in both failure modes. With the function of the concrete strength in the shear failure process understood, it is possible to introduce the spatial variability of concrete strength in the failure process.

The variation of concrete strength over the concrete body means the existence of peaks and valleys regarding concrete strength in space. The local valleys may be considered as **weak spots** in the structure. Taking a tensile element as an example, the effect of local weak spots influences the overall behaviour of the element in several ways as illustrated in Fig. 6.1. In the longitudinal direction, the subsequent cross sections of the element may be considered as a serial system. The overall capacity of the system is determined by the weakest section. This type of failure can be described with Weilbull's model proposed in (Weilbull 1951). On the other hand, within the critical section, the effect of the weak spot is very much dependent on the post peak behaviour of the material. For a plastic material, after the strength of the weak spot has been reached ($\sigma_{u,i}$ in Fig. 6.1), the stiffness of the whole element is reduced, but the total force applied on the element will still increase. The ultimate capacity of the section is defined by the mean strength of material over the whole section.

$$P_u = \iint \sigma_u(x,y)dxdy \,/\, A \quad \text{(continuous)}$$
$$P_u = \sum \sigma_{u,i} A_i \,/\, \sum A_i \quad \text{(discrete)}$$

where

A: is the total area of the cross section. A_i is the area of a part of the cross section.

σ_u: is the local strength of the material.

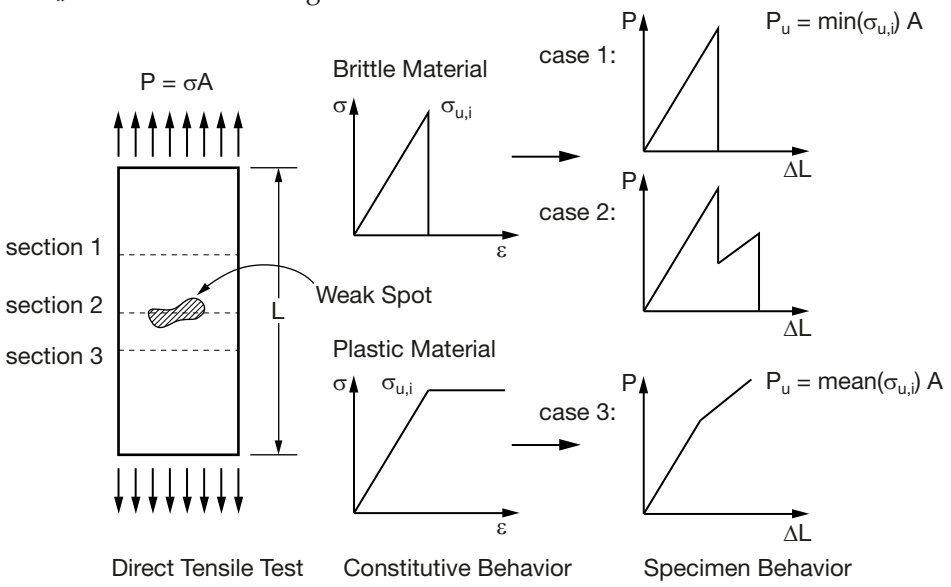

Fig. 6.1. Relation of material constitutive behaviour to the behaviour of tensile element with weak spot.

If the material is extremely brittle, the stress level at the weak spot goes to zero immediately after it reaches $\sigma_{u,i}$, see Fig. 6.1. The ultimate capacity of the section is then dependent on the distribution of the material strength σ_u. Assume that the **cumulative strength distribution function** of the material is represented by: $\Phi_\sigma(\sigma)$. $\Phi_\sigma(\sigma)$ varies from 0 to 1 when σ varies from 0 to ∞, its corresponding **partial distribution function** is denoted as $\varphi_\sigma(\sigma)$. At $\sigma = \sigma_{u,i}$ the area of the cross-section that has not failed yet is $A_i(\sigma) = A \cdot [1- \Phi_\sigma(\sigma_{u,i})]$. The relationship between the total force and the average stress level over the critical cross-section is

$$P_b(\varepsilon) = A_i(\sigma) \cdot \sigma = AE\varepsilon\left(1 - \Phi_\sigma(E\varepsilon)\right)$$

The ultimate load of the tensile member is calculated by finding the peak value of that equation. In the discrete case, the weak spot of the material occupies a certain area. After its strength has been reached, the part of the total force carried

by the weak spot has to be taken over by the remaining part of the section. An example of such situation is shown in Fig. 6.1, case 2. After the failure of the weak spot, an increment of stress is also expected in the remaining section under the same total force P. This may result in the failure of the whole cross-section immediately if the increment of the stress is large enough. An example of such a case is shown in Fig. 6.1, case 1.

For a plastic material, when the stress in a part of the cross-section reaches the yielding strength σ_u, the stress there remains σ_u. Therefore the total force P of the cross-section at a given deformation ε shall be calculated by the integration over the whole cross section:

$$\begin{aligned} P_p(\varepsilon) &= \int_0^{\sigma} A_i(\sigma_u)\cdot\sigma_u d\sigma_u + \int_{\sigma}^{\infty} A_i(\sigma_u)\cdot\sigma d\sigma_u \\ &= A\int_0^{\sigma} \varphi_\sigma(\sigma_u)\cdot\sigma_u d\sigma_u + A\sigma\int_{\sigma}^{\infty} \varphi_\sigma(\sigma_u) d\sigma_u \\ &= A\int_0^{E\varepsilon} \varphi_\sigma(\sigma_u)\cdot\sigma_u d\sigma_u + AE\varepsilon\left(1-\Phi_\sigma(E\varepsilon)\right) \end{aligned}$$

Compared to the ideal brittle material, an additional term is added in case of an ideal plastic material. The overall load – displacement relationship of an ideal plastic material loaded in tension is shown in Fig. 6.1 as case 3. For a general quasi-brittle material with a certain softening property, the value of σ_u in the first term should be replaced by the softening function of the material $\sigma_{soft}(\sigma_u, \varepsilon)$. As expected, the total force P at a given average strain ε should be between $P_b(\varepsilon)$ and $P_p(\varepsilon)$.

$$P(\varepsilon) = A\int_0^{E\varepsilon} \varphi_\sigma(\sigma_u)\cdot\sigma_{soft}(\sigma_u,\varepsilon) d\sigma_u + AE\varepsilon\left(1-\Phi_\sigma(E\varepsilon)\right)$$

For shear failure, the mechanism is more complex than failure in pure tension. Nonetheless, a similar strategy may be followed. The influence of material variability can be discussed in longitudinal, depth and width directions.

Longitudinal Direction (*x* Direction)

The beam can be treated as a serial system similar to the tension element in the longitudinal direction. When the shear force over the span is constant in case of point loaded beams, the cracked section in the span which has the lowest shear resistance will be the location from where the critical inclined crack develops. The variation of concrete strength in the longitudinal direction results in an uncertainty of the crack initiation positions. Sections closer to the support but with lower concrete tensile strength might crack earlier. Besides, the loading history or the variation of loading condition may generate cracks at random positions. The presence of a crack due to an earlier loading case in the loading history may initiate the development of an inclined crack as well. The uncer-

tainty of the position of the critical inclined crack may result in an unexpected failure mode. The effect of this type of variation in the longitudinal direction will be discussed in section 6.2.

Height Direction (*z* Direction)

In the beam height direction, the variation of concrete strength is important at certain locations. First of all, a crack always develops towards the direction with the smallest σ/f_{ct} ratio at its tip. Other than that, only the concrete strength along the crack path and at the top of the uncracked compressive zone is of importance. For the uncracked concrete between the flexural cracks, its strength is not relevant anymore. Secondly, even at the sensitive areas, the concrete property plays a different role at different locations. The strength of concrete in the compressive zone decides the capacity of the residual arch structure formed by the inclined crack. Along the crack path, the shear force is transmitted by aggregate interlock. When calculating the aggregate interlocking force V_{ai} at a given shear displacement Δ, a large part of the crack profile shares the same tangential displacement Δ. Thus the crack path can be considered as a parallel system, the shear stresses along which are calculated based on the same Δ. Besides, since the aggregate interlocking functions on the basis of compression contact between aggregate and cement matrix, plastic constitutive behaviour is expected.

Width Direction (*y* direction)

Last but not least, the variation of concrete strength in width direction is only pronounced when the width of the structural member is large. In that case the structure can be considered as a parallel system. If the critical crack surface is located at the same position in the longitudinal direction, the shear failure process may be described in the same manner as in the tension element. Otherwise, an additional geometric effect has to be taken into account.

Little experimental research has been carried out to investigate the three aspects mentioned above. Nevertheless, the experimental research carried out by the author in several research programs is related to these aspects. Therefore, the background of those experiments and their rationality within this chapter will be explained respectively in the following sections together with the conclusions derived through the experiments. The referred experimental research was carried out in the Stevin Lab at Delft University of Technology.

6.2 INFLUENCE OF EXISTING FLEXURAL CRACKS

6.2.1 Introduction

It has been discussed previously, that in the longitudinal direction of a beam structure variation of material property and pre-existing cracks within the shear span may result in an unexpected crack pattern. This is especially true when dealing with existing structures, the load history of which is mostly unknown. The influence of existing cracks has been studied by several researchers.

Hamadi and Regan reported a comparative study in (Hamadi & Regan 1980). The loading procedure of their specimens is shown in Fig. 6.2. Flexural cracks were generated in a 4 points bending test. Afterwards, 3 point loading was applied after having one of the supports moved closer. In all the tests, shear failure was only observed in virgin shear spans, which indicates that the presence of flexural cracks seems to increase the shear capacity.

Pimanmas and Tisavipat observed a similar behaviour in their experimental research reported in (Pimanmas & Tisavipat 2005). In their tests, vertical cracks generated by pre-cracking loading were across the whole beam height, and along the whole span of the shear testing stage, see Fig. 6.3. In the shear tests, the ultimate capacity of the specimens being pre-cracked were between 17.8% and 48.8% higher than the reference virgin specimen. Besides, it was reported that the presence of the flexural cracks changed the failure mode of the specimen.

In those tests, the preloading process was achieved by changing the supporting condition of the specimens. This type of change of loading condition is not common for a simply supported structural element. Thus it is of limited practical significance. For simply supported beams subjected to point loads, the moment

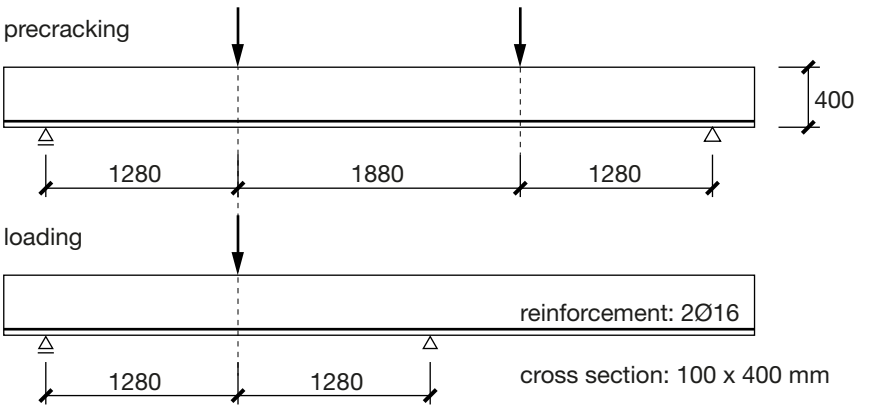

Fig. 6.2. Loading arrangement for Hamadi and Regan's beam tests with existing flexural cracks (Hamadi & Regan 1980).

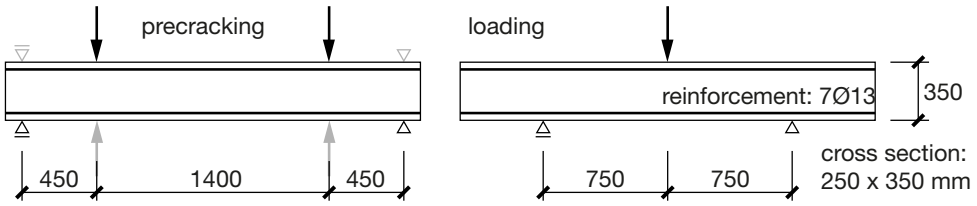

Fig. 6.3. Loading arrangement for Pimanmas and Tisavipat's beam tests. Adapted from (Pimanmas & Tisavipat 2005).

distribution does not change significantly without changing the supporting condition. Therefore, the loading history cannot result in a substantial variation of crack pattern. The pre-cracking procedure practiced in the research programs mentioned above is quite extreme. Besides, they are shown to give results at the safe side.

On the other hand, for beams with relatively more complex boundary conditions, such as continuous beams, the influence of existing cracks may be more pronounced. Examples have been shown in Chapter 5. In the span of a continuous beam a point of inflection may be present where the bending moment is zero. However, the shear force may be rather high at that location. This type of local force distribution prevents the development of flexural cracks in the vicinity of the point of inflection when the beam is loaded for the first time. Thus, no inclined crack will develop from a flexural major crack there. According to the shear failure process described in Chapter 3, the formation of a major crack due to a bending moment is vital to the shear failure process. Thus, the suppression of the development of flexural cracks will result in a higher shear capacity. Unlike simply supported beams, for a continuous beam, the variation of the position of a point load along the beam span will directly lead to shifting of the point of inflection, which changes the moment distribution drastically. If, due to the load history, a crack already exists in the vicinity of the point of inflection and the shear force level is quite high, the chance of having an inclined crack starting from the existing crack may be increased. Consequently, an unusual position and profile of the critical inclined crack will influence the formation of the arch structure. The ultimate bearing capacity of the structure is influenced eventually. In real structures such as continuous concrete slab bridges, the presence of existing cracks is quite likely to happen at various locations due to, for example, heavy traffic loads, uneven foundation settlements, or restrained volume changes.

The influence of the existing cracks on the shear capacity of continuous reinforced concrete beams without shear reinforcement is studied by a series of comparative experiments. These experiments are part of the extended test

program investigating the shear capacity of continuous beams presented in Chapter 4 and in (Yang, den Uijl et al. 2011). The tests are designed in such a way that the situation described above is simulated in the laboratory. The influence of an existing crack on the shear capacity of continuous reinforced concrete beams is evaluated.

6.2.2 Loading Procedure

The problem of the influence of existing cracks was first noticed in test C11b123 of the continuous beam test series. The test was carried out on a specimen that had been tested previously at the other end. It was test C11a091 in Table 5.1. The maximum moment reached at the boundary of the critical shear span of C11a091 (see Fig. 6.4) during the previous test was 166.9 kNm. Since the cracking moment of the cross-section is only M_{cr} = 61.3 kNm (f_{ct} = 4.9 MPa), several flexural cracks had been observed before the next test started. The crack pattern of the specimen is shown in Fig. 6.4. At first, it was assumed that the presence of those cracks would not affect the behaviour of test C11b123. However, the ultimate bearing capacity of the beam was significantly lower than what was found in the rest of the test series. For that reason two additional experiments were added as series 4 in Table 5.1. They were executed on the same specimen (Beam 16). C16a123 is the reference test, evaluating the shear capacity of a virgin specimen, while C16b123 is designed to investigate the influence of existing cracks in a more controlled way. No visible crack was observed in the critical span before loading was started.

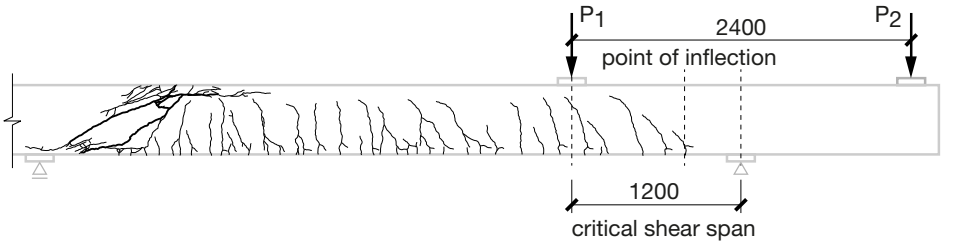

Fig. 6.4. Crack pattern of C11b123 before loading.

The test setup and the specimen have already been explained in Chapter 5, for instance the sketch of the setup is plotted in Fig. 5.5. The specimens are identified as C11b123, C16a123 and C16b123. The test number indicates the length of the critical shear span a = 1200 mm. One may check Fig. 5.9 for the full explanation of the coding rules. During the test, the ratio between P_1 and P_2 was kept constant: P_1/P_2 = 2.97, which makes the ratio between the maximum hogging moment and sagging moment M^-/M^+ = 2/3. Thus the maximum M/Vd in the shear span is 1.60.

In test C11b123 and C16a123 the loading procedure consists of two stages. First, the hydraulic jacks were force controlled. The loading procedure is the same as described in section 5.3.2.3. In this stage, the loading process was subdivided into several steps. For each load step a maximum load level was defined based on the shear force in the measuring span. The forces of the jacks P_1 and P_2 were increased with a constant loading rate until predefined load levels. The loading rate of P_1 was fixed at 0.2 kN/s, and the loading rate of P_2 followed accordingly. After reaching the predefined load level, the forces were kept constant for 10 minutes to stabilize the deformation of the specimen, and to provide sufficient time for crack marking and other measurements.

The force controlled loading procedure was ended when a potentially unstable inclined crack developed, or when the specimen showed significant change of flexural stiffness. Then, the hydraulic jack P_1 was switched to displacement control, while the load applied by P_2 was still controlled by the real-time measured force P_1, so that the value of P_1/P_2 was still kept constant. The load level was increased stepwise up to failure of the specimen.

In test C16b123 an additional pre-cracking stage was added before the loading procedure described above started to generate the existing crack for the next load stage in a more controlled way. In the stage, the beam was only loaded by actuator P_1 with the same supporting condition. The actuator P_1 was driven by force control. It was intended to have three load steps in the preloading stage, with the maximum shear force by the end of each load steps V = 50, 100 and 125 kN, respectively. However, due to an error in the controlling system, the loading rate of P_1 in the first load step was faster than planned, which yielded a maximum shear force of 102.4 kN in that step, see Fig. 6.5. Because the designed maximum load level in the preloading stage was not exceeded yet, the cracking process was not influenced by this accident, and the test was continued. The maximum load level in this test was P_1 = 164.5 kN (V = 125 kN). It is about 66% of the maximum shear load at that boundary conditions according to the previous tests carried out in the extended test program. With the cracking moment M_{cr} = 61.3 kNm, development of flexural cracks is expected at about 560 mm from the intermediate support. In the subsequent test, the point of inflection is at 480 mm from the support. Therefore, flexural cracks were expected to develop in the vicinity of the point of inflection in the preloading stage. This is verified by the observation of the crack pattern after the pre-cracking stage; see Fig. 6.6. After the third load step, the load applied by P_1 was reduced to zero with the same loading rate, and kept for 10 minutes before the real loading procedure discussed previously started. The loading history of both P_1 and P_2 is given in Fig. 6.5.

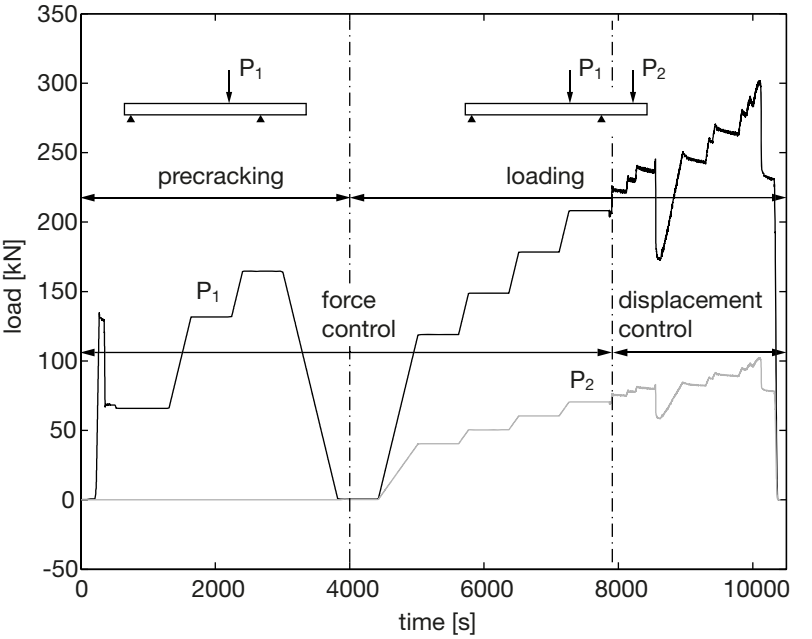

Fig. 6.5. Loading procedure of test C16b123.

6.2.3 Test Results

Despite the identical boundary conditions in the three tests, a transition from shear compression failure to flexural shear failure is clearly observed because of the introduction of pre-cracking. The test results are summarized in Table 6.1. The load (P_1) -deflection relationships of the three tests are plotted in Fig. 6.7. The programs of the experiments are explained as follows:

In the reference test C16a123, flexural cracks developed first under the loading point. At P_1 = 200.0 kN, a dowel crack started to develop along the tensile reinforcement from one of the flexural cracks which is marked in Fig. 6.6 (left) as inclined crack 1. Limited additional deformation was observed in the load-deflection relationship at that load level, and the stiffness of the beam was not influenced very much by then. At P_1 = 339.5 kN, the second inclined crack developed, see Fig. 6.6 (left). The loading procedure was switched to displacement control. The load level was able to be increased further, while the propagation of the cracks was quite stable. At P_1 = 611.8 kN, the load could not be increased any further. The concrete strut reached the maximum compressive strain. This is typically defined as shear compression failure.

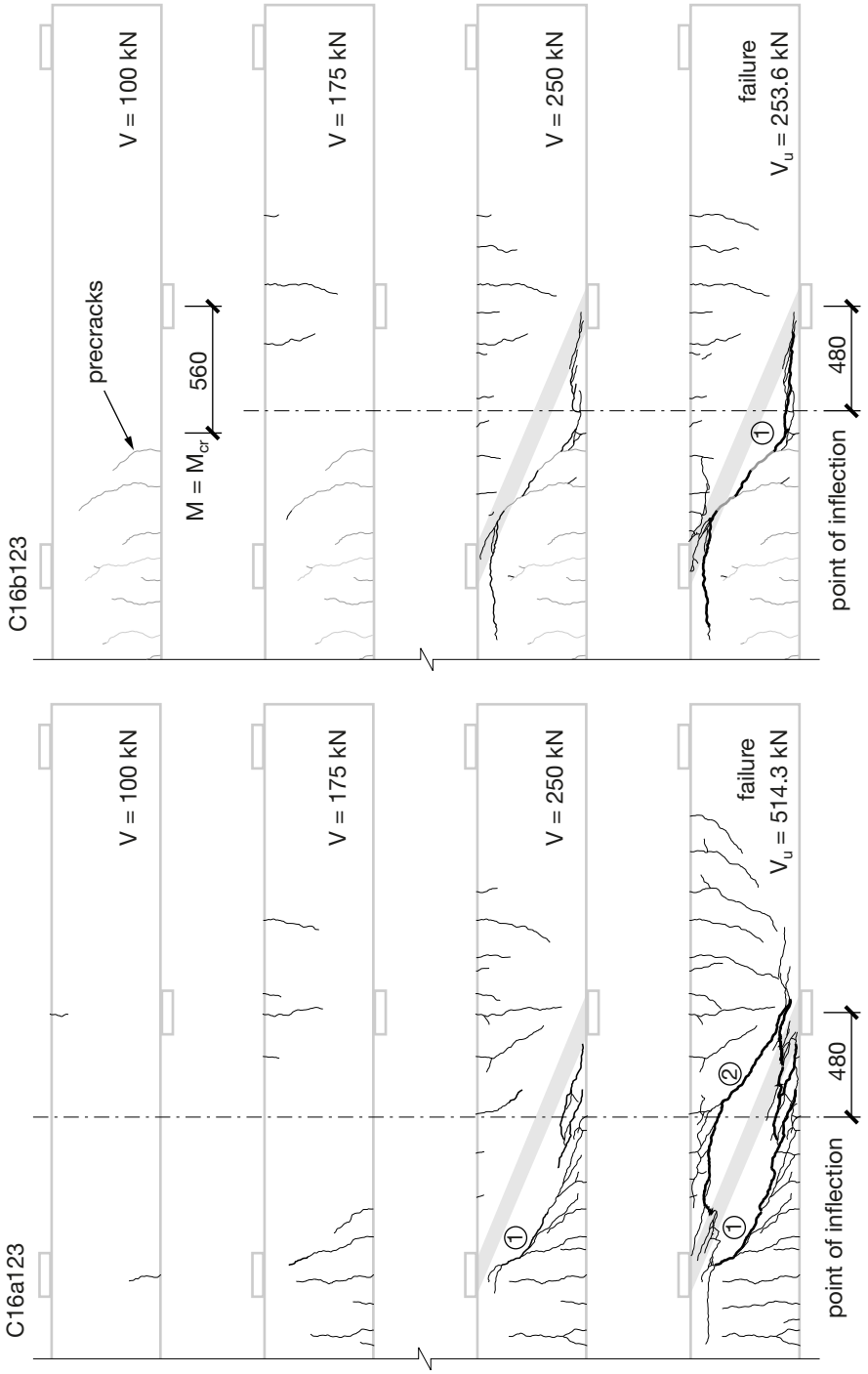

Fig. 6.6. Crack development of (left) test C16a123 and (right) test C16b123 (the existing cracks in C16b123 are marked by grey lines).

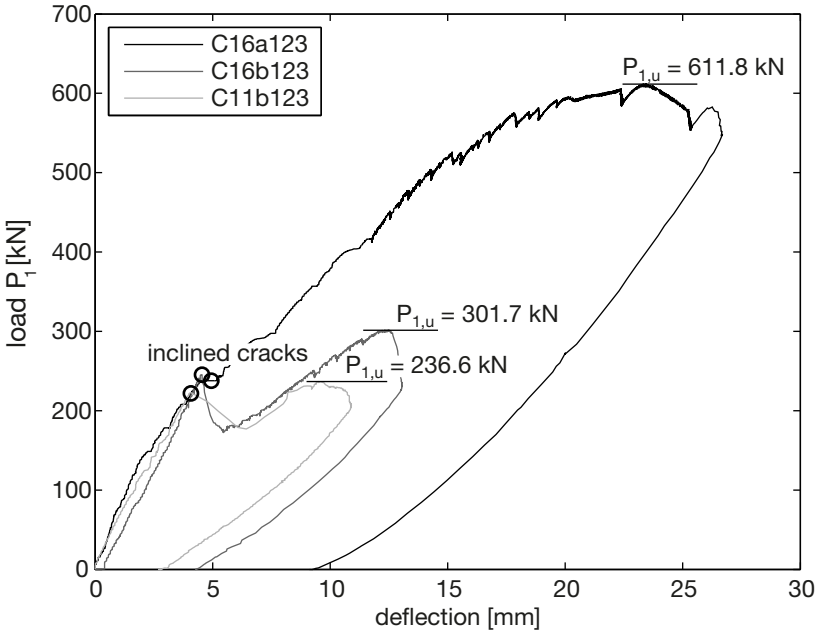

Fig. 6.7. Load-deflection relationship of pre-cracking tests series.

Table 6.1. Summary of the precracking test results.

Test No.	Pre-cracking	Age [days]	Failure Mode[1]	$P_{1,u}$[2] [kN]	V_u[3] [kN]	$P_{1,cr}$[2] [kN]	V_{cr}[3] [kN]
C16a123	No	50	SC	611.8	514.3	237.9	200.0
C16b123	Yes	56	FS	301.7	253.6	245.3	206.2
C11b123	Yes	41	FS	236.6	198.9	222.8	187.3

[1] SC stands for shear compression failure, FS stands for flexural shear failure;

[2] Subscript *u* stands for ultimate load. Subscript *cr* stands for inclined cracking load.

[3] The shear force does not include the self-weight. The shear force generated by the self-weight of the specimens is about 8.82 kN. It has to be taken into account during the evaluation process.

On the other hand, in the pre-cracked tests not many new flexural cracks developed when the load level was low. Instead, the existing flexural cracks continued to propagate. For example, in test C16b123 at about P_1 = 200 kN the secondary crack branches developed at the compressive side from the tips of the existing cracks and made them joining the critical inclined crack; see Fig. 6.6 (right). At the tensile side of the crack, dowel crack was developed along the longitudinal reinforcement. This process was accompanied by large deformation in the critical shear span, and the load level dropped quickly in Fig. 6.7. After increasing the displacement of the actuators the load level could be recovered and even increased to a certain extent. The maximum load reached was 301.7 kN, which was less than half of the ultimate bearing capacity in the reference test. In

test C11b123 the failure process was similar, but its capacity was even lower. The failure mode of these two tests can be defined as flexural shear failure.

6.2.4 Discussion

The first impression is that the experimental results on continuous beams with pre-cracking and the ones reported in literature (Hamadi & Regan 1980; Pimanmas & Tisavipat 2005) are contradictory. In the tests reported in both publications, the presence of existing cracks increased the shear capacity, while in the continuous beam tests they reduced the ultimate capacity. However, both can be explained with the same theory presented in Chapter 3.

First of all, despite the failure modes, in almost all the load cases in the continuous test program, the development of an inclined major crack, and the subsequent opening of a dowel crack along the longitudinal rebar have been observed at a certain load level. That load level is defined as inclined cracking load as was discussed previously in Chapter 3. As shown in Fig. 6.7 in the continuous beam tests, the inclined cracking load of the tests with different failure modes is actually quite stable. The inclined cracking load is not clearly mentioned in either Hamadi & Regan's tests or Pimmanmas & Tisavipat's tests. Nevertheless, in Pimmanmas & Tisavipat's tests, V_{cr} can still be distinguished from the load-deflection relationship because of the reduction of the overall stiffness when the longitudinal bar is detached from the concrete beam. Regarding the inclined cracking load, a slight offset of the position of the inclined crack does not affect the value of V_{cr} significantly, this conclusion is confirmed in the crack pattern shown in Fig. 6.6, and in section 5.3.5 as well.

Secondly, the presence of the existing cracks influences the position of the major cracks and their profiles; both aspects eventually determine the profile of the critical inclined crack, especially the tip of the inclined crack, which eventually governs the failure modes. Based on the procedure described in section 3.5.2, with the boundary conditions of the experiment presented in this section, the critical compressive zone is at $a_{c,c}$ = 180 mm from the edge of the loading point. Taking into account the cracking moment M_{cr} = 61.3 kNm, the actual available length of the locations where a critical inclined crack may develop is only about 133.5mm when the measured inclined cracking load was reached. Considering the average major crack spacing of 232 mm, the chance of having flexural shear failure in such a load configuration is small. However, the presence of the flexural crack in C16b123 already defined the positions of the major crack before the load was applied. Besides, unlike the simply supported beam tests, the existing cracks in the continuous tests were generated at sections with small M/Vd ratio, the profiles of the cracks from previous loading case already had a pronounced inclination. Consequently the tip of the inclined crack may be

located outside the critical compressive zone, thus the flexural shear failure mode becomes possible.

In the simply supported tests in literature, the situation is different. First of all, the cracks generated in the precracking tests are pure flexural cracks. They are perpendicular to the longitudinal direction of the beam. The force needed to open an inclined crack (shear resistance) is related to the profile of the crack itself, see Fig. 3.38. A more inclined crack may deliver less shear force through aggregate interlock action, thus results in a smaller shear capacity. That explains why in the Hamadi and Regan's test series, the critical inclined crack always developed at the virgin shear span, where it is still possible to generate an inclined crack due to the combined effect of moment and shear force.

Moreover, for a beam with only vertical cracks, such as the Pimmanmas beams, a very large shear resistance is expected due to the aggregate interlock in cracks with this type of profile. In their experiments, the shear capacity of the existing flexural cracks is so high that an additional inclined crack with lower capacity was still able to develop in the uncracked concrete between the flexural cracks.

Besides, the Pimanmas' tests also show that despite the fact that the existing cracks in those beams are over the whole beam height, the compressive zone of the beams seems not to be affected. The height of the arch still equals z_c at the section of the existing flexural crack. If the distance of the flexural crack and the loading point is small, it is still possible to have shear compression failure which is then influenced by the position of the kink between the major crack and the secondary crack branches. In Pimanmas' tests it turns out that this postion is still defined by the locations of the existing cracks due to the crack arrest mechanism shown in Fig. 6.8. Since in this test series, the a/d ratio of the specimens is only 2.42, the space left for another critical inclined crack is limited. When the critical inclined crack develops from the existing flexural crack located within $a_{c,c}$ from the centre of the loading point, a stronger residual structure is formed by the profile of the critical inclined crack, thus the failure mode may switch from flexural shear to shear compression.

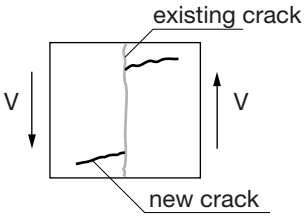

Fig. 6.8. Crack arresting mechanism, adopted from (Pimanmas & Tisavipat 2005).

The discussion above leads to the following conclusions regarding the presence of cracks or other type of weaker sections along the longitudinal direction of a beam. First of all, the location of the existing crack will influence the location and profile of the critical inclined crack, and thus the aggregate interlock in the crack and the capacity of the residual concrete arch formed by it. Consequently the uncertainty of the existing cracks makes the failure mode unpredictable when both failure modes are possible in the span (a/d between 2 to 3 for example).

Because of the uncertainty of the failure modes if the clear beam span is not exceptionally small (a/d <2, also for continuous beam), it is at the safe side to use the inclined cracking load as a lower bound for the shear capacity before the shear compression failure is guaranteed when the shear span is smaller than the lower bound defined by the crack path function as shown in Fig. 3.42. In case of a continuous beam it is more vulnerable to shear flexural failure, thus the conclusion has to be strictly followed.

6.3 INFLUENCE OF CONCRETE STRENGTH ALONG A CRACK

6.3.1 Introduction

Section 6.2 reveals the influence of the randomness regarding to the weaker sections along the longitudinal direction of a beam due to the variation of the material properties. The following question may be raised: at a given critical cracked section, will the material variability further influence the development of the crack and eventually the shear capacity of the beam? The classical answer is: Yes, since by definition, the opening of a crack is related to the strength of the concrete. Variation of concrete properties such as tensile strength makes the crack follow the direction in which σ_1/f_{ct} is minimum. The presence of a weak spot in the concrete section will result in earlier occurrence of the critical crack. However, the moment when the crack develops at a specific section is in principle not so much dependent on the material variability. Once the cracking process starts, it reaches s_{cr} quickly to fulfil the cross-sectional force equilibrium. This process usually will not result in immediate failure of the cross section. Eventually the shear force that is able to be transmitted across the crack under the critical shear displacement Δ_{cr} is decisive to the shear capacity for the cracked section.

The effect of variability of concrete to the shear resistance of a cracked section can be summarized into two aspects: the influence of the crack profile and the yielding strength of the cement matrix according to Walraven's formula (Walraven 1980). Numerical simulations with the non-linear-finite-element program Atena 2D have been carried out to investigate the influence of material

variability to the shear failure process of structures (Tanaka 2008). The analysis shows that the variability of the concrete strength influences the location of the critical inclined crack and thus affects the failure mode, which has been treated in the preceding section. Regarding the capacity of the structure, its influence is limited. However, there is no experimental proof explicitly supporting this conclusion yet. In this section the experimental research on a comparative study on the shear capacity of 50-years old and new concrete beams is presented. Compared to freshly cast concrete in the laboratory, there are a considerable number of cracks and other weak spots in the old concrete beams, causing large spatial variability regarding the material properties, which will be demonstrated in this section later. Thus the direct comparative study on the shear tests of an old and similar new concrete beam with the same conditions should provide a conclusive answer to the problem.

6.3.2 Background of the Test Program

The experimental research program presented in this section started from a discussion on the concrete strengths measured through core samples drilled from several existing concrete bridges in the Netherlands. Compressive tests of those core samples showed that the compressive strength of the concrete in the bridges has increased considerably compared to the design strength when the bridges were constructed. This would involve a higher shear capacity according to current codes like the Eurocode and the ACI code. However, the tensile strength from direct tension tests on the same set of cores was reported to be about 50% lower compared to what is normally expected for the compressive strength of fresh hardened concrete, although the splitting tensile strength

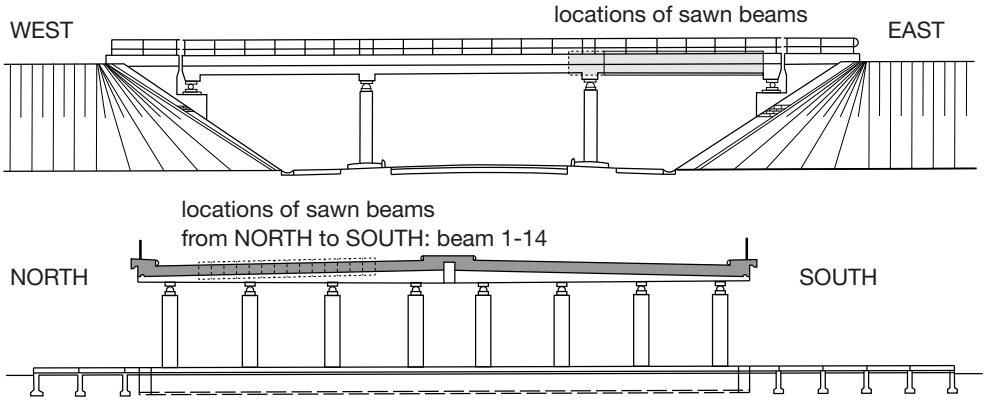

Fig. 6.9. Geometries of the deck of Gestelsstraat Bridge and the location of the test specimens in the bridge deck.

showed the same relation to the compressive strength as is found in new concrete. This can be attributed to the presence of weak spots in the old concrete samples. Considering the difference in the concrete strength from different testing methods, the question was raised by Rijkswaterstaat (Dutch Ministry of Infrastructure and Environment), whether the tested compressive strength of the old concrete can be used to evaluate the shear capacity of the bridge deck, or to use the direct tensile strength is more appropriate?

To answer that question, the ministry of transportation intended to evaluate the shear capacity of an old bridge by testing it to failure. The bridge Gestelsestraat in the motorway surrounding Eindhoven was chosen. It was built in 1961, and would be demolished in 2008, due to the reconstruction of that motorway. It is a three span flat slab bridge without shear reinforcement in the bridge deck. The only vertical reinforcing elements are bent-up bars in the flexural reinforcement and steel profiles used as the supports of the topside reinforcing bars. See Fig. 6.9 for the geometry of the bridge. The bridge has a skewness of 75 degrees.

The initial plan was to check the shear capacity of an entire span by loading the bridge in situ to failure. However, preliminary non-linear finite element simulations showed that the chance to generate shear failure of the deck was too small because of the low amount of flexural reinforcement. Moreover, the available time for testing was very short. Therefore it was decided to saw beams from the bridge deck, which would be subjected to shear loading tests under laboratory conditions. In total 14 beams were sawn in the end, and a selection of those beams were tested in Stevin Lab of Delft University of Technology by the author. The test program is presented in this section.

6.3.3 Test Specimens and Setups

6.3.3.1 Specimens

The original arrangement of the longitudinal reinforcement in the slab is shown in Fig. 6.10. In the width direction four repetitive longitudinal reinforcement design layers can be distinguished. The spacing between each layer is 150 mm. That determines the average width of the beams as 600 mm. The beams were cut from the east side span (see Fig. 6.9 for the definition of the directions. In the present section, the **bottom side** of the beam refers the original bottom side of the bridge) to avoid the larger amount of bent bars at the middle span. Out of the 14 beams, 4 beams include the intermediate support in the west end, see Fig. 6.9. They are numbered as Beam 6—Beam 9. The length of those beams is 8800 mm. The remaining beams were sawn before the intermediate support, thus have the dimensions of about 7000 mm long, 500 mm deep and 600 mm wide. The beams are not totally prismatic. The side surface is curvy along the longitudinal direction. The cross sections of the specimens were measured at every 1000 mm and

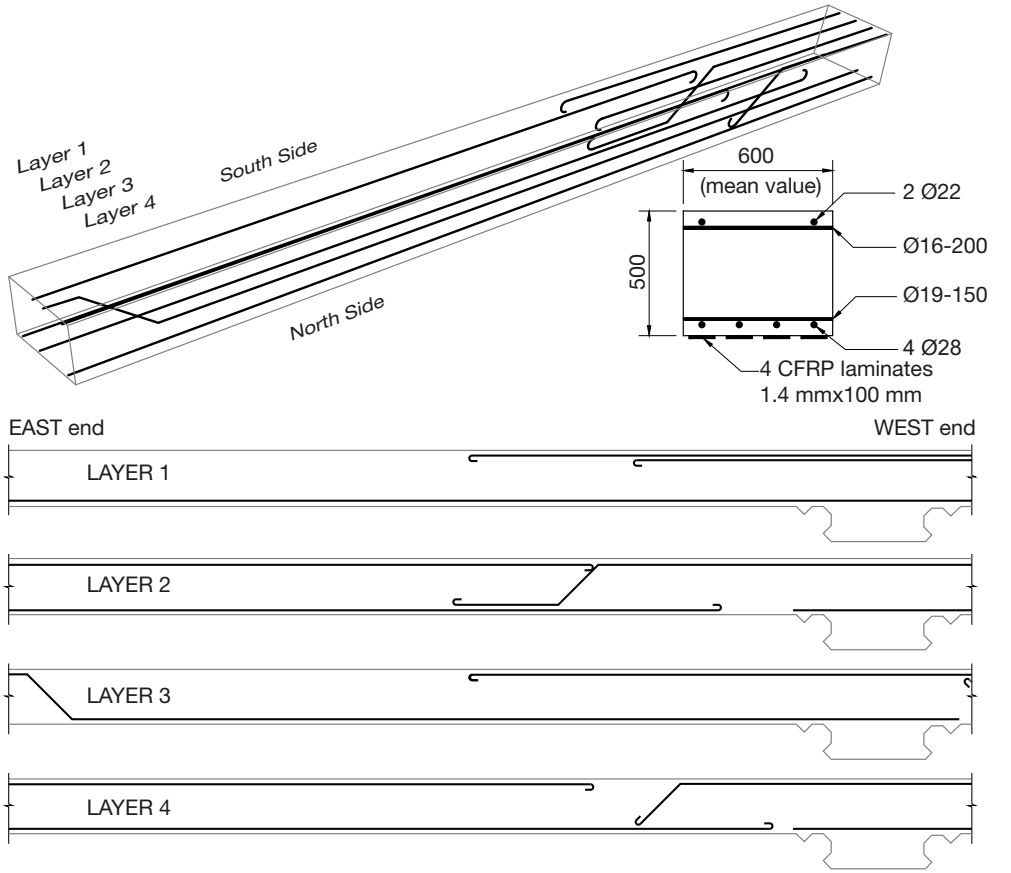

Fig. 6.10. Reinforcement layout of the old beams sawn from the Gestelsstraat bridge.

reported in (den Uijl & Yang 2009; Yang & Den Uijl 2012). Because of the sawing operation, the tensile longitudinal rebars of Beam 14 were damaged; therefore it was not tested. Besides, Beam 4 was damaged by accidental loading, no results were recorded. These two specimens were not tested.

Close to the intermediate support at the west end, some of the bars were bent from the top reinforcement layer to the bottom layer. This procedure was common at that time, to optimize the usage of reinforcement with regard to the moment distribution of the structure. The arrangement of reinforcement ensures that there are 4Ø28 mm tensile bars at the bottom of the beam in the sagging moment span, and 5Ø28 mm tensile bars in the top reinforcement layer in the hogging moment span close to the intermediate support. Thus, for simply supported tests, the critical shear span has to be arranged in such way that the bend ups of the rebars are avoided. For continuous beam tests, the loading

conditions of the test had to generate similar moment distributions as the original reinforcement was designed for.

Because the original reinforcement could not provide sufficient flexural capacity, to increase the flexural strength of the beams, four Carbon Fibre Reinforced Polymer (CFRP) laminates, each with a cross-section of 1.4×100 mm, were glued onto the tensile surface of the specimens. The laminates were placed beyond the position of loading plates when possible, so that both ends of the laminates are clamped by the loading/supporting plates during the test. The applied CFRP laminates behaviour is linear elastic up to failure at 1850 MPa (S&P Clever Reinforcement Company AG 2007). Because of the rather high strength, they are expected to behave as a perfect linear elastic material up to the failure of the beam. When the critical shear crack develops, debonding of the CFRP may occur. The failure of the beam may be caused by a combination of the opening of a dowel crack or the debonding longitudinal rebar CFRP. The bond behaviour between the CFRP laminates and concrete is quite different compared to the development of dowel crack along the longitudinal rebar under dowel force. The combined action makes it even more difficult to determine a failure criterion. Therefore it is not appropriate to compare this set of test directly with the results of beams with only steel bars reported in literature. Therefore, for some of the tests on old beams, reference tests were performed on new beams with the same dimensions, type and layout of the longitudinal reinforcement and the skew shear reinforcement, CFRP strengthening, concrete composition (type of cement, type and distribution of aggregates), and compressive concrete strength.

The whole test program was composed of two series. The first series comprised comparative tests between old and new specimens. It included 6 tests on simply supported old beams and on 6 new beams with the same boundary conditions. The second series is the additional test program, on the four beams with intermediate support. The test series comprised 5 simply supported tests and 4 continuous beam tests.

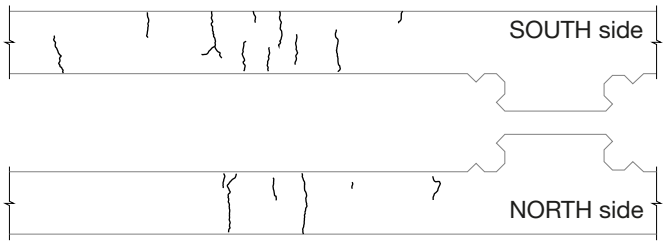

Fig. 6.11. Existing cracks in Beam 6.

The additional target in the second test series was to investigate the influence of real-life concrete variability on the shear behaviour. As was expected, the loading history of the bridge introduced a certain degree of damage to the beams. Visible cracks were found on the sawn surfaces of the beams. An example of the existing crack pattern across a tested shear span is plotted in Fig. 6.11. For all the tested specimens, the visible crack distribution before the experiments was recorded in (den Uijl & Yang 2009; Yang & Den Uijl 2012).

Besides, the concrete mixture showed a substantial sedimentation effect during casting. That generated a lot of air bubbles under the reinforcing bars and large aggregate, see Fig. 6.12. They became voids after the concrete was hardened.

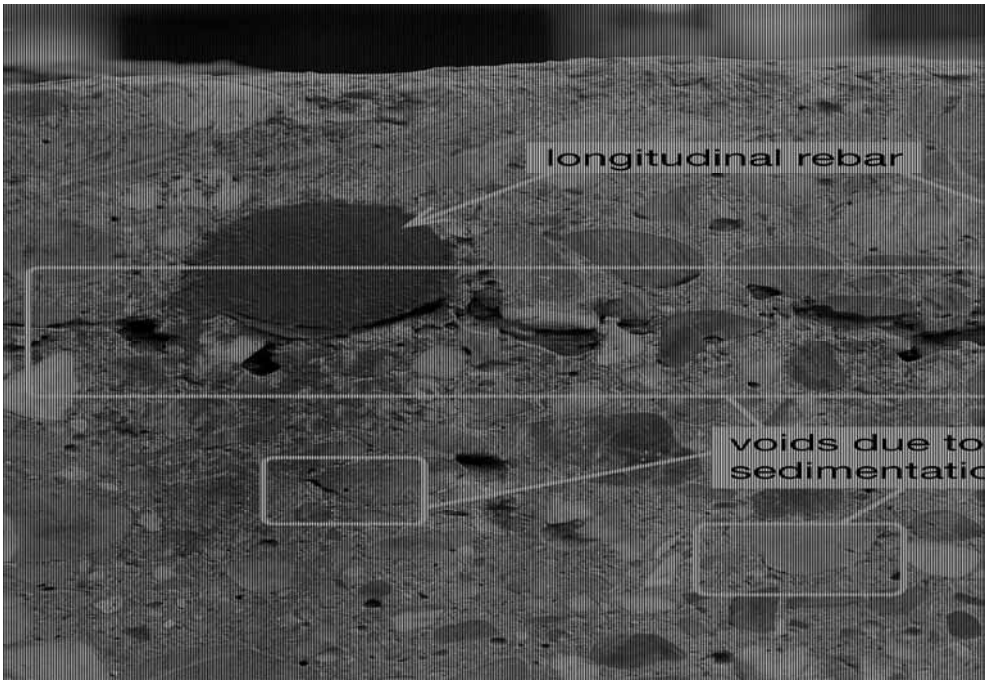

Fig. 6.12. Voids observed in a section of concrete beam specimen.

6.3.3.2 Material Properties

The Gestelsestraat Bridge was designed for a 28-days cube strength of about 35 MPa. To determine the concrete strength after almost 50 years, 24 cylinders with 100 mm diameter were drilled in-situ. After the first test series, two additional large concrete cores with a diameter of 290 mm were drilled from the Beam 4 at the part of the span that was not affected by the accidental loading. These cores were positioned close to each other with the axis perpendicular to

the side face of the beam. From those large cores, 100 mm diameter cylinders were drilled from vertical direction and longitudinal direction of the beam to evaluate the directional difference of the concrete strength. To guarantee that the measured concrete strengths are comparable, the same procedure has been followed with regard to the new concrete beams. The material properties are summarized in Table 6.2, in which $f_{cm,cube}$ is the equivalent cube compressive strength (cylinder Ø100-100 mm), $f_{ctm,s}$ is the splitting tensile strength, and $f_{ctm,dt}$ is the direct tensile strength (cylinder Ø100-200 mm; end faces glued to displacement controlled loading plates, thus rotation free). The reference beams were cast at different times, which resulted in a relatively large variation between the strengths of different beams. More detailed results are reported in (den Uijl & Yang 2009).

Table 6.2. Concrete strength (reference beams: cube compressive and splitting tensile strength measured at time of beam test, direct tensile strength measured 4 to 8 weeks after beam test).

Sample Sources	Specimen	$f_{cm,cube}$ [MPa]	$f_{ctm,s}$ [MPa]	$f_{ctm,dt}$ [MPa]	$f_{ctm,dt}/f_{ctm,s}$ [%]
Gestelsstraat Bridge	Site[1]	81.9	4.54	2.1	46.2
	B4E	68.0	4.01	2.1	52.4
Directional Strength:	$f_{cm,cube,h}$:	64.4	$f_{cm,cube,v}$:	71.6	
Reference Beams	B1N	82.4	4.9	3.5	71
Directional Strength:	$f_{cm,cube,h}$:	80.3	$f_{cm,cube,v}$:	90.6	
	B2N	69.9	4.7	3.2	68
	B3N	67.5	4.3	2.9	68

[1] Derived from the 100 mm diameter cylinders directly drilled from the bridge.

[2] $f_{cm,cube,h}$ is the concrete cube strength derived from samples drilled in horizontal direction; $f_{cm,cube,v}$ is the concrete cube strength derived from samples drilled in vertical direction.

The comparison of $f_{ctm,dt}/f_{ctm,s}$ between the old concrete specimens and the new concrete specimens in Table 6.2 clearly shows the problem stated in section 6.3.2 that for the old concrete in the existing bridges, the tensile strength derived from direct tensile tests is indeed considerably lower than in the case of newly cast concrete.

Another phenomenon that is worthwhile to be mentioned is that the concrete cube strength of samples drilled in vertical direction is always more than 10% higher than the ones drilled in the horizontal direction. This phenomenon is observed in the specimens of both old and new concrete. A possible explanation is the sedimentation effect described shown in Fig. 6.12. It is a more general effect not only found in the existing concrete structures but also in the newly cast

structures. The presence of the horizontal cracks weakens the compressive strength of concrete when the compressive stresses are parallel to the horizontal cracks. That was the case when the cylinders in compression tests were drilled horizontally. This phenomenon is illustrated in Fig. 6.13.

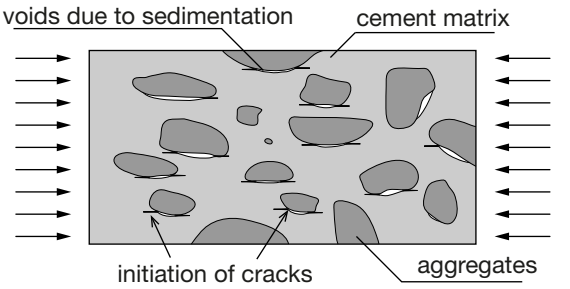

Fig. 6.13. Cracks generated by sedimentation voids under aggregates during compressive tests.

The diameters of the reinforcing bars in the old beams are Ø16, Ø19, Ø22, and Ø28 as shown in Fig. 6.10. They are all plain bars. The measured yield stress of the steel used in the longitudinal bars was 292 MPa, and the ultimate tensile strength was 402 MPa. In the ends of the beams steel plates were welded onto the longitudinal rebars, to ensure sufficient bond capacity. To make the reference beams comparable, plain bars of the lowest graded steel available on the market (S235) were chosen. The measured yield stress of the longitudinal bars was 303 MPa, and the ultimate tensile strength 420 MPa.

The measured elastic modulus of the CFRP laminates was 165 GPa. Tests showed that in most cases, the bond strength between CFRP and concrete was stronger than the tensile strength of the concrete (Yang & Den Uijl 2012). A weaker bond strength was observed in the first two continuous beam tests, in which the original asphalt surface layer was not completely removed.

6.3.3.3 Test Setup

In principle the test setup is the same as explained for the continuous test program presented in Chapter 5. In the first test series, all the specimens are simply supported, thus, the main variable in the test series is the shear span a. In the second test continuous beams were involved. Accordingly more variables were included, which are the moment ratio in the shear span M^-/M^+, and whether or not the beam is reinforced by FRP. A list of the configuration of the tested specimens is given in Table 6.3 and Table 6.4, where the experiments are identified by the number of the beam, the concrete type and the loading type. In the first test series, the beams are numbered as BxxNx. The first letter and the two

digits stand for the beam number. The second letter stands for the type of concrete, which may vary between E (existing concrete) and N (newly cast concrete). The last digit indicates the test sequence of the same beam. The specimens in the second series are identified slightly differently in the format of ExSx. Here, Ex stands for the beam number, whereas the second letter indicates the boundary conditions. C means continuous tests and S means simply supported tests. The last digit indicates the test sequence for the same beam as well.

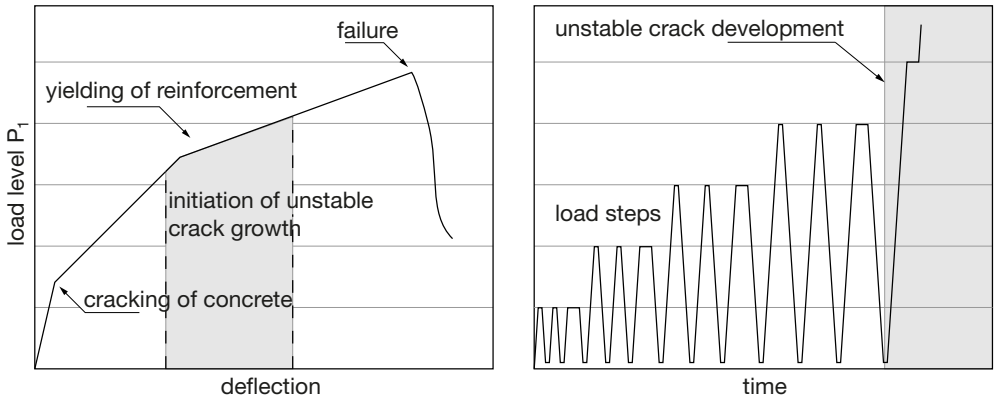

Fig. 6.14. Illustration of loading scheme of P_1.

In some of the old beam tests, Acoustic Emission (AE) sensors were installed, to monitor the elastic wave emitted during the cracking process of the concrete, thus to monitor the damage level of the specimen. To serve for the AE measurement, a different loading procedure including additional load cycles was designed. During the loading process, the actuators were under force control in most part of the tests. The load levels in the actuators were increased stepwise. The maximum load level in each loading step was designed with respect to the critical structural stages of the specimen. For example, the first load step was set a bit lower than the flexural cracking load, to open the existing cracks before new cracks are created. Within each load step, the force P_1 (see Fig. 5.5) was increased at a constant loading rate of 0.2 kN/s. After the designated load level was reached, the forces were kept constant for 2 min, and then reduced with the same loading rate to a force level of about 15 kN for P_1 and kept constant for 2 min to finish the load cycle. In total three load cycles were executed within each load step. The holding time in the last cycle was 10 min for crack marking and photogrammetry measurement. This type of load scheme stops as soon as an unstable inclined crack develops. It guarantees the full development of cracks during the tests. In the first test series, after the load cycles, the actuator P_1 was switched to displacement control. The load level was increased step-wisely until failure. In the second test series, after the development of the critical inclined

crack, P_1 was still under force control and increased step-wise, but no load cycle was performed anymore. Meanwhile, a strict displacement safety threshold was applied over the actuator, which made sure that as soon as the deformation of the specimen became unstable, the loading procedure would be stopped. An example of the loading scheme of P_1 is given in Fig. 6.14.

6.3.4 Test Results and Discussions

A summary of the results of all the 21 executed tests is listed in Table 6.3 and Table 6.4.

Table 6.3. Summary of configurations and results of tests on old and new concrete specimens.

Test No.[1]	d [mm]	b [mm]	a [mm]	a/d [-]	l [m]	FRP[2]	V_u/bd^3 [MPa]	$V_{c,fl}/bd^3$ [MPa]	Failure mode[3]
Series 1									
B13E1	426	600	1000	2.35	5000	Y	1.41	1.34	S
B10E1	456	550	1265	2.77	5000	Y	1.50	1.02	S
B05E1	438	585	1260	2.88	5000	Y	1.69	1.23	S
B03E1	441	588	1540	3.49	5000	Y	1.32	1.07	S
B12E1	431	590	1510	3.50	5000	Y	1.25	1.14	F
B11E1	426	600	1765	4.14	5000	Y	1.05	0.77	F
B02N1	456	600	1000	2.19	5000	Y	1.82	1.18	S
B03N1	456	600	1250	2.74	5000	Y	1.32	1.14	S
B01N1	456	600	1250	2.74	5000	Y	1.45	1.24	S
B01N2	456	600	1509	3.29	5000	Y	1.25	1.24	S
B03N2	456	600	1500	3.31	5000	Y	1.28	1.20	S
B02N2	456	600	1530	3.36	5000	Y	1.19	-	F
Series 2									
E6S1	447	598	750	1.68	3000	Y	2.67	1.69	O,F
E7S1	446	567	750	1.68	5000	Y	2.36	1.37	O,F
E8S1	447	599	500	1.12	5000	N	2.31	2.13	F
E8S2	447	599	500	1.12	4500	N	2.21	-	F
E9S1	446	596	500	1.12	5000	Y	3.2	1.71	O,F

Table 6.4. Summary of configurations and results of tests on old concrete specimens (continuous tests).

Test No.[1]	d [mm]	b [mm]	a [mm]	a/d [-]	M/Vd [-]	M^-/M^+ [-]	V_u/bd^3 [MPa]	V_{cr}/bd^3 [MPa]	Failure mode[4]
E6C1	447.4	598.4	1250	2.79	2.09	3.0	2.51	1.70	SC
E7C1	446.4	567.4	1250	2.80	1.68	1.5	2.35	1.72	O
E8C2	446.8	599.0	1000	2.24	1.68	3.0	2.63	1.26	O
E9C1	445.6	595.6	1500	3.37	2.02	1.5	1.76	1.58	O,F

[1] Identification code, explanation of it is referred to 6.3.3.1;

[2] Y indicates that the specimen was reinforced by CFRP laminates, N indicates no reinforcement;

[3] The shear forces are measured values, they do not include the self-weight.

[4] Failure mode of the test, S stands for shear failure: because of the complex reinforcement configuration, it is difficult to distinguish the specific failure mode. Nevertheless, when it is distinguishable SC stands for shear compression failure. F stands for flexural failure due to the yielding of reinforcement. O stands for other failure such as the in sufficient bond between CFRP and the specimen.

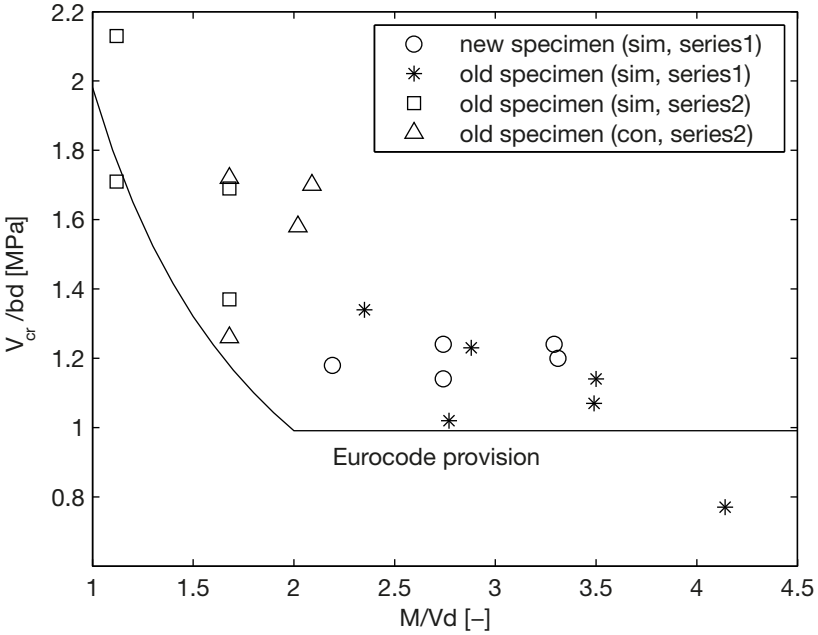

Fig. 6.15. Comparison of V_{cr}/bd derived from specimens made of old concrete and new concrete. In the legend, sim stands for simply supported specimens, con stands for continuous supported specimens

Within the test program, different failure types have been observed. Nevertheless in most of the tests an inclined crack together with a certain level of

detachment of either the reinforcement or the CFRP laminates were observed, from which the inclined cracking force V_{cr} was defined.

Because of the complexity regarding the reinforcement arrangement, a clear definition of the critical shear displacement Δ_{cr} is not available for this type of specimens. Thus it is not possible to predict the shear capacity properly with the same procedure as specified in Chapter 4. Nevertheless, the same reinforcing arrangement of both the new beams and the old ones ensures the same failure criteria within this research program. By comparing the performance of the two groups, it is still possible to evaluate the difference between the old and new concrete specimens. Accordingly, the question raised by Rijswaterstaat on whether it is possible or not to evaluate the shear capacity of existing concrete structures with the measured concrete compressive strength from cylinder specimens can be answered.

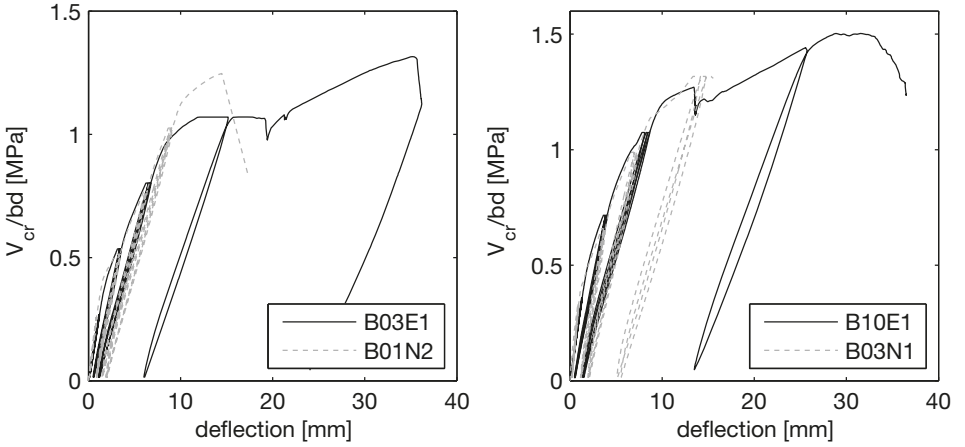

Fig. 6.16. Comparison of shear stress - deflection relationships between old and new beams.

In Fig. 6.15 the measured inclined cracking load V_{cr} of all the tests in this research program is plotted against the maximum M/Vd ratio of the critical shear span. With respect to V_{cr}, the comparison shows that the difference between specimens consisting of old or new concrete is quite limited. Similarly, the overall stiffness of the specimens is quite comparable as well when the shear force is nominalized by the measured cross sectional area of the specimen. Two examples of such a comparison from the shear stress-deflection relationship are shown in Fig. 6.16. It shows that the influence of the weak spots in the old concrete specimens was only pronounced at the stage when the flexural cracks were developed. After the flexural cracks were stabilized, the stiffness of both old beams and new beams were comparable. That also indicates that once a

major crack is fully developed, the shear force that can be transferred per vertical displacement Δ is not affected by the local weak spots along the crack anymore.

This conclusion was further validated afterwards by comparing the surfaces of the critical inclined cracks of Beam 4E and Beam 1N. The failures of both beams were due to the large opening of inclined cracks, thus can be treated as flexural shear failure. After the tests, the specimens were broken along the critical inclined crack, and the longitudinal reinforcing bars were sawn so that the crack surfaces were exposed to be examined. The photos of both crack surfaces are shown in Fig. 6.17, in which the difference of colour was due to the different type of cement paste. In both cases the crack surface developed through the course aggregates. That indicates that the cement matrix strengths of both old concrete and the new one are higher than the aggregates. It confirms with the decision in section 4.5.2 to take into account the effect of aggregate fracture when the concrete strength is higher than 60 MPa. Because of that, the surface roughness played an important role to generate aggregate interlocking force. In that case, only a limited part of the crack faces had contact, which generated the shear resistance of V_{ai}, whereas the local voids or cracks in the old concrete did not contribute to V_{ai} or weaken it at all. To the contrary, the observation shows that the presence of the local cracks may even increase the roughness of the cracked surface, thus increase the shear force that is transferred through the cracked surface in certain concomitances.

In addition, the influence of existing cracks to the shear failure modes addressed in 6.2 was also found in this test program. However, since it is difficult to quantify both the material properties and the boundary conditions of the old specimens, it is not discussed further. For more detailed information reference is made to (Yang et al. 2012).

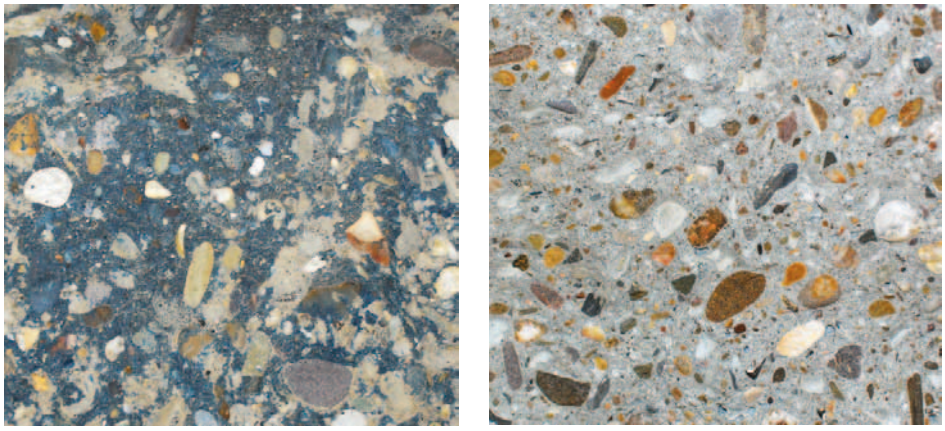

Fig. 6.17. Surface of inclined crack in Beam 4E (left) and Beam 1N (right).

Last but not least, to give a direct answer to the practical question raised from Rijkswaterstaat, the results of the Eurocode provision as also shown in Fig. 6.15. The reinforcement ratio of the specimens is determined by converting the area of CFRP strips into steel bars according to their elastic modules. The concrete cylinder strength f_{cm} of 60 MPa was used as a general approximation based on the measured concrete compressive strength reported in Table 6.2. The original formula was adjusted to predict the mean value of the test results, see Chapter 2. Despite the inaccuracy introduced into the assumptions, the comparison shows that for design practice, it is still safe to use the measured concrete compressive strength to estimate the shear capacity of the existing structures with Eurocode provision.

6.4 INFLUENCE OF CONCRETE STRENGTH VARIABILITY IN WIDTH DIRECTION

6.4.1 Introduction

In principle, a specimen having identical boundary conditions in the transverse direction can always be considered as a parallel system composed of a set of specimens in the transverse direction. According to this assumption the boundary conditions of the set of paralleled specimens are identical in the transverse direction, and the contribution of each specimen in the transverse direction is the same as well, so that the same failure section applies. As discussed in section 6.1.3, in a parallel system, the overall capacity of the whole set of the specimens is determined by the post peak behaviour of each component of the system. However, the post peak behaviour of a reinforced concrete beam after shear failure is complicated. It was shown in Fig. 3.40 that depending on the position of the critical inclined crack the residual behaviour of the beam may be quite different. In addition, the presence of existing cracks can cause the transition of the failure mode from flexural shear to shear compression, which has been shown in section 6.2 already. Because of the uncertainty of the behaviour of the beam after inclined cracking, when dealing with structural elements with large width and material variation in width direction, it is difficult to define how the variability should be taken into account in the evaluation of the overall structural behaviour.

On the other hand, when the concrete strength of an existing structure is determined on the basis of drilled core samples, a large scatter is often observed. Shear failure is usually regarded as a brittle failure mode, considering the parallel system theory discussed before, the weakest spot of the parallel system is believed to govern the bearing capacity of the structure. With this principle an over-conservative prediction of the bearing capacity of the existing structure

may be obtained. Since an investigation of the existing concrete slab decks in the Dutch highway system have shown that their concrete strength has a large scatter (Steenbergen et al. 2010; Vervuurt et al. 2013), and some of those structures even showed local damage (Lantsoght & van der Veen 2012; Yang, den Uijl et al. 2012), an appropriate evaluation of those structures is important.

For that reason, experimental studies have been carried out in the Stevin Laboratory at Delft University of Technology to investigate the influence of the concrete strength variation in transverse direction on the shear capacity of the slabs. The test program and several preliminary conclusions derived from the results are reported in (Yang & den Uijl 2012). In this section, the experimental research will be presented, and based on the results of that research, the one way shear behaviour of structural elements with a large width and significant concrete strength variability is discussed.

6.4.2 Test Specimens and Setup

6.4.2.1 Design of Test Specimens

The dimensions and the arrangement of the concrete strips for the chosen slab layout are shown in Fig. 6.18. The slabs are 4200 mm long, 2500 mm wide and 300 mm thick. They are composed of seven strips of two different concrete mixtures. The ones at the sides are 250 mm wide and are made of high strength concrete, whereas the central strips are 400 mm wide. That makes the volume ratio between high strength concrete and low strength concrete about 52%-48%. Taking into account the inaccuracy of the casting process, the ratio between the two concrete mixtures can be approximated to 50%-50%.

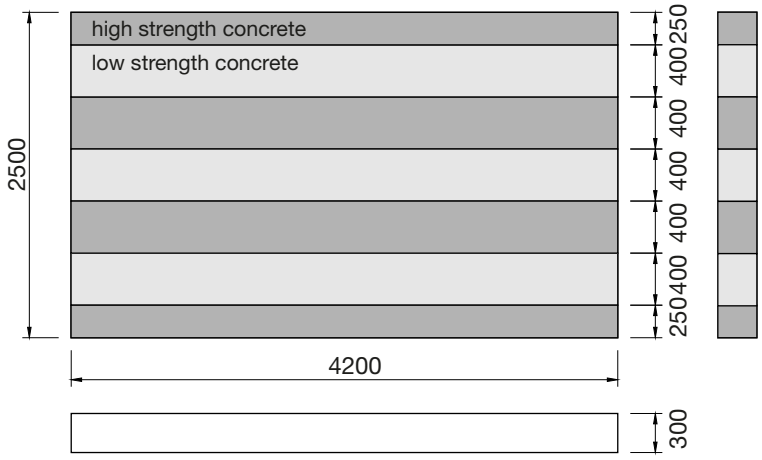

Fig. 6.18. Dimensions and layout of test specimens with mixed strengths.

6.4.2.2 Concrete Properties

In order to maximize the difference of concrete strength, the strengths of the two concrete mixtures used in the same slab shall be clearly different. The concrete mixtures used in the test program are C53/65 and C20/25. The high strength concrete mixture is a commercial mixture delivered by a concrete plant that has been used in the tests regarding the continuous beams subject to a point load in the research program, see section 5.3. This enables the comparison with former test series. The cube strength can reach as high as 87 MPa (Yang & den Uijl 2011). The low strength mixture was designed in the lab. In order to minimize the concrete strength, while preventing segregation, limestone powder and fly ash were used to partly replace cement. The compositions of the mixtures are given in Table 6.5 and Table 6.6.

Because of the complexity of casting the mixed slabs, only one slab with two different concretes was cast at once. Despite the great effort being made to ensure consistent concrete mixtures among the different casts, scatter still exists among the concrete strength of the different casts, especially for the low strength mixtures. On average, the low strength concrete is stronger than the design value. Cube tests were performed at the date that the tests were carried out. The results of the aforementioned tests are summarized in Table 6.8 together with the configurations of the test setups.

Table 6.5. Composition of the high strength concrete mixture.

Content	Mass [kg]
CEM I 52.5	280
CEM III 42.5	145
Sand 0-4 mm	775
Gravel 4-16 mm	900
Fly Ash	60
SPL VC 1550	3.541
VTR VZ 1	1.213
Water	171
Total	2336

Table 6.6. Composition of the low strength concrete mixture

Content	Mass [kg]
CEM I 42.5	150
Limestone Powder	80
Fly Ash	100
Sand 0-4 mm	872
Gravel 4-16 mm	907
Water	185
Total	2294

Table 6.7. Comparison between control cube tests and cylinder tests (Ø100×100 mm) drilled from the tested specimens (Measured compressive strength; unit: MPa).

Cast No.	1	2	3	4	5	6	7	8
Cube	30.5	80.3	90.1	45.0	81.3	40.3	83.9	39.8
Cylinder	32.6	97.4	90.7	38.4	89.7	43.0	78.5	34.5

Table 6.8. Configurations of tested specimens (cylinder strength f_{cm} = 0.85 $f_{c,cube}$, concrete cube strength measured at the day of testing).

Test No.[1]	a [mm]	Cast No. [-]	$f_{cm,l}$[2] [MPa]	Cast No. [-]	$f_{cm,h}$[2] [MPa]	f_{cm} [MPa]	age [days]
L016A	600	1	23.2	-	-	23.2	61
H026A	600	-	-	2	61.0	61.0	29
M036A	600	4	30.6	3	69.7	50.2	43
M046A	600	6	25.6	5	64.8	45.2	38
M056B	600	8	31.0	7	73.1	52.0	85
L018B	800	1	26.3	-	-	26.3	126
H028B	800	-	-	2	67.8	67.8	117
M038B	800	4	37.3	3	72.9	55.1	112
M048B	800	6	31.2	5	69.0	50.1	105
M058A	800	8	31.0	7	68.7	49.9	79

[1] Identification code, concrete strength: L-low, H-high, M-mixed; Slab number: 01-05; Shear span: 6 = 600 mm, 8 = 800 mm; Test order: A = first, B = second.

[2] $f_{cm,l}$: is the tested cylinder strength of the low strength concrete; $f_{cm,h}$: is the tested cylinder strength of the high strength concrete;

Moreover, Ø100 mm cores were drilled after the specimens were tested to check if the casting process was executed properly. Splitting tensile tests and compressive tests were applied on them. The cylinders from the cores drilled from the specimens have the dimension of Ø100×100 mm, which is considered to be equivalent to cube tests. Since in the Eurocode the cylinder strength (Ø150×200) is utilized, the tested cube strengths are translated to cylinder strength with a factor 0.85. These results are used as an indication of the real concrete strength of the slabs. Those test results are consistent to the cube tests. The comparison between cube strength and original cylinder strength are shown in Table 6.7.

6.4.2.3 Reinforcement Configuration

The reinforcement arrangement is consistent with other slab tests in the same research project (Lantsoght, van der Veen et al. 2011). The bottom reinforcement mesh is composed of 21Ø20 mm ribbed bars in longitudinal direction and 34Ø10 mm in transverse direction. The top reinforcement mesh consists of 9Ø12 mm in longitudinal direction and 15Ø12 mm in transverse direction. The concrete cover is 25 mm, which makes the effective depth of the slab d = 265 mm. The reinforcement ratio of the longitudinal bottom bars in is 0.97%.

For the bottom reinforcement mesh, some steel bars are bent up to support the top reinforcement at the edges of the specimen. Since the bent ups of the transverse rebars may be considered as shear reinforcement, they may influence

the shear capacity of the specimens. However, since the area of these bars is quite limited compared to the cross sectional area of the slab and the anchorage length of these bars is very short, the tensile force that can be built up in these bars is quite limited. Therefore, the influence of the reinforcement arrangement on the shear capacity of the specimens is negligible.

6.4.2.4 Casting Process

In order to get a concrete slab with two different concrete mixtures in different regions maintaining the connectivity between the various parts, the two types of concrete have to be cast at more or less the same time to be able to harden together. To achieve this, the mould was separated into strips by removable partitions. These removable elements consist of two panels spaced 380 mm with a hoist beam mounted on top to lift the elements right after the concrete has been cast and vibrated. Slots are made in the panels to place the transverse bottom reinforcement. The top mesh rests on rows of steel wire supports, and was placed after the removable moulds had been lifted out. The whole casting procedure is described by the following steps:

- Clean the mould and oil it. Place the removable mould units. Record the actual distance between the panels;
- First, cast high strength concrete filling the respective moulds up to around 100 mm;
- Cast the low strength concrete filling those strips completely. Try to make the level of the fresh concrete 15 mm higher than 300 mm;
- Finally complete the casting of high strength concrete. Make the level of the fresh concrete 15 mm higher than 300 mm. Compact the concrete with internal vibrators;
- Lift the removable moulds one after another;
- Place the top reinforcement mesh. Vibrate the concrete carefully and add some high strength concrete on top if needed;
- Flatten the surface and remove spilled concrete.

An overview of the concrete mould is given in Fig. 6.19, together with a photo of the concrete specimen after the casting procedure. Immediately after the casting, the differences in the concrete type are clearly shown by colour in the photo. The lower strength concrete has a higher water/cement ratio therefore it is more reflective than the higher strength concrete.

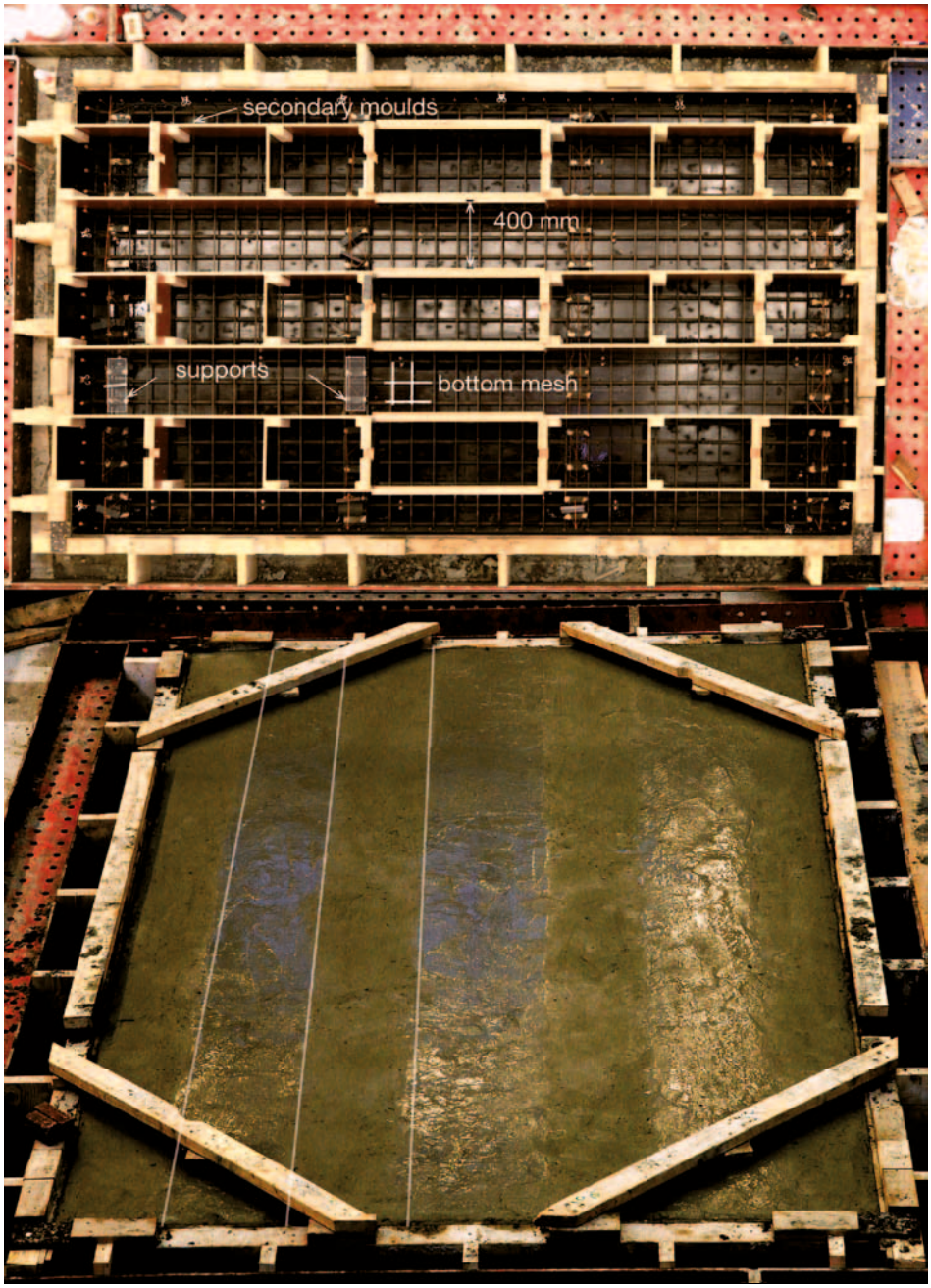

Fig. 6.19. Overview of concrete mould (top), prepared specimen after casting (bottom).

6.4.2.5 Test Setup

A sketch of the test setup is plotted in Fig. 6.20. The specimens were simply supported and loaded by a hydraulic actuator. A 1000 mm high, and 2500 mm long steel distributing beam was used to transmit the force from the actuator to the slab. The large stiffness of this beam ensured a homogeneous displacement along the width direction, with the additional plaster layer between the load distributing beam and the specimen, a line load was simulated. The centre-to-centre distance between the line load and the main support was 600 mm or 800 mm. The main span of the slab was 3600 mm. An ideal simply support condition was created by a roller support and a fixed hinge. In order to measure the reaction force of the support in the critical span, 7 support units including load cells were installed at the main support. 7 pairs of laser displacement sensors were placed at the centre of each strip, to measure both top and bottom displacement. The displacement differences of each laser sensor pair indicate the crack opening in vertical direction at the centre of each strip.

During the experiments, the main actuator was under force control in the first loading stage. A loading scheme was designed for each test. It follows the same principle as was presented in Chapter 5. The force applied by the actuator is increased stepwise. The maximum load level in each load step was designed with respect to the critical structural stages of the specimen.

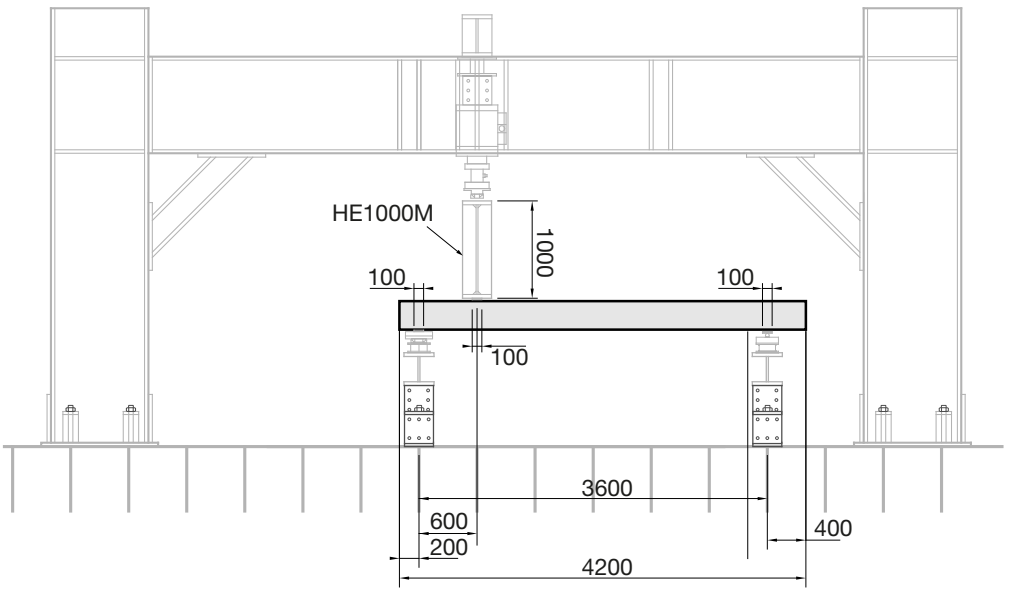

Fig. 6.20. Test setup of specimens with concrete strength variability in width direction.

6.4.3 Test Results and Discussions

All the five specimens were tested at both ends. These ten tests were subdivided into two test series with different shear spans: series 1 with a shear span of 600 mm, series 2 with a shear span of 800 mm. From Slabs 1 to 4, the first test had a shear span a = 600 mm and were tested with a = 800 mm on the other side. Slab 5 was used for additional tests. It was first tested with a = 800 mm, to check if there is any influence from the order of testing. The results of the tests are summarized in Table 6.9. In the table, the tests are categorized by the shear span.

The name of the test specimens is explained as follows: the first letter indicates the type of concrete being tested, which varies among L, H and M, representing Low strength, High strength and Mixed strength concrete. The following two digits stand for the number of the slab, while the last digit stands for the length of the shear span, which varies between 6 (600 mm) and 8 (800mm). The last letter of the name indicates the test sequence in the same specimen.

Table 6.9. Summary of test results investigating concrete variability (unit: kN).

Test No.	P_{cr}	P_u	V_{cr}[1]	V_u[1]	$V_{EC,m}$	V_{cal}[4]	$V_{cr}/V_{EC,m}$	V_{cr}/V_{cal}
L016A	1007.0	1445.8	862.5	1228.2	524.2	716.5	1.65	1.20
H026A[2]	1200.0[3]	1659.5	1286.4	1406.3	723.8	950.6	1.78	1.35
M036A	1200.0	1833.3	1023.4	1551.1	678.1	900.3	1.51	1.14
M046A	1199.5	1701.8	1022.9	1441.5	654.8	872.6	1.56	1.17
M056B	1176.0	1211.0	1003.4	1032.5	686.3	909.8	1.46	1.10
L018B	1071.2	1071.2	855.0	855.0	546.7	666.5	1.56	1.28
H028B	1297.6	1297.6	1031.1	1031.1	749.7	863.0	1.38	1.19
M038B	1132.8	1165.5	902.8	928.3	699.5	832.4	1.29	1.08
M048B	1195.2	1195.2	951.4	951.4	677.7	808.8	1.40	1.18
M058A	1153.0	1166.1	928.8	928.8	676.8	807.8	1.37	1.15

[1] Self-weight has been taken into account to compare with the calculated results.

[2] Test was terminated at this load level due to unbalanced movement of the loading beam.

[3] The opening of the inclined crack started at the end of the 3rd load step at one side of the slab. It developed towards the other side at P = 1515.6 kN. This was caused by the additional torsional moment in the main support.

[4] V_{cal} is calculated with the procedure proposed in Chapter 4.

In test H026A, shortly after the inclined crack developed, the loading plate between the distributing beam and the concrete surface slipped away, because of the large displacement. The test had to be terminated for safety reasons. Therefore, the maximum load of that test is relatively low.

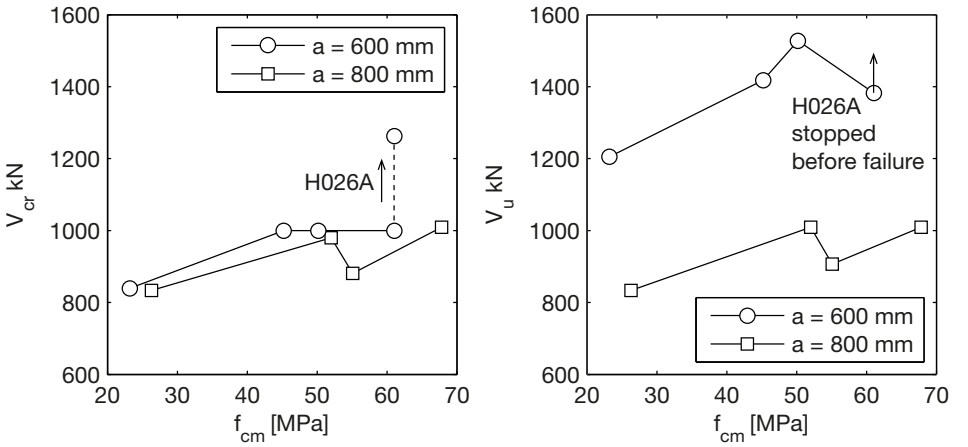

Fig. 6.21. Relationship between concrete mean strength f_{cm} and inclined cracking force V_{cr} (left) and ultimate shear capacity V_u (right).

The ultimate capacity of the slabs and the inclined cracking load are plotted against the mean concrete strength (see Table 6.8) in Fig. 6.21. The results show that in test series 2 (a = 800 mm) the concrete strength has a very consistent influence on the shear capacity. The results are quite repeatable among the three tests: M038B, M048B and M058A. However, the results derived from test series 1 (a = 600 mm) lead to a contradictory conclusion. The three mixed specimens have a quite different ultimate capacity. Among them, test M036A reached the yielding moment, while in M056B the maximum shear force was as low as 1009.2 kN, which is only 66% of the highest one.

The rather large scatter shown in Fig. 6.21 regarding the ultimate shear capacity is due to the unstable failure modes of the specimens in test Series 1 (a = 600 mm); the influence of the concrete strength on the shear capacity was suppressed by the switch of the failure modes. On the other hand, Fig. 6.21 shows that despite the variation of the failure modes, the inclined cracking load was quite stable. In most cases the inclined cracking load is in line with the mean concrete strength of the slab. Therefore the inclined cracking load can still be calculated with the mean concrete strength over the width. Besides, the conclusion stated in section 6.2 is still valid with respect to slab structures, saying that for structures which do not have a fixed failure mode, one may use the inclined cracking load as a lower bound. For that reason, special attention is paid to the inclined cracking load of each test.

Table 6.9 provides the comparison of the measured V_{cr} with the Eurocode provision and the calculated shear capacity with the formula proposed in this research. Both calculation results are derived using the mean concrete strength f_{cm} of the whole slab. The comparison shows that by adapting the mean concrete

strength both methods are able to follow the increment of shear capacity properly. Regarding accuracy, the prediction given by the method proposed in this section is better. Compared to the test result, it gives a consistent prediction. Nevertheless, both methods underestimated the tested shear capacity.

It has to be mentioned that in Table 6.9 the inclined cracking load is defined as the load level at which unstable cracks started to develop in diagonal direction. During the loading process, the vertical displacement of the slab in the middle of the shear span is monitored by an array of laser displacement sensors. This has been explained in section 6.4.2.5. The vertical component of the crack opening is derived by subtracting the top and bottom displacement. The inclined cracking load is derived from the real-time measured vertical crack opening versus load relationship when the crack opening in vertical direction starts from at least one pair of the sensors in width direction. Detailed information is given in the test report (Yang & den Uijl 2012).

Unlike beam specimens, a clear definition of the inclined cracking load is not always possible. In some of the specimens, a clear plateau was not found in the vertical crack opening-load curve of all the laser sensor pairs, in some other ones no clear difference in vertical crack opening was distinguishable. An example is shown in Fig. 6.22. It plots the vertical crack opening – load relationship of test M038B at the middle of the shear span in the seven strips. Although the final failure mode was flexural shear, the opening of the vertical crack did not start at the same load level along the transverse direction. Relating to the shear failure mechanism explained in Chapter 3, this indicates that for a slab structure, despite the fact that a certain part of the critical inclined crack in transverse direction reaches Δ_{cr}, the remaining part of the slab will not always follow. Only

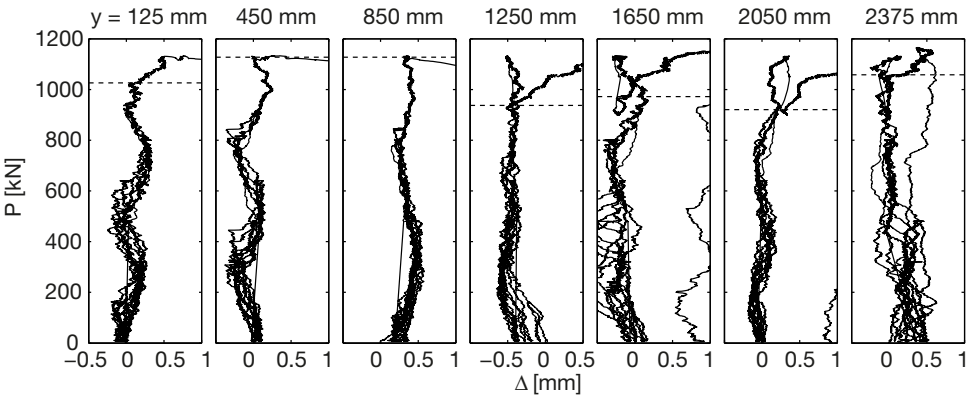

Fig. 6.22. Load-vertical displacement relationship at different locations in width direction of test M038B

when the vertical displacement Δ of the majority of the section reaches Δ_{cr}, the splitting dowel crack can developed, eventually, failure of the section is possible. The failure load is most likely to be the average of the whole section.

A possible reason for the inhomogeneous vertical displacement could be that the position of the inclined crack is not identical along the width direction. To illustrate this, the crack pattern at both sides of slab 1-4 after failure is plotted in Fig. 6.25, where both the shape and the position of the critical inclined crack at the sides of the specimen are not the same. This phenomenon is observed not only on slabs with mixed strength but also on homogeneous slabs. It is not directly related to the material variability.

In order to check the integrity of the slabs with mixed strips, the crack patterns of four specimens in the same test series under the same load level P = 800 kN are marked in Fig. 6.24. The graphs show that the cracked areas of L016A and H026A do not vary significantly, despite the two times higher strength of the latter one. The furthest cracks in both specimens are located at almost the same distance to the line load. On the other hand, the crack spacing clearly changes with the concrete strength. In the low strength slab L016A, about nine cracks are visible over a distance of 1 meter, while in the high strength slab H026A, only around seven cracks can be found within the same distance. This is

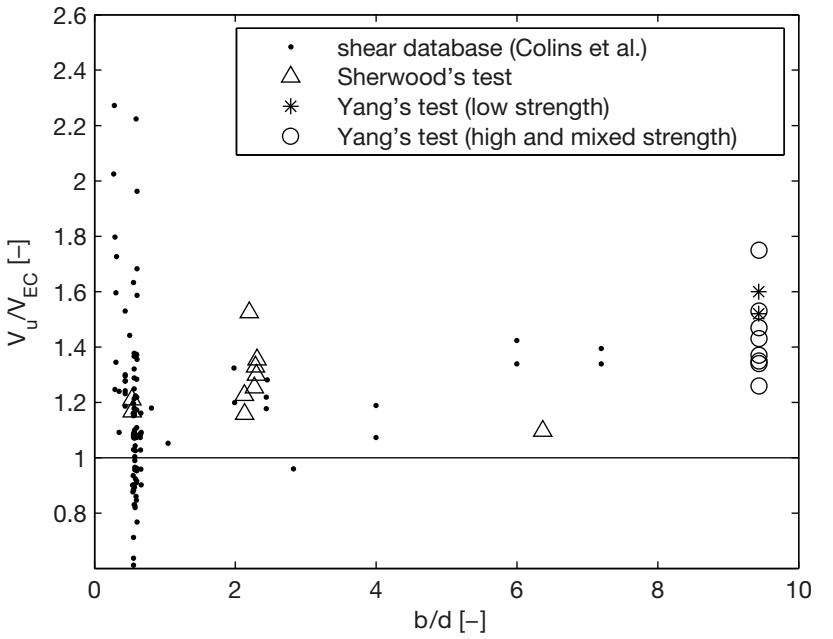

Fig. 6.23. Width depth ratio versus shear capacity prediction with Eurocode.

certainly due to the lower concrete tensile strength. The crack patterns of the mixed specimens fall in between these two reference cases. It is noted that the strips of different concrete strengths in the mixed slabs behave as if it was a homogeneous slab. The formation of the crack pattern did not vary significantly with regard to the concrete strength variation in the transverse direction. This is also observed from other measurements, such as AE emission, and vertical crack opening-load relationships at different strips.

Other than the finding that the weaker concrete spots in the transverse direction of the mixed slab do not determine the overall shear capacity of the whole slab, an additional conclusion may be drawn from the set of tests. In Table 6.9, the comparison between test results and predictions shows that in general the shear capacity of the slabs seems to be always higher than the predicted capacity based on beam test results.

To check the influence of the width of the specimen to its shear capacity, a more extensive study on experiments reported in literature has been carried out. Shear tests with configurations similar to the tests presented in this study in the shear test database reported by Collins, Bentz et al. (Collins, Bentz et al. 2008) are collected. The adopted original database has been used to determine the critical shear displacement Δ_{cr} for the proposed shear design procedure in Chapter 4 already. In this part of the research a different selection of tests has been made. It is based on the following criteria: concrete strength f_{cm} between 15 MPa and 40 MPa, effective depth d between 250 mm and 300 mm, reinforcement ratio ρ between 0.5% and 1.5%, and shear slenderness ratio a/d larger than 2.7 to ensure shear flexural failure. These results comparable with the low strength slab tests. A summary of these tests are indicated in Appendix III in combine with the ACI-DAfStd database. Besides, the wide beam tests reported by Sherwood et.al in (Edward G. Sherwood 2006) are included in the comparison as well. Note that according to Sherwood et al.'s description, the boundary conditions of their widest specimen are different from an ideal one-way slab. They applied three parallel point loads and 3 point supports in the transverse direction of the specimen to replace a real line load and line support: that configuration may course stress localization and eventually influence the shear capacity of the specimen.

The aforementioned data are plotted together with the results presented in this section in Fig. 6.23, in which the y axis is the normalized measured capacity by Eurocode prediction. The x axis is the ratio between specimen width b and the effective depth d. The comparison shows the tendency that the average normalized shear capacity is indeed increasing with the width of the specimen. Regarding this, several explanations are proposed in the following section.

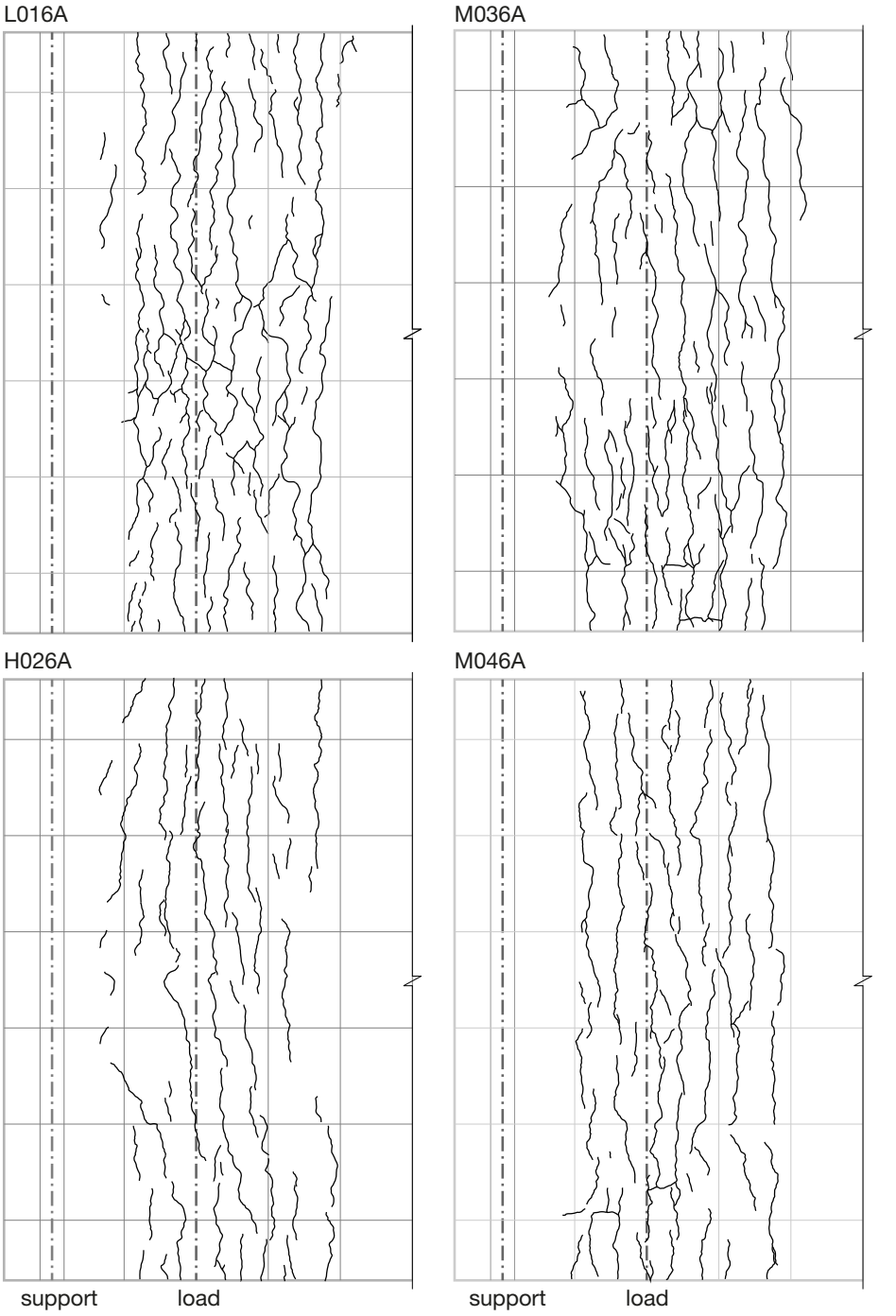

Fig. 6.24. Bottom crack patterns of series 1 at P = 800 kN.

Fig. 6.25. Comparisons of crack patterns of side surfaces of slab 1-4 after failure.

Other than the increase of mean shear strength, although the amount of data points between the narrow and wide specimens are not comparable, Fig. 6.23 still shows the tendency that the narrow specimens have larger scatter than the wide ones. This can be explained by the fact that the narrow specimens are more vulnerable to the local variation of the concrete strength. The shear capacity of the whole specimen is easily influenced by the weak spots in the shear span. However, for a wide member, the local shear failure does not result in an overall collapse, the load can still be carried though the redistribution mechanism in the transverse direction. The wider the specimen is, the smaller is the variation of the expected concrete mean strength in the transverse direction. If the shear capacity of the mixed specimen can be estimated by the average strength, the scatter of the shear capacity of one-way slabs with width-depth ratio of 10 shall be considerably less than that of beams with width-depth ratio of 0.5. In practise, most slab bridge decks have a width over depth ratio larger than 10. However, this ratios for most specimens in literature is close to 0.5 (beam specimens). Further than this study, the widest specimen in literature has a width-depth ratio of 7.2. Taking into account that the design formula of the shear capacity of a beam is derived from a regression study of relatively narrow beam tests with remarkably large scatter, the safety for the shear capacity of a slab factor needs to be adjusted, if the same β value (reliability factor) has to be achieved.

6.4.4 Influence of Specimen Width

The comparison study of slabs with concrete strength varying in width direction shows that basically the shear failure of reinforced concrete structures can still be considered as quasi-brittle behaviour, thus considering it as a parallel system making it possible to calculate the shear capacity by taking the average concrete strength in the transverse direction. On the other hand, it was found that despite the strength variability, the shear capacity of a slab structure with larger width-depth ratio has a relatively higher shear capacity than beam specimens. This conclusion is also confirmed by comparison of experimental results reported in some literature, like Conforti, Minelli et al. (Conforti et al. 2013) in their shallow specimens. Although no direct experimental comparison has been carried out to validate it, the observation on higher shear capacity of one way slab specimens turns out to be a more general phenomenon. In this section it is attempted to explain this within the theoretical framework presented in the previous chapters.

For a homogeneous one way slab structure, any strip of the slab in the span direction should be equivalent in theory, since the structural performance and the boundary conditions of each strip are the same. So does the shear capacity of any strip taken along the transverse direction, which shall be of no difference

compared to the whole slab. The additional increment of the shear capacity has to come from the inhomogeneity of the structure in the transverse direction. Ignoring the variation of the boundary conditions, it is the variability of the concrete property (strength) in transverse direction that raises the shear capacity of slab structures.

Compared to beam elements with relatively small width, the larger width-depth ratio allows a difference regarding the deformation of the slab along the transverse direction. Consequently, unlike beam elements which always have cracks throughout the whole specimen width once a local spot of the structure cracks, cracking of weak spots locally will not spread over the whole width. For a one way slab, the crack development in width direction is the result of the connection of local fracture at weak spots over the concrete slab. The random distribution of the weak spots shapes the transverse cracks of one way slabs into a curve with random waves. The wavy shape of the crack influences the force transferred through aggregate interlock effect in two possible ways:

- Firstly, the wavy crack profile increases the length of the crack profile, so that the shear force transferred through the aggregate interlock effect V_{ai} is increased by:

$$V'_{ai} = \frac{b_{cr}}{b} V_{ai} \tag{6.1}$$

  where b_{cr} is the real length of the critical crack.

- Secondly, the wavy crack profile results in the shift of the crack position in longitudinal direction. Assuming that the uncracked part of the beam is a rigid body, under the same rotation around the crack tip, the vertical displacement at the level of longitudinal reinforcement varies. Since the dowel action is a plastic mechanism, only when the shear displacements Δ of most parts of the cross-section reach Δ_{cr} the dowel crack along the rebar will develop. Therefore more rotation is needed, and the value of critical shear displacements Δ_{cr} is increased due to the crack profile.

$$\Delta' = \theta(x_{cr} + d\tilde{x}_{cr}) = \Delta_{cr}(1 + \frac{d\tilde{x}_{cr}}{x_{cr}}) \tag{6.2}$$

where

x_{cr} : is the length of the inclined crack in longitudinal direction,

$d\tilde{x}_{cr}$: is the average variation of the transverse crack profile in longitudinal direction, in other words the average wave amplitude of the crack profile.

Both aspects strongly rely on the configuration of the crack profile in the transverse direction. Assuming the crack profile to be a random triangular wave for its simple geometry, the average period and amplitude defines the character of the profile.

Amplitude

The amplitude of the transverse crack profile A_p is related to the crack spacing. There has to be a crack within the maximum crack spacing defined by the bond between concrete and reinforcing bars. Thus the variation of the crack profile cannot be larger than the maximum crack spacing. The average amplitude can be defined as the average crack spacing $l_{cr} = \Psi_s l_t$, with $\Psi_s = 1.5$ and l_t defined by Eq. (3.4).

Wave Length

The period of the crack profile curve can be considered as a random 1D signal, how to determine the average wave length can be converted to the following question: within how much distance a crack generated by a local weak spot will influence the remaining part of the uncracked zone. Outside the affected zone, the position of a newly developed crack will not be influenced by the adjacent one, where the next peak in the wave profile may be formed. The distance between the two peaks can be considered as half the average wave length (or the period) of the curve. Based on that consideration, the problem is translated into investigating the length of the influencing zone of a local crack in the width direction.

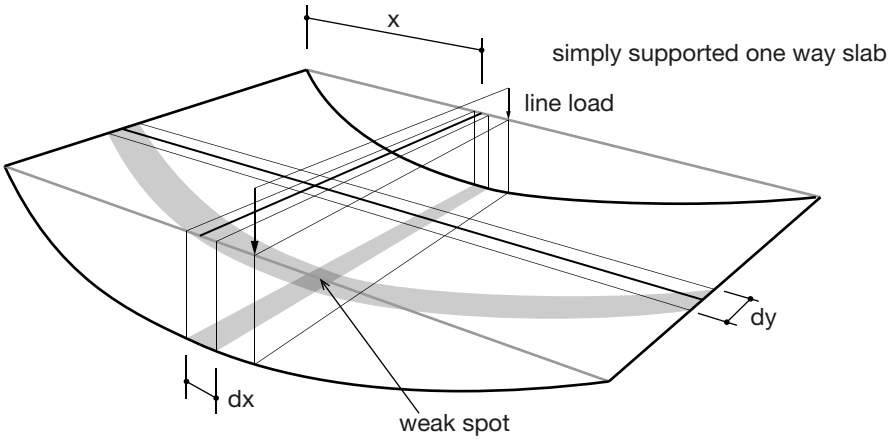

Fig. 6.26. Simplified model to consider the influence of weak spot in a one way slab.

If a slice of a one way slab with width dx in the transverse direction is taken out, see Fig. 6.26, the slice of the slab and its relationship between the remaining part of the slab can be considered as a beam on a distributed elastic foundation.

The stiffness of the foundation is the deflection stiffness per width of the slab in longitudinal direction. The opening of a crack locally results in the reduction of flexural stiffness at the cross-section locally. Therefore that cracked longitudinal strip tends to generate a larger deflection. On the other hand the remaining uncracked part along the width direction has to carry a larger part of the shear force. This is equivalent to superimpose a reversed force at the cracked spot of the transverse slice. Thus the research question is further simplified to evaluating the influenced area of a local force in a beam on elastic foundation.

Considering the longitudinal strip of a simply supported one way slab, the deflection stiffness of the section at a distance x from the support is

$$k_w = \frac{3EI_y l}{x^2(l-x)^2} \tag{6.3}$$

where

I_y : is the moment of inertia of a strip of the slab in longitudinal direction;
l : is the length of the slab;
x : is the distance of the weak spot to the support.

In the other direction, k_w is considered as the elastic stiffness of the transverse slice of the slab cut at x from the support.

Assuming that the length of the crack in transverse direction generated by the weak spot is still small compared to the width of the whole slab, the boundary conditions of the transverse slice can be described by an infinite beam on elastic foundation loaded by a point load. The solution of such a problem is (Timoshenko 1930):

$$\begin{aligned} y &= \frac{P}{8\beta^3 EI_x} e^{-\beta x}(\cos\beta x + \sin\beta x); \\ M &= -\frac{P}{4\beta} e^{-\beta x}(\sin\beta x - \cos\beta x) = -\frac{P}{4\beta} e^{-\beta x}\phi_\beta. \end{aligned} \tag{6.4}$$

where

P : is the compensation load for the cracked area;
I_x : is the moment of inertia of the transvers strip;
β : is the stiffness factor, which is expressed by

$$\beta = \sqrt[4]{\frac{k_w}{4EI_x}} \tag{6.5}$$

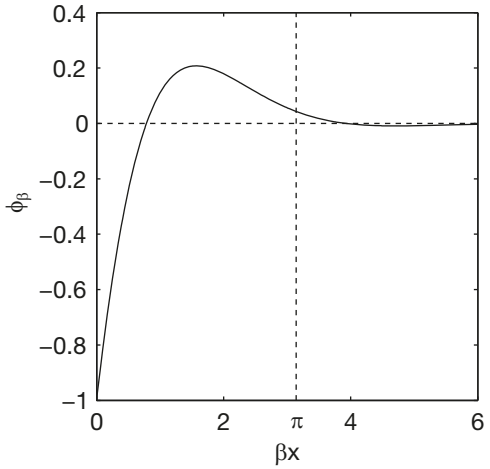

Fig. 6.27. Relationship between $\phi_\beta = e^{-\beta x}(\sin\beta x - \cos\beta x)$ and βx.

Despite the fact that the value of P is unknown, the distribution of moment over the beam is determined by the function: $\phi_\beta = e^{-\beta x}(\sin\beta x - \cos\beta x)$, the value of which decreases with the distance from the loading point, see Fig. 6.27. The value of ϕ_β approaches zero at $\beta x = \pi$. Thereafter, its value becomes negligible compared to the rest part of the curve. Based on that consideration, one may conclude that the influencing length of a weak spot of a slab is:

$$l_w = \pi \sqrt[4]{\frac{4EI_x}{k_w}} = \pi \sqrt[4]{\frac{4 \cdot x^2 (l-x)^2 dx}{3l}} \tag{6.6}$$

where

dx: is the width of the transverse strip, which can be considered as the average crack spacing l_{cr}.

Thus the expected average wave length of the crack profile can be estimated by $2l_w$, Assuming it is the dominating frequency, further evaluation on its influence to the shear capacity can be continued.

With the estimation of the crack profile, the effects of the two proposed influencing aspects regarding the length of the crack and the critical shear displacement are evaluated. Taking the configuration of the high strength concrete slab test H028B presented in this chapter as an example, the amplitude A and the period T of the crack profile are calculated with Eq. (3.4) and Eq. (6.6); they are A = 107.1 mm and T = 504.9 mm respectively, having average bond stress $\tau_{bm} = 2.0\, f_{ctm}$, and critical crack located at x = 400 mm.

The actual crack length is therefore easily calculated with

$$b_{cr} = b\frac{T}{\sqrt{T^2 + A_p^2}} \tag{6.7}$$

In H028B, the increasing factor from the width of the beam to the actual crack length is only 1.02. Because of the large period and small amplitude, the increment of the crack length is negligible in most cases.

On the other hand, the increment of the critical vertical displacement Δ_{cr}, is calculated with Eq. (6.2), where the average additional length $d\tilde{x}_{cr} = A_p/2 = 53.6$ mm. Furthermore, it is assumed that the total length of the critical inclined crack in longitudinal direction is $x_{cr} = h = 200$ mm (from the measurement of the specimen). Both values are inserted into Eq. (6.2). The critical vertical displacement Δ_{cr} for the slab should be increased by 1.27. Taking the increment into account, the shear capacity of the slab is recalculated with the standard procedure described in Chapter 4. The calculated shear capacity is then $V'_{cal} = 970.2$ kN. The original prediction which neglects the variation of critical crack position, yields $V = 863.0$ kN. The prediction taking into account the increase of vertical displacement results are 12.4% higher value than the original prediction. Considering the actual tested shear capacity being 1031.1 kN, one may conclude that the alternative of increase of the critical vertical displacement is the governing factor of the two proposed mechanisms regarding the width effect of slabs. The same procedure has been applied to all other tests in the same experimental program. The results are listed in Table 6.10, where it is clearly shown that by taking into account the misalignment of the crack path in the width direction, the model is able to predict the shear capacity of all the slab specimens more accurately.

However, the choice of the total length of the critical inclined crack length x_{cr} still needs to be investigated further. If the actual crack length is much larger than h, the increase of Δ_{cr} has to be reduced, which might be the case when the slab is loaded by a uniformly distributed load, the crack inclination is increased remarkably according to Chapter 5. Consequently, the total length of the inclined crack increases as well. As Eq. (6.2) shows, the same additional length $d\tilde{x}_{cr}$ cannot increase Δ_{cr} to the same level anymore. The influence of the specimen width to the shear capacity may become less prominent. Further experimental evidence is still needed to validate this proposition.

Nevertheless for most slab structures, the shear critical load cases are multiple point loads or line loads. To deal with these types of loading conditions, the procedure proposed in this section can be used as a good estimation. Based on the limited amount of evaluation of the test results presented in this section, an average increase of 18.2% is observed if the additional shear displacement is implemented, which appears to be quite stable for all the cases (COV = 8%). Following an engineering approach, a rough width factor of $\gamma_w = 1.1$ can be

assumed for a more accurate evaluation regarding the shear capacity of concrete slabs.

Table 6.10. Comparison of the model prediction with test results (unit: kN).

Test No.	L016A	H026A	M036A	M046A	M056B	L018B	H028B	M038B	M048B	M058A
V_{cr} [1]	862.5	1286.4	1023.4	1022.9	1003.4	855.0	1031.1	902.8	951.4	928.8
V_{cal} [2]	716.5	950.6	900.3	872.6	909.8	666.5	863	832.4	808.8	807.8
V_{cr}/V_{cal}	1.20	1.35	1.14	1.17	1.10	1.28	1.19	1.08	1.18	1.15
V'_{cal} [2]	829.4	1097.5	1040.0	1008.4	1050.9	767.3	989.6	956.4	929.7	928.6
V_{cr}/V'_{cal}	1.04	1.17	0.98	1.01	0.95	1.11	1.04	0.94	1.02	1.00

[1] Self-weight has been taken into account.

[2] V_{cal} is the calculated shear capacity with the original method; V_{cal}' is the calculated shear capacity taking into account the two effects explained in the section.

6.5 CONCLUSIONS

This chapter discusses the influence of spatial variability of material properties to the shear failure process. It is mainly focused on the variability of concrete strength.

According to the theoretical framework proposed in this research both concrete tensile strength and compressive strength influence the shear failure process. The concrete tensile strength mainly affects the shear failure modes, while the concrete compressive strength influences the shear capacity.

Inspired by investigating the influence of the concrete tensile strength in direct tension tests by the material spatial variability, its effect on the shear capacity of a concrete member is discussed in three dimensions: longitudinal direction, vertical direction and transverse direction.

Longitudinal Direction

The presence of existing cracks due to the loading history or other type weak section in longitudinal direction of the concrete member may influence the position and the profile of the critical inclined crack, thus the capacity of the concrete arch formed by it. Consequently this effect makes the failure mode of the member unpredictable when both failure modes are still possible in the span.

Because of the uncertainty of the failure modes, it is on the safe side to use the inclined cracking load as the lower bound of the shear capacity unless the shear compression failure is guaranteed when the shear span is smaller than the lower bound defined by the crack path function for shear compression failure.

Vertical Direction

The spatial variability of concrete strength only influences the crack path locally. Besides, it determines the strength of the residual concrete arch structure formed by the inclined crack.

Other than that, since only limited parts of the cracked surface have contacts, the influence of the weak spots along the critical crack does not influence the overall shear capacity of the beam.

Width Direction

When the concrete strength varies along the width direction of a concrete slab, the inclined cracking load of the specimen can be calculated with the mean strength in the width direction.

Contrary to narrow beam specimens, the opening of the critical inclined crack in a slab specimen shows certain ductility. The overall capacity of the beam can still be maintained before the dowel crack along the longitudinal rebar develops over the most part of the beam in width direction.

The maximum shear stress of a one way slab is on average larger than that of a beam. This effect is also valid for slabs with homogeneous materials. It can be explained by two aspects:

- The wavy crack profile increases the length of the crack profile; accordingly the shear force transmitted through aggregate interlock V_{ai} is increased.
- The wavy crack profile results in a shift of the crack position in longitudinal direction. As a result, at the same rotation at the crack tip, the vertical displacement at the bottom of the crack varies in width direction. Only when the vertical displacement D of the utmost part of the cross-section reaches Δ_{cr}, the dowel crack may develop.

The crack path in width direction can be simplified by a wave function. On the basis of that assumption, the influence of both effects to shear capacity is studied. The results show that the second one is the main reason of the increase of the shear capacity. Although further study is still needed regarding the evaluation of the crack length x_{cr} at different boundary conditions etc. the proposed method provides a simplified tool based on the shear design procedure proposed in Chapter 4, which is able to predict the effect of the width of the concrete specimen on its shear capacity with a pleasing accuracy.

Following an engineering approach, an approximated width factor of $\gamma_w = 1.1$ can be assumed for a more accurate evaluation regarding the shear capacity of concrete slabs.

Chapter 7

Retrospective View

7.1 INTRODUCTION

The research work presented in this dissertation is dedicated to a rather classic problem, namely, the shear capacity of reinforced concrete members without shear reinforcement. Looking back to the task set in the beginning of the dissertation, the research work presented in the dissertation has provided an adequate solution. A new theory on the shear failure mechanism has been established, which provides a fundamental insight into the phenomenon from a quite different perspective from the classical theories. Based on this new theory, a simplified shear evaluation procedure is proposed. The good accuracy obtained from comparison with test results reported in literature confirms that the theory reflects the mechanism properly.

In this chapter, both the shear failure mechanism and the design procedure based on it are reviewed. Moreover, several topics which are strongly related to the theory developed in this thesis, but have not yet been fully studied due to lack of time, are mentioned. Additional research which may lead to a better understanding of those topics is proposed.

7.2 SHEAR FAILURE MECHANISM

The theory proposed in this research attributes flexural shear failure to the opening of dowel cracks at the tip and the level of tensile reinforcement of a flexural crack. Therefore the development of flexural cracks in reinforced concrete beams without shear reinforcement is strongly related to their shear failure process. According the theory, the flexural cracks that develop above the centroid line of the beam section are defined as major cracks, which should be treated differently from the cracks that develop at the level of tensile bars due to bonding cracking. It is assumed that the height of the major cracks will be stabilized quickly to a value s_{cr} after the cross sectional moment M has exceeded M_{cr}. The pattern of the major cracks is defined by the crack height, spacing and profile. The crack height s_{cr} can be calculated from the requirement of cross sectional equilibrium; the crack spacing is determined by s_{cr}, whereas the profile of a crack is related to the ratio M/Vd of the cracked cross section and crack spacing.

However, it is shown that only based on the opening of the major cracks described by the crack pattern and formed at M_{cr} not sufficient shear capacity can be developed. Additional shear displacement along the crack faces is necessary to generate larger shear resistance through aggregate interlock. This is only possible when allowing the development of a secondary crack branch at the tip

of the existing major cracks. With the increase of the shear displacement, the development of the secondary crack branch at the level of longitudinal reinforcement (also defined as dowel crack) will become unstable. Consequently the opening of one of the major cracks increases considerably, and the shear resistance provided by the aggregate interlock of the crack drops. The load level by then is usually defined as the inclined cracking load in experiments. After the formation of the inclined crack, the load bearing system of the beam becomes an arch structure formed by the critical crack. When the capacity of the resultant arch structure is less than the inclined cracking load, the beam collapses. The corresponding failure mode is denoted as flexural shear failure. On the other hand, if the residual arch structure is capable to carry the load that causes the inclined cracks, the capacity of the beam is higher than the inclined cracking load. The collapse of the beam is determined by crushing of the concrete arch.

The description of shear failure process shows that the unstable development of dowel cracks can be considered as a criterion for the inclined cracking load and flexural shear failure. It is proposed in this research that the shear displacement of a critical major crack at the level of the tensile reinforcement can be used as a criterion for unstable development of the dowel cracking and eventually shear failure.

The mechanism described above forms the foundation of the theory presented in this research. To convert it into a procedure that can be applied in design practice, several simplifications have been made in the dissertation. The procedure proposed in the research proofs to be able to generate accurate prediction with respect to the overall shear capacity of concrete beams. Nevertheless, some of the simplifications do not fully reflect the experimental observations or require further experimental evidence. They are discussed in the sequel.

Definition of Critical Inclined Crack

It is assumed in the theory that when the beam is loaded by point loads, the critical inclined crack is located in the vicinity of the loading point. This assumption is derived from the comparison of the shear displacement Δ of cracks at different positions subjected to the same shear force, see Fig. 3.33. The shear force needed to generate the critical shear displacement in a cracked section is determined by the crack opening w and the profile of the crack. When the cracked section has a large M/Vd ratio, its profile can be approximated by a vertical plane. In that case, the shear resistance is mainly influenced by the crack width. A larger M/Vd ratio results in a smaller cross sectional shear resistance. Nevertheless, the variation of the shear capacity due to M/Vd is quite limited. Those two conclusions were also proven by the experimental observations in

Section 5.3.5. Based on this, it can be considered as a safe choice to assume the critical crack at the maximum possible M/Vd location in the span.

However, for beams with moderate shear slenderness ratio, cracks with M/Vd smaller than 2.0 may develop as well. As discussed before, the shear resistance of those cracks can be lower than those closer to the loading point. The situation described in Fig. 3.38 may become different. The actual lowest point of the shear resistance line might switch to a section closer to the support. It has been argued that the difference between the shear resistance of the two sections is usually quite limited, in the cases when the critical section closer to the support becomes critical to the ultimate capacity. Nevertheless, it has to be remarked that the evaluation procedure proposed in Chapter 4 does not include the influence of the crack profile (see the calculated shear resistance line marked in Fig. 7.1), thus is not able to determine the critical section closer to the support. That explains the difference between the location of the critical inclined crack between the experimental observations and the theory presented. This might cause a certain inaccuracy in more complex situations.

To be able to evaluate the actual shear resistance line shown in Fig. 7.1, two options have been proposed in Chapter 5 of the dissertation. The crack profile is taken into account by assuming an inclined crack plain with an inclination angle α or by reduction the actual crack height s_{cr}. Because of the limitation in the available test results, both procedures could not be evaluated sufficiently. Thus they can only be applied in very limited occasions. To derive a curve as proposed in Fig. 7.1, more research is still needed.

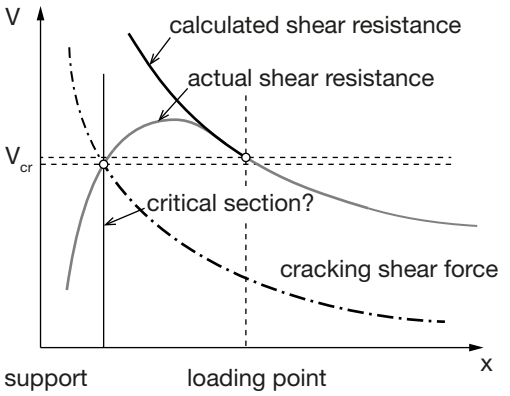

Fig. 7.1. Determination of the critical section in a span with relatively small shear slenderness ratio.

Shear Failure at Small *M/Vd*

For structural members with a small shear slenderness ratio, further than the difficulty of determining the location of the critical inclined crack, it is also difficult to accurately evaluate the shear force contribution in the compressive zone. Because the small shear span limits the development of the major crack, the hypothesis needed to generate Mörsch's stress distribution is not valid anymore. Besides, the steep drop of the shear resistance line influenced by the crack profile makes the shear resistance very sensitive to the crack location, which is still a random variable within the maximum crack spacing. The last point is that for beams with smaller shear span, the reduction of beam stiffness after the unstable opening of the inclined crack is limited. Therefore, it is more difficult to observe the inclined cracking load in experiments as well. Taking the aforementioned aspects into account, the accurate prediction of the inclined cracking load at small shear spans is less relevant.

Nevertheless, there are still several interesting topics to be discussed. For example, the theory assumes that in general the fracture energy of concrete does not influence the shear resistance of a cracked section, since the pattern of the major cracks has already fully developed before the critical shear displacement is reached. However, when the critical inclined crack is located at a section with a very small M/Vd, Δ_{cr} is reached before the crack develops fully. In that case the tension softening relationship becomes important. It defines the force needed to get a fully developed major crack. The fracturing process of the critical inclined crack becomes more important to the inclined cracking load in that situation, which can be evaluated by the fracture mechanics of concrete.

Influence of Fracture Energy

Similar to the effect of the tensile strength of concrete discussed in Chapter 6, the direct influence of the fracture energy of concrete to the shear capacity of the structural member is limited other than in the situation discussed in the preceding section. The experimental proof of this conclusion is that the shear capacities of concrete beams with old concrete or existing cracks have the same inclined cracking load as new beams. Nevertheless the influence still exists indirectly. One of the aspects which may be influenced by the fracture energy is the definition of the critical shear displacement Δ_{cr}. A brief discussion on this has been given in Section 3.4.3. Further quantitative evaluation is still standing out.

Further than the influence of fracture energy, the role of other parameters such as the rebar configuration and the concrete type are not completely clear yet. When there are multiple layers of reinforcement with heavy reinforcement ratio, or very high strength concrete in compine with small maximum aggregate size, it is still not very clear how the the related variables should be adjusted.

Examples of test on members with such specimens are the test BRH100 in (Podgorniak-Stanik 1998) for the first case and the test series reported by Sneed and Ramirez in (Sneed & Ramirez 2010) for the second case. It showns that more refined research work is still needed to complete the theoretical framework.

Aggregate Interlock at Small Crack Width

In the dissertation, it has been clearly declared that the shear stress generated by aggregate interlock at a small crack width is very important for the overall shear capacity of the whole structural member. Taking that into account, Fig. 4.29 indicates a possibility to replace the complex shear stress distribution in a crack by a block of shear stress within a characteristic length from the crack tip, so that the shear stress distribution at ultimate limit state can be treated with this simplified shear stress block in the part of the crack with small crack width, as is done with the bending resistance of beams in design codes.

However, the effect of aggregate interlock at small crack widths still needs to be discussed. In this research, it implies that Walraven's formula on aggregate interlock still works when the normal crack width ranges between 0.01 mm and 0.1 mm. This assumption is probably overestimating the shear stress that can be generated in reality. That explains why in the design method presented in Chapter 4 the evaluated critical shear displacement Δ_{cr} is more close to the lower bound of the experimental observations.

Very little experimental research has been carried out regarding aggregate interlock at very small crack widths. Walraven's experiments started from a minimum crack width of 0.1 mm (Walraven 1980); Keuser and Walraven's tests (Keuser & Walraven 1989) did not reach a very large tangential displacement; while van Mier's tests (van Mier, Nooru-Mohamed et al. 1991) ended up mostly with opening of mode I cracks in different directions. As a result, most current theories made their own simplifications on this effect. For example, in most non-linear finite element method, the shear stress - tangential displacement relationship is assumed to be linear (Rots & Blaauwendraad 1989), with the shear stiffness related to the normal crack width.

Apparently, more research is required on this topic. The questions to be answered are: Is it possible to keep such small crack widths while having significantly larger tangential (shear) displacement under the complex stress stage as in the crack tip? If not, what type of crack width distribution can describe the situation best? Also it is important to investigate the shear stress-tangential displacement relationship of a crack with small normal crack width after the crack has opened first and closed again (which is the case for shear cracks).

7.3 SHEAR CALCULATION PROCEDURE

Based on the critical shear displacement Δ_{cr} criterion described in this dissertation, a shear capacity calculation procedure has been proposed. It has been discussed in Chapter 4 regarding simply supported beams with point load, and then been extended to deal with different concrete types and boundary conditions in the following chapters. In this section a summarized shear design procedure is given to cover the conditions discussed in the whole dissertation.

Before Evaluation

Step 1: Check the loading conditions of the member.

Check the boundary conditions of the member. If the structural member is loaded by a point load or uniformly distributed load, and there is no distributed support on the beam, the procedure is discussed in the dissertation. Otherwise check the following three questions:

- Whether or not a similar crack path can be obtained at a given moment/shear force ratio?
- With the same crack path and crack opening, do the shear force components change?
- Where is the critical section?

With respect to each question, adjustments have to be made accordingly. On the other hand for beams with point loads, when the shear span is shorter than 2.0 d, the calculating M/Vd has to be taken as 2.0.

Step 2: Determine the critical section.

The critical section is used to calculate the value of moment and crack width in the shear capacity calculation. Depending on the boundary conditions, there can be more than one critical sections.

For members loaded by point loads, the centre of the loading point or the support can be used as the critical section for crack width calculation.

When the member is subjected to a uniformly distributed load, the position of the critical section should be calculated differently. In the part of the member with a sagging moment (deflection is in the same direction of the load), it is calculated with $x_{ct} = (0.14l/d + 0.3)d$, where l is the length between two adjacent points of inflection. In the hogging moment part (deflection is in the opposite direction of the load, usually close to the intermediate support), the critical section is set to be at d from the intermediate support.

In case of more general loading conditions, it is necessary to calculate the shear resistance of the whole length of the member and compare it with the shear force distribution to determine the critical sections.

Step 3: Check the dimensions of the member

If the width of the member is larger than $2l_w$, an additional width effect has to be taken into account. l_w is expressed by Eq. (6.6):

$$l_w = \pi\sqrt[4]{\frac{4l_{cr} \cdot x^2(l-x)^2}{3l}} \tag{6.6}$$

The beam height should be higher than 200 mm. Otherwise, the average crack spacing $l_{cr,m}$ has to be adjusted to l_{cr} at the tension reinforcement level.

Step 4: Check the concrete type

Check whether the member is made of high strength concrete with f_{cm} > 60 MPa, or lightweight aggregate concrete. Calculate the aggregate interlock reduction factor R_a. Unless a specific evaluation is made, R_a = 0.75 for LWA concrete, $f_{cm} \leq$ 60 MPa. For ultra-high strength concrete, an additional R_a is needed, Eq. (4.11) is suggested with further calibration in advance.

In case of existing structures or other types of structures, of which the strength of the concrete is not known, compressive tests are recommended on cylinders drilled from the same structure. The existing faults or cracks do not influence the shear capacity significantly.

Evaluation Procedure

Step 5: Calculate the equivalent rebar diameter with

$$\phi_{eq} = \sum \phi_i^2 / \sum \phi_i \tag{4.16}$$

Step 6: Calculate the maximum shear force carried by dowel action:

$$V_{d\max} = 1.64 b_n \phi \sqrt[3]{f_c} \tag{3.28}$$

Step 7: Start with a shear force value V_u, calculate the moment at the design cross section, and the crack width w_b at that cross section:

$$M_d = V_u d \frac{M}{Vd},\ w_b = \frac{M_d}{zA_s E_s} l_{cr,m} \tag{4.8}$$

Step 8: Determine the critical transverse displacement Δ_{cr}:

$$\Delta_{cr} = \frac{25d}{30610\phi_{eq}} + 0.0022 \leq 0.025 \text{ mm} \tag{4.15}$$

In case the rebar configuration is not known, a rough estimation can be made with Eq. (4.9).

$$\Delta_{cr} = \frac{d}{29800} + 0.005 \leq 0.025 \tag{4.9}$$

When the member is loaded by a uniformly distributed load, the critical transverse displacement should be reduced by $\sin\alpha$, with $\alpha = 36^{o}$.

When the width of the specimen is larger than l_w, the value of Δ_{cr} has to be increased by a factor expressed by Eq. (6.2).

Step 9: Evaluate the shear force carried by aggregate interlock effect with the calculated Δ_{cr} and w_b

For an accurate evaluation, it is recommended to calculate V_{ai} through integrating the shear stress derived from Walraven's formula over the crack height s_{cr}. This could be done with the Matlab code attached in Appendix I.

$$V_{ai} = R_a \sigma_{pu} s_{cr} b \int_0^1 A_x\left(\Delta, w(s')\right) - \mu A_y\left(\Delta, w(s')\right) ds'$$

A simplified estimation is also provided with the following equation:

$$V_{ai} = R_a f_c^{0.56} s_{cr} b \frac{0.03}{w_b - 0.01}(-978\Delta_{cr}^2 + 85\Delta_{cr} - 0.27)$$

where, R_a is 1.0 for normal concrete.

Step 10: Calculate the shear force carried in the concrete compressive zone. z is expressed by Eq. (3.26):

$$V_c = \frac{2}{3}\frac{z_c}{z}V$$

When the tip of the critical inclined crack is confined, for example, when the crack tip is close to the intermediate support of a continuous member loaded by a uniformly distributed load, the teeth structure cannot be developed in front of the critical inclined crack. Then V_c has to be increased. In continuous members loaded by a uniformly distributed load, V_c is suggested to be increased to $2.5V_c$.

Step 11: Update the overall shear force V_u of the whole cross section, and repeat from Step 7 to Step 11 till the value of V_u converges.

$$V_u = V_c + V_d + V_{ai}$$

Step 12: For members loaded by point loads, with a shear span smaller than $2.0d$, the calculated V_u is based on $M/Vd = 2.0$, the value of V_u still has to be multiplied by $\beta = 2(M/Vd)^{-1}$.

References

AASHTO. (2004). *AASHTO LRFD Bridge Design Specifications*. Washington D.C., American Association of State Highway and Transportation Officials (AASHTO).

ACI-ASCE Committee 426. (1973). "The Shear Strength of Reinforced Concrete Members." *Journal of the Structural Division, ASCE* **99**(6): 1091-1187.

ACI-ASCE Committee 445. (1998). "Recent Approaches to Shear Design of Structural Concrete." *Journal of Structural Engineering, ASCE* **124**(12): 1375-1417.

ACI Committee 318. (2004). *Building Code Requirements for Structural Concrete and Commentary*. ACI 318.

ACI Committee 446. (1989). *Fracture Mechanics of Concrete: Concepts, Models and Determination of Material Properties*.ACI 446.1R-91.

Adebar, P. & M. P. Collins. (1996). "Shear Strength of Members without Transverse Reinforcement." *Canadian Journal of Civil Engineering* **23**: 30-41.

Amir, S. (2012). "Punching Shear Strength of Transversely Prestressed Concrete Decks." *Structural Faults and Repair -2012*. Edinburgh.

Barenblatt, G. I. (1996). *Scaling, Self-Similarity, and Intermediate Asymptotics*. Cambridge, Cambridge University Press.

Baumann, T. & H. Rüsch. (1970). "Versuche zum Studium der Verdübelungswirkung der Biegezugbewehrung eines Stahlbetonbalkens." *Deutscher Ausschuss für Stahlbeton*(Heft 210).

Bažant, Z. P. (2004). "Discussion on 'Shear Database for Reinforced Concrete Members without Shear Reinforcement'." *ACI Structural Journal* **101**: 139-140.

Bažant, Z. P. (2005). *Scaling of Structural Strength*, Elsevier Science.

Bažant, Z. P. & P. Gambarova. (1980). "Rough Cracks in Reinforced Concrete." *Journal of the Structural Division, ASCE* **106**(4): 819-842.

Bažant, Z. P. & M. T. Kazemi. (1991). "Size Effect on Diagonal Shear Failure of Beams without Stirrups." *ACI Structural Journal* **88**(3): 268-276.

Bažant, Z. P. & J.-K. Kim. (1984). "Size Effect in Shear Failure of Longitudinal Reinforced Beams." *ACI Journal* **81**(5): 456-468.

Bažant, Z. P. & H. Ohtsubo. (1977). "Stability of Conditions for Propagation of a System of Cracks in a Brittle Solid." *Mechanics Research Communication* **4**(5): 353-366.

Bažant, Z. P. & J. Planas. (1998). *Fracture and Size Effect in Concrete and Other Quasibrittle Materials*.

Bažant, Z. P. & J. Planas. (1998). *Fracture and Size Effect in Concrete and Other Quasibrittle Materials*, CRC Press.

Bažant, Z. P. & A. B. Wahab. (1980). "Stability of Parallel Cracks in Solids Reinforced by Bars." *International Journal of Solids Structures* **16**: 97-105.

Bažant, Z. P., Y. Xi & S. G. Reid. (1991). "Statistical Size Effect in Quasi-Brittle Structures: I. Is Weibull Theory Applicable?" *Journal of Engineering Mechanics* **117**(11): 2609-2622.

Bažant, Z. P. & Q. Yu. (2005). "Designing Against Size Effect on Shear Strength of Reinforced Concrete Beams Without Stirrups: I. Formulation." *Journal of structural Engineering, ASCE* **131**(12): 1877-1885.

Bažant, Z. P. & Q. Yu. (2005). "Designing Against Size Effect on Shear Strength of Reinforced Concrete Beams Without Stirrups: II. Verification and Calibration." *Journal of structural Engineering, ASCE* **131**(12): 1886-1897.

Bentz, E. C., F. J. Vecchio & M. P. Collins. (2006). "Simplified Modified Compression Field Theory for Calculating Shear Strength of Reinforced Concrete Elements." *ACI Structural Journal* **103**(4): 614-624.

Bergkvist, H. & L. Guex. (1979). "Curved Crack Propagation." *International Journal of Fracture* **15**(5): 429-441.

Bhal, N. S. 1968. *Über den Einfluss der Balkenhöhe auf die Schubtragfähighkeit van einfeldrigen Stalbetonbalken mit und ohne Schubberwehrung*. PhD Dissertation, Universität Stuttgart.

Borosnyói, A. & G. L. Balázs. (2005). "Models for Flexural Cracking in Concrete: the State of the Art." *Structural Concrete* **6**(2): 53-61.

Bosco, C. & A. Carpinteri. (1992). "Fracture behavior of beam cracked across reinforcement." *Theoretical and Applied Fracture Mechanics* **17**(1): 61-68.

Braam, C. R. 1990. *Control of Crack Width in Deep Reinforced Concrete Beams*. PhD Dissertation, Delft University of Technology.

Bresler, B. & J. G. MacGregor. (1967). "Review of Concrete Beams Failing in Shear " *Journal of the Structural Division, ASCE* **93**(1): 343-372.

Broberg, K. B. (1999). *Cracks and Fracture*. Cambridge, Academic Press.

Bryant, R. H., A. C. Bianchini, J. J. Rodriguez & C. E. Kesler. (1962). "Shear Strength of Two-Span Continuous Reinforced Concrete Beams with Multiple Point Loading." *ACI Journal* **59**(44): 1143-1177.

Caldentey, A. P., P. Padilla, A. Muttoni & M. F. Ruiz. (2012). "Effect of Load Distribution and Variable Depth on Shear Resistance of Slender Beams without Stirrups." *ACI Structural Journal* **109**(5): 595-603.

Campana, S., A. Anastasi, M. F. Ruiz & A. Muttoni. (2013). "Analysis of shear-transfer actions on one-way RC members based on measured cracking pattern and failure kinematics." *Magazine of Concrete Research* **65**(6): 386-404.

Carpinteri, A. (1984). "Stability of Fracturing Process in RC Beams." *Journal of structural Engineering, ASCE* **110**(3): 544-558.

Carpinteri, A. (1989). "Decrease of apparent tensile and bending strength with specimen size: Two different explanations based on fracture mechanics." *International Journal of Solids and Structures* **25**(4): 407-429.

Červenka, V. & L. Jendele. (2009). *ATENA Program Documentation Part 1: Theory*. Prague.

Chana, P. S. (1981). *Some Aspects of Modeling the Behavior of Reinforced Concrete under Shear Loading*.Technical Report 543, Cement and Concrete Association.

Chana, P. S. (1987). "Investigation of the mechanism of shear failure of reinforced concrete beams." *Magazine of Concrete Research* **39**(141): 196-204.

Choi, K.-K. & H.-G. Park. (2007). "Unified Shear Strength Model for Reinforced Concrete Beams - Part II: Verification and Simplified method." *ACI Structural Journal* **104**(2): 153-161.

Choi, K.-K., H.-G. Park & J. K. Wight. (2007). "Unified Shear Strength Model for Reinforced Concrete Beams - Part I: Development." *ACI Structural Journal* **104**(2): 142-152.

Collins, M. P. (1978). "Towards a Rational Theory for RC Members in Shear." *Journal of the Structural Division, ASCE* **104**(4): 649-666.

Collins, M. P., E. C. Bentz & E. G. Sherwood. (2008). "Where is Shear Reinforcement Required? Review of Research Results and Design Procedures." *ACI Structural Journal* **105**(5): 590-600.

Collins, M. P., E. C. Bentz, E. G. Sherwood & L. Xie. (2008). "An adequate theory for the shear strength of reinforced concrete structures." *Magazine of Concrete Research* **60**(9): 635-650.

Collins, M. P. & D. A. Kuchma. (1999). "How Safe are Our Large, Lightly Reinforced Concrete Beams, Slabs, and Footings?" *ACI Structural Journal* **96**(4): 482-490.

Collins, M. P., D. Mitchell & E. C. Bentz. (2008). "Shear Design of Concrete Structures." *The Structural Engineer* **86**(10): 32-39.

Commission of Inquiry. (2007). *Report of the Commission of inquiry into the collapse of a portion of the de la Concorde overpass*, Montréal, Commission of Inquiry into the Collapse of the de la Concorde Overpass,.

Conforti, A., F. Minelli & G. A. Plizzari. (2013). "Shear and Flexure Behaviour of Shallow-Wide Beams Reinforced with Steel Fibres." *fib Symposium* Tel Aviv**:** 277-280.

CSA. (2004). *Design of Concrete Structures*. A23.3-04 Canadian Standards Association.

CUR. (1978). *Scheurvorming door krimp en temperatuur - wisseling in wanden (Cracking due to shrinkage and temperature variation in walls)*.Rapport 85.

de Saint-Venant, P. M. (1856). "Mémoir sur la flexion des prismes." *Journal de mathématiques pures et appliquées 2e série* **1**: 89-189.

Delatter, N. J. (2009). *Beyond Failure: Forensic Case Studies for Civil Engineers*. Reston, Virginia, American Society of Civil Engineers.

den Uijl, J. A. & Y. Yang. (2009). *Comparative Study of Shear Capacity on Beams of 50-years Old and New Concrete – Measuring Report*.Report 25.5-09-06, Delft, Delft University of Technology.

Edward G. Sherwood, A. S. L., Evan C. Bentz, and Michael P. Collins. (2006). "One-Way Shear Strength of Thick Slabs and Wide Beams." *ACI Structural Journal* **103**(6): 794-803.

Emiko, L., W. T. Huan, V. Thamaraikkannan & T. Thangayah. (2011). "Shear Transfer in Lightweight Concrete." *Magazine of Concrete Research* **63**(6): 393-400.

Erdogan, F. & G. C. Sih. (1963). "On the Crack Extension in Plates under Plane Loading and Transverse Shear." *Journal of Basic Engineering* **85**: 519-527.

Eurocode 1. (2003). *Actions on Structures - Part 2: Traffic Loads on Bridges*. NEN-EN 1991-2

Eurocode 2. (2004). *Design of Concrete Structures: General Rules and Rules for Buildings*. NEN-EN 1992-1-1

Evans, R. H. & M. S. Marathe. (1968). "Microcracking and stress-strain curves for concrete in tension." *Matériaux et Constructions* **1**(1): 61-64.

Fenwick, R. C. & T. Paulay. (1968). "Mechanisms of shear resistance of concrete beams." *Journal of the Structural Division, ASCE* **94**(10): 2235-2350.

fib. (1993). *fib Model Code for Concrete Structures 1990*. Lausanne, Thomas Telford.

fib. (2012). *fib Model Code for Concrete Structures 2010*. Lausanne, Ernst & Sohn.

Frosch, R. (1999). "Another Look at Cracking and Crack Control in Reinforced Concrete." *ACI Structural Journal* **96**(3): 437-442.

Gambarova, P. (1981). "On Aggregate Interlock Mechanism in Reinforced Concrete Plates with Extensive Cracking." *IABSE Colloquium on Advanced Mechanics of Reinforced Concrete, Final Report*. Delft.

Gastebled, O. J. & I. M. May. (2001). "Fracture Mechanics Model Applied to Shear Failure of Reinforced Concrete Beams without Stirrups." *ACI Structural Journal* **98**(2): 184-190.

Griffith, A. A. (1921). "The Phenomena of Rupture and Flow in Solids." *Philosophical Transactions of the Royal Society of London. Series A.* **221**: 163-197.

Gustafsson, P. J. & A. Hillerborg. (1988). "Sensitivity in Shear Strength of Longitudinally Reinforced Concrete Beams to Fracture Energy of Concete." *ACI Structural Journal* **85**(3): 286-294.

Hamadi, Y. D. & P. E. Regan. (1980). "Behaviour in Shear of Beams with Flexural Cracks." *Magazine of Concrete Research* **32**(111): 67-78.

Hamadi, Y. D. & P. E. Regan. (1980). "Behaviour of normal and lightweight aggregate beams with shear cracks." *The Structural Engineer* **58B**(4): 71-79.

Hanson, J. A. (1961). "Tensile Strength and Diagonal Tension Resistance of Structural Lightweight Concrete." *ACI Journal* **58**(1): 1-39.

Hillerborg, A., M. Modeer & P.-E. Petersson. (1976). "Analysis of Crack Formation and Crack Growth in Concrete by Means of Fracture

Mechanics and Finite Elements." *Cement and Concrete Research* **6**(6): 773-782.

Hordijk, D. A. 1991. *Local Approach to Fatigue of Concrete*. PhD Dissertation, Delft University of Technology.

Houde, J. & M. S. Mirza. (1974). "A Finite Element Analysis of Shear Strength of Reinforced Concrete Beams." *ACI Special Publication* **42**: 103-128.

IBBC-TNO. (1977a). *Resultaten van de eerste serie dwarskrachtproeven*.Rapport B-77-128, Delft.

IBBC-TNO. (1977b). *Resultaten van de tweede serie dwarskrachtproeven*.Rapport B-77-190, Delft.

IBBC-TNO. (1977c). *Experimenteel onderzoek met betrekking tot de dwarskrachtcapaciteit van liggers met een rechthoekige doorsnede*.Rapport BI-77-17, Delft.

IBBC-TNO. (1985). *Dwarskracht*.Rapport B-84-522, Delft.

Irwin, G. R. 1958. Fracture. *Handbuch der Physik*. Flügge Ed. Berlin, Springer-Verlag. 6.

Ivey, D. L. & E. Buth. (1967). "Shear Capacity of Lightweight Concrete Beams." *ACI Journal* **64**(10): 634-643.

Jenq, Y. S. & S. P. Shah. (1985). "A Two Parameter Fracture Model for Concrete " *Journal of Engineering Mechanics* **111**(4): 1227-1241.

Jenq, Y. S. & S. P. Shah. (1988). "Mixed-mode fracture of concrete." *International Journal of Fracture* **38**(2): 123-142.

Jenq, Y. S. & S. P. Shah. (1990). "Shear Resistance of Reinforced Concrete Beams--A Fracture Mechanics Approach." *ACI Special Publication* **118**: 237-258.

Jourawski, D. J. (1856). "Sur le Résistance d'un Corps Prismatique et d'une Pièce Composée en Bois ou on Tôle de Fer à une Force Perpendiculaire à leur Longeur." *Annales des Ponts et Chauseés, Mémoires et Documents, 3rd Series,* **12**(2): 328-355.

Kani, G. N. J. (1964). "The Riddle of Shear Failure and Its Solution." *ACI Journal* **61**(28): 441-467.

Kani, G. N. J. (1967). "How Safe are Our Large Reinforced Concrete Beams." *ACI Journal* **64**(3): 128-141.

Keuser, W. & J. C. Walraven. (1989). "Fracture of Plain Concrete Under Mixed Mode Conditions." *Proceedings of Recent Developments in the Fracture of Concrete and Rock*. Cardiff**:** 625-634.

Kim, W. & R. N. White. (1991). "Initiation of Shear Cracking in Reinforced Concrete Beams with No Web Reinforcement." *ACI Structural Journal* **88**(3): 301-308.

Kim, W. & R. N. White. (1999). "Shear-Critical Cracking in Slender Reinforced Concrete Beams." *ACI Structural Journal* **96**(5): 757-765.

Kittl, P. & G. Díaz. (1988). "Weibull's Fracture Statistics, or Probabilistic Strength of Materials: State of the Art." *Res Mechanica* **24**: 99-207.

Kittl, P. & G. Díaz. (1990). "Size Effect on Fracture Strength in the Probabilistic Strength of Materials." *Reliability Engineering and System Safety* **28**: 9-21.

Klatter, H. E. & J. M. van Noortwijk. (2003). "Life-Cycle Cost Approach to Bridge Management in the Netherlands." *9th International Bridge Management Conference*. Orlando, Florida. E-C049**:** 179-188.

König, G. & J. Fischer. (1995). *Model Uncertainties concerning Design Equations for the Shear Capacity of Concrete Members without Shear Reinforcement*.CEB Bulletin No. 224.

Krefeld, W. & C. Thurston. (1966). "Studies of the SHear and Diagonal Tension Strength of Simply Supported Reinforced Concrete Beams." *ACI Journal* **63**(4): 449-476.

Krefeld, W. J. & C. W. Thurston. (1966). "Contribution of Longitudinal Steel to Shear Resistance of Reinforced Concrete Beams." *ACI Journal* **63**(3): 325-344.

Krips, M. (1985). "Rißbreitenbeschränkung im Stahlbeton under Spannbeton." *Mitteilungen aus dem Institut fur Massivbau der Technischen Hochschule Darmstadt*(Heft 33): 84-85.

Lantsoght, E. 2013. *Shear in Reinforced Concrete Slabs under Concentrated Load close to Supports*. PhD Dissertation, Delft University of Technology.

Lantsoght, E. & C. van der Veen. (2012). "Residual Capacity from aggregate interlock of cracked reinforced concrete slab bridge." *IABMAS*. Villa Erba, Lake Como**:** 3368-3375.

Lantsoght, E., C. van der Veen & J. C. Walraven. (2011). "Experimental Study of Shear in RC One-Way Slabs Subjected to Concentrated Loads." *fib Symposium*. Prague 1**:** 551-554.

Leonhardt, F. 1978. Shear in Concrete Structures. *CEB Bulletin: Shear and Torsion, Explanatory and Viewpoint papers on Model Code chapters 11 and 12*. 126**:** 67-124.

Leonhardt, F. & R. Walther. (1962). "Schubversuche an einfeldrigen Stahlbetonbalken mit und ohne Schubbewehrung." *Deutscher Ausschuss für Stahlbeton*(Heft 151): 83.

Lubell, A. S., E. C. Bentz & M. P. Collins. (2009). "Influence of Longitudinal Reinforcement on One-Way Shear in Slabs and Wide Beams." *Journal of Structural Engineering, ASCE* **135**(1): 78-87.

MacGregor, J. G. & A. R. V. Walters. (1967). "Analysis of Inclined Cracking Shear in Slender Reinforced Concrete Beams." *ACI Journal* **64**(10): 644-653.

Marti, P. (1985). "Basic Tools of Reinforced Concrete Beam Design." *ACI Journal* **82**(4): 46-56.

Mattock, A. H., W. K. Li & T. C. Wang. (1976). "Shear Transfer in Lightweight Reinforced Concrete." *PCI Journal* **21**(1): 20-39.

Mechtcherine, V. (2009). "Fracture mechanical behavior of concrete and the condition of its fracture surface." *Cement and Concrete Research* **39**(7): 620-628.

Mechtcherine, V. & H. S. Müller. (2002). "Fracture Behaviour of high-performance concrete." *Finite Elements in Civil Engineering Applications*. Tokyo, Swets & Zeitlinger**:** 35-43.

Melin, S. (1992). "Directional stability of an originally straight crack." *International Journal of Fracture* **53**: 121-128.

Mihaylov, B. I., E. C. Bentz & M. P. Collins. (2013). "Two-Parameter Kinematic Theory for Shear Behavior of Deep Beams." *ACI Structural Journal* **110**(3).

Millard, S. G. & R. P. Johnson. (1984). "Shear Transfer across Cracks in Reinforced Concrete due to Aggregate Interlock and to Dowel Action." *Magazine of Concrete Research* **36**(126): 9-21.

Millard, S. G. & R. P. Johnson. (1985). "Shear Transfer in Cracked Reinforced Concrete." *Magazine of Concrete Research* **37**(130): 3-15.

Mörsch, E. (1909). *Der Einsenbetonbau (Published in English as: Concrete-Steel Construction)*, Engineering News Publishing Co.

Muttoni, A. (2003). "Shear and Punching Strength of Slabs without Shear Reinforcement (Schubfestigkeit und Durchstanzen von Platten ohne Querkraftbewehrung)." *Beton- und Stahlbetonbau* **98**(2): 74-84.

Muttoni, A. & M. F. Ruiz. (2008). "Shear Capacity of Members without Transverse Reinforcement as Function of Critical Shear Crack Width." *ACI Structural Journal* **105**(2): 163-172.

Nawy, E. G. (2009). *Reinforced Concrete: A Fundamental Approach*, Pearson Prentice Hall.

Nederlands Normalisatie-Instituut. (1995). *NEN 6720 Voorschriften Beton Constructieve eisen en rekenmethoden (Regulations for concrete Structural requirements and calculation methods)* NEN 6720.

Niwa, J., K. Yamada, K. Yolozawa & H. Okamura. (1987). "Revolution of the Equation for Shear Strength of Reinforced Concrete Beams without Web Reinforcement." *Concrete Library of JSCE* **9**: 65-83.

Noakowski, P. (1985). "Verbundorientierte, kontinuierliche Theorie zur Ermittlung der Rißrbreite." *Beton- und Stahlbetonbau* **80**(7): 185-190.

Perera, S. V. T. J. & H. Mutsuyoshi. (2013). "Shear Behavior of Reinforced High-Strength Concrete Beams." *ACI Structural Journal* **110**(5): 43-52.

Petersson, P.-E. 1981. *Crack Growth and Development of Fracture Zones in Plain Concrete and Similar Materials*. PhD Dissertation, Lund Institude of Technology.

Pimanmas, A. & J. Tisavipat. (2005). "Effect of Existing Cracks on Shear Failure Behaviour of Reinforced Concrete Members." *Magazine of Concrete Research* **57**(8): 485-495.

Podgorniak-Stanik, B. A. 1998. *The Influence of Concrete Strength, Distribution of Longitudinal Reinforcement, Amount of Transverse Reinforcement and Member Size on Shear Strength of Reinforced Concrete Members* MSc Thesis, University of Toronto.

Pruijssers, A. F. 1988. *Aggregate Interlock and Dowel Action under Monotonic and Cyclic Loading*. PhD Dissertation, Delft University of Technology.

Rafla, K. (1971). "Empirische Formeln zur Berechnung der Schubtragfähigkeit von Stahlbetonbalken (Empirical formulas for the calculation of shear capacity of reinforced concrete beams)." *Strasse Brücke Tunnel* **23**(12): 311-320.

Rankin, G. I. B. & A. E. Long. (1997). "Arching action strength enhancement in laterally-restrained slab strips." *Proceedings of the Institution of Civil Engineers: Structures and Buildings* **122**(4): 461-467.

Regan, P. E. (1993). "Research on Shear a Benefit to Humanity or a Waste of Time." *The Structural Engineer* **71**(19): 337-347.

Regan, P. E. & H. Rezai-Jorabi. (1988). "Shear Resistance of One-way Slabs Under Concentrated Loads." *ACI Structural Journal* **85**(2): 150-157.

Reineck, K.-H. (1991). "Ultimate Shear Force of Structural Concrete members without Transverse Reinforcement Derived from a Mechanical Model." *ACI Structural Journal* **88**(5): 592-602.

Reineck, K.-H., E. C. Bentz, B. Fitik, D. A. Kuchma & O. Bayrak. (2013). "ACI-DAfStb Databases of Shear Tests on Slender Reinforced Concrete Beams without Stirrups." *ACI Structural Journal* **110**(5): 867-875.

Reineck, K.-H., D. A. Kuchma, K. S. Kim & S. Marx. (2003). "Shear Database for Reinforced Concrete Members without Shear Reinforcement." *ACI Structural Journal* **100**(2): 240-249.

Reinhardt, H. W. & D. A. Hordijk. (1986). "Tensile Tests and Failure Analysis of Concrete." *Journal of Structural Engineering, ASCE* **112**(11): 2462–2477.

Remmel, G. 1992. *Zum Zugtragverhalten hochfester Betone und seinem Einfluss auf die Querkrafttragfahigkeit von schlanken Bauteilen ohne Schubbewehrung*. PhD Dissertation.

Rots, J. G., B. Belletti & S. Invernizzi. (2008). "Robust modeling of RC structures with an "event-by-event" strategy." *Engineering Fracture Mechanics* **75**(3-4): 590-614.

Rots, J. G. & J. Blaauwendraad. (1989). "Crack Models for Concrete: Discrete or Smeared? Fixed, Multi-Directional or Rotating?" *Heron* **34**(1): 1-33.

Rots, J. G. & S. Invernizzi. (2004). "Regularized sequentially linear saw-tooth softening model." *International Journal for Numerical and Analytical Methods in Geomechanics* **28**(7-8): 821-856.

S&P Clever Reinforcement Company AG. (2007). *Technical data of S&P Laminates CFK*.

Sagaseta, J. & R. L. Vollum. (2011). "Influence of Aggregate Fracture on Shear Transfer through Cracks in Reinforced Concrete." *Magazine of Concrete Research* **63**(2): 119-137.

Sarkhosh, R. (2012). "Shear Capacity of Concrete Beams under Sustained Loading." *fib International PhD Symposium*. Karlsrhue.

Schlaich, J., K. Schäfer & M. Jennewein. (1987). "Toward a Consistent Design of Structural Concrete." *Journal of the Prestressed Concrete Institute* **32**(3): 74-150.

Schlangen, E. & E. J. Garboczi. (1996). "New method for simulating fracture using an elastically uniform random geometry lattice." *International Journal of Engineering Science* **34**(10): 1131-1144.

Schlangen, E. & J. G. M. van Mier. (1992). "Simple lattice model for numerical simulation of fracture of concrete materials and structures." *Materials and Structures* **25**(9): 534-542.

Shah, S. P., E. S. Stuart & C. Ouyang. (1995). *Fracture Mechanics of Concrete*. New York, John Wiley & Sons, Inc.

Sherwood, E. G., E. C. Bentz & M. P. Collins. (2007). "Effect of Aggregate Size on Beam-Shear Strength of Thick Slabs." *ACI Structural Journal* **104**(2): 180-190.

Shioya, T. (1989). *Shear Properties of Large Reinforced Concrete Member*, Shimizu Corporation.

Sih, G. C. (1974). "Strain Energy Density Factor Applied to Mixed Mode Crack Problems." *International Journal of Fracture* **10**: 305-321.

Slobbe, A. T., M. A. N. Hendriks & J. G. Rots. (2012). "Sequentially linear analysis of shear critical reinforced concrete beams without shear reinforcement." *Finite Elements in Analysis and Design* **50**: 108-124.

Slobbe, A. T., M. A. N. Hendriks & J. G. Rots. (2013). "Systematic Assessment of Directional Mesh Bias with Periodic Boundary Conditions: Applied to the Crack Band Model." *Engineering Fracture Mechanics* **109**: 186-208.

Slobbe, A. T., M. A. N. Hendriks & J. G. Rots. (2014). "A delayed C^1 - continuous propagation algorithm for smeared cracks." *Engineering Fracture Mechanics*(to be published).

Sneed, L. H. & J. A. Ramirez. (2010). "Influence of Effective Depth on Shear Strength of Concrete Beams--Experimental Study." *ACI Structural Journal* **107**(5).

Stamenkovic, H. (1977). "Inflection points as statical supports are responsible for structural failure of AMC warehouse in Shelby, Ohio, 1955." *Matériaux et Constructions* **10**(60): 375-384.

Steenbergen, R. D. J. M., E. A. C. Neeft & A. H. J. M. Vervuurt. (2010). *Material Research Existing Civil Structures / Materiaalonderzoek Bestaande Kunstwerken (in Dutch)*, TNO Buildings and Infrastructure/TU Delft.

Strifors, H. C. (1974). "A generalized force measure of conditions at crack tips." *International Journal of Solids and Structures* **10**(12): 1389-1404.

Tada, H., P. C. Paris & G. R. Irwin. (2000). *The Stress Analysis of Cracks Handbook*. New York, The American Society of Mechanical Engineers.

Tanaka, Y. (2008). *Numerical Study on Tensile Strength of Concrete with Weak Spot*.Report 25.5-07-11, Delft, Delft University of Technology.

Taylor, H. P. J. 1971. *Fundamental behaviour in bending and shear of reinforced concrete* Thesis.

Taylor, H. P. J. (1974). "The Fundamental Behaviour of Reinforced Concrete Beams in Bending and Shear." *ACI Special Publication* **42**: 43-77.

Taylor, R. & R. S. Brewer. (1963). "The Effect of the Type of Aggregate on the Diagonal Cracking of Reinforced Concrete Beams." *Magazine of Concrete Research* **15**(44): 87-92.

Timoshenko, S. (1930). *Strength of Materials-Advanced Theory and Problems*.

Timoshenko, S. (1956). *Strength of Materials*. New York, Van Nostrand.

TNO-DIANA. (2011). http://tnodiana.com/DIANA-manuals. "DIANA User's Manual (release 9.4.4)."

van Mier, J. G. M. (2013). *Concrete Fracture: A Multiscale Approach*, CRC Press.

van Mier, J. G. M., M. B. Nooru-Mohamed & G. Timmers. (1991). "An Experimental Study of Shear Fracture and Aggregate Interlock in Cementbased Composites." *Heron* **36**(4): 1-45.

Vecchio, F. J. & M. P. Collins. (1986). "The Modified Compression-Field Theory for Reinforced Concrete Elements Subjected to Shear." *ACI Journal* **83**(2): 219-231.

Vervuurt, A., W. Courage & R. D. J. M. Steenbergen. (2013). "Strength Characteristics for the Structural Assessment of Existing Concrete Structures." *IABSE*. Rotterdam.

Vintzeleou, E. N. & T. P. Tassios. (1986). "Mathematical Models for Dowel Action Under Monotonic and Cyclic Conditions." *Magazine of Concrete Research* **38**(134): 13-22.

Walraven, J. 1980. *Aggregate Interlock: A theoretical and experimental analysis.* PhD Dissertation, Delft University of Technology.

Walraven, J. (1981). "fundamental Analysis of Aggregate Interlock." *Journal of structural Engineering, ASCE* **107**(ST11): 2245 - 2270.

Walraven, J. & N. Lehwalter. (1994). "Size Effects in Short Beams Loaded in Shear." *ACI Structural Journal* **91**(5): 585-593.

Walraven, J. C. (1978). *The Influence of Depth on the Shear Strength of Lightweight Concrete Beams without Shear Reinforcement*.Report 5-78-4, Delft, Delft University of Technology.

Walraven, J. C. (2007). "Fracture Mechanics of Concrete and Its Role in Explaining Structural Behaviour." *FraMCos-6.* Catania(Italy)**:** 1265-1275.

Walraven, J. C., J. Frenay & A. Pruijssers. (1987). "Influence of Concrete Strength and Load History on Shear Friction Capacity of Concrete Members." *PCI Journal* **32**(1): 66-84.

Walraven, J. C. & N. Lehwalter. (1989). "Bearing capacity of concrete compression struts in strut and tie models, considering the example of short compact beams (Die Tragfaehigkeit von Betondruckstreben in Fachwerkmodellen am Beispiel von gedrungenen Balken)." *Beton- und Stahlbetonbau* **84**(4): 81-87.

Walraven, J. C. & W. P. M. Mercx. (1983). "The Bearing Capacity of Prestressed Hollow Core Slabs." *Heron* **28**(3): 1-46.

Walraven, J. C. & H. W. Reinhardt. (1981). "Theory and experiments on the mechanical behaviour of cracks in plain and reinforced concrete bujected to shear loading." *Heron* **26**(1).

Walraven, J. C. & H. W. Reinhardt. (1981). "Theory and Experiments on the Mechanical Behaviour of Cracks in Plain and Reinforced Concrete Subjected to Shear Loading." *Heron* **26**(1A): 1-68.

Walraven, J. C. & J. Stroband. (1994). "Shear Friction in High-Strength Concrete." *ACI Special Publication* **149**: 311-330.

Walraven, J. C. & J. Stroband. (1999). "The Behaviour of Cracks in Plain and Reinforced Concrete Subjected to Shear." *Utilization of High Strength/High Performance Concrete*. Sandefjord, Norway. 1**:** 701-708.

Walraven, J. C. & J. Stroband. (1999). "Shear Capacity of High Strength Concrete Beams with Shear Reinforcement." *Utilization of High Strength/High Performance Concrete* Sandefjord, Norway. 1**:** 701-708.

Walraven, J. C., E. Vos & H. W. Reinhardt. (1979). *Experiments on Shear Transfer in Cracks in Concrete. Part I: Description of Results*.Report 5-79-10, Delft, Delft University of Technology.

Weilbull, W. (1951). "A Statistical Distribution Function of Wide Applicability." *Journal of Applied Mechanics*: 293-297.

Westergaard, H. M. (1939). "Bearing Pressures and Cracks." *Journal of Applied Mechanics* **61**: A49-53.

Wight, J. K. & G. J. Parra-Momtesinos. (2003). "Strut-and Tie Model for Deep Beam Design." *ACI Concrtete International* **25**(5).

Xu, S., X. Zhang & H. W. Reinhardt. (2012). "Shear Capacity Prediction of Reinforced Concrete Beams without Stirrups Using Fracture Mechanics Approach." *ACI Structural Journal* **109**(5): 705-714.

Xu, X.-P. & A. Needleman. (1994). "Numerical Simulations of Fast Crack Growth in Brittle Solids." *Journal of the Mechanics and Physics of Solids* **42**(9): 1397-1434.

Yang, Y. (2009). *Photogrammetric Measurement on Shear Tests of Old and New Concrete Beams*.Report 25.5-09-07, Delft, Delft University of Technology.

Yang, Y. (2009). *Preliminary Study on Shear Strength of Beams Cut from a Reinforced Concrete Bridge Deck*.Report 25.5-09-01, Delft, Delft University of Technology.

Yang, Y. & J. A. Den Uijl. (2010). *Post-Diction Report of Comparison Study of Old and New Concrete Beams*.Report 25.5-10-02, Delft, Delft University of Technology.

Yang, Y. & J. A. den Uijl. (2011). *Report of Experimental Research on Shear Capacity of Beams Close to Intermediate Supports*.Report 25.5-11-10, Delft, Delft University of Technology.

Yang, Y. & J. A. Den Uijl. (2012). *Report of Comparison Study on Shear Capacity of Old Concrete Beams with Continuous Supported Conditions*.Report 25.5-12-01, Delft, Delft University of Technology.

Yang, Y. & J. A. den Uijl. (2012). *Shear Capacity of Concrete Structures Influenced by Concrete Strength Variation in Width Direction*.Report 25.5-12-07, Delft, Delft University of Technology.

Yang, Y., J. A. den Uijl, G. Dieteren & A. de Boer. (2010). "Shear Capacity of 50 Years Old Reinforced Concrete Bridge Decks without Shear Reinforcement." *The 3rd Congress of the International Federation for Structural Concrete*. Washington DC.

Yang, Y., J. A. den Uijl & J. Walraven. (2011). "Shear Capacity of Continuous RC Beams without Shear Reinforcement." *fib Symposium* Prague. 2**:** 763-766.

Yang, Y., J. A. den Uijl & J. Walraven. (2012). "Residual shear capacity of continuous reinforced concrete beams." *ICCRRR 2012: Concrete Repair, Rehabilitaion and Retrofitting III*. Cape Town, Taylor & Froncis Group**:** 297-298.

Yang, Y., J. A. den Uijl & J. Walraven. (2012). "Shear Capacity of Reinforced Concrete Beams under Complex Loading Conditions." *the 9th fib International PhD Symposium in Civil Engineering*. Karlsruhe, Karlsruhe Institude of Technology**:** 43-48.

Yang, Y., J. A. den Uijl & J. C. Walraven. (2010). "Testing and Monitoring Shear Behaviour of 50 Years Old Concrete Beams." *8th fib PhD Symposium* Lyngby, DenMark**:** 623-628.

Yang, Y., J. A. Den Uijl & J. C. Walraven. (2011). "Shear Capacity of Continuous RC Beams without Shear Reinforcement." *fib Symposium Prague* Prague**:** 763-770.

Yang, Y., J. A. den Uijl & J. C. Walraven. (2013). "Residual Shear Capacity of 50 years Old RC Solid Slab Bridge Decks." *International IABSE Conference: Assessment, Upgrading and Refurbishment of Infrastructures*. Rotterdam. 538-539.

Zararis, P. D. & G. C. Papadakis. (2001). "Diagonal Shear Failure and Size Effect in RC Beams without Web Reinforcement." *Journal of Structural Engineering, ASCE* **127**(7): 733-742.

Zararis, P. D. & L. P. Zararis. (2009). "Shear Strength of Reinforced Concrete Slender Beams with or without Axiao Forces - A Generalized Theory." *ACI Structural Journal* **106**(6): 782-789.

Zhang, J.-P. (1997). "Diagonal cracking and shear strength of reinforced concrete beams." *Magazine of Concrete Research* **49**(178): 55-65.

Zsutty, T. C. (1971). "Shear Strength Prediction for Separate Categories of Simple Beam Tests." *ACI Journal* **68**(2): 138-143.

Notation

Roman Upper Case

A	total cross sectional area
$A_{c,eff}$	effective concrete area surrounding the tensile reinforcement in a beam
A_p	amplitude of the transverse crack profile
$A_x,\ A_y$	projected contact areas for a unit crack length, which are functions of the normal and tangential displacement (n,t) of the two crack faces
C_{Rd}	regression factor in Eurocode shear formula to calculate the design shear resistance of a member without shear reinforcement
C_{Rm}	regression factor in Eurocode shear formula to calculate the mean shear resistance of a member without shear reinforcement from experiments
C^i	indicate the i^{th} derivative of the expression is a continuous function
D	aggregate size
D_{max}	maximum aggregate size
E	elastic modules
E_c	elastic modules of concrete in linear elastic stage
E_s	elastic modules of steel in linear elastic stage
G_f	fracture energy, the subscript I or II stand for the corresponding fracture mode
$G_I,\ G_{II}$	strain energy release rate for the corresponding fracture mode
G_1-G_4	functions in Walraven's aggregate interlock formula

I	moment of inertia of a given cross-section
K_I, K_{II}	stress intensity factor at given crack tip, the subscription stands for the corresponding fracture mode
M	flexural moment
M^+, M^-	maximum positive moment (sagging moment) and negative moment (hogging moment) of the span
M_{cr}	cracking moment, the moment that makes the stress at a edge of the beam cross-section higher than the tensile strength of the material
N_c	resultant compressive force in the uncracked compressive zone
N_{ai}	resultant compressive force component carried by aggregate interlock
$O(x)$	higher order terms that can be ignored
P_1,P_2	forces measured though the corresponding load cells
R^2	coefficient of determination
R_a	reduction factor of aggregate interlock, for high strength concrete or lightweight aggregate concrete
R_s	surface roughness index
T_s	resultant tensile force in the reinforcement
U	strain energy of a structural member
U^*	complimentary strain energy of a structural member
V	shear force
V_{ai}	resultant shear force component carried by aggregate interlock
V_E	expected shear force at corresponding cross section
V_R	shear resistance at corresponding cross section
V_c	resultant shear force component carried in the uncracked concrete compression zone
V_{cr}	inclined cracking load, the shear force needed to generate the critical inclined crack

$V_{cr,m}$ shear force needed to open a major crack at x_0 from the support

V_d resultant shear force component carried by the dowel action

V_u maximum shear force in the span before the collapse of the structural member

Roman Lower Case

a centre to centre distance between a loading point and the first support of a beam next to it

a_0 uncracked span length of the member from the support

a_c length of the secondary branch

$a_{c,c}$ length of the critical compressive zone, when the tip of the major crack is located in the zone, the residual structure formed by which can generate sufficient capacity after V_{cr}

a_v edge to edge distance between a loading plate and the support of a beam, used in Eurocode shear formula

b width of the structural member

b_{cr} length of a crack in the transverse direction of a slab

b_n clear width of the beam

c thickness of the concrete cover

d effective height of a beam cross section, it is defined as the distance from the centroid of the tensile reinforcement to the edge fibre of the cross-section in the compressive edge

d_0 a constant defined in Bažant's shear design formula, see Chapter 2

$d\tilde{x}_{cr}$ average width of the transverse crack profile, which can also be considered as the average wave amplitude

e_c offset of the resultant compressive force to the centroid of the compressive zone

f_c concrete compressive strength (through cylinder tests with diameter 150 mm)

f_{cm} mean concrete compressive strength (through standard cylinder tests)

$f_{cm,cube}$	mean concrete compressive strength (through standard cube tests)
f_{ctm}	mean tensile strength of concrete
$f_{ctm,s}$	mean tensile strength of concrete (through splitting tests)
$f_{ctm,dt}$	mean tensile strength of concrete (through direct tensile tests)
f_t	tensile strength of a material
f_x, f_y	resultant normal stresses in longitudinal and vertical direction
h	total height of the member
h_i, h_j	position of the layers in the layered model
k_α	crack inclination factor to take into account the reduction of the crack height
k_c	slope of the stress line to distribute localized load/deformation to the whole section
k_{cr}	factor between the height of major crack and the effective beam height
k_h	size effect factor in Eurocode formula
k_r	stiffness of the residual structure formed by the inclined crack
k_s	slope of the secondary crack branch
k_w	deflection stiffness of a transverse strip of a concrete slab member
l_0	the length of the secondary crack branch
l_{ch}	characteristic length in the layered model to convert crack width to strain
l_{cr}	mean crack spacing along the reinforcement, $l_{cr,max}$ is the maximum crack spacing along the reinforcement
$l_{cr,m}$	mean crack spacing of the major cracks (at the mid-height of the beam section)
l_t	minimum crack spacing, or the stress transmit length between rebar and concrete
l_w	influencing length of a weak spot of a slab

m	ratio between the sagging moment and the maximum moment differemce in the span of a continuous supported beam with uniformly distributed load, $m = M_2/(M_1+M_2)$
n_e	elastic stiffness ratio between E_s and E_c
n,t	normal and tangential displacement of the crack at the crack profile
r_{excl}	distance surrounding an already cracked root element in which no more crack can develop from another root element in CPA
s	distance of a point of the crack profile to the tensile edge of the beam, thus it can also be considered the height of the crack at certain stage of the crack development
s_{cr}	the height of the crack after it is stabilized
t_c	slope of the major crack $t_c = s_{cr}/x$
$w,\ w_b$	crack opening at the level of the tensile reinforcement in the longitudinal direction
w_t	crack opening at the tip of the major crack in the longitudinal direction
x_0	distance between the centre of the support and the root of the crack profile
x_{cr}	distance between the tip and the root of the major crack in longitudinal direction
x_{ct}	distance between the tip of the crack and the centre of the support, also defined as the position of the critical section
y	deflection of a beam
z	length of the internal level arm between the loading point of the equivalent compressive force and the centroid of the tension force in tensile reinforcement
z_0	location of the neutral axis of a beam cross-section from the tension edge
z_c	is the height of the uncracked compressive zone at tip of the major crack
z_c'	is the height of the uncracked compressive zone at tip of the secondary crack

Greek Upper Case

Δ, Δ_b	relative displacement of the crack faces at the level of tensile reinforcement in the vertical direction
Δ_0, Δ_t	relative displacement of the crack faces at the tip of the crack in the vertical direction
Δ_{cr}	the critical shear displacement of the crack faces at the level of the tensile reinforcement for the opening of the dowel crack
Δ_α	shear displacement of the crack faces along the crack faces
ΔT_s	difference of tensile force in reinforcement between two major cracks
Φ_σ	the cumulative strength distribution function of the material
Ψ_s	the ratio between the minimum crack spacing and the mean factor of the crack spacing at reinforcement level

Greek Lower Case

α	first derivative of the crack profile, when assuming the crack profile as a plain, alpha stand for the slope of the crack plain
β	stiffness factor in the expression of beams on elastic foundation
β_a	shear slenderness factor defined in Eurocode shear formula
δ_{cr}	normalized crack spacing, $\delta_{cr} = l_{cr}/h$
ε	normal strain, or average strain of the cross-section in certain direction
ε_{sm}, ε_{cm}	average strain of the reinforcement and concrete between two adjacent major cracks respectively
γ_w	width factor for slab members
κ	curvature at given location of the beam in longitudinal direction
κ_B	aggregate factor in Bažant's formula
κ_r	function in the expression of the residual structure stiffness
λ	length of the dowel crack along the tensile reinforcement

μ	coefficient of the friction between aggregate and the matrix material
ϕ	diameter of rebar
ϕ_{eq}	equivalent diameter of the reinforcement configuration
ϕ_{β}	function used to calculate the moment of a beam on elastic foundation loaded by a point load
ψ_M, ψ_T, ψ_I, ψ_{II}	regression functions in the expression of stress intensity factors, which do not have an analytical expression
ρ_{eff}	effective reinforcement ratio when calculating crack spacing at the level of reinforcement of a beam
ρ_s	reinforcement ratio, ratio of reinforcing bar area over effective area of the beam cross-section $\rho_s = A_s/bd$
σ	normal stress
σ_c	normal stress at the outer fibre of the compressive zone
σ_{pu}	crushing strength of the cement matrix under confinement
σ_{sr}	cracking stress of reinforcement at the onset of the formation of a new crack
σ_u	maximum stress of a material
τ	shear stress
τ_{bm}	average friction between rebars and concrete
τ_u	average shear stress in the beam cross-section at failure
τ_1, τ_2	shear resistance corresponding to the two failure modes specified in IBBC-TNO shear design method
θ	relative rotation of the crack faces around the tip of the crack
θ, r	coordinates in a polar coordinate system with the origin at the tip of the crack and the principal axis along the axis of the crack
ξ	normalized crack coordinate in height direction, $\xi = s/h$
ξ_σ	partial distribution function of a material strength

ζ	normalized crack coordinate in longitudinal direction, ζ = *x/h*

Subscriptions

ai	effect caused by aggregate interlock
c	effect in the uncracked compressive zone in the member
cal	values calculated with the corresponding theory
cr	values relating to the opening of the inclined crack
d	effects caused by dowel action
I, II	mode of fracture
m	mean value of the notation
$test$	values measured in the tests
u	values relating to the ultimate capacity
x	longitudinal direction of the member
y	transvers direction of the member

Appendix I

Matlab Code

In this appendix, a Matlab code designed for the implementation of the alternative procedure of Step 4 Eq. (4.4) in Section 4.4.1 is presented. In the program, the influence of rebar configuration to the value of Δ_{cr} is calculated with Eq. (4.15) in Section 4.6.2. The influences of the other aspects such as the fracture of aggregates, the loading conditions etc. have not been implemented in the code, users may include these aspects according to the suggestion given in the dissertation, or use their own validated formulation.

```
function [V] = CSDM(mvd, da, fc, d, bw, rho, Re)
%CSDM  Evaluation shear capacity based on Critical Shear Displacement
%
%   V = CSDM(mvd, da, fc, d, bw, rho, Re), is the implementation of the
%   critical shear displacement method proposed in Y.Yang (2014). "Shear
%   behaviour of reinforced concrete members without shear reinforcement
%   -A new look and an old problem." The equation numbers in the file is
%   in accordance to the reference.
%   The input variables are explained as follow:
%   mvd is the maximum value of M/Vd in the calculated span in [-];
%   da is the maximum aggregate size in [mm];
%   fc is the compressive strength of concrete in [MPa];
%   d is the effective depth of the beam in [mm];
%   bw is the width of the beam in [mm], here the beam is assumed to be
%   prismatic, the program has not checked for T beams or I beams.
%   rho is the reinforcement ratio of the beam, the percentage is not.
%   needed Re is the rebar configuration. It is a cell, each array stands
%   for the configuration of a beam, which is a two columns matrix. The
%   first column is the number of rebar, the second one is the diameter
%   in [mm].
% Example
%   For two beams with maximum a/d ratio = 3.0, concrete compressive
%   strength 34.2 MPa and 34.8 MPa, effective depth of 420 mm and 720 mm,
%   width of 200 mm, reinforcement ratio of 0.74% and 0.79%, rebar
%   configuration being 1 Ø 14 + 2 Ø 20 and 3 Ø 22(Walraven's A2 and A3
%   beams), the inputs are:
%
%   mvd = [3; 3];
%   da = [16; 16];
%   fc = [34.2; 34.8];
%   d = [420; 720];
%   bw = [200; 200];
%   rho = [.0074; .0079];
%   Re = {[1 14; 2 20];[3 22]};
%   V = CSDM(mvd, da, fc, d, bw, rho, Re);
```

```
%Last modified by Yuguang Yang on April 04 2014. Copy right reserved.

CoreNum = 4; % when parallel calculation is available on the computer,
% determine the number of cores that is available
global Es Ec

Es = 210000; % elastic modules of steel in MPa
Ec = 40000; % elastic modules of concrete in MPa, only effecting the
% crack height calculation, thus a rough estimation is sufficient.
% validation, it is recommended to make Ra = 0.75 for LWA concrete;
% and keep Ra = 1.0, while reduce fc back to 60 MPa for HSC
n = numel(d);       % number of tests
As = rho.*bw.*d;    % reinforcement area
Ra = ones(n,1);     %reduction factor for special concrete types such as
% HSC or LWA concrete.
br = zeros(n,1);D = br;
if nargin > 6
    for l = 1:n
        br(l) = sum(Re{l}(:,1).*Re{l}(:,2)); % the part of width occupied
        % by rebar for dowel force Vdw calculation (only applicable when
        % all the rebars are in one layer)
        D(l) = sum(Re{l}(:,1).*Re{l}(:,2).^2)/sum(Re{l}(:,1).*Re{l}(:,2));
        % equivalent rebar diameter Deff, calculated with eq..(4.16)
    end
else
    % When rebar configuration is not available, assuming there are four
    % bars in one layer, calculate the rebar diameter accordingly.
    Re = ones(n,1)*[4 4];
    Re(2) = (As/pi).^.5;
    br = 4*Re(:,2); D = Re(:,2);
end
Vdw = V_dw(bw, br, fc, D);   % calculate the contribution of dowel action
V = zeros(n,1);

%Initialize Matlab Parallel Computing Environment
if matlabpool('size')<=0 % check parallel computing environment
matlabpool('open','local',CoreNum);
% start parallel computing environment
end

for l = 1:n
    V(l) = Vm(mvd(l), da(l), fc(l), d(l), bw(l), As(l), Vdw(l), ...
    D(l), rho(l), Ra(l));
    % calculation of the maximum shear resistance of each tests
end
matlabpool close
end
%-------------------------------------------------------------------------
--
function V = Vm(mvd, da, fc, d, bw, As, Vdw, rho, D, Ra)

global Es Ec

ne = Es/Ec; % ratio between Es and Ec for crack height calculation
delta = min((3.267e-5.*d*25/D+.002204), .025);
scr = (1+rho.*ne-(2*rho.*ne+(rho.*ne).^2).^.5).*d;   % major crack height
lcrm = scr./1.28;       % average crack spacing of major cracks
z = (2*d + scr)/3;      % internal level arm
V1 = 1.5*d*bw;          % first guess of shear resistance
V0 = 0; count = 0;      % initiation of iteration
```

```
while abs(V0-V1) > 10
    M0 = V1*d*mvd;      % cross sectional moment
    w = M0/z/As/Es*lcrm;    % estimation of average crack width eq..(4.8)
    V0 = V1;

    Vai = V_ai(delta, w, da, scr, fc, bw);  % aggregate interlock
    Vc = V_c(z,d, V0);          % shear force in compression zone
    V1 = Ra*Vai + Vc + Vdw;     % summation of total shear force

    V = V1;
    if count == 20  % maximum iteration number is 20
        break
    end
    count = count+1;
end
if mvd < 2
    V = V*2/mvd0;
end
% fctm = (fc<58).*.3.*(fc-8).^(2/3)+(fc>=58).*2.12.*log(1+(fc/10));
end
%-------------------------------------------------------------------------
--
function Vai = V_ai(delta, w, da, scr, fc, bw)
% shear resistance contributed by aggregate interlock, based on eq..(4.4)
w0 = 0.01;  % crack width at crack tip
dw = (w0-w)/100;   % increment of crack width in the linear crack profile
CrackProfile = (w: dw: w0);    % crack profile, divided into 100 sections
n = numel(CrackProfile);
L = scr/n;
fc = min(fc,60);    % limitation for high strength concrete
tau = zeros(size(CrackProfile));
parfor l = 1:n
    [~,tau(l)]=AI_walraven(CrackProfile(l), delta, da, fc);
    % Walraven's aggregate interlocking formula eq..(3.30)
end
Vai = -sum(tau.*L )*bw;
% alternative simplified AI formula: eq..(4.7), much faster than
% Walraven's formula:
% Vai = (-978*delta.^2+85*delta-.27).*fc.^.56.*bw.*.03./(w-.01).*scr;
end
%-------------------------------------------------------------------------
--
function Vdw = V_dw(bw, br, fc, D)
% maximum dowel action force, based on eq..(3.28)
Vdw = 1.64*(bw-br).*D.*(fc).^.333;
end
%-------------------------------------------------------------------------
--
function Vc = V_c(z, d, V)
% shear force contrition in compression zone, based on eq..(3.26)
Vc = 2*(d-z)/z*V;
end
%=========================================================================
==
function [sig,tau]=AI_walraven(w0, D0, da, fc)
%AI_Walraven Walraven's formula for aggregate interlock eq..(3.30)
%   [sig,tau]=AI_walraven(w0, D0, da, fc), calculated the shear and
%   normal stresses [MPa] generated due to aggregate interlock when the
%   normal or shear displacement at the crack faces is given. The
%   function only allows the input of single values. If you have an array
```

```
%   please do it through iteration. This function has to be a separate
%   file named 'AI_walraven.m'. The inputs of the function are:
%   normal crack opening w0 [mm],
%   shear crack opening D0 [mm],
%   maximum aggregate size da [mm],
%   concrete compressive strength fc [MPa].
%Exmaple
%   [sig,tau]=AI_walraven(0.01,0.02,16,34.2);

%Last modified by Yuguang Yang on April 04 2014. Copy right researved.

global dm pk u w D
w = w0*(w0>0);  % normal crack opening
D = abs(D0);    % shear crack opening
dm = da;        % maximum aggregate size
% situation when there is no contact between crack faces
if w > dm
    sig = 0;
    tau = 0;
% situation when the shear displacement is larger than Dmax
else if D > dm
    [sig,tau]=AI_walraven_u(w0, da, fc);
    else
% normal situation
pk = 0.75;
u = .4;     % friction coefficient
fcc = fc;
sig_pu = 6.39*fcc^(.56);    % crush strength of the cement matrix
if D > w
    Ay = quad(@ay,2*w,dm);
    Ax = quad(@ax,2*w,dm);
else
    if (w^2+D^2)/D<dm
    Ay = quad(@ay,(w^2+D^2)/D,dm);
    Ax = quad(@ax,(w^2+D^2)/D,dm);
    else
    Ay = 0;
    Ax = 0;
    end
end
sig = sig_pu*(Ax-u*Ay);
tau = sig_pu*(Ay+u*Ax)*(-D/D0);
    end
end
end
function [sig,tau]=AI_walraven_u(w0)
% Walraven's formula when the shear displacement is larger than Dmax
% aggregate size.
global dm pk u w
w = w0;     % crack opening [mm]
dm = 16;    % maximum aggregate size [mm]
pk = 0.75;  % percentage of aggregate
u = .4;     % friction
fcc = 40;   % concrete compressive strength [MPa]
sig_pu = 6.39*fcc^(.56);    % yield strength of concrete under three
% dimensional loading
if w*2 < dm
Ay = quad(@ayu,2*w,dm);
Ax = quad(@axu,2*w,dm);
sig = sig_pu*(Ax-u*Ay);
tau = sig_pu*(Ay+u*Ax);
```

```
else
sig = 0;
tau = 0;
end
end
function [F] = F(d0,dm)
% aggregate size distribution function F(D), see eq..(3.30)
d = d0/dm;
F = .532*d.^.5-.212*d.^4-.072*d.^6-.036*d.^8-.025.^10;
end
function [G1] = G1(d,D,w)
% function G1(n,t,D), see eq..(3.30)
um = UM(w,D,d);
G1 = d.^(-3).*((d.^2-(w^2+D.^2)).^.5.*D./(w^2+D.^2).^.5.*um-w.*um-um.^2);
end
function [G2] = G2(d,D,w)
% function G2(n,t,D), see eq..(3.30)
um = UM(w,D,d);
G2 = d.^(-3).*((D-(d.^2-w^2-D.^2).^.5*w./(w^2+D.^2).^.5.*um +...
    (um+w).*(d.^2/4-(w+um).^2).^.5 - w*(d.^2/4-w^2).^.5)+...
    d.^2/4.*asin((w+um)./d*2) - d.^2/4.*asin(2*w./d));
end
function [G3] = G3(d,w)
% function G3(n,t,D), see eq..(3.30)
G3 = d.^(-3).*(d/2-w).^2;
end
function [G4] = G4(d,w)
% function G4(n,t,D), see eq..(3.30)
G4 = d.^(-3).*(d.^2*pi/8-w*(d.^2/4-w^2).^.5-d.^2/4.*asin(2*w./d));
end
function um = UM(w,D,d)
% calculation of umax in G1 and G2
um = (-w/2*(w^2+D^2)+(w^2*(w^2+D^2)^2-(w^2+D^2)*((w^2+D^2)^2- ...
D^2*d.^2)).^.5/2)/(w^2+D^2);
end
function [ay] = ay(d)
% projected contact area Ax in x direction in eq..(3.30)
global dm pk w D
if D > w
    if w == 0
        D0 = dm;
    else
        D0 = (w^2+D^2)/w;
    end
d1 = d(d <= D0);
ay1 = pk*4/pi.*F(d1,dm).*G3(d1,w);
d2 = d(d > D0);
ay2 = pk*4/pi.*F(d2,dm).*G1(d2,D,w);
ay = [ay1,ay2];
else
  ay = pk*4/pi.*F(d,dm).*G1(d,D,w);
end
end
function [ax] = ax(d)
% projected contact area Ax in x direction in eq..(3.30)
global dm pk w D
if D > w
    if w == 0
        D0 = dm;
    else
        D0 = (w^2+D^2)/w;
```

```
    end
d1 = d(d <= D0);
ax1 = pk*4/pi.*F(d1,dm).*G4(d1,w);
d2 = d(d > D0);
ax2 = pk*4/pi.*F(d2,dm).*G2(d2,D,w);
ax = [ax1, ax2];
else
  ax = pk*4/pi.*F(d,dm).*G2(d,D,w);
end
end
function [ay] = ayu(d)
% projected contact area Ay in y direction when the shear displacement is
% larger than maximum aggregate size D > dm
global dm pk w
ay = pk*4/pi.*F(d,dm).*G3(d,w);
end
function [ax] = axu(d)
% projected contact area Ax in x direction when the shear displacement is
% larger than maximum aggregate size D > dm
global dm pk w
ax = pk*4/pi.*F(d,dm).*G4(d,w);
end
```

Appendix II

Results of FEM Models for the Crack Profile Study

This appendix provides the additional information of the FEM models utilized in deriving the crack profile expression in Chapter 3, section 3.2.4. Other than the basic configurations of the models which have been introduction in the dissertation, in this appendix, the differences of 23 models used in the parametric study are presented. The main variables of the models includes the crack position x_0, the crack spacing, the height of the existing crack, the tensile properties of concrete, the thickness of the concrete cover, the reinforcement ratio, etc. The resultant crack paths of each model are reported in the appendix as well.

Table II.1. Material properties of the normal concrete elements in a basic model (Model 1-5 in Table II.2).

Elastic Modules:	4.000000E+04 MPa
Poison's ratio:	0.4
Crack model:	Total strain fixed crack model
Tensile strength:	3 MPa
Fracture energy:	0.125 kN/m
Tension softening curve:	Linear softening
Saw-tooth model:	Ripple model
Number of saw-tooth:	25
Crack band width model:	Oliver model
Crack track algorism:	PROFLD (see explanations in main text Section 3.2.4)
Excluding distance r_{excl}:	8.0 m
Shear retention factor:	0.05 (constant)

The properties of the normal concrete elements for the reference models (Model 1-5) are listed in Table II.1. In the basic models, a simplified concrete tensile behaviour was employed, some of the properties were rough approximations see Table II.1. From Model 6 the material properties were improved by adapting the fib Model Code 1990 based on concrete class C40. The improved material properties are mentioned in Table II.2. However, a comparison between

Model 1 and Model 6 showed that the influence from the differences of the material properties is very limited.

Table II.2. Configurations of FEM models.

Model No.	Parameter	Misc.
Model 1.	Basic model, with x_0 = 605 mm, M/Vd = 1.32	Influence of the M/Vd value at the crack root.
Model 2	Basic model, with x_0 = 805 mm, M/Vd = 1.75	
Model 3	Basic model, with x_0 = 1005 mm, M/Vd = 2.18	
Model 4	Basic model, with x_0 = 1205 mm, M/Vd = 2.62	
Model 5	Basic model, with x_0 = 1405 mm, M/Vd = 3.05	
Model 6	Based on Model 1, with more realistic concrete properties of C30: f_{ct} = 2.8 MPa, G_f = 7.08 ·10-2, E_c = 3.4 ·10⁴ MPa, shear retention factor S_F = 20. Hordijk softening model.	Influence of the concrete tensile properties.
Model 7	Based on Model 6, load step size is doubled.	Influence of the load step size.
Model 8	Based on Model 7, load step size is doubled again.	
Model 9	Based on Model 8, reinforcement area is reduced to 1/3 of Model 8: 1Ø32	Influence of the reinforcement ratio.
Model 10	Basic model, with x_0 = 1605 mm, M/Vd = 3.49	Extended series on the influence of the M/Vd value at the crack root.
Model 11	Basic model, with x_0 = 1805 mm, M/Vd = 3.92	
Model 12	Basic model, with x_0 = 405 mm, M/Vd = 0.88	
Model 13	Basic model, with x_0 = 205 mm, M/Vd = 0.45	
Model 14	Based on Model 6, half of the nodal coordinate values	Influence of the size effect.
Model 15	Based on Model 1, double the mesh size in the critical zone	Influence of the mesh size.
Model 16	Based on Model 1, smaller crack spacing $l_{cr,m}$ = 100 mm	Influence of the major crack spacing $l_{cr,m}$.
Model 17	Based on Model 1, smaller crack spacing $l_{cr,m}$ = 300 mm	
Model 18	Based on Model 6, 10 times the reinforcement area	Extended series on the influence of reinforcement ratio.
Model 19	No reinforcement	
Model 20	Based on Model 6, the height of the existing crack height $s_{cr,e}$ reduced from 400 mm to 300 mm	Influence of existing crack height.
Model 21	Based on Model 6, $s_{cr,e}$ = 200 mm	
Model 22	Based on Model 6, $s_{cr,e}$ = 100 mm	
Model 23	Based on Model 6, half the concrete cover thickness, c = 20 mm	Influence of concrete cover thickness.

Regarding the root element, as explained in the main text, the properties of which has to be designed such that a crack will always develop from that element rather than any other part of the model. To serve that purpose, the tensile strength of the root element f_{ct} was reduced to 0.001 MPa, and the fracture energy G_f became 0.00125 kN/m. The other properties of the element were the same as the normal concrete elements.

The coordinates of the resultant crack paths of all the 23 models are given in the following tables.

Table II.3. Model 1

x	y
605.2	13.3
606.0	26.7
607.2	40.0
609.8	50.2
610.1	50.9
613.1	60.4
616.2	70.7
619.8	81.2
620.8	83.9
623.8	92.0
628.4	103.0
632.3	111.6
633.5	114.1
639.2	125.4
645.9	137.4
647.7	140.5
655.8	153.4
658.7	158.0
664.6	167.2
669.5	174.6
673.7	180.9
680.1	190.3
683.2	195.0
691.0	206.8
692.1	208.4
699.8	220.3
702.4	224.3

Table II.4. Model 2

x	y
805.2	13.3
805.8	26.7
806.9	40.0
809.0	50.2
810.1	53.9
811.9	60.4
814.6	70.8
817.7	81.4
821.2	92.2
821.2	92.3
825.2	103.5
829.8	114.9
833.5	123.2
835.0	126.4
841.0	138.5
847.7	151.1
848.5	152.5
856.7	166.4
858.7	169.6
865.2	179.7
869.5	186.3
873.9	193.5
879.6	202.7
883.2	208.9
890.4	220.7
892.1	223.3
897.6	232.3

Table II.5. Model 3

x	y
1005.0	13.3
1006.0	26.7
1007.0	40.0
1008.0	50.2
1010.0	58.4
1011.0	60.4
1013.0	70.9
1016.0	81.5
1019.0	92.5
1022.0	98.8
1023.0	103.8
1028.0	115.3
1032.0	127.0
1035.0	131.6
1038.0	139.1
1045.0	152.6
1048.0	158.0
1052.0	166.1
1059.0	177.1
1060.0	179.1
1068.0	192.4
1069.0	194.2
1078.0	208.8
1079.0	209.7
1080.0	211.3
1085.0	221.3

707.3	232.1
713.1	241.7
714.6	244.1
721.6	256.0
723.7	259.8
728.4	268.0
734.5	279.0
735.2	280.0
741.9	292.0

903.0	240.8
905.0	244.1
912.0	256.1
913.0	257.9
919.0	268.0
924.0	275.4
926.0	280.0
934.0	292.0

Table II.6. Model 4

x	y
1205.0	13.3
1206.0	26.7
1206.0	40.0
1208.0	50.2
1210.0	60.5
1210.0	60.8
1212.0	70.9
1215.0	81.6
1218.0	92.7
1222.0	104.0
1222.0	105.5
1226.0	115.7
1230.0	127.5
1235.0	139.7
1236.0	141.1
1241.0	152.8
1248.0	165.7
1248.0	166.1
1254.0	178.6
1259.0	186.7
1261.0	191.4
1268.0	204.5
1269.0	205.0
1274.0	214.8
1278.0	222.6

Table II.7. Model 5

x	y
1405.0	13.3
1406.0	26.7
1406.0	40.0
1408.0	50.2
1410.0	60.5
1410.0	63.2
1412.0	70.9
1414.0	81.7
1417.0	92.8
1420.0	104.2
1423.0	111.4
1424.0	116.0
1428.0	127.9
1433.0	140.1
1436.0	148.4
1438.0	152.9
1444.0	165.7
1448.0	173.4
1450.0	178.3
1457.0	190.8
1459.0	194.5
1463.0	203.6
1467.0	211.2
1469.0	214.7
1473.0	223.8

Table II.8. Model 6

x	y
605.2	13.3
605.9	26.7
607.2	40.0
609.8	50.2
610.1	51.0
613.2	60.4
616.6	70.7
620.5	81.2
620.6	81.6
624.8	91.9
629.5	102.8
632.0	107.9
635.0	113.9
640.8	125.0
647.5	136.3
647.8	136.9
648.0	137.1
658.7	153.8
658.7	153.8
668.2	167.6
669.5	169.4
678.2	181.5
680.2	184.4
687.6	195.3
691.0	200.6

1283.0	229.1
1286.0	232.9
1291.0	244.4
1293.0	248.6
1297.0	256.2
1303.0	264.3
1306.0	268.1
1313.0	279.3
1314.0	280.0
1321.0	292.0

1474.0	225.8
1479.0	233.8
1481.0	245.0
1484.0	249.9
1489.0	256.4
1493.0	261.4
1498.0	268.2
1503.0	275.3
1507.0	280.1
1513.0	288.3

695.8	208.3
702.3	219.0
703.0	220.2
710.0	232.1
713.0	237.2
716.9	244.1
723.3	256.0
723.7	256.8
729.8	268.0
734.5	277.4
735.9	280.0
741.9	292.0

Table II.9. Model 7

x	y
605.2	13.3
605.9	26.7
607.3	40.0
610.1	50.1
610.1	50.2
613.6	60.4
617.0	70.7
620.6	80.5
620.9	81.2
625.0	91.9
629.8	102.8
631.9	107.0
635.3	113.8
641.0	124.9
647.4	135.8
647.9	136.7
648.2	137.2
658.6	153.8
658.7	153.9
667.9	167.6
669.5	170.0
677.3	181.4

Table II.10. Model 8

x	y
605.2	13.3
605.9	26.7
607.3	40.0
610.1	50.1
610.1	50.2
613.6	60.4
617.0	70.7
620.6	80.5
620.9	81.2
625.0	91.9
629.8	102.8
631.9	107.0
635.3	113.8
641.0	124.9
647.4	135.8
647.9	136.7
648.2	137.2
658.6	153.8
658.7	153.9
667.9	167.6
669.5	170.0
677.3	181.4

Table II.11. Model 9

x	y
605.3	13.3
606.1	26.7
607.5	40.0
609.7	50.2
610.1	51.8
612.3	60.4
615.1	70.8
618.5	81.3
621.0	88.0
622.6	92.1
627.0	103.2
632.2	114.4
632.6	115.3
638.0	125.7
644.4	137.7
647.7	143.4
653.5	153.2
658.7	161.6
662.1	167.0
669.5	177.9
671.5	180.6
680.1	192.0

680.1	185.7
686.6	195.3
691.0	201.5
695.6	208.3
702.3	218.6
703.3	220.2
710.6	232.1
713.0	235.8
718.1	244.0
723.7	253.8
725.0	256.0
731.8	268.0
734.5	272.6

680.1	185.7
686.6	195.3
691.0	201.5
695.6	208.3
702.3	218.6
703.3	220.2
710.6	232.1
713.0	235.8
718.1	244.0
723.7	253.8
725.0	256.0
731.8	268.0
734.5	272.6

682.3	195.0
691.0	207.0
692.0	208.4
700.1	220.3
702.4	223.4
708.0	232.1
713.1	240.8
714.9	244.1
721.6	256.0
723.7	259.3
728.8	268.0
734.5	279.0

Table II.12. Model 10

x	*y*
1605.0	13.3
1605.0	26.7
1606.0	40.0
1608.0	50.2
1610.0	60.0
1610.0	60.5
1612.0	70.9
1615.0	81.7
1617.0	92.8
1620.0	104.2
1623.0	112.4
1624.0	116.0
1627.0	128.1
1631.0	140.4
1635.0	153.1
1637.0	157.1
1639.0	165.7
1643.0	178.0
1648.0	189.0
1648.0	190.1
1653.0	202.1

Table II.13. Model 11

x	*y*
1805.0	13.3
1805.0	26.7
1806.0	40.0
1808.0	50.2
1810.0	60.5
1810.0	64.7
1811.0	71.0
1814.0	81.7
1816.0	92.9
1819.0	104.5
1822.0	116.3
1823.0	120.6
1825.0	128.4
1829.0	140.6
1833.0	153.2
1837.0	164.1
1837.0	165.6
1841.0	177.9
1846.0	190.0
1848.0	195.0
1850.0	201.9

Table II.14. Model 12

x	*y*
405.3	13.3
406.2	26.7
407.8	40.0
410.1	48.2
410.9	50.2
414.9	60.3
418.9	70.6
420.4	74.0
423.5	81.0
428.4	91.5
431.1	96.8
434.0	102.2
440.0	112.9
442.8	117.6
446.4	123.3
451.9	131.8
457.8	140.6
459.1	142.3
468.0	154.8
469.4	156.7
478.2	168.8

1658.0	212.8	1854.0	213.3	480.2	171.5
1658.0	213.6	1858.0	220.5	488.2	182.6
1662.0	224.4	1860.0	224.4	491.0	186.6
1666.0	231.5	1863.0	235.3	497.2	195.7
1669.0	235.0	1866.0	241.4	501.9	202.8
1672.0	245.9	1870.0	246.1	505.3	208.1
1675.0	251.6	1873.0	257.5	512.8	220.1
1679.0	257.0	1875.0	263.0	512.9	220.3
1684.0	264.1	1880.0	268.7	520.2	232.0
1687.0	268.4	1884.0	273.2	523.7	238.2
1693.0	276.2	1889.0	280.3	526.8	244.0
1696.0	280.2			533.1	256.0

Table II.15. Model 13

x	y
205.3	13.3
206.4	26.7
208.5	40.0
210.0	44.9
212.2	50.2
217.2	60.3
220.2	65.7
222.9	70.5
228.8	80.7
230.5	83.6
235.0	91.0
240.9	100.2
241.7	101.3
248.6	111.4
251.6	115.6
255.5	120.9
260.7	127.7
262.9	130.7
269.6	139.3
272.5	143.0
280.1	152.5
283.3	156.5

Table II. 16. Model 14

x	y
252.6	6.7
252.9	13.3
253.5	20.0
255.0	24.9
255.1	25.1
257.3	30.2
259.4	35.3
260.2	37.3
261.6	40.5
264.0	45.8
265.6	49.1
266.7	51.1
269.6	56.5
271.6	60.0
272.7	61.8
275.6	66.4
277.9	69.9
279.5	72.3
283.1	77.3
284.7	79.5
288.2	84.3
290.1	86.9

Table II.17. Model 15

x	y
605.2	13.3
605.9	26.7
607.1	40.0
609.5	50.6
610.6	53.9
612.9	61.3
616.6	72.6
621.4	85.6
625.0	94.5
628.1	101.2
628.8	102.9
641.5	127.5
644.9	133.3
656.8	151.9
665.1	163.5
676.3	178.9
684.9	190.4
695.6	205.7
703.1	216.8
711.4	230.9
719.9	244.9
725.8	255.5

291.0	166.0
294.4	170.4
301.9	180.1
304.5	183.6
312.7	195.0
313.4	196.0
321.7	208.0
323.7	211.0
329.3	220.0
334.5	229.1
336.1	232.0
342.5	244.0

293.2	91.2
295.5	94.4
297.8	97.8
301.0	102.5
302.0	104.1
305.8	110.1
306.5	111.1
309.5	116.0
311.9	120.0
313.0	122.0
316.2	128.0
317.3	129.8
319.5	134.0

736.3	274.0
739.6	279.8
752.2	303.1
752.6	303.9
764.8	327.8
767.5	332.9
776.9	351.7

Table II. 18. Model 16

x	*y*
604.8	13.3
604.6	26.7
604.6	40.0
606.7	50.3
610.1	59.6
610.4	60.5
614.6	70.8
619.6	81.0
619.9	81.4
625.6	91.7
627.5	95.0
633.5	105.0
635.4	108.1
643.0	120.6
644.7	123.8
649.8	134.6
655.2	146.6
655.6	147.4
660.1	159.6
664.1	171.7
666.5	178.1

Table II. 19. Model 17

x	*y*
605.2	13.3
605.8	26.7
606.9	40.0
609.2	50.6
610.3	54.1
612.3	61.3
615.3	71.9
618.6	82.6
621.3	90.2
622.5	93.4
626.6	104.2
631.3	115.1
633.3	119.3
636.5	126.0
642.4	137.5
647.7	146.9
650.4	151.3
658.1	163.3
658.7	164.1
667.0	176.1
668.6	178.2

Table II. 20. Model 18

x	*y*
605.2	13.3
605.9	26.7
607.2	40.0
609.8	50.2
610.1	51.0
613.2	60.4
616.6	70.7
620.5	81.2
620.6	81.6
624.8	91.9
629.6	102.8
632.0	107.8
635.0	113.9
640.8	125.0
647.5	136.3
647.9	136.8
648.0	137.1
658.7	153.8
658.7	153.8
668.1	167.6
669.5	169.5

668.0	183.8
670.9	195.8
673.8	207.8
676.9	219.8
677.7	222.8
679.0	231.9
680.7	243.9

676.1	187.7
679.3	191.6
685.8	199.3
690.2	204.4
696.4	211.2
701.0	216.0
708.7	223.9
711.3	226.4
721.1	235.8
723.9	238.5
730.9	245.5
739.6	253.5
740.7	254.5
750.7	263.4
754.8	267.3
760.9	273.0
768.6	280.0
771.4	282.6

678.1	181.5
680.2	184.5
687.5	195.3
691.0	200.7
695.7	208.3
702.3	219.2
702.9	220.2
710.0	232.1
713.0	237.3
716.8	244.1
723.2	256.0
723.7	256.9
729.8	268.0
734.5	277.4
735.9	280.0
741.9	292.0

Table II. 21. Model 19

x	y
605.3	13.3
606.1	26.7
607.6	40.0
609.3	50.2
610.1	55.0
611.1	60.4
613.3	70.9
615.9	81.6
619.3	92.5
621.6	99.3
623.3	103.8
627.6	115.3
632.7	127.0
634.5	130.6
638.4	139.1
645.1	152.6

Table II. 22. Model 20

x	y
605.2	13.3
606.0	26.7
607.4	40.0
610.1	49.5
610.4	50.2
614.0	60.4
617.6	70.7
620.5	78.1
621.7	81.1
626.2	91.8
631.2	102.5
631.6	103.2
636.9	113.5
643.0	124.4
645.4	128.4
649.5	135.1

Table II. 23. Model 21

x	y
605.2	13.3
605.9	26.7
607.2	40.0
610.0	50.2
610.1	50.3
613.6	60.4
616.9	70.7
620.6	80.9
620.7	81.2
625.0	91.9
629.9	102.7
631.9	106.6
635.4	113.7
641.2	124.7
647.3	135.2
647.9	136.2

647.8	157.1
652.7	166.1
658.8	176.3
660.8	179.2
666.5	192.2
669.1	197.0
679.4	204.7
684.3	208.9
681.7	219.5
674.1	221.7
666.7	218.4
663.1	214.0
659.5	202.9

651.1	137.8
660.5	151.9
661.8	153.7
672.7	168.2
673.0	168.6
683.9	182.2
684.4	182.8
694.5	194.9
695.0	195.4
703.9	206.0
705.9	208.7
712.0	216.8
716.6	223.3
719.6	227.5
727.4	238.1
727.5	238.2
735.7	248.7
738.3	251.8

648.2	136.7
657.4	151.9
658.7	153.9
664.5	163.0
670.8	172.8
672.6	175.7
681.6	190.5
682.2	191.6
691.7	208.0
692.3	209.0
700.0	222.6
702.7	227.6
707.1	235.7
713.1	245.9
714.4	248.0
722.9	260.0
723.7	261.0
732.9	272.0
734.5	273.9
744.4	284.0
745.4	285.0
756.3	294.7
757.9	296.0
767.2	303.3
774.1	308.0
778.1	310.6

Table II. 24. Model 22

x	y
605.1	13.3
605.5	26.7
606.2	40.0
608.1	50.2
610.2	58.8
610.5	60.4
612.7	70.9
615.0	81.6

Table II. 25. Model 23

x	y
615.2	10.0
615.7	20.0
618.0	30.1
620.1	36.4
621.4	40.2
624.6	50.4
628.1	60.7
630.9	67.8

617.8	92.7
621.0	104.1
622.3	108.4
624.5	115.8
628.4	127.8
632.8	140.1
636.4	149.1
638.0	152.8
643.5	165.4
648.0	174.5
649.6	177.7
656.0	189.7
658.9	194.6
663.1	201.5
669.6	211.6
670.8	213.3
679.2	225.1
680.3	226.5
688.7	236.8
691.0	239.5
698.9	248.4
701.8	251.5
710.2	259.9
712.7	262.3
722.7	271.4
723.6	272.2
734.5	281.3
736.4	282.9
745.4	289.8
751.6	294.3
756.3	297.4
767.2	304.3
769.5	305.7

632.2	70.8
636.6	80.7
640.7	89.0
641.3	90.2
647.4	101.3
649.6	105.0
654.7	113.2
660.0	121.4
662.3	124.9
669.9	136.1
670.0	136.2
676.1	144.9
682.0	153.2
683.7	155.5
690.4	164.9
694.4	170.7
700.1	179.0
703.5	184.2
710.7	196.1
711.4	197.2
718.6	210.0
721.6	215.0
725.5	222.7
731.3	235.4
732.7	237.9
737.4	248.0

Appendix III

Shear Databases

This appendix includes several collections of shear test data which have been used in this research for different purposes. Considering the fact that great efforts have been made by other researchers to collect the shear test data from literature. It is the intention to make the maximum use of those databases. In this appendix, the ACI-DAfStd database is employed as a reference, it is the most updated and comprehensive database by the time this dissertation is written. All the tests in that database, which the shear evaluation procedure presented in Chapter 4 is applicable to, are listed in this appendix. The criteria are as follow:

- Normal rebar type, $\phi_{max} > 6$ mm;
- Effective depth $d > 100$ mm;
- Flexural shear failure mode ($a/d > 2.5$ and no shear compression failure is reported);
- Prismatic cross section;

In total 668 tests are included in this collection. Even with the whole set of the data, model is still able to deliver very good accuracy. The COV of V_{cal}/V_u for the whole data set is as low as 13.8% (excluding the 8 tests from Sneed). Nevertheless, as pointed out in Section 2.4, evaluating a model with unselected data may lead to unjustified conclusions. Therefore, that conclusion is not discussed in the main text.

The test number listed in Table III.1. is consistent with the ACI-DAfStd, for readers who want to check additional information of the data or the original reference, the paper (Reineck, Bentz et al. 2013) is referred to. The information that is included in the tables are:

- The number of the test in ACI-DAfStd database when applicable;
- The reference of the tests in author-year format;
- The name of the test in the reference;
- The width of the test specimen b;
- The length of the critical shear span of the test specimen (centre to centre distance between loading point to support in case of simply supported beams;

- The maximum M/Vd in the critical shear span, equivalent to a/d for simply supported beams;
- The effective depth of the specimen d;
- The mean concrete compressive strength f_{cm};
- The reinforcement ratio ρ_s;
- The actual rebar configuration of the specimen;
- The measured ultimate shear force V_u;
- The calculate shear capacity V_{cal} with the evaluation procedure presented in this research;
- The ratio between V_{cal}/V_u;
- The data collection where that data point is used in this dissertation.
- The span of beams with uniformly distributed loads L;
- The ratio between the sagging moment and the maximum moment difference in the span of a continuous supported beam with uniformly distributed load m.

Other than Table III.1, three more data collections are included in this appendix, among which, Table III. 2 consists of the additional shear tests with point loads which are not included in ACI-DAfStd database but also being used in the dissertation; Table III. 3 is a database of shear tests on lightweight aggregate concrete beams; Table III. 4 collects shear tests with uniformly distributed load. Because the study is mostly focused on the tests reported by Krefeld and Thurston (Krefeld & Thurston 1966), see Section 5.4.3.2, only this set of tests is included in this database; Table III. 5 presents the shear tests reported by IBBC-TNO (IBBC-TNO 1985) in Section 5.4.4.2.

The explanations of the abbreviations of databases in the tables are as follow:

- **kf**: the adjusted database of König & Fischer (König & Fischer 1995), see Section 4.4.2 and 4.6.2.
- **hsc**: the collection of tests to evaluation the influence of fracture of aggregate in high strength concrete beams, see Section 4.5.2.
- **d12 - d25**: the collection of shear tests on specimens reinforced with single type of reinforcement, see Section 4.6.2. The last two digits represent the normalized rebar diameter in mm.
- **bw**: the data collection to evaluate the influence of specimen width, see Section 6.4.4. The original data collection was from the database of Collins et.al. in (Collins, Mitchell et al. 2008). The relevant data is selected in the ACI-DAfStd. Some of the data points might be missing in the current table.
- **lwa**: the collection of shear tests carried out on specimens with lightweight aggregate concrete, see Section 4.5.2. In addition, the specimens marked by **lwar** are reference tests on specimens with normal concrete.

Table III.1. Shear tests with point loads in ACI-DAfStb database (selected).

No.	Lit.	Name	b	a	M/Vd	d	f_{cm}	ρ_s	Rebar	V_u	V_{cal}	V_{cal}/V_u	database
-	-	-	mm	mm	-	mm	MPa	%	Configuration	kN	kN	-	
1	Acharya;	ER1b	101.6	304.8	2.53	120.7	24.9	2.07	2 #4	24.6	22.6	0.92	
6	Kemp (1965)	AR2b	76.2	279.4	3.91	71.4	31.9	2.62	2 #3	11.5	11.6	1.01	
7		AR3b	76.2	228.6	3.20	71.4	28.9	2.62	2 #3	13.5	12.2	0.90	
10		BR6a	101.6	304.8	2.64	115.3	33.3	3.24	3 #4	39.6	28.3	0.72	
15		DR3b	101.6	304.8	3.25	93.7	30.4	4.16	2 #5	31.8	22.5	0.71	d16
17		AR1a	76.2	228.6	3.33	68.6	28.8	7.58	2 #5	22.4	17.1	0.76	d16
18		AR2a	76.2	304.8	4.44	68.6	34.1	7.58	2 #5	15.6	16.1	1.03	d16
20		AR4a	76.2	381.0	5.56	68.6	34.9	7.58	2 #5	13.5	14.9	1.10	d16
21	Adebar (1989) +	ST1	360.0	812.5	2.92	278.0	49.9	1.57	5 Ø20	128.6	147.7	1.15	
22	Adebar;	ST2	360.0	812.5	2.92	278.0	49.9	1.57	6 Ø20	119.8	147.7	1.23	
23	Collins (1994) +	ST3	290.0	812.5	2.92	278.0	46.8	1.95	7 Ø20	108.6	127.9	1.18	
24	Adebar;	ST8	290.0	812.5	2.92	278.0	43.9	1.95	8 Ø20	81.5	125.5	1.54	
25	Collins (1996)	ST16	290.0	812.5	4.56	178.0	48.9	3.04	9 Ø20	75.7	89.8	1.19	
28	Ahmad;	A1	127.0	812.8	4.00	203.2	59.3	3.93	2 #8	58.3	51.3	0.88	kf,hsc,d25
29	Kahloo	A2	127.0	609.6	3.00	203.2	59.3	3.93	2 #8	69.3	57.5	0.83	kf,hsc,d25
30	Poveda (1986)	A3	127.0	548.6	2.70	203.2	59.3	3.93	2 #8	69.3	60.0	0.87	
34		A7	127.0	832.1	4.00	208.0	59.3	1.77	2 #5 + 1 #3	47.2	43.1	0.91	kf,hsc
35		A8	127.0	624.1	3.00	208.0	59.3	1.77	2 #5 + 1 #3	49.3	48.7	0.99	kf,hsc
36		A9	127.0	561.7	2.70	208.0	59.3	1.77	2 #5 + 1 #3	80.4	51.0	0.63	
40		B1	127.0	806.7	4.00	201.7	65.3	5.03	2 #9	51.7	55.6	1.08	kf,hsc,d28
41		B2	127.0	605.0	3.00	201.7	65.3	5.03	2 #9	69.3	62.2	0.90	kf,hsc,d28
42		B3	127.0	544.5	2.70	201.7	65.3	5.03	2 #9	100.4	64.9	0.65	
46		B7	127.0	832.1	4.00	208.0	65.3	2.25	3 #5	45.0	46.8	1.04	kf,hsc,d16
47		B8	127.0	624.1	3.00	208.0	65.3	2.25	3 #5	47.1	52.9	1.12	kf,hsc,d16
48		B9	127.0	561.7	2.70	208.0	65.3	2.25	3 #5	80.4	55.4	0.69	
52	Ahmad;	C1	127.0	736.6	4.00	184.2	62.7	6.64	4 #7	54.7	59.8	1.09	kf,hsc,d22
53	Kahloo	C2	127.0	552.5	3.00	184.2	62.7	6.64	4 #7	76.0	68.4	0.90	kf,hsc,d22
54	Poveda (1986)	C3	127.0	497.2	2.70	184.2	62.7	6.64	4 #7	69.3	71.9	1.04	

No.	Lit.	Name	b	a	M/Vd	d	f_{cm}	ρ_s	Rebar	V_u	V_{cal}	V_{cal}/V_u	database
-	-	-	mm	mm	-	mm	MPa	%	Configuration	kN	kN	-	
58	Ahmad;	C7	127.0	826.0	4.00	206.5	62.7	3.26	3 #6	45.8	51.6	1.13	kf,hsc
59	Kahloo	C8	127.0	619.5	3.00	206.5	62.7	3.26	3 #6	44.9	58.4	1.30	kf,hsc
60	Poveda (1986)	C9	127.0	557.6	2.70	206.5	62.7	3.26	3 #6	45.7	61.2	1.34	
88		B7N	102.0	658.6	3.70	178.0	41.4	1.40	2 #4	27.0	26.4	0.98	d12
89		B8N	102.0	658.6	3.70	178.0	41.4	1.40	2 #4	31.9	26.4	0.83	d12
96		B7H	102.0	658.6	3.70	178.0	74.2	1.40	2 #4	27.1	29.8	1.10	d12
97		B8H	102.0	658.6	3.70	178.0	76.8	1.40	2 #4	27.1	29.8	1.10	d12
123	Angelakos;	DB0530	300.0	2662.0	2.88	925.0	30.4	0.50	2 M 30	167.9	160.0	0.95	
124	Bentz;	DB120	300.0	2662.0	2.88	925.0	20.0	1.01	4 M 30	181.9	186.0	1.02	
125	Collins (2000)	DB130	300.0	2662.0	2.88	925.0	30.4	1.01	4 M 30	187.9	210.5	1.12	
126		DB140	300.0	2662.0	2.88	925.0	36.1	1.01	4 M 30	182.9	221.5	1.21	
127		DB165	300.0	2662.0	2.88	925.0	61.8	1.01	4 M 30	187.9	258.1	1.37	
128		DB180	300.0	2662.0	2.88	925.0	76.0	1.01	4 M 30	174.9	259.9	1.49	
129		DB230	300.0	2662.0	2.97	895.0	30.4	2.09	8 M 30	259.9	279.6	1.08	
131	Koch (1974)	2	1000.0	920.0	3.68	250.0	25.6	0.64	41Ø7	221.6	232.8	1.05	kf,hsc,bw
132		3	1000.0	920.0	3.68	250.0	26.0	0.91	29Ø10	226.1	271.6	1.20	kf,hsc,bw
134		11	1000.0	1825.0	3.65	500.0	23.3	0.46	30Ø10	279.7	277.4	0.99	kf,hsc
135		12	1000.0	1825.0	3.65	500.0	26.0	0.65	41Ø10	342.5	334.7	0.98	kf,hsc
136		16	1000.0	2750.0	3.67	750.0	28.8	0.42	28Ø12	432.6	349.5	0.81	kf,hsc
161	Lubell; Sherwood;	AT-1 - East	2016.0	2662.0	2.91	916.0	60.9	0.76	20 M 30	1194.2	1536.5	1.29	
162	Bentz; Collins	AT-1 West	2016.0	2662.0	2.91	916.0	61.4	0.76	20 M 30	1287.8	1536.9	1.19	
163	(2004)	AT-2 / 250N	250.0	1262.0	2.89	437.0	35.8	0.92	2Ø25	116.8	104.1	0.89	
164	Sherwood (2008)	AT-2/ 250W	252.0	1262.0	2.87	439.0	36.6	0.90	2Ø25	113.7	105.6	0.93	
165		AT-2 /1000W	1002.0	1262.0	2.87	439.0	37.1	0.91	8Ø25	479.3	422.6	0.88	
166		AT-2/1000N	1002.0	1262.0	2.88	438.0	36.0	0.91	8Ø25	448.0	418.2	0.93	
167		AT-2/3000	3005.0	1262.0	2.87	439.0	38.6	0.91	24Ø25	1308.4	1282.7	0.98	
168		AT-3/N1	697.0	1001.9	3.26	307.0	35.6	0.93	4Ø25	240.2	214.1	0.89	d25
169		AT-3/N2	706.0	1001.9	3.27	306.0	35.2	0.93	4Ø25	261.3	214.7	0.82	d25

No.	Lit.	Name	b	a	M/Vd	d	f_{cm}	ρ_s	Rebar	V_u	V_{cal}	V_{cal}/V_u	database
-	-	-	mm	mm	-	mm	MPa	%	Configuration	kN	kN	-	
170		AT-3/T1	700.0	1001.9	3.27	306.0	35.9	0.93	4Ø25	256.4	214.7	0.84	d25
171		AT-3/T2	706.0	1001.9	3.26	307.0	35.2	0.92	4Ø25	252.3	215.2	0.85	d25
181	Bernhardt;	S9A	150.0	550.0	3.46	159.0	78.0	5.27	4Ø20	80.7	63.3	0.78	kf,hsc
182	Fynboe (1986)	S9B	150.0	550.0	3.46	159.0	78.0	5.27	4Ø20	65.7	63.3	0.96	kf,hsc
183		S9C	150.0	550.0	3.46	159.0	92.3	5.27	4Ø20	68.7	63.9	0.93	kf,hsc
184	Bhal (1968)	B1	240.0	881.3	2.94	300.0	22.0	1.26	2Ø24	71.0	72.6	1.02	bw
185		B2	240.0	1762.5	2.94	600.0	28.1	1.26	4Ø24	119.5	138.1	1.16	
186		B3	240.0	2643.8	2.94	900.0	26.1	1.26	6Ø24	166.4	168.3	1.01	
187		B4	240.0	3525.0	2.94	1200.0	23.9	1.26	8Ø24	187.1	185.5	0.99	
188		B5	240.0	1762.5	2.94	600.0	25.3	0.63	2Ø24	106.9	100.4	0.94	
189		B6	240.0	1762.5	2.94	600.0	23.5	0.63	8Ø12	115.4	93.5	0.81	
190		B7	240.0	2643.8	2.94	900.0	25.9	0.63	3Ø24	140.0	125.4	0.90	
191		B8	240.0	2643.8	2.94	900.0	26.3	0.63	12Ø12	127.6	116.6	0.91	
192	Bresler;	0A-1	309.9	1752.6	3.80	461.0	21.4	1.81	4 #9	170.7	131.3	0.77	d28
193	Scordelis (1963)	0A-2	304.8	2209.8	4.74	466.1	22.5	2.27	5 #9	184.4	131.7	0.71	d28
194		0A-3	307.3	3124.2	6.77	461.5	35.7	2.73	6 #9	195.8	138.7	0.71	d28
195	Cladera;	H 50/1	200.0	1042.5	2.90	360.0	47.4	2.23	2Ø32	100.8	104.3	1.04	
196	Mari (2002)	H 50/5	200.0	1042.5	2.90	360.0	47.4	2.23	2Ø32	178.7	104.3	0.58	
197		H 60/1	200.0	1042.5	2.90	360.0	57.8	2.23	2Ø32	109.2	110.6	1.01	
198	Cladera (2002)	H 75/1	200.0	1042.5	2.90	360.0	65.5	2.23	2Ø32	101.0	112.5	1.11	
199		H 100/1	200.0	1042.5	2.90	360.0	82.7	2.23	2Ø32	118.9	114.5	0.96	
200		H 100/5	200.0	1042.5	2.90	360.0	82.7	2.23	2Ø32	141.2	114.5	0.81	
201	Cao (2000)	SB 2012/0	300.0	5325.0	2.89	1845.0	26.1	1.52	12Ø30	418.4	318.1	0.76	
203	Cederwall; Hedman;	734-34	135.0	800.0	3.42	234.0	27.8	1.07	1Ø12 + 2Ø12	42.1	37.0	0.88	
204	Losberg (1974)	734-40	134.0	600.0	2.56	234.0	24.1	1.08	1Ø12 + 2Ø12	42.1	40.2	0.95	
205	Chana (1981)	2.1a	203.0	1068.0	3.00	356.0	37.0	1.74	4Ø20	96.0	97.3	1.01	
206		2.1b	203.0	1068.0	3.00	356.0	37.0	1.74	4Ø20	97.1	97.3	1.00	
207		2.2a	203.0	1068.0	3.00	356.0	31.2	1.74	4Ø20	87.4	92.7	1.06	

No.	Lit.	Name	b	a	M/Vd	d	f_{cm}	ρ_s	Rebar	V_u	V_{cal}	V_{cal}/V_u	database
-	-	-	mm	mm	-	mm	MPa	%	Configuration	kN	kN	-	
208	Chana (1981)	2.2b	203.0	1068.0	3.00	356.0	31.2	1.74	4Ø20	94.4	92.7	0.98	
209		2.3a	203.0	1068.0	3.00	356.0	33.9	1.74	4Ø20	99.4	94.9	0.96	
210		2.3b	203.0	1068.0	3.00	356.0	33.9	1.74	4Ø20	96.4	94.9	0.98	
241	Chang;	IA1	101.6	558.8	4.09	136.7	26.2	2.89	2 #5	20.0	22.8	1.14	d16
243	Kesler (1958)	IB1	101.6	355.6	2.60	136.7	26.2	1.86	2 #4	19.6	24.1	1.23	
245		IC1	101.6	457.2	3.35	136.7	26.2	2.37	5 #3	19.7	26.5	1.35	
246		IC2	101.6	457.2	3.35	136.7	26.2	2.37	5 #3	17.9	26.5	1.48	
249		IIB1	101.6	558.8	4.09	136.7	16.8	2.37	5 #3	16.7	21.3	1.27	
251		IIC1	101.6	355.6	2.60	136.7	16.8	2.89	2 #5	17.9	24.1	1.35	
267		4-21a	101.6	508.0	3.72	136.7	36.7	1.86	2 #4	21.2	22.9	1.08	d12
268		4-21b	101.6	508.0	3.72	136.7	36.7	1.86	2 #4	24.7	22.9	0.93	d12
269		4-22a	101.6	508.0	3.72	136.7	30.3	1.86	2 #4	21.5	21.7	1.01	d12
270		4-22b	101.6	508.0	3.72	136.7	30.1	1.86	2 #4	23.5	21.6	0.92	d12
271		4-23a	101.6	508.0	3.72	136.7	30.6	1.86	2 #4	21.7	21.7	1.00	d12
272		4-23b	101.6	508.0	3.72	136.7	30.6	1.86	2 #4	22.6	21.7	0.96	d12
277		5-21a	101.6	508.0	3.72	136.7	30.6	2.89	2 #5	29.0	24.7	0.85	d16
278		5-21b	101.6	508.0	3.72	136.7	30.6	2.89	2 #5	27.6	24.7	0.90	d16
279		5-22a	101.6	508.0	3.72	136.7	29.6	2.89	2 #5	22.5	24.5	1.09	d16
280		5-22b	101.6	508.0	3.72	136.7	29.6	2.89	2 #5	26.0	24.5	0.94	d16
281		5-23a	101.6	508.0	3.72	136.7	30.5	2.89	2 #5	24.6	24.7	1.00	d16
282		5-23b	101.6	508.0	3.72	136.7	30.5	2.89	2 #5	23.5	24.7	1.05	d16
295	Collins;	B100	300.0	2662.0	2.88	925.0	34.2	1.01	4 M30	227.9	217.9	0.96	hsc
296	Kuchma (1999)	B100H	300.0	2662.0	2.88	925.0	93.1	1.01	5 M30	193.0	261.9	1.36	hsc
297		B100B	300.0	2662.0	2.88	925.0	37.1	1.01	6 M30	206.9	223.2	1.08	hsc
298		B100L	300.0	2662.0	2.88	925.0	37.1	1.01	14 M15	225.9	207.5	0.92	hsc
299		B100-R	300.0	2662.0	2.88	925.0	34.2	1.01	4 M30	251.9	217.9	0.87	hsc
300		B100HE	300.0	2662.0	2.88	925.0	93.1	1.01	4 M30	219.9	261.9	1.19	hsc
301		B100L-R	300.0	2662.0	2.88	925.0	37.1	1.01	14 M15	237.9	207.4	0.87	hsc

No.	Lit.	Name	b	a	M/Vd	d	f_{cm}	ρ_s	Rebar	V_u	V_{cal}	V_{cal}/V_u	database
-	-	-	mm	mm	-	mm	MPa	%	Configuration	kN	kN	-	
303	Diaz de Cossio;	A-2	152.4	838.2	3.30	254.0	29.9	0.98	3 #4	42.4	44.0	1.04	d12,bw
304	Siess (1960)	A-3	152.4	1092.2	4.30	254.0	18.5	0.98	3 #4	34.9	34.1	0.98	d12,bw
305		A-4	152.4	1346.2	5.30	254.0	25.5	0.98	3 #4	36.0	34.3	0.95	d12,bw
308		A-12	152.4	838.2	3.30	254.0	25.4	3.33	2 #9	59.5	56.8	0.95	d28
309		A-13	152.4	1092.2	4.30	254.0	21.0	3.33	2 #9	47.6	48.5	1.02	d28
310		A-14	152.4	1346.2	5.30	254.0	26.1	3.33	2 #9	55.5	47.8	0.86	d28
311		A-15	152.4	1600.2	6.30	254.0	23.8	3.33	2 #9	50.3	43.7	0.87	d28
312	Drangsholt;	B11	150.0	663.0	3.00	221.0	51.3	1.82	3Ø16	58.9	57.1	0.97	d16
314	Thorenfeld (1992)	B13	150.0	828.0	4.00	207.0	51.3	3.24	5Ø16	71.1	61.1	0.86	d16
315		B14	150.0	621.0	3.00	207.0	51.3	3.24	5Ø16	83.4	69.8	0.84	d16
317		B21	150.0	663.0	3.00	221.0	73.9	1.82	3Ø16	68.7	60.4	0.88	d16
319		B23	150.0	828.0	4.00	207.0	73.9	3.24	5Ø16	78.5	64.4	0.82	d16
320		B24	150.0	621.0	3.00	207.0	73.9	3.24	5Ø16	83.4	73.3	0.88	d16
322		B43	150.0	828.0	4.00	207.0	82.1	3.24	5Ø16	86.8	64.6	0.74	d16
323		B44	150.0	621.0	3.00	207.0	82.1	3.24	5Ø16	107.9	73.6	0.68	d16
325		B51	150.0	663.0	3.00	221.0	92.8	1.82	3Ø16	56.9	61.1	1.07	d16
327		B53	150.0	828.0	4.00	207.0	92.8	3.24	5Ø16	77.5	64.9	0.84	d16
328		B54	150.0	621.0	3.00	207.0	92.8	3.24	5Ø16	78.5	73.8	0.94	d16
330		B61	300.0	1326.0	3.00	442.0	73.9	1.82	3Ø32	186.2	182.2	0.98	d32
332		B63	300.0	1656.0	4.00	414.0	73.9	3.24	5Ø32	234.7	190.1	0.81	d32
333		B64	300.0	1242.0	3.00	414.0	73.9	3.24	5Ø32	286.7	215.2	0.75	d32
335	Elzanaty;	F7	177.8	1092.2	4.00	273.1	19.7	0.52	2 #4	34.6	34.2	0.99	kf,hsc,d12,bw
336	Nilson;	F11	177.8	1079.5	4.00	269.9	19.7	1.19	2 #6	45.1	43.2	0.96	kf,hsc,bw
337	Slate (1986)	F12	177.8	1073.2	4.00	268.3	19.7	2.44	3 #7	54.3	55.4	1.02	kf,hsc,d22
338		F8	177.8	1092.2	4.00	273.1	38.0	0.93	2 #4 + 1 #5	46.1	51.4	1.11	kf,hsc,bw
339		F13	177.8	1079.5	4.00	269.9	38.0	1.19	2 #6	49.0	52.6	1.07	kf,hsc,bw
340		F14	177.8	1073.2	4.00	268.3	38.0	2.44	3 #7	64.8	67.1	1.04	kf,hsc,d22
341		F1	177.8	1079.5	4.00	269.9	62.2	1.19	2 #6	58.8	60.5	1.03	kf,hsc

No.	Lit.	Name	b	a	M/Vd	d	f_{cm}	ρ_s	Rebar	V_u	V_{cal}	V_{cal}/V_u	database
-	-	-	mm	mm	-	mm	MPa	%	Configuration	kN	kN	-	
342	Elzanaty;	F2	177.8	1073.2	4.00	268.3	62.2	2.44	3 #7	67.0	76.9	1.15	kf,hsc
343	Nilson;	F10	177.8	1066.8	4.00	266.7	62.2	3.21	3 #8	76.2	82.6	1.08	kf,hsc,d25
344	Slate (1986)	F9	177.8	1073.2	4.00	268.3	75.3	1.63	2 #7	63.7	67.2	1.06	kf,hsc,d22
345		F15	177.8	1073.2	4.00	268.3	75.3	2.44	3 #7	67.7	77.8	1.15	kf,hsc,d22
348		F5	177.8	1619.3	6.00	269.9	60.3	1.19	2 #6	45.0	47.0	1.04	kf,hsc
349		F6	177.8	1609.7	6.00	268.3	60.3	2.44	3 #7	62.1	58.4	0.94	kf,hsc,d22
351	Feldman;	L-2	152.4	762.0	3.02	252.5	20.4	3.35	2 #9	76.4	55.2	0.72	d28
352	Siess (1955)	L-2A	152.4	762.0	3.02	252.5	34.9	3.35	2 #9	80.9	64.4	0.80	d28
353		L-3	152.4	1016.0	4.02	252.5	26.6	3.35	2 #9	54.3	53.2	0.98	d28
354		L-4	152.4	1270.0	5.03	252.5	24.5	3.35	2 #9	52.0	47.7	0.92	d28
355		L-5	152.4	1524.0	6.04	252.5	26.5	3.35	2 #9	52.2	45.8	0.88	d28
360		L3R	152.4	977.9	3.87	252.5	26.6	3.35	2 #9	62.4	54.0	0.86	d28
385	Ferguson (1956)	F2	100.8	609.6	3.23	189.0	27.8	2.08	2 #5	22.5	28.9	1.29	d16
390		SAR3	200.0	1100.0	4.23	260.0	130.2	3.09	8 M16	108.0	101.2	0.94	d16
391		HP1	200.0	800.0	4.00	200.0	132.1	3.02	6 M16	109.1	82.9	0.76	d16
392		HP3	200.0	800.0	4.00	200.0	118.8	4.02	8 M16	102.1	92.6	0.91	d16
393		HP5	200.0	800.0	4.00	200.0	102.6	4.02	9 M16	109.6	92.3	0.84	d16
397	Ghannoum (1998)	N90 (N)	400.0	162.5	2.50	65.0	32.5	1.92	5 M10	76.2	59.3	0.78	
398		N90 (S)	400.0	162.5	2.50	65.0	32.5	1.15	3 M10	42.8	47.4	1.11	
399		N155 (N)	400.0	318.8	2.50	127.5	32.5	1.96	5 M15	112.5	95.0	0.84	
400		N155 (S)	400.0	318.8	2.50	127.5	32.5	1.18	3 M15	85.2	77.4	0.91	
401		N220 (N)	400.0	475.0	2.50	190.0	32.5	1.97	5 M20	123.7	123.2	1.00	
402		N220 (S)	400.0	475.0	2.50	190.0	32.5	1.18	3 M20	104.6	101.2	0.97	
403		N350 (N)	400.0	781.3	2.50	312.5	32.5	2.00	5 M25	180.8	178.5	0.99	
404		N350 (S)	400.0	781.3	2.50	312.5	32.5	1.20	3 M25	160.2	145.5	0.91	
405		N485 (N)	400.0	1100.0	2.50	440.0	32.5	1.99	5 M30	219.1	225.7	1.03	
406		N485 (S)	400.0	1100.0	2.50	440.0	32.5	1.19	3 M30	191.2	184.0	0.96	
407		N960 (N)	400.0	2222.5	2.50	889.0	32.5	1.97	10 M30	398.6	401.1	1.01	

No.	Lit.	Name	b	a	M/Vd	d	f_{cm}	ρ_s	Rebar	V_u	V_{cal}	V_{cal}/V_u	database
-	-	-	mm	mm	-	mm	MPa	%	Configuration	kN	kN	-	
408	Ghannoum (1998)	N960 (S)	400.0	2222.5	2.50	889.0	32.5	1.18	6 M30	379.1	320.3	0.84	
409		H90 (N)	400.0	162.5	2.50	65.0	55.6	1.92	5 M10	77.7	69.3	0.89	
410		H90 (S)	400.0	162.5	2.50	65.0	55.6	1.15	3 M10	52.4	56.6	1.08	
411		H155 (N)	400.0	318.8	2.50	127.5	55.6	1.96	5 M15	105.6	111.0	1.05	
412		H155 (S)	400.0	318.8	2.50	127.5	55.6	1.18	3 M15	77.3	90.8	1.17	
413		H220 (N)	400.0	475.0	2.50	190.0	55.6	1.97	5 M20	136.3	144.1	1.06	
414		H220 (S)	400.0	475.0	2.50	190.0	55.6	1.18	3 M20	106.9	118.9	1.11	
415		H350 (N)	400.0	781.3	2.50	312.5	55.6	2.00	5 M25	191.8	208.7	1.09	
416		H350 (S)	400.0	781.3	2.50	312.5	55.6	1.20	3 M25	159.5	170.8	1.07	
417		H485 (N)	400.0	1100.0	2.50	440.0	55.6	1.99	5 M30	202.7	264.0	1.30	
418		H485 (S)	400.0	1100.0	2.50	440.0	55.6	1.19	3 M30	202.2	216.0	1.07	
419		H960 (N)	400.0	2222.5	2.50	889.0	55.6	1.97	10 M30	349.9	468.1	1.34	
420		H960 (S)	400.0	2222.5	2.50	889.0	55.6	1.18	6 M30	329.2	374.9	1.14	
421	Grimm, R. (1997)	S 1.1	300.0	570.0	3.73	153.0	85.6	1.34	4Ø14	70.9	75.8	1.07	
422		S 1.2	300.0	570.0	3.75	152.0	86.6	2.20	5Ø16	75.9	88.9	1.17	d16
423		S 1.3	300.0	570.0	3.90	146.0	89.0	4.22	3Ø28	99.3	109.7	1.10	d28
424		S 2.2	300.0	1230.0	3.53	348.0	86.7	1.88	4Ø25	194.0	151.3	0.78	d25
425		S 2.4	300.0	1230.0	3.75	328.0	89.4	3.75	6Ø28	233.2	178.4	0.77	d28
426		S 3.2	300.0	2630.0	3.66	718.0	89.0	1.72	6Ø28	270.2	250.5	0.93	d28
427		S 3.3	300.0	2630.0	3.53	746.0	89.7	0.83	3Ø28	215.1	198.7	0.92	d28
428		S 3.4	300.0	2630.0	3.81	690.0	89.4	3.57	12Ø28	393.1	320.7	0.82	d28
429		S 4.1	300.0	570.0	3.73	153.0	105.4	1.34	4Ø14	75.0	77.3	1.03	
430		S 4.2	300.0	570.0	3.75	152.0	105.4	2.20	5Ø16	91.0	90.5	0.99	d16
431		S 4.3	300.0	570.0	3.90	146.0	105.4	4.22	3Ø28	123.0	112.7	0.92	d28
436	Hallgren (1994)	B90SB5-2-33	156.0	700.0	3.66	191.3	31.2	2.27	6Ø12	56.6	50.4	0.89	d12
437		B90SB6-2-33	156.0	700.0	3.61	193.9	31.2	2.24	6Ø12	54.1	51.0	0.94	d12
438		B90SB9-2-31	156.0	700.0	3.65	191.8	29.5	2.27	6Ø12	49.6	49.7	1.00	d12
439		B90SB10-2-31	157.0	700.0	3.63	192.8	29.5	2.20	6Ø12	54.1	49.7	0.92	d12

No.	Lit.	Name	b	a	M/Vd	d	f_{cm}	ρ_s	Rebar	V_u	V_{cal}	V_{cal}/V_u	database
-	-	-	mm	mm	-	mm	MPa	%	Configuration	kN	kN	-	
440	Hallgren (1994)	B90SB13-2-86	163.0	700.0	3.65	191.8	81.9	2.17	6Ø12	83.1	62.9	0.76	d12
441		B90SB14-2-86	158.0	700.0	3.61	193.9	81.9	2.21	6Ø12	77.1	62.4	0.81	d12
442		B90SB17-2-45	157.0	700.0	3.66	191.3	42.7	2.26	6Ø12	59.6	55.3	0.93	d12
443		B90SB18-2-45	155.0	700.0	3.61	193.9	42.7	2.26	6Ø12	63.6	55.6	0.87	d12
444		B90SB21-2-85	155.0	700.0	3.61	193.9	80.4	2.26	6Ø12	69.6	61.7	0.89	d12
445		B90SB22-2-85	158.0	700.0	3.63	192.8	80.4	2.23	6Ø12	76.1	62.1	0.82	d12
446		B91SC1-2-62	156.0	700.0	3.63	192.8	58.7	2.25	6Ø12	71.6	60.8	0.85	d12
447		B91SC2-2-62	155.0	700.0	3.57	196.1	58.7	2.23	6Ø12	70.1	61.5	0.88	d12
448		B91SC3-2-69	155.0	700.0	3.61	193.9	65.6	2.26	6Ø12	77.1	61.4	0.80	d12
449		B91SC4-2-69	156.0	700.0	3.59	195.0	65.6	2.23	6Ø12	74.6	61.9	0.83	d12
450		B91SD1-4-61	156.0	700.0	3.61	193.9	57.8	3.99	6Ø16	89.1	71.4	0.80	d16
451		B91SD2-4-61	156.0	700.0	3.59	195.0	57.8	3.96	6Ø16	90.5	71.8	0.79	d16
452		B91SD3-4-66	156.0	700.0	3.59	195.0	62.4	3.96	6Ø16	82.1	72.6	0.88	d16
453		B91SD4-4-66	155.0	700.0	3.59	195.0	62.4	3.99	6Ø16	79.6	72.4	0.91	d16
454		B91SD5-4-58	156.0	700.0	3.58	195.5	55.4	3.95	6Ø16	78.5	71.1	0.91	d16
455		B91SD6-4-58	150.0	700.0	3.58	195.5	55.4	4.11	6Ø16	83.1	69.6	0.84	d16
458		B3	262.0	550.0	2.64	208.0	87.8	0.74	2Ø16	76.1	75.1	0.99	
460		B5	283.0	550.0	2.61	211.0	86.7	1.05	2Ø20	104.2	91.6	0.88	
462		B7	337.0	550.0	2.64	208.0	80.8	0.57	2Ø16	89.3	87.8	0.98	
463	Hamadi (1976)	G1	100.0	1255.0	3.39	370.0	28.8	1.70	2Ø20	45.0	43.2	0.96	
464		G2	100.0	1255.0	3.37	372.0	22.3	1.08	2Ø16	41.4	35.5	0.86	d16
465		G3	100.0	1255.0	3.36	374.0	22.1	0.60	2Ø12	35.6	28.8	0.81	d12
466		G4a	100.0	2195.0	5.90	372.0	20.9	1.08	2Ø16	31.0	27.4	0.88	d16
467		G4b	100.0	1280.0	3.44	372.0	19.9	1.08	2Ø16	38.9	34.1	0.88	d16
473	Hanson (1961)	8A4	152.4	1320.8	4.95	266.7	19.9	1.25	4 #4	34.8	37.9	1.09	lwar,d12,bw
474		8B4	152.4	1320.8	4.95	266.7	29.4	1.25	4 #4	43.8	42.5	0.97	lwar,d12,bw
475		8BW4	152.4	1320.8	4.95	266.7	28.2	1.25	4 #4	41.0	41.9	1.02	lwar,d12,bw
476		8B2	152.4	1320.8	4.95	266.7	29.3	3.50	2 #7 + 2 #4	53.4	61.3	1.15	lwar

No.	Lit.	Name	b	a	M/Vd	d	f_{cm}	ρ_s	Rebar	V_u	V_{cal}	V_{cal}/V_u	database
-	-	-	mm	mm	-	mm	MPa	%	Configuration	kN	kN	-	
477		8B3	152.4	660.4	2.48	266.7	28.6	1.25	4 #4	46.8	57.4	1.23	lwar
478	Hedmann;	A4	152.0	1321.0	4.95	267.0	18.9	1.25	4 #4	34.5	37.3	1.08	d12,bw
479	Losberg (1978)	B4	152.0	1321.0	4.95	267.0	28.0	1.25	4 #4	43.5	41.8	0.96	d12,bw
480		BW4	152.0	1321.0	4.95	267.0	26.8	1.25	4 #4	40.7	41.3	1.01	d12,bw
481		B2	152.0	1321.0	4.95	267.0	27.8	2.22	2 #7 + 1 #4	53.1	47.1	0.89	
482	Islam; Pam;	M100-S0	150.0	800.0	3.94	203.0	79.1	3.22	2Ø25	65.6	58.7	0.89	d25
483	Kwan (1998)	M80-S0	150.0	800.0	3.94	203.0	68.6	3.22	2Ø25	58.6	57.9	0.99	d25
484		M60-S0	150.0	800.0	3.86	207.0	48.3	2.02	2Ø20	46.1	47.6	1.03	
485		M40-S0	150.0	800.0	3.90	205.0	32.7	3.19	2Ø25	55.6	48.2	0.87	d25
486		M25-S0	150.0	800.0	3.86	207.0	25.3	2.02	2Ø20	48.1	39.3	0.82	
487	Johnson; Ramirez (1989)	6	304.8	1670.1	3.10	538.7	53.1	2.49	5 #10	197.0	230.2	1.17	d32
488	Kani (1967)	40	151.6	747.3	5.35	139.7	25.1	2.59	2 #6	32.0	29.0	0.91	kf,hsc
490		43	151.4	812.8	5.93	137.2	26.6	2.73	2 #6	29.1	28.8	0.99	kf,hsc,sf
494		47	151.1	678.2	5.13	132.1	23.5	2.84	2 #6	28.2	28.7	1.02	
495		48	151.1	678.2	5.09	133.4	23.5	2.82	2 #6	27.1	28.9	1.07	kf,hsc
496		52	152.4	543.6	3.93	138.4	23.6	2.69	2 #6	28.9	32.2	1.11	kf,hsc,sf
499		55	150.4	406.4	3.02	134.6	23.8	2.80	2 #6	32.6	34.9	1.07	kf,hsc,sf
500		56	153.2	475.7	3.46	137.4	25.9	2.67	2 #6	28.0	34.4	1.23	kf,hsc
501		57	153.2	747.3	5.39	138.7	25.1	2.61	2 #6	31.6	29.2	0.93	kf,hsc
502		58	152.4	475.7	3.44	138.4	25.9	2.66	2 #6	28.9	34.5	1.19	kf,hsc
503		59	154.4	372.9	2.67	139.7	25.3	2.63	2 #6	50.2	38.3	0.76	
504		60	154.9	406.9	2.93	138.7	25.4	2.64	2 #6	39.3	37.0	0.94	
505		81	153.4	1627.6	5.93	274.3	26.1	2.76	2 #8 + 2 #3	51.2	47.7	0.93	kf,hsc
507		83	156.0	813.8	3.00	271.3	26.1	2.74	2 #8 + 2 #3	64.9	64.3	0.99	kf,hsc,sf
508		84	151.1	1085.1	4.00	271.0	26.1	2.84	2 #8 + 2 #3	55.4	55.6	1.00	kf,hsc,sf
510		91	154.4	1627.6	6.06	268.7	26.1	2.70	2 #8 + 2 #3	51.0	46.2	0.91	kf,hsc
512		93	154.9	1763.3	6.46	272.8	28.8	2.66	2 #8 + 2 #3	53.8	46.7	0.87	kf,hsc
515		96	153.2	1085.1	3.94	275.1	24.0	2.76	2 #8 + 2 #3	56.3	55.4	0.99	kf,hsc,sf

No.	Lit.	Name	b	a	M/Vd	d	f_{cm}	ρ_s	Rebar	V_u	V_{cal}	V_{cal}/V_u	database
-	-	-	mm	mm	-	mm	MPa	%	Configuration	kN	kN	-	
516	Kani (1967)	97	152.4	815.3	2.95	276.4	25.9	2.68	2 #8 + 2 #3	62.5	63.4	1.01	
518		99	152.4	679.5	2.50	271.8	24.9	2.73	2 #8 + 2 #3	77.2	67.0	0.87	
521		63	154.4	2170.2	4.00	542.8	24.9	2.77	2 #8 + 2 #9	93.2	92.8	1.00	
522		64	156.2	4340.4	8.03	540.5	24.4	2.75	2 #8 + 2 #9	79.0	67.2	0.85	kf,hsc
524		66	156.2	3255.3	6.01	541.3	25.1	2.75	2 #8 + 2 #9	90.7	77.3	0.85	kf,hsc,sf
528		71	154.9	1627.6	2.99	544.1	26.0	2.66	2 #8 + 2 #9	102.1	106.0	1.04	
530		74	152.4	1630.7	3.12	523.2	25.9	2.84	2 #8 + 2 #9	107.6	101.7	0.94	kf,hsc,sf
531		75	152.4	1630.7	3.11	524.0	25.9	2.84	2 #8 + 2 #9	107.9	101.9	0.94	kf,hsc
532		76	152.4	1358.9	2.63	517.7	29.2	2.87	2 #8 + 2 #9	114.8	113.7	0.99	
533		79	153.2	3804.9	6.84	556.3	24.8	2.72	2 #8 + 2 #9	83.6	72.6	0.87	kf,hsc
535		3042	153.9	2736.9	2.50	1094.7	25.1	2.70	2 #9 + 4 #10	236.9	181.2	0.77	
536		3043	153.7	3276.6	3.00	1092.2	25.6	2.71	2 #9 + 4 #10	165.0	166.2	1.01	kf,hsc,sf
537		3044	152.4	4363.7	3.98	1097.3	28.0	2.72	2 #9 + 4 #10	159.0	147.2	0.93	kf,hsc,sf
538		3045	154.9	5461.0	5.00	1092.2	26.9	2.70	2 #9 + 4 #10	152.3	131.1	0.86	kf,hsc,sf
539		3046	154.9	7681.0	7.00	1097.3	25.4	2.70	2 #9 + 4 #10	154.3	109.3	0.71	kf,hsc
540		3047	154.9	8757.9	8.00	1094.7	25.4	2.69	2 #9 + 4 #10	147.0	101.8	0.69	kf,hsc
541		271	611.1	1630.7	6.07	268.7	25.6	2.75	2 (2 #8 + 2 #9)	217.2	177.4	0.82	kf,hsc
542		272	610.9	1358.9	5.02	270.8	25.6	2.73	2 (2 #8 + 2 #9)	227.7	190.6	0.84	kf,hsc
543		273	612.1	1087.1	4.01	271.3	25.8	2.72	2 (2 #8 + 2 #9)	206.1	208.5	1.01	kf,hsc
544		274	612.1	815.3	3.02	270.3	25.8	2.73	2 (2 #8 + 2 #9)	250.1	232.9	0.93	kf,hsc
663		709	152.4	1359.4	4.87	279.1	25.5	2.72	2 #8 + 2 #3	52.0	51.5	0.99	
664		666	154.9	816.0	2.95	276.6	27.8	2.70	2 #8 + 2 #3	63.4	66.2	1.04	
665		675	152.4	816.7	2.95	276.9	25.3	2.74	2 #8 + 2 #3	56.7	63.8	1.13	
666		718	151.6	1358.8	4.85	280.2	25.2	2.72	2 #8 + 2 #3	54.3	51.4	0.95	
667		742	152.4	1359.2	5.02	270.8	33.2	2.80	2 #8 + 2 #3	54.5	54.1	0.99	
668		744	152.4	1358.4	5.05	269.0	34.7	2.82	3 #3 + 2 #8	52.5	54.6	1.04	
669		746	152.4	1357.2	5.06	268.2	29.5	2.83	4 #8 + 2 #3	53.2	52.0	0.98	
671		502	152.4	812.3	2.83	287.0	24.1	2.64	5 #8 + 2 #3	49.6	65.1	1.31	

No.	Lit.	Name	b	a	M/Vd	d	f_{cm}	ρ_s	Rebar	V_u	V_{cal}	V_{cal}/V_u	database
-	-	-	mm	mm	-	mm	MPa	%	Configuration	kN	kN	-	
673		504	150.9	813.7	2.98	273.1	24.9	2.81	6 #8 + 2 #3	62.1	62.5	1.01	
675	Kawano;	A-1a	105.0	900.0	3.00	300.0	23.6	1.28	2Ø16	34.0	35.6	1.05	d16,bw
676	Watanabe (1998)	A-1b	105.0	900.0	3.00	300.0	23.6	1.28	2Ø16	30.0	35.6	1.19	d16,bw
677		A-2a	176.0	1500.0	3.00	500.0	25.9	1.37	6Ø16	85.0	94.5	1.11	d16
678		A-2b	176.0	1500.0	3.00	500.0	25.9	1.37	6Ø16	104.0	94.5	0.91	d16
679		A-3a	350.0	2850.0	3.00	950.0	19.7	1.18	8Ø25	232.1	223.9	0.96	d25
680		A-3b	350.0	2850.0	3.00	950.0	19.6	1.18	8Ø25	253.6	223.6	0.88	d25
681		A-4a	600.0	6000.0	3.00	2000.0	21.1	1.20	15Ø35	721.4	561.0	0.78	
682		A-4b	600.0	6000.0	3.00	2000.0	21.9	1.20	15Ø35	670.9	567.7	0.85	
683	Kim,	CTL-1	170.0	810.0	3.00	270.0	49.4	1.87	3Ø19.1	71.3	73.2	1.03	kf,hsc
684	Park (1994)	CTL-2	170.0	810.0	3.00	270.0	49.4	1.87	3Ø19.1	72.3	73.2	1.01	kf,hsc
685		P1.0-1	170.0	816.0	3.00	272.0	49.4	1.01	3Ø14.1	58.9	61.6	1.05	kf,hsc
686		P1.0-2	170.0	816.0	3.00	272.0	49.4	1.01	3Ø14.1	57.1	61.6	1.08	kf,hsc
687		P3.4-1	170.0	801.0	3.00	267.0	49.4	3.35	3Ø25.4	78.7	85.6	1.09	kf,hsc,d25
688		P3.4-2	170.0	801.0	3.00	267.0	49.4	3.35	3Ø25.4	79.2	85.6	1.08	kf,hsc,d25
689		P4.6-1	170.0	765.0	3.00	255.0	49.4	4.68	4Ø25.4	90.4	94.6	1.05	kf,hsc,d25
690		P4.6-2	170.0	765.0	3.00	255.0	49.4	4.68	4Ø25.4	96.0	94.6	0.99	kf,hsc,d25
693		A4.5-1	170.0	1215.0	4.50	270.0	49.4	1.87	3Ø19.1	67.5	61.8	0.92	kf,hsc
694		A4.5-2	170.0	1215.0	4.50	270.0	49.4	1.87	3Ø19.1	64.7	61.8	0.96	kf,hsc
695		A6.0-1	170.0	1620.0	6.00	270.0	49.4	1.87	3Ø19.1	60.4	55.1	0.91	kf,hsc
696		A6.0-2	170.0	1620.0	6.00	270.0	49.4	1.87	3Ø19.1	62.2	55.1	0.89	kf,hsc
697		D142-1	170.0	426.0	3.00	142.0	49.4	1.87	3Ø13.9	41.2	46.1	1.12	kf,hsc
698		D142-2	170.0	426.0	3.00	142.0	49.4	1.87	3Ø13.9	39.5	46.1	1.16	kf,hsc
699		D550-1	300.0	1650.0	3.00	550.0	49.4	1.88	8Ø22.2	231.0	228.5	0.99	kf,hsc,d22
700		D550-2	300.0	1650.0	3.00	550.0	49.4	1.88	8Ø22.2	219.4	228.5	1.04	kf,hsc,d22
701		D915-1	300.0	2745.0	3.00	915.0	49.4	1.87	8Ø28.6	284.9	306.5	1.08	kf,hsc,d28
702		D915-2	300.0	2745.0	3.00	915.0	49.4	1.87	8Ø28.6	345.3	306.5	0.89	kf,hsc,d28
704	Kim W.;	2,5P1	100.0	625.0	2.50	250.0	18.6	1.08	1 #6	34.5	25.9	0.75	

No.	Lit.	Name	b	a	M/Vd	d	f_{cm}	ρ_s	Rebar	V_u	V_{cal}	V_{cal}/V_u	database
-	-	-	mm	mm	-	mm	MPa	%	Configuration	kN	kN	-	
705	Kim D.;	3P1	100.0	750.0	3.00	250.0	18.6	1.08	1 #6	28.1	24.1	0.86	bw
706	White R. (1997)	4P1	100.0	1000.0	4.00	250.0	18.6	1.08	1 #6	28.0	21.6	0.77	bw
708		2,5P2	100.0	625.0	2.50	250.0	18.6	1.93	1 #8	47.1	30.9	0.66	
709		3P2	100.0	750.0	3.00	250.0	18.6	1.93	1 #8	31.5	28.8	0.91	d25
710		4P2	100.0	1000.0	4.00	250.0	18.6	1.93	1 #8	32.2	25.9	0.80	d25
713		11A2	152.4	850.9	2.71	313.9	28.7	3.31	2 #10	74.4	73.2	0.98	
714		12A2	152.4	850.9	3.58	237.7	28.6	4.37	2 #10	64.7	58.7	0.91	d32
715		III-18A2	152.4	850.9	2.69	316.0	18.3	2.66	2 #9	64.0	61.3	0.96	
716		18B2	152.4	850.9	2.69	316.0	18.9	2.66	2 #9	73.0	61.8	0.85	
717		18C2	152.4	850.9	2.69	316.0	21.5	2.66	2 #9	73.9	64.2	0.87	
718		18D2	152.4	850.9	2.69	316.0	21.0	2.66	2 #9	60.9	63.7	1.05	
719		IV-13A2	152.4	850.9	2.67	319.0	18.9	0.80	1 #7	49.2	40.8	0.83	
720		14A2	152.4	850.9	3.50	242.8	19.7	1.05	1 #7	35.8	33.7	0.94	d22
721		15A2	152.4	850.9	2.69	316.0	19.1	1.33	1 #9	46.5	47.4	1.02	
722		15B2	152.4	850.9	2.69	316.0	19.7	1.33	1 #9	52.7	47.8	0.91	
723		16A2	152.4	850.9	3.55	239.8	21.1	1.75	1 #9	42.5	40.2	0.95	d28
724		17A2	152.4	850.9	3.50	242.8	20.9	2.10	2 #7	44.6	44.3	0.99	d22
725		18E2	152.4	850.9	2.69	316.0	18.8	2.66	2 #9	82.6	61.7	0.75	
726	Krefeld;	19A2	152.4	850.9	3.55	239.8	19.5	3.51	2 #9	46.8	49.9	1.07	d28
727	Thurston (1966)	20A2	152.4	850.9	3.58	237.7	20.0	4.37	2 #10	51.3	52.9	1.03	d32
728		21A2	203.2	850.9	3.58	237.7	18.9	4.92	3 #10	77.2	72.4	0.94	d32
730		2AC	152.4	1155.7	4.55	254.0	21.9	1.31	1 #8	38.3	35.6	0.93	d25,bw
731		3AC	152.4	1155.7	4.52	255.5	19.8	1.99	2 #7	45.1	40.3	0.89	d22
732		4AC	152.4	1155.7	4.55	254.0	15.7	2.62	2 #8	38.4	40.6	1.06	d25
733		5AC	152.4	1155.7	4.58	252.5	17.4	3.33	2 #9	42.7	44.6	1.04	d28
734		6AC	152.4	1155.7	4.61	250.4	21.7	4.15	2 #10	54.4	50.1	0.92	d32
737		3CC	152.4	1460.5	5.72	255.5	19.5	1.99	2 #7	36.5	36.7	1.01	d22
738		4CC	152.4	1460.5	5.75	254.0	19.5	2.62	2 #8	41.0	39.7	0.97	d25

No.	Lit.	Name	b	a	M/Vd	d	f_{cm}	ρ_s	Rebar	V_u	V_{cal}	V_{cal}/V_u	database
-	-	-	mm	mm	-	mm	MPa	%	Configuration	kN	kN	-	
739	Krefeld;	5CC	152.4	1460.5	5.78	252.5	19.3	3.33	2 #9	45.8	42.2	0.92	d28
740	Thurston (1966)	6CC	152.4	1460.5	5.83	250.4	19.5	4.15	2 #10	45.6	44.6	0.98	d32
742		4EC	152.4	1765.3	6.95	254.0	20.2	2.62	2 #8	42.6	37.4	0.88	d25
743		5EC	152.4	1765.3	6.99	252.5	18.5	3.33	2 #9	40.2	39.0	0.97	d28
744		6EC	152.4	1765.3	7.05	250.4	18.1	4.15	2 #10	42.9	40.8	0.95	d32
746		4GC	152.4	2070.1	8.15	254.0	20.0	2.62	2 #8	37.7	35.3	0.94	d25
747		5GC	152.4	2070.1	8.20	252.5	20.8	3.33	2 #9	42.6	38.2	0.90	d28
748		6GC	152.4	2070.1	8.27	250.4	20.3	4.15	2 #10	41.3	40.0	0.97	d32
753		VII-6C	152.4	850.9	3.37	252.5	19.1	3.33	2 #9	51.9	51.6	1.00	d28
754		VIII-3AAC	152.4	850.9	3.33	255.5	32.8	1.99	2 #7	56.4	52.7	0.93	d22
755		4AAC	152.4	850.9	3.35	254.0	27.7	2.62	2 #8	58.5	54.0	0.92	d25
756		5AAC	152.4	850.9	3.37	252.5	31.2	3.33	2 #9	57.6	59.5	1.03	
757		6AAC	152.4	850.9	3.40	250.4	32.7	4.15	2 #10	60.7	63.4	1.04	d32
758		3AC	152.4	1155.7	4.52	255.5	30.3	1.99	2 #7	54.1	45.7	0.84	d22
759		4AC	152.4	1155.7	4.55	254.0	29.0	2.62	2 #8	54.8	48.6	0.89	d25
760		5AC	152.4	1155.7	4.58	252.5	31.2	3.33	2 #9	55.3	52.9	0.96	d28
761		6AC	152.4	1155.7	4.61	250.4	32.4	4.15	2 #10	59.9	56.3	0.94	d32
762		4CC	152.4	1460.5	5.75	254.0	36.5	2.62	2 #8	53.7	47.8	0.89	d25
763		5CC	152.4	1460.5	5.78	252.5	35.6	3.33	2 #9	58.1	50.5	0.87	d28
764		6CC	152.4	1460.5	5.83	250.4	36.5	4.15	2 #10	63.8	53.6	0.84	d32
766		5EC	152.4	1765.3	6.99	252.5	35.6	3.33	2 #9	53.9	47.3	0.88	d28
767		6EC	152.4	1765.3	7.05	250.4	32.1	4.15	2 #10	50.0	48.4	0.97	d32
768		IX-3AAC	152.4	850.9	3.33	255.5	11.9	1.99	2 #7	41.1	39.2	0.95	d22
769		4AAC	152.4	850.9	3.35	254.0	12.3	2.62	2 #8	43.2	42.6	0.99	d25
770		5AAC	152.4	850.9	3.37	252.5	14.6	3.33	2 #9	51.0	47.8	0.94	d28
771		6AAC	152.4	850.9	3.40	250.4	12.7	4.15	2 #10	62.7	48.3	0.77	d32
772		3AC	152.4	1155.7	4.52	255.5	13.0	1.99	2 #7	37.5	35.7	0.95	d22
773		4AC	152.4	1155.7	4.55	254.0	12.3	2.62	2 #8	40.9	37.8	0.92	d25

No.	Lit.	Name	b	a	M/Vd	d	f_{cm}	ρ_s	Rebar	V_u	V_{cal}	V_{cal}/V_u	database
-	-	-	mm	mm	-	mm	MPa	%	Configuration	kN	kN	-	
774	Krefeld;	5AC	152.4	1155.7	4.58	252.5	14.6	3.33	2 #9	44.5	42.4	0.95	d28
775	Thurston (1966)	6AC	152.4	1155.7	4.61	250.4	11.8	4.15	2 #10	41.4	41.9	1.01	d32
776		3CC	152.4	1460.5	5.72	255.5	11.6	1.99	2 #7	31.8	31.5	0.99	d22
777		4CC	152.4	1460.5	5.75	254.0	16.2	2.62	2 #8	35.8	37.6	1.05	d25
778		5CC	152.4	1460.5	5.78	252.5	14.0	3.33	2 #9	35.6	38.3	1.08	d28
779		6CC	152.4	1460.5	5.83	250.4	13.0	4.15	2 #10	40.4	39.5	0.98	d32
782		X-C	203.2	1460.5	3.03	482.6	15.9	1.55	3 #8	86.8	87.5	1.01	d25
783		XI-PCA	152.4	1765.3	7.05	250.4	34.5	4.15	2 #10	53.9	49.4	0.92	d32
784		PCB	152.4	1765.3	7.05	250.4	34.5	4.15	2 #10	53.9	49.4	0.92	d32
785		s-I-OCa	152.4	1460.5	5.75	254.0	33.9	2.62	2 #8	49.1	46.7	0.95	d25
786		OCb	152.4	1460.5	5.75	254.0	37.1	2.62	2 #8	53.1	48.0	0.90	d25
787		s-II- Oca	254.0	1765.3	3.87	455.7	36.4	2.22	4 #9	150.0	133.7	0.89	d28
788		OCb	254.0	1765.3	3.87	455.7	36.4	2.22	4 #9	137.3	133.7	0.97	d28
791		C	140.0	500.0	2.50	200.0	18.6	0.56	2Ø10	26.9	27.0	1.01	
792		D	140.0	500.0	2.50	200.0	18.2	0.81	2Ø12	30.8	29.9	0.97	
793		E	140.0	500.0	2.50	200.0	17.9	1.10	2Ø14	43.4	32.5	0.75	
794		F	140.0	500.0	2.50	200.0	17.5	1.82	2Ø18	54.3	37.4	0.69	
795		D-1	140.0	500.0	2.50	200.0	20.6	0.81	2Ø12	43.3	31.0	0.72	
796		E-1	140.0	500.0	2.50	200.0	18.9	1.10	2Ø14	40.8	33.1	0.81	
799	Kuhlmann;	A6-L	402.0	715.0	2.86	250.0	47.1	1.56	5Ø20	199.9	149.7	0.75	
800	Ehmann (2001)	A6-R	402.0	1215.0	4.86	250.0	47.1	1.56	5Ø20	148.3	122.3	0.82	
801	Kuhlmann; Zilch;	B1/l	400.0	715.0	2.86	250.0	45.2	1.92	3Ø20 + 2Ø25	188.4	156.3	0.83	
802	Ehmann et. al. (2002)	B1/r	400.0	1215.0	4.86	250.0	45.2	1.92	3Ø20 + 2Ø25	151.7	127.8	0.84	
803		C3	400.0	965.0	3.86	250.0	41.3	1.57	5Ø20	139.7	127.7	0.91	
804		C6	400.0	965.0	3.86	250.0	42.1	1.57	5Ø20	140.0	128.4	0.92	
809		B4JL20-S	102.0	760.0	5.00	152.0	38.5	1.38	3 #3	19.7	21.4	1.09	
811		B3SE03-S	102.0	684.0	4.50	152.0	41.4	1.38	3 #3	23.2	22.9	0.99	
815		B3NO15-S	102.0	608.0	4.00	152.0	39.6	1.38	3 #3	22.8	23.8	1.04	

No.	Lit.	Name	b	a	M/Vd	d	f_{cm}	ρ_s	Rebar	V_u	V_{cal}	V_{cal}/V_u	database
-	-	-	mm	mm	-	mm	MPa	%	Configuration	kN	kN	-	
817		B3NO30-S	102.0	532.0	3.50	152.0	41.4	1.38	3 #3	24.4	25.6	1.05	
818		B3NO30-H	102.0	532.0	3.50	152.0	41.4	1.38	3 #3	27.5	25.6	0.93	
819	Laupa;	S1	152.4	1333.5	4.93	270.5	25.8	1.44	3 #5	38.2	41.5	1.09	d16,bw
820	Siess (1953)	S2	152.4	1295.4	4.82	268.7	25.6	2.09	3 #6	43.2	46.2	1.07	
821		S3	152.4	1295.4	4.89	265.2	30.7	2.51	2 #8	53.8	48.9	0.91	d25
822		S4	152.4	1295.4	4.92	263.4	29.3	3.20	2 #9	56.3	51.4	0.91	d28
823		S5	152.4	1295.4	4.95	261.9	28.4	3.97	2 #10	50.5	53.6	1.06	d32
824		S9	152.4	1295.4	4.76	272.3	14.0	0.92	3 #4	26.3	31.0	1.18	d12
825		S10	152.4	1295.4	4.82	268.7	14.9	1.39	2 #6	34.9	33.7	0.97	
826		S11	152.4	1295.4	4.85	267.0	14.0	1.91	2 #7	34.5	36.1	1.04	d22
827		S13	152.4	1295.4	4.95	261.9	24.9	3.97	2 #10	50.5	51.6	1.02	d32
828	Leonhardt;	P1	502.0	490.0	3.43	143.0	11.7	0.47	3Ø12	48.3	51.3	1.06	d12
829	Walther (1962)	P2	503.0	490.0	3.45	142.0	11.7	0.95	6Ø12	74.4	66.4	0.89	d12
830		P3	502.0	490.0	3.45	142.0	11.7	1.11	7Ø12	79.5	70.6	0.89	d12
831		P4	500.0	490.0	3.38	145.0	12.7	1.40	9Ø12	99.1	81.6	0.82	d12
832		P5	503.0	490.0	3.38	145.0	11.7	1.86	12Ø12	99.1	90.9	0.92	d12
833		P6	499.0	490.0	3.45	142.0	12.7	1.44	4Ø18	86.3	74.7	0.87	
834		P7	503.0	490.0	3.43	143.0	12.7	1.48	2Ø26	74.6	81.1	1.09	d25
835		P8	502.0	490.0	3.31	148.0	23.6	0.91	6Ø12	89.3	84.2	0.94	d12
836		P9	500.0	490.0	3.36	146.0	23.6	1.86	12Ø12	104.0	111.3	1.07	d12
837		P10	503.0	350.0	3.43	102.0	10.8	1.10	5Ø12	57.8	52.8	0.91	d12
838		P11	498.0	630.0	3.44	183.0	12.0	1.12	9Ø12	99.3	87.7	0.88	d12
847		5l	190.0	810.0	3.00	270.0	28.9	2.07	2Ø26	59.8	67.9	1.14	kf,hsc,d25
848		5r	190.0	810.0	3.00	270.0	28.9	2.07	2Ø26	75.8	67.9	0.90	kf,hsc,d25
849		6l	190.0	1100.0	4.07	270.0	28.9	2.07	2Ø26	59.7	60.6	1.01	kf,hsc,d25
851		7-1	190.0	1350.0	4.86	278.0	28.6	2.01	2Ø26	60.9	57.3	0.94	kf,hsc,d25
852		7-2	190.0	1350.0	4.86	278.0	28.6	2.01	2Ø26	67.0	57.3	0.86	kf,hsc,d25
853		8-1	190.0	1620.0	5.83	278.0	31.9	2.01	2Ø26	64.0	55.6	0.87	kf,hsc,d25

No.	Lit.	Name	b	a	M/Vd	d	f_{cm}	ρ_s	Rebar	V_u	V_{cal}	V_{cal}/V_u	database
-	-	-	mm	mm	-	mm	MPa	%	Configuration	kN	kN	-	
854	Leonhardt;	8-2	190.0	1620.0	5.91	274.0	31.9	2.04	2Ø26	64.2	55.1	0.86	kf,hsc,d25
859	Walther (1962)	EA1	190.0	750.0	2.78	270.0	19.4	1.89	2Ø24 + 1Ø6	59.2	63.8	1.08	127.6435245
860		EA2	190.0	750.0	2.78	270.0	19.4	1.88	3Ø16 + 2Ø14	75.5	71.3	0.95	142.6808432
861		D1/1	50.0	210.0	3.00	70.0	28.1	1.62	2Ø6	7.3	7.5	1.03	kf,hsc,sf
862		D1/2	50.0	210.0	3.00	70.0	28.1	1.62	2Ø6	7.2	7.5	1.04	kf,hsc,sf
863		D2/1	100.0	420.0	3.00	140.0	29.7	1.62	2Ø12	21.3	22.6	1.06	kf,hsc,sf,d12
864		D2/2	100.0	420.0	3.00	140.0	29.7	1.62	2Ø12	23.4	22.6	0.97	kf,hsc,sf,d12
865		D3/1	150.0	630.0	3.00	210.0	32.1	1.62	2Ø18	46.8	44.0	0.94	kf,hsc,sf
866		D3/2l	150.0	630.0	3.00	210.0	32.1	1.62	2Ø18	41.6	44.0	1.06	kf,hsc,sf
867		D3/2r	150.0	630.0	3.00	210.0	32.1	1.62	2Ø18	44.9	44.0	0.98	kf,hsc,sf
868		D4/1	200.0	840.0	3.00	280.0	32.8	1.68	2Ø24	75.1	71.6	0.95	kf,hsc,sf
869		D4/2l	200.0	840.0	3.00	280.0	32.8	1.68	2Ø24	75.0	71.6	0.95	kf,hsc,sf
870		D4/2r	200.0	840.0	3.00	280.0	32.8	1.68	2Ø24	69.6	71.6	1.03	kf,hsc,sf
871		C1	100.0	450.0	3.00	150.0	36.4	1.33	1Ø16	21.7	22.0	1.01	kf,hsc,sf,d16
872		C2	150.0	900.0	3.00	300.0	36.4	1.34	3Ø16	65.5	59.0	0.90	kf,hsc,sf,d17,bw
873		C3	200.0	1350.0	3.00	450.0	36.4	1.34	6Ø16	100.5	111.9	1.11	kf,hsc,sf,d18
874		C4	225.0	1800.0	3.00	600.0	36.4	1.34	9Ø16	150.8	142.6	0.95	kf,hsc,sf,d19
875		E6	190.0	750.0	2.78	270.0	26.9	2.40	2Ø20 + 3Ø16	92.0	81.1	0.88	
888	Marti;	PS6	400.0	640.0	3.83	167.0	27.9	1.84	8Ø14	113.4	94.5	0.83	
889	Pralong;	PS7	400.0	640.0	3.83	167.0	24.4	0.92	4Ø14	86.9	69.1	0.79	
890	Thürlimann (1977)	PS11	400.0	640.0	3.83	167.0	28.1	1.38	6Ø14	98.6	84.1	0.85	
907	Mathey;	IIIa-17	203.2	1524.0	3.78	402.8	27.8	2.54	2 #9 + 1 #10	90.4	94.5	1.04	kf,hsc
908	Watstein (1963)	IIIa-18	203.2	1524.0	3.78	402.8	23.9	2.54	2 #9 + 1 #10	83.1	90.5	1.09	kf,hsc
909		Va-19	203.2	1524.0	3.78	402.8	22.3	0.93	1 #5 + 2 #6	65.7	66.6	1.01	kf,hsc
910		Va-20	203.2	1524.0	3.78	402.8	24.3	0.93	1 #5 + 2 #6	68.3	68.3	1.00	kf,hsc
911		VIb-21	203.2	1143.0	2.84	402.8	24.8	0.84	2 #5 + 1 #6	73.3	75.6	1.03	
912		VIb-22	203.2	1143.0	2.84	402.8	24.5	0.84	2 #5 + 1 #6	64.3	75.3	1.17	
913		VIb-23	203.2	1143.0	2.84	402.8	29.0	0.84	2 #5 + 1 #6	77.0	79.2	1.03	

No.	Lit.	Name	b	a	M/Vd	d	f_{cm}	ρ_s	Rebar	V_u	V_{cal}	V_{cal}/V_u	database
-	-	-	mm	mm	-	mm	MPa	%	Configuration	kN	kN	-	
914	Mathey;	VIa-24	203.2	1524.0	3.78	402.8	25.0	0.47	3 #4	56.9	53.8	0.95	kf,hsc,d12
915	Watstein (1963)	VIa-25	203.2	1524.0	3.78	402.8	24.5	0.47	3 #4	52.3	53.5	1.02	kf,hsc,d12
929	Moody;	A1	177.8	774.7	2.96	261.6	28.8	2.17	1 #11	60.6	62.4	1.03	
930	Viest; Elstner;	A2	177.8	774.7	2.90	266.7	29.5	2.14	2 #8	67.3	65.2	0.97	
931	Hognestad (1954)	A3	177.8	774.7	2.89	268.0	29.5	2.23	2 #7 + 1 #6	76.2	69.5	0.91	
932		A4	177.8	774.7	2.87	270.0	29.9	2.37	4 #6	71.7	75.0	1.05	
933		B1	177.8	774.7	2.90	266.7	20.1	1.60	1 #8 + 2 #4	56.8	55.4	0.98	
934		B2	177.8	774.7	2.89	268.0	20.5	1.63	2 #7	60.6	54.4	0.90	
935		B3	177.8	774.7	2.87	270.0	18.3	1.60	2 #6 + 1 #5	56.1	55.5	0.99	
936		B4	177.8	774.7	2.85	271.5	15.9	1.64	4 #5	56.1	56.6	1.01	
937		C1	177.8	774.7	2.89	268.0	6.0	0.81	1 #7	20.6	29.0	1.41	
938		C2	177.8	774.7	2.85	271.8	5.8	0.82	2 #5	25.0	31.1	1.24	
939		C3	177.8	774.7	2.84	273.1	6.6	0.78	3 #4	25.9	34.0	1.31	
940		C4	177.8	774.7	2.82	274.3	6.4	0.81	2 #4 + 2 #3	25.7	35.9	1.40	
941		1	152.4	914.4	3.41	268.2	34.9	1.90	2 #7	58.8	54.2	0.92	d22
942		2	152.4	914.4	3.41	268.2	15.9	1.90	2 #7	36.6	43.1	1.18	d22
943		3	152.4	914.4	3.41	268.2	24.5	1.90	2 #7	53.3	48.9	0.92	d22
944		4	152.4	914.4	3.41	268.2	14.6	1.90	2 #7	41.5	42.1	1.01	d22
945		5	152.4	914.4	3.41	268.2	29.2	1.90	2 #7	53.1	51.4	0.97	d22
946		6	152.4	914.4	3.41	268.2	15.0	1.90	2 #7	35.5	42.4	1.19	d22
947		7	152.4	914.4	3.41	268.2	29.4	1.90	2 #7	52.2	51.5	0.99	d22
948		8	152.4	914.4	3.41	268.2	11.6	1.90	2 #7	32.2	39.3	1.22	d22
949		9	152.4	914.4	3.41	268.2	39.1	1.90	2 #7	54.4	56.1	1.03	d22
950		10	152.4	914.4	3.41	268.2	22.7	1.90	2 #7	49.9	47.8	0.96	d22
951		11	152.4	914.4	3.41	268.2	36.2	1.90	2 #7	61.1	54.8	0.90	d22
952		12	152.4	914.4	3.41	268.2	19.2	1.90	2 #7	48.2	45.5	0.95	d22
953		13	152.4	914.4	3.41	268.2	35.9	1.90	2 #7	56.6	54.7	0.97	d22
954		14	152.4	914.4	3.41	268.2	21.4	1.90	2 #7	44.2	47.0	1.06	d22

No.	Lit.	Name	b	a	M/Vd	d	f_{cm}	ρ_s	Rebar	V_u	V_{cal}	V_{cal}/V_u	database
-	-	-	mm	mm	-	mm	MPa	%	Configuration	kN	kN	-	
955		15	152.4	914.4	3.41	268.2	35.5	1.90	2 #7	52.2	54.5	1.04	d22
956		16	152.4	914.4	3.41	268.2	15.5	1.90	2 #7	38.8	42.8	1.10	d22
983	Morrow;	B40 B4	304.8	1104.9	3.00	368.3	33.0	1.89	2 #6 + 4 #7	157.6	148.3	0.94	
984	Viest (1957)	B56 B2	304.8	1511.3	4.10	368.3	14.0	1.89	2 #6 + 4 #7	102.6	100.7	0.98	
985		B56 E2	304.8	1511.3	4.10	368.3	14.0	0.58	2 #4 + 2 #5	82.1	67.7	0.82	
986		B56 A4	304.8	1511.3	4.03	374.7	23.7	2.45	2 #7 + 4 #8	140.4	128.8	0.92	
987		B56 B4	304.8	1511.3	4.10	368.3	25.9	1.89	2 #6 + 4 #7	124.8	120.4	0.96	
988		B56 E4	304.8	1511.3	4.10	368.3	27.0	1.27	5 #6	111.5	106.3	0.95	
989		B56 A6	308.1	1511.3	4.25	355.6	37.9	3.87	2 #8 + 5 #9	180.5	161.8	0.90	
990		B56 B6	304.8	1511.3	4.07	371.6	43.4	1.87	2 #6 + 4 #7	139.3	142.8	1.03	
991		B70 B2	304.8	1866.9	5.11	365.3	15.5	1.91	2 #6 + 4 #7	92.0	94.1	1.02	
992		B70 A4	304.8	1866.9	5.07	368.3	25.9	2.50	2 #7 + 4 #8	135.4	118.8	0.88	
993		B70 A6	304.8	1866.9	5.25	355.6	42.7	3.91	2 #8 + 5 #9	181.0	151.3	0.84	
994		B84 B4	304.8	2222.5	6.11	363.5	25.9	1.92	2 #6 + 4 #7	114.8	101.0	0.88	
995		B113 B4	304.8	2959.1	8.10	365.3	31.0	1.91	2 #6 + 4 #7	109.0	95.1	0.87	
996		B113 B4R	304.8	2959.1	8.03	368.3	27.3	1.89	2 #6 + 4 #7	89.2	92.2	1.03	
997	Mphonde;	AO-3-3b	152.4	1041.4	3.49	298.5	20.2	3.34	3 #8	65.3	61.0	0.94	kf,hsc,d25
998	Frantz (1984)	AO-3-3c	152.4	1041.4	3.49	298.5	26.4	2.33	2 #7 + 1 #6	67.5	60.2	0.89	kf,hsc
999		AO-7-3a	152.4	1041.4	3.49	298.5	36.7	3.34	3 #8	82.8	72.4	0.87	kf,hsc,d25
1000		AO-7-3b	152.4	1041.4	3.49	298.5	40.6	3.34	3 #8	83.5	74.5	0.89	kf,hsc,d25
1001		AO-11-3a	152.4	1041.4	3.49	298.5	73.0	3.34	3 #8	90.4	84.1	0.93	kf,hsc,d25
1002		AO-11-3b	152.4	1041.4	3.49	298.5	72.7	3.34	3 #8	90.0	84.0	0.93	kf,hsc,d25
1003		AO-15-3a	152.4	1041.4	3.49	298.5	79.3	3.34	3 #8	94.1	84.4	0.90	kf,hsc,d25
1004		AO-15-3b	152.4	1041.4	3.49	298.5	91.3	3.34	3 #8	100.7	84.9	0.84	kf,hsc,d25
1005		AO-15-3c	152.4	1041.4	3.49	298.5	89.5	3.34	3 #8	98.5	84.9	0.86	kf,hsc,d25
1025	Podgorniak-Stanik	BRL100	300.0	2662.5	2.88	925.0	89.3	0.51	2 M30	165.6	202.8	1.22	
1026	(1998)	BRH100	300.0	2662.5	2.97	895.0	89.3	3.14	12 M30	690.4	405.9	0.59	
1027		BN100	300.0	2662.5	2.88	925.0	35.2	0.76	3 M30	193.6	196.1	1.01	

No.	Lit.	Name	b	a	M/Vd	d	f_{cm}	ρ_s	Rebar	V_u	V_{cal}	V_{cal}/V_u	database
-	-	-	mm	mm	-	mm	MPa	%	Configuration	kN	kN	-	
1028		BH100	300.0	2662.5	2.88	925.0	94.1	0.76	4 M30	195.0	235.0	1.20	
1029		BN50	300.0	1312.5	2.92	450.0	35.2	0.81	2 M20 + 1 M25	132.4	123.9	0.94	
1030		BH50	300.0	1312.5	2.92	450.0	94.1	0.81	3 M20 + 1 M25	132.0	149.3	1.13	
1031		BN25	300.0	663.5	2.95	225.0	35.2	0.89	3 M15	73.0	79.3	1.09	
1032		BH25	300.0	663.5	2.95	225.0	94.1	0.89	3 M15	85.2	95.9	1.13	
1033		BN12.5	300.0	325.5	2.96	110.0	35.2	0.91	3 M10	40.2	48.3	1.20	
1044	Regan (1971)	R1	152.0	888.9	3.27	272.0	24.6	1.46	3Ø16	46.5	49.9	1.07	d16,bw
1045		R2	152.0	888.9	3.27	272.0	24.6	1.46	3Ø16	48.5	49.0	1.01	d16,bw
1046		R3	152.0	888.9	3.27	272.0	23.3	1.46	3Ø16	46.5	48.2	1.04	d16,bw
1050		R7	152.0	888.9	3.27	272.0	26.4	1.46	3Ø16	56.5	50.0	0.88	d16,bw
1051		R29	152.0	888.9	3.27	272.0	28.4	1.46	3Ø16	54.5	51.1	0.94	d16,bw
1053		N17	152.0	1525.0	5.61	272.0	31.7	1.46	3Ø16	82.9	42.0		bw
1054	Rehm; Eligehausen; Neubert (1978)	P 1	900.0	1000.0	3.19	313.0	22.5	1.21	36Ø11	333.1	334.8	1.01	
1055	Reineck;	N5	500.0	567.5	2.50	227.0	25.6	0.44	6Ø10	106.9	106.3	0.99	
1056	Koch;	N6	500.0	565.0	2.50	226.0	24.5	0.79	8Ø12	120.4	127.7	1.06	
1057	Schlaich (1978)	N7	500.0	562.5	2.50	225.0	23.4	1.39	10Ø14	142.4	154.8	1.09	
1058		N8	500.0	791.0	3.50	226.0	24.5	0.79	8Ø12	104.1	110.7	1.06	d12
1060	Remmel (1991)	2	150.0	504.9	3.06	165.0	80.8	1.87	3Ø14	48.2	49.2	1.02	
1061		3	150.0	660.0	4.00	165.0	80.8	1.87	3Ø14	46.7	44.2	0.95	
1063		5	150.0	489.6	3.06	160.0	80.3	4.09	2Ø25	60.4	59.5	0.98	d25
1064		6	150.0	640.0	4.00	160.0	80.3	4.09	2Ø25	58.0	54.3	0.94	d25
1069	Rosenbusch;	1.2 / 1	200.0	875.0	3.37	260.0	41.3	3.55	3Ø 28	91.2	89.2	0.98	d28
1073	Teutsch (2002)	2.6 / 1	200.0	1025.0	3.94	260.0	38.3	1.81	3Ø 20	75.9	67.5	0.89	
1074	Ruesch;	X	90.0	400.0	3.60	111.0	21.9	2.65	3Ø10.6	14.7	18.2	1.23	
1075	Haugli (1962)	Y	120.0	716.8	3.60	199.0	21.9	2.65	3Ø16.4	30.6	35.3	1.15	
1076		Z	180.0	947.2	3.62	262.0	23.0	2.64	3Ø23	56.0	61.6	1.10	
1079	Salandra;	LR-2.59-NS	101.6	444.1	2.59	171.5	52.0	1.45	2 #4	26.9	32.2	1.20	
1080	Ahmad (1989)	LR-3.63-NS	101.6	622.4	3.63	171.5	50.4	1.45	2 #4	22.1	27.7	1.25	d12

No.	Lit.	Name	b	a	M/Vd	d	f_{cm}	ρ_s	Rebar	V_u	V_{cal}	V_{cal}/V_u	database
-	-	-	mm	mm	-	mm	MPa	%	Configuration	kN	kN	-	
1083	Salandra;	HR-2.59-NS	101.6	444.1	2.59	171.5	64.7	1.45	2 #4	30.0	33.7	1.12	
1084	Ahmad (1989)	HR-3.63-NS	101.6	622.4	3.63	171.5	66.6	1.45	2 #4	20.3	29.3	1.44	d12
1086	Scholz (1994)	A-2	200.0	1116.0	3.00	372.0	76.6	0.81	3Ø16	85.3	89.2	1.05	d16
1087		A-3	200.0	1488.0	4.00	372.0	76.6	0.81	3Ø16	82.9	79.4	0.96	d16
1089		B-2	200.0	1104.0	3.00	368.0	80.3	2.00	3Ø25	127.3	114.8	0.90	d25
1090		B-3	200.0	1472.0	4.00	368.0	80.3	2.00	3Ø25	111.9	102.1	0.91	d25
1092		C-2	200.0	1098.0	3.00	366.0	79.7	3.36	4Ø28	123.3	136.7	1.11	d28
1093		C-3	200.0	1464.0	4.00	366.0	79.7	3.36	4Ø28	108.0	120.5	1.12	d28
1095		D-2	200.0	1086.0	3.00	362.0	92.0	1.94	7Ø16	123.3	127.8	1.04	d16
1096		D-3	200.0	1448.0	4.00	362.0	92.0	1.94	7Ø16	123.0	111.9	0.91	d16
1146	Taylor (1968)	1A	203.2	1117.6	3.02	369.9	27.4	1.03	2 #7	65.3	72.0	1.10	d22
1147		2A	203.2	1117.6	3.02	369.9	31.6	1.55	3 #7	95.1	88.5	0.93	d22
1148		3A	203.2	1117.6	3.02	369.9	30.0	1.03	2 #7	111.1	73.9	0.67	d22
1149		4A	203.2	1473.2	3.98	369.9	33.6	1.03	2 #7	94.7	68.7	0.73	d22
1151		6A	203.2	1295.4	3.50	369.9	26.4	1.03	2 #7	90.0	67.1	0.75	d22
1152		1B	203.2	1117.6	3.02	369.9	27.4	1.03	2 #7	79.0	72.0	0.91	d22
1153		2B	203.2	1117.6	3.02	369.9	31.6	1.55	3 #7	103.9	88.5	0.85	d22
1154		3B	203.2	1117.6	3.02	369.9	30.0	1.03	2 #7	79.5	73.9	0.93	d22
1155		4B	203.2	1473.2	3.98	369.9	33.6	1.03	2 #7	89.8	68.7	0.76	d22
1157		6B	203.2	1295.4	3.50	369.9	26.4	1.03	2 #7	81.1	67.1	0.83	d22
1158	Taylor (1972)	A1	400.0	2800.0	3.01	930.0	27.3	1.35	4Ø40	358.4	292.4	0.82	
1159		A2	400.0	2800.0	3.01	930.0	21.5	1.35	4Ø40	328.4	272.4	0.83	
1160		B1	200.0	1400.0	3.01	465.0	25.5	1.35	4Ø20	104.3	97.0	0.93	
1161		B2	200.0	1400.0	3.01	465.0	20.9	1.35	4Ø20	87.3	91.6	1.05	
1162		B3	200.0	1400.0	3.01	465.0	27.0	1.35	4Ø20	85.3	98.6	1.16	
1168	van den Berg (1962)	D-1	228.6	1257.3	3.50	359.2	39.6	4.32	7 #8	154.2	144.5	0.94	d25
1169		D-2	228.6	1257.3	3.50	359.2	34.1	4.32	7 #8	134.2	138.6	1.03	d25
1170		D-3	228.6	1257.3	3.50	359.2	28.7	4.32	7 #8	131.9	132.0	1.00	d25

No.	Lit.	Name	b	a	M/Vd	d	f_{cm}	ρ_s	Rebar	V_u	V_{cal}	V_{cal}/V_u	database
-	-	-	mm	mm	-	mm	MPa	%	Configuration	kN	kN	-	
1171	van den Berg (1962)	D-4	228.6	1257.3	3.50	359.2	28.2	4.32	7 #8	147.5	131.4	0.89	d25
1172		D-5	228.6	1257.3	3.50	359.2	34.1	4.32	7 #8	134.2	138.6	1.03	d25
1173		D-6	228.6	1257.3	3.50	359.2	32.8	4.32	7 #8	143.0	137.1	0.96	d25
1174		D-7	228.6	1257.3	3.50	359.2	25.6	4.32	7 #8	143.0	127.8	0.89	d25
1175		D-8	228.6	1257.3	3.50	359.2	20.3	4.32	7 #8	120.8	119.7	0.99	d25
1176		D-9	228.6	1257.3	3.50	359.2	12.0	4.32	7 #8	91.9	103.2	1.12	d25
1177		D-10	228.6	1257.3	3.50	359.2	21.2	4.32	7 #8	129.7	121.2	0.93	d25
1178		D-11	228.6	1257.3	3.50	359.2	15.2	4.32	7 #8	111.9	110.3	0.99	d25
1179		D-12	228.6	1257.3	3.50	359.2	18.5	4.32	7 #8	109.7	116.6	1.06	d25
1180		D-13	228.6	1257.3	3.50	359.2	16.5	4.32	7 #8	102.1	113.0	1.11	d25
1181		D-14	228.6	1257.3	3.50	359.2	19.0	4.32	7 #8	109.7	117.5	1.07	d25
1182		D-15	228.6	1257.3	3.50	359.2	17.7	4.32	7 #8	105.2	115.3	1.10	d25
1183		D-16	228.6	1257.3	3.50	359.2	20.6	4.32	7 #8	114.1	120.2	1.05	d25
1184		D-17	228.6	1257.3	3.50	359.2	17.6	4.32	7 #8	107.5	115.0	1.07	d25
1185		D-18	228.6	1257.3	3.50	359.2	19.4	4.32	7 #8	107.5	118.2	1.10	d25
1186		D-19	228.6	1257.3	3.50	359.2	21.8	4.32	7 #8	118.6	122.2	1.03	d25
1187		D-20	228.6	1257.3	3.50	359.2	19.2	4.32	7 #8	109.7	117.9	1.08	d25
1188		E-1	228.6	1524.0	4.24	359.2	52.2	4.32	7 #8	151.6	142.6	0.94	d25
1189		E-2	228.6	1524.0	4.24	359.2	37.5	4.32	7 #8	147.2	129.9	0.88	d25
1190		E-3	228.6	1524.0	4.24	359.2	32.9	4.32	7 #8	131.6	125.1	0.95	d25
1191		E-4	228.6	1524.0	4.24	359.2	28.8	4.32	7 #8	131.6	120.5	0.92	d25
1192		E-5	228.6	1524.0	4.24	359.2	15.9	4.32	7 #8	100.5	101.9	1.01	d25
1193		A4-1	228.6	990.6	2.76	359.2	34.6	4.32	7 #8	181.2	156.1	0.86	
1194		A4-2	228.6	1371.6	3.82	359.2	30.9	4.32	7 #8	136.2	129.3	0.95	d25
1195		A4-3	228.6	1447.8	4.03	359.2	33.2	4.32	7 #8	137.0	128.5	0.94	d25
1196		A4-4	228.6	1524.0	4.24	359.2	30.9	4.32	7 #8	137.6	122.9	0.89	d25
1197		A4-5	228.6	1257.3	3.50	359.2	31.4	4.32	7 #8	136.4	135.4	0.99	d25
1198		A4-6	228.6	1524.0	4.24	359.2	35.7	4.32	7 #8	145.0	128.0	0.88	d25

No.	Lit.	Name	b	a	M/Vd	d	f_{cm}	ρ_s	Rebar	V_u	V_{cal}	V_{cal}/V_u	database
-	-	-	mm	mm	-	mm	MPa	%	Configuration	kN	kN	-	
1199		A4-7	228.6	1257.3	3.50	359.2	40.0	4.32	7 #8	145.3	144.9	1.00	d25
1200		A4-8	228.6	1600.2	4.46	359.2	34.0	4.32	7 #8	127.1	123.4	0.97	d25
1201		A4-9	228.6	1676.4	4.67	359.2	37.8	4.32	7 #8	133.7	124.4	0.93	d25
1202		A4-10	228.6	1752.6	4.88	359.2	28.2	4.32	7 #8	124.7	112.0	0.90	d25
1204		A4-12	228.6	990.6	2.76	359.2	34.9	4.32	7 #8	181.2	156.5	0.86	
1205		A5-1	304.8	1257.3	3.50	359.2	35.3	3.24	7 #8	188.5	164.9	0.88	d25
1206		A5-2	228.6	1257.3	3.50	359.2	16.2	3.67	5 #5 + 4 #8	103.0	111.4	1.08	
1207		A5-3	228.6	1257.3	3.50	359.2	18.7	2.70	4 #5 + 5 #6	98.6	107.5	1.09	
1208		A5-4	228.6	1257.3	3.50	359.2	18.2	2.49	4 #6 + 2 #5 + 4 #4	98.6	105.8	1.07	
1209		A -5	228.6	990.6	2.76	359.2	19.8	1.77	7 #4 + 2 #6	105.5	108.2	1.02	
1210		A5-6	228.6	990.6	2.76	359.2	21.4	2.23	3 #6 + 3 #5 + 3 #4	123.3	118.1	0.96	
1211		A5-7	228.6	1257.3	2.81	448.1	21.0	3.46	7 #8	157.0	148.0	0.94	
1212	Walraven (1978)	A1	200.0	375.0	3.00	125.0	22.9	0.83	2Ø10 + 1Ø8	30.3	30.5	1.01	kf,hsc,lwar,sf
1213		A2	200.0	1260.0	3.00	420.0	22.9	0.74	1Ø20 + 2Ø14	72.8	70.3	0.97	kf,hsc,lwar,sf
1214		A3	200.0	2160.0	3.00	720.0	23.2	0.79	3Ø22	105.8	98.9	0.94	kf,hsc,lwar,d22,sf
1226	Xie; Ahmad;	NNN-3	127.0	631.8	2.93	215.9	36.5	2.08	2 #6	36.9	43.8	1.19	
1229	Yu (1994)	NHN-3	127.0	631.8	2.93	215.9	95.9	2.08	2 #6	46.0	52.1	1.13	
1230	Yoon;	N1-S	375.0	2112.5	3.23	655.0	34.2	2.88	10 Ø30	256.4	315.3	1.23	
1231	Cook;	M1-S	375.0	2112.5	3.23	655.0	63.7	2.88	10 Ø30	303.4	365.8	1.21	
1232	Mitchell (1996)	H1-S	375.0	2112.5	3.23	655.0	82.7	2.88	10 Ø30	334.4	361.5	1.08	
1233	Yoshida; Bentz; Collins (2000)	YB2000/0	300.0	5327.0	2.82	1890.0	31.9	0.74	6 M30	289.4	257.6	0.89	
1234	Lubell (2006)	AW1	1170.0	1773.8	3.30	538.0	35.1	0.79	10 M25	604.3	512.6	0.85	d25
1235		AW4	1168.0	1773.8	3.51	506.0	37.9	1.69	20 M25	744.6	656.9	0.88	d25
1236		AW8	1169.0	1812.0	3.57	507.0	37.4	1.69	21 M25	819.3	647.2	0.79	d25
1237		AX6	703.0	1002.0	3.48	288.0	39.0	1.73	7 M25	282.5	256.2	0.91	d25
1238		AX7	704.0	1002.0	3.49	287.0	39.0	1.04	7 M20	250.5	219.5	0.88	bw
1239		AX8	705.0	1002.0	3.47	289.0	39.0	1.72	7 M25	272.0	257.3	0.95	d25
1241	Sherwood (2008)	L-10N1	300.0	4012.0	2.87	1400.0	36.5	0.83	3 + 2 Ø 30	270.6	245.1	0.91	hsc

No.	Lit.	Name	b	a	M/Vd	d	f_{cm}	ρ_s	Rebar	V_u	V_{cal}	V_{cal}/V_u	database
-	-	-	mm	mm	-	mm	MPa	%	Configuration	kN	kN	-	
1242	Sherwood;	L-10N2	300.0	4012.0	2.87	1400.0	38.3	0.83	3 + 2 Ø 30	247.9	248.7	1.00	hsc
1243	Bentz;	L-10H	300.0	4012.0	2.87	1400.0	69.9	0.83	3 + 2 Ø 30	240.4	285.9	1.19	hsc
1244	Collins (2007)	L-20N1	300.0	4012.0	2.87	1400.0	29.8	0.83	3 + 2 Ø 30	268.4	230.9	0.86	hsc
1245		L-20N2	300.0	4012.0	2.87	1400.0	31.5	0.83	3 + 2 Ø 30	272.5	234.7	0.86	hsc
1246		L-40N1	300.0	4012.0	2.87	1400.0	26.7	0.83	3 + 2 Ø 30	245.0	223.4	0.91	hsc
1247		L-40N2	300.0	4012.0	2.87	1400.0	27.1	0.83	3 + 2 Ø 30	290.7	224.3	0.77	hsc
1248		L-50N1	300.0	4012.0	2.87	1400.0	39.0	0.83	3 + 2 Ø 30	274.3	250.0	0.91	hsc
1249		L-50N2	300.0	4012.0	2.87	1400.0	38.1	0.83	3 + 2 Ø 30	299.1	248.3	0.83	hsc
1250		L-50N2R	300.0	4012.0	2.87	1400.0	38.1	0.83	3 + 2 Ø 30	331.2	248.3	0.75	hsc
1251		S-10N1	122.0	779.5	2.78	280.0	39.8	0.83	2 *2 # 3	36.7	44.9	1.22	hsc,bw
1252		S-10N2	122.0	779.5	2.78	280.0	39.8	0.83	2 *2 # 3	38.3	44.9	1.17	hsc,bw
1253		S-10H	122.0	779.5	2.78	280.0	73.4	0.83	2 *2 # 3	37.7	50.8	1.35	hsc
1254		S-20N1	122.0	779.5	2.78	280.0	37.2	0.83	2 *2 # 3	39.2	44.0	1.12	hsc,bw
1255		S-20N2	122.0	779.5	2.78	280.0	36.2	0.83	2 *2 # 3	38.3	43.7	1.14	hsc,bw
1256		S-40N1	122.0	779.5	2.78	280.0	27.6	0.83	2 *2 # 3	41.7	40.4	0.97	hsc,bw
1257		S-40N2	122.0	779.5	2.78	280.0	27.6	0.83	2 *2 # 3	34.9	40.4	1.16	hsc,bw
1258		S-50N1	122.0	779.5	2.78	280.0	41.3	0.83	2 *2 # 3	38.5	45.4	1.18	hsc
1259		S-50N2	122.0	779.5	2.78	280.0	41.3	0.83	2 *2 # 3	40.6	45.4	1.12	hsc
1262	Thiele (2010)	T1_ohne	400.0	1030.0	4.15	248.0	24.3	0.93	8 Ø 12	107.4	95.9	0.89	
1263		T7_70_oben	400.0	1030.0	3.47	297.0	23.4	1.35	8 Ø 16	130.9	129.3	0.99	d16,bw
1264		T9_ohne	400.0	830.0	4.97	167.0	39.7	2.41	8 Ø 16	112.2	101.9	0.91	d16
1265		T13_ohne	400.0	830.0	3.82	217.0	40.4	1.85	8 Ø 16	127.8	127.2	0.99	d16
1266		T10_40_oben	400.0	830.0	4.97	167.0	39.7	2.41	8 Ø 16	102.4	101.9	1.00	d16
1267	Injaganeri (2007)	H20-0-0	150.0	464.3	2.88	161.0	47.9	2.50	3 Ø 16	56.2	49.6	0.88	
1268		H40-0-0	150.0	1016.3	2.95	345.0	55.6	2.33	6 Ø 16	120.8	97.8	0.81	
1269		H60-0-0	150.0	1589.3	2.97	536.0	55.6	3.13	8 Ø 20	171.8	152.9	0.89	
1270	Winkler (2011)	SB 2	150.0	781.8	3.91	200.0	33.3	1.19	(2 Ø10 +1 Ø8) + 3 Ø8	42.0	41.0	0.98	
1271		SB 3	150.0	1175.0	3.92	300.0	33.3	1.18	(2 Ø12 +1 Ø10) + 2 Ø12	52.4	54.9	1.05	bw

No.	Lit.	Name	b	a	M/Vd	d	f_{cm}	ρ_s	Rebar	V_u	V_{cal}	V_{cal}/V_u	database
-	-	-	mm	mm	-	mm	MPa	%	Configuration	kN	kN	-	
1272	Winkler (2011)	SB 4	225.0	1768.8	3.93	450.0	33.3	1.20	6 Ø12 + (2 Ø12+4 Ø10)	93.4	104.8	1.12	
1273		SB 5	300.0	2362.5	3.94	600.0	33.3	1.20	(6 Ø16 +1 Ø10) + (2 Ø16+6 Ø10)	165.7	158.9	0.96	
1274		SB 6	450.0	3550.0	3.94	900.0	33.3	1.20	10 Ø20 +(4 Ø20+3 Ø14)	304.2	291.9	0.96	
1281	Rosenbusch (2003)	1.1-1	200.0	875.0	3.37	260.0	41.3	0.65	4 Ø22	50.6	43.7	0.86	
1282		2.1-1	200.0	875.0	3.37	260.0	41.3	3.55	4 Ø28	91.1	85.2	0.94	d28
1283	Tureyen;	V-S-1	457.2	1181.1	3.28	360.4	38.9	0.96	8 #5	179.1	179.1	1.00	d16
1284	Frosch (2002)	V-S-2	457.2	1181.1	3.28	360.4	39.3	1.92	16 #5	203.0	244.9	1.21	d16
1286	Bentz;	SBB1.1	104.0	235.0	2.80	84.0	33.8	1.63	2 #3	14.5	17.2	1.19	
1287	Buckley (2005)	SBB1.2	105.0	235.0	2.80	84.0	33.8	1.61	2 #3	18.5	17.3	0.93	
1288		SBB1.3	104.0	235.0	2.80	84.0	33.8	1.63	2 #3	15.0	17.2	1.15	
1289		SBB2.1	106.0	482.5	2.87	168.0	32.6	1.59	2 x 2 #3	28.9	32.4	1.12	
1290		SBB2.2	105.0	482.5	2.87	168.0	32.6	1.61	2 x 2 #3	30.6	32.3	1.05	
1291		SBB2.3	106.0	482.5	2.91	166.0	32.6	1.61	2 x 2 #3	29.8	32.1	1.07	
1292		SBB3.1	105.0	977.5	2.94	333.0	34.3	1.55	2 #3 + 2 M15	42.5	50.8	1.19	
1293		SBB3.2	101.0	977.5	2.94	333.0	34.3	1.61	2 #3 + 2 M15	41.0	49.7	1.21	
1294		SBB3.3	101.0	977.5	2.94	333.0	34.3	1.61	2 #3 + 2 M15	43.3	49.7	1.15	
1358	Sneed (2007);	1-1	304.8	679.5	2.91	233.3	62.8	1.20	3 #6	131.1	107.6	0.82	
1359	Sneed, Ramirez (2008);	1-2	306.3	1536.7	2.89	531.7	62.8	1.24	4 #8	139.3	200.9	1.44	
1360	Sneed, Ramirez (2010)	1-3	304.8	1965.3	2.89	681.0	61.8	1.24	4 #9	146.5	237.4	1.62	
1361		1-4	306.3	2374.9	2.89	822.1	71.0	1.60	4 #10	165.2	305.8	1.85	
1362		2-1	203.2	679.5	2.89	234.9	65.1	1.24	3 #5	57.3	76.2	1.33	
1363		2-2	407.9	1536.7	2.92	527.1	61.6	1.20	4 #9	155.0	253.9	1.64	
1364		2-3	508.0	1965.3	2.87	684.2	64.7	1.30	7 #9	260.8	405.9	1.56	
1365		2-4	612.9	2374.9	2.90	820.3	69.3	1.60	8 #10	344.2	610.2	1.77	

Table III.2. Collection of shear tests with point loads not included in ACI-DAFStb

No.	Author	Name	b	d	M/Vd	d_a	$f_{c,cyl}$	ρ_s	Reinforcement Configuration	V_u	V_{cal}	V_{cal}/V_u	database
-	-	-	mm	mm	-	mm	MPa	%		kN	kN	-	
1	Thorenfeldt;	B11	150	663.0	3	221	54.0	1.82	2Ø16	58.01	57.97	1.00	kf,hsc
2	Drangshold (1990)	B13	150	828.0	4	207	54.0	3.23	5Ø16	70.48	61.96	1.14	kf,hsc
3		B14	150	621.0	3	207	54.0	3.23	5Ø16	82.59	70.69	1.17	kf,hsc
4		B21	150	663.0	3	221	77.8	1.82	5Ø16	67.96	60.52	1.12	kf,hsc
5		B23	150	828.0	4	207	77.8	3.23	5Ø16	77.94	64.39	1.21	kf,hsc
6		B24	150	621.0	3	207	77.8	3.23	5Ø16	82.59	73.36	1.13	kf,hsc
7		B43	150	828.0	4	207	86.4	3.23	5Ø16	86.01	64.63	1.33	kf,hsc
8		B44	150	621.0	3	207	86.4	3.23	5Ø16	107.12	73.59	1.46	kf,hsc
9		B51	150	663.0	3	221	97.7	1.82	3Ø16	56.02	61.23	0.91	kf,hsc
10		B53	150	828.0	4	207	97.7	3.23	5Ø16	76.69	64.91	1.18	kf,hsc
11		B54	150	621.0	3	207	97.7	3.23	5Ø16	77.63	73.87	1.05	kf,hsc
12		B61	300	1326.0	3	442	77.7	1.82	3Ø32	180.34	182.90	0.99	kf,hsc
13		B63	300	1656.0	4	414	77.7	3.23	5Ø32	222.32	190.34	1.17	kf,hsc
14		B64	300	1242.0	3	414	77.7	3.23	5Ø32	280.69	215.34	1.30	kf,hsc
15	Bhal (1967)	B1	240	891.0	3	297	24.2	1.29	2Ø24	71.28	74.29	0.96	kf,hsc,sf
16		B2	240	1800.0	3	600	30.9	1.28	4Ø24	119.52	142.02	0.84	kf,hsc,sf
17		B3	240	2700.0	3	900	28.7	1.28	6Ø24	164.16	172.98	0.95	kf,hsc,sf
18		B4	240	3600.0	3	1200	26.4	1.28	8Ø24	181.44	190.61	0.95	kf,hsc,sf
19		B5	240	1800.0	3	600	27.8	0.64	2Ø24	106.56	103.32	1.03	kf,hsc,sf
20		B6	240	1800.0	3	600	25.8	0.60	8Ø12	113.76	93.17	1.22	kf,hsc,sf
21		B7	240	2700.0	3	900	28.5	0.64	3Ø24	138.24	128.95	1.07	kf,hsc,sf
22		B8	240	2700.0	3	900	26.3	0.64	12Ø12	127.63	116.47	1.10	sf
23		s1_1	150	660.0	4	165	85.1	1.87	3Ø14	46.28	44.35	1.04	kf,hsc
24		s1_2	150	504.9	3.06	165	85.1	1.87	3Ø14	48.02	49.37	0.97	kf,hsc
25		s1_3	150	640.0	4	160	87.4	4.09	3Ø20	57.60	55.23	1.04	kf,hsc
26		s1_4	150	489.6	3.06	160	87.4	4.09	3Ø20	60.24	61.41	0.98	kf,hsc
27		s1.1	300	570.7	3.73	153	90.1	1.34	3Ø16	70.23	75.69	0.93	kf,hsc
28		s1.2	300	570.0	3.75	152	91.2	2.21	3Ø20	75.24	89.27	0.84	kf,hsc

No.	Lit.	Name	b	a	M/Vd	d	f_{cm}	ρ_s	Rebar	V_u	V_{cal}	V_{cal}/V_u	database
-	-	-	mm	mm	-	mm	MPa	%	Configuration	kN	kN	-	
29	Bhal (1967)	s1.3	300	569.4	3.9	146	93.7	4.22	3Ø28	98.55	110.63	0.89	kf,hsc
30		s2.1	300	1228.5	3.51	350	94.4	0.60	3Ø16	126.00	107.83	1.17	kf,hsc
31		s2.2	300	1231.9	3.54	348	91.3	1.88	3Ø28	191.05	150.86	1.27	kf,hsc
32		S2.3	300	1231.9	3.54	348	93.7	0.94	3Ø20	124.24	122.24	1.02	kf,hsc
33		s2.4	300	1230.0	3.75	328	94.1	3.76	3Ø40	230.26	173.42	1.33	kf,hsc
34		s3.1	300	4132.5	5.51	750	91.3	0.42	3Ø20	137.25	126.59	1.08	kf,hsc
35		s3.2	300	2627.9	3.66	718	93.7	1.72	3Ø40	258.48	233.81	1.11	kf,hsc
36		s3.3	300	2633.4	3.53	746	94.4	0.83	3Ø28	201.42	199.60	1.01	kf,hsc
37		s3.4	300	2628.9	3.81	690	94.1	3.57	3Ø56	380.88	272.49	1.40	kf,hsc
38		s4.1	300	570.7	3.73	153	110.9	1.34	3Ø16	74.36	77.59	0.96	kf,hsc
39		s4.2	300	570.0	3.75	152	110.9	2.21	3Ø20	90.29	91.62	0.99	kf,hsc
40		s4.3	300	569.4	3.9	146	110.9	4.22	3Ø28	122.20	113.75	1.07	kf,hsc
41	Janaka-Perera;	NSC40-I	200	750.0	3	250	38.0	2.95	3Ø25	75.00	84.32	0.89	hsc
42	Mutsuyoshi (2013)	NSC40-II	200	875.0	3.5	250	38.0	2.95	3Ø25	78.00	79.18	0.99	hsc
43		NSC40-III	200	1000.0	4	250	36.0	2.95	3Ø25	76.50	73.90	1.04	hsc
44		HA100-I	200	750.0	3	250	133.0	2.95	3Ø25	85.50	101.73	0.84	hsc
45		HA100-II	200	875.0	3.5	250	116.0	2.95	3Ø25	85.00	94.93	0.90	hsc
46		HA100-III	200	1000.0	4	250	114.0	2.95	3Ø25	85.00	90.21	0.94	hsc
47		HA120	200	1000.0	4	250	138.0	2.95	3Ø25	82.50	91.76	0.90	hsc
48		HA160-I	200	1000.0	4	250	165.0	2.95	3Ø25	81.00	93.31	0.87	hsc
49		HA160-II	200	1000.0	4	250	194.0	2.95	3Ø25	77.00	94.83	0.81	hsc
50		HA160-III	200	1000.0	4	250	183.0	2.95	3Ø25	75.00	94.27	0.80	hsc
51		LA120	200	1000.0	4	250	155.0	2.95	3Ø25	120.50	92.76	1.30	hsc
52	Matsui;	A1	100	450.0	3	150	32.3	2.65	2#5	27.44	28.12	0.98	hsc
53	Yuichi et.al. (1995)	A2	100	450.0	3	150	32.3	2.65	2#5	26.46	28.12	0.94	hsc
54		B1	100	450.0	3	150	38.3	2.65	2#5	29.30	29.52	0.99	hsc
55		B2	100	450.0	3	150	38.3	2.65	2#5	27.44	29.52	0.93	hsc
56		C1	100	450.0	3	150	48.6	2.65	2#5	29.60	31.61	0.94	hsc

No.	Lit.	Name	b	a	M/Vd	d	f_{cm}	ρ_s	Rebar	V_u	V_{cal}	V_{cal}/V_u	database
-	-	-	mm	mm	-	mm	MPa	%	Configuration	kN	kN	-	
57	Matsui;	C2	100	450.0	3	150	48.6	2.65	2#5	32.24	31.61	1.02	hsc
58	Yuichi et.al. (1995)	D1	100	450.0	3	150	70.9	2.65	2#5	33.32	33.92	0.98	hsc
59		D2	100	450.0	3	150	70.9	2.65	2#5	33.91	33.92	1.00	hsc
60		E1	100	450.0	3	150	83.3	2.65	2#5	38.22	34.28	1.12	hsc
61		E2	100	450.0	3	150	83.3	2.65	2#5	42.43	34.28	1.24	hsc
62		F1	100	450.0	3	150	127.4	2.65	2#5	34.40	35.32	0.97	hsc
63		L1	100	675.0	3	225	124.4	2.55	2#6	43.51	46.17	0.94	hsc
64		L2	100	675.0	3	225	124.4	2.55	2#6	40.96	46.17	0.89	hsc
65		M1	100	787.5	3.5	225	124.4	2.55	2#6	43.32	43.38	1.00	hsc
66		M2	100	787.5	3.5	225	124.4	2.55	2#6	43.71	43.38	1.01	hsc
67		N1	100	900.0	4	225	124.4	2.55	2#6	41.26	41.14	1.00	hsc
68		N2	100	900.0	4	225	124.4	2.55	2#6	38.81	41.14	0.94	hsc
69		S1	100	900.0	3	300	127.4	2.58	2#7	51.35	56.57	0.91	hsc

Table III.3. Collection of shear tests with point loads on lightweightaggregate concrete beams

No.	Lit.	Name	b	a	M/Vd	d	f_{cm}	ρ_s	Rebar	V_u	V_{cal}	V_{cal}/V_u	database
-	-	-	mm	mm	-	mm	MPa	%	Configuration	kN	kN		
1	Walraven (1978)	B1	200.0	375	3.00	125.0	32.0	0.83	2Ø10 + 1Ø8	29.8	29.9	0.99	lwa,sf***
2		B2	200.0	1260	3.00	420.0	32.0	0.56	1Ø20 + 2Ø14	60.5	59.9	1.01	lwa,sf***
3		B3	200.0	2160	3.00	720.0	29.5	0.79	3Ø22	79.2	92.9	0.85	lwa,sf***
4		C1	200.0	375	3.00	125.0	33.3	1.52	2Ø12 + 1Ø14	35.0	36.4	0.96	lwa,sf***
5		C2	200.0	1260	3.11	405.0	33.3	1.56	1Ø18 + 5Ø16	86.7	90.9	0.95	lwa,sf***
6		C3	200.0	2160	3.09	700.0	30.7	1.58	1Ø20 + 5Ø22	106.4	122.9	0.87	lwa,sf***
7	Taylor;	A1	190.5	711	3.22	220.7	27.5	1.88	4#5**	48.3	59.68	0.81	lwar
8	Brewer (1963)	A2	190.5	711	3.22	220.7	30.0	1.88	4#5**	45.8	61.22	0.75	lwar
9		A3	190.5	711	3.22	220.7	27.5	1.88	4#5**	46.3	59.68	0.78	lwar
10		A4	190.5	711	3.22	220.7	28.4	1.88	4#5**	39.9	60.23	0.66	lwar
11		A5	190.5	711	3.22	220.7	36.7	1.88	4#5**	53.3	64.87	0.82	lwar
12		A6	190.5	711	3.22	220.7	33.3	1.88	4#5**	49.3	63.07	0.78	lwar
13		A7	190.5	711	3.22	220.7	33.3	1.88	4#5**	49.3	63.07	0.78	lwar
14		A8	190.5	711	3.22	220.7	37.2	1.88	4#5**	43.3	65.11	0.67	lwar
15		A9	190.5	711	3.20	222.3	28.4	1.20	4#4	46.3	53.27	0.87	lwar
16		A10	190.5	711	3.20	222.3	30.0	1.20	4#4	40.4	54.16	0.75	lwar
17		A11	215.9	711	3.20	222.3	36.7	1.06	4#4	49.8	61.59	0.81	lwar
18		A12	241.3	711	3.20	222.3	37.2	0.94	4#4	45.8	65.88	0.70	lwar
19		B1	190.5	711	3.22	220.7	23.9	1.88	4#5**	37.9	50.6	0.75	lwa
20		B2	190.5	711	3.22	220.7	23.9	1.88	4#5**	37.9	50.6	0.75	lwa
21		B3	190.5	711	3.22	220.7	23.9	1.88	4#5**	36.9	50.6	0.73	lwa
22		B4	190.5	711	3.22	220.7	26.6	1.88	4#5**	39.4	52.3	0.75	lwa
23		B5	190.5	711	3.22	220.7	35.8	1.88	4#5**	42.3	56.9	0.74	lwa
24		B6	190.5	711	3.22	220.7	34.7	1.88	4#5**	47.3	56.4	0.84	lwa
25		B7	190.5	711	3.22	220.7	34.7	1.88	4#5**	37.9	56.4	0.67	lwa
26		B8	190.5	711	3.22	220.7	37.6	1.88	4#5**	39.9	57.7	0.69	lwa
27		B9	190.5	711	3.20	222.3	26.6	1.20	4#4	34.4	46.1	0.75	lwa
28		B10	190.5	711	3.20	222.3	23.9	1.20	4#4	35.9	44.7	0.80	lwa

No.	Lit.	Name	b	a	M/Vd	d	f_{cm}	ρ_s	Rebar	V_u	V_{cal}	V_{cal}/V_u	database
-	-	-	mm	mm	-	mm	MPa	%	Configuration	kN	kN		
29	Taylor;	B11	215.9	711	3.20	222.3	35.8	1.06	4#4	35.4	54.0	0.66	lwa
30	Brewer (1963)	B12	241.3	711	3.20	222.3	37.6	0.94	4#4	38.4	58.4	0.66	lwa
31		C1	190.5	711	3.22	220.7	24.9	1.88	4#5**	37.4	51.2	0.73	lwa
32		C2	190.5	711	3.22	220.7	26.4	1.88	4#5**	41.8	52.1	0.80	lwa
33		C3	190.5	711	3.22	220.7	24.9	1.88	4#5**	42.3	51.2	0.83	lwa
34		C4	190.5	711	3.22	220.7	25.9	1.88	4#5**	41.8	51.8	0.81	lwa
35		C5	190.5	711	3.22	220.7	32.4	1.88	4#5**	46.8	55.3	0.85	lwa
36		C6	190.5	711	3.22	220.7	37.0	1.88	4#5**	51.3	57.4	0.89	lwa
37		C7	190.5	711	3.22	220.7	37.0	1.88	4#5**	46.3	57.4	0.81	lwa
38		C8	190.5	711	3.22	220.7	32.9	1.88	4#5**	45.8	55.5	0.83	lwa
39		C9	190.5	711	3.20	222.3	25.9	1.20	4#4	37.4	45.7	0.82	lwa
40		C10	190.5	711	3.20	222.3	26.4	1.20	4#4	36.4	46.0	0.79	lwa
41		C11	215.9	711	3.20	222.3	32.4	1.06	4#4	39.4	52.4	0.75	lwa
42		C12	241.3	711	3.20	222.3	32.9	0.94	4#4	41.8	56.2	0.74	lwa
43	Hanson (1961)	2B4	152.4	1118	4.19	266.7	34.1	1.25	4#4	25.6	41.8	0.61	lwa
44		3B4	152.4	1118	4.19	266.7	30.3	1.25	4#4	25.7	40.5	0.64	lwa
45		4B4	152.4	1118	4.19	266.7	35.3	1.25	4#4	29.2	42.3	0.69	lwa
46		6B4	152.4	1118	4.19	266.7	33.4	1.25	4#4	28.9	41.6	0.69	lwa
47		10B4	152.4	1118	4.19	266.7	33.4	1.25	4#4	27.6	41.6	0.66	lwa
48		13B4	152.4	1118	4.19	266.7	35.5	1.25	4#4	29.4	42.3	0.69	lwa
49		10BW4	152.4	1118	4.19	266.7	31.2	1.25	4#4	25.8	40.8	0.63	lwa
50		2B2	152.4	1118	4.19	266.7	33.6	2.49	2#8	33.4	47.8	0.70	lwa
51		3B2	152.4	1118	4.19	266.7	31.3	2.49	2#8	35.6	46.8	0.76	lwa
52		4B2	152.4	1118	4.19	266.7	35.2	2.49	2#8	35.6	48.5	0.73	lwa
53		5B2	152.4	1118	4.19	266.7	34.0	2.49	2#8	44.0	48.0	0.92	lwa
54		6B2	152.4	1118	4.19	266.7	34.5	2.49	2#8	37.8	48.2	0.78	lwa
55		7B2	152.4	1118	4.19	266.7	34.2	2.49	2#8	48.9	48.1	1.02	lwa
56		10B2	152.4	1118	4.19	266.7	30.5	2.49	2#8	37.0	46.5	0.80	lwa

No.	Lit.	Name	b	a	M/Vd	d	f_{cm}	ρ_s	Rebar	V_u	V_{cal}	V_{cal}/V_u	database
-	-	-	mm	mm	-	mm	MPa	%	Configuration	kN	kN		
57	Hanson (1961)	13B2	152.4	1118	4.19	266.7	34.9	2.49	2#8	38.4	48.4	0.79	lwa
58		2B3	152.4	559	2.10	266.7	33.0	1.25	4#4	59.9	56.4	1.06	lwa
59		6B3	152.4	559	2.10	266.7	33.2	1.25	4#4	42.3	56.5	0.75	lwa
60		7B3	152.4	559	2.10	266.7	33.6	1.25	4#4	55.6	56.7	0.98	lwa
61		13B3	152.4	559	2.10	266.7	34.6	1.25	4#4	57.8	57.2	1.01	lwa
62		2A1	152.4	559	2.10	266.7	25.4	2.49	2#8	82.3	57.9	1.42	lwa
63		3A1	152.4	559	2.10	266.7	22.8	2.49	2#8	44.0	56.1	0.78	lwa
64		4A1	152.4	559	2.10	266.7	20.5	2.49	2#8	55.0	54.4	1.01	lwa
65		5A1	152.4	559	2.10	266.7	24.1	2.49	2#8	48.3	57.0	0.85	lwa
66		6A1	152.4	559	2.10	266.7	25.3	2.49	2#8	44.6	57.8	0.77	lwa
67		7A1	152.4	559	2.10	266.7	22.1	2.49	2#8	56.6	55.6	1.02	lwa
68		7A1X	152.4	559	2.10	266.7	29.2	2.49	2#8	88.4	60.3	1.47	lwa
69		8A1X	152.4	559	2.10	266.7	25.5	2.49	2#8	80.4	65.24	1.23	lwar
70		8A1	152.4	559	2.10	266.7	27.7	2.49	2#8	57.7	66.81	0.86	lwar
71		2B1	152.4	559	2.10	266.7	36.9	2.49	2#8	96.1	64.4	1.49	lwa
72		3B1	152.4	559	2.10	266.7	28.2	2.49	2#8	48.9	59.6	0.82	lwa
73		4B1	152.4	559	2.10	266.7	33.7	2.49	2#8	83.8	62.8	1.34	lwa
74		5B1	152.4	559	2.10	266.7	33.0	2.49	2#8	48.7	62.4	0.78	lwa
75		6B1	152.4	559	2.10	266.7	33.6	2.49	2#8	70.2	62.7	1.12	lwa
76		7B1X	152.4	559	2.10	266.7	32.3	2.49	2#8	79.0	62.0	1.27	lwa
77		7B1	152.4	559	2.10	266.7	35.9	2.49	2#8	87.6	63.9	1.37	lwa
78		10B1	152.4	559	2.10	266.7	33.5	2.49	2#8	95.6	62.7	1.53	lwa
79		13B1	152.4	559	2.10	266.7	34.1	2.49	2#8	88.7	63.0	1.41	lwa
80		8B1	152.4	559	2.10	266.7	37.1	2.49	2#8	90.4	72.64	1.24	lwar
81		9C1	152.4	559	2.10	266.7	47.6	2.49	2#8	113.0	69.4	1.63	lwa
82		4C1	152.4	559	2.10	266.7	48.3	2.49	2#8	109.2	69.6	1.57	lwa
83		8C1	152.4	559	2.10	266.7	58.0	2.49	2#8	127.3	73.4	1.73	lwa
84		4D1	152.4	559	2.10	266.7	56.3	2.49	2#8	119.0	72.8	1.63	lwa

No.	Lit.	Name	b	a	M/Vd	d	f_{cm}	ρ_s	Rebar	V_u	V_{cal}	V_{cal}/V_u	database
-	-	-	mm	mm	-	mm	MPa	%	Configuration	kN	kN		
85		8D1	152.4	559	2.10	266.7	73.6	2.49	2#8	165.5	84.41	1.96	lwar
86	Ivy, Buth (1967)	(1)1	152.4	533	2.00	266.7	31.0	1.25	4#4	100.8	56.6	1.78	lwa
87		(1)2	152.4	889	3.33	266.7	31.0	1.25	4#4	39.1	45.0	0.87	lwa
88		(1)3	152.4	1321	4.95	266.7	32.3	1.25	4#4	33.4	38.3	0.87	lwa
89		(23)1	152.4	889	3.33	266.7	27.9	0.93	4#4	36.0	38.5	0.94	lwa
90		(23)2	152.4	889	3.33	266.7	28.8	1.25	4#4	37.4	44.0	0.85	lwa
91		(23)3	152.4	889	3.33	266.7	28.7	1.46	3#5	40.9	44.3	0.92	lwa
92		(23)1S	152.4	889	3.33	266.7	25.7	0.93	3#4	34.2	37.6	0.91	lwa
93		(23)2S	152.4	889	3.33	266.7	26.7	1.25	4#4	39.6	43.1	0.92	lwa
94		(23)3S	152.4	889	3.33	266.7	28.0	1.46	3#5	39.6	44.0	0.90	lwa
95		(27)1	152.4	533	2.00	266.7	23.2	1.25	4#4	73.0	52.1	1.40	lwa
96		(27)2	152.4	889	3.33	266.7	25.6	1.25	4#4	39.1	42.6	0.92	lwa
97		(27)3	152.4	1321	4.95	266.7	23.6	1.25	4#4	27.6	35.0	0.79	lwa
98		(23)4	108.0	627	3.33	188.5	24.5	1.25	2#4	16.9	22.2	0.76	lwa
99		(23)5	152.4	889	3.33	266.7	29.6	1.25	4#4	36.5	44.4	0.82	lwa
100		(23)6	152.4	1110	3.34	332.7	26.3	1.56	4#5	58.7	53.5	1.10	lwa
101		(23)7	190.5	1318	3.34	395.0	25.9	1.52	4#6	75.6	72.1	1.05	lwa
102		(23)8	152.4	533	2.00	266.7	20.9	0.93	3#4	49.9	44.3	1.13	lwa
103		(23)9	152.4	533	2.00	266.7	20.4	1.25	4#4	62.7	50.2	1.25	lwa
104		(23)10	152.4	533	2.00	266.7	22.4	1.46	3#5	62.2	51.5	1.21	lwa
105		(23)11	152.4	533	2.00	266.7	20.8	2.10	3#6	83.8	56.1	1.50	lwa
106		(23)12	152.4	800	3.00	266.7	22.5	2.10	3#6	54.3	48.1	1.13	lwa
107		(23)13	152.4	1067	4.00	266.7	22.1	2.10	3#6	38.3	42.3	0.91	lwa
108		(23)14	152.4	1321	4.95	266.7	19.2	2.10	3#6	39.8	37.1	1.07	lwa
109		(23)15	152.4	889	3.33	266.7	22.8	0.93	3#4	33.5	36.3	0.92	lwa
110		(23)16	152.4	889	3.33	266.7	19.2	1.25	4#4	39.2	39.2	1.00	lwa
111		(23)17	152.4	889	3.33	266.7	23.2	2.43	5#5	39.8	52.0	0.77	lwa

Table III. 4. Collection of shear tests with uniformly distributed load from (Krefeld and Thurston, 1966).

No.	Name	b	L	d	f_{cm}	ρ_s	Rebar	V_u	V_{cal}	V_{cal}/V_u	f_{cm}
-	-	mm	mm	mm	MPa	%	Config.	kN	kN	-	MPa
1	4A1	203.2	1829	390.1	29.2	2.06	2 #10	405.2	169.0	140.7	0.83
2	4B1	203.2	1829	390.1	27.5	2.06	2 #10	438.6	191.2	138.4	0.72
3	5A1	203.2	1829	390.1	29.4	3.09	3 #10	549.8	213.5	167.1	0.78
4	5B1	203.2	1829	390.1	29.6	3.09	3 #10	625.4	191.2	167.3	0.87
5	4A2	203.2	1829	390.1	28.1	2.06	2 #10	428.3	180.1	139.1	0.77
6	5A2	203.2	1829	390.1	29.4	3.09	3 #10	636.5	180.1	167.0	0.93
7	11A1	152.4	1829	313.9	27.0	3.42	2 #10	268.7	112.6	101.7	0.90
8	15A1	152.4	1829	316.0	19.2	1.34	1 #9	156.2	72.5	62.0	0.85
9	16A1	152.4	1829	239.8	21.0	1.76	1 #9	106.5	58.9	55.2	0.94
10	17A1	152.4	1829	242.8	18.3	2.10	2 #7	123.4	58.9	51.5	0.87
11	17B1	152.4	1829	242.8	21.0	2.10	2 #7	129.2	63.4	53.4	0.84
12	19A1	152.4	1829	239.8	21.2	3.53	2 #9	161.2	85.6	71.2	0.83
13	3AU	152.4	2438	255.5	22.7	1.99	2 #7	94.1	67.8	50.4	0.74
14	4AU	152.4	2438	254.0	17.9	2.62	2 #8	91.8	70.0	54.4	0.78
15	5AU	152.4	2438	252.5	20.6	3.35	2 #9	111.4	72.3	64.7	0.90
16	2CU	152.4	3048	254.0	20.8	1.31	1 #8	55.4	50.0	42.1	0.84
17	3CU	152.4	3048	255.5	20.5	1.99	2 #7	72.7	50.0	45.1	0.90
18	4CU	152.4	3048	254.0	20.5	2.62	2 #8	80.7	56.7	52.1	0.92
19	5CU	152.4	3048	252.5	20.4	3.35	2 #9	83.8	67.8	59.3	0.87
20	6CU	152.4	3048	250.4	20.5	4.28	2 #10	78.9	74.5	67.6	0.91
21	4EU	152.4	3658	254.0	20.2	2.62	2 #8	74.0	56.7	48.6	0.86
22	5EU	152.4	3658	252.5	19.3	3.35	2 #9	78.5	54.5	54.6	1.00
23	6EU	152.4	3658	250.4	20.1	4.28	2 #10	69.6	63.4	62.7	0.99
24	5GU	152.4	4267	252.5	21.3	3.35	2 #9	66.9	56.7	53.1	0.94
25	4JU	152.4	4877	254.0	22.2	2.62	2 #8	58.0	50.0	45.2	0.90
26	6U	152.4	1829	252.5	20.4	4.25	2 #10	171.5	85.6	83.2	0.97
27	4AAU	152.4	1829	254.0	36.4	2.62	2 #8	184.4	90.1	74.5	0.83
28	6AAU	152.4	1829	250.4	34.4	4.28	2 #10	215.9	90.1	95.6	1.06
29	4AU	152.4	2438	254.0	31.6	2.62	2 #8	118.5	76.7	64.0	0.83
30	5AU	152.4	2438	252.5	31.6	3.35	2 #9	133.6	94.5	73.0	0.77
31	6AU	152.4	2438	250.4	34.1	4.28	2 #10	155.9	90.1	85.0	0.94
32	4CU	152.4	3048	254.0	32.3	2.62	2 #8	98.5	74.5	59.3	0.80
33	5CU	152.4	3048	252.5	32.3	3.35	2 #9	96.3	85.6	67.5	0.79

No.	Name	b	L	d	f_{cm}	ρ_s	Rebar	V_u	V_{cal}	V_{cal}/V_u	f_{cm}
-	-	mm	mm	mm	MPa	%	Config.	kN	kN	-	MPa
34	6CU	152.4	3048	250.7	36.8	4.28	2 #10	108.7	92.3	79.8	0.86
35	3AAU	152.4	1829	255.5	12.5	1.99	2 #7	129.2	58.9	47.7	0.81
36	4AAU	152.4	1829	254.0	12.3	2.62	2 #8	112.7	54.5	54.9	1.01
37	6AAU	152.4	1829	250.4	13.4	4.28	2 #10	135.0	78.9	73.9	0.94
38	3AU	152.4	2438	255.5	13.7	1.99	2 #7	98.1	50.0	43.7	0.87
39	4AU	152.4	2438	254.0	12.7	2.62	2 #8	82.5	45.6	49.4	1.08
40	6AU	152.4	2438	250.4	12.4	4.28	2 #10	80.3	63.4	64.2	1.01
41	3CU	152.4	3048	255.5	12.2	1.99	2 #7	60.3	45.6	38.9	0.85
42	4CU	152.4	3048	254.0	17.1	2.62	2 #8	71.8	50.0	49.4	0.99
43	5CU	152.4	3048	252.5	14.7	3.35	2 #9	81.6	54.5	54.0	0.99
44	6CU	152.4	3048	250.4	13.7	4.28	2 #10	72.7	54.5	60.3	1.11
45	4EU	152.4	3658	254.0	14.3	2.62	2 #8	51.4	45.6	43.9	0.96
46	5EU	152.4	3658	252.5	15.1	3.35	2 #9	65.1	50.0	50.8	1.02
47	6EU	152.4	3658	250.4	12.8	4.28	2 #10	62.9	50.0	55.1	1.10
48	3GU	152.4	4267	255.5	13.5	1.99	2 #7	48.7	40.2	35.5	0.88
49	5GU	152.4	4267	252.5	11.2	3.35	2 #9	49.6	41.1	44.1	1.07
50	U	203.2	3048	482.6	21.1	1.55	3 #8	254.3	158.2	107.6	0.68
51	OU	254.0	3658	455.7	37.2	2.23	4 #9	286.4	216.5	163.8	0.76

Table III. 5. Collection of shear tests with uniformly distributed load from (TNO, 1977).

No.	Name	b	L	d	m	f_{cm}	ρ_s	Rebar	V_u	V_{cal}	V_{cal}/V_u
-	-	mm	mm	mm	-	MPa	%	Config.	kN	kN	-
1	A1L	150.0	900	150	0.00	20.1	2.05	3Ø14	98.8	88.0	0.89
2	A1R	150.0	900	150	0.00	20.1	2.05	3Ø14	129.8	93.9	0.72
3	A2L	150.0	900	150	0.25	22.2	2.05	3Ø14	95.0	82.8	0.87
4	A2R	150.0	900	150	0.25	22.2	2.05	3Ø14	104.9	81.6	0.78
5	A3L	150.0	900	150	0.50	21.5	2.05	3Ø14	85.3	58.5	0.69
6	A3R	150.0	900	150	0.50	21.5	2.05	3Ø14	77.9	70.1	0.90
7	A4L	150.0	900	150	0.75	23.6	2.05	3Ø14	58.1	83.2	1.43
8	A4R	150.0	900	150	0.75	23.6	2.05	3Ø14	77.6	53.3	0.69
9	A5L	150.0	900	150	1.00	24.7	2.05	3Ø14	88.0	57.5	0.65
10	A5R	150.0	900	150	1.00	24.7	2.05	3Ø14	55.6	66.3	1.19
11	B1L	150.0	1350	150	0.00	20.2	2.05	3Ø14	56.5	75.0	1.33
12	B1R	150.0	1350	150	0.00	20.2	2.05	3Ø14	56.5	85.0	1.51
13	B2L	150.0	1350	150	0.25	20.8	2.05	3Ø14	78.3	50.8	0.65
14	B2R	150.0	1350	150	0.25	20.8	2.05	3Ø14	66.4	60.8	0.92
15	B3L	150.0	1350	150	0.50	22.8	2.05	3Ø14	66.8	51.8	0.77
16	B3R	150.0	1350	150	0.50	22.8	2.05	3Ø14	61.7	66.5	1.08
17	B4L	150.0	1350	150	0.75	23.9	2.05	3Ø14	52.0	49.5	0.95
18	B4R	150.0	1350	150	0.75	23.9	2.05	3Ø14	52.0	82.8	1.59
19	B5L	150.0	1350	150	1.00	20.5	2.05	3Ø14	48.2	94.0	1.95
20	B5R	150.0	1350	150	1.00	20.5	2.05	3Ø14	60.8	108.9	1.79
21	C1L	150.0	1800	150	0.00	23.2	2.05	3Ø14	42.5	75.6	1.78
22	C1R	150.0	1800	150	0.00	23.2	2.05	3Ø14	41.0	85.9	2.10
23	C2L	150.0	1800	150	0.25	19.5	2.05	3Ø14	51.3	101.0	1.97
24	C2R	150.0	1800	150	0.25	19.5	2.05	3Ø14	60.3	62.8	1.04
25	C3R	150.0	1800	150	0.50	26.4	2.05	3Ø14	69.8	54.9	0.79
26	C4L	150.0	1800	150	0.75	24.3	2.05	3Ø14	53.6	95.1	1.78
27	C5L	150.0	1800	150	1.00	26.0	2.05	3Ø14	37.4	95.1	2.55
28	C5R	150.0	1800	150	1.00	26.0	2.05	3Ø14	42.1	87.0	2.07
29	A10L	150.0	900	150	0.00	24.3	2.05	3Ø14	93.2	86.9	0.93
30	A10R	150.0	900	150	0.00	24.3	2.05	3Ø14	91.6	79.4	0.87
31	A50R	150.0	900	150	1.00	25.1	2.05	3Ø14	56.3	79.2	1.41

About the Author

Yuguang YANG 杨宇光 was born in Jiaxing, Zhejiang, China on March 27, 1983. He received his BSc degree on Civil Engineering at Shanghai Jiao Tong University in 2005. From 2005 to 2007 he studied in Delft University of Technology supported on scholarship from TU Delft. He got his MSc degree with honour in 2007, and the graduation work was "Bending behaviour of a high performance concrete overlay on an orthotropic steel deck".

In October 2007, he became a Ph.D. candidate (Assistent in opleiding AIO) in the group of concrete structure, TU Delft under the supervision of Prof. Joost Walraven. The research topic was initially "Interaction between conventional reinforcement and high performance concrete". From 2008, he started the research on "Residual shear capacity of existing bridges" supported by Rijkswaterstaat (Dutch ministry of infrastructure and environment). The basic concepts of the theory presented in this dissertation were developed in this research. He continued his career as a Postdoc in the group of concrete structure, TU Delft with Prof. Dick Hordijk from Feb 2014.

By the moment this dissertation is finished, his research interests are shear behaviour of reinforced concrete structures, non-linear FEM modelling of concrete structures, and structural application of high performance concrete.

Shear loading on structures has been recognized as one of the most relevant actions determining structural safety since the 19th century. In the case of reinforced concrete structures, despite the great efforts that have been made through experimental and theoretical research over many years, the nature of the shear failure process of a reinforced concrete beam without shear reinforcement has always, for a substantial part, remained a riddle. The present research work takes a new look at this old problem. The mechanism of flexural shear failure for a reinforced concrete beam without shear reinforcement is explained fundamentally, based on which a new failure criterion is proposed. The study leads to a shear evaluation procedure that is in excellent agreement with test results.

ISBN 978-94-6169-516-1

TU Delft